

Confidential - Property of GlaxoSmithKline

Copying not permitted. Return to GSK



## **New Chemical Approaches for the Development of Targeted Protein Degradation**

Hannah Lithgow, MSci.

Industrial Supervisors: Ian E. D. Smith, Dr Markus Queisser

Academic Supervisor: Prof. Glenn A. Burley

## Contents

<b>DECLARATION .....</b>	<b>5</b>
<b>ABSTRACT .....</b>	<b>6</b>
<b>SCIENTIFIC ACKNOWLEDGEMENTS.....</b>	<b>8</b>
<b>PERSONAL ACKNOWLEDGEMENTS.....</b>	<b>9</b>
<b>1.1 ABBREVIATIONS .....</b>	<b>10</b>
<b>1.2 GLOSSARY .....</b>	<b>16</b>
<b>2. INTRODUCTION .....</b>	<b>17</b>
2.1 THE UBIQUITIN PROTEASOME SYSTEM .....	17
2.2 THE PROTAC APPROACH .....	20
2.2.1 <i>PROTACs and their Utility in Drug Discovery</i> .....	20
2.2.2 <i>Development of Peptidic PROTACs</i> .....	22
2.2.2.1 VHL recruiting PROTACs .....	22
2.2.2.2 KEAP1 recruiting PROTACs .....	23
2.2.3 <i>Development of Small Molecule PROTACs</i> .....	24
2.2.3.1 VHL recruiting PROTACs .....	24
2.2.3.2 Cereblon Recruiting PROTACs .....	36
2.2.3.3 MDM2 Recruiting PROTACs.....	43
2.2.3.4 IAP Recruiting PROTACs .....	44
2.2.3.5 DCAF15 Recruiting PROTACs .....	50
2.2.3.6 Current State of the Art.....	52
<b>3. OVERALL AIMS FOR THE RESEARCH.....</b>	<b>54</b>
<b>4. EXPANDING THE PROMISCUOUS TOOLBOX FOR EXAMINING NEW E3 LIGASES.....</b>	<b>59</b>
4.1 INTRODUCTION.....	59
4.1.1 <i>Building a Promiscuous Toolbox to Evaluate New E3 Ligases</i> .....	59
4.1.2 <i>Bromosporine and the Promiscuous Toolbox</i> .....	60
4.1.3 <i>Analysing the Protein Degradation from the Promiscuous Toolbox</i> .....	62
4.2 BROMOSPORINE PROTACs PROJECT AIMS AND OBJECTIVES .....	66
4.3 RESULTS AND DISCUSSION .....	68
4.3.1 <i>Design of Bromosporine PROTACs recruiting VHL and cereblon</i> .....	68
4.3.2 <i>Synthesis of Bromosporine PROTACs</i> .....	71
4.3.3 <i>Biological Evaluation of Bromosporine PROTACs</i> .....	75
4.4 SUMMARY AND FUTURE WORK .....	91
<b>5. INVESTIGATING DCAF15 AS A POTENTIAL E3 LIGASE FOR THE PROTAC APPROACH .....</b>	<b>95</b>
5.1 INTRODUCTION – THE E3 LIGASE DCAF15 .....	95
5.2 DCAF15 PROTACs PROJECT AIMS AND OBJECTIVES.....	96
5.3 RESULTS AND DISCUSSION .....	98
5.3.1 <i>Design of DCAF15 Recruiting PROTACs</i> .....	98
5.3.2 <i>Synthesis of DCAF15 Recruiting PROTACs</i> .....	101
5.3.4 <i>Biological Evaluation of DCAF15 Recruiting PROTACs</i> .....	105
5.3.4.1 Biological Evaluation of Indisulam Analogue.....	105
5.3.4.2 Biological Evaluation of RIPK2 Targeting DCAF PROTACs.....	106
5.3.4.3 Biological Evaluation of BTK DCAF PROTACs .....	108

5.3.4.4 Biological Evaluation of JQ1 derived DCAF PROTACs .....	110
5.3.4.5 Evaluation of the Lack of Degradation of the DCAF15 Recruiting PROTACs.....	112
5.4 SUMMARY AND FUTURE WORK .....	114
<b>6. VALIDATION OF A HIGH-THROUGHPUT GFP DEGRADATION ASSAY UTILISING HALOPROTACS TO KNOWN E3 LIGASES .....</b>	<b>117</b>
6.1 INTRODUCTION.....	117
6.2 HALOPROTACS PROJECT AIMS AND OBJECTIVES.....	119
6.3 RESULTS AND DISCUSSION .....	123
6.3.1 <i>Design and Synthesis of HaloPROTACs</i> .....	123
6.3.2 <i>Synthesis of HaloPROTACs</i> .....	127
6.3.2 <i>Biological Evaluation of VHL Recruiting HaloPROTACs</i> .....	132
6.3.3 <i>Biological Evaluation of IAP Recruiting HaloPROTACs</i> .....	136
6.3.4 <i>Biological Evaluation of KEAP1 Recruiting HaloPROTACs</i> .....	141
6.3.5 <i>Biological Evaluation of DCAF15 Recruiting HaloPROTACs</i> .....	143
6.3.6 <i>Biological Evaluation of Cereblon Recruiting HaloPROTACs</i> .....	144
6.4 SUMMARY AND FUTURE WORK .....	145
<b>7. HALOCOMPOUNDS AND THE SEARCH FOR NEW E3 LIGASES USING HTE.....</b>	<b>147</b>
7.1 INTRODUCTION – HIGH-THROUGHPUT EXPERIMENTATION.....	147
7.2 HIGH-THROUGHPUT SYNTHESIS OF HALOCOMPOUNDS PROJECT AIMS AND OBJECTIVES.....	149
7.3 RESULTS AND DISCUSSION .....	153
7.3.1 <i>In-Situ HaloPROTACs – Validation of Testing Reaction Mixtures</i> .....	153
7.3.2 <i>Computational Chemistry Selection for the HaloTag® Degradation Screen</i> .....	160
7.3.2.1 Optimisation Set – Selecting 300 amines .....	160
7.3.2.2 Validation Set – Selecting 3000 amines.....	163
7.3.3 <i>High-Throughput Chemistry for HaloCompound Synthesis</i> .....	166
7.3.3.1 HTE Optimisation – VHL as a Standard Amine.....	166
7.3.3.2 HaloCompound In-Situ Synthesis for the Optimisation Set.....	167
7.3.3.3 Computational Analysis of the Chemistry Optimisation Set .....	177
7.3.3.4 Further Chemistry Optimisation for HTE for the Validation Set.....	182
7.3.3.5 HaloCompound In-Situ Synthesis for the Validation Set .....	191
7.3.3.6 Computational Analysis of the Validation Set .....	194
7.3.4 <i>Biological Evaluation of the In-Situ HaloCompounds</i> .....	200
7.3.4.1 Biological Evaluation of the Chemistry Optimisation Set .....	200
7.3.4.2 Hit Evaluation from the Chemistry Optimisation Set .....	207
7.3.4.3 Biological Evaluation of the Validation Set.....	212
7.3.4.4 Hit Evaluation from the Validation Set.....	218
7.4 SUMMARY AND FUTURE WORK .....	223
<b>8 CONCLUSIONS .....</b>	<b>227</b>
<b>9 EXPERIMENTAL .....</b>	<b>229</b>
9.1 <i>General Methods</i> .....	229
9.2 <i>Synthetic Procedures</i> .....	231
9.2.1 Bromosporine-based PROTAC synthesis .....	232
9.2.2 DCAF15-based PROTAC synthesis .....	242
9.2.3 HaloPROTAC synthesis .....	264
9.3 <i>High-Throughput Chemistry Experiments</i> .....	277
9.3.1 General Considerations .....	277

9.3.2 General Procedures .....	278
9.3.3 Nanoscale Synthetic Procedures .....	280
<b>9.4 Supplementary Figures .....</b>	<b>292</b>
<b>9.5 Biological Experiments.....</b>	<b>296</b>
9.5.1 Cell culture .....	296
9.5.2 Compound preparation .....	296
9.5.3 Cell lysis .....	297
9.5.4 Protein Concentration Measurement .....	297
9.5.5 PAGE Electrophoresis .....	298
9.5.6 Western Blotting Experiments .....	298
9.5.7 Western Blot Quantification .....	298
9.5.8 GFP Degradation Assay .....	299
9.5.9 Fluorescence measurements in 384 well assay plates .....	299
<b>10 REFERENCES .....</b>	<b>301</b>
<b>11. SUPPLEMENTARY INFORMATION .....</b>	<b>312</b>

## Declaration

This thesis is the result of the author's original research. It has been composed by the author and has not been previously submitted for examination which has led to the award of a degree.

The copyright of this thesis belongs to GSK in accordance with the author's contract of engagement with GSK under the terms of the United Kingdom Copyright Acts. Due acknowledgement must always be made of the use of any material contained in, or derived from, this thesis.

Signed:

Date:

## Abstract

Proteolysis targeting chimeras (PROTACs) are heterobifunctional small molecules which induce targeted protein degradation by redirecting the ubiquitin-proteasome system. PROTACs simultaneously bind to both a protein of interest and an E3 ubiquitin ligase. The proximity of the target protein and the E3 ligase complex allows transfer of ubiquitin onto the target protein, after which the protein can be recognised and then degraded by the proteasome. The PROTAC mechanism-of-action offers a number of potential advantages over small molecule inhibition for the development of new medicines. Efficacy maybe achieved from low doses, extended duration of action is possible, arising from pharmacokinetic-pharmacodynamic disconnects, and challenging targets may become tractable through the identification of suitable affinity binders.

In this research, the development of PROTAC technology is explored. In order to expand the breadth of E3 ligases that are currently recruited using this approach, a promiscuous toolbox was established to prosecute new chemical matter for E3 ligases. In order to further elaborate the promiscuous toolbox already known for the degradation of kinases, investigation of a promiscuous bromodomain PROTAC was explored. After assessment of bromosporine derived PROTACs in multiple cell lines with two validated E3 ligases, it was deemed an unsuitable binder for the toolbox. The PROTACs were unable to induce potent nor promiscuous bromodomain degradation. As a result, a known BET bromodomain binder was selected for the promiscuous toolbox in addition to the known promiscuous kinase binder and a RIPK2 binder for new E3 ligase validation.

With a promiscuous toolbox in hand, a new E3 ligase was evaluated. Indisulam, a small molecule “molecular glue”, was found to bind to the E3 ligase DCAF15. Indisulam derived PROTACs were synthesised and evaluated with a range of linker lengths and multiple protein binders. These studies conclusively demonstrated that protein degradation was not achieved using these PROTACs. The indisulam derived binder was subsequently found not to be suitable for the PROTAC approach without further investigation to determine DCAF15 recruitment.

Given the lack of degradation with the initial, empirically selected E3 ligases from the literature, a distinct E3 ligase agnostic approach to protein degradation was developed. A high-throughput phenotypic screen was established using green fluorescent protein (GFP) as the protein of interest, where cellular fluorescence levels correlate with protein degradation. High-throughput chemistry techniques were implemented and optimised to synthesise thousands of HaloCompounds *in-situ* by amide coupling. The compounds were tested directly in cells to find new chemical matter for the induction of protein degradation. This strategy allowed

identification of several potential hits from a 3000-amine screen, with one high-confidence hit currently being further evaluated. For this effort the screen was optimised successfully and can potentially be employed for a target-agnostic high-throughput screening campaign of hundreds of thousands of compounds for new E3 ligases to employ in future protein degradation strategies.

## Scientific Acknowledgements

Thank you to my supervisor Ian Smith for supervision and initial training. Also thank you for generating the images presented in this thesis.

For the bromosporine work, I'd like to thank Marcel Mülbaier and Mark Rackham for the initial idea of setting up a promiscuous bromodomain project. I'd like to thank the biology students Abigail Jones, for running my Western blots and guiding me through the process. To Jade Morgan, who supervised me running my very own blots. To Nico Zinn for the proteomics analysis and the affinity enrichment proteomics.

For the DCAF15 work, I'd like to thank Markus Queisser and Jess Eden for running the Western blot analysis.

For the HaloTag projects, I'd like to thank Marcel Mülbaier and Markus Queisser, for the idea of running a phenotypic screen. I'd really like to say thank you for allowing me to lead, manage and execute this amazing idea into my own project when it came to overall decision making. I'd like to thank Peter Stacey and Agnieszka Konopacka, for the development of the GFP mutant control cell line. Also, I'd like to thank Peter for his supervision and guidance in helping me run my GFP biological assays independently through this thesis.

I'd like to thank Blandine McKay, for acquiring the Mosquito liquid handling, and coordinating the calibration and set-up of the machine. I'd like to thank David Battersby, for the introduction to HTE and the many references he provided (and the proof reading afterwards!).

To Georgina Green and Steve Besley, for their help with the analytical LCMS set-up, and help streamlining the output for thousands of LCMS data points into excel.

To Xiao Lewell for her help with all the great and thorough computational analysis, including the compound selection, the pK<sub>a</sub>H calculations and the resulting reaction analysis.

To David Battersby for his guidance and introduction to HTE and experimental write up.

I've learned an amazing amount of biology, high-throughput chemistry, project management and computational chemistry throughout, and now have complete respect for the intricacies in running HTS screens, so thank you to everyone involved.

## Personal Acknowledgements

I must start by thanking my supervisors Ian Smith, Markus Queisser and Glenn Burley for all their support over the last 3 years. None of this would have been possible without their guidance, direction and reassurance that everything was going to work out just fine (after a year and a half of no results, this was a hard task!). I thank them for all their hard work and advice and helping me start to become more confident in myself and my own abilities. I'd like to thank the Protein Degradation department, for the amazing fun over the last three years, you've become like a family to me, and I'm really going to miss that. Specifically, Chris Tinworth and Rob Law who helped me immensely in the lab. To Jenny Borthwick, Mark Rackham and Chris Tame who were there for me when I needed someone to talk to. In addition, the other PhDs (GSK and Strathclyde), who all go through the ups and downs of a PhD and who have helped me through the process and made it enjoyable.

I also must thank the PhD programme itself for the unique opportunity of a PhD in GSK. I'd like to thank Harry Kelly and Billy Kerr immensely for this and everything they have done for me, and Andrea Malley and Laura Paterson for their effort to make this happen.

I'd like to thank Dr. Watson, my amazing flatmate, who always had time to listen and binge watch Netflix on bad days, to Erin who was available for reassuring hugs as Mo was not a hugger... To Abby Whitnall my angel without wings (so a person) who randomly rang my doorbell with flowers when writing wasn't going as planned. My weird and wonderful friends, Olga, Kate and Emma (aka PupperSquad), for always sending me dog pictures to cheer me up and accompanying me in amazing places in the world on adventures. To Matthew, my wonderfully patient and kind boyfriend, who always believed I could do it even when I didn't and got me through it in one piece and even sang to me through the sleepless nights. I'd also like to thank my family, for support and help throughout (despite making fun of me at every step of the way).

And finally, thanks to the very few people who will read this, this was a huge effort from myself and my supervisors correcting it, so thank you. I cannot wait until this lies in a cupboard gathering dust and I never have to see it again.

## 1.1 Abbreviations

% wt	percentage weight
[M+H] <sup>+</sup>	mass plus proton
A375	human cell line derived from malignant melanoma
AAK1	AP2-associated protein kinase 1
ABL	Abelson murine leukemia viral oncogene homolog 1
Ac	Acetyl
AGC	protein kinase families A, C and G
ALK	Anaplastic lymphoma kinase
Aq.	aqueous
AR	androgen receptor
ATP	adenosine triphosphate
AURK	aurora kinases
BCL	B-cell lymphoma
BCR	breakpoint cluster region
BCR-ABL	fusion gene of BCR and ABL
BD1/2	bromodomain 1/2
BET	bromodomain and extra terminal domain
BL	Burkitt lymphoma
Boc	<i>tert</i> -butyloxycarbonyl
BRD4	bromodomain-containing protein 4
BTK	Bruton's tyrosine kinase
c-ABL	Abelson tyrosine kinase
CAD	charged aerosol detector solubility
Calcd	calculated
Cas9	CRISPR associated protein 9
cChromLogD	calculated chromatographic LogD
CCL7	C-C motif chemokine 7
CDK	Cyclin-dependent kinase
BCL	B-cell lymphoma
CECR2	Cat eye syndrome critical region protein 2
ChromLogD	chromatographic LogD
clAP1	cellular inhibitor of apoptosis protein-1
clAP2	cellular inhibitor of apoptosis protein-2
CK1	casein kinase 1
ClipTACs	clicked chemistry derived PROTACs
CLK	cdc2-like kinase
CLND	chemiluminescent nitrogen detection
clogP	calculated LogP
c-Met	proto-oncogenic Mesenchymal to Epithelial Transition kinase
CMKC	Calcium/calmodulin-dependent protein kinase
<i>c-MYC</i>	regulator gene that encodes transcription factors

CPME	cyclopentyl methyl ether
CPP	cell penetrating peptide
CRABPs	cellular retinoic acid-binding proteins
CRBN	Cereblon (gene)
CRISPR	clustered regularly-interspaced short palindromic repeats
CRL	Cullin–RING E3 ubiquitin ligase
CSK	C-terminal Src kinase
c-Src	cellular Src kinase
CuAAC	Cu(I)-catalyzed azide-alkyne cycloaddition
Cul4A	Cullin-4A
dba	tris(dibenzylideneacetone)
DC <sub>50</sub>	half maximal degradation concentration
DCAF	DDB1 and CUL4 associated factors
DC <sub>max</sub>	concentration at which maximal degradation is achieved
DDA1	DET1- and DDB1-associated protein 1
DDB1	DNA binding protein 1
DIAD	diisopropyl azodicarboxylate
DIPEA	<i>N,N</i> -diisopropylethylamine
DMAP	4-(dimethylamino)pyridine
DMF	<i>N,N</i> -dimethylformamide
DMSO	dimethylsulfoxide
DNA	deoxyribonucleic acid
Dppf	1,1'-bis(diphenylphosphino)ferrocene
DUBs	deubiquitinating enzymes
EG	ethylene glycol
EGFR	Epidermal growth factor receptor
ELT	encoded library technology (DNA specifically)
ER	estrogen receptor
ERK	extracellular regulated kinase
ERR $\alpha$	estrogen-related receptor alpha
ER $\alpha$	estrogen receptor alpha
ESI	electrospray ionisation mass spectrometry
Et	ethyl
FCC	flash column chromatography
FDA	Food and Drug Administration
Fer	kinase encoded by Fer gene
Fes	kinase encoded by Fes gene
Fgf8	fibroblast growth factor 8
FKBP	FK506 binding protein
FLT3	fetal liver tyrosine kinase 3.
For	formic
FP assay	fluorescence polarization assay
GAK	G-associated kinase

Confidential – Do Not Copy

GCN5	general control of amino-acid synthesis
GFP	green fluorescent protein
Gly	glycine
GSK	GlaxoSmithKline
GSK3	glycogen synthase kinase-3
GTP	guanosine-5'-triphosphate
h	hour
H3122	human derived cell line from lung adenocarcinoma
HaloPROTAC	HaloTag® targeting PROTACs
HATU	(1-[bis(dimethylamino)methylene]-1H-1,2,3-triazolo[4,5-b]pyridinium3-oxid hexafluorophosphate
Hba	hydrogen bonding acceptor
Hbd	hydrogen bonding donator
HDAC	Histone Deacetylase
HECT	homologous to the E6-AP carboxyl terminus
HEK293	human derived cell line from embryonic kidney cells
HeLa	human derived cell line from cervical cancer (Henrietta Lacks)
HER2	human epidermal growth factor receptor 2
HIF1 $\alpha$	hypoxia-inducible factor-1alpha
HMBC	heteronuclear multiple bond correlation
HOBt	hydroxybenzotriazole
HomoPROTAC	PROTAC targeting its own E3 ligase for degradation
HPH	high pH
HPLC	high performance liquid chromatography
HRMS	high resolution mass spectrometry
HSQC	heteronuclear single quantum correlation
HTE	high-throughput experimentation
HTS	high-throughput screening
IAP	inhibitor of apoptosis
IC <sub>50</sub>	half maximal inhibitory concentration
IkBa	nuclear factor of kappa light polypeptide gene enhancer in B-cells inhibitor, alpha
IKK $\epsilon$	IkB kinase- $\epsilon$
IKZF	gene that encodes Ikaros family zinc finger protein 1
IKZF1	Ikaros
IKZF3	Aiolos
IL-6	interleukin 6
Ilk1	Integrin-linked kinase 1
IMiD	immunomodulatory drug
IP (dose)	Intraperitoneal injection
IPA	isopropyl alcohol
IR	infrared spectroscopy

Confidential – Do Not Copy

ITK	interleukin-2-inducible T-cell kinase
FRET	fluorescence resonance energy transfer
IV	intravenous
JQ1	thienotriazolodiazepine, a potent inhibitor of the BET family bromodomains
K <sub>d</sub>	dissociation constant
KEAP1	Kelch-like ECH-associated protein 1
KDAC	targeting lysine deacetylases
LBD	ligand binding domain
LCMS	liquid chromatography mass spectrometry
LHS	left hand side
LPS	lipopolysaccharide
m/z	mass / charge
MALDI-TOF	matrix assisted laser desorption ionization - time of flight
MAPK	mitogen-activated protein kinase
MCP1	monocyte chemoattractant protein-1.
MDA-MB-231	human derived cell line from breast cancer
MDAP	mass directed automated preparative HPLC
MDM2	mouse double minute 2 homologs
MDP	muramyl dipeptide
Me	methyl
MEIS2	meis homeobox 2
MetAP2	methionyl aminopeptidase 2
min	minute
MOLM-14	human derived cell line from acute myeloid leukemia
Ms	mesyl
MUT	GFP-HaloTag® mutant control cell line
MV4-11	human acute monocytic cell line
MW	molecular weight
NCS	<i>N</i> -chlorosuccinimide
NHS	<i>l</i> -hydroxysuccinimide esters
NMM	<i>N</i> -methylmorpholine
NMP	<i>N</i> -methyl-2-pyrrolidone
NMR	nuclear magnetic resonance
Nrf2	Nuclear factor erythroid 2-related factor 2
NUT	gene which encodes for nuclear protein in testis
OAc	acetate
ODD	oxygen-dependent degradation domain
P53	tumor suppressor protein that in humans is encoded by the TP53 gene
PAINS	pan-assay interference compounds
PB	protein binding
PBMC	peripheral blood mononuclear cell
PC3	human derived cell line from prostate cancer
PCAF	P300/CBP-associated factor

Confidential – Do Not Copy

PEG	polyethylene glycol
PFI	property forecast index (log D7.4 + aromatic ring count)
PG	protecting group
pIC <sub>50</sub>	pIC <sub>50</sub> = -log(IC <sub>50</sub> )
PIM	proviral insertion in murine
PK	pharmacokinetics
PKa	negative base-10 logarithm of the acid dissociation constant (Ka)
PKA	protein kinase A
PKG	protein kinase G
PKC	protein kinase C
POI	protein of interest
PPI	protein-protein interactions
PROTAC	proteolysis-targeting chimera
PTK2 (FAK)	protein tyrosine kinase 2 (focal adhesion kinase)
PTK2B	protein tyrosine kinase 2 beta
Pypy	pyrimidine pyrazole
QC	quality control
RBM39 (CAPERα)	recombinant mouse RNA-binding protein 39
RFMS	rapid fire mass spectrometry
RHS	right hand side
RING	interesting new gene
RIPK2	receptor-interacting serine/threonine-protein kinase 2
RNA	ribonucleic acid
ROCO	GTPase domain
RPS6KA	ribosomal protein s6 kinase alpha.
RS4;11	human derived cell line from acute lymphoblastic leukemia bone marrow
rt	room temperature
SAR	structure activity relationship
SARM	selective androgen receptor modulators
sat.	saturated
SCF	Skp1–Cul1–F-box-protein
SCX	strong cation exchange
SEM	[2-(trimethylsilyl)ethoxy]methyl
Ser	serine
SGC	Structural Genomics Consortium
siRNA	small interfering ribonucleic acid
Sirt	Sirtuin
SM	starting material
SMAC	Second mitochondria derived activator of caspase
SMARCA2	SWI/SNF related, matrix associated actin dependent regulator of chromatin
SMILES	simplified molecular-input line-entry system
SMKI	small molecule kinase inhibitors
smMLCK	calcium/calmodulin-dependent myosin light chain kinase

Confidential – Do Not Copy

SNAR	nucleophilic aromatic substitution
SNIPERs	specific and nongenetic (IAPs)-dependent protein eraser
SPE	solid phase extraction
SPLAMs	splicing inhibitor sulfonamides
STE	sterile
T3P	propylphosphonic anhydride
TAF1	TBP-associated factor 1
TBK1	TANK-binding kinase 1
TBME	methyl <i>tert</i> -butyl ether
tBu	<i>tert</i> -butyl
TCO	trans-cyclooctene
TFA	trifluoroacetic acid
THF	tetrahydrofuran
THP-1	human leukemia monocytic cell line
TK	tyrosine kinase
TKL	tyrosine kinase-like
TMT	tandem mass tag
TNF	tumour necrosis factor
Tpsa	topological polar surface area
TRIM24	tripartite motif 24
Tz	tetrazine
UHT	ultra high-throughput
UPLC	ultra performance liquid chromatography
UPS	ubiquitin proteasome system
UV	ultraviolet
VCaP	human derived cell line from prostate cancer
VCB	VHL-elonginB-elonginC
VHL	Von Hippel-Lindau
VT NMR	variable temperature NMR
XIAP	X-linked Inhibitor-of-Apoptosis Protein
Xphos	2-dicyclohexylphosphino-2',4',6'-triisopropylbiphenyl

## 1.2 Glossary

(p)IC <sub>50</sub>	<p><i>Binding Potency</i>: The half maximal inhibitory concentration measured <i>in vitro</i> for a specified protein using for example Fluorescence Polarization (FP) or Fluorescence Resonance Energy Transfer (FRET) binding assays.<sup>1</sup></p> <p><i>Cellular Potency</i>: The half maximal inhibitory concentration following compound administration to cells and subsequent measurement of for example a reduction in cytokine release as a result of inhibition of the targeted protein.<sup>2,3</sup></p> <p>(The “p” prefix denotes the negative logarithmic value)</p>
DC <sub>50</sub>	The half maximal concentration of the degradation of a specified protein measured following administration to cells following a specified incubation time, and measured by for example Western Blotting analysis, fluorescence based assays, or proteomics. <sup>4,5</sup>
ChromLogD	<p>Lipophilicity of the compounds:</p> <p>Chromatographic LogD = (Chromatographic Hydrophobicity Index (CHI) * 0.857) – 2.00</p> <p>CHI is measured using reverse phase HPLC at pH 7.4, and derived from gradient retention time by using calibration lines obtained for standard compounds.<sup>6</sup></p>
Solubility	<p>Kinetic aqueous solubility is measured from a DMSO solution of the compound by addition into water and subsequent filtration. The concentration of the compound in the filtrate is quantified by either:</p> <p>CLND: Chemiluminescent Nitrogen Detection, or</p> <p>CAD: Charged Aerosol Detection.<sup>6</sup></p>

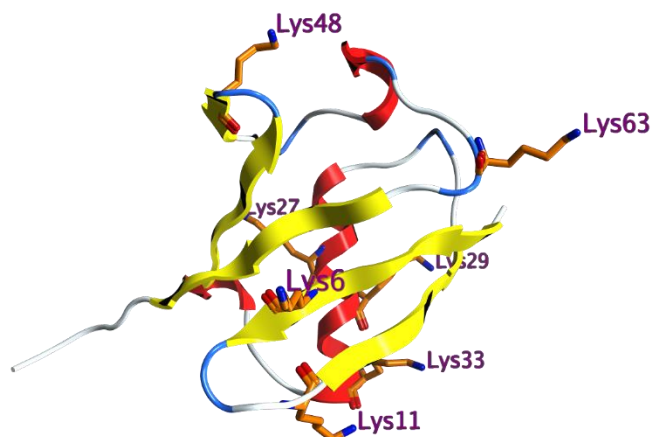
## 2. Introduction

### 2.1 The Ubiquitin Proteasome System

Degradation of proteins is an essential biological process required for the regulation of homeostasis, cell differentiation and proliferation.<sup>7</sup> Within cells, proteins are continuously being degraded by amide hydrolysis into short peptides and then recycled. The two main methods of achieving protein degradation are by proteolysis in lysosomes and via the ubiquitin-proteasome system (UPS).<sup>8,9</sup> The UPS operates via a complex and selective process of “tagging” a target protein for subsequent recognition, trafficking and degradation by the 26S proteasome (**Figure 1A**).<sup>10,11</sup>

The conjugation of ubiquitin to a protein, known as ubiquitination, is the process by which the UPS recognises which proteins are destined for destruction.<sup>10</sup> Proteins are “tagged” with polymeric chains of Ubiquitin. Ubiquitin is an 8.5 kDa protein which is highly conserved in eukaryotes and regulates various cellular processes through covalent conjugation to specific proteins (**Figure 1A**). Tagging occurs by the covalent conjugation of an activated ubiquitin to the side-chain amine function of a surface lysine residue or an N-terminal methionine.<sup>12</sup> This process begins with the activation of ubiquitin by an E1 enzyme (also known as the ubiquitin activating enzyme) via adenylation and the formation of a thioester bond from a cysteine residue to the C-terminus of ubiquitin (**Figure 1B**).<sup>13</sup> Ubiquitin is subsequently transferred to an E2 enzyme (also known as the ubiquitin conjugating enzyme) through transthioesterification.<sup>9,14</sup> An E3 ligase then interacts with the E2 enzyme in one of two ways depending on the class of E3 ligase to which it belongs. The target protein will then be ubiquitinated through a reaction between a surface lysine residue with the thioester, resulting in the monoubiquitination of the protein. An E3 ligase can also catalyse the polyubiquitination of the target in the same way as for monoubiquitination. Ubiquitin has eight attachment sites that can be used to couple to another ubiquitin molecule to form this poly-ubiquitinated chain (via 1 of 7 lysines, shown in **Figure 1A** or the N-terminal methionine). The combination of E2 enzyme and the E3 ligase determines the type of ubiquitin chain that is formed, which can either be branched or linear and reside on the 8 distinct ubiquitin attachment sites. Each type of chain formed has different properties and mediates different cellular functions.<sup>12</sup> Polyubiquitination at Lys48 of ubiquitin acts as the main signal for protein trafficking to the proteasome resulting in protein degradation.<sup>15</sup> This process can also be reversed through the action of deubiquitinating enzymes (DUBs).<sup>16,17</sup>

A)



B)

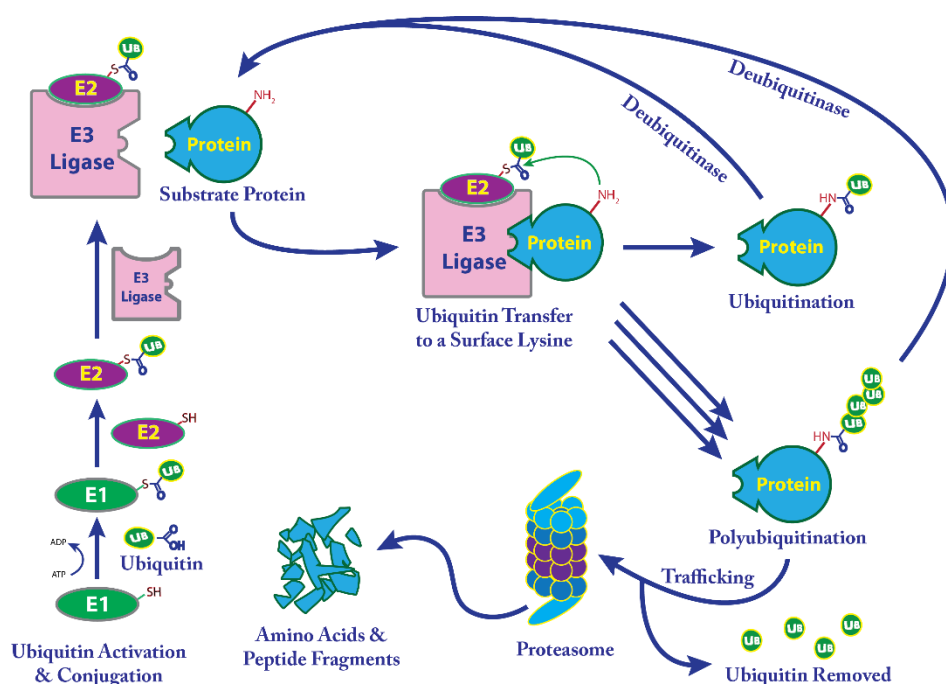


**Figure 1:** Molecular model of ubiquitin protein, highlighting the secondary structure (A).  $\alpha$ -helices are coloured in red and  $\beta$ -strands in yellow. The sidechains of the 7 lysine residues are indicated by orange sticks. (Image was created using MOE from PDB 1ubi). Ubiquitination of a target protein and subsequent cascade leading to proteasomal degradation (B).

There are two major forms of E3 ligases known, which have subtle mechanistic differences. A RING (really interesting new gene) E3 ligase acts as a scaffold between the ubiquitinated E2 enzyme and the target protein, bringing the two in close proximity to facilitate the transfer of ubiquitin to a lysine residue directly on the surface of the target protein (**Figure 2**).<sup>18</sup> By comparison, the HECT (homologous to E6-associated protein C-terminus) E3 ligases have a direct role in the catalysis, by forming an intermediate thioester-linked ubiquitin which is subsequently transferred to the target substrate.<sup>19</sup>

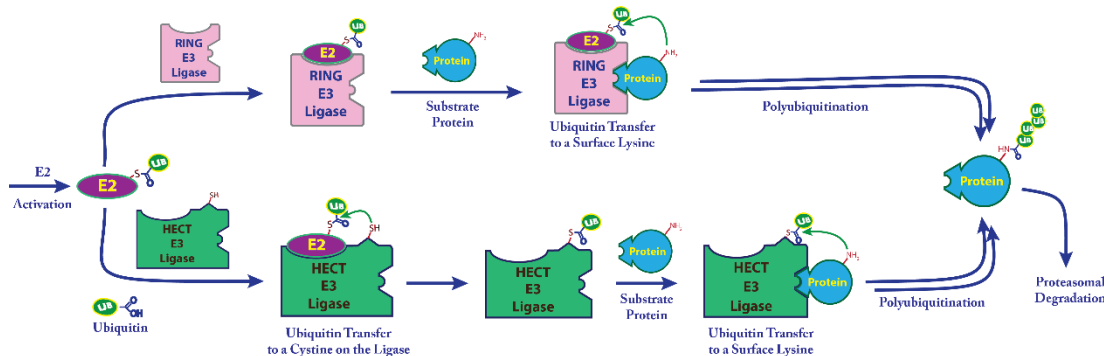


**Figure 2:** Comparing the mechanisms of action of HECT and RING E3 ligases in the UPS.

The proteasome is a multi-subunit enzyme which facilitates protein hydrolysis of the ubiquitinated substrates. The 26S proteasome consists of two components, a 20S core and 19S cap.<sup>10</sup> The 19S cap consists of 19 proteins which are made up of a base and a lid complex (**Figure 3**).<sup>20,21</sup> This acts as the recognition site for the appropriately-linked polyubiquitin tags which are then removed by DUBs. The 20S core is the site of protein degradation and consists of two types of subunits:  $\alpha$ -subunits and  $\beta$ -subunits. Both types of subunits are made up of seven proteins, which organise into a hollow chambered structure which allows for protein processing. The  $\alpha$ -rings are required for structural and gatekeeping purposes and the  $\beta$ -ring contain the protease active sites. In the internal core, subunits  $\beta_2$ ,  $\beta_5$  and  $\beta_1$  have proteolytic activity, exhibiting trypsin-like, chymotrypsin-like, and caspase-like peptidase activity respectively. Protein degradation then occurs by cleaving peptide substrates at basic, hydrophobic, and acidic sites. This gives rise to small peptide fragments which can then be further degraded to amino acids and recycled.<sup>10,22</sup>

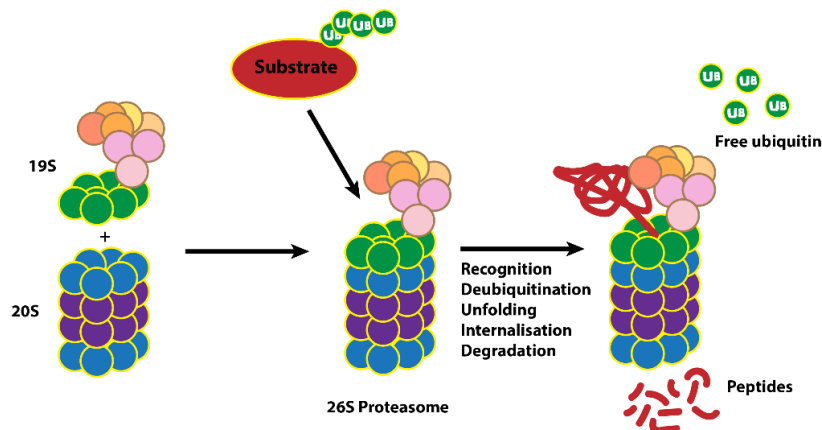


**Figure 3:** Composition of the 26S proteasome (19S: base complex in green, and the lid in pink/orange, 20S:  $\alpha$ -rings in blue,  $\beta$ -ring in purple (with seven subunits in each ring)).

## 2.2 The PROTAC Approach

### 2.2.1 PROTACs and their Utility in Drug Discovery

Induction of protein degradation promises to become a powerful new therapeutic modality for drug discovery. There are limitations to conventional small molecule modulation of biological targets which could be mediated through the protein degradation approach. The requirement to engage the target *in vivo* at relatively high drug concentrations and maintaining this efficacious concentration for the duration of the effect is a challenge for orally-dosed small molecules.<sup>23</sup> Upon clearance of the small molecule drug from the system, biological function is regained and the desired therapeutic effects are lost without a subsequent dose. As a result, new approaches to drug discovery such as complete protein removal from the cell are being investigated. This would mean that all of the protein's functions will be diminished until it has been resynthesised. The rate of protein resynthesis depends on protein type and localisation, and can range from minutes to days.<sup>24</sup>

Previous methods for protein removal in drug discovery have primarily involved the use of biological agents. RNA interference is used to knockdown proteins and alter expression levels in the cell. This is achieved by using small interfering, double-stranded RNAs (siRNA).<sup>25</sup> However, this technique has inherent issues, such as generally low cellular permeability siRNA molecules leading to low levels of agent at the desired site of action. Furthermore, siRNA molecules tend to preferentially distribute to specific organs such as liver and spleen, which may be undesired.<sup>26,27</sup> Another example of protein removal from cells is the CRISPR-Cas9 technique of genetic editing and knockout with CRIPSR first reported in the 1990s.<sup>28,29</sup> This technique has developed significantly since being reported for gene editing in 2005 with the modification of genes in organisms such as plants, zebra fish and mice. At present, off-target effects have been observed in the alteration of DNA in human cells.<sup>28,29</sup> As a result, many challenges must still be addressed before this can be considered a safe and efficacious technique for the treatment of diseases.<sup>30</sup>

An alternative method to decrease cellular protein levels in cells involves the use of PROTACs (PROteolysis TArgeting Chimeras). These heterobifunctional molecules are designed to harness the UPS to specifically target selected proteins for degradation (**Figure 4**).<sup>13,31,32</sup> PROTAC molecules consist of two binders: one for the protein of interest and the other for an E3 ligase which are linked together to give a structure that brings the target protein and the selected E3 ligase into close proximity for ubiquitin transfer.<sup>33,34</sup> It is believed that the mechanism of action of these molecules is the non-canonical polyubiquitination of a surface lysine of the target protein and subsequent degradation. This is thought to be achieved through

the formation of a non-covalent ternary complex of the PROTAC binding to its two respective binding partners<sup>35</sup> thereby creating a close proximity environment between the ubiquitin on an E3 ligase and a lysine residue of the target protein, analogous to the native UPS.<sup>4</sup> In order for this approach to be viable, the protein must have a surface lysine available for ubiquitination, and the ternary complex must adopt the correct orientation for effecting this transfer. In the PROTAC mechanism of action the PROTAC acts as a catalyst for the degradation process. As binding to each target is reversible, one molecule of PROTAC may be able to induce degradation of multiple molecules of protein and can continue until the PROTAC is cleared or all of the protein is removed.<sup>32</sup>

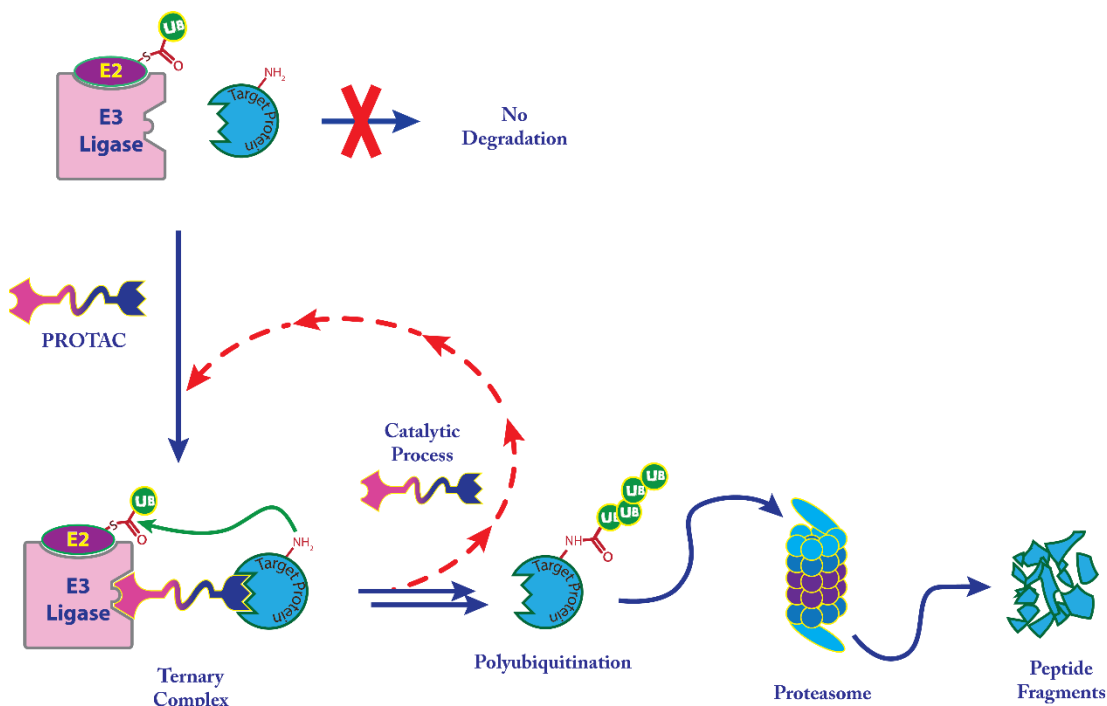


**Figure 4:** The PROTAC approach to protein degradation.

Since the conception of targeted protein degradation in the late 1990s and the early 2000s,<sup>31</sup> methods for validating the PROTAC approach for drug discovery have subsequently been the focus of industrial and academic research and will be discussed in the following section. In order for the approach to be viable as a method of therapeutic intervention, it must deliver drug candidates which are efficacious, tolerated and safe and additionally provide advantages over small molecule oral compounds and other methods of protein knockdown or knockout.

Small molecule PROTACs can have additional advantages over siRNA and CRISPR-Cas9 for the knock-down of proteins in cells. Use of suitably optimised small molecules leads to more cell-permeable protein knock-down agents than siRNA, where the largest impediment to clinical utility is poor exposure.<sup>27</sup> In comparison, PROTACs should induce very selective target knock-down through the incorporation of a selective target protein binder into the PROTAC

molecule.<sup>4,36</sup> Another potential advantage of this approach is the titratability of PROTACs. After dosing, the PROTAC drug would be cleared by metabolism and excreted and the target protein would be resynthesised. This contrasts with gene modification which leads to long term, or even permanent protein knockout, with potential for toxicity.<sup>28</sup>

The PROTAC approach in drug discovery will have a number of other advantages over conventional small molecule target inhibitors. The catalytic nature of PROTACs should lead to a low efficacious dose. Depending on the resynthesis rate of the protein and the pharmacokinetics of the PROTAC, this could result in a longer duration of action which may lead to more efficacious therapeutics.<sup>32,36</sup>

Although there are many potential advantages to a PROTAC medicine, there may also be limitations of the PROTAC approach in comparison to conventional small molecule inhibitors/antagonists. Due to their larger molecular weight, typically 800 Da or more, it may be more difficult to achieve routine oral bioavailability, although this has been achieved with some large molecular weight macrocycles.<sup>37</sup> However, with infrequent dosing, parenteral routes may be acceptable compared to oral administration. The large size and flexibility of PROTACs may also reduce the probability of achieving blood brain barrier permeability.<sup>38</sup> As a result, lead compounds for the PROTAC approach may require significant optimisation to achieve suitable drug-like qualities depending on target organs and drug delivery modality.

One perceived advantage of the PROTAC approach, in comparison to occupancy-based small molecule inhibition, is that a functional binding site is not required; only affinity binding is required to allow ternary complex formation between the protein of interest and the E3 ligase.<sup>14</sup> In contrast, a functional binding site is required for conventional small molecule approaches to achieve inhibition of the target pharmacology. For example, in the case of kinase inhibitors a small molecule inhibitor competes for the ATP binding site and good target selectivity is often difficult to achieve due to large sequence and structural conservation in the ATP domains between various kinases.<sup>39,40</sup>

## **2.2.2 Development of Peptidic PROTACs**

### **2.2.2.1 VHL recruiting PROTACs**

PROTAC molecules were first synthesised by Craig Crews and co-workers in the early 2000s, utilising peptidic binders to E3 ligases.<sup>31,33,41-44</sup> Von Hippel-Lindau protein (VHL) was one of the first E3 ligase utilised in the PROTAC approach to test the initial hypothesis of protein degradation using heterobifunctional molecules. VHL is a RING E3 ligase with a known

endogenous substrate, hypoxia-inducible factor 1 $\alpha$  (HIF1 $\alpha$ ) which is recognised by VHL upon hydroxylation of a critical proline residue by HIF prolyl-hydroxylases under normoxic conditions.<sup>45</sup> An ER degrading PROTAC **1** was first designed by conjugating a steroidal ER inhibitor to a hydroxylated amino acid pentamer, LAhypYI, which binds to VHL in the same manner as hydroxylated HIF1 $\alpha$  (**Figure 5**).<sup>33,46</sup> This was shown to give a functional and cell permeable PROTAC recruiting VHL, albeit showing degradation only at relatively high concentrations (>10  $\mu$ M). The pentamer containing PROTACs were the first reported examples of cellularly active PROTACs and confirmed their potential utility as bifunctional molecules which could induce cellular protein degradation.

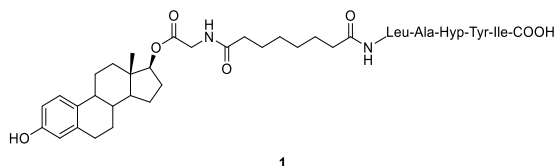


**Figure 5:** ER targeting PROTAC **1** based on a peptidic VHL binder.

#### 2.2.2.2 KEAP1 recruiting PROTACs

In an attempt to assess the utility of another E3 ligase for the PROTAC approach, the Kelch-like ECH-associated protein-1 (KEAP1) was investigated using novel peptidic PROTACs.<sup>47</sup> KEAP1 targeting peptides were synthesised and conjugated to a peptide that recognises and binds to the protein of interest, Tau (**Figure 6**). In order to achieve cell permeability, the compound **2** was designed by conjugating the two warheads to a cell-penetrating peptide poly-d-arginine (CPP). The PROTAC **2** was shown to degrade Tau in concentration and time-dependent manners (20  $\mu$ M required for potent knockdown). Degradation was prevented in the presence of MG132, a proteasome inhibitor, establishing that protein degradation was via PROTAC-induced ubiquitination. Although there are no small molecule KEAP1 recruiting PROTACs, this research demonstrated that KEAP1 is a viable E3 ligase to employ for future PROTAC design.

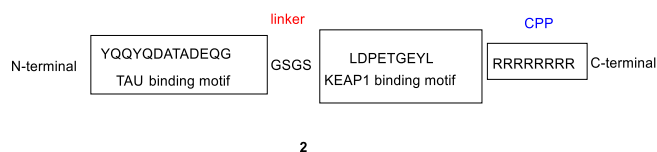


**Figure 6:** KEAP1 peptidic (CPP) PROTAC **2**.

In order to demonstrate KEAP1's utility in the PROTAC approach, the use of non-peptidic binders would be required. In recent drug discovery efforts, there have been attempts to develop small molecule inhibitors of KEAP1, such as **3**, **4**, and **5** (**Figure 7**). This includes the covalent inhibitor bardoxolone **3**, CDDO, which has been shown to have unwanted side effects

which may limit its utility.<sup>48-54</sup> In addition, multiple drug discovery efforts have developed reversible compounds, such as **4** (EC<sub>50</sub> 29 nM) and **5** (IC<sub>50</sub> 15 nM).<sup>55,56</sup> However, the compounds have yet to been utilised in the PROTAC approach and their ability to recruit KEAP1 as an E3 ligase is not yet known. As a result, the value of KEAP1 as an E3 ligase for the PROTAC approach is currently not established.

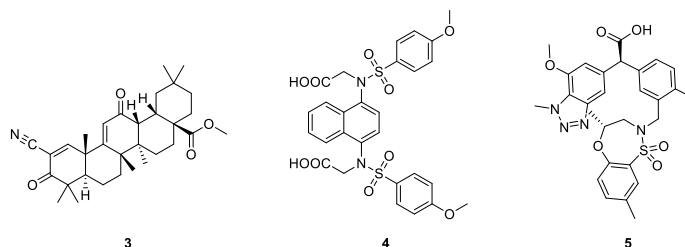


**Figure 7:** Small molecule inhibitors of the KEAP1 (**3**, **4**, **5**).

Overall, these peptidic PROTACs for VHL and KEAP1 were able to demonstrate the potential for redirecting the UPS to achieve targeted protein degradation. The peptides utilised showed the first cellular targets degraded by the PROTAC approach and inspired the development of PROTACs as small molecule degraders for the ultimate goal of medicine development.

### 2.2.3 Development of Small Molecule PROTACs

In order to develop PROTACs into more therapeutically-relevant molecules, the peptidic E3 ligase binder had to be replaced. PROTAC medicines would require drug-like physicochemical properties such as good permeability and longer biological half-lives than the peptides could offer.<sup>4,35</sup> The development of small molecules aimed at binding to E3 ligases had previously been difficult as a result of having to compete with binding proteins in order to access the binding sites of these E3 ligases.<sup>57</sup> Currently only four E3 ligases (out of the available 600) have been reported in the literature for the successful design and preparation of functional PROTACs, and these are discussed below. As a result, the PROTAC approach is currently limited by the number of E3 ligases that have been successfully employed. It is anticipated that expansion of this E3 ligase repertoire will be required in order to fully capitalise on the potential of PROTAC medicines.

#### 2.2.3.1 VHL recruiting PROTACs

Following the success of peptidic VHL recruiting PROTACs in Section 2.2.2, further development has enabled the production of potent small molecule PROTACs. It has been shown that the strong primary protein-protein interaction between HIF1 $\alpha$  and VHL is focused on a single hydroxylated proline residue.<sup>58</sup> As a result, Crews and co-workers were able to

create a small molecule binder **6** containing a hydroxyproline core, which competed with a HIF1 $\alpha$  derived ligand in an *in vitro* FP assay pIC<sub>50</sub> of 5.4 (**Figure 8**).<sup>45,59</sup>

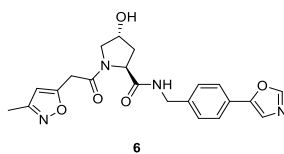


**Figure 8:** Small molecule inhibitor of VHL **6**.

The VHL binder **6** was then further co-developed by GSK and Craig Crews' group (**Figure 9A**).<sup>60,61</sup> By modifying the isoxazole fragment into either a *tert*-butyl derived amide **7** or an isopropyl derived isoindolinone **8**. The modifications led to sub micromolar binding affinity with VHL pIC<sub>50</sub> of 6.5. X-ray crystal analysis structure of **7** bound to VHL suggested that derivitisation of the amide (red) and of the aryl ring (red) would be tolerated and could be employed in PROTAC synthesis without compromising VHL potency.<sup>60,61</sup>

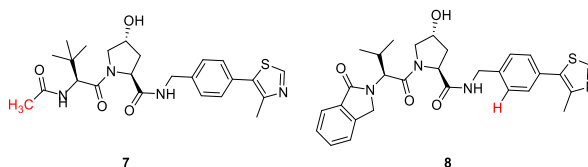


**Figure 9:** VHL binders **7** and **8** based on a hydroxy-proline core.

Moving on from the successful *in vitro* degradation of ER by the peptidic VHL recruiting PROTAC **1**<sup>33</sup> through the use of these new VHL binders, next generation small molecule ER VHL recruiting PROTACs **9** were synthesised (**Figure 10**). The molecules reported in the literature were the first examples of potent cellular protein degraders using this modality.<sup>62</sup> Biochemical assays were used to confirm that these PROTACs were able to potently engage both ER and VHL with respective pIC<sub>50</sub> values in FP assays of 7.4 and 6.5. The PROTAC **9** was tested in a cellular assay for ER protein levels, and was found to have a DC<sub>50</sub> (the concentration at which 50% of the protein is degraded) of 5 nM and achieved an 80% reduction in ER protein level at non-cytotoxic concentrations.

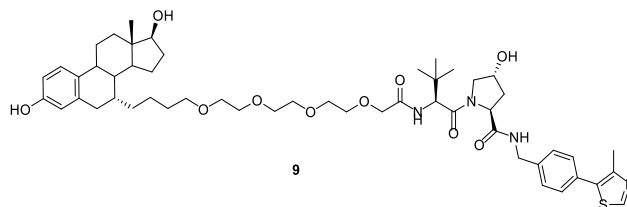


**Figure 10:** ER targeting PROTAC **9** employing VHL as the E3 ligase.

In order to support the hypothesis that degradation is a direct result of engagement of VHL, a negative VHL control **10** was also synthesised, utilising the diastereomeric VHL binder that

has a VHL binding affinity (FP)  $pIC_{50}$  of less than 4.0 but a very similar physicochemical profile (**Figure 11**). Following treatment with the control, the level of ER remained between 70–100%, inferring that the degradation was VHL mediated. The reduction in protein levels observed with the inactive PROTAC at higher concentrations was most likely due to cytotoxicity and not as a direct result of UPS-mediated degradation.

This early work on the ER VHL recruiting PROTAC **9** showed the potential for successful degradation of disease-causing proteins. Future work would be required to develop ER targeting PROTAC medicines, such as developing good physicochemical properties and PK profiles to show good *in vivo* activity and illustrate the benefits of an ER degrader versus an ER small molecule inhibitor.

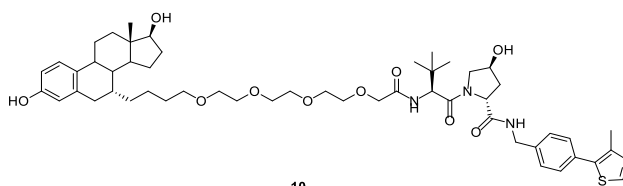


**Figure 11:** Negative VHL enantiomer control ER targeting PROTAC **10**.

In the initial assessment of the small molecule PROTAC approach, PROTACs targeting a protein construct for Green Fluorescent protein (GFP) and a HaloTag® fusion protein were also developed and termed HaloPROTACs (**Figure 12**).<sup>63</sup> This protein construct recognises and binds to chloroalkanes which in turn allows E3 ligase recruitment to ubiquitinate GFP leading to its degradation. Molecules **7** and **8** incorporating both VHL binders were synthesised and tested. The resulting compounds **11a/b** and **12a/b** were shown to degrade GFP with low nM potency with more potent degradation observed with shorter linkers and VHL II binder **8**. This work illustrated the ability to use VHL to degrade a novel protein, in addition to subtle difference in linker lengths impacting degradation. This approach will be discussed further in Chapters 6 and 7.

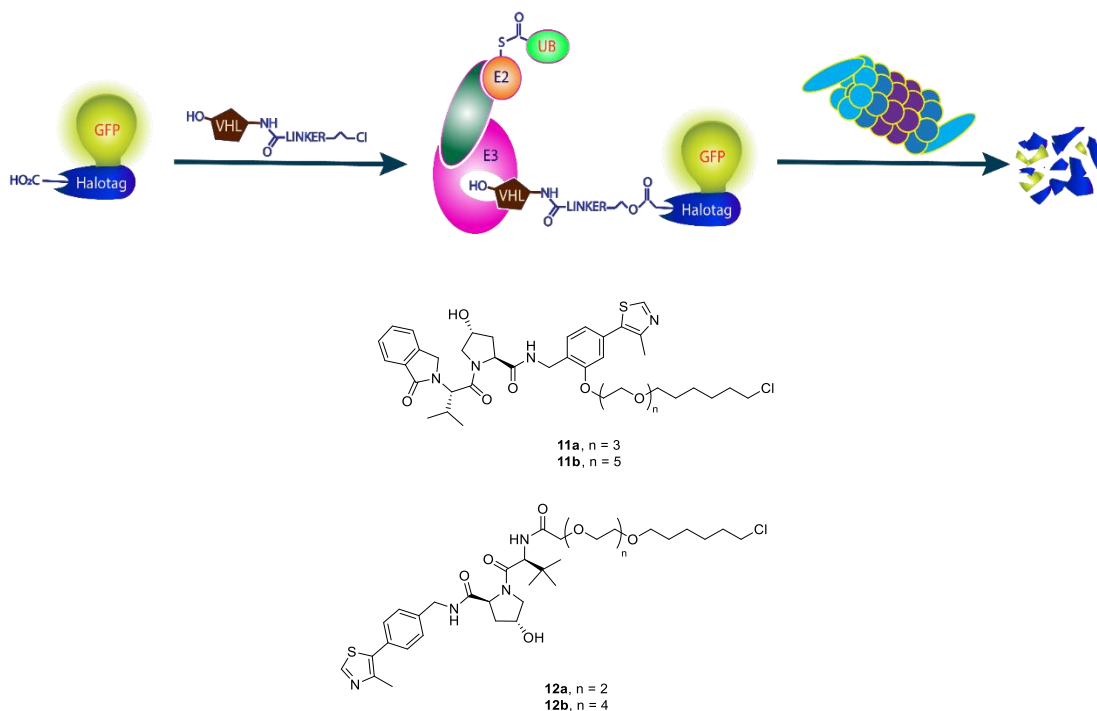


**Figure 12:** HaloPROTACs **11–12** degrading the GFP-HaloTag® fusion protein.

Further demonstration of the utility of VHL recruiting PROTACs is in the targeted degradation of receptor-interacting serine/threonine-protein kinase 2 (RIPK2), an important signaling enzyme in the innate immune system. Using a small molecule inhibitor of RIPK2 discovered at GSK,<sup>64</sup> a RIPK2 VHL recruiting PROTAC **13** was prepared (**Figure 13**). In a biochemical assay, PROTAC **13** was found to have a RIPK2 binding potency  $pIC_{50}$  7.8. When a degradation assay was conducted with PROTAC **13**, the  $DC_{50}$  in THP-1 cells was found to be 1.4 nM after 16 h incubation and the RIPK2 protein levels were >95% reduced at 10 nM.<sup>4</sup>

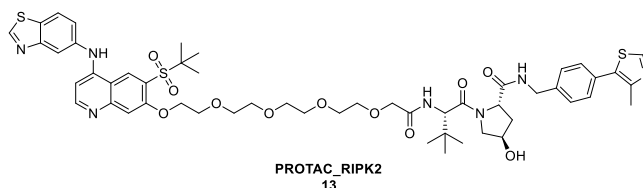


**Figure 13:** RIPK2 VHL recruiting PROTAC **13** (PROTAC\_RIPK2).

Another interesting aspect of PROTAC mechanism of action that was observed in the RIPK2 VHL example is the “hook effect”. This can be seen in **Figure 14**, where an increase in PROTAC **13** concentration above 10  $\mu$ M caused a decrease in the degradation of RIPK2. This is a consequence of ternary kinetics where the ratio of PROTAC **13** to the two binding partners has an optimal concentration. At higher concentrations, the binary complexes between the

PROTAC **13** and the two binding partners dominates, resulting in decreased ternary complex formation, decreased degradation, and increased levels of remaining protein.

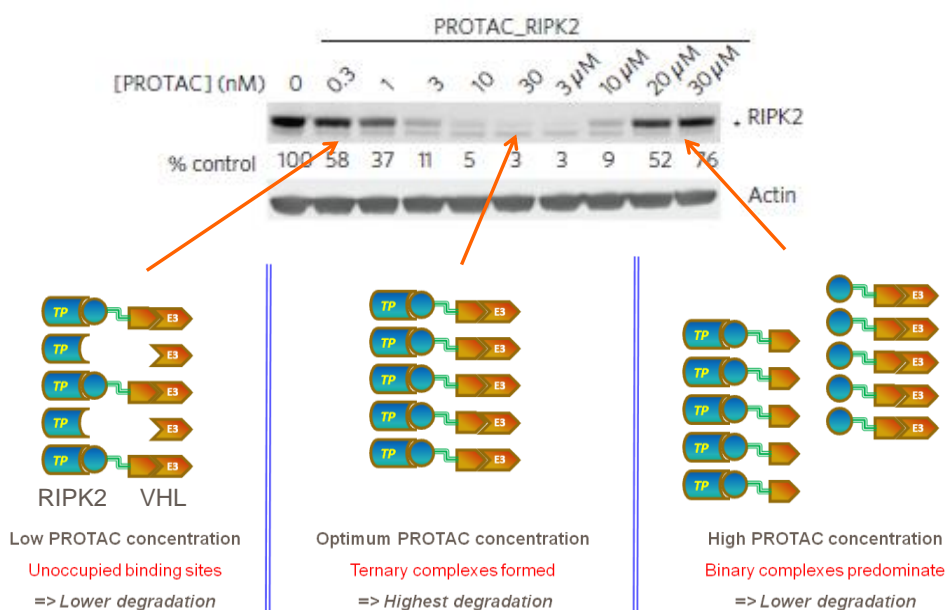


**Figure 14:** Ternary complex formation and the “hook effect” with PROTAC **13** (TP = target protein; E3 = E3 ligase).

The RIPK2 targeting PROTAC work was also able to provide evidence to support the hypothesis that PROTACs act via a catalytic mechanism. Since PROTAC-induced degradation is event-driven rather than occupancy-driven, it was envisaged that one PROTAC molecule can cause the degradation of multiple molecules of the targeted protein. This hypothesis arose as a way to explain the observation that early PROTACs had more potent DC<sub>50</sub> values relative to their binding affinities.<sup>40</sup> For RIPK2, the degradation stoichiometry was determined to be 1.0:3.4 by a ubiquitination assay. One picomole of the RIPK2 VHL recruiting PROTAC **13** resulted in 3.4 picomoles of ubiquitinated RIPK2. This was an important discovery, as the catalytic nature of PROTACs may lead to high degradation efficiency and the potential for a low efficacious dose for PROTAC-based medicines.<sup>4</sup>

One important consideration in the use of VHL in PROTAC design is the potential for competition between the PROTAC and the canonical VHL substrate HIF1α. Inhibition of HIF1α ubiquitination may result in its accumulation, potentially triggering the hypoxic response as an undesired E3 ligase-dependent effect. Importantly, in the RIPK2 targeting PROTAC **13** study, no hypoxia response effects were observed at concentrations up to 3 μM, although at 30 μM partial hypoxia was observed. This suggests at least a 1000-fold window between RIPK2 degradation and HIF1α stabilisation for PROTAC **13**, indicating a low potential for undesired effects using VHL binders in conjunction with potent target binders for PROTAC design. This work shows the real possibility of utilising VHL as an E3 ligase for PROTAC-based medicines,

with catalytic activity and a potential window between degradation and VHL inhibition-driven toxicity. Future work in developing potent RIPK2 targeting PROTACs *in vivo* would further illustrate the use of VHL recruiting PROTACs for medicine development.

The small molecule VHL binder **7** has also been utilised to construct PROTACs that degrade BRD4. BRD4 is an example of the BET (bromodomain and extra terminal domain) protein family which recognises acetyl-lysine residues on proteins.<sup>65</sup> As shown in **Figure 15**, the pan-BET inhibitor JQ1 **14** was linked by a PEG chain to the VHL binder **7**. Interestingly, two molecules of varying linker length were shown to degrade BRD4 successfully (**15a** and **15b**), but the shorter chain MZ1 **15a** PROTAC (n=2) was found to induce faster degradation than the longer chain PROTAC MZ2 **15b** and to have higher degradation efficacy overall. Surprisingly, some selective degradation of BRD4 over the other BET family members was observed at lower concentrations with both PROTACs, despite the unselective nature of the parent binder. This suggests there may be possibility of generating selective degraders with an unselective target binder. Other reports have also disclosed BET targeting PROTACs with investigations directed toward understanding the subtle effects of the linker on the efficiency and selectivity of BRD4 protein degradation.<sup>66</sup>

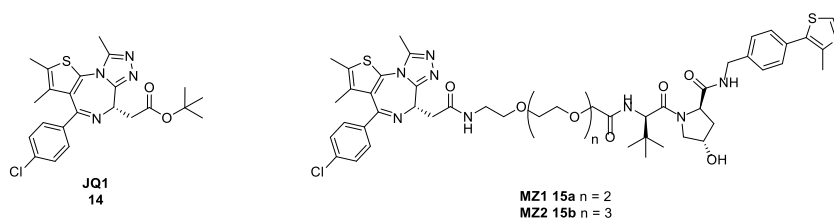


**Figure 15:** JQ1 **14** and JQ1 derived VHL recruiting PROTACs MZ1 **15a** and MZ2 **15b**.<sup>65</sup>

Another JQ1 **14** derived VHL recruiting PROTAC ARV\_771 **16** (**Figure 16**) has been described as a potential treatment for metastatic castration-resistant prostate cancer and has been demonstrated to produce *in vivo* pharmacology.<sup>67</sup> This BET targeting PROTAC, which employs a VHL binder containing an additional chiral methyl group, induces BRD2/3/4 degradation with a  $DC_{50} < 5$  nM resulting in downstream c-MYC inhibition following 16 h treatment in 22Rv1 cells. In a 22Rv1 murine xenograft model, ARV\_771 **16** treatment resulted in a dose-dependent decrease in tumour size. However, once a day dosing was not tolerated, indicating the potential for significant compound-related toxicity which is likely to be a direct result of BET protein degradation rather than inhibition. Alternating the compound dosing regimen to every 3 days resulted in 60% tumour growth inhibition over a 2-week period, although toxicity was also observed with this dosing regimen. This result illustrated the potential for *in vivo* tumour regression in animal models through the PROTAC approach, although it also highlights some of the challenges associated with developing safe and efficacious PROTAC molecules in future.

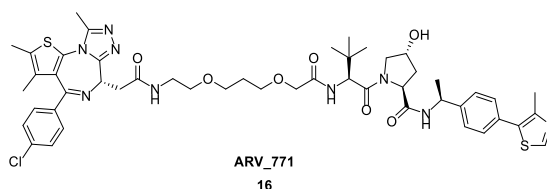


**Figure 16:** Structure of BET VHL recruiting PROTAC ARV\_771 **16** employing a modified VHL binder containing a chiral methyl group.

With the BET family of proteins showing good degradation via the PROTAC approach, they have been the subject of analysis of the impact of warhead selection and the subsequent ternary complex formation on protein degradation efficiency.<sup>68</sup> To assess this impact, PROTACs were prepared with the same linker and E3 ligase VHL binder, but with different BRD-binding warheads. Using JQ1 **14** and I-BET726 warheads, comparison of two different exit vectors for the BET family were investigated (MZ2 **15b** versus MZP-55 **17**, **Figure 17**). JQ1 **14** binds to BRD4 with 100 nM  $K_d$  and I-BET726 binds with 4 nM  $K_d$ . Using the small molecule X-ray crystal structures, two clear exit vectors could be identified in order to link the BRD binders to the VHL binder. MZ2 **15b** showed degradation selectivity for BRD4 and BRD3 over BRD2, whereas MZP-55 **17** was more selective for BRD4 degradation. In investigations studying the ternary complex formation, MZ2 **15b** showed more cooperative protein-protein interactions and consequently better ternary complex formation between the two binding partner proteins than the single proteins alone. In contrast, MZP-55 **17** induced destabilising protein-protein interactions between the two proteins (negative cooperativity). Despite MZP-55 **17** being a more potent BRD4 binder, these destabilising interactions lead to a similar BRD4 degradation profile to the less potent warhead for MZ2 **15b**. These results show that the exit vector selected for linker attachment may be critical for the degradation profile of PROTAC molecules. One caveat in comparing both the molecules directly in a cellular assay is the physicochemical properties such as solubility and permeability that may influence the cellular degradation profiles. Therefore, the compounds cannot be directly compared in terms of generating selectivity from a vector. It may be advantageous to compare different exit vectors from a single compound in future to assess the exit vector's true impact on degradation and selectivity profiles, and how this may be utilised in generating potent molecules for drug discovery efforts.

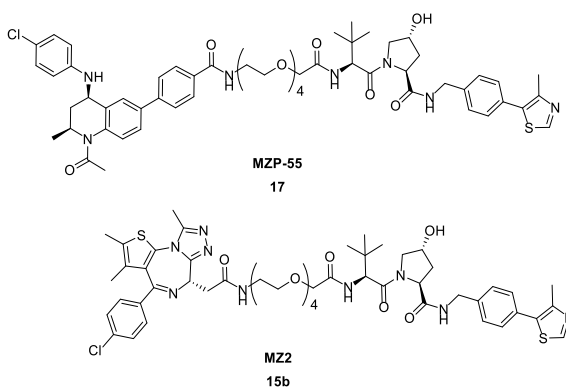


**Figure 17:** Comparing two BRD4 binders for PROTAC-mediated degradation.

Another report exploring the cooperativity effect in ternary complex formation disclosed the rational design of AT1 **18** with a different exit vector for VHL.<sup>69-71</sup> In a crystal structure of the previous molecule MZ1 **15a**, it was observed that the molecule was folded in a manner which could be optimised. Through rationale design, it was envisaged to alter the exit vector of VHL to the *tert*-leucine side-chain, giving rise to AT1 **18** (**Figure 18**). This new exit vector is proposed to create positive cooperativity to enable more efficient BRD4 degradation. The compound was less potent than the corresponding AT1 **18**, with potent degradation now in the micromolar range, suggesting that despite the positive cooperativity in the ternary complex, the mechanism of PROTAC action relies on more than just favourable ternary complex formation. AT1 **18** also showed good levels of selectivity (only up to 3  $\mu$ M is described), once again confirming that a non-selective inhibitor can become a selective degrader. The publication shows that rational design can be employed for the preparation of optimised PROTACs and may be used to design selective degraders from non-selective binders. However, although promising in principle, this effect has yet to be demonstrated *in vivo*.

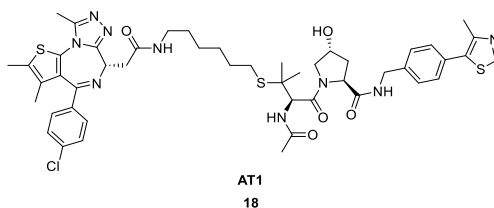


**Figure 18:** JQ1 derived selective degrader AT1 **18**.

In addition to the BET family of bromodomains, a non-BET bromodomain, TRIM24 was shown to be degraded through a PROTAC approach, providing the first example of a non-functional inhibitor to be converted into a functional degrader (**Figure 19**).<sup>70</sup> Small molecule inhibitors of the non-BET bromodomain were developed as potential therapeutics, as TRIM24 has been shown to be an important dependency for a number of cancer types. However, functional inhibition of TRIM24 led to no evident pharmacological effect.<sup>72</sup> The TRIM24 degrading

PROTAC **19** showed anti-proliferative effects in leukemia derived cell lines in comparison to the small molecule inhibitor and the DMSO vehicle, showing TRIM24 structural dependency for the cell lines tested. This shows the power of the PROTAC approach in using non-efficacious small molecules to recapitulate protein knock-down that results in efficacious *in vitro* effects which could be a powerful advantage in future PROTAC derived medicines.

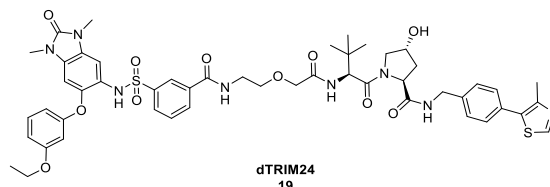


**Figure 19:** TRIM24 degrader **19** recruiting VHL.

In addition to the degradation of the BET family and RIPK2, early PROTACs targeting tyrosine kinases were also developed. A number of PROTACs featuring different small molecule inhibitors of the tyrosine kinases for BCR-ABL were synthesised and evaluated. Bosutinib **20**, dasatinib **21** and imatinib **22** PROTACs recruiting VHL were designed and prepared (**Figure 20**).<sup>73</sup> With both VHL recruiting PROTACs, no BCR-ABL degradation was observed despite evidence of target engagement. Only the dasatinib derived PROTAC **21** proved to be an active degrader, demonstrating ABL knockdown exclusively (maximal degradation of 65% was observed following 24 h incubation with 1  $\mu$ M PROTAC). Surprisingly, all attempts to incorporate imatinib **22** and bosutinib **20** into VHL recruiting PROTAC resulted in no degradation of either ABL or BCR-ABL, despite evidence of target engagement. However, these compounds have different physicochemical profiles, permeability, and solubility and their cellular degradation performance cannot be directly compared. These combined results highlight the subtle interplay between target protein binders chosen in the PROTAC design, as certain combinations may result in mismatched protein orientations of the ternary complex, or differences in binding affinities to the desired target, preventing effective target protein ubiquitination and subsequent degradation. It may also highlight the issues of having a limited number of E3 ligases for specific target degradation, as different targets may be more efficiently degraded by some E3 ligases and less effectively by others.

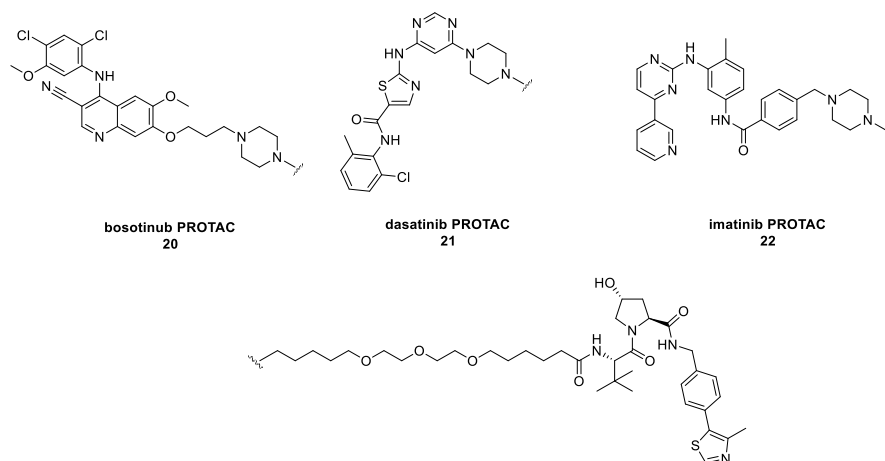


**Figure 20:** Bosutinib dasatinib and imatinib based VHL recruiting PROTACs.

Additional PROTACs targeting the degradation of kinases have been developed and assessed. PROTACs for EGFR, a receptor tyrosine kinase, were developed based on a number of warheads (**Figure 21**).<sup>74</sup> PROTACs based on lapatinib **23** were able to degrade EGFR with almost complete degradation at 250 nM. Interestingly, this compound was also active in degrading HER2 kinase (lapatinib is a dual HER2/EGFR inhibitor). HER2 degradation with lapatinib was mitigated with a longer linker, showing the possibility of tuning selectivity with linker selection. Degradation selectivity *in vivo* from an unselective binder has not yet been explored and would need to be fully evaluated to determine if this is a viable approach for mitigating the unwanted degradation of other targets.

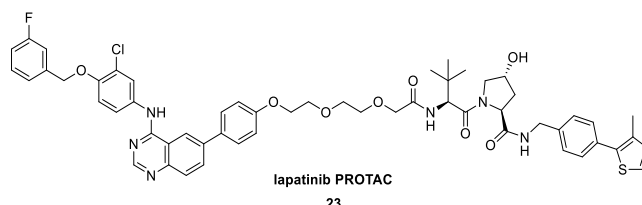


**Figure 21:** PROTAC based on lapatinib **23** recruiting VHL.

In order to validate a number of targets in one experiment, Crews utilised a promiscuous kinase binder approach recruiting VHL.<sup>75</sup> In order to assess a number of kinases simultaneously, a PROTAC containing the c-Met inhibitor foretinib was prepared and tested (**Figure 22**).<sup>75-79</sup> Foretinib also has broad spectrum kinase activity against 133 different kinases, and conjugating this inhibitor to VHL **25** (and cereblon, see later) led to a compound that was found to bind to 52 kinases (most likely due to exit vector tolerance for the linker portion of the molecule). Using protein dynamics experiments to evaluate the proteome and protein degradation, only nine kinases were found to be degraded >20% by the foretinib derived PROTAC **25**. The greatest reduction in protein was observed for c-Met and RIPK2 (a

previously degraded target) which have known high affinity binding to foretinib itself. In addition, a relatively weakly bound protein, p38 $\alpha$  ( $K_D = 11 \mu\text{M}$ ) was found to be degraded with a  $DC_{50}$  of 210 nM, illustrating the non-linear correlation between binding affinity and degradation efficiency. The publication illustrated that the degraded proteins formed stable ternary complexes with the PROTAC and VHL, indicating the importance of protein-protein interactions. With powerful structural biology tools, PROTACs could theoretically be designed to have good degradation selectivity with unselective binders. This approach is highlighted in a positive manner with respect to selectivity, but this could also be an important caveat for PROTAC design, as 133 kinases were bound by foretinib, yet only 9 were degraded by the foretinib derived PROTAC. This suggests that the E3 ligases that are currently employed may not be suitable for more specific protein of interests in the wider proteome, and the expansion of the E3 ligases currently in use would be beneficial to help increase the scope of degradable proteins.

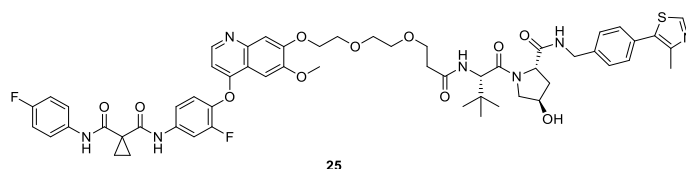
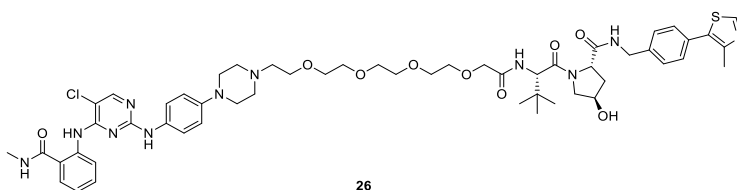


**Figure 22:** Promiscuous Kinase PROTAC **25** based on foretinib recruiting VHL.

In an analogous manner, our laboratory carried out a similar promiscuous kinase experiment using an alternative target binder (**Figure 23**).<sup>80</sup> This was achieved by incorporating a linkable analogue of the potent broad spectrum kinase inhibitor CTx-0294885 **26**,<sup>81</sup> which engages over 100 kinases. As expected with the addition of the linker, the binding affinity of the PROTAC was reduced compared to the parent binder for kinases with  $pIC_{50}$  values between 5 and 6. Targets with high binding potency for the parent inhibitor were largely found to also have high binding potency to the PROTAC **26**. As with the Crews experiment, the number of degraded targets was greatly reduced as compared to inhibited targets. Only one out of 21 kinases that bound to the PROTAC **26** with  $pIC_{50} > 6$  was degraded at 1  $\mu\text{M}$  PROTAC concentration, and many proteins which had good kinase occupancy with this molecule were not degraded. This lack of degradation despite target engagement could be a result of 1) poor ternary complex formation as a result of linker geometry or length, 2) decreased efficiency of the degradation of membrane bound proteins via the PROTAC approach or, 3) lack of available surface lysine residues for the ubiquitin transfer to occur.<sup>80</sup> Interestingly, four other kinases with  $pIC_{50}$  values of less than 6 were degraded using this PROTAC. However, only one linker length was studied as a part of these investigations, so future proteomic analysis on linker length differentiation between PROTACs would be extremely valuable to determine the effects of linker length on degradation efficiency. This does however show that target binding potency may not be the main driver for PROTAC induced protein degradation. This

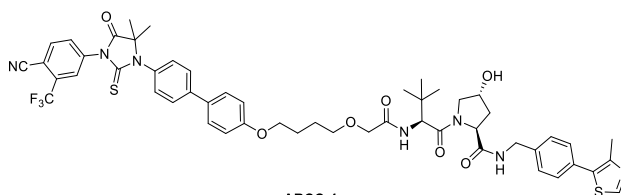
work, in addition to Crews' and co-workers', also highlights that not all PROTACs based on a given E3 ligase to a specific target will be able to induce protein degradation.



26

**Figure 23:** Promiscuous Kinase PROTAC **26** based on CTx-0294885 recruiting VHL.

More recently, an AR targeting PROTAC has shown good *in vitro* effects compared to its small molecule inhibitor counterpart.<sup>82</sup> An example of a AR targeting PROTAC recruiting VHL is ARCC-4 **27**, which is based on the small molecule enzalutamide (**Figure 24**). The PROTAC shows more potent effects *in vitro* in VCaP cells by inducing apoptosis compared to the small molecule inhibitor. Using *in vitro* drug resistance models, it was demonstrated how the PROTAC approach can outperform a small molecule inhibitor which is prone to the development of resistance. In cell lines with AR overexpression, which is a common resistance mechanism against small molecule inhibitors, the PROTAC **27** is able to degrade over 95% of the protein. The PROTAC **27** is also less susceptible to AR binding pocket mutations, which also lead to resistance. This shows that the effects of potent degradation may lead to superior efficacy compared to an inhibitor, and future work is envisaged to be able to evaluate these differences in disease models.

ARCC-4  
27

**Figure 24:** AR targeting PROTAC ARCC-4 **27**.

VHL has proven to be a useful E3 ligase for PROTAC design and use, and VHL recruiting PROTACs have been shown to degrade multiple proteins with good to excellent degradation potency. VHL recruiting PROTACs have demonstrated utility both *in vitro* and *in vivo*, outperforming some small molecule inhibitors for efficacy (AR).<sup>82</sup> In addition, it has been shown that non-functional small molecule binders (TRIM24)<sup>70</sup> can be converted into potent pharmacologically active VHL recruiting PROTACs. Despite this promise, there is very little description about the physicochemical properties or PK profiles of these molecules in the literature, including their use as *in vivo* drug candidates. Future work to showcase oral bioavailability, solubility, and potency in the clinic would therefore illustrate the utility of the VHL recruiting PROTAC approach.

### 2.2.3.2 Cereblon Recruiting PROTACs

Thalidomide, infamously known for its teratogenicity, has proven an unlikely, yet powerful tool in the development of the PROTAC approach. Efforts to better understand the mechanism of action of thalidomide showed that it binds to cereblon, a constituent of a cullin-RING ubiquitin ligase (CRL) complex. Cereblon forms an E3 ubiquitin ligase complex with damaged DNA binding protein 1 (DDB1) and Cul4A that is important for limb development and degradation of the fibroblast growth factor Fgf8 and MEIS2.<sup>83,84</sup>

Lenalidomide **29**, and the other IMiD members of the family, act as “molecular glues” to cereblon.<sup>85</sup> “Molecular glues” are small molecules which can promote new protein-protein interactions which would not otherwise form without the presence of the small molecule. This occurs through either direct binding interactions between both protein targets and the small molecule directly at the protein-protein interface, or through allosteric conformational change of the first protein structure that promotes the formation of a neosurface which recognises and binds to secondary proteins. More recently, thalidomide **28** and its analogues lenalidomide **29** and pomalidomide **30** (**Figure 25**), which are collectively known as IMiDs, have been shown to inhibit cereblon and cause the degradation of Ikaros (IKZF1) and Aiolos (IKZF3); transcription regulators important for the generation of lymphocytes.<sup>86</sup> The degradation of Ikaros/Aiolos by cereblon only occurs in the presence of the IMiDs, as these molecules lead to ternary complex formation between cereblon, the IMiD, and Ikaros/Aiolos.<sup>85,87</sup> As well characterised E3 ligase binders, IMiDs have also more recently been incorporated into PROTACs to give a series of efficient, functional PROTACs with lower molecular weight compared to VHL recruiting PROTACs.<sup>73,88,89</sup>

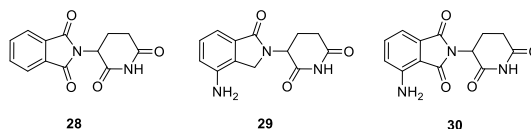


**Figure 25:** Thalidomide **28** and its analogues lenalidomide **29** and pomalidomide **30**.

Incorporation of small molecule BRD4 inhibitors into cereblon recruiting PROTACs showcases the possible advantages of the PROTAC approach versus their conventional small molecule inhibitor counterparts. Crews developed the BET targeting heterobifunctional molecule ARV-825 **31** (**Figure 26**), linking together JQ1 **14** and pomalidomide **30**.<sup>73</sup> Treatment of BL cell lines with ARV-825 **31** resulted in almost complete BRD4 protein degradation at 10 nM within 6 h, with DC<sub>50</sub> below 1 nM. Pronounced down regulation of c-MYC was observed with ARV-825 which was not fully suppressed by the parent JQ1 **14** even at high concentrations. However, this has not been confirmed as a PROTAC-mediated effect, as the parent cereblon binder may

also have an effect on c-MYC levels, so further investigation is required to determine the full cause of c-MYC reduction. In a closely-related approach, Bradner also developed a similar cereblon recruiting PROTAC dBET1 **32** based on O-linked thalidomide and BRD4 inhibitor JQ1 **14**.<sup>89</sup> Interestingly, despite the structural similarities between dBET1 **32** and ARV-825 **31**, the degradation of BRD4 is more efficient with ARV-825 **31**, which is most likely a linker-driven effect as a result of increased length and lipophilicity. This work shows the possible advantages of degradation in comparison to inhibition, but also the importance of linker optimisation to induce potent degradation efficiency.

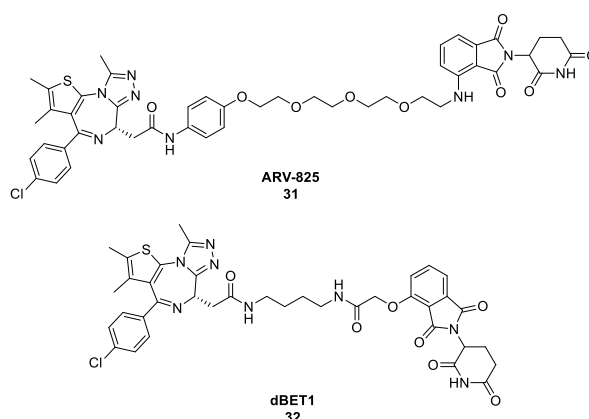


**Figure 26:** JQ1 derived PROTACs ARV-825 **31** and dBET1 **32** recruiting cereblon.

As part of the effort to optimise ternary complex formation for BRD4 in favour of the other BET isoforms, a second exit vector from JQ1 **14** was investigated.<sup>90</sup> Using *in silico* docking of BRD4 and cereblon to reveal low-energy binding modes, ZXH-3-26 **33** was rationally designed to be able to discriminate between the homologues of the BET family in favour of BRD4 (**Figure 27**). As the interactions between the compound and the two desired proteins are highly specific, gaining BRD4 selectivity was hypothesised to be as a result of unfavourable ternary complex formation. However, the hook effect is prominent with this PROTAC **33**. This was the first reported example of BRD4-selective degradation achieved over BRD2/3 degradation, but *in vivo* studies are still required to determine if the toxicity associated with non-selective BET degradation<sup>67</sup> can be mitigated through isoform-selective degradation. This may be more difficult to achieve with thalidomide derived binders due to expected poor PK profiles (and will be further discussed).

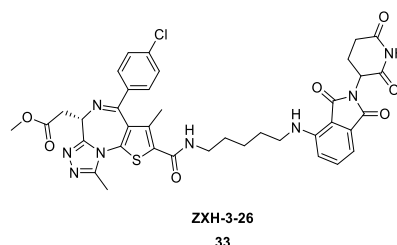


**Figure 27:** JQ1 derived PROTAC ZXH-3-26 **33**.

A more recent cereblon recruiting BET targeting PROTAC has shown extremely potent BET family degradation.<sup>91</sup> QCA570 **34**, with a pyrazole alkyne derived linker, has shown picomolar degradation of BRD2/3/4 in RS4;11 cells in 3 h (**Figure 28**). Interestingly, A PROTAC with a single atom shorter linker was found to be 10-fold less potent in cell growth inhibition assays of three cancer cell lines. **QCA570 34** was also efficacious *in vivo* showing potent anti-proliferative effects compared to vehicle control following a single 1 mg/kg IV dose. Animal weight was shown to decrease after the compounds were administered with a 5–10% difference observed in the vehicle control group after 3 weeks post administration, but they claimed there were no other signs of toxicity in all the treatment groups. This study suggests that there may be a therapeutic window between BET driven toxicity (observed with JQ1-VHL recruiting PROTAC previously **16**)<sup>67</sup> and efficacious anticancer effects. Further studies are required to address longer term BET degradation pharmacology and toxicity, especially in non-oncology settings.

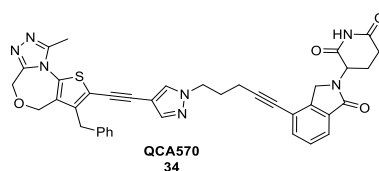


**Figure 28:** BET targeting PROTAC QCA570 **34**.<sup>91</sup>

In addition to the BET family of proteins, other non-BET bromodomain derived PROTACs were also investigated to determine if they had additional efficacy compared to their parent inhibitors. One example is a cereblon recruiting PROTAC to degrade PCAF/GCN5 **35** (**Figure 29**).<sup>92</sup> PCAF and GCN5 have previously been implicated in a number of immuno-inflammation conditions, with knockout models showing reduced ability to produce cytokines upon stimulation with lipopolysaccharide (LPS). However, a small molecule inhibitor was shown to have little efficacy in any of the models tested. In order to recapitulate the observed knockout phenotype, a PCAF PROTAC (dual inhibitor for GCN5) was designed and synthesised to give GSK983 **35**. The PROTAC **35** was able to prevent differentiation of monocytes into macrophages and inhibit cytokine production (including IL-6, CCL7 and TNF) after LPS stimulation. This shows the powerful potential of the PROTAC approach in drug discovery to produce differential pharmacology compared to conventional small molecule inhibitors.

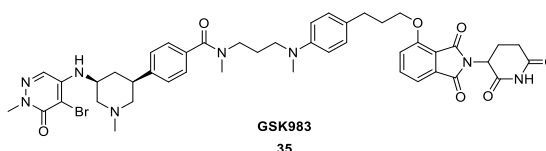


**Figure 29:** PCAF/GCN5 PROTAC recruiting cereblon **35**.

In a similar fashion, a PROTAC for BRD9 was investigated to determine if the non-functional inhibitor iBRD9 could be converted into a functional degrader.<sup>93</sup> Two compounds were developed with different linkers to lenalidomide **29**. BRD9 compound **36** had an amide and alkyl chain linker, and dBRD9 had a tertiary amine PEG derived linker (**Figure 30**). They were both potent degraders of BRD9 (degradation observed at just 50 nM) but had very different selectivity profiles. Compound **36** was shown to produce a stable ternary complex with BRD7 and BRD4 in addition to BRD9, leading to potent degradation of these proteins. In comparison, dBRD9 **37** had a much more selective profile with no degradation observed of either off-target. The results show the differential selectivity profiles available through linker adaptation. As a result, the first potent, and selective degrader of BRD9 was developed which will be useful as a chemical biology tool for subsequent biological evaluation of BRD9 function.

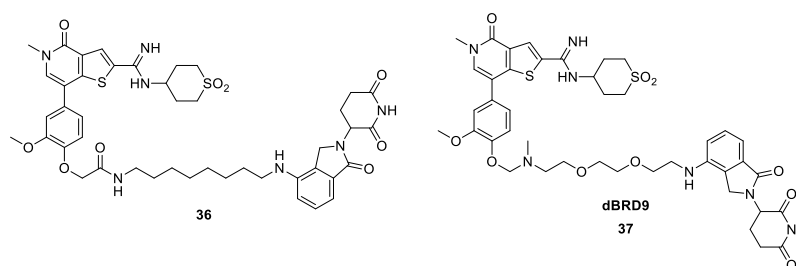


**Figure 30:** BRD9 PROTACs recruiting cereblon BRD9 compound **36** and dBRD9 **37**.

In addition to the extensive work reported using cereblon recruiting PROTACs to degrade epigenetic targets, kinase degrading PROTACs employing cereblon binders have also been widely investigated. Crews has developed multiple BCR-ABL PROTACs using cereblon recruitment in addition to previously mentioned VHL recruiting PROTACs. In this work, Crews linked BCR-ABL inhibitors (imatinib, bosutinib, and dasatinib) to pomalidomide **38–40** (**Figure 31**). In the case of imatinib **38**, no degradation was observed for either c-ABL or BCR-ABL despite nanomolar target engagement. The dasatinib cereblon recruiting PROTAC **40** successfully degraded c-ABL (>85% at 1  $\mu$ M) but also induced BCR-ABL degradation (>60% at 1  $\mu$ M). Bosutinib cereblon recruiting PROTAC **39** was also successful in degrading c-ABL (>90%) and BCR-ABL (>80%) degradation at 2.5  $\mu$ M. Interestingly, the bosutinib derived VHL recruiting PROTAC **39** did not possess similar activity, and in all cases BCR-ABL was not degraded with VHL recruiting ligands. This work may give an insight into the importance of the ternary complex formation, as the linking vector may not allow the correct orientation to ubiquitinate a surface lysine on the target protein.

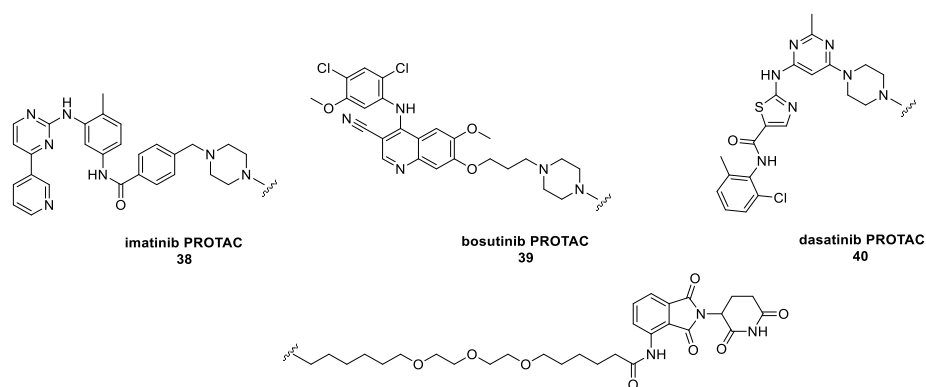


**Figure 31:** Imatinib **38**, bosutinib **39**, and dasatinib **40** PROTACs recruiting cereblon.

An early example of a potent kinase degrading cereblon recruiting PROTAC is based on the RIPK2 protein, which has previously shown good degradation with VHL recruiting PROTACs (**Figure 32**).<sup>94</sup> This compound **41** was found to be an extremely potent RIPK2 degrader in multiple cell lines. However, due to similar potency as the VHL recruiting PROTAC, in addition to the potential teratogenicity risk associated with lenalidomide **29**, this compound was deemed a good PROTAC tool but was not carried forward into medicine design.

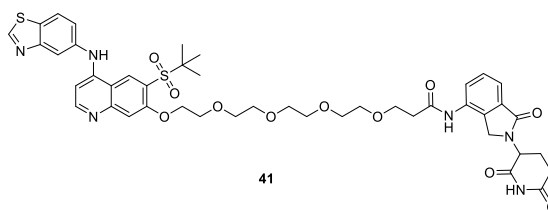


**Figure 32:** RIPK2 targeting PROTAC **41** recruiting cereblon.

In the same manner that was achieved with the VHL recruiting PROTACs, Crews used a promiscuous kinase PROTAC **42** to assess the degradability of the kinome with the E3 ligase cereblon (**Figure 33**).<sup>75</sup> Using the same warhead based on foretinib and the same linker (as in **Figure 22**), the compound was conjugated to lenalidomide **29** (**Figure 33**). In total, the PROTAC **42** engaged 62 kinases, and was able to degrade 14 (9 kinases degraded by VHL PROTAC **25**, with 6 in common). Common kinases degraded by both compounds include RIPK2 (a known degradable target), c-Met (the primary target for the small molecule inhibitor), p38 $\alpha$  and c-Abl (a known degradable target). Selective cereblon recruiting PROTAC degradation was observed with c-Src and CSK, among others. This could be due to interactions between the kinases and the E3 ligase leading to a differential degradation profile. This suggests that the E3 ligase chosen for elaboration of protein binders into PROTACs may be crucial to conferring success in degradation. However, it could also be a result of negative protein-protein interactions as a result of linker length, and different linkers would need to be assessed to determine if the E3 ligase is suitable for recruitment for a particular protein of

interest. This work also highlights the difference between a potent inhibitor versus a potent degrader, and that not every E3 ligase may be suitable to degrade a protein of interest.

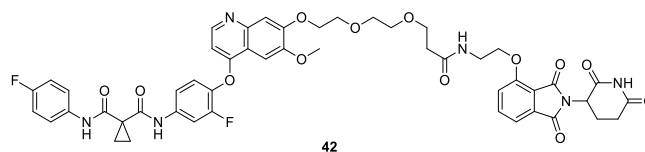


**Figure 33:** Promiscuous kinase cereblon recruiting PROTAC **42** based on foretinib.

Our laboratories also developed a promiscuous kinase PROTAC **43** in order to compare degradability to the other available E3 ligases (**Figure 34**).<sup>80</sup> In comparison to the VHL example **26** shown previously, the cereblon recruiting PROTAC was able to induce the degradation of more proteins using the same linker and warhead. In total, 15 kinases were degraded in this experiment (compared to 5 with VHL recruiting PROTAC **26**). It was found that 15 of the 30 kinases which bound to the PROTAC **43** with  $pIC_{50} > 6$  were degraded in this experiment, with no degradation of kinases with PROTAC binding of  $pIC_{50} < 6$ . This illustrates that cereblon may require proteins to have increased binding potency, although further studies to confirm this are required. In addition, the compound was found to be a more potent degrader than the VHL recruiting PROTAC **43** at lower concentrations (VHL recruiting PROTAC **26** only induced degradation at 1  $\mu$ M, while the cereblon recruiting PROTAC **43** induced the degradation of 12 proteins at 100 nM). Kinases such as AAK1, AURKA/B, BTK, IRAK3, PTK2/2B, TEC were found to be degraded in this experiment, and this work helped to determine the PROTAC-mediated degradability of novel targets such as PTK2, BTK and IRAK3. This further shows that cereblon is an extremely useful E3 ligase in assessing the initial degradability of a target and that cereblon recruiting PROTACs may be more likely to induce degradation of kinase targets than the corresponding VHL recruiting PROTAC counterpart.

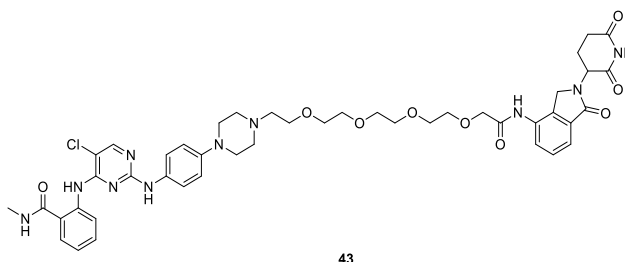


**Figure 34:** Promiscuous kinase Cereblon recruiting PROTAC **43** based on CTx-0294885.

In an analogous approach, the Gray lab also demonstrated a promiscuous kinase degradation approach with cereblon recruiting PROTACs.<sup>95</sup> In this example, a broad-spectrum kinase inhibitor was employed to prepare PROTAC TL12-186 **44** (**Figure 35**). The compound inhibited 193 kinases over 90% at a screening concentration of 1  $\mu$ M. Upon compound treatment (100 nM) in MOLM-14 cells, 12 kinases were shown to be downregulated by at least

25%: AAK1, AURKA, AURKB, BTK, CDK12, FLT3, FES, FER, PTK2 (also known as FAK), PTK2B, ULK1, and TEC. This method has allowed for the discovery of newly tractable targets for the PROTAC approach, for example, BTK and FAK which were first published as a result of this experiment. This has initiated multiple drug discovery programs for these targets for the PROTAC approach.<sup>96-98,97</sup>

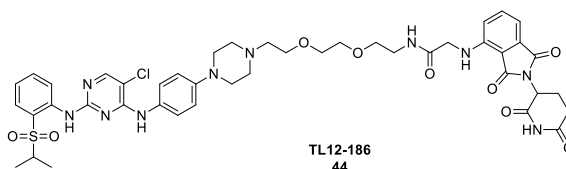


**Figure 35:** TL12-186 Promiscuous cereblon recruiting PROTAC **44**.

Although cereblon recruiting PROTACs have shown promise in target degradability, there are a number of issues associated with these compounds with respect to medicine development. A possible risk associated with the potential use of IMiD derived PROTACs as therapeutics is the inherent instability of the E3-binding motif.<sup>99</sup> The IMiD derived binders readily undergo non-enzymatic amide hydrolysis and are susceptible to hydrolytic cleavage at pH > 6 (**Figure 36, 45–47**).<sup>100</sup> More stable motifs may be required to observe the maximal degradation potential of cereblon recruiting PROTACs over extended incubation periods. This hydrolysis is also apparent *in vivo* with the IMiDs **45–47**, and may be related to the main clearance pathway for pomalidomide **30**, including cytochrome P450-mediated hydroxylation followed by glucuronidation, glutarimide hydrolysis and renal clearance.<sup>101</sup> The excreted half-lives of the IMiD compounds is between 3 and 9.5 h (with the racemisation half-lives of less than 2 h).<sup>102</sup> Further research to discover more stable cereblon binders is required in order to create a viable cereblon recruiting PROTAC therapy with a prolonged duration of action,.

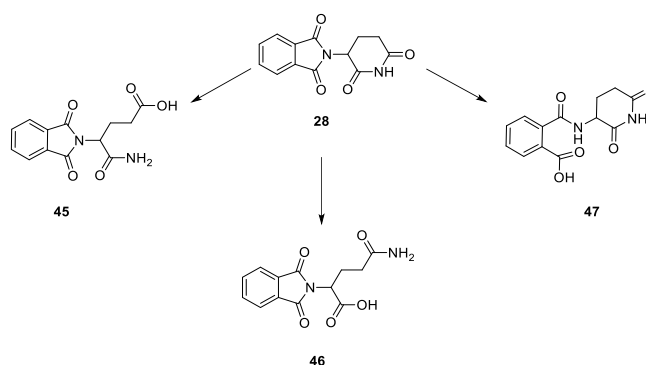


**Figure 36:** Primary hydrolytic degradation of thalidomide in aqueous solutions at pH > 6.<sup>103</sup>

Another possible risk associated with the development of cereblon recruiting PROTACs into therapeutics is the potential for IMiD-induced teratogenicity. Whilst the exact mechanism of IMiD-induced teratogenicity has not been definitively identified, it is thought to be mediated by IMiD-induced modulation of cereblon function through either the degradation of neosubstrates

such as Ikaros and Aiolos through creation of a neomorphic protein binding surface<sup>86</sup> or else via inhibition of endogenous substrate degradation such as MEIS2 and SALL4.<sup>104</sup> PROTACs making use of cereblon-binding moieties may also carry this teratogenicity risk, although if efficient degradation can be achieved through very low equilibrium occupancy of the ligase, then it may be possible to establish a viable therapeutic index. Ultimately, this is a risk which can only be extensively addressed through *in vivo* teratogenicity testing, and the clinical benefit must be deemed to outweigh the potential risks.

### 2.2.3.3 MDM2 Recruiting PROTACs

MDM2 (murine double minute-2) is an E3 ligase which has been the centre of multiple small molecule drug discovery efforts in oncology. This protein is the main degradation regulator of p53, which has been established as a key regulator of the cell cycle and of cellular proliferation. Inhibitors of MDM2 have been investigated in order to increase p53 protein levels, and small molecule imidazoline inhibitors (nutlins) of the MDM2-p53 PPI, are currently in the clinic for multiple oncology indications.<sup>105,106</sup>

Employing the known chemical matter that binds to MDM2, the first examples of non-peptidic small molecule PROTACs were synthesised by the Crews group.<sup>44</sup> Crews was able to degrade the androgen-receptor (AR) by compounds **48**, which consists of an AR inhibitor<sup>107</sup> linked to the nutlin derived MDM2 binder (**Figure 37**). Degradation was only reported above concentrations of 10  $\mu$ M, although this was shown to be a result of the proteasome dependent degradation, as the effect was not observed in the presence of a proteasome inhibitor. As a result, more efforts would be required to develop potent PROTAC molecules suitable for further medicine development.

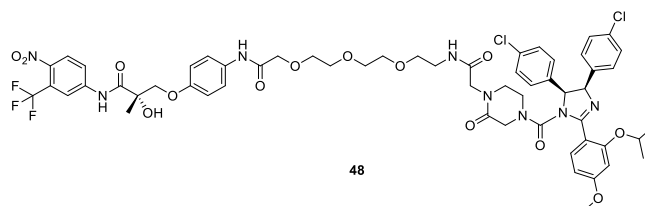


**Figure 37:** Structure of SARM-MDM2 recruiting PROTAC **48**.

More recently, through the use of the highly substituted MDM2-binder idasanutlin, potent degradation of BRD4 with a JQ1 **14** warhead has been observed with compound **49** (**Figure 38**).<sup>108</sup> Degradation of BRD4 was observed at nM levels with good knockdown achieved at just 100 nM with a short linker between the two moieties. The compound was active *in vitro*, with cell viability greatly reduced in cancer cell lines. However, due to toxicity observed with BET inhibitors, the *in vivo* tolerability of the PROTAC molecule **49** is a key question.

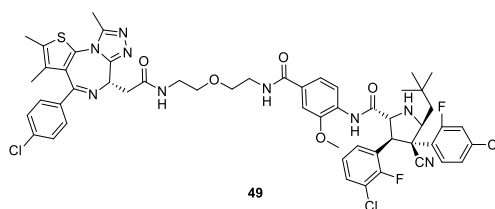


**Figure 38:** JQ1 derived MDM2 recruiting PROTAC **49**.

MDM2 has been speculated to be useful for the design and construction of PROTACs for some time, yet there were very few examples of functional PROTACs harnessing MDM2 until 2018.<sup>108,109</sup> The reasons for this are not known, but a promiscuous PROTAC approach utilising MDM2 would be extremely advantageous to showcase the utility of this E3 ligase. However, it may be possible that idasanutlin may not be suitable in developing good properties for PROTAC molecules. Idasanutlin is highly lipophilic and resulting PROTACs may have inherent solubility issues in development. However, dual inhibition of the p53-MDM2 complex and degradation of a desired target may be a useful therapeutic strategy for oncology indications in the future provided the physicochemical properties of the PROTAC can be appropriately tuned. Further work into potent and selective *in vivo* recruitment of MDM2 for a number of targets would be required to ensure its applicability in the PROTAC approach.

#### 2.2.3.4 IAP Recruiting PROTACs

Inhibitor of apoptosis proteins (IAPs), are another class of E3 ligases that are currently under investigation for clinical use in oncology, with multiple small molecule drug discovery efforts ongoing.<sup>55,110-112</sup> Inhibitor of apoptosis (IAP) proteins are a family of eight proteins which regulate caspases and apoptosis, which have been shown to be dysregulated in a number of cancers. In the mammalian IAP family, this includes: cIAP1, cIAP2 and XIAP. These proteins contain three BIR (baculovirus IAP repeat) domains, BIR1/2/3, and a RING finger domain.<sup>113</sup> IAP-targeting therapeutics designed to mimic the endogenous IAP antagonist, SMAC (second mitochondrial activator of caspases) bind to these domains and are currently undergoing clinical evaluation. These compounds induce apoptosis by preventing IAP interactions with caspases. In the cases of cIAP1 binding, this causes cIAP1 dimerisation, autoubiquitination and subsequent degradation of the protein, or “self-degradation”, perpetuating the apoptosis cascade.<sup>114</sup>

The first example of utilising IAP in the PROTAC approach was through the use of SNIPERs (specific and nongenetic IAPs-dependent protein erasers), or IAP recruiting PROTACs.<sup>115</sup> Hashimoto was able to convert the small molecule bestatins, known to recruit cIAP1 (cellular inhibitor of apoptosis protein 1),<sup>116</sup> into PROTACs that degraded a number of targets including

CRABP-II **50** (cellular retinoic acid binding proteins) and the ER **51** (**Figure 39**). As with the other previous examples of using peptidic binders, the cellular potency of **50/51** were weak, likely due to poor permeability. Another concern with the development of the SNIPER molecules was their specificity. Before bestatins were discovered to recruit cIAP1 they were previously developed as aminopeptidase inhibitors. This activity may lead to various undesired effects in addition to protein degradation.<sup>117</sup> A further concern with small molecule binders of cIAP1 (which includes their inclusion into PROTACs) is that engagement of cIAP1 leads to its autoubiquitination and subsequent degradation leading to apoptosis.<sup>114</sup> This may be an issue when developing these molecules into therapeutics where apoptosis is undesirable.<sup>13</sup>

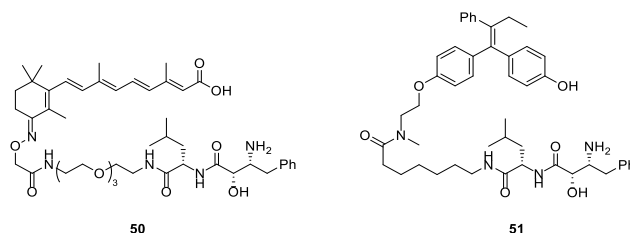


**Figure 39:** CRABP-II IAP recruiting PROTAC **50** and bestatins-containing ER $\alpha$  PROTAC **51**.

More recently, in 2017, Naito published a “second generation” CRABP-II SNIPER utilising a pan-inhibitor of cIAP1/cIAP2/XIAP coined MV-1 **52** (**Figure 40**).<sup>118</sup> This compound **52** was envisaged to be much more cell penetrant, and was able to induce degradation at 300 nM after just 6 h. This was shown to be proteasome dependent as proteasome inhibitor MG132 removed all degradation activity. The compounds were also shown to degrade cIAP1 as predicted. This compound was the first known IAP recruiter to be able to induce targeted protein degradation at nM levels.

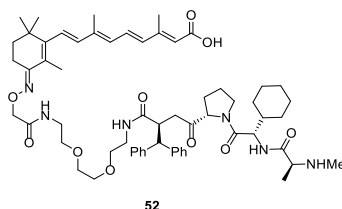
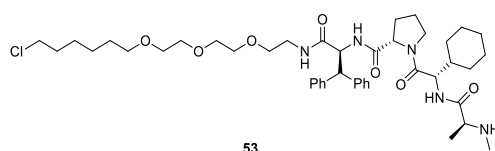


**Figure 40:** SNIPERs targeting CRABP-II using MV-1 **52** to recruit IAP.

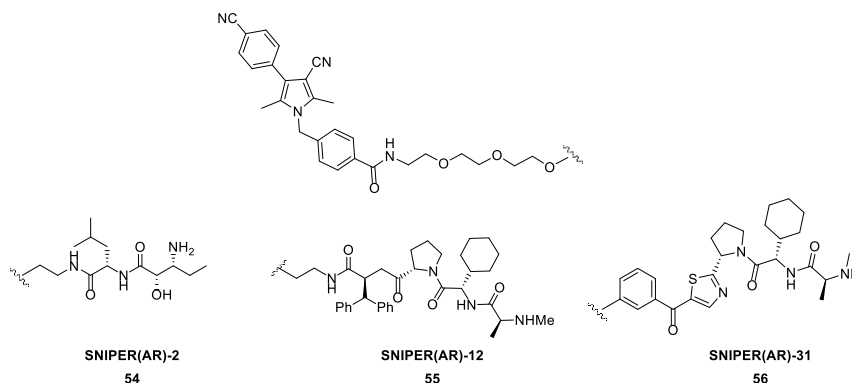
HaloPROTACs targeting IAP were designed and synthesised using this second generation IAP binder (**Figure 41**).<sup>119</sup> HaloTag $\text{®}$  fusion to TNF $\alpha$  in HEK293 cells was used to investigate IAP degradation of the HaloTag $\text{®}$  fusion system. This compound **53** was shown to degrade the constructs at 1  $\mu\text{M}$  and longer linkers than shown were inactive. The compounds were also shown to degrade the HaloTag $\text{®}$  protein without fusion of TNF $\alpha$  at 1  $\mu\text{M}$ . This shows that HaloTag $\text{®}$  protein constructs may not be a useful approach to determine target tractability of a protein of interest (without a known ligand) as the HaloTag $\text{®}$  mediated protein degradation could give false positives.



53

**Figure 41:** HaloPROTAC recruiting IAP **53**.

With a more cell permeable binder, new PROTACs based on IAP recruitment were developed. In addition to the IAP binders previously discussed, a third IAP binder was also developed as a PROTAC based on LCL-161 **56** and was used to directly compare the IAP ligands for the degradation of AR (**Figure 42**).<sup>120</sup> Using the same warhead and linker, SNIPER(AR)-2 **54**-12 **55**/31 **56** were developed and assessed. SNIPER(AR)-2 **54** was found to degrade the target at high concentrations of 30  $\mu\text{M}$  (52% degradation), which is weak as a likely consequence of poor permeability. SNIPER(AR)-12 **55** degraded the target at 10  $\mu\text{M}$  (40% degradation) and the best performing PROTAC in the series SNIPER(AR)-31 **56** was active at 3  $\mu\text{M}$  (57% degradation). All three compounds were shown to degrade cIAP as expected. The high concentrations required may be due to poor permeability of the PROTAC, as IAP requires a basic amine for protein binding, but this does not explain the incomplete degradation observed. In comparison to the potent VHL recruiting PROTACs (albeit with a different AR recruiting motif), the incomplete degradation with IAP recruiting PROTACs, along with the high concentrations required raises questions regarding the suitability of IAP recruiting PROTACs for the degradation of AR.



SNIPER(AR)-2  
**54**

SNIPER(AR)-12  
**55**

SNIPER(AR)-31  
**56**

**Figure 42:** AR IAP recruiting PROTACs with different IAP binders **54–56**.

In addition to the AR, the IAP binder based on LCL-161 has been shown to be successfully used for the degradation of BRD4.<sup>121,122</sup> SNIPER(BRD4)-1 **57** was developed using a 4-EG chain (longer in length than cereblon dBET1 **32** and VHL MZ1 **15a** (**Figure 43**)). This compound **57** was shown to induce BRD4 degradation at just 3 nM (60% degradation). Interestingly, unlike the other E3 ligases recruited, complete knockdown is not observed with a  $\text{DC}_{\text{max}}$  of 77% (30 nM) and a prominent hook effect at just 300 nM. The reason for this is unknown, but

it has also been previously observed with the AR targeting PROTACs based on IAP binders. This effect would have to be studied *in vivo*, as it is not yet known whether full degradation is required to elicit a desired pharmacological response and may limit to utility of IAP recruiting PROTACs.

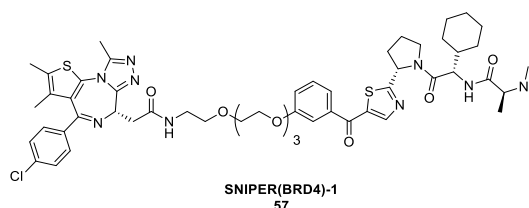


**Figure 43:** BRD4 targeting PROTAC recruiting IAP **57**.

In contrast to the previous cases, there are examples where potent protein degradation is achieved exclusively through IAP recruitment, not observed with VHL (**Figure 20**) or cereblon (**Figure 31**). IAP recruitment was utilised to degrade BCR-ABL using dasatinib based SNIPER(ABL)-39 **58** (**Figure 44**).<sup>109</sup> The compound **58** was shown to have very potent knockdown at just 10 nM, in stark comparison to the previous PROTACs developed recruiting VHL (no degradation) and cereblon (modest degradation).<sup>73</sup> This provides further evidence that differences in linker composition and E3 ligase binders could control the selectivity and degradability of a given target. This result shows IAP may be a useful family of E3 ligases for specific protein degradation, in contrast to the poor results observed for the degradation of AR and BRD4 using IAP recruiting PROTACs.

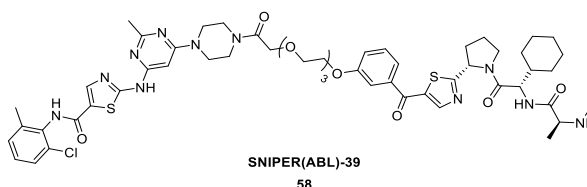


**Figure 44:** BCR-ABL PROTAC recruiting IAP **58**.<sup>123</sup>

IAP recruiting PROTACs degrading the ER $\alpha$  have also been developed and evaluated *in vivo* (**Figure 45**).<sup>122,124</sup> These compounds were based on the previously discussed scaffolds leading to SNIPER(ER)-87 **59**. Utilising a new IAP binder in the PROTAC approach leads to the development of SNIPER(ER)-110 **60**. Both compounds **59** and **60** showed excellent knockdown of ER $\alpha$  *in vitro* compared to the peptidic PROTAC **51** and were tested in a xenograft model. The compounds were found to be potent in the xenograft study compared to vehicle in reducing tumour size, weight and volume. In order to ascertain whether this effect was PROTAC-mediated, both binding partners (ER binder and IAP binder) would need to be evaluated in this experiment to ensure the effects were not caused by the small molecule inhibition. This work shows the potential for IAP as an E3 ligase for the PROTAC approach,

although further *in vivo* studies with other targets are required to show the utility of these IAP binders for use in overall PROTAC design.

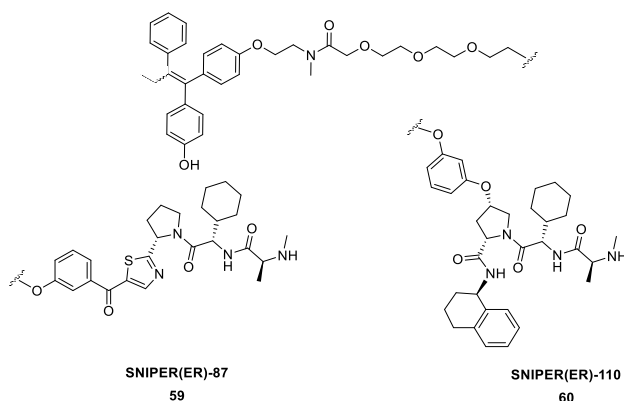


**Figure 45:** SNIPER targeting PROTACs SNIPER(ER)-87 **59** and SNIPER(ER)-110 **60**.

In addition to the SNIPERs synthesised previously, an increasing number of small molecule inhibitors of IAP have been published. One example is tetrahydroisoquinoline derived bivalent heterodimeric IAP antagonist **61** (Figure 46).<sup>125</sup> Compound **61** showed potent inhibition of cIAP1 binding in an FP binding assay ( $IC_{50} = 13$  nM).

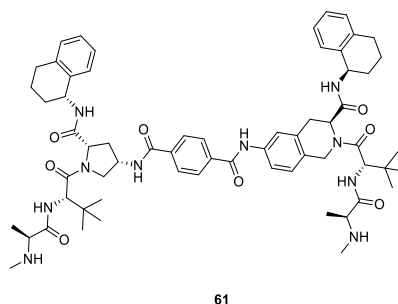
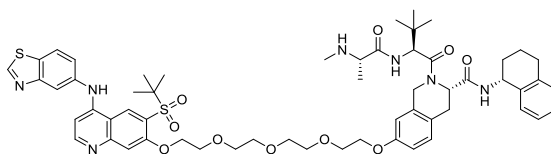


**Figure 46:** Heterodimeric IAP antagonist **61**.

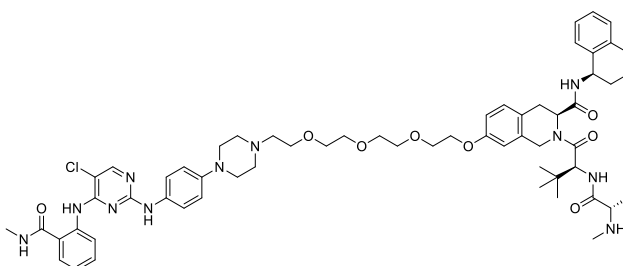
By synthesising RIPK2 targeting PROTACs by linking off one of the monomeric units of this IAP binder, a potent RIPK2 degrader was synthesised **62** (Figure 47).<sup>94</sup> In unpublished results, compound **62** was found to be extremely potent in the degradation of RIPK2 in THP-1 cells, with a  $DC_{50}$  of 150 pM after 16 h, (Figure 47), which compares favorably to the VHL recruiting PROTAC **13** which has a  $DC_{50}$  of 1.4 nM. Further work is being carried out within our laboratories with IAP binders and their use as an E3 ligase in the PROTAC approach using this binder both *in vitro* and *in vivo*.



62

**Figure 47:** RIPK2 targeting PROTAC recruiting IAP **62**.

In order to assess the wider utility of IAP as an E3 ligase for the wider kinase family, a promiscuous IAP recruiting PROTAC **63** was assessed by our group, in addition to the VHL **26** and cereblon recruiting PROTACs **43**.<sup>80</sup> Combining a promiscuous kinase warhead with an IAP binder from a published structure using a 4-EG linker unit, the promiscuous kinase IAP recruiting PROTAC **63** was designed and prepared (**Figure 48**). A significant portion of the kinases bound by the parent kinase inhibitor were found to not have the same affinity for the PROTAC **63**, which could be a result of presence of the linker or as a result of the poor physicochemical properties of the PROTAC. This experiment illustrated that IAP is a robust E3 ligase for kinase degradation with 50% of significantly engaged and quantified kinases degraded, and a total of 8 degraded proteins. Degradation of BTK and RPS6KA are all shown to have significant degradation despite having moderate kinase activity as measured in a Kinobead experiment.<sup>126,127</sup> Moderately bound kinases TEC, GAK and PTK2B all show good degradation with this compound. PTK2, AURKA and MAPK2 also show moderate to good degradation with the PROTAC **63**, in-line with their good kinase potency. This work, in conjunction with the other E3 ligases tested, may suggest that not every E3 ligase can be recruited for specific protein degradation and that multiple E3 ligases should be tested with a protein of interest for drug discovery.



63

**Figure 48:** Promiscuous IAP recruiting PROTAC **63** based on CTx-0294885.

In addition to the previously discussed IAP binders, there are a number of other IAP inhibitors, with varying selectivity profiles, which could be utilised in the PROTAC approach (**Figure 49**). This includes the clinical candidate ASTX660 **64**,<sup>55</sup> which is a pan-IAP inhibitor, as well as the novel binder **65** developed at GSK which has a differentiated IAP domain selectivity profile

(selectivity for XIAP BIR2 pIC50 ~7 over the BIR3 domain, in addition to cIAP1 BIR3 binding ~6.5).<sup>94</sup> In addition, the binder **66** is a selective compound for XIAP.<sup>128</sup> It would therefore be interesting to develop and investigate a number of different IAP recruiting PROTACs with differential selectivity profiles for a given PROTAC to determine if selectivity may influence the PROTAC's potency or safety profiles in future.

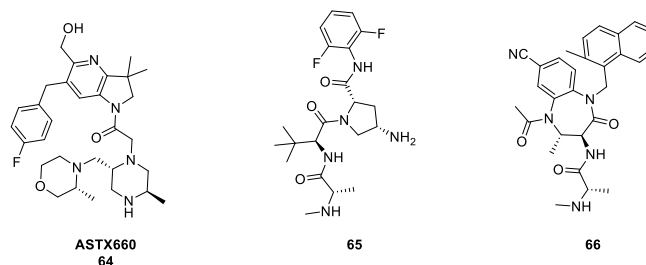


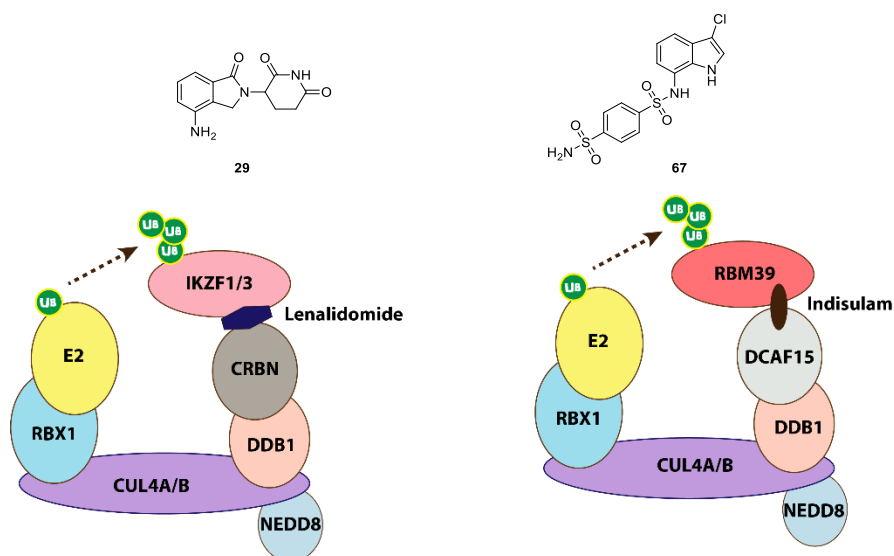
**Figure 49:** Small molecule IAP binders for potential use in the PROTAC approach.

IAP binders have shown increasing utility in PROTAC design, with recent examples providing potent and robust degradation both *in vitro* and *in vivo*. However, possible caveats to the use of IAP binders in PROTAC design include the necessity for the small molecule IAP binder to have a basic amine required for IAP binding, which may impair PROTAC permeability. In addition to the basic centre, recent IAP binders all have highly lipophilic groups, including cyclohexyl rings and tetrahydronaphthalenes which may contribute to poor physicochemical properties or compound half-lives and will need to be further evaluated in PK models. The IAP “self” degradation upon inhibition may also be cause for concern, as cIAP1 autoubiquitination and degradation leads to apoptosis, which may be unsuitable for PROTACs for use in non-oncology applications and would require in-depth evaluation.

### 2.2.3.5 DCAF15 Recruiting PROTACs

Another E3 ligase which could be utilised in the PROTAC approach is DCAF15.<sup>83,84,129-134</sup> In an analogous manner to cereblon and thalidomide **28**, it was recently discovered that indisulam **67**, a molecule that has shown anticancer effects, is also molecular glue for the E3 ligase DCAF15 (**Figure 50A**).<sup>135,136</sup> Indisulam is an aryl sulfonamide discovered in a phenotypic screen testing for anticancer activity, however indisulam **67** therapy in clinical trials resulted in only a small number of responding patients.<sup>135-137</sup> In order to assess its biological function, with aims to improve its efficacy, indisulam's **67** mechanism of action was investigated. It was then shown that indisulam **67** promotes the degradation of CAPER $\alpha$  and that the loss of the protein from the cell was the cause of cell death. Degradation of CAPER $\alpha$  was also observed with analogues **68** and **69** (**Figure 50B**), also known as SPLAMs (for SPLicing inhibitor sulfonAMides). Similar to the IMiDs function, degradation of CAPER $\alpha$  is not achieved by DCAF15 without the presence of the small molecule molecular glues.

A)



B)

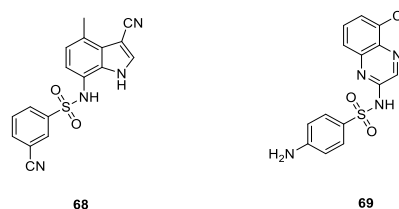


**Figure 50:** Lenalidomide **29** binding to Ikaros and CRBN complex and Indisulam **67** binding to RBM39 and DCAF15 complex (A). Structures of the other SPLAMs **68** and **69** (B).

In 2018, a report on BRD7/9 targeting PROTACs with a number of E3 ligases also featured compounds based on indisulam **67** (Figure 51). Two compounds were featured, with a 2-EG and 4-EG linker **70a/b** respectively. However, the compounds did not show any degradation of the desired targets, nor was there evidence of binding activity to DCAF15. As a result, more PROTACs based on this scaffold should be further investigated to demonstrate the utility of DCAF15 as an E3 ligase in the PROTAC approach, as this remains inconclusive.

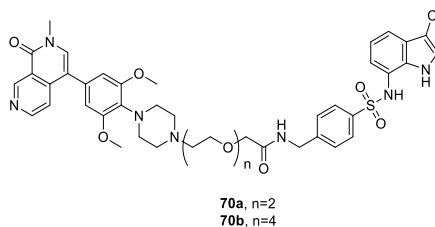


**Figure 51:** BRD7/9 targeting PROTACs based on indisulam.

### 2.2.3.6 Current State of the Art

Development of the small molecule protein degradation platform has advanced immensely from the early 2000's from the initial application of peptidic PROTACs to the more drug-like molecules which have the potential to become transformational medicines. In future PROTAC research will require the balance of potency, selectivity and good physicochemical properties for PROTACs to ensure the protein degradation approach is a viable and novel therapeutic approach.

The current research has primarily focused on protein target tractability, with overall aims of medicine discovery. Four of the E3 ligases described, VHL (example binder **71**), cereblon (example binder **72**), MDM2 (example binder **73**) and IAP (example binder **74**) have shown utility in the PROTAC approach in supporting the hypothesis that PROTAC-based medicines may provide advantages over small molecules (**Figure 52**). Many publications have shown the degradability of multiple targets with one or more E3 ligases (illustrating the importance of testing multiple E3 ligases for target tractability), and PROTAC molecules have shown good pharmacological effects both *in vitro* and *in vivo*, including low efficacious doses and even the creation of functional PROTACs from non-functional binders. A number of publications have illustrated the potential of these molecules as therapeutics, but others have also demonstrated that not every E3 ligase can be employed to degrade a target of interest and that some E3 ligases are more successful for the degradation of specific proteins than others.

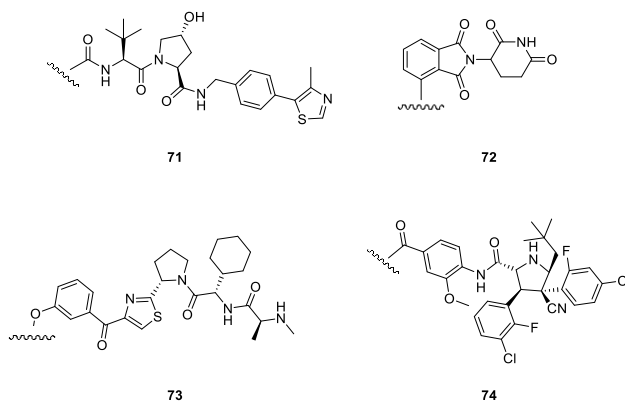


**Figure 52:** Exemplar structures of E3 ligase binders currently utilised in the PROTAC approach.

One current limitation of the approach is the underutilisation of other E3 ligases, of which there are over 600.<sup>32,36</sup> A number of E3 ligases which are not currently employed in the approach are tissue and cell type specific, which may be extremely advantageous in targeting a PROTAC therapy specifically to disease relevant tissue/cells.<sup>11,138</sup> Additionally, as demonstrated in the number of publications, not every E3 ligase can degrade a specific target

of interest, so the four that are currently used, may not be sufficient for more undruggable and desirable targets. A number of E3 ligases mentioned in the introduction, such as DCAF15 and KEAP1 are also examples of E3 ligases of interest for the PROTAC approach, however utility with functional small molecule PROTACs has not yet been demonstrated. This could be a result of failure of incorporation of the binders into PROTACs, or successful results not yet published. Reasons for failure of recruitment of E3 ligases is not well understood or documented in the literature. For example, in cases where one E3 ligase was able to degrade a specific protein of interest, but another was not, there are currently no exact methods to determine the reason for failure. This could be a result of poor ternary complex formation, binding of either part of the PROTAC not being sufficient, surface lysine availability, among many others. This is a disadvantage of the PROTAC approach, in cases where degradation cannot be achieved, it would require a lot of experiments to determine the true cause for this. As a result, it will be useful to evaluate many E3 ligase binders in order to determine their utility in the PROTAC approach and in drug discovery.

In addition to this, there are a number of concerns about the four E3 ligases currently used. Cereblon has teratogenicity risks associated with the small molecule thalidomide, which may prevent its wider use in non-oncological indications. In addition, IAP drives cell apoptosis upon cIAP1 inhibition, which will need to be further evaluated *in vivo* to determine if this may cause unwanted effects and may also limit the PROTACs to oncology indications. MDM2 has not yet been demonstrated as a widely applicable E3 ligase and has only been shown in a small number of examples with nanomolar protein degradation, which is required for good efficacy in a potential medicine. Therefore, there is a need to expand the scope of E3 ligases used in protein degradation in the future.

### 3. Overall Aims for the Research

As previously discussed in the introduction section, the E3 ligases which are available for recruitment for the PROTAC approach are limited in number and there are potential concerns regarding their suitability for incorporation in potential PROTAC medicines. In addition, it has been shown that not every E3 ligase can be recruited to successfully degrade a given target of interest, so this may result in tractable targets for the PROTAC approach not being fully evaluated. Therefore, new E3 ligase recruitment in the PROTAC approach would be advantageous to protein degradation drug discovery. There are over 600 E3 ligases which are yet to be exploited in PROTAC development. The aim of the current work is to expand the protein degradation platform through the investigation of new E3 ligases for subsequent PROTAC recruitment, with overall aims to expand the E3 ligase repertoire for novel PROTAC medicine development.

In order to evaluate novel E3 ligases for the PROTAC approach a “promiscuous toolbox” would be established (**Figure 53**). This promiscuous toolbox would consist of binders to multiple proteins and protein families, which have previously been validated through existing E3 ligases for the PROTAC approach for new E3 ligase validation. In the introduction section, kinases and the bromodomain protein families were shown to be degradable by a number of E3 ligases. The promiscuous kinase experiments illustrated in the introduction were used to assess target validation using the E3 ligases VHL, cereblon and IAP. This promiscuous kinase approach (targeting over 100 kinases) would therefore be redesigned and utilised to further investigate novel E3 ligases for the protein degradation platform and will be discussed in Chapters 4 and 5. In addition, to expand the toolbox to encompass a promiscuous bromodomain binder, a pan-bromodomain inhibitor would be selected from the literature and evaluated for the PROTAC approach. The current bromodomain PROTACs only target the four proteins from the BET family, and more promiscuous PROTACs would allow the future E3 ligases to be evaluated against more proteins, increasing the chance of finding a successful hit. In order to validate the selected binder for the promiscuous toolbox, PROTACs based on known E3 ligases VHL and cereblon would be designed and evaluated. In order for the promiscuous bromodomain inhibitor to be valuable in the toolbox, it would be required to be as efficacious as the current BET targeting PROTACs, and expand the proteins degraded into the non-BET bromodomain family. The design, synthesis and evaluation of the promiscuous bromodomain PROTACs will be discussed in Chapter 4. Once the toolbox is established, it can then be utilised to assess novel E3 ligase binder for the PROTAC approach, which would enable the expansion of E3 ligases used for future PROTAC medicine development.

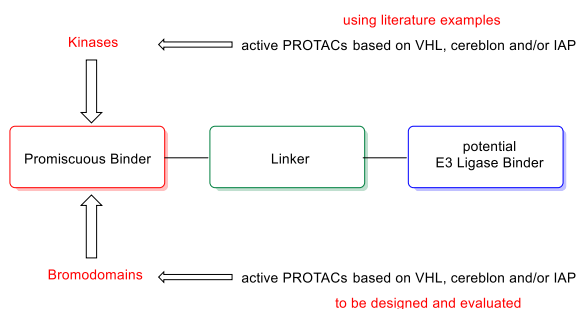


**Figure 53:** Design of a promiscuous toolbox for new E3 ligases, using binders that have been validated for the PROTAC approach using the current E3 ligases available (VHL, cereblon and/or IAP).

With a promiscuous toolbox in hand for evaluating new E3 ligases, a novel E3 ligase for the PROTAC approach will be investigated. In recent literature, DCAF15, an E3 ligase, has shown to have a small molecule binder, indisulam **67**, which binds to the protein, in an analogous manner to cereblon. PROTACs recruiting DCAF15 could prove useful if degradation could be achieved similar to that of cereblon but DCAF15 would the benefit of potentially mitigating the inherent stability and teratogenicity risks associated with cereblon. Therefore, to test whether DCAF15 could be a useful E3 ligase, PROTACs recruiting DCAF15 will be designed using the toolbox (**Figure 54**). Indisulam **67** would therefore be evaluated for derivitisation, including an appropriate exit vector, for subsequent PROTAC synthesis. The PROTACs designed would encompass a number of different targeted proteins of interest, in addition to multiple linker lengths for the indisulam analogues. These would then be evaluated for protein degradation to determine if DCAF15 is a suitable E3 ligase for the PROTAC approach and this will be discussed in Chapter 5. If successful degradation was achieved, further PROTACs could be designed and analysed to determine if indisulam **67** had potential to be elaborated into PROTAC drug candidates.

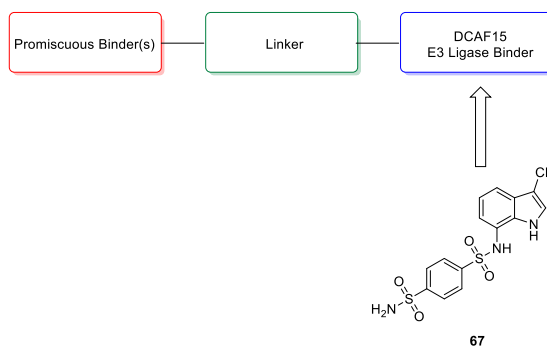


**Figure 54:** PROTACs targeting DCAF15 will be investigated utilising the promiscuous toolbox.

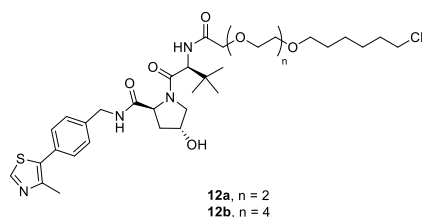
The promiscuous toolbox method allows specific E3 ligases to be evaluated for the PROTAC approach but is not suitable for use where no known chemical matter for a given E3 ligase

exists. As previously discussed, there are over 600 E3 ligases available for incorporation into PROTACs but this has been dramatically underutilised in the drug discovery efforts in protein degradation. Efforts to find new chemical matter for E3 ligases is a resource intensive task. Specific E3 ligase binders would need to be determined using techniques such as ELT, HTS, literature precedence or developing small molecules from endogenous binders to the E3 ligase (as utilised in search of small molecule VHL binders). After small molecule determination, complex efforts to determine appropriate exit vectors, linker lengths and evaluating protein levels after PROTAC incubation are required. The promiscuous toolbox could therefore not be utilised to expand the E3 ligases utilised unless the chemical matter is already established for a given protein of interest or efforts to find chemical matter are undertaken. As a result, it was envisaged that a method to assess multiple E3 ligases at once for protein degradation could be extremely powerful for the PROTAC approach and could accelerate the process into drug discovery. A high-throughput assay would ideally be used to test many thousands of PROTAC molecules to find chemical matter which induces protein degradation specifically. A cellular phenotypic protein degradation assay, for example, would therefore be E3 ligase agnostic, and able to detect chemical matter that induces degradation, irrespective of the E3 ligase recruited. Testing potential PROTAC molecules in this assay would mitigate the need to determine an appropriate exit vector, as this should theoretically be known from the parent molecule tested and should accelerate the process of E3 ligase validation for the PROTAC approach.

Inspired by HaloPROTACs ability to degrade GFP-HaloTag® (**Figure 55A**), a GFP degradation assay was designed to search for novel chemical matter for induced protein degradation (**Figure 55B**). By drawing on fluorescence reduction correlating to GFP degradation shown by **12a/b**, this approach could be amenable to high-throughput fluorescence read-out techniques not achievable through traditional protein degradation assays, such as Western blotting or proteomics. With aims to use an assay in a HTS format in evaluating chemical matter for several E3 ligases at once, the GFP degradation assay had to be validated. In order to establish this assay as robust and fluorescence reduction specific to protein degradation only and was not cytotoxicity-driven, a GFP-HaloTag® control cell line, not previously reported in the literature, was harnessed and will be discussed. In this cell line, the GFP-HaloTag® was mutated which would not allow binding to the HaloPROTAC and therefore degradation would not occur, and fluorescence reduction only correlates to cytotoxicity. With aims of GFP degradation assay validation, HaloPROTACs based on known E3 ligase binders were designed, synthesised and evaluated using the two GFP-HaloTag® cell lines, which will be discussed in Chapter 6. This would also include cytotoxic compounds to assess the ability to distinguish degradation from cytotoxicity (or non-specific fluorescence reduction) in the two cell lines. This work would highlight the utility of using a phenotypic

cellular assay for protein degradation and illustrate the potential power of then using the screen for finding new chemical matter for E3 ligases which otherwise could not be achieved.

A)



B)

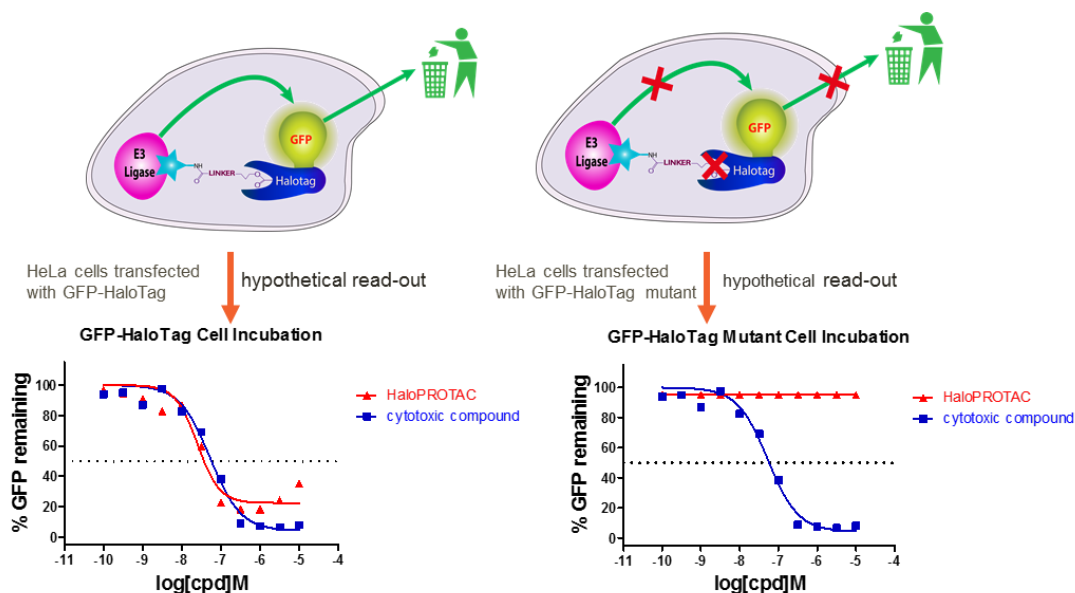


**Figure 55:** Exemplar VHL recruiting HaloPROTAC able to induce GFP degradation (A). Development of a GFP degradation screen to investigate new E3 ligases. HaloPROTACs target and degrade a GFP-HaloTag® construct which correlates to fluorescence reduction through E3 ligase recruitment. This would then be compared to a GFP-HaloTag® mutant control cell line which would delineate HaloPROTAC-driven fluorescence reduction and cytotoxicity. Example illustrations of fluorescence reduction in response to a HaloPROTAC (red) and a cytotoxic compound (blue) are shown below the respective cell line (B).

With aims to employ the GFP degradation screen in a HTS screening format for the search for new E3 ligases, a strategy encompassing high-throughput chemistry had to be explored. In order to generate thousands of HaloPROTACs *in-situ*, high-throughput amide coupling techniques would be investigated and established, which will be discussed in Chapter 7 (**Figure 56**). The aims were two-fold, to develop high-throughput chemistry to synthesise and screen many thousands of molecules to search for new E3 ligases, and through this work, establish that the assay would be suitable for a larger HTS test-set of up to 100,000 molecules. The compounds which were synthesised in order to establish the chemistry was robust with thousands of molecules would also be tested in the high-throughput GFP degradation assay

to search positive hits for E3 ligases. Any hits that were established through this smaller screening set could then be further evaluated. By using the promiscuous toolbox, the applicability of the compound for additional protein degradation of kinases and BET proteins could be demonstrated, and future work could assess any hits for their utility in drug discovery efforts.

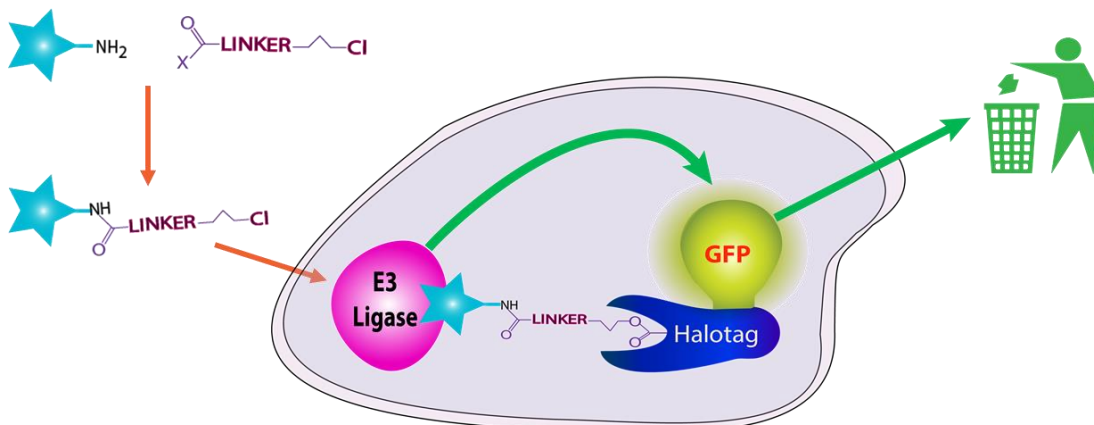


**Figure 56:** Development of a high-throughput amide coupling reaction to generate many HaloPROTACs *in-situ* to then test GFP degradation screen to investigate new E3 ligases.

## 4. Expanding the Promiscuous Toolbox for Examining New E3 ligases

### 4.1 Introduction

#### 4.1.1 Building a Promiscuous Toolbox to Evaluate New E3 Ligases

In order to establish and expand a promiscuous binder toolbox for assessing novel E3 ligases for protein degradation, the approach was to utilise a well-established class of proteins known to be degradable by PROTACs. Using this method, new E3 ligases could be tested using the promiscuous binders, and through subsequent biological evaluation, protein degradation as a result of novel E3 ligase recruitment could be assessed. An appropriate small molecule E3 ligase binder could be addressed from, for example, literature, ELT or HTS campaigns for a specific E3 ligase of interest.<sup>139-142</sup> After an appropriate exit vector is identified, through X-ray crystallography or another suitable approach, PROTACs would be designed using this toolbox and tested in biological assays, such as Western blotting or proteomics experiments. If the E3 ligase binder was able to induce protein degradation specifically, this could then be further evaluated for its wider utility in the PROTAC approach in drug discovery. This may include determining the structure activity relationship of the small molecule and potentially improving the physicochemical properties of the binder, to develop a molecule suitable for use in an overall PROTAC medicine.

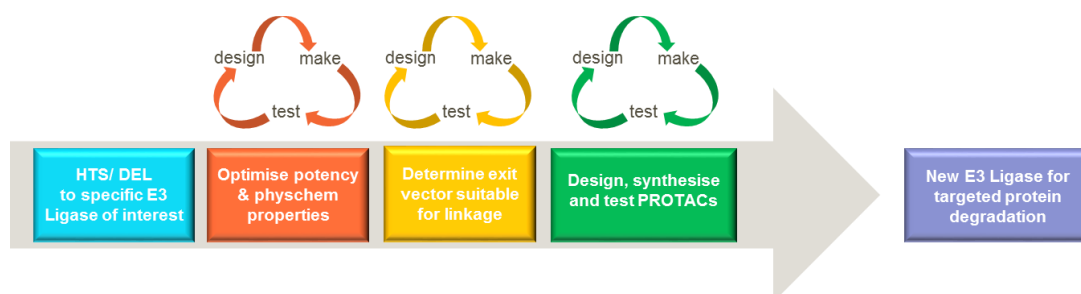


**Figure 57:** Workflow to identify and test new E3 ligases for the PROTAC approach.

To build the promiscuous toolbox, proteins which were validated as degradable for the PROTAC approach would be included. The kinase family are an example of a class of proteins which have been successfully degraded via the PROTAC approach.<sup>4,36,73,75,96,97,143</sup> Examples include the RIPK2 binder **75** which has shown degradability with three out of four E3 ligases tested. Promiscuous kinase experiments have also illustrated kinase degradability with 5–15 kinases with VHL, cereblon and IAP using the warhead **76**. (**Figure 58**). Together, these proteins form a promiscuous kinase toolbox for evaluating new E3 ligases. Drawing on easily degraded targets by the small number of validated E3 ligases in the literature, this will form a toolbox of proteins which can be utilised to investigate new chemical matter for E3 ligases.

Expansion of this toolbox to include other non-kinases would also be advantageous and will be discussed.

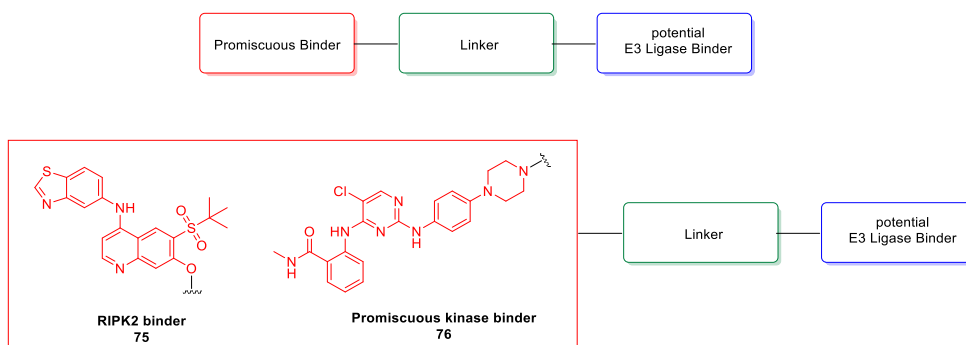


**Figure 58:** Promiscuous kinase PROTAC toolbox for assessing new E3 ligases.

#### 4.1.2 Bromosporine and the Promiscuous Toolbox

In order to build on the promiscuous protein toolbox mentioned (RIPK2, promiscuous kinase), it was envisaged to utilise the bromodomain family of proteins. PROTACs targeting the BET family have been developed and extensively described in the introduction section. In order to access multiple bromodomain proteins at once, not just the BET family of bromodomains, it was envisaged to assess a more promiscuous bromodomain protein binder than JQ1 **14**. The promiscuous kinase binder, for example, binds to over 100 kinases, and Tinworth has shown the degradability of up to 15 of those using multiple E3 ligases.<sup>80</sup> In comparison, JQ1 **14** only binds to 4 proteins, the BET family of bromodomains. Therefore, PROTACs based on a more promiscuous bromodomain inhibitor were designed and assessed in order to expand the proteins degradable by the toolbox, thereby, increasing the chances of finding a valuable E3 ligase hit.

In order to access a promiscuous bromodomain inhibitor, established compounds from the literature were evaluated. A review of bromodomain inhibitors by Conway and co-workers, illustrated two compounds with multi-domain inhibition of several bromodomains developed by the SGC (**Figure 60**).<sup>144</sup> The compounds had similar core structures, but differential binding profiles. Compound **77** was found to bind to BRD4, BRD9 and CREBBP. Further iterations lead to the discovery of bromosporine **78**, a pan-bromodomain compound deemed a useful tool probe for the bromodomain family.<sup>145,146</sup>

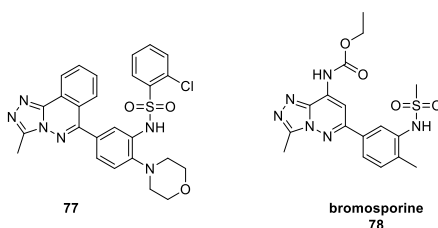


**Figure 59:** Compound **77**, a bromodomain inhibitor, and subsequently discovered bromosporine **78**, a promiscuous bromodomain inhibitor both developed by the SGC.

As a pan-bromodomain inhibitor, bromosporine was an ideal candidate for the promiscuous toolbox, and further analysis into bromosporine's binding profile was assessed. In our in-house assays, bromosporine **78** was found to bind to the BET proteins BRD2/3/4 with a  $pIC_{50} \sim 6.5$ , and the non-BET proteins BRD9, BRPF1, CECR2 and TAF1 with  $pIC_{50} > 5.5$  (**Figure 60A**). Bromosporine **78** was the first known compound with  $\mu M$  potency for CECR2 and TAF1. However, it is worth noting that the SMARCA2/SMARCA4 potency shown in the figure is hypothesised to be indirect via BRD9.<sup>147</sup> ITC has also been performed on bromosporine externally **78** and  $K_d$  values are reported in the **Figure 60B**, showing good correlation between the two methods of binding determination. In the ITC, bromosporine **78** has good binding  $K_d$  values to other non-BET bromodomains as expected, such as: CECR2, TAF1 and TAF1L and BRD9.<sup>146</sup> SMARCA2/4 was not found in this analysis, so was deemed an indirect effect in the in-house binding assays. Therefore, it was hypothesised based on previous experience within the group and literature evidence, that PROTACs with  $\mu M$  activity could successfully degrade the protein of interest.<sup>94</sup> As a result, PROTACs based on the bromosporine **78** could potentially degrade the BET family, in addition to a number of non-BET bromodomains. This would be a useful addition to the toolbox for the testing of novel E3 ligases in future, if bromosporine could be harnessed as a successful degrader. Therefore, bromosporine derived PROTACs would be assessed to determine the utility of bromosporine **78** as a promiscuous bromodomain binder for the PROTAC approach.

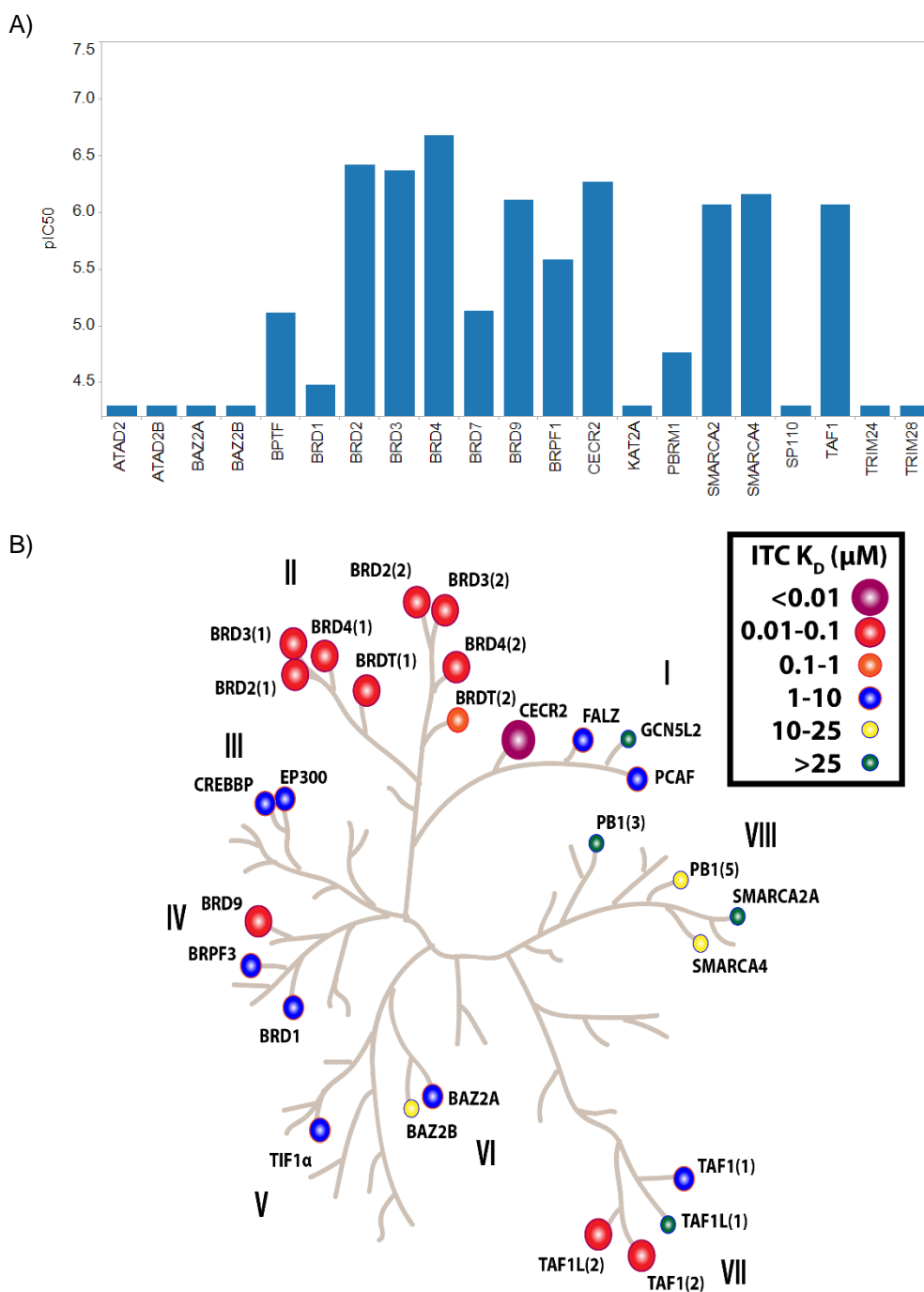


**Figure 60:** pIC<sub>50</sub> values to the bromodomain family by bromosporine **78** (A) and the phylogenetic tree showing ITC K<sub>d</sub> values (B).

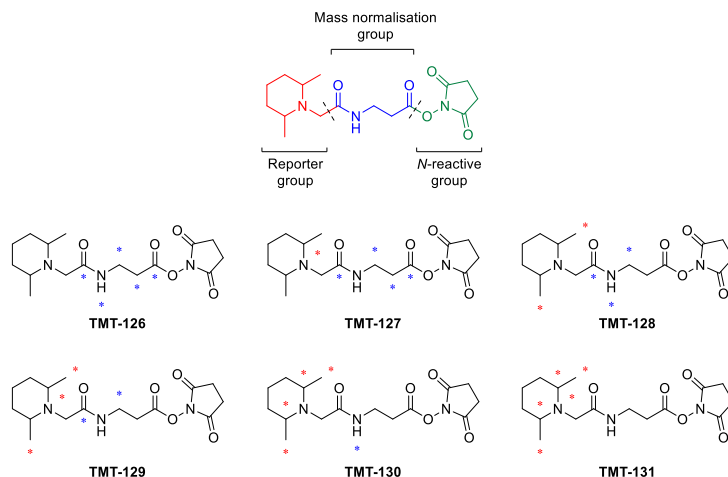
#### 4.1.3 Analysing the Protein Degradation from the Promiscuous Toolbox

In order to determine proteins degraded using the promiscuous toolbox, biological evaluation would be required. Multiple research groups, including our own laboratories, have investigated the degradability of multiple proteins in one experiment via a proteomic approach.<sup>95,148</sup> This

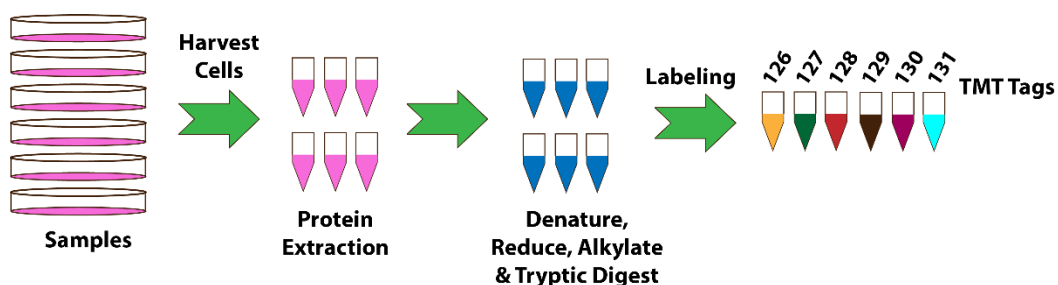
approach could therefore be a useful method to investigating new E3 ligases with a promiscuous warhead.

In order to determine down-regulated proteins through proteomics, Tandem Mass Tag (TMT) labelling strategies can be used (**Figure 61**).<sup>4, 80, 149</sup> The TMT tags are chemically identical tags but contain different isotopes substituted at a number of points in the molecule, which can be identified using MS-based techniques.<sup>80,150</sup> The tags can be conjugated to proteins in cell lysate samples previously treated by a PROTAC, which can be then compared to DMSO controls to determine qualitative protein levels of the soluble proteome. The **TMT** tag consists of a dimethylpiperazine mass reporter group and an cleavable *N*-hydroxysuccinimide (NHS) moiety separated by a mass normalisation linker (**Figure 61A, TMT126–TMT131**). Points of the molecules are then tagged with varying the substituents with the labelled <sup>13</sup>C/<sup>15</sup>N as a reporter isotope and mass balancing isotopes (shown in the figure by red or blue asterisks respectively). The reactive NHS ester group of TMT isobaric mass tags allows labelling of the *N*-termini and lysine residues of peptides directly from cell lysates for both compounds treated and control samples (**Figure 61B**). These samples are then combined and analysed by LCMS/MS (**Figure 61C**),<sup>80</sup> allowing separation of the distinct peptides. Following MS/MS, the detailed fragmentation patterns of the individual peptides can be deconvoluted and corresponded to their full protein counterparts (via sophisticated computational methods). Simultaneously, fragmentation of the TMT label occurs in the MS/MS, resulting in release of distinct dimethylpiperazine reporter group ions between  $m/z = 126–131$  which can therefore be linked back to the sample where the specific report was used. The relative intensities of each of the six reporter group ion correlates directly to the relative amount of each peptide in the treated or control samples and can therefore be used as a relative quantification technique for protein levels. This experiment is done in at least one additional replicate, to ensure sample variability is mitigated. For example, in a PROTAC treated sample, the TMT label ion peak should be observed as much less intense peak than the control sample, and therefore relative protein degradation can be determined for each protein in comparison to the DMSO control.

A)



B)



C)

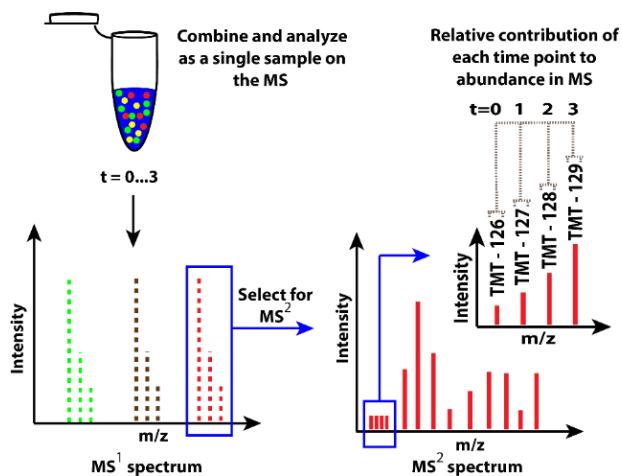


**Figure 61:** Structure of TMT reagents used in expression proteomics as isobaric labelling and isotopic labelling patterns of TMT 6-plex reagents (A) (red Asterix = <sup>13</sup>C/<sup>15</sup>N reporter isotope, blue Asterix = <sup>13</sup>C/<sup>15</sup>N mass balancing isotope) and the TMT assay workflow overview (B). Example MS readout from a TMT labelling experiment (C).

In proteomic analysis of the PROTACs, protein degradation can be visualised using log<sub>2</sub> plots of one replicate compared to another. If specific protein levels are found to be significantly reduced in a compound treated sample compared to the untreated DMSO control sample this will be observed in the lower left quadrant highlighted in blue in **Figure 62**. Combined with target engagement, for example, using pIC<sub>50</sub> determined by biochemical efforts, this can determine if the proteins are degraded directly (or possibly indirectly) via the PROTAC. This is therefore an extremely useful method in identifying protein degradation where multiple proteins can be assessed in a single experiment. This is an extremely powerful resource for identifying protein degradation from a promiscuous protein binder and will be utilised in this research.

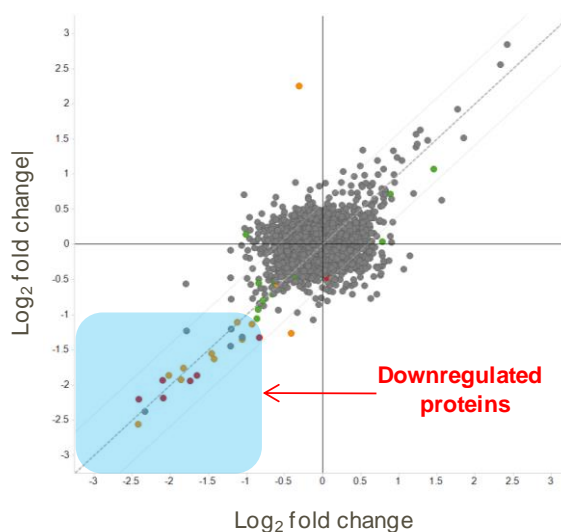


**Figure 62.** An active PROTAC should induce protein degradation in both replicates leading to downregulated proteins ending in the lower left quadrant of the log<sub>2</sub> fold change plots.<sup>80</sup>

In combination with TMT labelling approaches, another method of isotopic labeling can be utilised to differentiate protein degradation of mature and nascent (newly synthesised) proteins, coined multiplexed protein dynamics. This approach utilises Stable Isotope Labeling by Amino acids in Cell culture (SILAC) which utilises two isotopically differentiated amino acid media to create two populations of cells in culture (**Figure 63**). One media used, termed “light” has unlabeled amino acids, whereas the other media contains a “heavy” amino acid, where <sup>13</sup>C or <sup>15</sup>N is used, for example <sup>13</sup>C<sub>6</sub>-lysine, which in MS experiments have a 6 Da difference to the light amino acid. Protein synthesis then incorporates the amino acids found in the media, which results in proteins with either non-labelled amino acids in the “light” media, or “heavy” labelled amino acids in proteins. This creates chemically indistinguishable but isotopically different protein samples.

In order to utilise the SILAC approach in protein degradation experiments to distinguish mature and nascent proteins, the media used for cell culture can be exchanged at the same time as PROTAC treatment. For example, if the cells were cultured using the non-labelled “light” media, the cells would be treated with the PROTAC and incubated overnight with the “heavy” media. As a result, all mature proteins, synthesised in the cell culture, would contain the unlabeled amino acids. Nascent proteins would contain the labelled amino acids, as these would be resynthesised using the amino acids from the new “heavy” media. This can be confirmed by MS experiments in the same way as the TMT labelling. These results would show the PROTAC’s effect on not only mature proteins, but also downstream effects of the proteins loss. This approach will therefore be utilised as a standard PROTAC-treated proteomic approach. This would combine the power of TMT labelling to determine relative protein knockdown compared to DMSO controls, with the SILAC approach, to give information on protein degradation and downstream effects. Multiplex protein dynamics is therefore an excellent and information rich experiment for assessing protein degradation using the promiscuous toolbox.

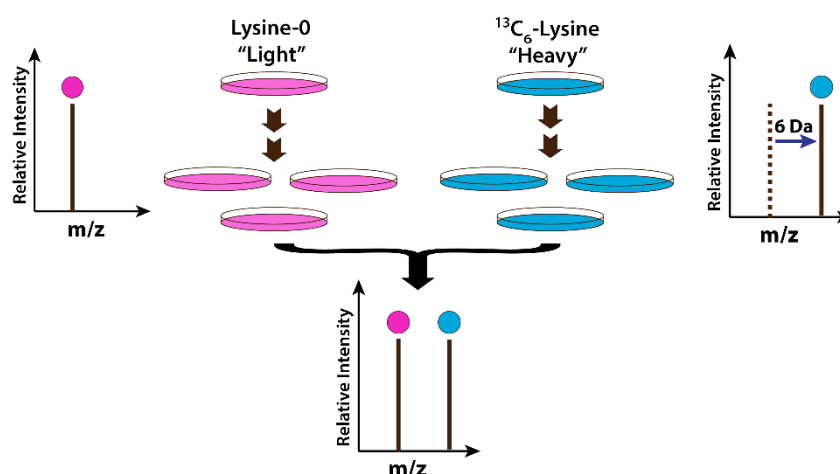


**Figure 63:** SILAC approach using “light” and “heavy” media containing unlabelled or labelled lysine which can then be corresponded to distinguishable MS-readouts.

## 4.2 Bromosporine PROTACs Project Aims and Objectives

To evaluate the tractability of a new E3 ligase in the PROTAC approach, it would be advantageous to target many proteins at once using a promiscuous toolbox, and then use proteomics experiments – namely multiplex protein dynamics - to quantify protein degradation. In an analogous manner to the promiscuous kinase approach, the aim of this project was to investigate whether bromosporine **78**, a promiscuous bromodomain binder, could be utilised to expand the number of bromodomain proteins that can be degraded in a single experiment.

VHL and cereblon, known for their degradation potential with the BET family, would be utilised to assess the degradation of the BET bromodomains and the non-BET bromodomains targeted by bromosporine **78** (**Figure 64A**). This would be used in conjunction with two possible vectors, to assess if either of the vector approaches were successful in degradation of the non-BET bromodomain family. PROTACs would be designed with one linker, two vectors and two E3 ligases to give four PROTACs **79a/b–80a/b** in total to assess the biological effects. Assessing the degradation capability of these PROTACs would be performed using a number of different biological assays, such as Western blotting experiments, imaging assays, multiplex protein dynamics. In addition to these experiments, affinity enrichment proteomics experiments would also be carried out, to determine binding to the bromodomain proteins by each vector. In order for bromosporine **78** to be a useful promiscuous binder for the toolbox, PROTACs **79–80** would be compared to the known degradable BET targeting PROTACs based on JQ1, MZ1 **15a**, in its efficiency to degrade BRD2/3/4 and expand this further into the non-BET family (**Figure 64B**).

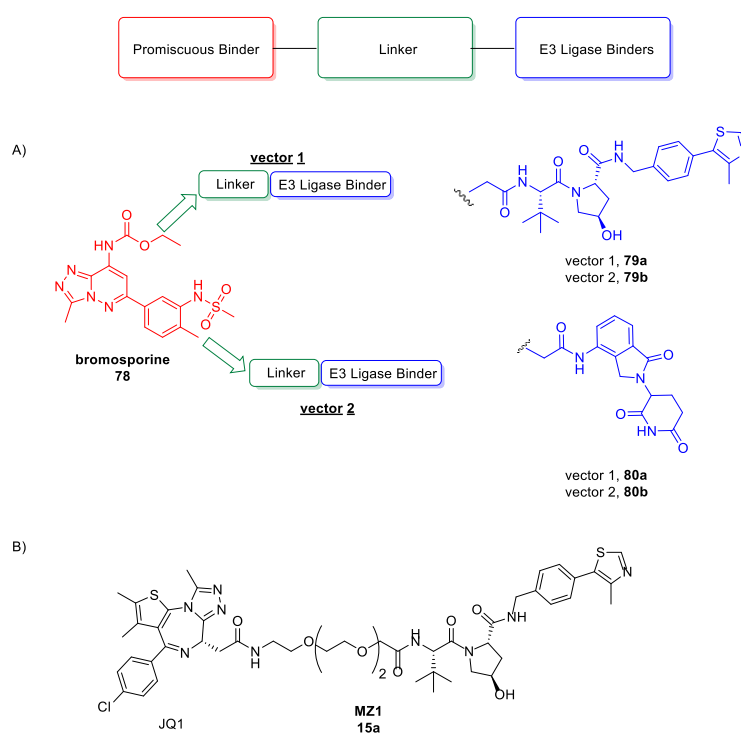


**Figure 64:** Promiscuous bromosporine PROTACs based on two vectors and two E3 ligases VHL **79a**, **79b** and cereblon **80a**, **80b** (A). These would be compared to MZ1 **15a** in biological evaluation, a known BET targeting PROTAC targeting VHL (B).

It was envisaged that bromosporine **78** elaboration into PROTACs may provide a more promiscuous BET targeting PROTAC than the JQ1 analogues and may be suitable for future prosecution of new E3 ligases to a wider range of proteins (**Figure 65**). By increasing the number of proteins that the PROTAC can bind to would give greater chance of identifying a

successful E3 ligase for the future PROTAC approach. If the degradation profile of bromosporine derived PROTACs was not as efficacious as the JQ1 derived PROTAC MZ1 **15a** for the BET family, or if no additional non-BET bromodomains were degraded, JQ1 linked compound **81** would therefore be added to the promiscuous binder toolbox. This would be to ensure the BET family of proteins could be assessed with new potential E3 ligases with JQ1 if bromosporine **78** was not a suitable BET and non-BET protein degrader.

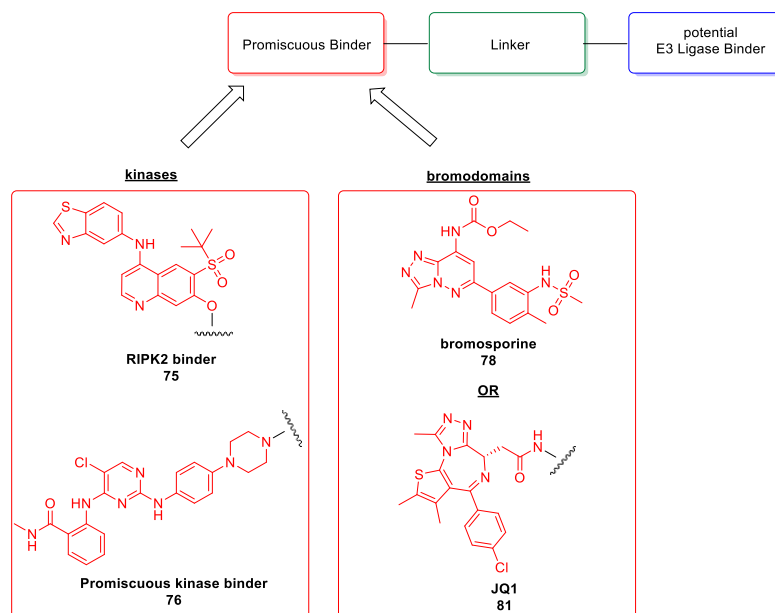


**Figure 65:** Promiscuous toolbox, utilising the kinase binders for RIPK2 **75** and the promiscuous binder **76** and the addition of a bromodomain binder, either bromosporine **78** or JQ1 linked binder **81** depending on the outcome of the bromosporine PROTACs synthesised in the following section.

## 4.3 Results and Discussion

### 4.3.1 Design of Bromosporine PROTACs recruiting VHL and cereblon

To evaluate bromosporine **78** as a promiscuous PROTAC binder for the promiscuous toolbox, PROTACs based on the known E3 ligases VHL and cereblon were designed and synthesised. Evaluation and comparison of bromosporine derived PROTACs recruiting VHL and cereblon to the known degrader MZ1 **15a** would elucidate whether bromosporine **78** would be a useful promiscuous binder to investigate new E3 ligases in the future. This was chosen to test the hypothesis of bromosporine PROTACs, as it has been previously shown that both E3 ligases have successfully degraded the BET family with a number of linkers. If VHL and cereblon could successfully degrade the BET family to the same levels as JQ1 allowed, in addition to any

non-BET bromodomains, this would give confidence that bromosporine **78** would be useful in the future use of E3 ligase for PROTAC determination.

When designing PROTACs, the main factors to consider are: an appropriate solvent exposed exit vector which can successfully retain binding to the protein of interest, linker length to the E3 ligase (varies on protein class, and protein location in the cell) and predicted lipophilicity (which can be used as a surrogate for permeability in the design stage). The crystal structure of bromosporine **78** has been published and is shown in **Figure 66**, which can be utilised in the design of PROTACs. The bound structure indicates two main solvent exposed vectors which would be suitable for elaboration into PROTACs. The first vector identified looks at conjugating bromosporine through the carbamate (vector 1 shown in blue, recommended by the SGC as a linking point) and the aromatic methyl (vector 2 shown in pink). The carbamate shown in blue, is hypothesised to be the exit vector used for the majority of JQ1 derived PROTACs.<sup>147</sup> There are no computational methods at present which can effectively predict which vector may be more favourable for the ternary complex of the multiple proteins involved in the PROTAC mechanism, therefore both vectors were evaluated for bromosporine.

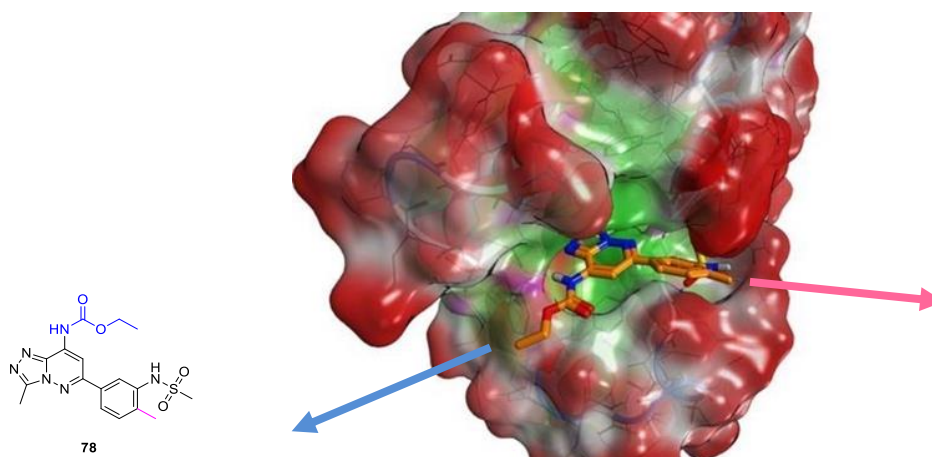


**Figure 66:** X-ray crystal structure of bromosporine **78** (orange) in BRD4, showing two exit vectors from the protein in blue and pink (MOE, PDB 5IGK).

In addition to the exit vector determination, lipophilicity and linker length were evaluated to design compounds which would permit cell permeability. Bromosporine **78** has a ChromLogD of 3.37, and internal learnings from our group suggested that PROTACs should have ChromLogD of between 5–7 initially to ensure good permeability. ChromLogD, Chromatographic LogD, is a measured LogD value derived directly from the compound's retention time on a C18 column (and calibrated using a standard compound) which is transformed to give the lipophilicity of the compound.<sup>36,151-154</sup> Calculating ChromLogD was found to not correlate well with measured values so was not used in this instance. Due to the

high number of hydrogen bond donors and acceptors in bromosporine **78** which could impair permeability, particularly the acidic sulfonamide and the carbamate, a lipophilic methylene linker was designed to promote permeability for the resulting PROTACs. The length of 10 carbon atoms has been shown to be optimal in BET programs internally, so these were employed in the initial hit PROTAC generation. In addition, Western blotting and multiplex protein dynamics experiments were resource intensive, so only a small number of compounds could be profiled using these methods, and it was decided to evaluate a number of vectors rather than linkers as a result. The chosen linker, together with the known E3 ligase cereblon, this gives compounds **82** from vector 1 (compound shown in blue) and **83** from vector 2 (compound shown in pink) which should retain binding affinity to the BET proteins, and cellular permeability (

**Figure 67**).

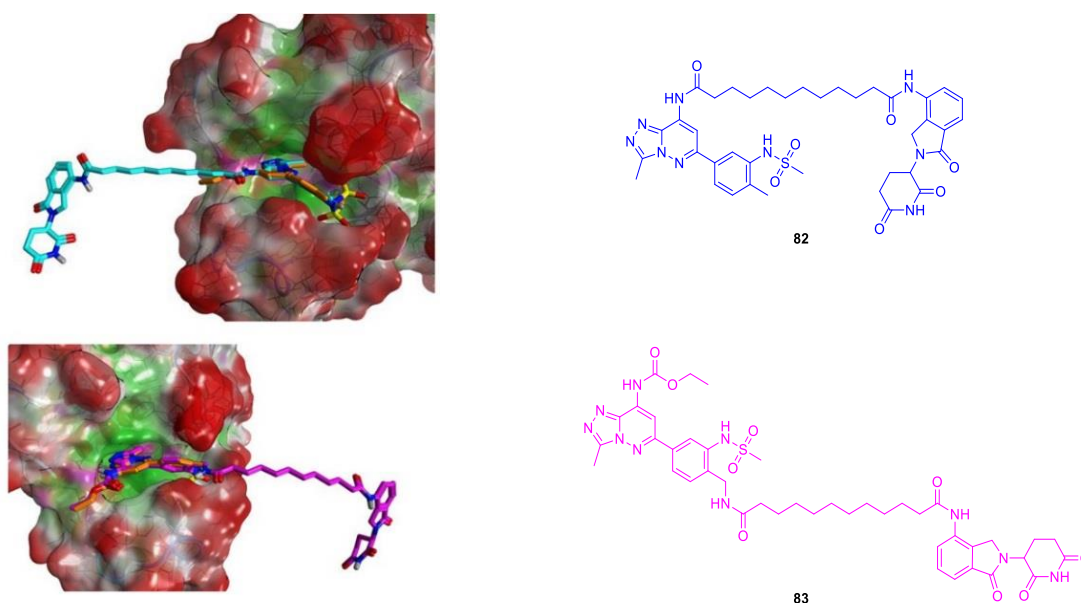


**Figure 67:** Bromosporine-cereblon recruiting PROTACs from each vector (**82** vector 1, blue and **83** vector 2, pink) docked using MOE into the BRD4 protein with bromosporine **78** overlay. Compounds docked in BRD4 shown with two vectors (**82** vector 1, blue and **83** vector 2, pink).<sup>155</sup>

The same bromosporine and linker moieties employed with the cereblon recruiting PROTACs can be also conjugated to VHL to give compounds **84** and **85** to compare the two E3 ligases with each vector (**Figure 68**). Both VHL and cereblon have shown robust and consistent degradation of the BET family with the JQ1 **14** protein binder. IAP was not employed in the first instance, as our laboratories were unable to replicate the degradation observed with JQ1-IAP recruiting PROTACs (based on **57**) with multiple BET binders and linker lengths.<sup>121</sup> Therefore, the assessment of bromosporine **78** as a promiscuous binder would use only VHL and cereblon in comparison to the known JQ1 PROTAC **15a** for two E3 ligases.

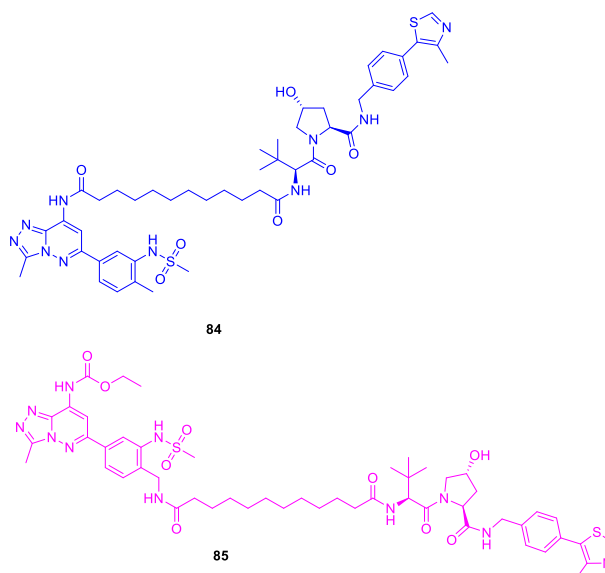
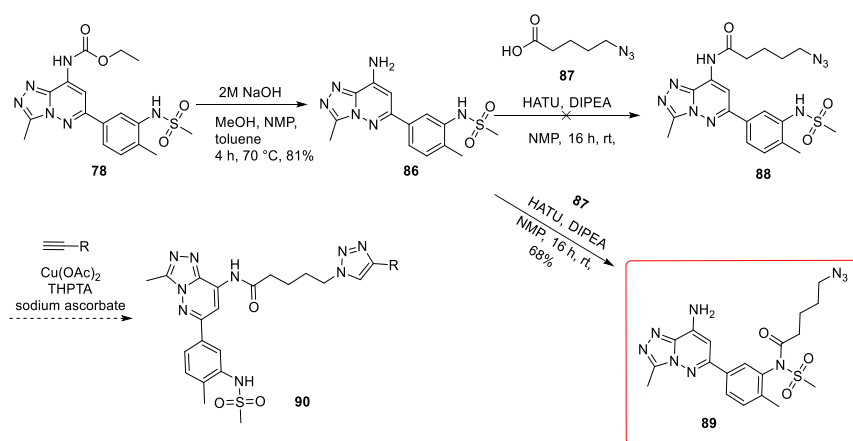


**Figure 68:** VHL derivatives of bromosporine PROTACs, (**84** vector 1, blue and **85** vector 2, pink).

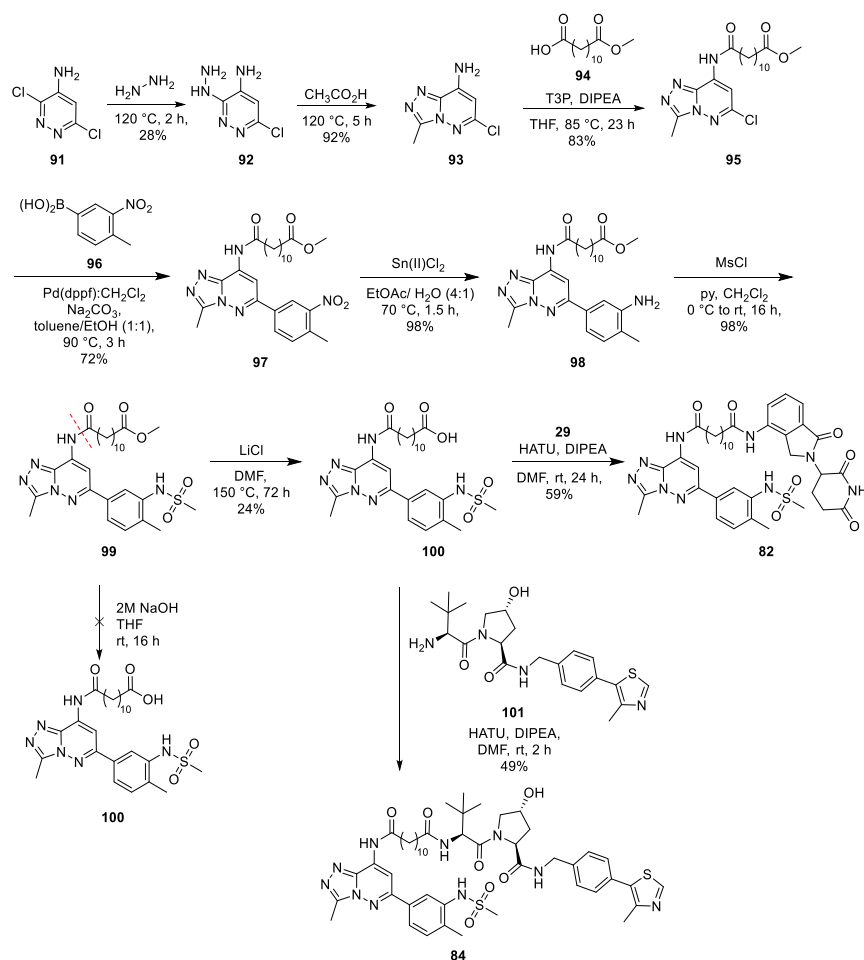
#### 4.3.2 Synthesis of Bromosporine PROTACs

An initial strategy to synthesise compounds from the first vector in bromosporine **78** through the carbamate was to hydrolyse the carbamate of bromosporine **78** itself (**Scheme 1**). The amine **86** could then be derivatised through an amide coupling. The initial synthesis was attempted including a functional handle azide as an example acid before conducting the synthesis of **82–85**. An azide could be further functionalised through CuAAC chemistry to install multiple functional moieties, including E3 ligase binders to give triazoles like compound **90**. This linking vector was recommended in the functionalisation of bromosporine **78** by the SGC, so bromosporine **78** was first hydrolysed to give the free amine **86** in 81% yield. Amine coupling with an acid derived azide **87**, HATU and DIPEA did not yield the desired product **88**, but instead functionalisation occurred on the acidic sulfonamide nitrogen **89**. At this stage, it was clear that amide coupling on the desired nitrogen would be challenging in the presence of the sulfonamide. The aromatic amine has a similar nature to DMAP and will be relatively deactivated, so more forcing conditions would be required to install an amide on this position. Due to previous issues with cereblon binders in the presence of sulfonamide protecting groups,<sup>94</sup> this was not deemed an appropriate strategy moving forward. In addition, because of the increased polarity of the triazole, all other compounds were synthesised with initially proposed methylene derived linkers to promote cellular permeability. As a result, a new synthetic method was required for PROTAC synthesis from this vector.



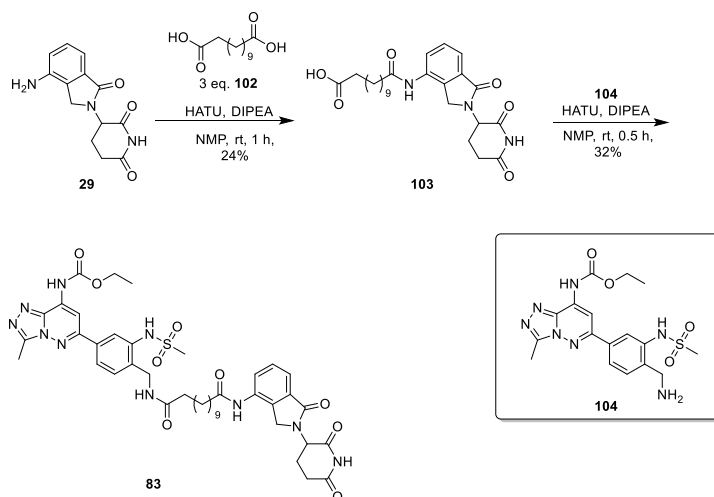
**Scheme 1:** Attempted synthesis of bromosporine vector 1 azide derivatives from bromosporine **78**.

To synthesise the desired PROTACs, the synthetic route was reassessed. To functionalise the deactivated amine to link from in bromosporine **78**, the core was synthesised and functionalised with the linker before the sulfonamide was in place (**Scheme 2**). This order of synthesis would prevent the reaction of the sulfonamide and alleviate the need for protecting groups. The synthesis started with hydrazine functionalisation of 3,6-dichloropyridazin-4-amine **91** to give **92** in a 28% yield. This was then cyclised with acetic acid to form the amine core **93** in 92% via recrystallisation from ethanol and water. An amide coupling was carried out with ester protected acid **95** using T3P and DIPEA. This had to be done at 85°C and further equivalents had to be added to drive conversion to get the linked core **95** in an 83% yield. Suzuki coupling with the nitro derived boronic acid **96**, nitro reduction of **97** and mesylation or **98** were carried out in good yields to afford the linked bromosporine **99**. Ester hydrolysis using traditional sodium hydroxide conditions proved to be too harsh to deprotect the acid, and instead, hydrolysed the relatively weak amide bond of **99** (**Scheme 2**, marked in red). Lithium chloride was used as an alternative method to deprotect the ester, yielding the acid **100** in 24% yield. This was then conjugated with the E3 ligase amines of VHL **101** and cereblon **29** using HATU, DIPEA amide coupling conditions to give **82** and **84** in 59% and 49% yield respectively.



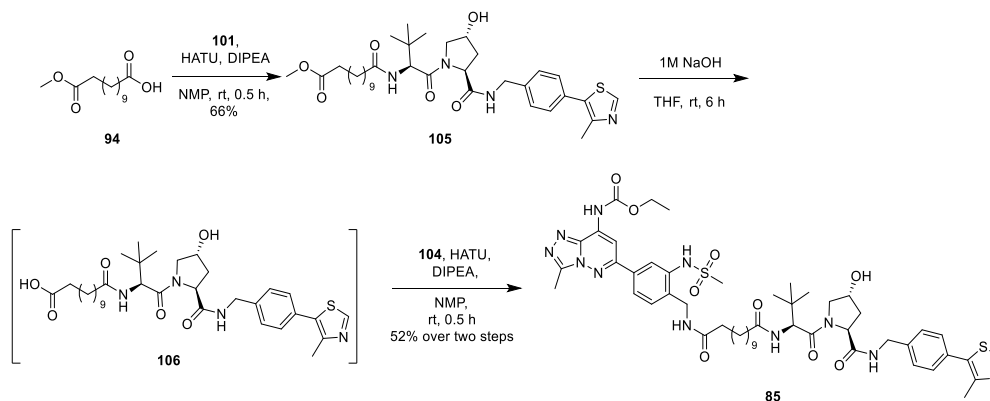
**Scheme 2:** Synthesis of vector 1 bromosporine VHL and cereblon recruiting PROTACs **82**, **84**.

For the synthesis of the second vector, the synthesis was carried out with the bromosporine derived amine **104** synthesised for another project, so was used in this project in parallel (**Scheme 3**). Due to the documented instability of both lenalidomide **29** and bromosporine **78** to base the cereblon recruiting PROTAC was synthesised using a protecting group free strategy. To avoid any deprotection steps, the di-acid was used in large excess and coupled to lenalidomide **29** to give the acid **103** in a moderate 24% yield. This was then directly coupled to the bromosporine derived amine **104** to give the bromosporine vector 2 cereblon recruiting PROTAC **83** in 32% yield.



**Scheme 3:** Synthesis of vector 2 bromosporine cereblon recruiting PROTAC **83**.

For the synthesis of the second vector, the amine **104** was also utilised (**Scheme 4**). Due to the base instability of the carbamate in amine **78** basic deprotection was also avoided in the synthesis of the VHL PROTAC **85**. The linker **94** was coupled to the VHL amine **101** to give **105** in a 66% yield. This was then deprotected and coupled to the amine linked bromosporine **104** to give the bromosporine vector 2 VHL recruiting PROTAC **85** in 52% over two steps.



**Scheme 4:** Synthesis of vector 2 bromosporine VHL recruiting PROTAC **85**.

The compounds designed were synthesised in moderate yields, giving sufficient material for biological testing. The synthesis for vector 2 PROTACs **83**, **85** was more amenable to derivitisation, as the core is developed, and a number of linkers could be added. This was not carried out due to insufficient material, and linkers were designed based on known degradation profiles for other BET targeting PROTACs. In addition, biological experiments were resource intensive, so only a small number of compounds could be synthesised when using these methods. In addition, further derivitisation of vector 1 **82**, **84** was deemed synthetically

challenging, as the linker moiety had to be installed early in the synthesis due to competition with the derivations of the amine reactivity versus the sulfonamide. As a result, the compounds synthesised would then be further evaluated for BET and non-BET bromodomain degradation.

#### 4.3.3 Biological Evaluation of Bromosporine PROTACs

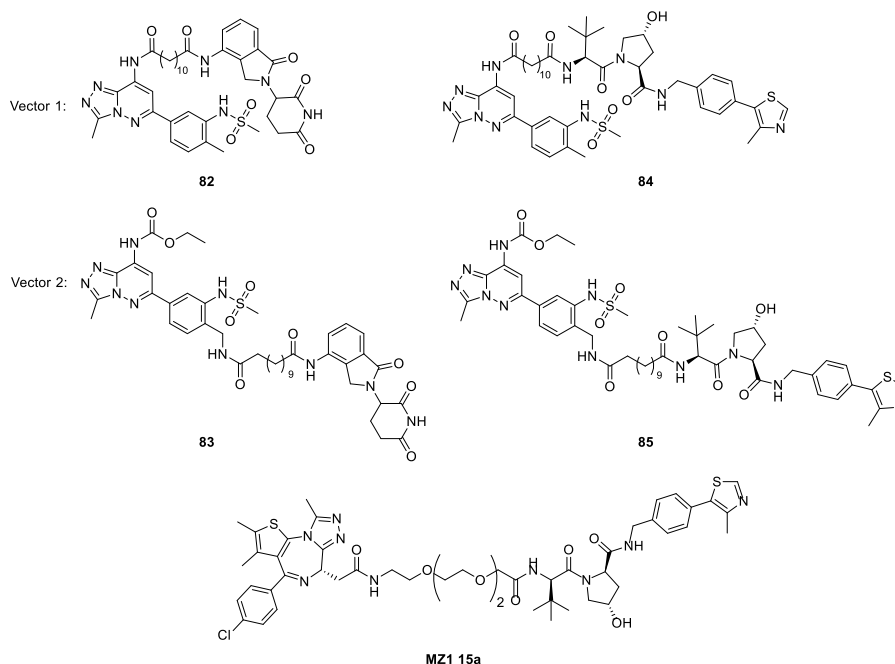
To evaluate the compounds which were synthesised, the compound's binding potencies and physicochemical properties were initially investigated.  $pIC_{50}$  values were generated in two conditions to determine if the compounds were still able to engage BRD4 with the addition of the linker and E3 ligase binder, which was investigated *in vitro* and in a cellular system. A biochemical binding FRET assay was used to measure binding to BRD4 BD1 and BD2. Additionally, to ensure the compounds were binding to the target in the cell (and indirectly determining if the compounds were cell permeable)  $pIC_{50}$  values were also measured via a PBMC-based assay by measuring MCP1 levels after LPS stimulation. This pathway is dependent on BRD4, and if BRD4 is inhibited successfully in the cell, MCP1 levels are reduced concentration dependently despite LPS stimulation. Physicochemical properties were also measured to ensure the compounds would be sufficient tools for the biological assessment of bromodomain degradation. ChromLogD, Chromatographic LogD, was also measured for the compounds as previously described it is a measured value which correlates the compound's retention time on a C18 column, with its lipophilicity. For ideal tool PROTACs, ChromLogD values of between 5–7 are desirable to ensure the compounds have sufficient lipophilicities to result in cell permeability. Kinetic aqueous solubility of the compounds were also measured from the compound's DMSO stock solution using the shake-flask method and determined using either CAD (charged aerosol detection) or CLND (chemiluminescent nitrogen detection). At tool generation stage, solubility is desirable but not a necessity, with a number of PROTACs generating positive degradation results despite being insoluble in aqueous media.

Both the cereblon **82, 83** PROTACs and bromosporine VHL **84, 85** from each vector retained most of potency to BRD4 BD2 as shown in **Table 1** with a  $pIC_{50}$  around 6.5. The PROTACs **82–85** were able to maintain the majority of the binding to BRD4 BD1, in comparison to the  $pIC_{50}$  of 7 for bromosporine **78** the PROTACs were between  $pIC_{50}$  of 5.8 and 6.7. The binding potency loss observed with some of the molecules was expected, as this is typical for PROTAC efforts and can be due to the linker affecting the binding. This suggests both vectors, as predicted by X-ray crystallography and molecular modelling,<sup>155</sup> are suitable exit vectors for the PROTAC approach. The ChromLogD values of the compounds **82–85** are in a suitable range for tool molecules, with the VHL compounds **84, 85** having ChromLogD values of over 5, and the cereblon compounds **82, 83** over 4. This shows the need for methylene derived linkers in these PROTACs to ensure good lipophilicity for these tool molecules, as the PEG derived

linkers traditionally used in PROTACs would have much lower lipophilicity and would most likely suffer from poor permeability. As commonly experienced in large permeable compounds, aqueous kinetic solubility has been compromised in the generation of these tools, decreasing from 361  $\mu\text{M}$  for bromosporine **78** to moderate/poor solubility for cereblon compounds **82**, **83** (15  $\mu\text{M}$  and 90  $\mu\text{M}$  respectively) and poor solubility for the VHL compounds **84**, **85** (23  $\mu\text{M}$  and <1  $\mu\text{M}$  respectively). This solubility loss is a known consequence of incorporating the VHL binder into PROTACs; nevertheless poorly soluble compounds have shown excellent levels of degradation both *in vitro* and *in vivo* previously,<sup>94</sup> so should not lessen the utility of these PROTACs as tool molecules.

The compounds **82–85** were also tested in cellular assays to determine cell permeability (**Table 1**). The compounds **82–85** also retained potency in a cell-based assay in human PMBCs, as they inhibited MCP1 cytokine production after LPS stimulation, which is characteristic of BET inhibition.<sup>156,157</sup> This also confirms the compounds are cell permeable in this cell line as they show activity to an intracellular target. Cellular activity is currently used by our group as a surrogate for permeability, as at present, data from permeability assays does not correlate well with PROTAC's cellular activity.<sup>94</sup> In comparison to the known BET targeting PROTAC MZ1 **15a**, MCP1 inhibition is more potent, despite similar binding to BRD4. This may be a result of more potent protein degradation leading to better efficacy in MCP1 production than inhibition alone, which will be evaluated further in the next section. With the results in hand, the tools are suitable for further characterisation in protein degradation assays.

**Table 1:** Biochemical data and physicochemical properties of bromosporine **78** and bromosporine derived PROTACs **82–85** and JQ1 PROTAC MZ1 **15a**. †Solubility measured by CLND therefore direct comparison may be impaired. \*denotes testing (n=1) \*\* denotes testing (n=3).

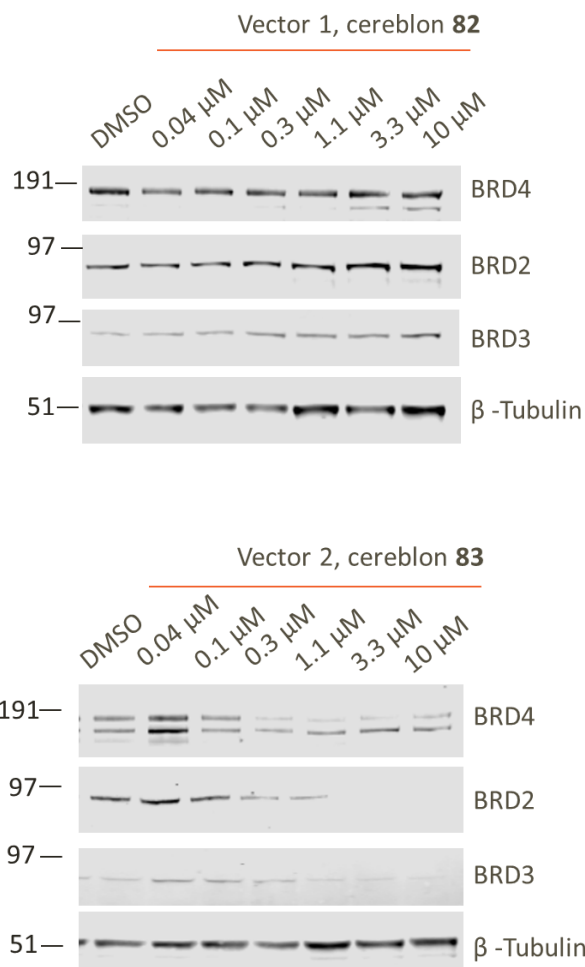


	Bromosporine <b>78</b>	Vector 1 cereblon <b>82</b>	Vector 2 cereblon <b>83</b>	Vector 1 VHL <b>84</b>	Vector 2 VHL <b>85</b>	MZ1 <b>15a</b>
BRD4 BD1 pIC <sub>50</sub> (n=2)	7.0	6.7**	6.3*	5.5	6.3	7.0*
BRD4 BD2 pIC <sub>50</sub> (n=2)	6.5	7.1	6.3*	6.1	6.3	7.1*
MCP1 production PMBC LPS stimulated pIC <sub>50</sub> (n=2)	7.4	6.7	6.7*	6.9	6.8*	8.4
ChromLogD (pH 7.4) (n=2)	3.37	4.45	4.23	5.27	5.15	5.03
Solubility CAD (μM) (n=1)	361	15	90	23	<1	164†

The compounds **82–85** were then tested for degradation of the BET bromodomains using Western blotting analysis. The cereblon recruiting PROTACs **82**, **83** were incubated with THP-1 cells overnight over a concentration range up to 10 μM (**Figure 69A**). In a number of the Western blotting experiments, two bands are visible around the BRD4 mass range, this can be due to unspecific binding of the antibody or post-translational modification or alternative protein splicing.<sup>158</sup> The higher band, corresponding to 191 kDa, is the band for BRD4 and was

used in protein quantification in the Western blot analysis. The cereblon bromosporine PROTAC **82** from vector 1 showed no decrease in any of the BET proteins after incubation overnight in THP-1 cells. Cereblon vector 2 bromosporine PROTAC **83** showed good knockdown of BRD2 (almost complete knockdown with 18% remaining at  $DC_{max}$  3.3  $\mu$ M, **Figure 69B**), BRD3 (<1% remaining at  $DC_{max}$  10  $\mu$ M) and of BRD4 (33% remaining at  $DC_{max}$  1  $\mu$ M). This work shows the importance of the correct exit vector orientation in protein degradation mediated by PROTAC molecules, and that very similar compounds with different exit vectors could have very different degradation profiles.

A)



B)

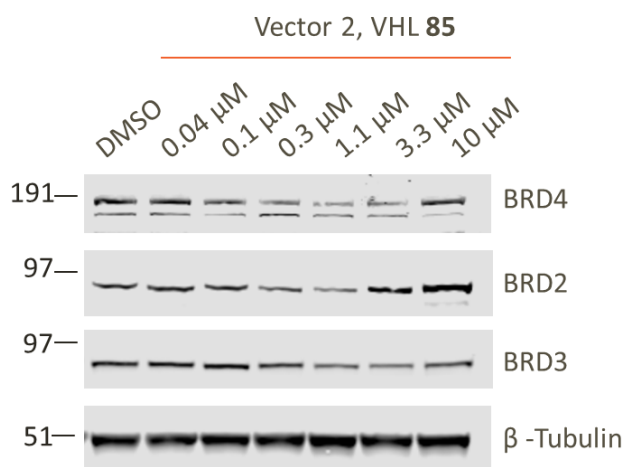
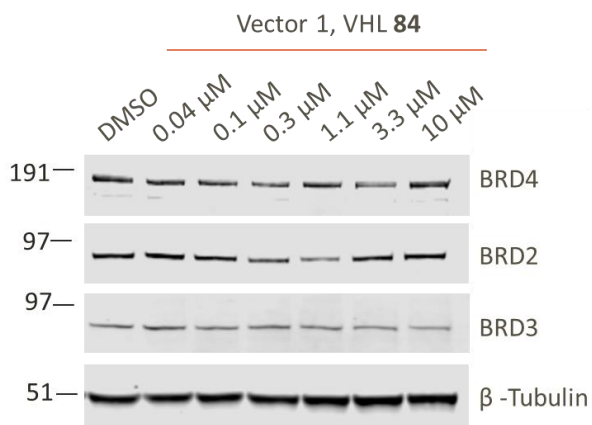
Concentration of <b>83</b> ( $\mu$ M)	0.04	0.1	0.3	1.1	3.3	10
BRD4 (%)	137%	81%	54%	33%	53%	50%
BRD2 (%)	109%	106%	83%	94%	18%	35%
BRD3 (%)	161%	134%	99%	51%	71%	0.4%

**Figure 69:** Western blot analysis of BRD4/2/3 after incubation of THP-1 cells after 16 h with increasing concentration of cereblon recruiting PROTACs **82**, **83** (A). Table shows protein quantification compared to DMSO vehicle and normalised to loading control  $\beta$ -tubulin for the above blot with compound **83** (B).

VHL recruiting compounds **84**, **85** were also tested in THP-1 cells (**Figure 70A**). VHL vector 1 **84** showed no significant degradation of any of the BET containing bromodomains at any of the concentrations. VHL vector 2 **85** showed around 50% reduction of BRD4 by protein quantification compared to the DMSO and loading controls (39% remaining at  $DC_{max}$  1.1  $\mu$ M, with the hook effect evident at higher concentrations **Figure 70B**). With this compound **85** there was also a slight decrease in BRD2 (62% remaining at 1.1  $\mu$ M) but only visible at a single concentration, so not reliable. BRD3 showed a 50% protein reduction at 1.1  $\mu$ M with the hook effect apparent at higher concentrations. These results show that the vector 2 VHL recruiting PROTAC is active, but the levels of degradation were lower than expected. This is surprising, given that vector 1 was deemed a suitable exit vector shown from the JQ1 derived VHL recruiting PROTACs. Further evaluation in different cell lines and using other methods of protein detection was deemed suitable as Western blotting experiments have previously shown larger errors in weak degraders due to sensitivity in the technique.<sup>94</sup> The approach employing vector 1 did not successfully work with either VHL or cereblon in these experiments, suggesting there could be a potential clash with either E3 ligases and the BRD proteins. Further evaluation of these compounds was then undertaken in different cell lines and different protein quantification strategies.

The bromosporine derived PROTACs were then compared to the known degrader MZ1 **15a**. This compound has previously shown excellent degradation of the BET bromodomain proteins, with  $DC_{50}$  (half maximal degradation concentration) of ~ 5 nM, with complete degradation of BRD2/3/4 at just 100 nM in an in-house Western blotting experiment in THP-1 cells.<sup>94</sup> This degrader shows superior protein degradation to the bromosporine derived PROTACs **82–85**, which may explain the greater effect on the MCP1 inhibition in PBMCs (**Table 1**). If the protein is crucial in MCP1 signaling, the removal of the protein should have a more profound effect than inhibition alone. The MCP1 and degradation correlations will also be time dependent, and the JQ1 derived compound **15a** may degrade the BET proteins faster than the bromosporine derivatives, leading to the pronounced effect. The results from the Western blotting and the MCP1 inhibition were carried out in different cell lines (THP-1 and PBMCs respectively). As a result, further analysis of the PROTACs would be carried out in PBMC cells. However, these results could elucidate that JQ1 VHL recruiting PROTAC MZ1 **15a** may be a more effective degrader than bromosporine derived PROTACs.

A)



B)

Concentration of <b>85</b> (μM)	0.04	0.1	0.3	1.1	3.3	10
BRD4 (%)	110%	81%	61%	39%	58%	77%
BRD2 (%)	138%	107%	82%	62%	162%	275%
BRD3 (%)	110%	112%	84%	50%	59%	68%

**Figure 70:** Western blot analysis of BRD4/2/3 after incubation of THP-1 cells after 16 h with increasing concentrations of VHL recruiting PROTACs **84**, **85** (A). Table shows protein quantification compared to DMSO vehicle and normalised to loading control  $\beta$ -tubulin for the above blot for compound **85** (B).

Degradation with all four bromosporine compounds **82–85** was then tested in a BRD4 immunofluorescent imaging assay in human PMBCs (**Figure 71**). In order to image BRD4 in cells, a BRD4 antibody with a fluorescent tag<sup>159</sup> is added to the PMBC cells after the PROTAC treatment, then an image is taken under the microscope and BRD4 fluorescence from the antibody bound to it is quantified, with low levels of fluorescence corresponding to BRD4 degradation. As the compounds were tested in individual donor's PBMCs, there is variability in the data, so the results could not be compared directly to one another. As a result, the compounds would be categorised as degraders or non-degraders. MZ1 **15a** shows potent BRD4 knockdown in this experiment as expected. Good degradation was observed with both cereblon vector 2 **83** (individual donor, DC<sub>50</sub> 36 nM) and VHL vector 2 **85** (individual donor, DC<sub>50</sub> 500 nM), consistent with the effect in THP-1 cells, although the degradation was more significant in the PBMC primary cells. Cereblon vector 1 PROTAC **82** is still inactive as per the THP-1 cell experiment, as expected. However, VHL vector 1 PROTAC **84** shows potent BRD4 knockdown in this assay (individual donor, DC<sub>50</sub> 120 nM), which was not replicated in the THP-1 experiment. Reasons for variability in protein degradation in the two methods could be due to the mixed population of human PBMCs,<sup>160</sup> compared to the monoclonal cell line THP-1, where different compounds have different permeability in different cells (due to diverse levels of transporters, cell membrane constituents, for example).<sup>154</sup> Another hypothesis, which is not yet established, could be due to varying levels of BRD4 or E3 ligase protein levels in each of the cell lines, this gives differential degradation.

It is also worth noting the effects seen in the PMBC pIC<sub>50</sub> in the previous **Table 1** elucidates that the MCP1 inhibition potency must be driven as an effect of BRD4 inhibition in cells rather than through BRD4 degradation. The bromosporine PROTACs **82–85** are all equipotent in binding but have different degradation profiles in the imaging assay. The imaging assay is an overnight incubation, which may be required for BET degradation, and the MCP1 inhibition may be a result of initial inhibition, before degradation has occurred in the cells. A time course study would be required in both imaging and MCP1 inhibition to confirm this hypothesis.

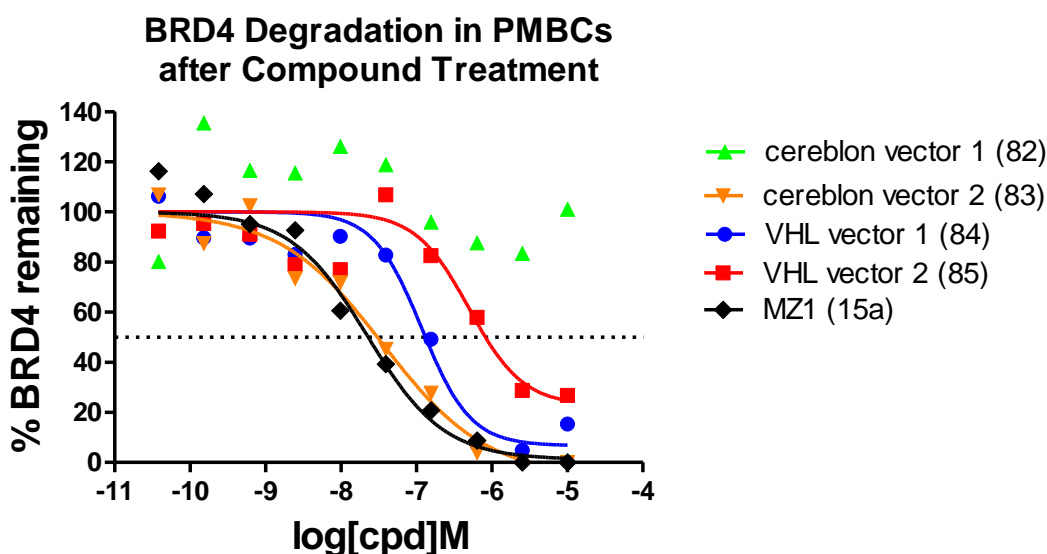


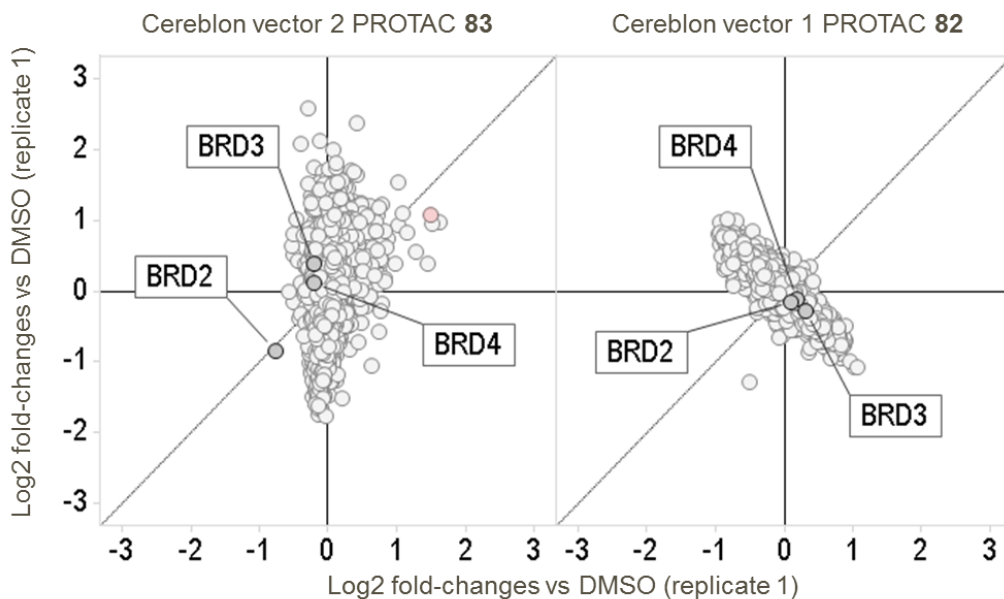
**Figure 71:** Degradation of BRD4 in human PMBCs. Human PMBCs are treated with BRD4 PROTAC overnight **82–85** or **15a** (18 h), then adhered, stained with a BRD4 conjugated antibody, then the nuclear fluorescence is quantified using an Array Scan. NB/ all five compounds were treated in different donors PMBCs therefore variability is expected, and direct comparison will be impaired. %BRD4 remaining is normalised to a potent in house BRD4 degrader with its  $DC_{max}$  set to “0% remaining” visualisation in this graph.

Given the variability shown in the previous experiments, it was decided to monitor all four compounds **82–85** in a proteomics experiment. As previously described, proteomics experiments are a good method to evaluate protein degradation of multiple proteins in one experiment using TMT labelling approaches.<sup>80,149,150</sup> Therefore, with all four PROTACs **82–85**, multiplex protein dynamics profiling<sup>161</sup> were carried out in THP-1 cells. PMBCs could not be used in this assay, due to their immediate isolation and use requirement. SILAC approach requires cells to be cultured in either “light” or “heavy” media for a long duration, and as a result, a monoclonal cell line such as THP-1 cells was deemed more suitable. This was performed to determine if any of the bromosporine PROTACs **82–85** caused degradation of any of the non-BET bromodomains to validate if bromosporine **78** was a useful protein binder to evaluate degradation of the wider bromodomain family.

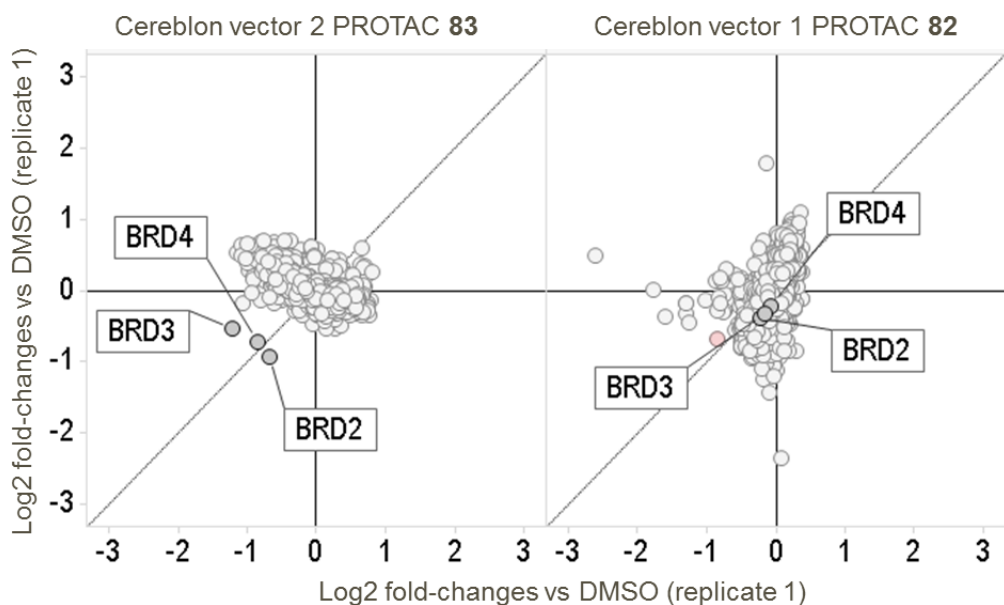
The cereblon recruiting PROTACs **82, 83** were evaluated by treatment in THP-1 cells at 1  $\mu$ M at both 6 h (**Figure 72A**) and 24 h (**Figure 72B**). Mass spectrometry analysis was carried out using a TMT labelling approach, in combination with SILAC elucidated which mature proteins were downregulated. Mature proteins were investigated in this experiment, as only the direct targets of bromosporine derived PROTACs were required to evaluate the compounds. Unfortunately, during the experiment, variability in background protein levels in the experiment affected the quality of the experiments. Replicates of background protein levels showed a

broader distribution than normal, and this directly affected the quantification of downregulated proteins. However, the data are still deemed as qualitative and should provide information on overall protein degradation with the compounds. Analogous to the BRD4 imaging assay and Western blot experiments (**Figure 70**, **Figure 69**, **Figure 71**), vector 1 PROTAC **82** shows no activity at either time point in any of the BET or non-BET bromodomains. Vector 2 PROTAC **83** shows slight reduction in BRD2 at 6 h, and BRD2/3/4 are reduced (albeit not significantly due to experimental conditions) at the 24 h timepoint. No downregulation of any of the non-BET bromodomains was observed.

A) Proteomic profiling of THP-1 cells after PROTAC treatment for 6 h

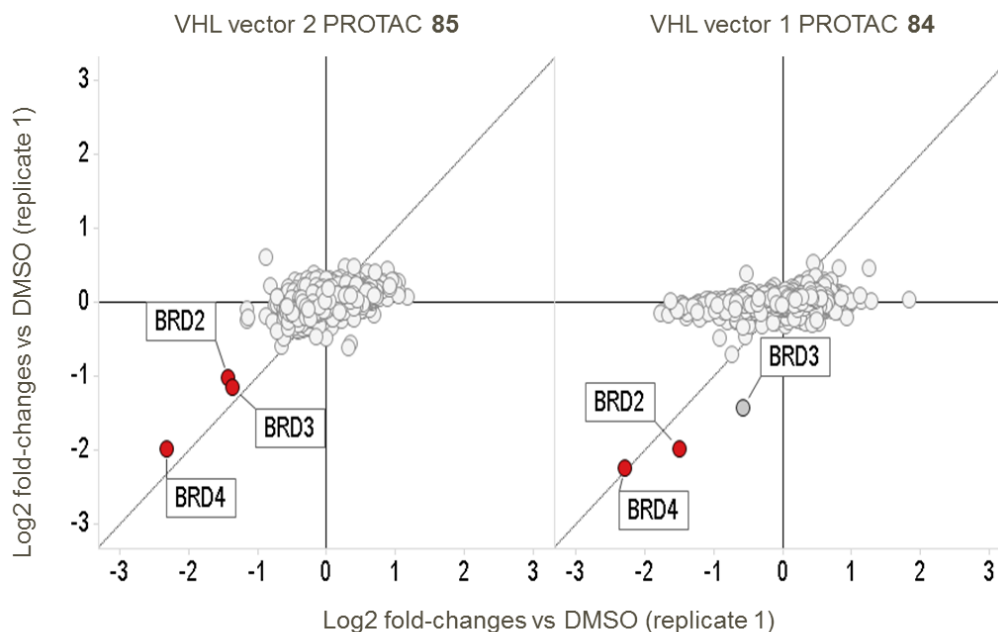
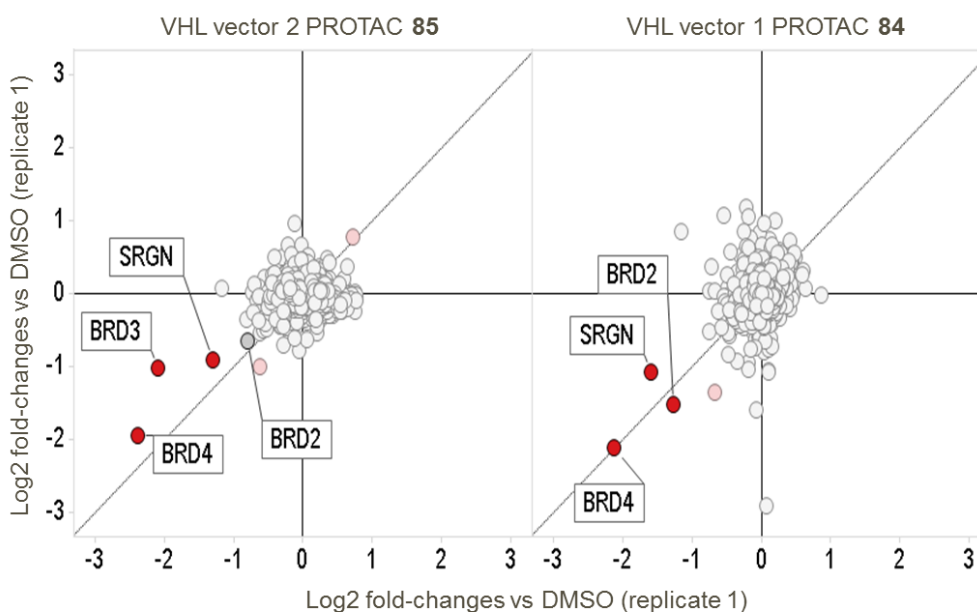


B) Proteomic profiling of THP-1 cells after PROTAC treatment for 24 h



**Figure 72:** Proteomic profiling of THP-1 cells upon compound treatment. THP-1 cells were incubated with either cereblon recruiting PROTAC vector 2 **83** (1  $\mu$ M) or cereblon recruiting PROTAC vector 1 **82** (1  $\mu$ M) for 6 h (A) or 24 h (B). The graphs show fold change values (log2 scale) of abundance compared to the vehicle control of replicate 2 over replicate 1 for each condition for the mature proteins. Marked in red are the proteins significantly regulated in at least one condition (fold change  $\geq$  50 % and p value  $\leq$  0.05).

The experiments were repeated with the VHL recruiting PROTACs. THP-1 cells were treated with the VHL recruiting PROTACs (VHL vector 1 **84** and 2 **85**) at a concentration of 1  $\mu\text{M}$  for 6 h (**Figure 73A**) and for 24 h (**Figure 73B**). In both experiments, analogous to the cereblon recruiting PROTACs, variation in the assay limited the analysis to qualitative protein knockdown. The VHL compounds, vector 1 **84** and vector 2 **85** are shown after 6 and 24 h. As with the BRD4 imaging assay in a different cell line, both VHL vectors **84**, **85** were active in reducing BRD4 levels in this experiment. This contrasts with the lack of degradation observed in the Western blot experiments (also in THP-1 cells) potentially showing a limitation of the BRD4 Western data where the compounds did not show significant degradation and could be a result of false negatives in this assay. BRD2 and BRD3 were downregulated by both PROTACs **84**, **85** at 6 h. At 24 h, vector 2 PROTAC **85** did not have a significant effect on BRD2 but did knockdown BRD3. Also, at 24 h, vector 1 PROTAC **84** had significant knockdown of BRD2 but BRD3 was not quantified. Although exact quantification is not possible due to the variability in this experiment, it does elucidate that the bromosporine VHL recruiting PROTACs **84**, **85** directly degrade the BET family of proteins, with no other non-BET proteins downregulated at either time points as observed with the cereblon based PROTACs. Despite the variability in the experiment there was an expectation to see downregulation of the non-BET proteins, which was not observed at any time points with any of the four PROTACs **82–85**.

A) Proteomic profiling of THP-1 cells after PROTAC **85**, **84** treatment for 6 hB) Proteomic profiling of THP-1 cells after PROTAC treatment **85**, **84** for 24 h

**Figure 73:** Proteomic profiling of THP-1 cells upon compound treatment. THP-1 cells were incubated with either VHL recruiting PROTAC vector 2 **85** (1  $\mu$ M) or VHL recruiting PROTAC vector 1 **84** (1  $\mu$ M) for 6 h (A) or 24 h (B). The graphs show fold change values (log<sub>2</sub> scale) of abundance compared to the vehicle control of replicate 2 over replicate 1 for each condition for the mature proteins. Marked in red are the proteins significantly regulated in at least one condition (fold change  $\geq$  50 % and p value  $\leq$  0.05).

In order to assess whether the lack of degradation of the non-BET bromodomains by any of the bromosporine PROTACs **82–85** was due to disruption in the binding caused by the linker, affinity enrichment proteomics was carried out.<sup>162</sup> This approach uses quantitative mass spectrometry techniques to assess which proteins are bound by each of the linked analogues (**Figure 74**). This is achieved using linkable analogues, utilised in the same manner as the PROTAC synthesis, using compounds **100** and **104** to represent each vector. These are then amide coupled on to an insoluble matrix which is then utilised in the proteomics experiments. Using the linkable derivatives, (acid for vector 1 **100** and amine for vector 2 **104**) these are immobilised to a matrix and cell lysates are incubated with the immobilised compounds. The proteins bound by the matrix can be competed off with increasing concentrations of bromosporine **78**. The matrix is filtered off and the proteins bound to the matrix are eluted. The proteins are then digested and analysed after TMT labelling in MS:MS experiments. Proteins that are bound to the matrix are analysed and pIC<sub>50</sub> values can be generated through the competition experiment, where concentration dependent reduction in protein levels are observed as a result of bromosporine **78** binding in place of the matrix compounds. Those non-BET proteins which are not captured by each of the matrix bound analogues but are known targets of bromosporine **78** shows that the compounds did not retain with the linked analogue due to the linker. As a result, no degradation can occur with compounds no longer bound to the protein.

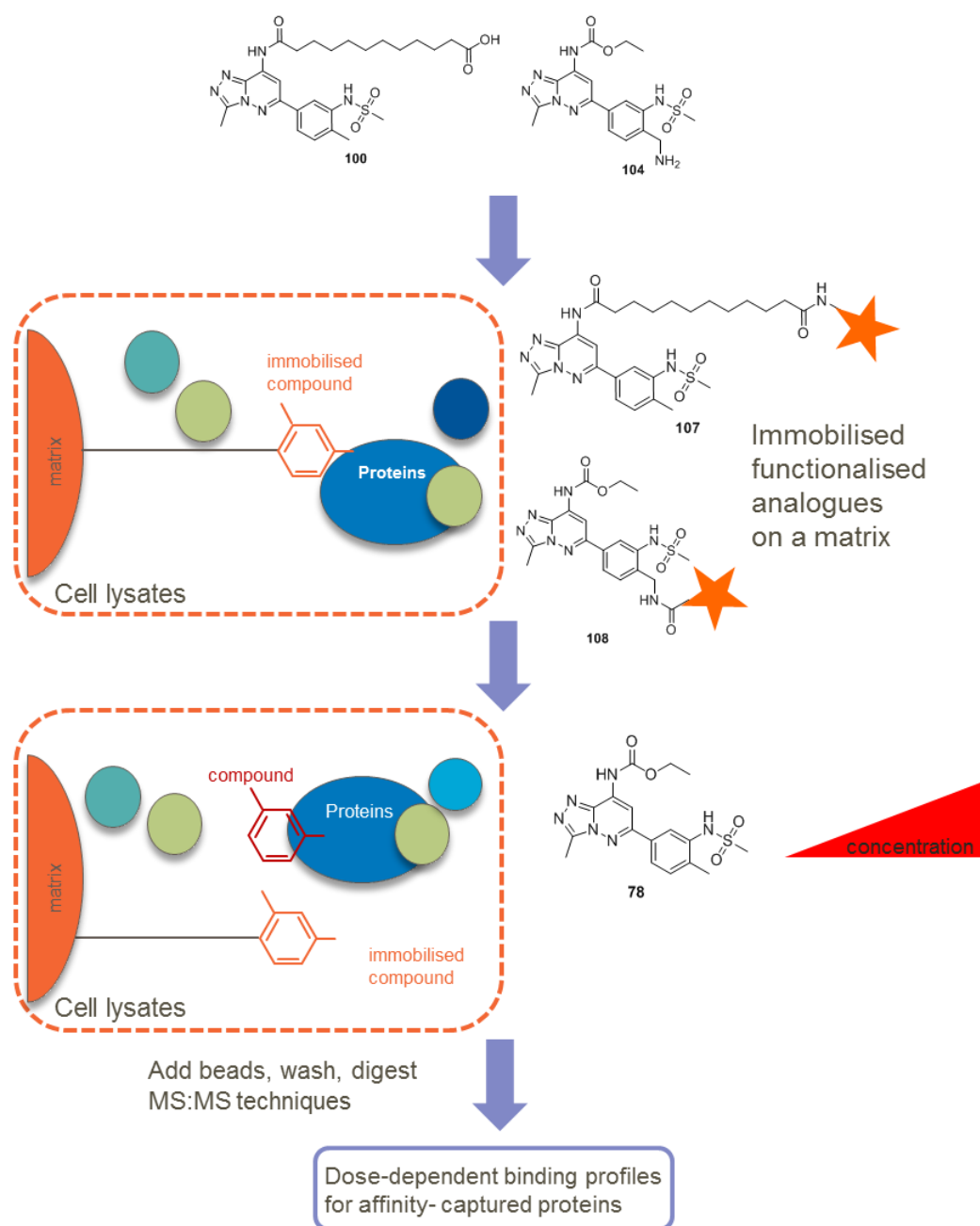


**Figure 74:** Affinity enrichment proteomics: compounds **100** and **104** were immobilised onto a matrix. THP-1 cell lysates are incubated with immobilised derivatives (vector 1 **107** and vector 2 **108**, 1 mM). This is then incubated with increasing amounts of bromosporine **78** (concentrations starting with 50  $\mu\text{M}$  in a 5-fold dilution series). Bromodomain binding proteins are captured upon incubation with the immobilised compounds. Bound proteins are digested with trypsin and labelled with isobaric mass tags (TMT, previously described) enabling relative quantification in the subsequent mass spectrometric analysis. Target bromodomains of the tested bromosporine **78** will display a dose-dependent reduction in binding.

Affinity enrichment proteomics experiments show binding of the two vectors for bromosporine **78** to the various bromodomains (**Table 2**). The potency of the BET compounds BRD2/3/4 and BRD9 is consistent across both vectors **107**, **108** with  $pIC_{50}$  5.5. Decreased binding is expected in cell lysates with PROTACs as the compounds can often bind non-specifically to lipophilic membrane proteins, so is usually lower than the biochemical result. The binding affinity for BRD7 is maintained for vector 2 linked compound **108** but 10-fold drop off for vector 1 linked compound **107**. BRPF1 and CECR2 binding was detected for vector 2 linked compound **108** ( $pIC_{50}$  5.6, 5.4 respectively) but not vector 1 linked **107**. TAF1 binding was moderate for both vectors ( $pIC_{50}$  4.7, 5.5 respectively). This work suggests vector 2 is better tolerated across most of the proteins for elaboration into PROTACs in comparison to vector 1. For vector 2, with binding to BRD7/9, BRPF1, CECR2 and SMARCA2 having similar binding potencies to the BET family, degradation would be expected with either VHL or cereblon. The same can be said for vector 1 with BRD9 and TAF1. At the time of this result, BRD9 PROTACs were published in the literature, showing that BRD9 is a degradable protein by the PROTAC approach.<sup>93</sup>

It is not entirely clear why the compounds did not show any reduction in any of the non-BET bromodomains. This could be a result of protein-protein clashes in the ternary complex formation, but it would be highly unlikely that all the proteins failure was a direct result of this. The other possible reason for failure of degradation with some of the non-BET bromodomains (not including BRD9) could be the accessibility of the surface lysines near the site of binding. However, this result does suggest, with binding retained to several non-BET and BET proteins and no further degradation achieved, that bromosporine **78** does not confer any advantages over the use of JQ1 **14** derived promiscuous PROTACs at present for inclusion into the promiscuous toolbox for new E3 ligases.

**Table 2:** Affinity enrichment proteomics of bromosporine linked compounds (**107** and **108**) in competition with bromosporine **78**. N.d. = not detected in the pull downs of any conditions.

Gene name	Vector 1 <b>107</b> pIC <sub>50</sub>	Vector 2 <b>108</b> pIC <sub>50</sub>
BRD2	5.6	5.6
BRD3	5.5	5.2
BRD4	5.5	5.4
BRD7	4.3	5.8
BRD9	6.2	5.7
BRPF1	n.d.	5.6
CECR2	n.d.	5.4
KAT2B	n.d.	4.9
SMARCA2	4.3	6.2
TAF1	5.5	4.7

#### 4.4 Summary and Future Work

In addition to the promiscuous kinase experiments that can be used for identifying new E3 ligases, bromosporine **78** was hypothesised to access a number of BET and non-BET bromodomains for degradation. JQ1 **14** derived PROTACs have previously shown robust degradation with multiple E3 ligases (IAP, cereblon and VHL), and bromosporine **78** was assessed with cereblon **82, 83** and VHL **84, 85** (**Figure 75**). Due to the complexity in synthesis from vector one (where the linker had to be installed before the molecule was fully intact) this was not modular and not directly amenable to linker optimisation as with a traditional PROTAC approach where one warhead can be derivatised to give multiple molecules. In addition to the resource intensive biological evaluation, four compounds were designed from two vectors with two E3 ligases, encompassing one linker length to assess bromosporine **78** to elucidate whether it could offer any additional non-BET proteins used in future experiments.

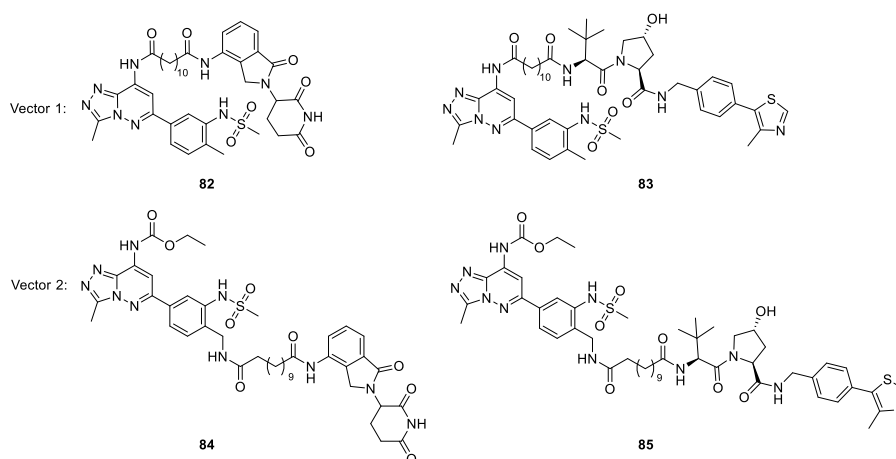


**Figure 75:** Bromosporine PROTACs synthesised and evaluated recruiting cereblon (**82**, **83**) and VHL (**84**, **85**).

The four compounds **82–85** were tested and evaluated in a number of different biological assays. Analysis of the compounds from the first vector were analysed for the two E3 ligases. Vector 1 cereblon recruiting PROTAC **82** was unsuccessful in degrading any proteins in all of the experiments, showing this vector was not suitable for degradation through cereblon. However, it did elicit a response in the PBMC binding assay showing reduction in MCP1 cytokine levels, showing the compound is cell-permeable, and could be a result of inferior ternary complex formation. Binding was shown to be equipotent for BRD2/3/4 from the affinity enrichment proteomics for this vector. For the BET proteins vector 1 VHL recruiting PROTAC **84** showed successful degradation of the BET proteins in PBMCs (50% BRD4 degradation at 1  $\mu$ M). BRD2/4 degradation was observed in THP-1 cells in the proteomics experiment (BRD3 degradation was present in one replicate but not in the other, so cannot be confirmed). This was not replicated in the Western blotting experiments as no degradation was observed in THP-1 cells which is currently not well understood. The affinity enrichment proteomics elucidated that the vector was not as well tolerated as vector 2, therefore this vector would not be utilised in further PROTAC efforts. This result is surprising due to the degradability of many of the BET proteins from JQ1 **14** derived PROTACs utilising this vector.

In addition, the compounds from the second vector were analysed for the two E3 ligases. For the BET proteins vector 2 VHL recruiting PROTAC **85** showed successful degradation in PBMCs (>80% BRD4 degradation at 1  $\mu$ M) and of BRD2/3/4 in THP-1 cells in the proteomics approach and was more robust than the first vector in these experiments. This was also observed in the THP-1 Western blotting experiment, although was only active in degrading around 50% of BRD2/3/4 at 1.1  $\mu$ M. Vector 2 cereblon recruiting PROTAC **83** was successful in degrading the BET family. It showed successful degradation in PBMCs (the most potent compound in this assay with >80% BRD4 degradation at 1  $\mu$ M) and of BRD2/3/4 in THP-1

cells in the proteomics approach, although absolute quantities were unable to be generated due to the variability in the background. Degradation was also observed in THP-1 cells in the Western blotting experiment, with almost complete knockdown of BRD3 and good knockdown of BRD2/4 observed. Binding was shown to be equipotent for BRD2/3/4 from the affinity enrichment proteomics for this vector. As a result, this vector was more efficient in degradation of the BET family with the use of bromosporine in PROTACs. The compounds however, were not as active as degrader MZ1 **15a** in BET degradation, which was not expected. This could be a result of using only one linker and could be further explored. It may also be a result of lower binding affinity to the BET bromodomain family, but this remains unknown.

The absence of degradation for the non-BET bromodomains to which bromosporine **78** binds was unexpected. During the completion of this work, degraders for BRD9 were identified in the literature utilising VHL and cereblon, and it would be expected that bromosporine derived PROTACs **82–85** could induce degradation of this protein in addition to the BET family. The lack of BRD9 degradation may be due to unfavourable protein-protein interactions in the ternary complex or may be due to insufficient binding potency to form this ternary complex. As a result of non-robust degradation seen with the BET bromodomains (variability in different cell types and relatively weak degradation not observed with other PROTACs targeting the BET family), and no additional degradation of the non-BET bromodomains with these compounds despite target engagement, bromosporine derived PROTACs were not further pursued with regards to assessing new E3 ligases.

In order to fully prosecute bromosporine **78** as a pan-bromodomain degrader, a toolbox of compounds with different linkers to VHL and cereblon could be synthesised based on the more successful vector 2 determined in these experiments. This could include different linker lengths such as **109** and **110** (**Figure 76**). Physicochemical properties would have to be monitored due to the polar nature of the warhead which may impair permeability. In addition, it was hypothesised with the number of promiscuous kinase degraders<sup>75,80,95</sup> that were published after this experiment was carried out, in which a degrader bound to 150 kinases and degraded 10, that the likelihood of bromosporine **78** having promiscuous degradation with another linker may be unlikely. However, lack of degradation could be a result of unfavourable ternary complex formation. For example, the linker may cause steric clashes between the two proteins, and as a result the correct orientation required for ubiquitination may not be achieved. Additionally, the lack of degradation may be a result of suboptimal binding potencies to the desired targets. This hypothesis could be evaluated using a number of linkers to ensure ternary complex formation was not impeded and could therefore address whether the binding potencies to the other non-BET bromodomains was sufficient to induce degradation. This would also have to be performed in multiple cell lines due to variability observed in the experiments between THP-1 cells and PBMCs observed with previous compounds. This would

therefore determine the wider utility of a pan-bromodomain degrader for use in promiscuous experiments for finding new E3 ligases.

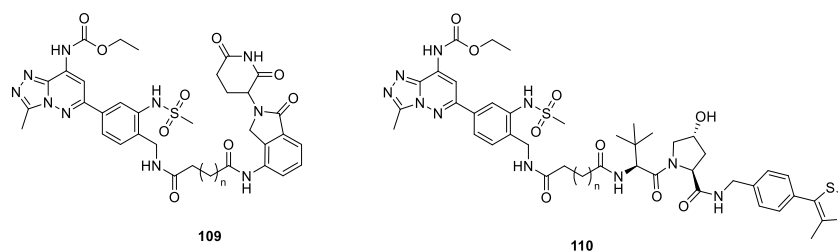


**Figure 76:** Design of future bromosporine PROTACs, utilising different linker lengths to determine bromosporine's **78** utility as a promiscuous degrader. (where n = a range of integers, to determine ideal linker lengths for the compounds).

As a result of the lack of degradation observed with the bromosporine based PROTACs, a promiscuous toolbox approach to assessing new E3 ligases would encompass JQ1 derived analogues **81** (**Figure 77**). This warhead shows robust protein binder for the BET family of proteins, which has shown to be successful in inducing degradation with VHL, cereblon and IAP. The toolbox would also include the RIPK2 protein binder **75**, previously described, as this has shown extremely facile degradation with all of the established E3 ligases, with low nanomolar and even picomolar degradation achieved. Lastly, the promiscuous kinase binder **76** will be useful in a promiscuous approach as it binds and degrades up to 15 different proteins with the E3 ligases known, with the opportunity to degrade many more due to target engagement dependence on the final PROTAC molecules' properties. With these three binders in hand, new E3 ligases can be prosecuted with multiple linkers, with hopes of finding successful degraders for the PROTAC approach for future drug discovery efforts.

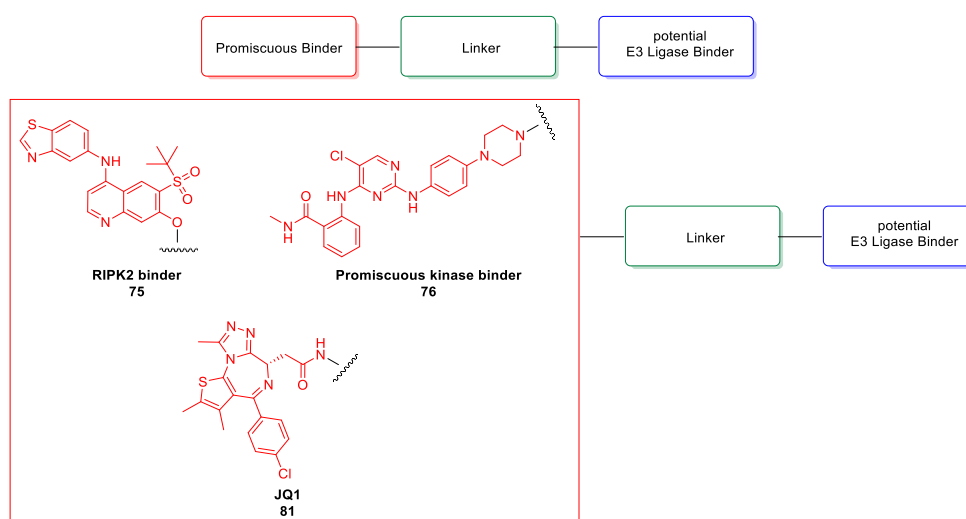


**Figure 77:** The promiscuous protein binder toolbox for assessing new E3 ligases for the PROTAC approach.

## 5. Investigating DCAF15 as a Potential E3 ligase for the PROTAC approach

### 5.1 Introduction – The E3 Ligase DCAF15

There are 600 E3 ligases known in eukaryotic cells, yet there are a relatively small number of E3 ligases that have small molecule binders or inhibitors to them.<sup>18,40,163-165</sup> One of the main reasons for the low small molecule tractability of these proteins is the strong protein-protein interactions that the molecules have to overcome to bind and inhibit the proteins.<sup>32,36</sup> Indisulam **67**, a small molecule, has recently been shown to bind and recruit DCAF15, in an analogous manner in which thalidomide **28** recruits cereblon. It was hypothesised that indisulam **67** could be utilised as an E3 ligase to recruit in the PROTAC approach.<sup>135</sup> Much like the IMiDs recruit cereblon to the desired protein of interest, indisulam has shown the same recruitment to DCAF15. The IMiD molecular glues, have shown to associate with cereblon independent of the neosubstrates Ikaros or Aiolos which indicates their utility as E3 ligase recruiter molecules.<sup>85</sup> However, indisulam binding could only be detected in the presence of both DCAF15 and Caper $\alpha$  (also known as RBM39). This observation suggests that indisulam binds with both proteins simultaneously. This may mean that using indisulam **67** may be more difficult to utilise in the PROTAC approach as the addition of a linker may disrupt this binding. However, when utilising photo-affinity labelling approaches to identify DCAF15, the researchers used a linked molecule **111** shown in **Figure 78**, which, despite having a linker in place to attach their photoaffinity group and biotin, binding to DCAF15 was not disrupted. They could successfully capture the E3 ligase and could also compete the label off with the small molecule's counterparts. This result indicates the possibility of retained binding to DCAF15 in a similar PROTAC approach, as the linked molecule could still engage the E3 ligase and ubiquitin transfer to the protein of interest may still be possible.

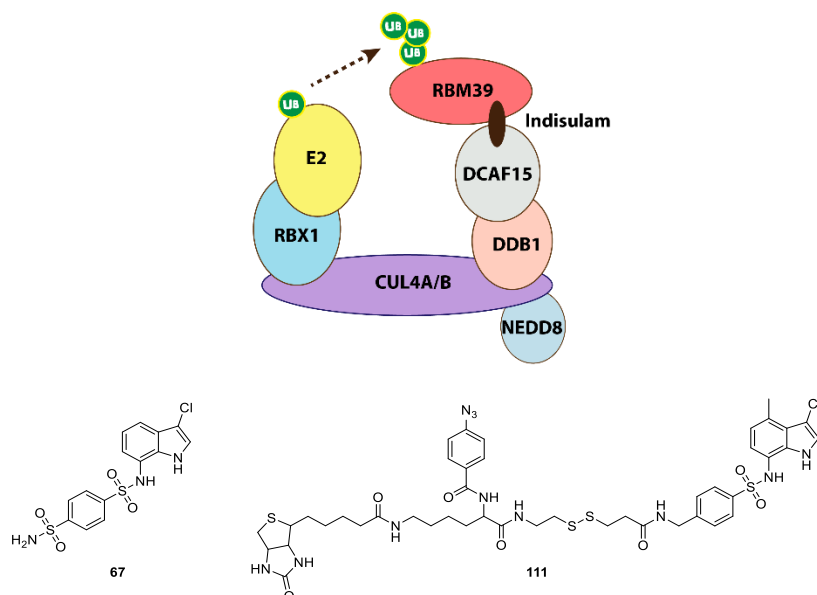


**Figure 78:** Indisulam **67** and its derivative **111** used to bind and capture DCAF15 using photoactivated cross linking and biotin/avidin pull down approaches.<sup>134-136</sup>

## 5.2 DCAF15 PROTACs Project Aims and Objectives

In order to expand the protein degradation platform, as previously described, new E3 ligase recruitment would be advantageous. The assessment of new E3 ligases from the literature can be achieved using a promiscuous toolbox approach to assess their utility in the PROTAC approach. The aim of this project will be to assess chemical matter that has been published which shows the recruitment of the E3 ligase DCAF15 and will assess the utility of the small molecule in the PROTAC approach. It was hypothesised that indisulam **67** could be utilised in the PROTAC approach analogous to the PROTACs which contain lenalidomide **29**. As a result of the similarity of the E2/E3 ligase complexes of both DCAF15 and cereblon, (**Figure 78**), there was a hypothesis that both small molecules indisulam **67** and lenalidomide **29** could potentially induce similar ternary complexes if utilised in PROTACs. Therefore, there was a reasonable expectation that DCAF15 recruiting PROTACs could induce protein degradation via a PROTAC approach analogous to cereblon recruiting PROTACs.

As previously described, it is valuable to test the chemical matter for the E3 ligase in conjugation with a promiscuous toolbox to assess many proteins for degradation (**Figure 77**). This includes the well described degradation of the kinases, for example, RIPK2 and BTK which have been validated internally and externally with multiple E3 ligases (VHL,<sup>4</sup> cereblon and IAP<sup>94</sup> for RIPK2, and cereblon<sup>96-98</sup> and IAP<sup>80</sup> for BTK). BTK is an example of a protein degraded by the promiscuous kinase binder chosen for the promiscuous toolbox, which showed excellent degradation by the cereblon recruiting PROTAC at low nM levels. As a result

of the similarity in complexes between DCAF15 and cereblon, BTK was hypothesised to be a useful protein for evaluation of promiscuous kinase PROTACs via Western blotting experiments in the first intent. The PROTAC's further evaluation could be expanded to proteomics experiments. In addition to the kinase family, the BET proteins have shown to be degradable through the same E3 ligases, again with varying linker lengths.<sup>65,66,69,88,166-169</sup> Therefore, a number of PROTACs targeting RIPK2 **75**, BTK **76** and BET proteins **81** and a number of different linkers **112–113**. This will give a good indication of the ability to recruit the new E3 ligase DCAF15 through a linkable analogue of indisulam **114** (**Figure 79**).

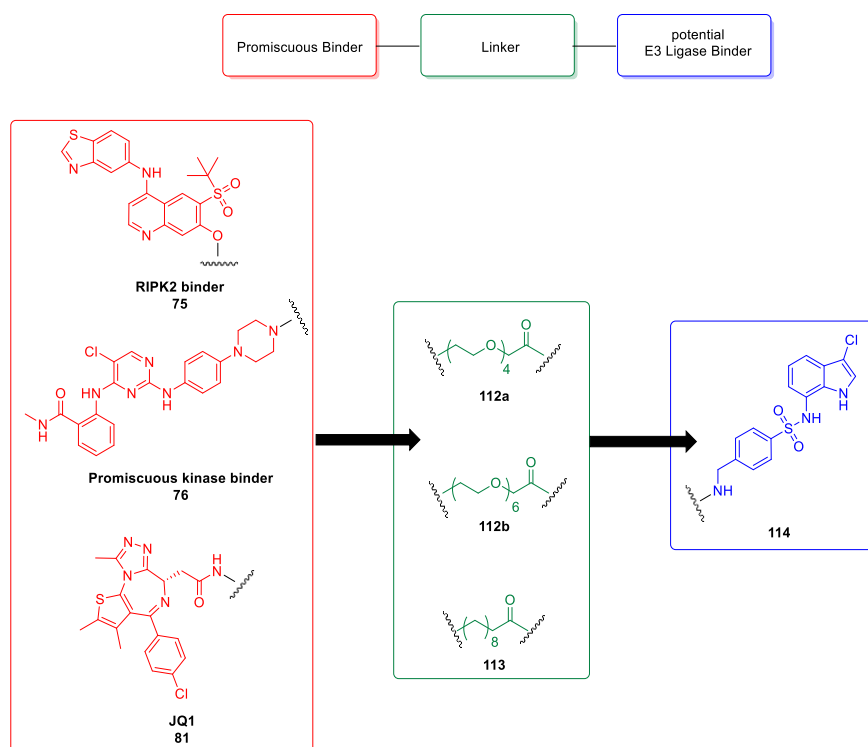


**Figure 79:** Design of a toolbox of DCAF15 derived PROTACs targeting multiple POI in red (BTK, BRD4 and RIPK2) with PEG and methylene derived linkers in green, with an indisulam derived linkable analogue in blue.

The synthesised compound's physicochemical properties would then be assessed to ensure cell permeability could be expected. They would also be assessed in a cellular targeting assay where available, which is routinely used in protein degradation efforts in place of artificial permeability measurements ensuring cellular permeability. Assessing the degradability of DCAF15 PROTACs would be performed using a number of different biological assays, such as Western blotting experiments and imaging assays. The results would then be compared to their cereblon counterparts to validate if indisulam derivatives would be a useful addition to the PROTAC toolbox targeting a new E3 ligase. If successful in degrading the well-established proteins for the approach, the promiscuous kinase derived compounds would then be fully

analysed by proteomics to determine the wider tractability of DCAF15 (in comparison to VHL, cereblon and IAP already determined using the warhead). If successful, indisulam derivatives **114** could be further assessed in drug discovery efforts, to determine the utility of the binder in potential drug candidates for specific proteins of interest.

## 5.3 Results and Discussion

### 5.3.1 Design of DCAF15 Recruiting PROTACs

In order to assess the recruitment of DCAF15 as an E3 ligase in the PROTAC approach, DCAF15 PROTAC molecules were designed and synthesised. Using a similar approach which was used in the photoaffinity labelling,<sup>136</sup> indisulam **67** was converted into a linkable analogue by replacing the terminal sulfonamide with a benzyl amine **115** which could be derivatised using an amide coupling (**Figure 80**). To confirm the compound **115** retains the same binding potency as **67**, compound **115** would be evaluated in its ability to degrade CAPER $\alpha$  in K562 cells (see page 104 for this confirmation, **Figure 84**).

In designing initial DCAF15 based PROTACs, one DCAF15 binder was chosen for elaboration into PROTACs in the first instance, to determine the tractability of the small molecule **115**. This has previously been achieved with cereblon recruiting PROTACs, where lenalidomide **29** and the structurally similar analogues have subtly different degradation potencies, but the overall ability to recruit the E3 ligase is unchanged. Indisulam derivatives were synthetically easily accessible and the synthesis will be discussed. Together with this linked analogue **115**, DCAF15 PROTACs were designed based on the promiscuous toolbox. As indisulam **67** binding to DCAF15 uses a similar protein complex to lenalidomide **29** in cereblon recruitment, it was envisaged to target proteins of interest which were degradable by cereblon, such as BTK, RIPK2 and BRD4. The PROTACs would therefore be synthesised and evaluated for protein degradation.

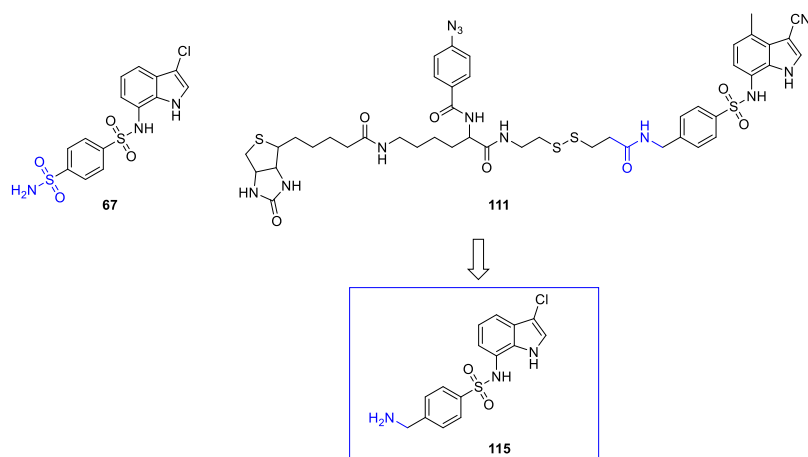


**Figure 80:** Design of a linkable analogue **115** of indisulam **67** using the same exit vector (shown in blue) that was utilised for the photoactivable probe used to identify DCAF15 binding.

For the compounds to achieve good permeability, and the possibility of a successful ternary complex formation, 2–3 linkers were used with each protein example. Four or six ethylene glycol units (**112a** and **112b**, **Figure 79**) were used as the inclusion of these moieties have no overall effect of the lipophilicity of the compounds, and should ensure enough flexibility in conformation between the two proteins in the ternary complex.<sup>32</sup> In addition, methylene derived linkers (**113**, **Figure 79**) are often preferred with highly hydrophilic protein binder warheads to ensure higher ChromLogD and as a result, cell permeability.

For the RIPK2 targeting PROTACs, these were based on a selective benzothiazole RIPK2 binder **75** utilised in PROTACs previously (**Figure 81**).<sup>4</sup> A methylene derived variant was not designed for the RIPK2 targeting compound, as all RIPK2 analogues with PEG chains achieve good degradation with the three E3 ligases tested, and the compounds with methylene derived linkers have previously been shown to reduce in cell binding to RIPK2 and subsequently result in poor RIPK2 degradation.<sup>94</sup> This is perhaps due to poor compound solubility or the compound's high lipophilicity (measured by ChromLogD) leading to the compounds being retained in the cell membrane. As a result, **116a** and **116b** were designed to assess potential RIPK2 degradation with DCAF15 recruitment.

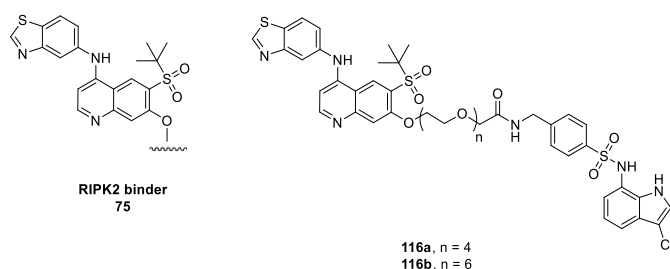


**Figure 81:** Design of RIPK2 TARGETING DCAF15 PROTACs **116a**, **116b** with PEG linkers.

A promiscuous kinase binder **76** which has shown BTK degradation with cereblon and IAP in house was utilised (**Figure 82**). Due to similarities in complexes between DCAF15 and cereblon, it was hypothesised that BTK could be degraded with the promiscuous kinase PROTACs.<sup>80</sup> If BTK degradation was achieved, the DCAF15 recruiting PROTAC could be further analysed in expression proteomics experiments to show the degradability of DCAF15 as an E3 ligase to the wider kinase family targeted by the promiscuous warhead. Three linkers were chosen to investigate BTK degradation with DCAF15 recruiting PROTACs **117–118** to give a range of linker lengths and lipophilicities, ensuring sufficient flexibility in the ternary complex, in addition to cellular permeability.

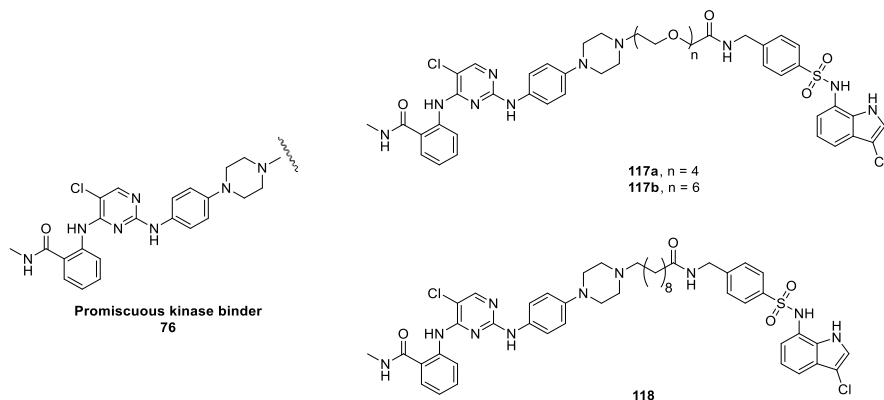


**Figure 82:** Design of promiscuous kinase derived DCAF15 PROTACs **117–118** with PEG linkers and a methylene derived linker **118**.

In the same manner for the promiscuous kinase derived DCAF15 PROTACs, for the BET family, JQ1 **81**, a pan-BET binder was used.<sup>67,88,170</sup> As previously observed with JQ1 derived cereblon recruiting PROTACs, short linkers can be utilised successfully to generate active PROTACs. As a result, four PROTACs were designed using JQ1 **81** to assess degradation of the BET proteins, in particular BRD4, with PEG chains **119a–119b**, and one example with methylene derived chain **120**, to ensure good permeability with a more lipophilic compound (**Figure 83**). With all these PROTACs designed, the interrogation of DCAF15 for the PROTAC approach could be achieved with a number of different proteins, with a number of different PROTACs, increasing the probability of success of validating DCAF15 for the PROTAC approach.

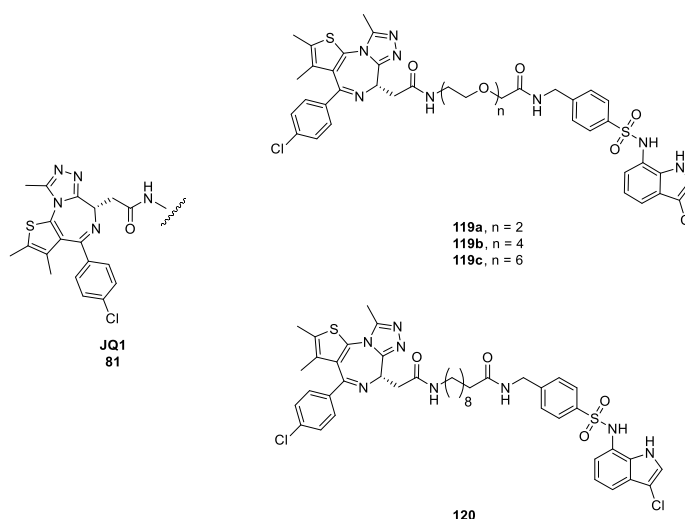
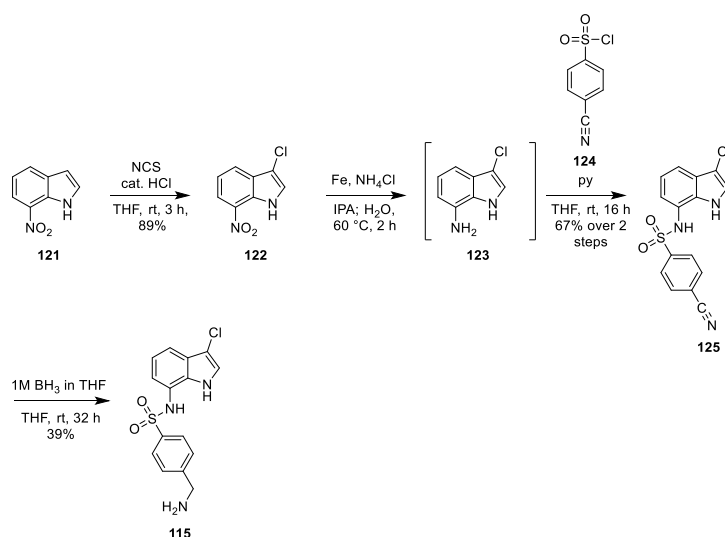


**Figure 83:** Design of JQ1 **81** derived DCAF15 PROTACs **119–120** with PEG linkers and a methylene derived linker PROTAC **120**.

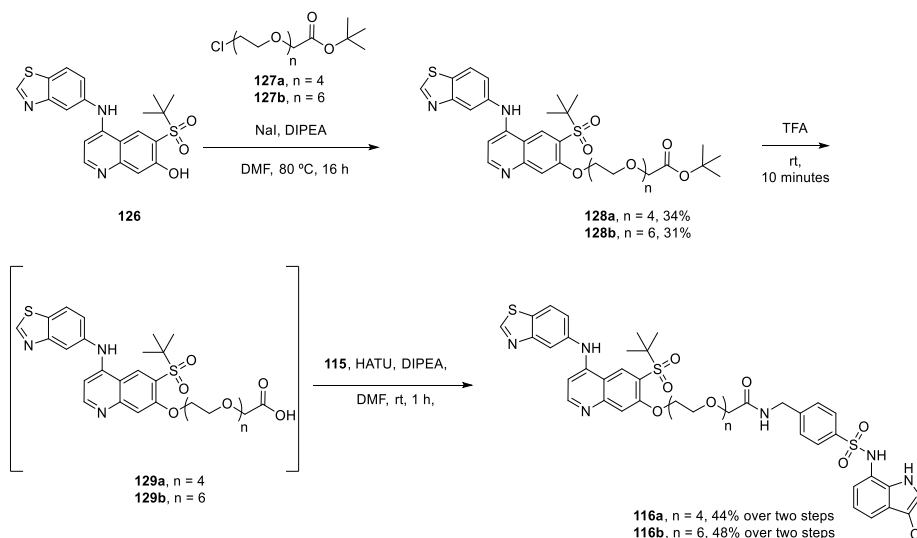
### 5.3.2 Synthesis of DCAF15 Recruiting PROTACs

Synthesis of linkable indisulam **115** molecules began with chlorination of 7-nitro-1*H*-indole **121** using NCS to give **122** in 89% yield (**Scheme 5**). This was then reduced using iron and ammonium chloride to give the amine **123** which was immediately reacted with 4-cyanobenzene-1-sulfonyl chloride **124** to give the sulfonamide **125** in 67% yield over two steps. Nitrile reduction with borane led to the unprotected indisulam analogue **115** in a 39% yield. This amine **115** could then be utilised in the synthesis of all DCAF15 recruiting PROTACs.



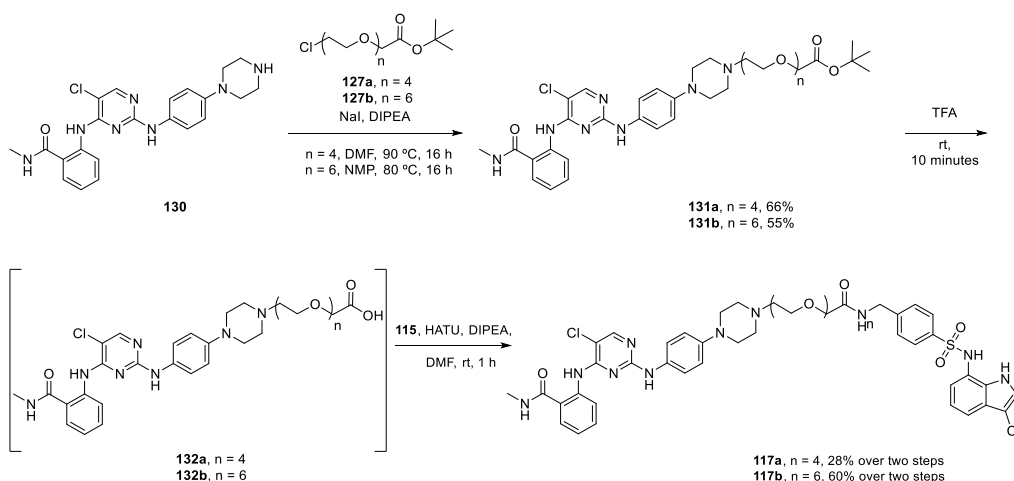
**Scheme 5:** Synthesis of indisulam linkable analogue **115**.

RIPK2 targeting PROTACs **116a/b** were synthesised using the chloropeglylated linkers **127a/b** respectively for derivitisation (**Scheme 6**).<sup>4,94</sup>  $S_N2$  of the linkers **127a/b** with the RIPK2 phenol **126** with sodium iodide gave the 4-EG and 6-EG *tert*-butyl esters **128a/b** in moderate yields respectively. The low isolated yields were a result of overalkylation on the aniline nitrogen occurring when using an excess of the linker, in order to prevent this, the reaction time can either be reduced, or use 1 eq. of the linker in future experiments. The *tert*-butyl ester **129a/b** were deprotected using TFA and amide coupled with the linkable amine **115** to give the RIPK2 targeting DCAF15 PROTACs **116a/b** in moderate yields.



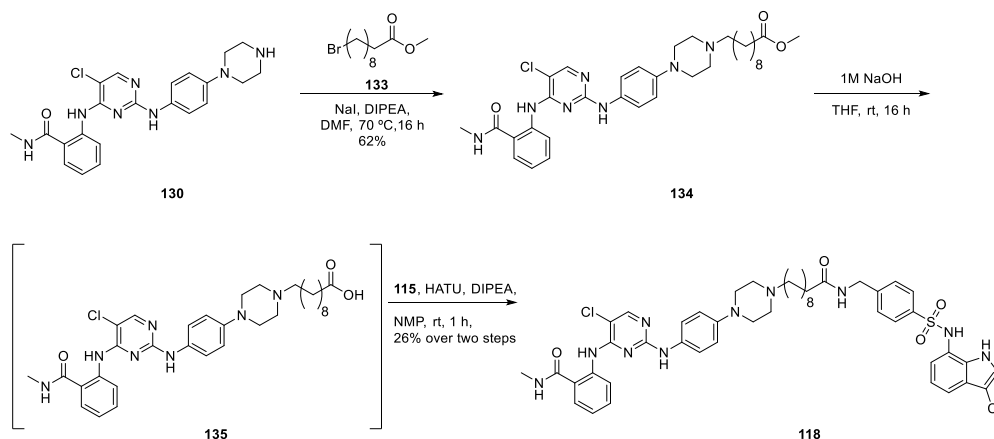
**Scheme 6:** Synthesis of RIPK2 targeting DCAF15 PROTACs **116a/116b**.

The BTK targeting DCAF15 PROTACs **117a/b** were synthesised in an analogous manner to the RIPK2 targeting PROTACs. The compounds were based on a promiscuous kinase binder **130** and were synthesised by an  $S_N2$  alkylation with the chloropeglylated linkers **127a/b** as previously described (**Scheme 7**).<sup>80</sup> The corresponding esters **131a/b** were deprotected with TFA and coupled to indisulam derived amine **115** in moderate to good yields to give the promiscuous kinase derived DCAF15 PROTACs **117a/b**.



**Scheme 7:** Synthesis of promiscuous kinase derived PEG linked DCAF15 PROTACs **117a/b**.

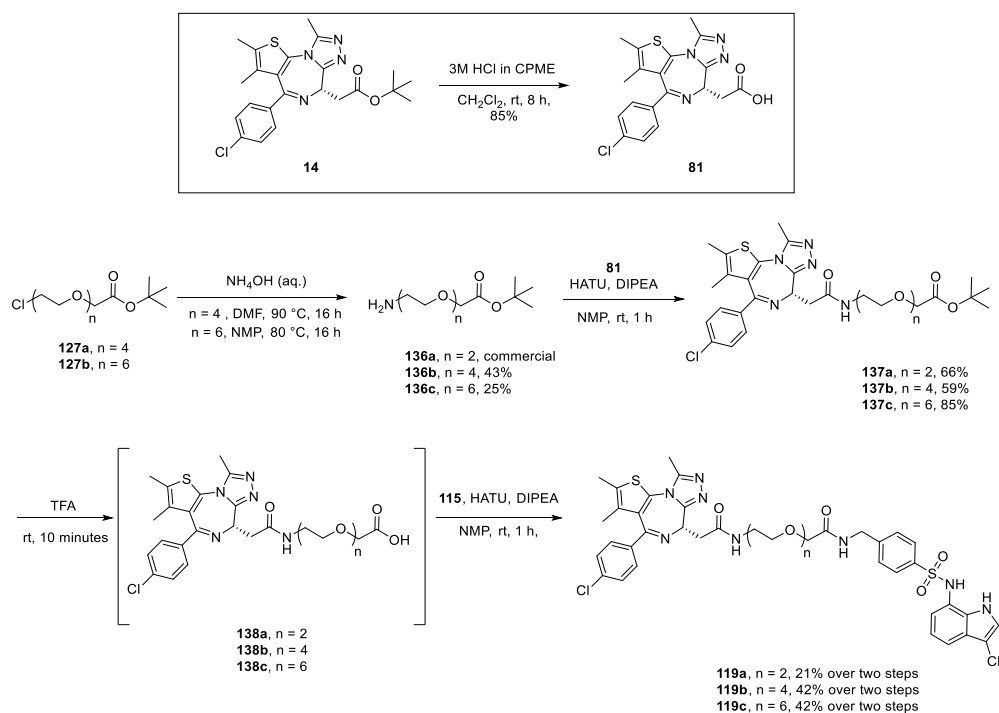
The synthesis of promiscuous kinase derived PROTAC **118** was performed in parallel. Synthesis was achieved through alkylation of the bromide linker **133** with the promiscuous kinase binder **130** to give the ester **134** in a 62% yield (**Scheme 8**). This was then deprotected and coupled to the indisulam derived amine **115** to give the methylene linked PROTAC **118** in a 26% yield over two steps.



**Scheme 8:** Synthesis of promiscuous kinase derived methylene linked DCAF PROTAC **118**.

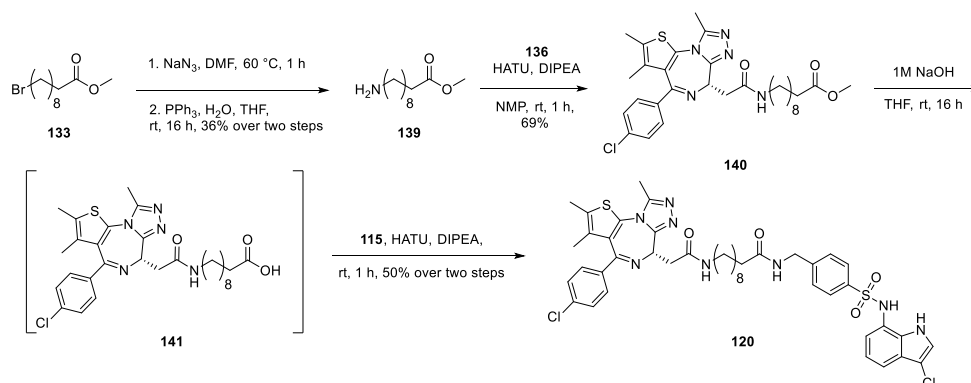
PROTACs based on JQ1 **14** were synthesised with multiple linker lengths and constituents. All compounds were derived from JQ1 **14** itself, which was hydrolysed with HCl in CPME to give the free acid **136** in an 85% yield (**Scheme 9**). Chloropeglyated linkers **127a/b** were converted to the free amine linkers by  $\text{S}_{\text{N}}2$  reaction with ammonium hydroxide that went in moderate yields **136b/c** (**136a** amine linker was commercial so didn't require synthesis from the chloro substituent). This was then coupled to JQ1 acid **81** using HATU and DIPEA that went in good yields for all amine derivatives. The *tert*-butyl esters **137a–137c** were

deprotected using TFA and a direct amide coupling with the indisulam amine **115** gave PROTACs **119a–119c** in moderate to good yields.



**Scheme 9:** Synthesis of JQ1 **14** derived PEG linked DCAF15 PROTACs **119a–119c**.

The synthesis of JQ1 PROTAC **120** was performed in parallel. Synthesis was achieved through Staudinger ligation of the bromide linker **133** with sodium azide to give the free amine **139** after triphenylphosphine deprotection in a 36% yield (**Scheme 10**). This was then coupled to the JQ1 acid **81** in a 69% yield. Ester deprotection and coupling to the indisulam free amine **115** gave the methylene derived PROTAC **120** in a 50% yield over two steps.



**Scheme 10:** Synthesis of JQ1 derived methylene linked DCAF15 PROTAC **120**.

With all the PROTACs in hand, DCAF15 could be evaluated biologically to determine its use as an E3 ligase in the PROTAC approach.

### **5.3.4 Biological Evaluation of DCAF15 Recruiting PROTACs**

#### **5.3.4.1 Biological Evaluation of Indisulam Analogue**

In order to assess if the linkable analogue of indisulam **115** still engaged DCAF15, Western blotting experiments were analysed to determine Capera $\alpha$  degradation in K562 cells. Experiments were conducted using K562 leukemia cells as high levels of DCAF15 were observed by proteomic analysis.<sup>147</sup> Compound **115** treatment for 24 h led to successful Capera $\alpha$  degradation, with a DC<sub>50</sub> of 227 nM (**Figure 84**). A non-specific band was visible in the Western blot above the desired mass range for Capera $\alpha$ , which was not considered for protein quantification. A number of treated samples had higher levels of Capera $\alpha$  control wells and were not included in the curve fitting for the DC<sub>50</sub> determination. These results suggest the amine **115** itself has good cellular permeability in K562 cells and is still engaging the E3 ligase DCAF15 despite removing the terminal sulfonamide, which was predicted in line with the photoactivatable probe used bearing the same amide.

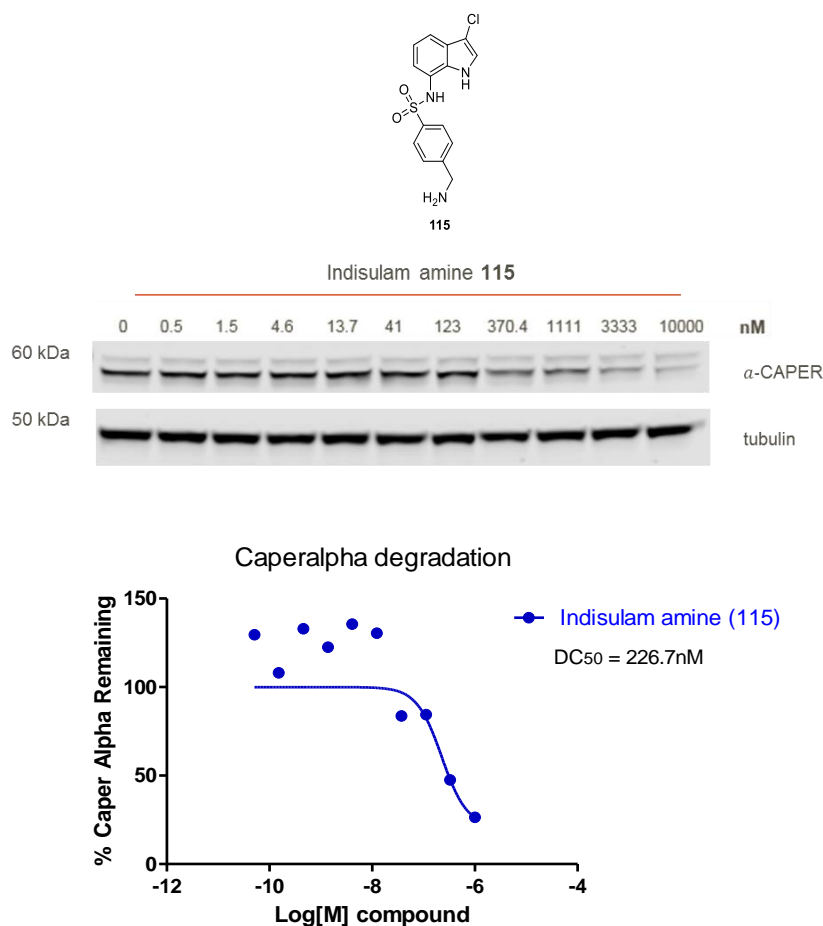


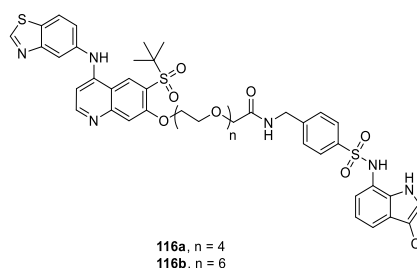
**Figure 84:** Western blotting analysis of Caper $\alpha$  in K562 cells after increasing concentration of compound **115** treatment for 24 h.  $\beta$ -Tubulin was used as a housekeeping protein and loading control for the experiment. NB/ Curve fixed to 100% to elucidate protein reduction compared to DMSO control and to obtain DC<sub>50</sub>. A few treated samples indicated higher levels of Caper $\alpha$  than the corresponding DMSO control wells, so the control wells were used as 100% protein level for the DC<sub>50</sub> fitting.

#### 5.3.4.2 Biological Evaluation of RIPK2 Targeting DCAF PROTACs

To evaluate the compounds which were synthesised, the compound's binding potencies (where possible) and physicochemical properties were initially investigated. DCAF15 targeting RIPK2 compounds show good biochemical and cellular potency with both the 4-EG **116a** and 6-EG **116b** linker (**Table 3**). To ensure the compounds were cell permeable, the compounds were tested in a functional in-cell assay to determine RIPK2 inhibition inside the cells. The compounds were tested in a challenge assay in human whole blood using MDP (Muramyl dipeptide)<sup>171,83</sup>, which is a component of both gram positive and gram-negative bacteria. In the presence of bacteria, RIPK2 signaling leads to release of cytokines such as TNF $\alpha$  as a result. When RIPK2 is inhibited successfully in the human blood, the release of these cytokines is

prevented even in the presence of MDP.<sup>172-175</sup> Both compounds **116a/b** are active in the MDP challenge assay, suggesting they are cell permeable and binding to RIPK2 intracellularly. The compounds were hypothesised to be cellular permeability as a result of their moderate measured ChromLogD of 5.6, which is estimated to give good permeable tool PROTACs. The measured kinetic solubility (determined by CAD) of the compounds were poor, but for tool generation, this was hypothesised to be acceptable, due to known, insoluble but potent PROTACs previously synthesised.

**Table 3:** Biochemical and physicochemical data for RIPK2 targeting DCAF15 PROTACs **116a/b**. \*denotes (n=3)



Compound	116a	116b
RIPK2 pIC <sub>50</sub> (n=2)	8.4	8.3
RIPK2 MDP challenge human whole blood pIC <sub>50</sub> (n=4)	7.2	6.6*
ChromLogD (pH 7.4) (n=2)	5.6	5.6
Solubility CAD (μM) (n=1)	8	9

Compounds **116a/b** were treated in K562 cells for 24 h with increasing concentrations to determine if the compounds were able to recruit DCAF15 for RIPK2 degradation. No degradation of RIPK2 was observed with either compound **116a/b** with any concentration (**Figure 85**). In this Western blot, there is a non-specific band observed underneath RIPK2 which was not used in the protein quantification. It was expected that some RIPK2 degradation would be observed, as RIPK2 has previously shown excellent utility and degradation with multiple E3 ligases, including cereblon.<sup>4,94</sup> The cereblon 4-EG counterpart **41** (introduction, **Figure 32**) shows excellent degradation in THP-1 cells at concentrations as low as 10 nM.<sup>94</sup> It was not expected that these compounds would not be successful, and as a result the other PROTACs synthesised were investigated to determine if RIPK2 was simply not a suitable protein for DCAF15 recruitment and subsequent degradation.

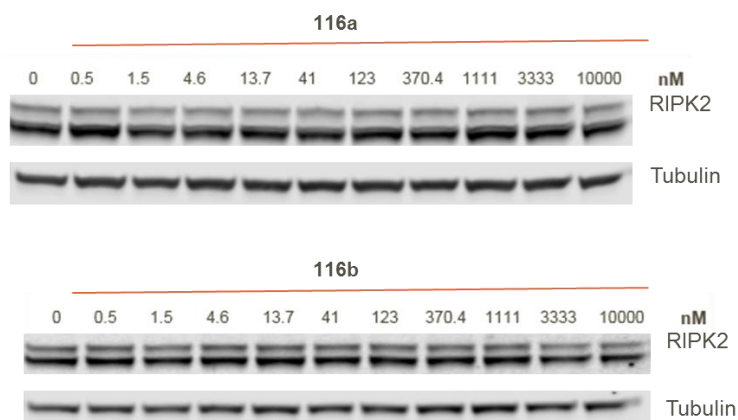


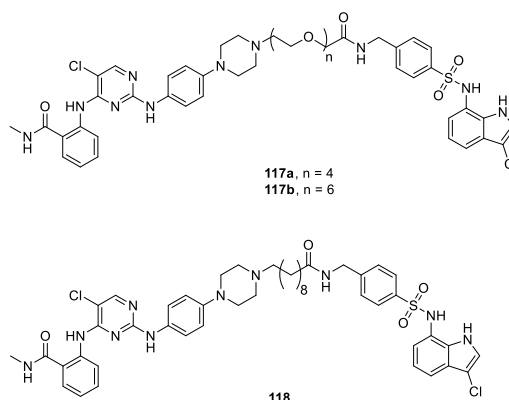
**Figure 85:** Western blotting analysis of RIPK2 in K562 cells after increasing concentration of compound treatment **116a/b** for 24 h.  $\beta$ -Tubulin was used as a housekeeping protein and loading control for the experiment.

#### 5.3.4.3 Biological Evaluation of BTK DCAF PROTACs

DCAF15 targeting BTK targeting PROTACs **117–118** were also evaluated. BTK binding assays were attempted to generate BTK binding potency of the three compounds, however the replicates were found to be inconsistent to one another (ranging in low nanomolar to micromolar) therefore were not reported, and binding was not determined. The promiscuous binder **76** used in the DCAF15 PROTACs has been previously used to degrade BTK using a 4-EG linker (e.g. cereblon compound **43**, **Figure 34**) so binding was assumed to be maintained using the same exit vector and linker construct in PROTACs **117–118**. In addition, the 4-EG and 6-EG compounds have ChromLogD values of 5.8 (**Table 4**) which should ensure permeability of the tool compounds. The methylene linked compound had a high ChromLogD of 7.3, which should also confer permeability. The compounds had poor kinetic solubility, although as previously suggested, this is not a concern at the tool generation stage. These compounds were therefore deemed suitable tools to investigate BTK degradation.

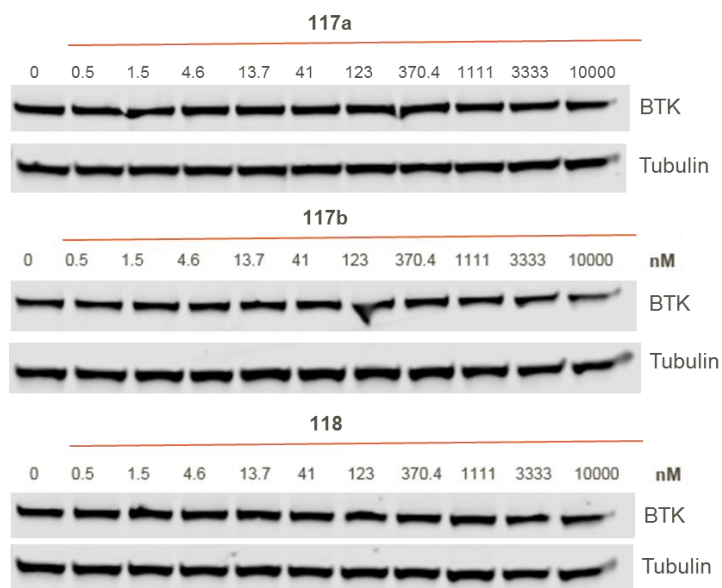
**Table 4:** Physicochemical data for promiscuous kinase DCAF15 PROTACs **117–118**.

\*denotes testing (n=4) \*\* denotes (n=2).



Compound	<b>117a</b>	<b>117b</b>	<b>118</b>
ChromLogD (pH 7.4) (n=2)	5.8	5.8	7.3*
Solubility CAD ( $\mu\text{M}$ ) (n=1)	10	<1	<1**

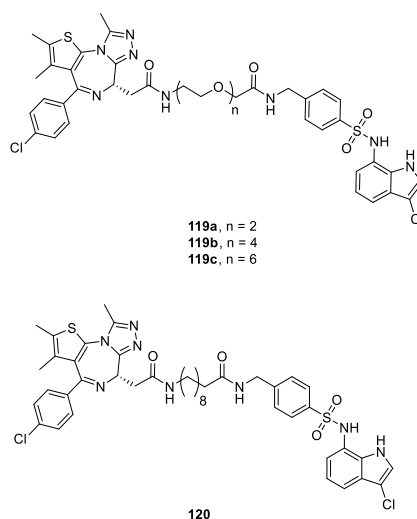
K562 cells were treated with compounds **117–118** for 24 h with increasing concentrations to determine if the compounds were able to recruit DCAF15 for BTK degradation. All three compounds **117–118** were tested in K562 cells with increasing concentrations (**Figure 86**). Western blotting analysis indicated that no BTK degradation was achieved with any of the three compounds **117–118** similar to the results with RIPK2 targeting PROTACs **116a/b**. It was expected that some BTK degradation would be observed, as the cereblon counterpart **43** shows excellent degradation in THP-1 cells at concentrations as low as 30 nM.<sup>80</sup> Therefore the binding to BTK should be sufficient for each of these PROTACs (utilising the same linker and exit vector) to induce BTK degradation with DCAF15, a similar E3 ligase construct.



**Figure 86:** Western blotting analysis of BTK in K562 cells after increasing concentration of compound **117–118** treatment for 24 h.  $\beta$ -Tubulin was used as a housekeeping protein and loading control for the experiment.

#### 5.3.4.4 Biological Evaluation of JQ1 derived DCAF PROTACs

The JQ1 based PROTACs were then evaluated. For the JQ1 derived DCAF15 PROTACs **119–120**, binding potency to BRD4 BD2 was mostly retained for compounds **119a–119c** (between 6.6–6.9), while for compound **120** this was reduced (6.2) (**Table 5**). The discrepancy in the binding affinity of **120** may be due to the insolubility of the compound as a result of the lipophilic methylene linker. **Compound 120** has a high ChromLogD of 7.0 and no measurable solubility, so may not be soluble enough in the assay to gain accurate binding data. In addition to biochemical potency, MCP1 cytokine production (which was described in the previous section) shows that the compounds **119–120** are cell permeable and engaging BRD4, which would be expected for the ChromLogD values of 5.9–7.0. BRD4 imaging degradation data (which was also described in the previous section) showed the compounds **119a–119c** did not degrade BRD4 in human PBMCs for any of the given compounds tested. Given the similarities in the ternary complexes between the E3 ligases DCAF15 and cereblon, and the cereblon recruiting molecules **31/32** (**Figure 26**) show excellent degradation in THP-1 cells and PBMCs at low concentrations, it was expected that some BRD4 degradation would be observed.<sup>88,89,94</sup> Compound **120** was not tested in this assay, as the compound was not synthesised in sufficient quantities, so was instead solely tested in Western blotting experiments. The other compounds were also tested in the analogous Western blotting experiment to the BTK and RIPK2 targeting PROTACs.

**Table 5:** Biochemical and physicochemical data for JQ1 derived DCAF15 PROTACs **119–120**. N.T. = not tested. \*denotes testing (n=1) \*\*denotes testing (n=3)

Compound	119a	119b	119c	120
BRD4 BD2 pIC <sub>50</sub> (n=2)	6.7	6.6*	6.9	6.2*
MCP1 Cytokine production PMBC LPS stimulated pIC <sub>50</sub> (n=2)	6.8	6.9	6.7*	6.5*
BRD4 human PBMC imaging pDC <sub>50</sub> (n=2)	<5	<5**	<5	N.T.
ChromLogD (pH 7.4) (n=2)	5.9	6.0	5.9	7.1
Solubility CAD (μM) (n=1)	1	11	16	<1

In addition to testing the compounds for degradation in the human PBMCs, compounds **119a/b** and **120** were incubated with K562 cells for 24 h at increasing concentrations (**Figure 87**). The Westerns for the BRD4 blots, had issues with the transfer from the gel from the electrophoresis onto the membrane used in the Western blot experiment, therefore in the first blot, the DMSO control lane had no apparent protein for BRD4 or tubulin present. Non-specific protein bands below BRD4 were also observed in some of the conditions, which were not used for protein quantification. No degradation was observed for any of the compounds analogous to results observed in the PBMC degradation assay. This, together with the lack of degradation in the PBMC imaging assay, elucidates that the DCAF15 PROTACs **119–120** were unable to degrade BRD4. None of the PROTACs synthesised recruiting DCAF15 were able to degrade their respective targeted proteins.

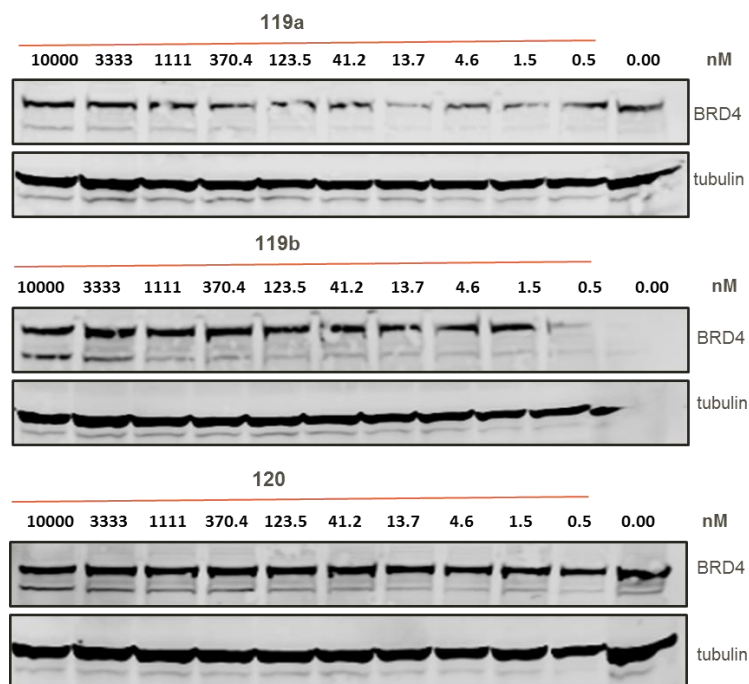


**Figure 87:** Western blotting analysis of BRD4 in K562 cells after increasing concentration of compound treatment **119a/b** and **120** for 24 h (NB/ the highest concentration is on the left-hand side and decreased to the right for the following Western blots).  $\beta$ -Tubulin was used as a housekeeping protein and loading control for the experiment.

#### 5.3.4.5 Evaluation of the Lack of Degradation of the DCAF15 Recruiting PROTACs

Before investigating the PROTACs using a proteomic approach for degradation of other proteins bound by the promiscuous binders, such as the 100 kinases from the promiscuous binder and the other 3 BET proteins, the lack of degradation of the current targets was examined. Lack of degradation observed with any of the PROTACs targeting DCAF15 as an E3 ligase may be a result of the PROTACs not binding sufficiently to DCAF15 in the ternary complex. It was previously highlighted that the binding event between indisulam **67** and DCAF15 only happened in the presence of CAPER $\alpha$ .<sup>135,136</sup> In the reported protein pull-down experiments, the compounds with a linker and biotin label **111** were still able to engage DCAF15. However, it is worth noting that the pull-down experiments used a covalent attachment to the DCAF15 protein.<sup>135</sup> This could be a result of weak binding to the DCAF15 leading to covalent binding required to capture the protein (the rationale for the covalent photoactivated portion is not mentioned in the publication). However, the linkable analogues of indisulam **115** were also shown to be active in degrading CAPER $\alpha$ , showing sufficient binding to the E3 ligase to induce this specific protein's degradation through a molecular glue interaction. Therefore, affinity enrichment proteomics based on the linkable analogue **115** was carried out by coupling it to an insoluble matrix and competed by indisulam **67**. Proteins which

were pulled down by the linkable analogue included a number of the components of the E3 ligase complex: DCAF15-DDB1-CUL4-RBX1. However, none of the components were directly competed by indisulam **67** and they were also not pulled down in every condition and deemed not reproducible following repeat experiments. No CAPER $\alpha$  was detected in any of the pull-down experiments. This result shows the compounds are able to bind to DCAF15 but does not give a clear result of the binding potency. The non-reproducible results could be a result of weak binding of the proteins to the linked analogue **115** when conjugated to the beads. This may mean that conjugating **115** into PROTACs may not be viable for DCAF15 recruitment in protein degradation.

In order to determine if the PROTACs were still able to engage DCAF15, SPR studies were carried-out in the presence of **116–120** with DCAF15, and additionally using the small molecule indisulam **67**. To determine if any of the compounds were able to bind to DCAF15 without the presence of Capera (RBM39), which was previously stated to be a requirement of indisulam's **67** DCAF15 binding (**Figure 88**). It was hypothesised that the PROTACs would still be able to engage DCAF15 as the photoaffinity probe **111** was able to still bind despite its conjugation to biotin. However, it was not clear if this compound **111** bound to DCAF15 alone, or in the presence of the DCAF15-Capera conjugate. The attempts to generate binding data to DCAF15 were unsuccessful with indisulam **67** or any of the PROTACs tested. This could be due to the need for Capera as a binding partner as previously described or could be a result of protein instability in the SPR studies. Although the compound **111** is still able to engage DCAF15 as illustrated by the pull-down experiments in the literature, it is not clear if this is applicable to all conjugated analogues or it is a specific case. Future SPR studies with the compounds with both DCAF15 and Capera are required to understand the relationship between binding with the proteins. As a result, it is not currently known whether the conjugated compounds **116–120** have sufficient affinity to DCAF15 in order for it to be recruited as an E3 ligase in the PROTAC approach.

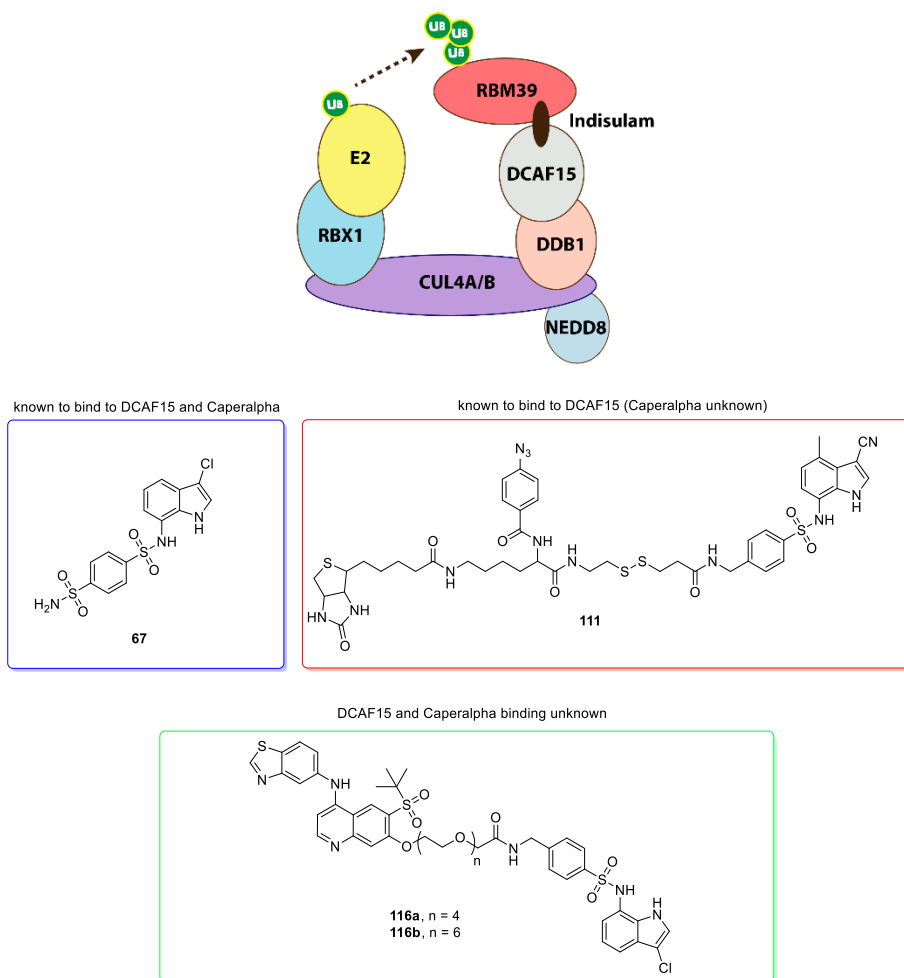


**Figure 88:** Compounds derived from indisulam **67** and whether they are known or not to DCAF15 and the molecular glue binding partner Capera.

Due to the intensive resources required for further proteomic experiments, and the lack of target engagement observed, it was decided not to proceed with any of the compounds into full proteomic analysis. As a result of no degradation, or any target engagement assay available, this project was terminated. In order to develop successful DCAF15 PROTACs in the future, binding and cellular target engagement assays would be required.

#### 5.4 Summary and Future Work

A toolbox of indisulam derived PROTACs (**116–120**) were synthesised and evaluated to determine if DCAF15 could be a useful E3 ligase for the PROTAC approach. Compounds were synthesised to assess three different proteins, BTK and RIPK2 from the kinase family, and BRD4 from the BET family, which have all previously shown good degradation with other known E3 ligase binders available. The compounds **116–120** were evaluated and shown to be active in cellular engagement assays where available and as they were deemed suitable

cell permeable tools to evaluate the E3 ligase. The compounds **116–120** were unable to achieve any degradation at any concentration tested with a number of different linker lengths. In attempts to determine target binding, the linkable analogue **115** was used in affinity enrichment proteomics and it was inconclusive if DCAF15 binding was retained, although the DCAF15 complex was identified in the experiments, it was not reproduced. With no target engagement determined with the PROTACs and/or associated degradation, indisulam derivatives were deemed not robust for the recruitment of DCAF15 and as a result for the PROTAC approach (**Figure 89**).

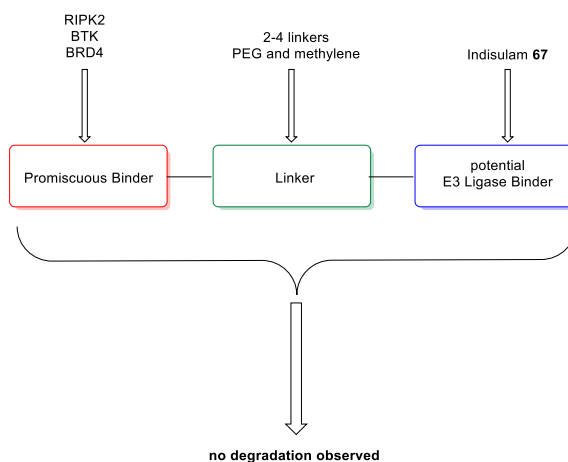


**Figure 89:** PROTACs synthesised based on indisulam **67** for DCAF15 using the promiscuous toolbox, resulting in no degradation.

Future work in ascertaining whether the PROTACs are still able to engage DCAF15 are required. There was no binding assay to complement DCAF15 small molecule binding retention in developing PROTACs (the pIC<sub>50</sub> of indisulam **67** to DCAF15 is not yet known). Despite the CAPER $\alpha$  degradation observed with the indisulam derivative **115**, it is not yet known whether DCAF15 binding in the PROTACs **116–120** is retained, and therefore cannot be deemed suitable for the PROTAC approach without target engagement assessment. This approach could be re-evaluated with a suitable cellular binding assay to DCAF15, in addition to X-ray crystallography, to ensure the PROTAC derivitisation was able to retain binding and target engagement for DCAF15 recruitment. This could include the suitable alternative exit-vector determinations of indisulam **67**, as well as investigation into other, even novel, DCAF15 binders which could be elaborated into PROTACs.

If it was established that the compounds were in fact binding successfully, there could be a number of other reasons for the failure in inducing protein degradation. At present, it is relatively difficult to assess PROTAC failure, which is a caveat of protein degradation in drug discovery. Target engagement and cellular permeability are two common methods to ascertain PROTAC failure, as binding in the cell is essential for activity. In addition, ternary complex

formation inside the cell may be a reason for failure, due to negative interactions between the protein pair. Investigation of ternary complex formation requires a lot of optimisation, for example using a nanoBRET assay (**Figure 90**).<sup>176-178</sup> This assay harnesses bioluminescent resonance energy transfer (BRET) by using a Luciferase fusion to the protein of interest, and a HaloTag fusion conjugated to a fluorophore to the E3 ligase, such as DCAF15. When a successful ternary complex forms, energy transfer occurs and can be measured. The execution of this assay requires a new cell line to be developed, and therefore confidence in DCAF15 binding would be required before this was initiated. Nevertheless, this assay would be very useful to ascertain whether a ternary complex is forming in the cells with the DCAF15 compounds synthesised. As the induced protein degradation field is relatively novel, there are unanswered questions as to why PROTACs fail, and these may require a more thorough biological investigation.

As a result of the complexities involved in determination of the PROTACs' failures, a new approach to evaluate new E3 ligase binders for drug discovery efforts would be beneficial and will be discussed.

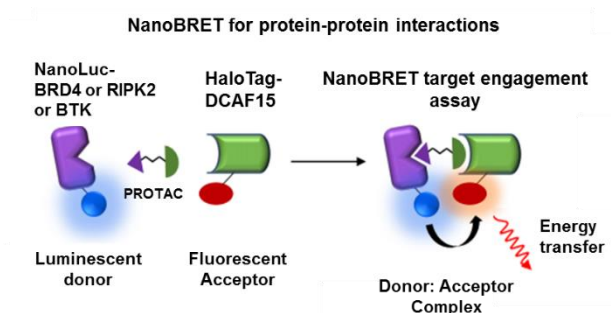


**Figure 90:** NanoBRET assay for the potential target engagement studies for the DCAF15 PROTACs.

## 6. Validation of a High-Throughput GFP Degradation Assay Utilising HaloPROTACs to Known E3 Ligases

### 6.1 Introduction

Evaluating different E3 ligases for the PROTAC approach in drug discovery can be achieved in a number of ways. One approach for the search for new E3 ligases for targeted protein degradation has previously been described. By utilising a potential E3 ligase binder from the literature, PROTACs can be designed and evaluated for their ability to successfully degrade known proteins of interest, such as the BET or kinase family of proteins, thereby validating the E3 ligase in targeted protein degradation. While successful in a number of occasions, this process is largely empirical which requires significant time and cost to execute. In addition, as observed with DCAF15, it may result in an unsuccessful incorporation into the PROTAC approach. There are approximately 600 E3 ligases known but by using this approach only one can be prosecuted at a time, which results in a resource intensive method to investigate a small number of E3 ligases. Therefore, the utilisation of a platform which would allow a non-biased biological experiment to assess multiple E3 ligases at once would be a more efficient method to find new chemical matter for E3 ligases. It is hypothesised that utilising a protein construct, such as green fluorescent protein, could allow an alternative fluorescence-based assay to labour-intensive Western blotting in order to quantify protein degradation. As a new method to finding binders for E3 ligases, a GFP-HaloTag® protein could be employed as a way of measuring protein degradation through novel HaloPROTACs. Once validated as a robust approach which will be discussed in this chapter, this could be assessed to evaluate and assess new E3 ligases for the PROTAC approach using high-throughput HaloPROTAC synthesis (which will be discussed in Chapter 7).

The use of HaloTag® proteins has been developed which has proved extremely useful in cellular imaging.<sup>179</sup> To bind specifically to a POI, such as GFP, the protein can be fused with a HaloTag® construct, developed by Promega.<sup>180-185</sup> This HaloTag® construct was inspired by a bacterial haloalkane dehalogenase, *Rhodococcus rhodochrous* which catalyzes the conversion of an alkyl chloride **142** to an alcohol **143a** through a aspartic acid addition to the chloroalkane and hydrolysis step mediated through histidine (**Figure 91**). In the same manner the HaloTag® construct recognises and binds to a chloroalkane moiety **142**, but instead of a catalytic hydrolysis, the process is now covalent leading to **143b**. This is achieved through enzyme mutation to remove the histidine, with the modification of the aspartic acid with the chloroalkane now being irreversible. This process allows rapid and irreversible tagging of the HaloTag® to the ligand and the resulting ester is protected from esterases (hypothesised due to its burial in the hydrophobic pocket of the protein).<sup>184</sup> This 33 kDa HaloTag® construct can be fused to a number of different proteins (N- or C-terminal fusions) to give a protein which

can now be efficiently labelled covalently using a chloroalkane derivative. The HaloTag® chloroalkane can be functionalised with various reporters such as dyes, peptides, E3 ligases, and are known as HaloTag® ligands. This HaloTag® label is therefore an extremely useful way to label a POI with a covalent ligand with multiple uses in cellular imaging and reporting and can be utilised in numerous high-throughput biological assays.

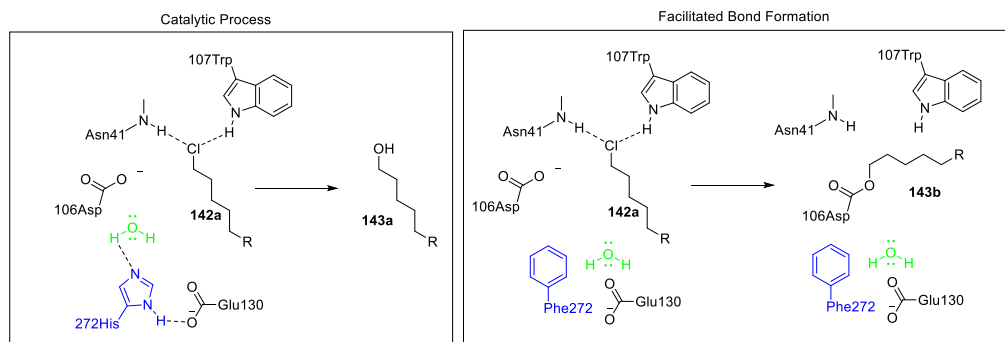
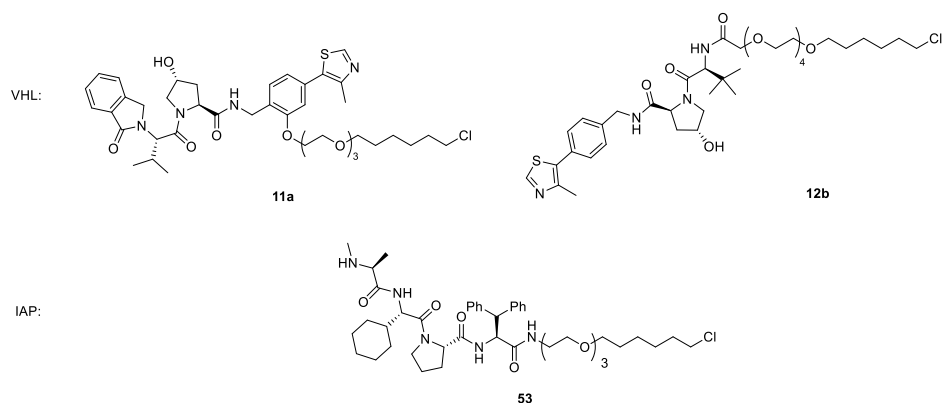


**Figure 91:** HaloTag® technology, developed by Promega. Inspired by Rhodococcus rhodochrous, a hydrolase enzyme which dehalogenates chloroalkanes catalytically through interactions with a water molecule (green) through histidine (blue) and glutamic acid. The histidine residue is mutated to phenylalanine (blue) in the HaloTag® removing the catalytic nature of the enzyme.

HaloPROTACs or “Chloroalkane PROTACs” targeting HaloTag® fusion proteins are known in the literature, developed first by Crews and GSK (see introduction).<sup>63</sup> HaloPROTACs implement a chloroalkane HaloTag® ligand conjugated to an E3 ligase binder (**Figure 92A**). HaloPROTACs allow a covalent modification of the GFP-HaloTag® fusion protein with an E3 ligase binder, which can recruit an E3 ligase, such as VHL **11a**, **12b** and IAP **53** (**Figure 92B**). However, Western blotting experiments were still required to ensure the degradation observed was PROTAC mediated, rather than cellular toxicity leading to the GFP reduction. Western blotting experiments are not high-throughput, therefore would present an issue in utilising HaloPROTACs for new E3 ligase investigation. If fluorescence could be used as a primary read-out for this experiment and cytotoxicity could be measured, it could be implemented in larger screening and could be a useful in a number of potential applications.

A)



B)

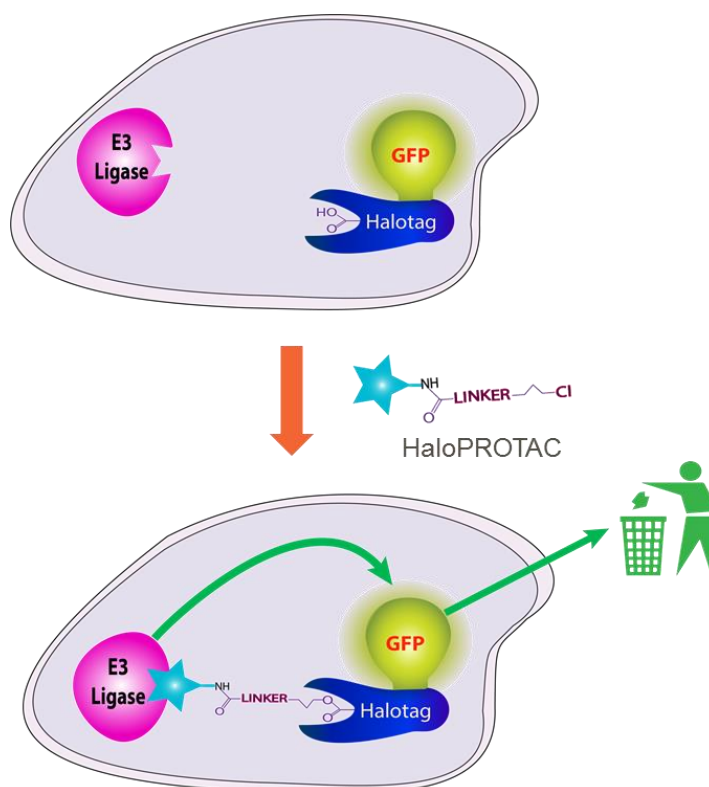


**Figure 92:** HaloPROTACs **11a**, **12b**, **53** degrading the GFP-HaloTag® fusion protein (A). Overview of HaloPROTAC induced degradation of the GFP-HaloTag® fusion protein through E3 ligase recruitment.

## 6.2 HaloPROTACs Project Aims and Objectives

In the following projects, the overall aim is to use an E3 ligase agnostic approach, through the implementation of a phenotypic, in-cell screen to search for new degraders irrespective of which E3 ligases are specifically recruited. The use of green fluorescent protein (GFP) as the protein of interest, combined with high-throughput PROTAC synthesis (see Chapter 7), would

allow the search for new E3 ligases in a cellular environment based on fluorescence reduction corresponding to protein degradation.

In order to implement a high-throughput experimentation screen, (which will be featured in Chapter 7) HaloPROTACs against the currently developed E3 ligases from the literature and in our laboratories will be investigated to assess the HaloPROTAC platform for its wider utility. It was hypothesised that a fluorescence reduction assay could be utilised to investigate new E3 ligases (with the correct controls in place to differentiate protein degradation and cellular toxicity). Due to the ease of fluorescence read-out in place of resource intensive Western blotting experiments, new E3 ligases could be evaluated more efficiently with a GFP-HaloTag® construct (**Figure 93**). To test a wide range of E3 ligases HeLa cells were selected as a cell line to transfect the GFP-HaloTag® construct, as they express around 50–60% of the 600 E3 ligases known, as elucidated by proteomic analysis by Cellzome.<sup>147</sup> In order to assess whether the degradation observed was due to the PROTAC approach and not an unrelated event, a HeLa cell line was also developed with a mutated GFP-HaloTag® control construct. The mutation no longer allowed covalent binding of the chloroalkane to the HaloTag® core (HaloTag® D106A). Therefore, any degradation of GFP observed, would be non-related, for example, could be as a result of cytotoxicity or compounds which inhibit cell growth. It could also be a result of proteasome activators or fluorescence quenching compounds, for example.

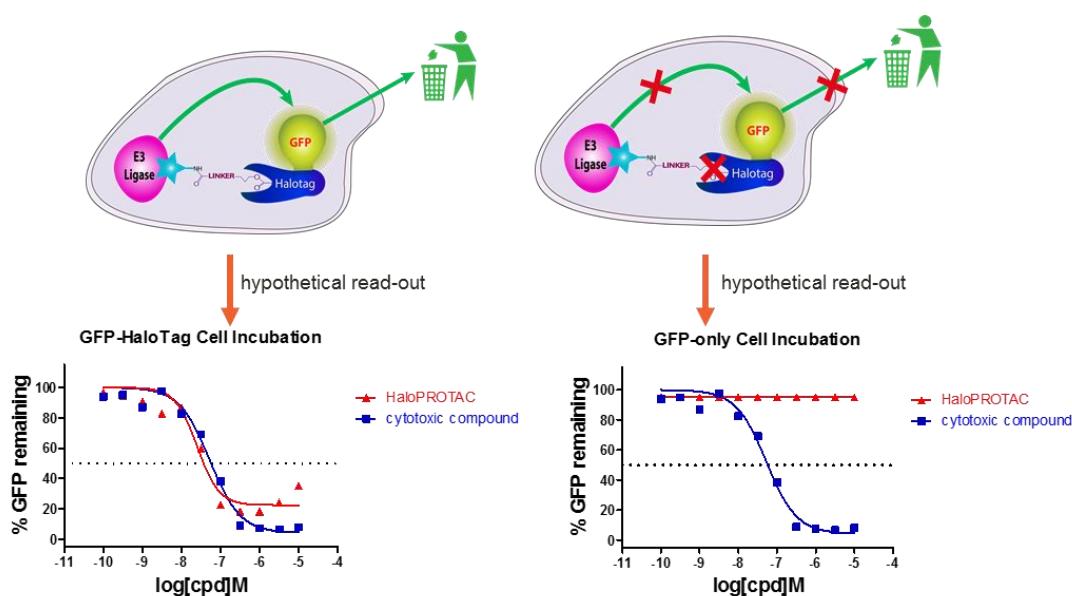


**Figure 93:** GFP-HaloTag® degradation mediated by the HaloPROTAC binding to the E3 ligase. Two HeLa cell lines were used in this assay: GFP-HaloTag® HeLa cells and additionally GFP-HaloTag® mutant control HeLa cells were developed with a mutation in the HaloTag® which would no longer bind the chloroalkane portion of the HaloPROTAC (HaloTag® mutant control (D106A)). Cells could therefore be used as a control to eliminate cytotoxic compounds which reduced the fluorescence without the PROTAC approach involved, exemplar readouts from potential HaloPROTACs (red) and potential cytotoxic compounds (blue) are shown.

In order to assess if the two cell types could confer robust and specific protein degradation through fluorescence read-outs, HaloPROTACs containing E3 ligases that were already utilised for the PROTAC approach could be used for assay validation. This was achieved by utilising HaloPROTACs which can bind to the HaloTag® fused to GFP protein, where degradation is correlated directly to fluorescence and should not change fluorescence in the GFP mutant control cell line (if not cytotoxic). As a result, a number of HaloPROTACs based on E3 ligases established would be investigated to probe the GFP degradation assay to investigate GFP degraders. In addition, a number of known non-degraders would also prove useful in this assay, to investigate how the cell lines would respond to non-functional HaloCompounds, to ensure false positives could be eliminated in a large assay format.

To validate the GFP degradation assay, VHL recruiting HaloPROTAC **11a**, an already established HaloPROTAC, would be synthesised and evaluated in this phenotypic assay set-up (**Figure 94A**). Based on the HaloPROTAC publication, an intermediate 3-EG linker would be used to synthesise the novel HaloPROTACs, such as **144** recruiting VHL.<sup>63</sup> Only one linker length would be used in this instance, as the aim was to validate the use of the two cell lines in the assay. Other validated E3 ligases would also be synthesised and evaluated, including IAP, which has a number of chemotypes with different selectivity profiles, **145–147**, which will

be investigated. Other E3 ligases which have chemical matter such as KEAP1 **148** and DCAF15 **149** would be tested to determine if they degrade GFP in contrast to their failed degradation with other proteins in our laboratories. In addition, the E3 ligase cereblon has not been published for its utility in the HaloPROTAC degradation of GFP, so a lenalidomide derived HaloPROTAC **150** would also be investigated.

A methylene-based linker of a similar length would be utilised in cases where cell permeability was hypothesised to be poor, to ensure the future HaloPROTACs with potentially hydrophilic binders could be assessed (**Figure 94B**). This linker will be assessed with VHL **151**, IAP **152** and cereblon **153** in the first intent, with aims to use this in future screens with polar amines in a potential HTS format.

The IAP **145** and KEAP1 **148** HaloPROTACs were of particular interest, as their small molecule counterparts are known to be cytotoxic at higher concentrations. This will be useful to test and assess cytotoxicity versus degradation of GFP, as both would result in fluorescence reduction. Therefore, these tools can be used to delineate if the fluorescence reduction is via a PROTAC approach by using both the GFP-HaloTag® and the GFP-HaloTag® mutant control cell line.

With the compounds in hand, the GFP degradation assay would be investigated. The aim would be to assess both cell lines described, with different methods of fluorescence detection where possible. This was envisaged to determine if the assay could be utilised in a larger phenotypic screen to search for novel degraders in future.

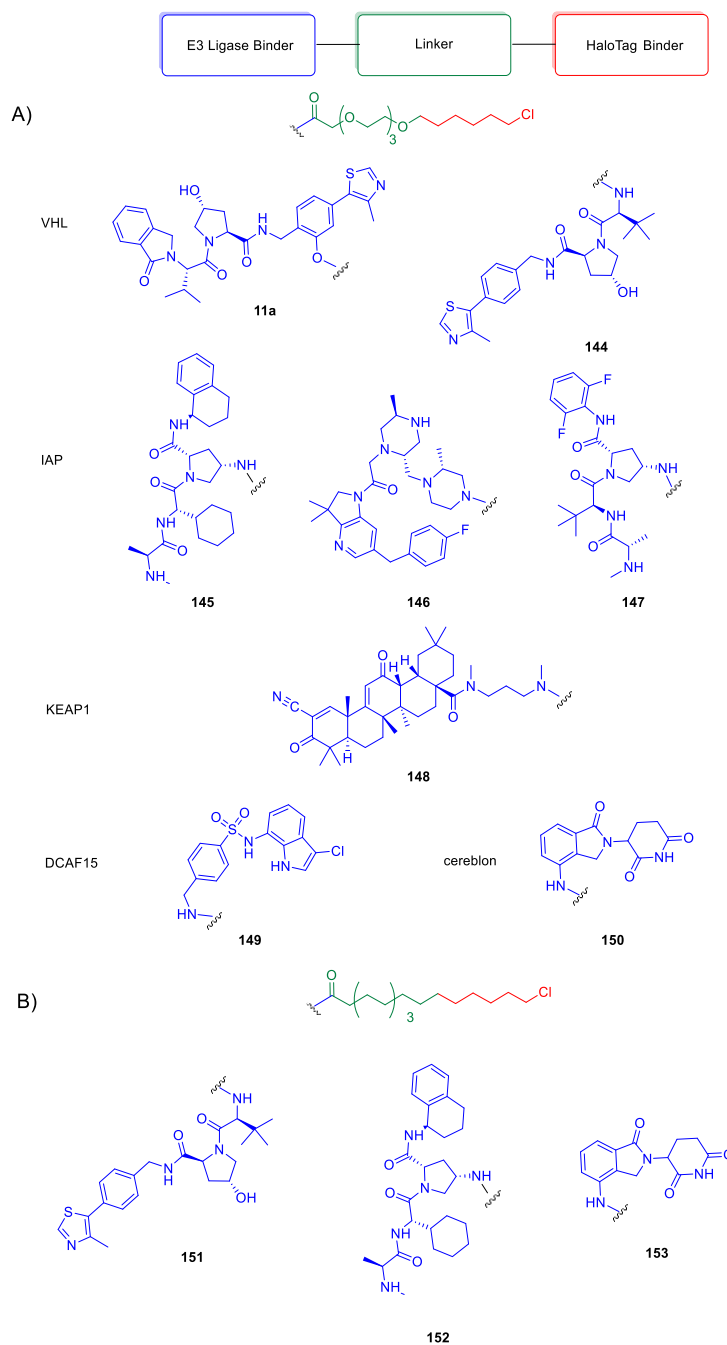


**Figure 94:** Utilising the GFP-HaloTag® technology to assess E3 ligases by synthesising chloroalkane derived HaloPROTACs which should cover both active and inactive degraders (A). In addition to the PEG derived compounds, methylene linked compounds for VHL, IAP and cereblon would also be assessed for possible use with future hydrophilic binders (B).

## 6.3 Results and Discussion

### 6.3.1 Design and Synthesis of HaloPROTACs

In order to optimise the GFP degradation assay in HeLa cells with both the GFP-HaloTag® and GFP-HaloTag® mutant constructs a number of HaloPROTACs were designed and synthesised. Two VHL standard compounds were designed as controls for the GFP degradation assay. Based on the HaloPROTAC publication,<sup>63</sup> an intermediate linker length was designed using 3-EG units for both VHL compounds **11a** and **144** to maintain good degradation observed in the HaloPROTAC publication with a consistent length between the two exit vectors (**Figure 95**). If a high-throughput assay was put into place with HaloPROTACs (see Chapter 7), one linker would be used in the initial experiments. The 3-EG was deemed a good starting point for this project as it has shown utility in the previous publications and works well with a number of PROTAC molecules in-house irrespective of POI or E3 ligase binder used. A methylene linker was also used in a number of examples, to validate if a very lipophilic linker could be used in examples with very polar binders. A methylene derived linker was therefore tested with this VHL binder, and the length of 15 methylene units was chosen. This was a result of the HaloTag® binder containing 6 methylene units, and the additional 8–10 carbons to give HaloPROTAC **151**. Further investigation into linker length optimisation could be performed in order to give a range of different molecules.

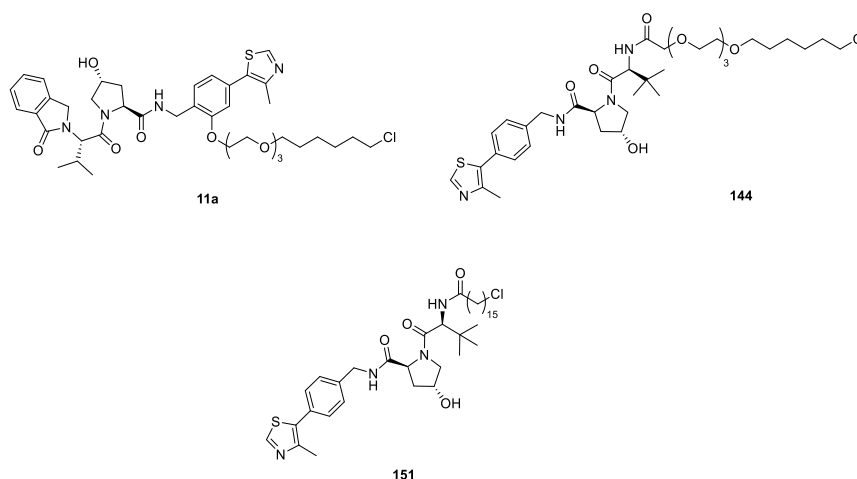


**Figure 95:** VHL recruiting HaloPROTACs **11a**, **144** and **151** used as controls for the assay development.

As previously described, IAP recruiting HaloPROTACs in the literature were synthesised and investigated for degradation of HaloTag®-TNF $\alpha$  with limited success (compound **53**, **Figure 41**).<sup>119</sup> It was hypothesised this could be due to the sub-optimal IAP binders/exit vectors for the approach. Therefore, additional IAP binders would be investigated for incorporation into HaloPROTACs and evaluated in the GFP degradation assay.

In addition to testing new IAP HaloPROTACs to determine their degradability, they were also used to explore the ability to distinguish GFP degradation and compound cytotoxicity. Inhibitor

of apoptosis (IAP) inhibitors are used in oncology indications to drive cells into apoptosis through cIAP1 self-degradation leading to the downstream release of caspases 3/7.<sup>110-112,125,186-188</sup> PROTACs have shown a good therapeutic window between degradation and apoptosis,<sup>94</sup> most likely as a result of the catalytic feature and low occupancy of the E3 ligase required to induce protein degradation. With the HaloPROTAC mechanism, this is no longer catalytic as the compounds are covalent, therefore any IAP compounds designed would be stoichiometric degraders of GFP. Therefore, it was hypothesised that these compounds may drive apoptosis in the GFP-HaloTag® cells. This would therefore be investigated using both the GFP-HaloTag® mutant control cell line, and cell imaging to investigate the effect on the cells morphological changes as a result of compound treatment. In addition, it would be possible, using both of the cell lines, to observe the activity window between protein degradation and apoptosis. As a result, a number of HaloPROTACs based on potent IAP inhibitors used within our group were therefore investigated **145–147 (Figure 96)**. The HaloPROTACs were designed using the small molecules as described in the introduction, HaloPROTAC **145** includes an IAP binder which is very potent at both cIAP1/XIAP BIR3. HaloPROTAC**146** includes a compound derived from ASTX660 which is active at cIAP1/XIAP BIR3. In addition, HaloPROTAC **147**, is derived from a small molecule which has lower affinity for cIAP1, which also binds to XIAP BIR2. It was hypothesised that this compound may have an increased activity window between GFP degradation and apoptosis as a result of the lower affinity to cIAP1 which may not be able to induce apoptosis until higher concentrations. Therefore, IAP-driven pharmacology was investigated comparing the GFP-HaloTag® cells and the GFP-HaloTag® mutant control cells using compounds **145–147** with different levels of cIAP1 and XIAP binding potencies.

In addition to the PEG derived compounds, an all-methylene linker was also used to generate HaloPROTAC **152**. This was in order to ensure the IAP recruiting compounds had sufficiently high lipophilicities to ensure permeability. IAP binders require a basic amine, which could impair permeability, and therefore a PEG and all-methylene compound would be synthesised and compared to ensure the assay could be assessed with potent and permeable IAP recruiters. All IAP derived HaloPROTACs would enable the assessment of the GFP degradation assay to determine GFP degradation versus cytotoxicity.

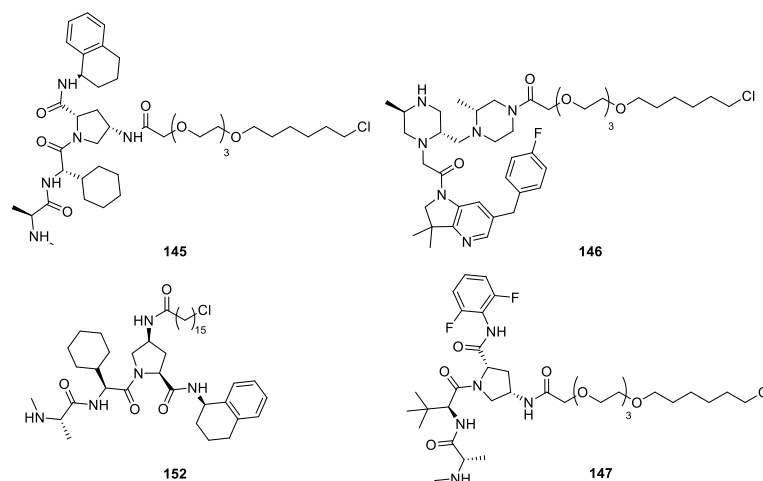


**Figure 96:** Design of IAP based HaloPROTACs with three IAP binders and two linkers.

In addition to the cytotoxic IAP recruiting HaloPROTACs designed, another positive cytotoxic control was designed using a KEAP1 inhibitor. Triterpenoid bardoxolone (also known as CDDO) is a promiscuous steroid which has been shown to bind to KEAP1 (compound **3**, **Figure 7**).<sup>53</sup> Bardoxolone **3**, in multiple cell lines at relatively moderate concentration ranges, has shown to be cytotoxic.<sup>50,51</sup> As a result, using the 3-EG linker, a HaloPROTAC **148** based on bardoxolone was designed (**Figure 97**). As this binder has not been featured in any potent PROTACs, an example exit vector was chosen for HaloPROTAC elaboration from the methyl ester in bardoxolone **3**. In addition to lack of KEAP1 binding assays available, the bardoxolone based HaloPROTAC **148** was not anticipated to be a potent degrader, but instead used in this assay as a positive cytotoxic control compound for the cellular screening.

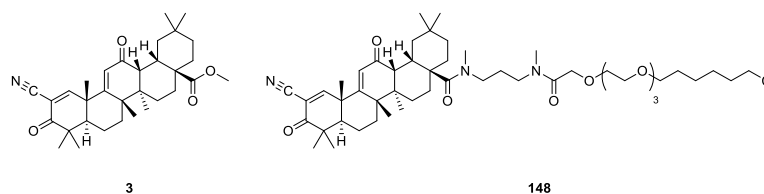


**Figure 97:** Design of bardoxolone based HaloPROTAC **148** featuring an 3-EG linker.

DCAF15 is an E3 ligase which was investigated for use in the PROTAC approach in the previous chapter. A HaloPROTAC **149** based on the indisulam **67** would therefore be investigated (**Figure 98**). This was used, with the standard 3-EG linker, in addition to the promiscuous toolbox used in Chapter 5, to determine if it was able to induce GFP degradation in the HeLa cells. Analogous to the previous chapter, DCAF15 binding was not determined as there was no suitable assay in place, therefore the HaloPROTAC was synthesised to complement the promiscuous toolbox. If GFP reduction was not observed, the reason for lack of degradation via DCAF15 recruitment would still not be known. This was also used as a non-

functional degrader in the GFP degradation assay, to ensure non-functional compounds would not interfere with the fluorescence.

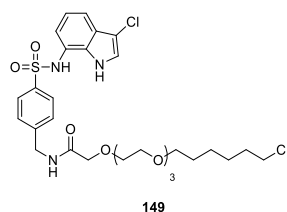


**Figure 98:** Design of indisulam based HaloPROTAC **149** featuring an 3-EG linker.

In addition to VHL and IAP, cereblon recruiting HaloPROTACs were investigated. There were no cereblon recruiting HaloPROTACs in the literature, so two compounds were designed. Using the standard 3-EG linker, a PEG derived compound **150** was deemed a suitable compound to determine cereblon recruitment for GFP degradation. In order to ensure cell permeability, for the compound the methylene derived linker was also designed **153** (**Figure 99**). Degradation of multiple proteins in HeLa cells has previously been achieved internally,<sup>94</sup> so it was hypothesised that cereblon could be recruited in HeLa cells to degrade the GFP-HaloTag®. The compounds designed in this chapter were utilised primarily to validate the cell lines and their use in a wider screening platform, so other linker combinations or other cereblon binding compounds were not synthesised at this stage. If investigating the degradability of GFP-HaloTag® with cereblon as an E3 ligase, more compounds would be synthesised in future efforts.

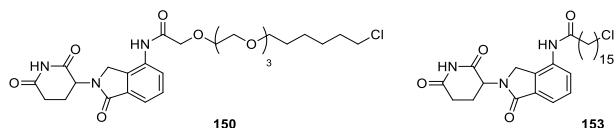
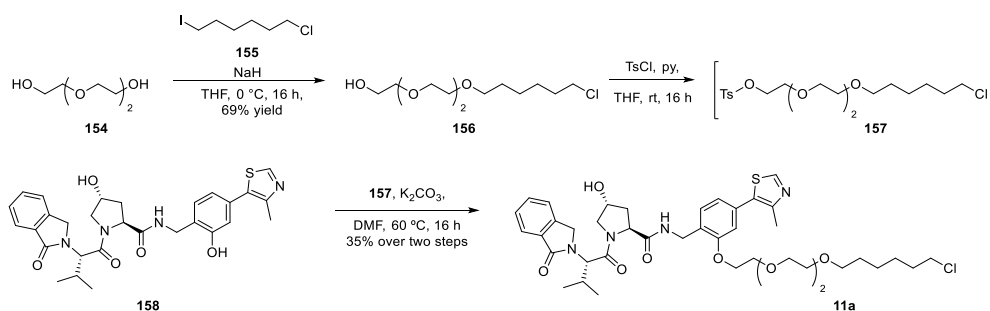


**Figure 99:** Design of lenalidomide based HaloPROTACs **150** and **153** featuring an 3-EG and all-methylene linker respectively.

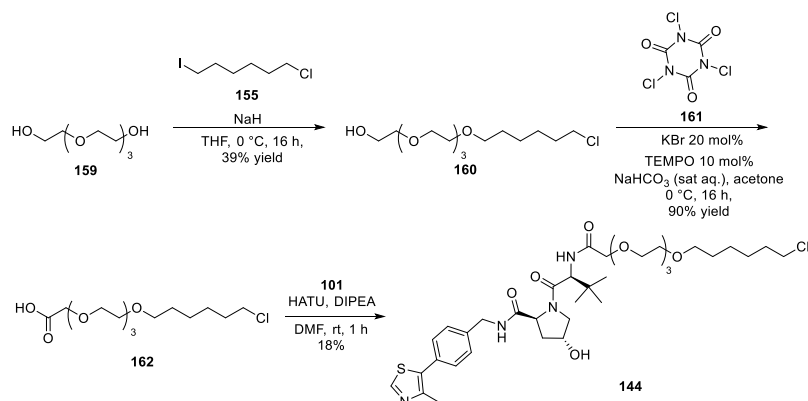
### 6.3.2 Synthesis of HaloPROTACs

In order to evaluate the designed compounds in the GFP degradation assay, the compounds were synthesised. The synthesis of the VHL recruiting HaloPROTAC 11a was achieved through alkylation of the 1-chloro-6-iodohexane **155** with excess of the 3-EG diol **154** to favour monoalkylation. This was successfully achieved in a 69% yield (**Scheme 11**). The product was then converted to the tosylate **157** and reacted with the VHL phenol **158** to give the HaloPROTAC **11a** in a 35% yield over two steps.



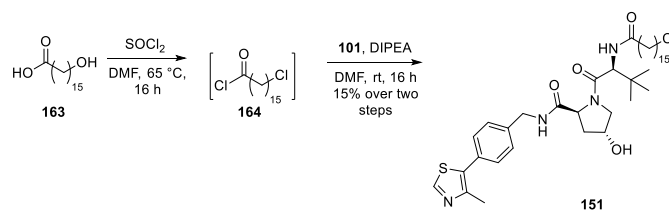
**Scheme 11:** Synthesis of standard VHL recruiting HaloPROTAC **11a**.

The second VHL recruiting HaloPROTAC **144** was also synthesised using a 3-EG linker, but this was now conjugated via an amide bond. The synthesis of the VHL recruiting HaloPROTAC **144** was achieved through alkylation of the 1-chloro-6-iodohexane **155** with excess of the 4-EG diol **159** to ensure monoalkylation which was achieved to give **160** in a 39% yield (**Scheme 12**). This was then oxidised to the corresponding acid **162** using trichloroisocyanuric acid **161** and TEMPO in a 90% yield. This was coupled to the VHL amine **101** using HATU and DIPEA to give the VHL recruiting HaloPROTAC **144** in an 18% yield. The acid **162** used in this experiment could be utilised in the synthesis of the remaining HaloPROTACs, as they all featured an amide bond in their structure.



**Scheme 12:** Synthesis of VHL standard HaloPROTAC **144**.

In addition, a VHL recruiting HaloPROTAC containing an all-methylene linker **151** was synthesised. This was achieved by converting the hydroxyalkyl acid **163** into the corresponding acid chloride **164** while simultaneously converting the alcohol to the chloride using thionyl chloride in a single step. This was concentrated *in vacuo* and used immediately. This was then reacted with the VHL amine **101** to give the corresponding HaloPROTAC **151** in a 15% yield over two steps (**Scheme 13**).



**Scheme 13:** Synthesis of VHL recruiting HaloPROTAC **151** with an all-methylene linker.

IAP recruiting HaloPROTACs **145** and **152** were synthesised in an analogous manner to VHL **144** and **151** utilising the common intermediates **162** and **164** respectively (**Scheme 14**). The HaloPROTAC was synthesised using an amide coupling of the chloroalkane acid **162** with the precursor amine **165** and subsequent HCl mediated Boc deprotection gave the desired compound **145** in 71% yield over two steps (**Scheme 14A**). The all-methylene derived variant **152** was also synthesised using the same method as with VHL with additional Boc deprotection affording the IAP all-methylene derived HaloPROTAC **152** (**Scheme 14B**).

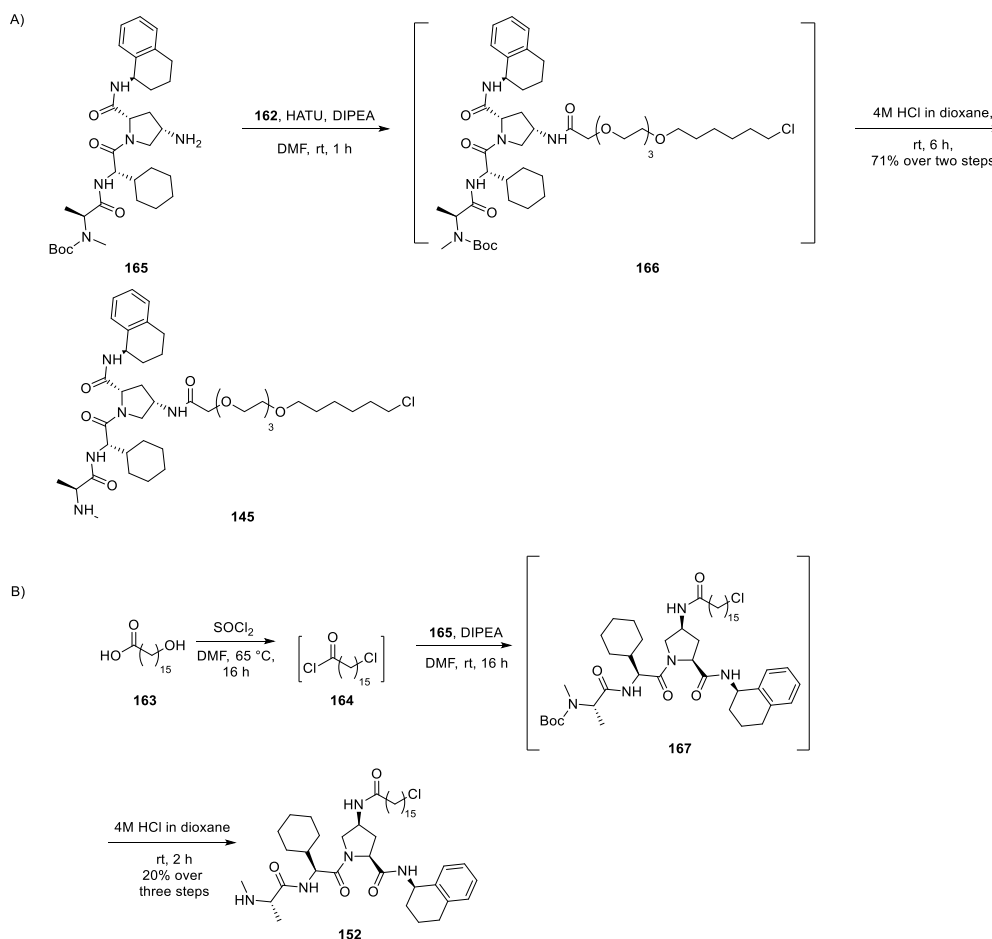
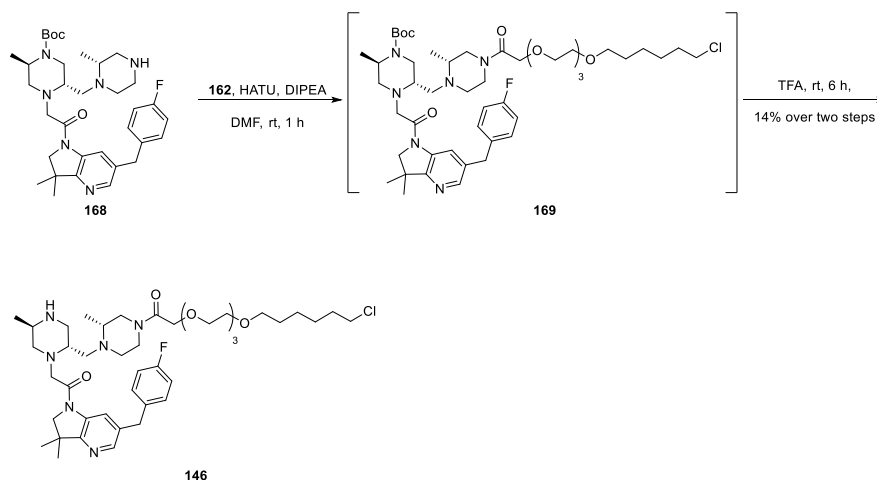


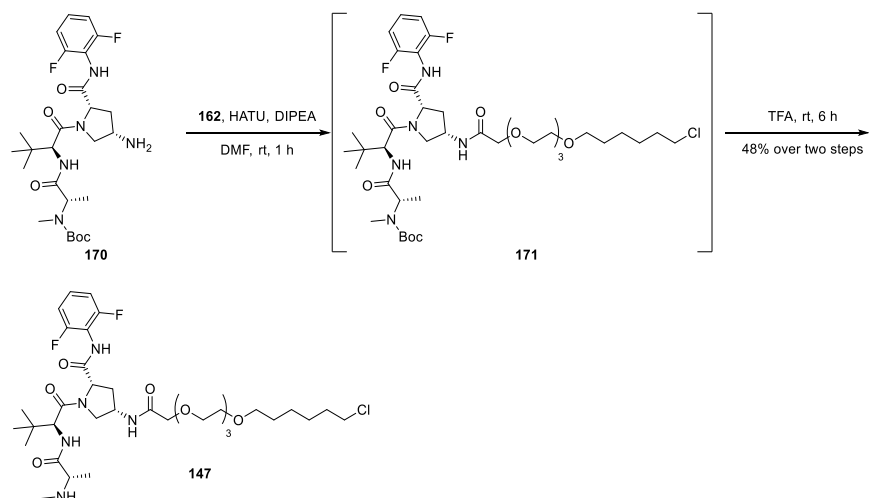
**Figure 100:** Synthesis of IAP recruiting HaloPROTACs **145** (A) and **152** (B).

The HaloPROTAC based on the dual inhibitor for XIAP and cIAP from Astex<sup>55</sup> was utilised to synthesise HaloPROTAC **146** in an analogous manner from a building block available in house **168** (Scheme 14). The amine **168** was amide coupled to **162** and Boc deprotected in a 14% yield over two steps to yield HaloPROTAC **146**.



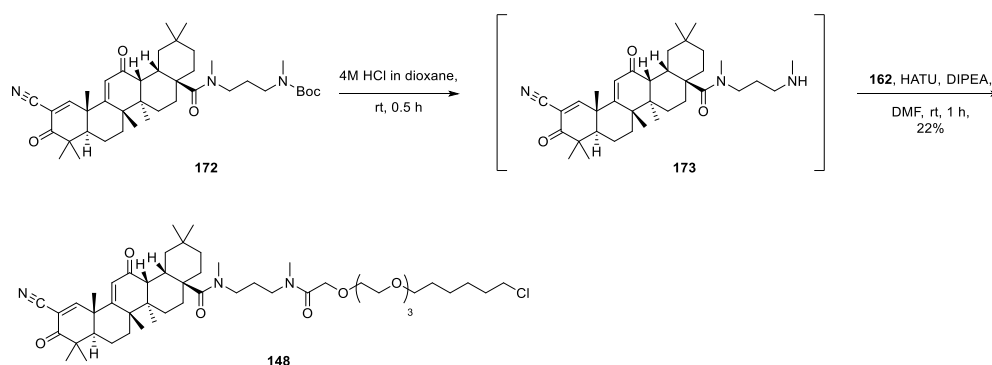
**Scheme 14:** Synthesis of IAP recruiting HaloPROTAC **146**.

And finally, the less potent cIAP1 inhibitor<sup>94</sup> based HaloPROTAC **147** was synthesised in 48% yield over two steps from an available building block used in house **170** (Scheme 15).



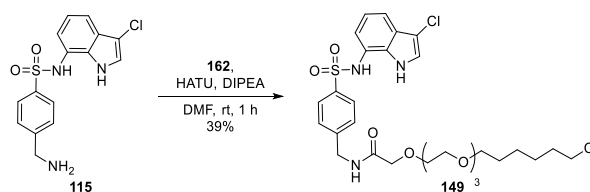
**Scheme 15:** Synthesis of IAP recruiting HaloPROTAC **147**.

A bardoxolone KEAP1 recruiting HaloPROTAC **148** was also synthesised as a positive cytotoxic control for the GFP degradation assay. This was achieved from a Boc-protected linkable analogue **172** that was available in house. Boc deprotection, followed by amide coupling with **162**, gave the desired compound **148** in 22% yield over two steps (Scheme 16).



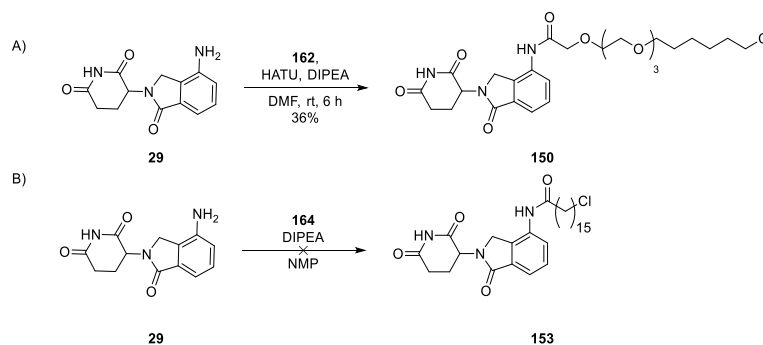
**Scheme 16:** Synthesis of a bardoxolone based KEAP1 recruiting HaloPROTAC **148**.

A HaloPROTAC based on a DCAF15 binder was also synthesised. Indisulam amine analogue **115** which was used in the previous chapter, was therefore converted into a HaloPROTAC as an analogous method of degradation assessment. This was achieved in a 39% yield from the chloroalkane acid **162** in an amide coupling to give the DCAF15 PROTAC **149** (**Scheme 17**).



**Scheme 17:** Synthesis of DCAF15 recruiting HaloPROTAC **149**.

Cereblon based HaloPROTACs were also designed and the synthesis for both compounds was attempted. The PEG derivative was synthesised from the acid **162** in an amide coupling to give the lenalidomide based HaloPROTAC **150** in 36% yield (**Scheme 18A**). The all-methylene cereblon HaloPROTAC **153** was also attempted to be synthesised in an analogous manner to the other all-methylene linked variants (**Scheme 18B**). The reaction went in a moderate conversion but attempts to purify the compound **153** (reverse phase chromatography, MDAP, and normal phase chromatography) all led to the glutarimide hydrolysis, and the desired compound could not be isolated and the compound **153** was abandoned due to chemical instability.



**Scheme 18:** Attempted synthesis of cereblon recruiting HaloPROTACs **150** (A) and **153** (B).

With all the HaloPROTACs **11a**, **144–153** in hand, the GFP degradation assay could therefore be evaluated and optimised for its potential as a novel phenotypic screen.

### 6.3.2 Biological Evaluation of VHL Recruiting HaloPROTACs

In order to evaluate the GFP degradation assay, the designed and synthesised HaloPROTACs were utilised to assess both the HeLa cell lines used for the assay: the GFP-HaloTag® cell line and the GFP-HaloTag® mutant cell line. The evaluation for known and validated E3 ligases would be used to determine if the two cell lines could be utilised in a HTS phenotypic screen to find new chemical matter for E3 ligase for the PROTAC approach.

The VHL recruiting HaloPROTAC **11a**, a known degrader of the GFP-HaloTag® was evaluated in both cell lines. In order to assess the efficiency of GFP degradation, a time course study was carried out with this HaloPROTAC **11a**. This was to determine the best pre-incubation time to facilitate good GFP knockdown and ensuring the longer incubations did not lead to cell viability issues as compound cytotoxicity would increase with time. The compound **11a** was therefore tested in both the GFP-HaloTag® and the GFP-HaloTag® mutant cell lines at 3 different time points, 18 h, 48 h, and 72 h (**Figure 101**). Fluorescence was measured using a PHERAstar end-point fluorescence reader, and then converted to a percentage of GFP remaining by normalising the effect between the DMSO control and removing the background fluorescence achieved using HeLa parental cells. It was found that the compound **11a** had concentration dependent reduction in GFP and pleasingly, the GFP-HaloTag® mutant cell line showed no effect as expected, indicating this was through the recruitment of VHL as a result of the chloroalkane HaloTag® covalent modification. It was also observed that good degradation was achieved at 18 h with 60% reduction with  $DC_{max}$  of 1  $\mu$ M, but incubation for 48 h gave robust and almost complete reduction in GFP with the compound **11a** with  $DC_{max}$  of >90% at 1  $\mu$ M and  $DC_{50}$  of 50 nM. 72 h also gave a robust knockdown of GFP, but this

incubation time may be too long in cases for additional compounds which might be cytotoxic, leading to cell viability issues.

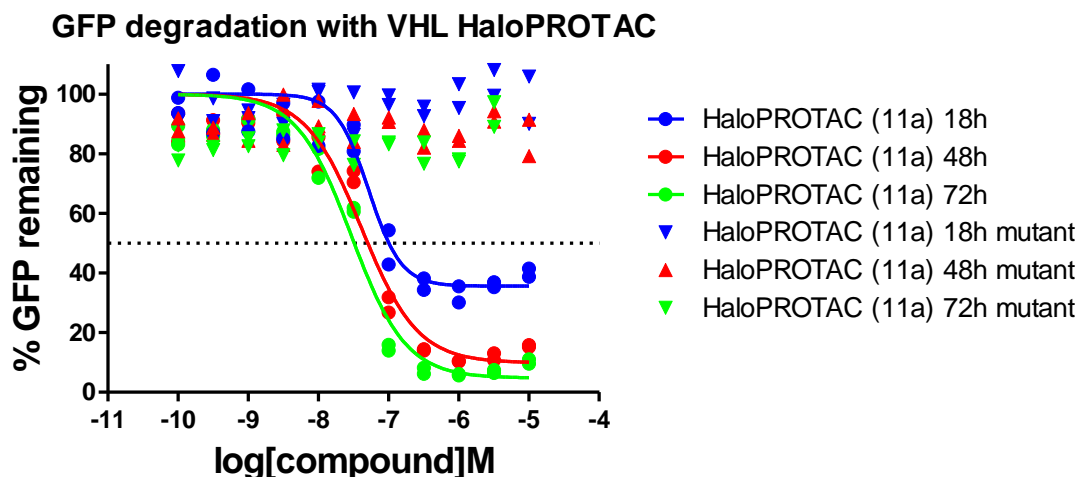
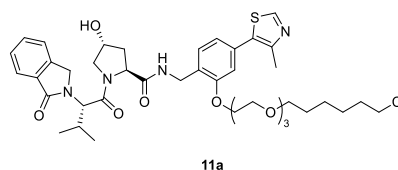
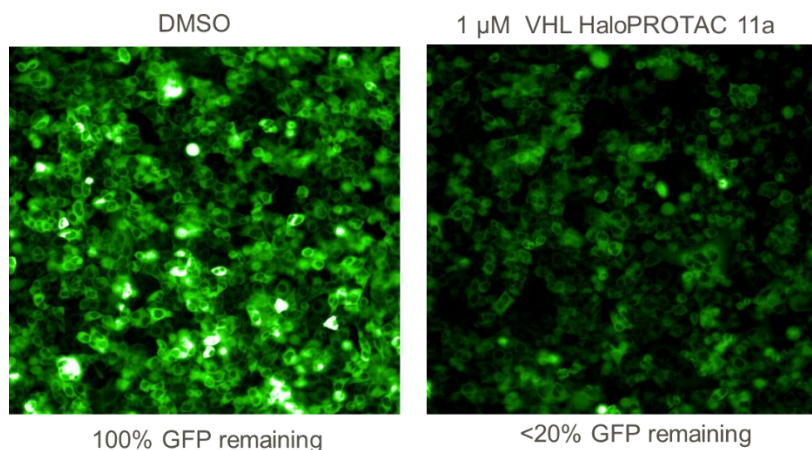


**Figure 101:** Degradation of GFP with VHL recruiting HaloPROTAC **11a** using PHERAstar endpoint reader, with time points 18 h, 48 h and 72 h using both the GFP-HaloTag® cells and the GFP-HaloTag® mutant control cells (n=2).

In addition to the end point fluorescence reader, the GFP degradation could also be measured by in-cell imaging (**Figure 102**). Fluorescence can be measured from images of the cells from the DMSO control and compared to the dosed cells with the compound **11a** (**Figure 102A**). The results from the in-cell imaging can be compared to the end point fluorescence reader and they show excellent correlation (**Figure 102B**). The end point reader is a simple fluorescence read out, which can be done on a 384-well plate in just 2 minutes, whereas the in-cell imaging takes photographs of the cells to analyse and takes 10 minutes per 384-well plate. As a result, moving forward, 48 h incubation will be used as standard, with the PHERAstar end point reader used unless specified. Imaging will be used to determine cell morphology and will be discussed further.

A)



B)

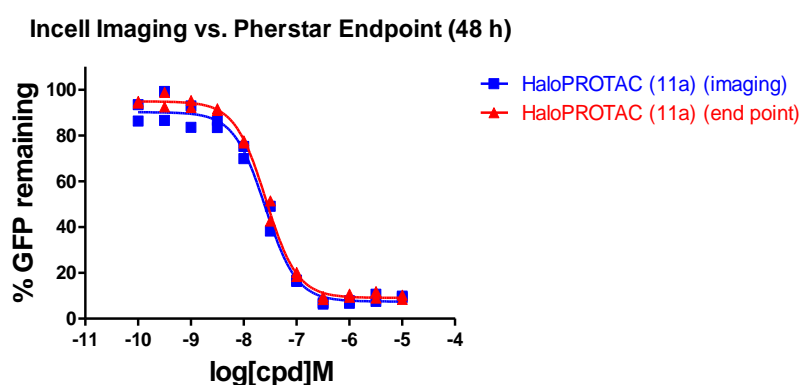
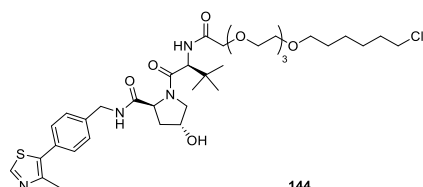
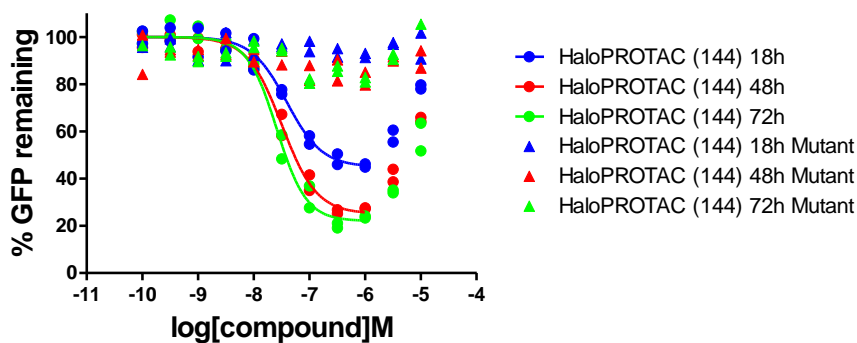


**Figure 102:** Images from the in-cell analyser show the effect of 1  $\mu\text{M}$  after 48 h VHL recruiting HaloPROTAC **11a** versus the DMSO control (A). Analysis in the end reader and the in-cell imaging were carried out for HaloPROTAC **11a** after 48 h incubation (B) (n=2).

The other VHL HaloPROTAC **144** was also incubated in the assay with the same time points. As previously observed with the VHL recruiting HaloPROTAC **11a**, there is a time dependence in GFP reduction with the VHL recruiting HaloPROTAC **144** (**Figure 103**). With 18 h incubation a  $\text{DC}_{\text{max}}$  of 65% at 1  $\mu\text{M}$  and  $\text{DC}_{50}$  of 208 nM was observed. Incubation for 48 h gave a more robust  $\text{DC}_{\text{max}}$  of 75% knockdown at 316 nM and  $\text{DC}_{50}$  of 53 nM. Interestingly, in this example, the hook effect is evident, whereas with the other VHL recruiting PROTAC **11a**, this is not observed. This is also observed in the publication of the HaloPROTACs with different linkers **12a/b**. This was hypothesised that this was due to the protein complex formation, and suboptimal binding of the two halves of the HaloPROTAC, leading the hook effect where binary binding may be preferred.<sup>63</sup>

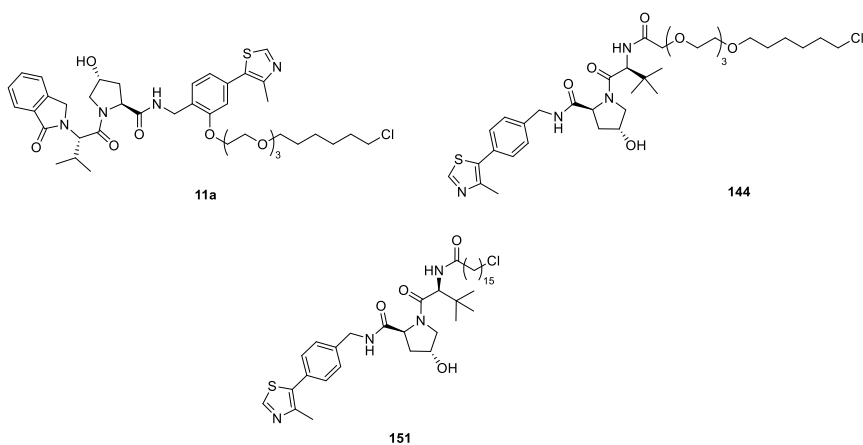


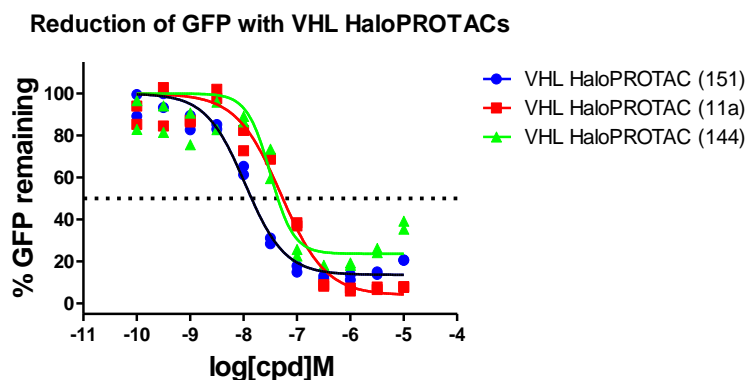
## GFP degradation with VHL HaloPROTAC



**Figure 103:** Degradation of GFP with VHL recruiting HaloPROTAC **144** using PHERAstar endpoint reader, with time points 18 h, 48 h and 72 h using both the GFP-HaloTag® cells and the GFP-HaloTag® mutant control cells (n=2).

The all-methylene derived-linked VHL recruiting HaloPROTAC **151** was also tested in the GFP degradation assay. This was also tested alongside the other VHL recruiting HaloPROTACs **11a** and **144** and gave excellent degradation, with an improved  $DC_{50}$  over the other PEG-linked counterparts of 14 nM (**Figure 104**). However, this compound **151** has a very high ChromLogD of 9.3 and no measurable solubility, so this linker was down prioritised unless cell permeability is viewed as a real concern. Despite the poor physicochemical parameters of the compound **151**, it does show good GFP knockdown, suggesting the compound **151** is freely available in the cell, and not only associated with the cell membrane - which is a common issue with highly lipophilic compounds. This led to an increased confidence that a range of linker lipophilicities can be employed where required for the syntheses of HaloPROTACs with good overall permeability in future.

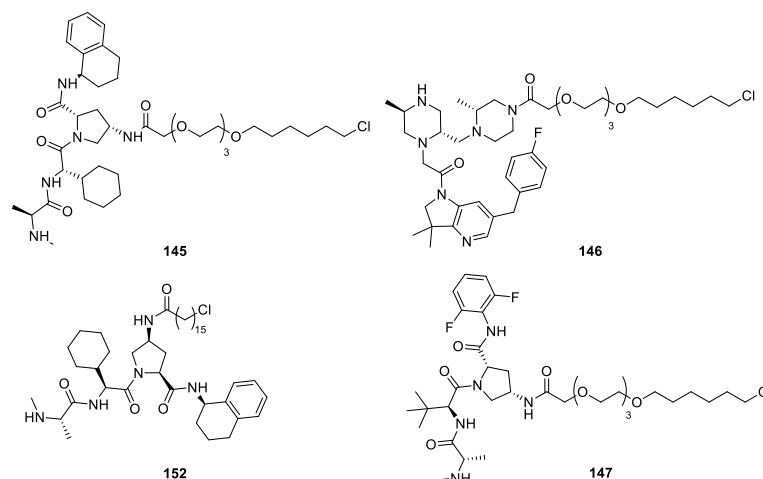




**Figure 104:** Degradation of GFP with all three VHL recruiting HaloPROTACs **151**, **11a**, **144** (n=2).

### 6.3.3 Biological Evaluation of IAP Recruiting HaloPROTACs

Before IAP evaluation in the GFP degradation assay, the compounds binding potencies were determined. The IAP recruiting HaloPROTACs **145–147** and **151** were therefore tested for binding to XIAP (BIR2 and BIR3 binding domain) and to cIAP1 (BIR3 binding domain), **Table 6**. In line with their expected binding from the small molecule counterparts, IAP recruiting HaloPROTACs **145**, **146** and **151** show binding to both XIAP and cIAP1 BIR3, with selectivity over the XIAP BIR2 domain. They bind to cIAP1 with high affinity, with a pIC<sub>50</sub> of ~8. The all-methylene derivative **151** has lower binding, possibly a result of low solubility (due to the methylene chain) which could impair the results (in-line with a reduction of all three binding potencies from the PEG chain derivative **145** with the same binder). The more XIAP selective HaloPROTAC **147** shows good binding to XIAP BIR2 with a pIC<sub>50</sub> of 6.9. This molecule **147** shows reduction in cIAP1 binding from the traditional IAP motifs which are typically around pIC<sub>50</sub> 8 to now just pIC<sub>50</sub> 6.4. This reduction in binding should be sufficient to prevent the cIAP1 self-ubiquitination at lower cellular concentrations. As cIAP auto-ubiquitination causes degradation of cIAP1 and subsequent cellular apoptosis,<sup>111</sup> this molecule **147** should be recruit XIAP and include a higher efficacious window between degradation and cytotoxicity.

**Table 6:** Biochemical potencies of IAP recruiting HaloPROTACs **145–147** and **151**.

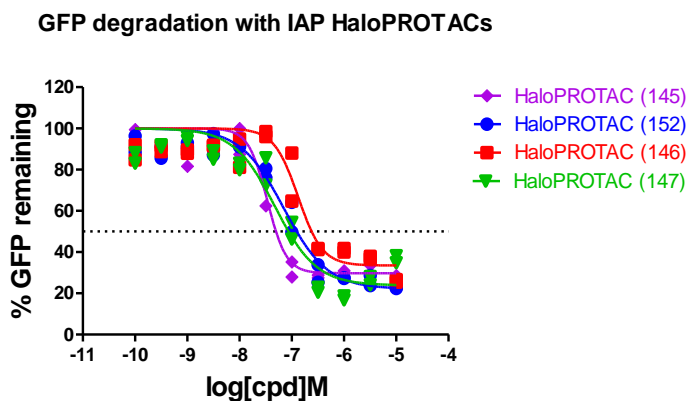
Compound	145	146	147	151
<b>BIR2 XIAP</b> <b>pIC<sub>50</sub> (n=2)</b>	5.7	<4	6.9	<4
<b>BIR3 XIAP</b> <b>pIC<sub>50</sub> (n=2)</b>	7.6	7.5	4.7	7.0
<b>BIR3 cIAP1</b> <b>pIC<sub>50</sub> (n=2)</b>	8.2	8.0	6.4	7.3

The IAP recruiting HaloPROTAC compounds **145–147** and **151** were then tested for the previously determined optimal time of 48 h in the GFP-HaloTag® cells with increasing concentrations (**Figure 105A**). The compounds **145–147** and **151** all show good levels of degradation in the GFP-HaloTag® cell line, with DC<sub>50</sub> of 41 nM for HaloPROTAC **145**, and between 100–150 nM for HaloPROTACs **146**, **147** and **151**. There is no additional GFP reduction observed with the all-methylene compound **151** suggesting the permeability of the PEG derived compound **145** is sufficient despite the basic amine centre which may have impaired this. This is hypothesised due to both the lipophilic side chains in the IAP binder, along with the lipophilic chloroalkane.

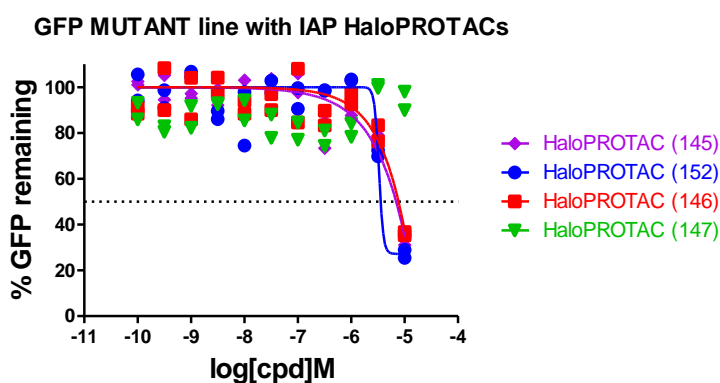
The compounds were also incubated in the GFP-HaloTag® mutant control cell line, to determine if GFP reduction was via a PROTAC or cytotoxic effect. The results from all HaloPROTACs are therefore compared to the mutant cell line, which pleasingly correlates very well with the IAP selectivity profiles (**Figure 105B**). The compounds which are bind to cIAP1 strongly (selective or dual with XIAP) **145**, **146** and **151** show apparent cytotoxicity with the

GFP-HaloTag® mutant cell line at high concentrations. The compounds **145**, **146** and **151** show degradation corresponding to likely apoptosis at 3  $\mu\text{M}$  and 10  $\mu\text{M}$ . In correlation with binding selectivity, the compound **147** which only binds to cIAP1 at higher concentrations shows little toxicity in the GFP-HaloTag® mutant. This adds to the hypothesis that the apparent toxicity is likely due to the cIAP1 pharmacology of apoptosis leading to cell death and GFP levels reducing. A fully XIAP selective compound would be required to confirm this effect. Despite the cytotoxicity observed at higher concentrations, the results show that there is a clear differentiation between PROTAC-driven GFP reduction, observed at lower concentrations, compared to cytotoxicity effects at higher concentrations. This illustrates there is an activity window between the PROTAC-driven effect and cytotoxicity as hypothesised. This suggests that evaluating cytotoxicity with future compounds at higher concentrations is essential to ensure the GFP reduction is a PROTAC specific event. In addition to the mutant cell line, other methods of cytotoxicity were then evaluated.

A)

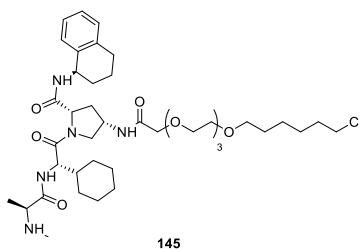


B)



**Figure 105:** Degradation of GFP with IAP recruiting HaloPROTACs **145–147** and **151** (A) (n=2). Testing the same compounds in the GFP-HaloTag® mutant line indicating some of the compounds are cytotoxic (B) (n=2).

By using incell imaging, the morphology of the cells can be investigated. With the IAP recruiting HaloPROTACs that showed nonspecific GFP reduction in the GFP-HaloTag® mutant cell line as a result of apoptosis, cell images were taken and analysed. An example in **Figure 106** shows the IAP recruiting HaloPROTAC **145**. As the images clearly show, the cells are very small and round, indicating apoptosis. This is a clear outcome that the IAP recruiting HaloPROTACs are cytotoxic at higher concentrations.



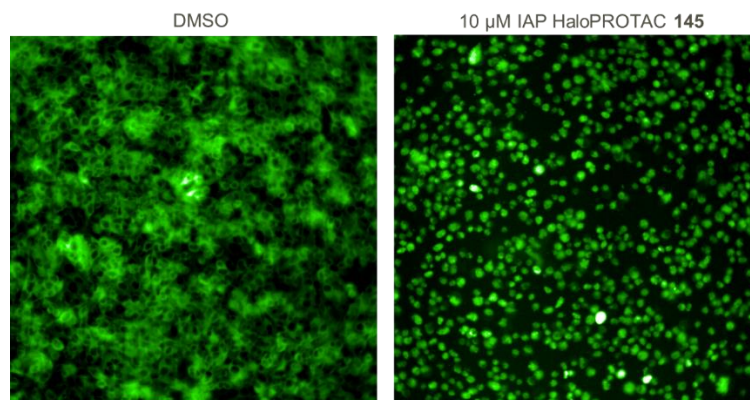
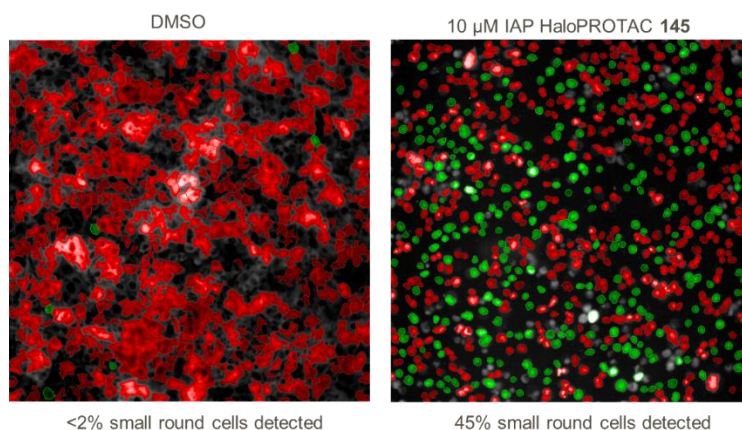


**Figure 106:** Analysis of GFP-HaloTag® HeLa cells, DMSO control (left) and 10 µM IAP recruiting HaloPROTAC **145** (right).

In order to establish if compounds are cytotoxic in this GFP-HaloTag® HeLa cell line without having to physically look at the images well by well, an imaging algorithm was used to detect small round cell morphology (**Figure 107A**). The images show the algorithm is able to distinguish between healthy cells (DMSO, red) and the small round apoptotic cells (green) after compounds treatment, with 45% small cell detected with 10 µM of IAP recruiting HaloPROTAC **145**. Using this algorithm to determine the cytotoxic effects of the IAP recruiting HaloPROTACs, can be displayed as a percentage of small cell formation after compound treatment (**Figure 107B**). This correlates well with the GFP-HaloTag® mutant cell line, where cytotoxicity as a result of apoptosis is observed predominately at the higher concentrations. At concentrations of 3 µM and 10 µM the compounds **145**, **146** and **151** are shown to be cytotoxic (with more than 25% small cells). At concentrations less than 500 nM, the compounds **145**, **146** and **151** are less likely to cause IAP-driven apoptosis. Compounds **145**, **146** and **151** have  $DC_{50}$  values below this level, indicating there is a window for degradation before apoptosis occurs. With the XIAP compound **147**, it is worth noting that in the GFP-HaloTag® mutant line, they showed no adverse effects, but in the imaging algorithm its clear the compound **147** is starting to induce apoptosis on a small population of the cells at 10 µM incubation. This is consistent with the binding profile of this compound, as at higher concentrations it's more likely to bind to cIAP1 and cause apoptosis as a result. This may be due to the GFP-HaloTag® mutant cell line not being a perfect control cell line, as the two cells lines are genetically very similar, but they may have slightly different responses to cytotoxic compounds due to their non-identical nature. The slight discrepancy between the two formats of determining cytotoxicity, suggests that both the GFP-HaloTag® mutant cell line and the imaging algorithm in the GFP-HaloTag® line should be used in parallel in future screens.

A)



B)

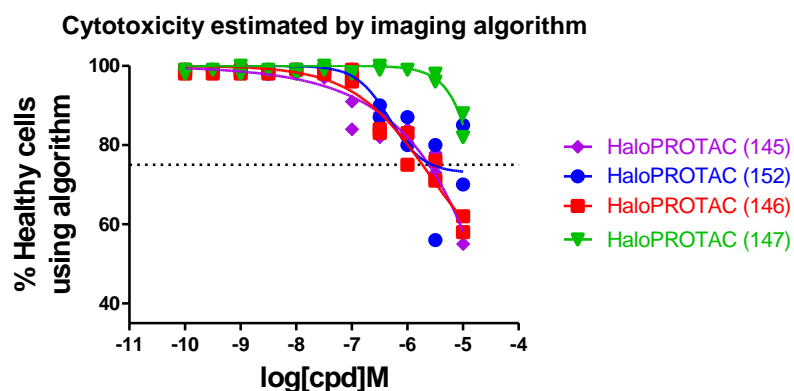
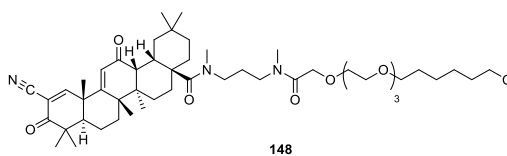


**Figure 107:** Imaging algorithm used to detect small round cells (green) with DMSO control and after treatment with IAP recruiting HaloPROTAC **145** (A). Imaging algorithm in % small cells of each of the IAP recruiting HaloPROTACs **145–147** and **151** (B) (n=2).

#### 6.3.4 Biological Evaluation of KEAP1 Recruiting HaloPROTACs

In addition to the IAP compounds, which were both active HaloPROTACs and cytotoxic, a positive cytotoxic HaloPROTAC control was investigated. The Bardoxolone based HaloPROTAC **148** was therefore tested in the GFP degradation assay. After 48 h incubation the compounds reduced GFP levels at less than 1  $\mu$ M in a concentration dependent manner (**Figure 108**). In the GFP-HaloTag® mutant cell line, the reduction was also observed, with no difference in the EC<sub>50</sub> for the molecule, suggesting the GFP fluorescence reduction is due to cytotoxicity exclusively, unlike the IAP counterparts **145–147**, where induced degradation and apoptosis were both involved. This was therefore deemed a good positive control for

cytotoxicity for the imaging algorithm development alongside the IAP recruiting HaloPROTACs.



**GFP degradation by KEAP1 HaloPROTACs**

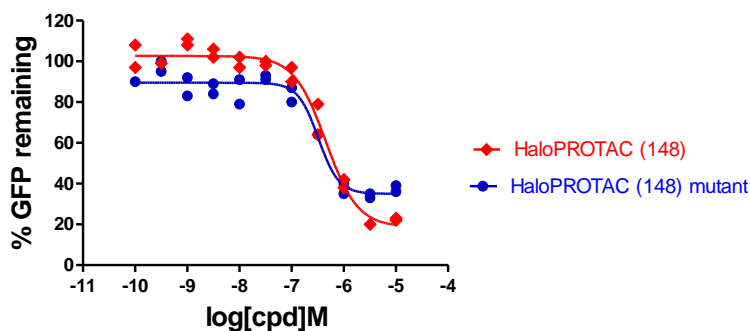


**Figure 108:** GFP levels after incubation of KEAP1 HaloPROTAC **148** in the GFP-HaloTag® and GFP HaloTag® mutant cell line after 48 h incubation (n=2).

The compound **148** was then tested in an imaging format to identify if the cells in the experiment had reduced in number or size (**Figure 109**). As expected, the cells had depleted in number and altered shape, changing from their usual morphology to small and round, indicative of apoptosis. This was also used as a tool to determine if the algorithm from the imaging analysis was able to identify those cells and was successful in drawing the conclusion that the cells were round (green) compared to the healthy cells (shown in red). This compound **148** proved a useful tool in the analysis preparation for a larger screen for this assay, and through the software analysis of KEAP1 and IAP recruiting HaloPROTACs, cytotoxic compounds could be recognised in future without searching for those compounds individually through the use of this imaging algorithm.

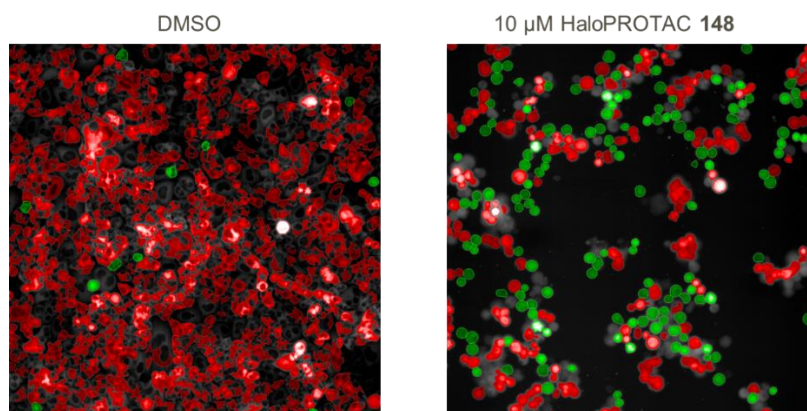
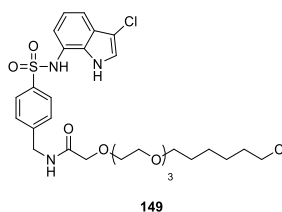


**Figure 109:** Imaging of GFP-HaloTag® cells after 48 h incubation with either DMSO or 10  $\mu$ M of the HaloPROTAC **148** to determine small round cells (green) versus healthy normal cells (red).

### **6.3.5 Biological Evaluation of DCAF15 Recruiting HaloPROTACs**

DCAF15, an E3 ligase investigated in the previous chapter, was investigated in this GFP degradation assay. As expected, correlating to the results in the previous chapter, no degradation was observed with the DCAF15 recruiting HaloPROTAC **149** (**Figure 110**). GFP reduction was observed at the higher concentrations, corresponding to the cytotoxicity observed with the small molecules in cancer cell lines. A hypothesis for the observed cytotoxicity may be due to CAPER $\alpha$  degradation as a result of DCAF15 and CAPER $\alpha$  forming a molecular glue binding pair leading to cell instability. This result illustrates further that this binder **115** is not suitable for use in the PROTAC approach, in an analogous manner to using the promiscuous toolbox. As previously described in Chapter 5, further investigations into DCAF15 binding and X-ray crystallography would be required to ensure the indisulam analogue could still bind to and recruit the E3 ligase DCAF15.



### GFP test with DCAF15 HaloPROTACs

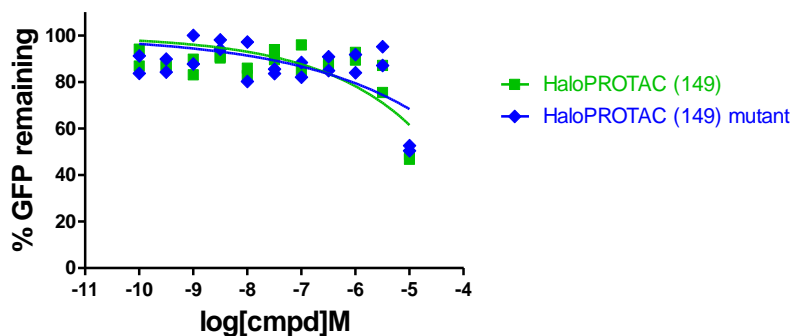
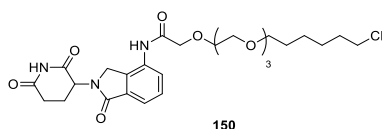


**Figure 110:** GFP levels after incubation of DCAF15 HaloPROTAC **149** in the GFP-HaloTag® and GFP HaloTag® mutant cell line after 48 h incubation (n=2).

### 6.3.6 Biological Evaluation of Cereblon Recruiting HaloPROTACs

As cereblon has previously not been utilised in GFP degradation, a cereblon recruiting HaloPROTAC was designed and tested in the GFP degradation assay. The PEG-linked compound **150** was incubated with both the GFP-HaloTag® cell line and the GFP-HaloTag® mutant line (**Figure 111**). Unfortunately, only minor degradation was observed, and was also observed in the mutant line, corresponding to either cytotoxicity or another protein synthesis/proteasome activating effect. This was not expected, as the traditional 3-EG linker has shown good activity in cereblon recruiting PROTACs previously, and lenalidomide **29** is not known to cause cellular cytotoxicity by binding alone. The lack of GFP degradation in this case could be a result of the instability of the lenalidomide binding motif in the cellular environment,<sup>100</sup> or could be a result of clashing protein-protein interactions in the ternary complex, not allowing for GFP ubiquitination and degradation to occur. This could also be a result of poor permeability of the compound **150**. The compound's ChromLogD was measured at 4.2, with excellent CAD solubility of >519  $\mu\text{M}$ . This was not in the desired tool generation of ChromLogD 5–7, however cereblon recruiting PROTACs have previously shown activity with ChromLogD values of 3–4. As there is lack of a cellular functional assay for cereblon to confirm this as the reason for failure therefore this remains inconclusive. As the aim of the project was to validate the GFP-Halotag cell lines, this was not further evaluated, and could be incorporated in future work with different linkers.



## GFP test with cereblon HaloPROTAC

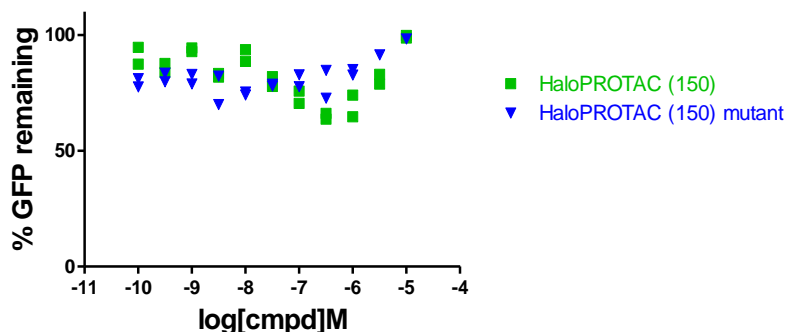


**Figure 111:** GFP levels after incubation of cereblon recruiting HaloPROTAC **150** in the GFP-HaloTag® and GFP HaloTag® mutant cell line after 48 h incubation (n=2).

#### 6.4 Summary and Future Work

The GFP degradation assay was analysed and validated with VHL, IAP and KEAP1 recruiting HaloPROTACs (**Figure 112**). VHL **11a**, **144** showed robust and reproducible degradation in the GFP-HaloTag® cell line and none in the GFP-HaloTag® mutant cell line, showing the latter would be an excellent control cell line for non-specific fluorescence reduction. IAP HaloPROTACs **145–147** and **151** exhibited a window between fluorescence reduction from the PROTAC approach, and reduction from apoptosis at higher concentrations. Together with the nonfunctional cytotoxic KEAP1 recruiting HaloPROTAC **148**, an imaging algorithm was validated to be useful in determining compounds which were causing apoptosis and could be used in future to identify false positives in the assay. As a number of the designed HaloPROTACs were non-functional compounds with regards to protein degradation, and as a result the future screening compounds will be coined HaloCompounds, with HaloPROTACs kept a term exclusively for active degrader molecules. As a result, the KEAP1 **148**, DCAF15 **149** and cereblon **150** compounds would also be deemed HaloCompounds in future.

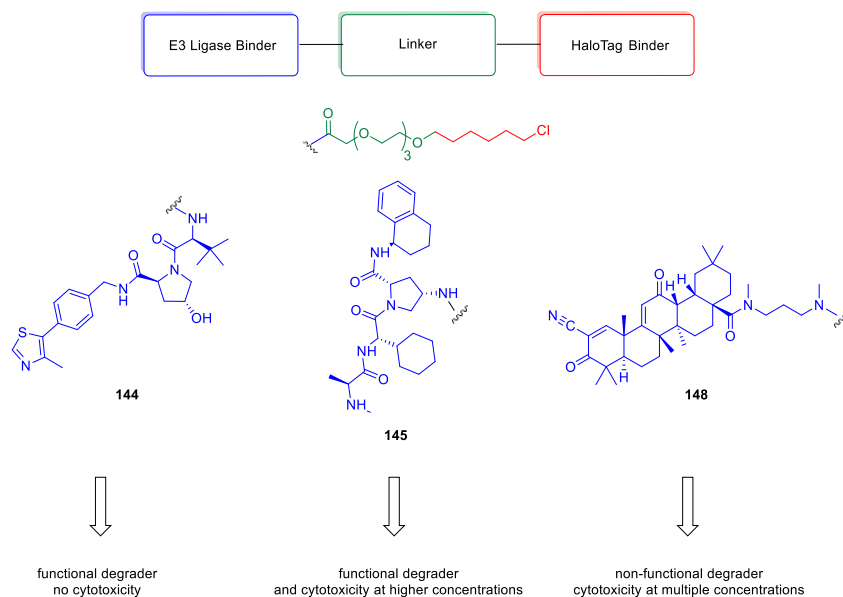


**Figure 112:** HaloPROTACs used to validate to validate the two cell lines in the GFP degradation assay.

The lack of degradation observed with the cereblon HaloCompound **150** is indeed a caveat of this approach, as one linker may not permit the degradation of GFP in the search for new E3 ligases in a larger screen. This could be further evaluated with a toolbox of Halo-linkers, including different linker lengths and chemical composition, which would increase the ChromLogD if permeability was the overall issue with the compound.

With the success of VHL and IAP with this 3-EG linker, it was hypothesised that the probability of finding new E3 ligase binders could be sufficient if the numbers of HaloCompounds tested was sufficiently large. As a result, the validation of the HaloCompound platform screening, utilising two cell lines, imaging cytotoxicity algorithms with several validated E3 ligases, was deemed successful. This could therefore be utilised with high-throughput experimentation to develop a HTS HaloCompound screen to expand the set of E3 ligases utilised for the PROTAC approach for drug discovery.

## 7. HaloCompounds and the Search for New E3 ligases Using HTE

### 7.1 Introduction – High-Throughput Experimentation

In order to synthesise many thousands of compounds in a time-efficient manner, high-throughput chemistry would be explored and utilised. High-throughput chemistry, also known as high-throughput experimentation (HTE) has been transformed in the last 20 years. This was originally established as combinatorial chemistry,<sup>189-192</sup> and more recently high-throughput chemical screening technology has been pioneered by both academia and industry.<sup>193-201</sup><sup>189,191,202-212</sup> In contrast, high-throughput screening in biological sciences has been embedded into the pharmaceutical industry, with many millions of compounds and numerous assay formats routinely used.<sup>213</sup> More recently this has started to be adopted into the chemical sciences. Cernak and others have shown the utility of screening 96-well plates in chemistry to be able to optimise and screen multiple catalysts/ligands/solvents to array the largest area of space to understand the specific chemical processes (**Figure 113**).<sup>205</sup> This can be performed with cheminformatics software and machine learning to gain a deeper understanding of chemical reactivity and to predict reactions which are more likely to work.<sup>206,214,215</sup> HTE was exploited at Merck as a method to screen for hydrogenations for the synthesis of drug candidates in process chemistry over 15 years ago,<sup>205</sup> and has since been embedded in their methodology toolbox for drug discovery. More recently, Cernak showed the extension to using 1536-well plates employing methods already adopted by the biological sciences to perform nanoscale synthesis<sup>216</sup> and be able to implement this in an ASMS screening cascade.<sup>217,218</sup> The ASMS strategy used unpurified reaction mixtures to test for compound binding which would be expected to be unsuitable in a traditional protein binding assay where by-products and catalysts could confound the result. This methodology has not yet been employed wider in biological screening, such as cellular screening, due to the logistical challenge of purifying hundreds of compounds.

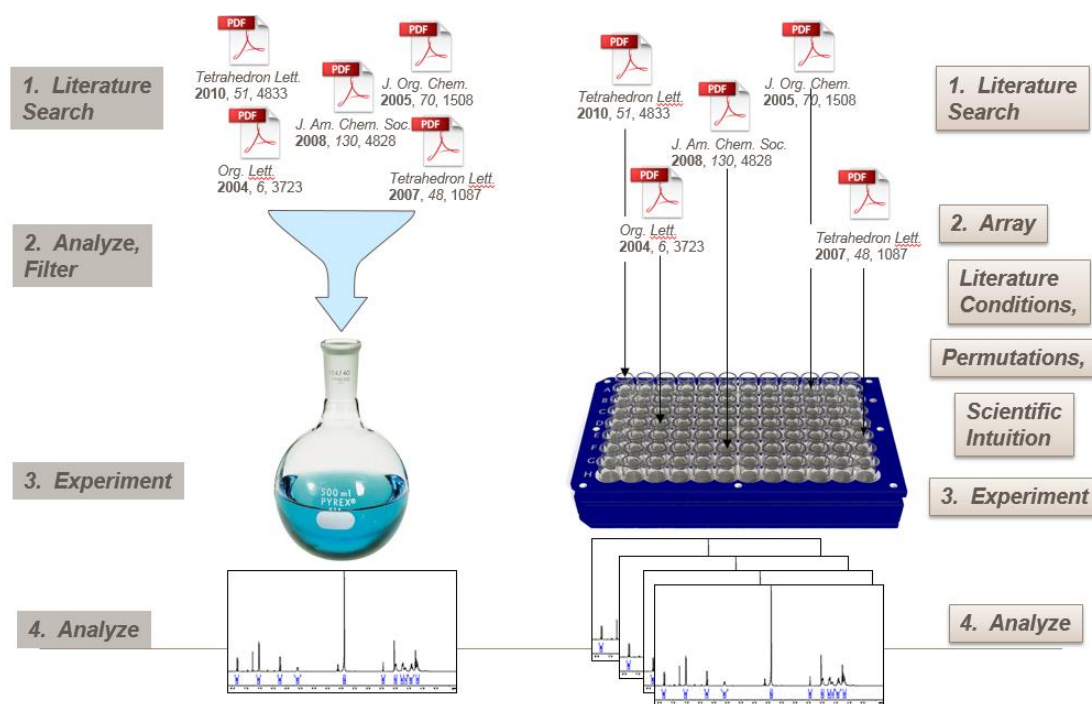


**Figure 113:** Traditional experimentation versus rationally designed HTE.

Plate-based chemistry is not without its challenges. Accurately weighing out small amounts of solid material is challenging. Robotics have been employed to dose solid materials with state-of-the-art weighing balances to control the accuracy. However, varying densities of solids mean that solid dispensing robotics are challenging to standardise. In addition, solids which are not a fine free-flowing powders pose issues during the dispense. As a result, dispensing stock solutions are preferred in place of solid dispensing and is featured in many HTE approaches. Application of liquid handling robots and automated electronic pipetting dispensers allow stock solutions to be used with ease with the caveat that this method can only be utilised for homogenous solutions with accuracy. Dispensing non-homogenous mixtures (such as catalyst slurries) can be performed, but absolute quantities of material in the reaction may not be known and may confound quantitative results. There are also limitations with respect to carrying out the reactions. For example, the majority of examples of HTE using 384- and 1536-well plates have been performed at room temperature using only high boiling solvents which are compatible with polypropylene based plates.<sup>204,205</sup> This has recently been addressed by the utilisation of glass plates which can be sealed and temperature controlled, but currently this is an extremely expensive and bespoke technique.<sup>217</sup> The surface area of the reaction mixtures also needs to be considered. The surface area to volume ratio increases with a decrease in scale resulting in increased sensitivity to atmospheric oxygen and water. Consequently HTE is generally carried out in a glovebox under a nitrogen or argon atmosphere to mitigate this issue<sup>216,218</sup> and highlights the careful consideration into

experimental design and procedures which needs to be considered when utilising plate-based chemistry.

Analytical and purification techniques are not yet developed sufficiently to cope with the capacity that high-throughput experimentation brings, although there is progress. In order to analyse many hundred to thousands of reactions, Merck & Co. frequently use MISER (Multiple Injections in a Single Experimental Run)<sup>206,218</sup> LCMS techniques. This generates qualitative data on reaction progress with a run time of just 10s per sample. More recently, academic groups have shown the use of MALDI-TOF methods to be able to analyse HTE rapidly.<sup>219</sup> Merck & Co. have recently utilised this along with mass spectrometry advancements in an ultra high-throughput fashion.<sup>217</sup> Using liquid handling robotics techniques from the reaction plates to the MALDI spotting plates (30 minutes per 1536-well plate) with a MALDI run time of just 11 minutes per plate using an ultra fast laser process developed by Bruker and GSK.<sup>220</sup> This, in conjunction with suitable internal standards, will allow semi-quantitative results based on molecular TOF. In order to achieve more quantitative data LCMS or HPLC techniques with a 2-minute run time have to be employed with internal standards (13 h per 384-well plate). This therefore would represent a bottle neck in the process with many thousands of reactions. As a result, a combination of qualitative (for all the reactions) and quantitative (for a small subset of the reactions) approaches could be utilised in order to reduce the analysis time. After plate analysis, many of the recent HTE publications do not feature purification techniques as these can be extremely difficult on many hundred to many thousands of molecules. However, as a result of progress during the combinatorial chemistry era, many methods are available for purification (although currently only suitable for up to hundreds of compounds) with extraction techniques,<sup>221-223</sup> ion-exchange cartridges to trap basic or acid compounds,<sup>224</sup> or automated preparative HPLC.<sup>225,226</sup>

There are many issues which need to be considered before the implementation of HTE. However, the established techniques offer the possibility of synthesising and characterising many thousands of compounds in a time efficient manner. This was not possible until recently and promises to become an extremely powerful technique for both reaction optimisation and compound synthesis for biological evaluation.

## **7.2 High-Throughput Synthesis of HaloCompounds Project Aims and Objectives**

The aim of this project was to exploit high-throughput experimentation (HTE) to search for chemical matter for new E3 ligase recruitment. In order to search for new chemical matter for the 600 known E3 ligases in an unbiased fashion, a phenotypic cellular screen could be

employed. An example assay cascade is shown in **Figure 114**. Synthesis of compounds could be achieved with the development and optimisation of HTE in 384-well plates, which will be discussed. The compounds could then be evaluated for GFP degradation by utilising the established GFP-HaloTag® HeLa cells. The cells were evaluated by proteomic assessment and were shown to include 50–60% of the known E3 ligases, which was deemed suitable for this assay. In order to differentiate which compounds were induced GFP degradation as a result of the PROTAC approach rather than another mechanism, the compounds would also be tested in the GFP-HaloTag® mutant control cell line. In addition, imaging software could also be utilised to assess the compounds' impact on the cellular morphology in order to remove cytotoxic compounds which cause the cells to become small and round, indicative of cellular apoptosis. The compounds which show specific fluorescence reduction and no cytotoxicity could then be analysed in target deconvolution studies, using the Cellzome platforms previously described. This could include using affinity enrichment proteomics to identify the proteins which are bound by the compound.<sup>126,127,161,162</sup> Hits could be further evaluated with additional PROTAC synthesis, performed using the promiscuous toolbox described in chapter 5. This would increase the confidence that the compounds which were found to degrade GFP, could degrade other POI, such as RIPK2, BTK or BRD4 as a result of potential new E3 ligase recruitment. This would therefore, be a fast and information rich method to identify chemical matter for E3 ligases for the PROTAC approach.

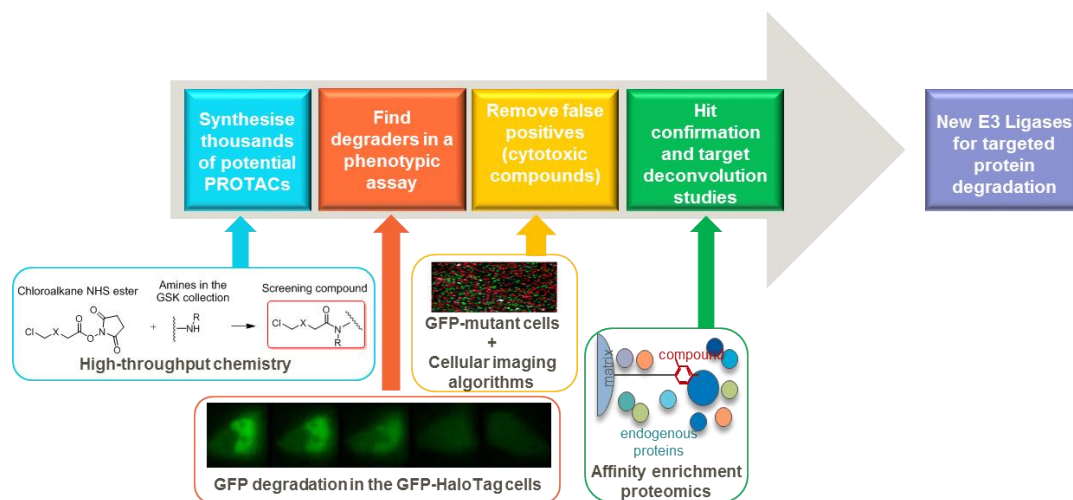


**Figure 114:** Assay cascade proposed for the search for new E3 ligases: *in-situ* synthesis of compounds using high-throughput chemistry, incubation with GFP-HaloTag® HeLa cells. Then use cellular imaging to determine GFP reduction and remove cytotoxic compounds by monitoring cellular morphological changes. Use Cellzome technology, for example affinity enrichment proteomics, for target deconvolution. Synthesise and test PROTACs based on hit compounds using the promiscuous toolbox.

In order for a high-throughput GFP degradation screen to be viable, high-throughput chemistry would require to be validated and subsequently employed to synthesise many thousands of

compounds (**Figure 115**). HTE has currently never been used in a phenotypic assay due to issues with purification of large numbers of compounds which would represent a bottleneck in the process. Consequently, it would be advantageous to test reaction mixtures in this GFP degradation assay to find degraders of GFP. As induced protein degradation is an event driven process, and can only result from fully formed HaloPROTAC molecules, it was hypothesised that degradation could be observed despite testing potentially impure reaction mixtures. If a successful HaloPROTAC was synthesised, but only partial conversion occurred, any unreacted starting materials, including the amine and the linker could compete with the PROTAC for the two binding proteins in the intermediate ternary complex. However, given that the potential E3 ligase binder amine would bind reversibly to the protein, and if the HaloPROTAC was present in sufficient quantity in the cells, the HaloPROTAC would still be able to competitively engage the E3 ligase and subsequently GFP degradation could occur. Impure reaction mixtures would thereby reduce the overall efficacy of the HaloPROTAC molecule, however, the GFP degradation and fluorescence reduction would still be observed. This therefore may be a viable method for finding hit HaloPROTAC molecules which degrade GFP in this assay. Furthermore, to ensure testing reaction mixtures would be suitable for the GFP degradation screen, reactions and different reaction components would be evaluated in the GFP-HaloTag® cells to evaluate the effect on the final outcome. It was envisaged that a high yielding reaction to form these HaloCompounds *in-situ* could be employed and developed. To this effect a high-throughput amide coupling to provide an efficient synthesis of the “HaloCompound” molecules would be explored. The aim of the HTE approach would be to utilise a small-scale reaction in a 384-well plate, such as using 0.100 µmol of the desired starting material (10 µL of a 10 mM stock solution for example). In order to achieve this small-scale chemistry, optimisation with a control amine, such as the amine used in the VHL recruiting HaloPROTAC **144** synthesis, would be used and developed for 384-well plates. Following optimisation, HTE could prove to be an extremely powerful method to synthesise many thousands of potential HaloPROTAC molecules to search for novel functional degraders of GFP.

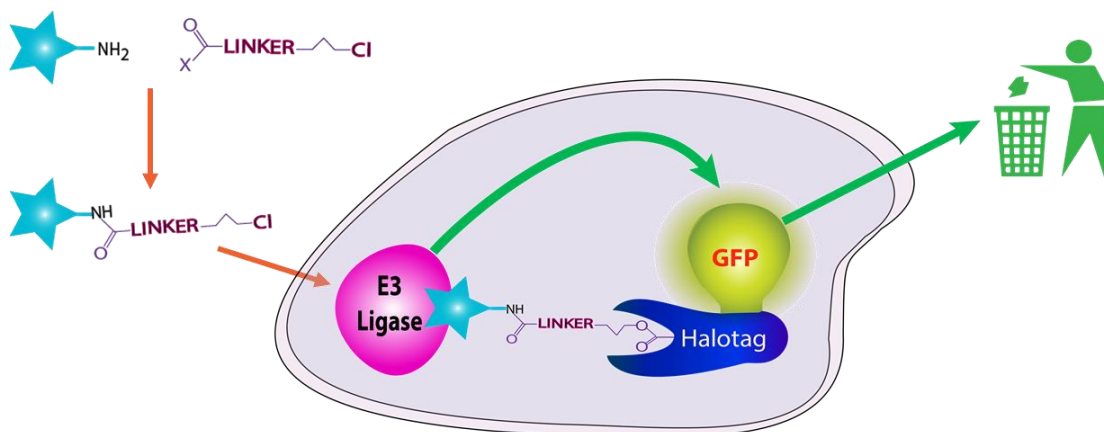


**Figure 115:** The search for new E3 ligases: *in-situ* synthesis of HaloCompounds from amine in the GSK compound collection with an activated ester to install the HaloTag® ligand, and then add compounds to GFP-HaloTag® HeLa cells to investigate GFP degradation as a loss of cellular fluorescence.

Once testing reaction mixtures in the cellular assay was deemed suitable and the chemistry was robust for an exemplar amine, the next aim would be to synthesise and test multiple novel HaloCompounds to screen for new E3 ligases. In order to validate the potential for an HTS screen, the amines required for testing would be split into three screening sets of increasing size to validate the HTE approach and the GFP degradation assay. This would include one to two linker molecules to validate the approach initially. The amines used in these reactions, and subsequent biological screens, would be selected from amines available in the GSK collection. The aim was to utilise physicochemical parameters and chemical diversity of the compounds as a method for selection. This could ensure the HaloCompounds had desired physicochemical properties for future elaboration in drug discovery and also to ensure the compounds would likely be cellularly permeable in order to engage and degrade GFP in the cells. The three sets include: the “optimisation set”, which contained up to 300 compounds, would be used to ensure the chemistry was robust and reproducible in plates for hundreds of compounds (**Figure 116**). The “validation set”, which contained up to 3000 compounds, would evaluate false positive rates and optimise biological test concentrations, to find a balance between good activity from likely suboptimal binders of the E3 ligases, and cytotoxicity. These two sets would then be validated and explored towards selecting the third and final “screening set” suitable for a HTS screen of up to 100,000 compounds to search for new E3 ligase binders. Any hits that arose from the two screening sets, the optimisation and the validation sets, would be evaluated further as previously described in the assay cascade, to determine if they were genuine E3 ligase binders useful for the PROTAC approach before embarking on the HTS screening set.

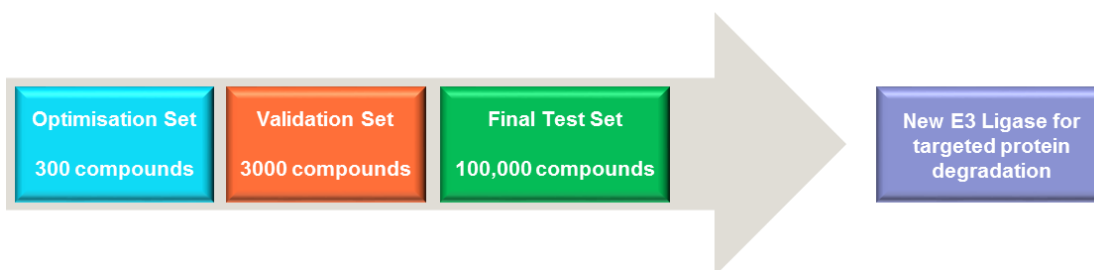


**Figure 116:** Optimisation, validation and final screening sets for the phenotypic screen for the GFP-HaloTag® assay.

## 7.3 Results and Discussion

### 7.3.1 *In-Situ* HaloPROTACs – Validation of Testing Reaction Mixtures

Before developing high-throughput chemistry for the GFP degradation screen, *in-situ* synthesis had to be validated to ensure it was compatible with the assay. Compound purification would not be possible on a large number of compounds, therefore testing reaction mixtures was envisaged as a suitable compromise. As GFP degradation via the PROTAC mechanism is not a binding assay, but instead a functional read-out as a result of event-driven induced protein degradation, it was hypothesised that incomplete reaction conversion would not prevent the compounds from inducing GFP degradation. Impurities may affect the apparent potency of compounds, leading to lower maximal degradation due to binding competition, but positive degraders should be able to be identified in a qualitative manner. As a result, components of the reactions (solvents, starting materials, bases and by-products) would be tested in the GFP-HaloTag® cells.

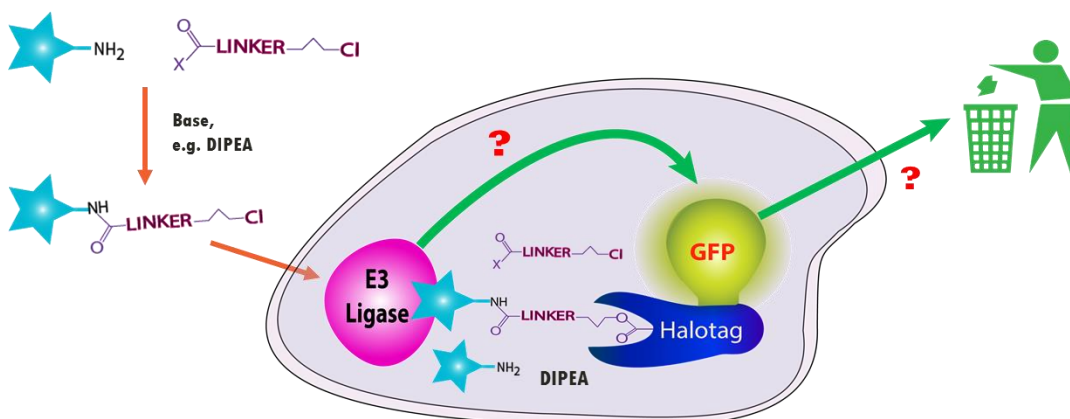


**Figure 117:** High-throughput synthesis of HaloCompounds from an amine and activated ester. This would be treated directly in the GFP cell lines, along with any unreacted amine, remaining activated ester and base and was unknown if it would influence the GFP reduction compared to the purified compound.

In order to develop an efficient reaction to synthesise many HaloCompounds **176** *in-situ*, an amide coupling was chosen with the aim of reacting multiple amines with a single activated ester to create the screening compound set. Following on from the success with the 3-EG linker length in the previous chapter, this was chosen for elaboration into an activated ester for the reaction proof of concept studies. The activated ester which has shown to be robust in amide coupling techniques in 96-well plate format by Cellzome, (used for their on-bead chemistry in affinity enrichment proteomics and TMT labelling)<sup>127,162,227,228</sup> is the *N*-hydroxysuccinimide ester. NHS esters are known to be stable to water hydrolysis, frequently stored in isopropanol and water, so was deemed a suitable ester for this approach. Amines in the GSK collection, as depicted by compound **174**, which would be used in the screen, are stored in DMSO, which is known for its hygroscopic nature, so an NHS ester would be a good choice for this screen to ensure ester hydrolysis was not an issue. As a result, amines **174** would be reacted with an NHS ester derived Halo-linker **175** to synthesise HaloCompounds **176** *in-situ* (Figure 118).

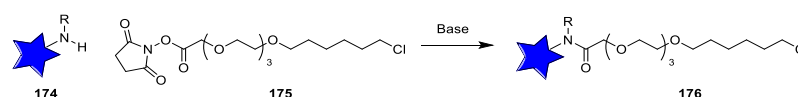
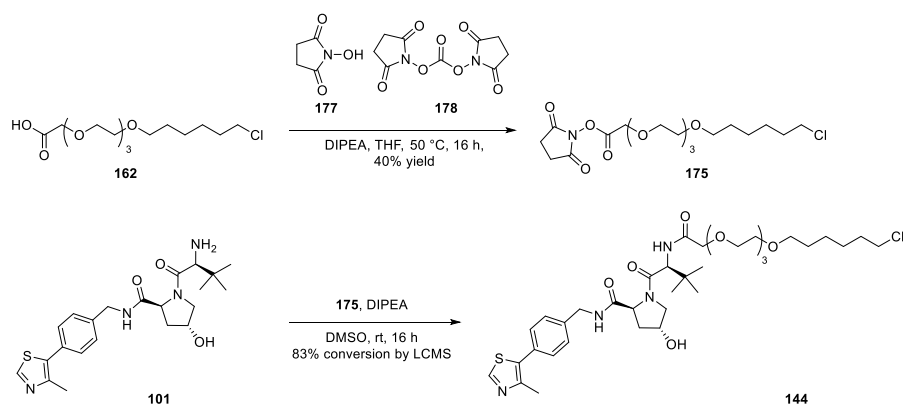


**Figure 118:** NHS Halo-linker **175** chosen for elaboration into HaloCompounds **176** for the GFP degradation screen.

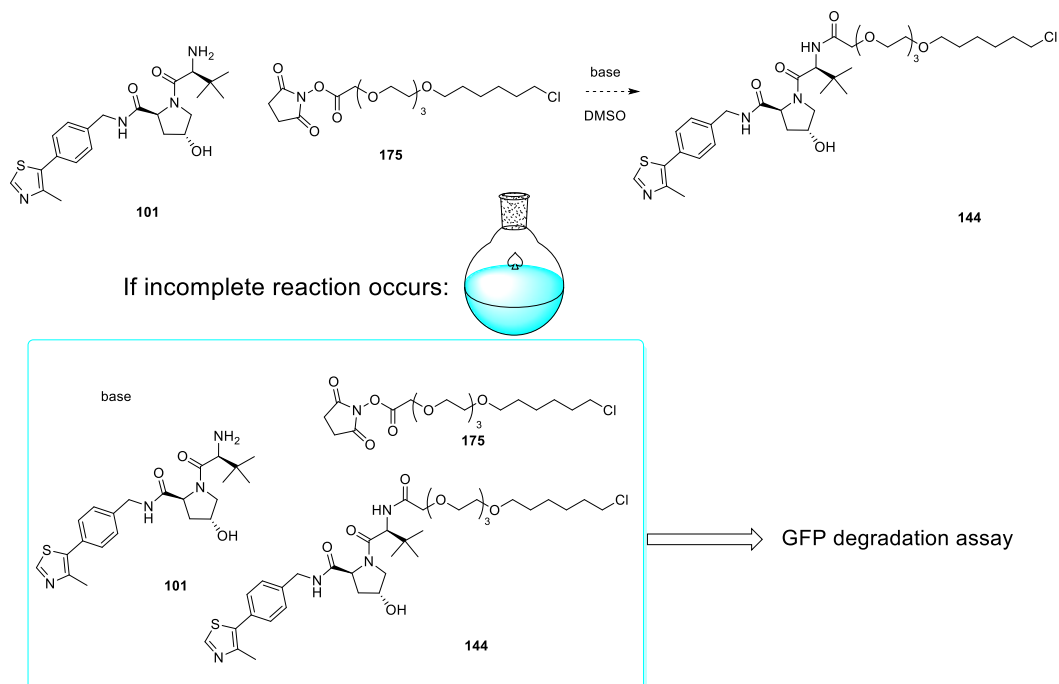
In order to evaluate reaction mixtures in the GFP degradation assay, the validated VHL recruiting HaloPROTAC **144** was synthesised *in-situ* and tested in the two GFP containing cell lines. The VHL recruiting HaloPROTAC **144** was synthesised *in-situ* from a reactive NHS ester Halo-linker **175**. This was prepared from the acid chloroalkane using a *N*-hydroxysuccinimide **177** and *N,N*-disuccinimidyl carbonate **178** to give the NHS ester Halo-linker **175** in a 40% yield (Scheme 19). On a 100  $\mu$ L scale, one equivalent of the VHL amine and 1.2 equivalents of the NHS ester Halo-linker **175** and 3 equivalents of DIPEA as a base were mixed in DMSO (final concentration 5 mM) for 16 h. This was used directly without further purification and analysed by LCMS showing 83% conversion to the desired HaloPROTAC **144**.



**Scheme 19:** Synthesis of *in-situ* VHL recruiting HaloPROTAC **144**.

In order to assess the impact of not purifying the HaloPROTACs, the prepared reaction mixture was tested in the GFP degradation assay alongside the individual reaction components. As the reaction to form the VHL recruiting HaloPROTAC **144** was incomplete and the NHS ester linker **175** was used in excess, the mixture which would therefore be tested in the GFP degradation assay would contain the starting materials, the product and the base (**Figure 119A**). This reaction mixture containing 83% VHL recruiting HaloPROTAC **144** was therefore tested in the GFP degradation assay for 72 h (**Figure 119B**). In addition, the reaction components, DIPEA, *N*-methylmorpholine (another potential base for the chemical reaction) and the NHS ester Halo-linker **175**, were also tested to ensure they would not affect the outcome of the assay (the starting amine was also tested in a subsequent experiment and will be discussed below). The bases and the NHS ester **175** caused no adverse effects on the cells or GFP levels in this experiment. The *in-situ* synthesis of the HaloPROTAC **144** showed potent GFP knockdown, with similar levels of knockdown between the purified and non-purified compounds. The DC<sub>50</sub> of the purified HaloPROTAC **144** is 6 nM and the DC<sub>50</sub> of the reaction mixture is 21 nM showing good GFP reduction despite being only 83% pure with excess linker. This gives good confidence that the assay will show effective GFP reduction in the presence of the starting materials and reaction components without purification.

A)



B)

## GFP degradation with Reaction Components

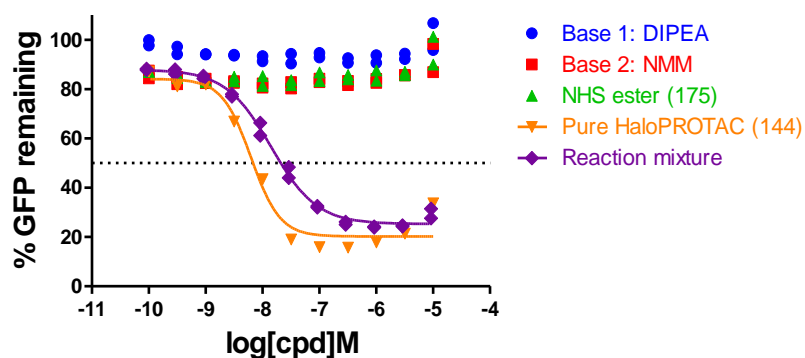


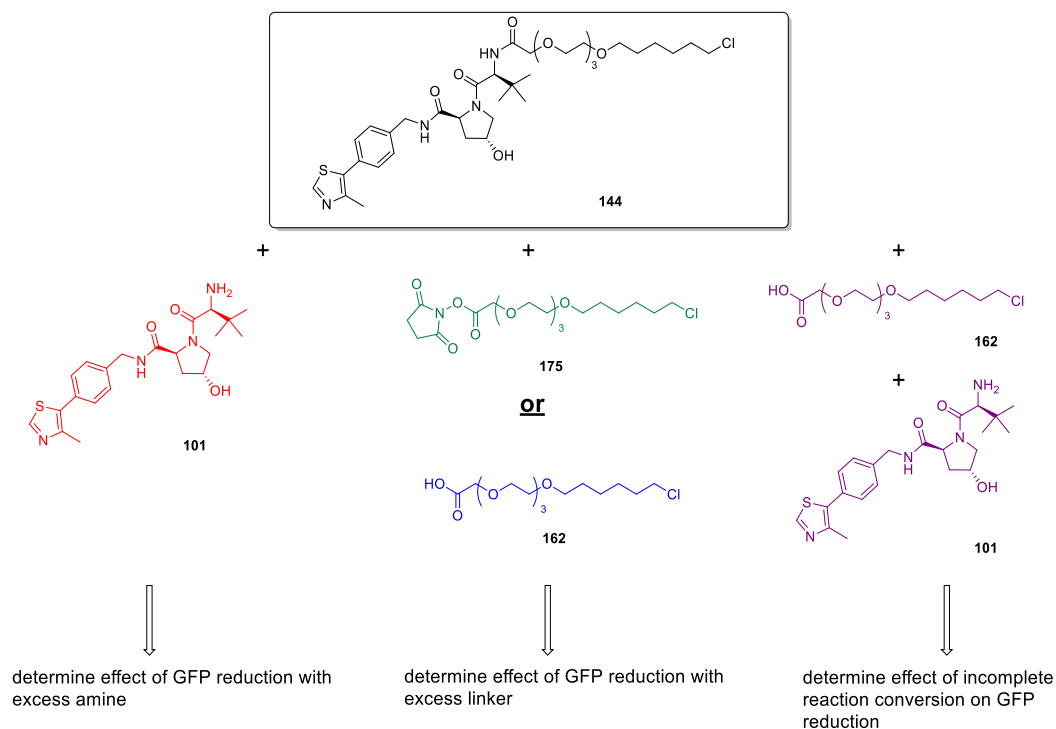
**Figure 119:** Synthesis of VHL recruiting HaloPROTAC **144**, and illustration of the components which would be in the reaction mixture if the conversion was incomplete (A). Testing reaction components versus purified VHL recruiting HaloPROTAC **144** in the GFP-HaloTag® HeLa cells after 72 h incubation (n=2) (B).

In order to assess the impact of different percentages of reaction conversion on the GFP reduction, a competition assay was developed. This experiment was carried out to mimic incomplete conversion for the VHL recruiting HaloPROTAC **144**, which would contain varying levels of the starting material amines **101** and ester **175** in addition to the HaloPROTAC **144** (**Figure 120A**). This would be important on a larger screening set as every reaction would progress to a different extent; this would help identify the estimated conversions required to

elicit a pharmacological response. From previous results, 1  $\mu\text{M}$  test concentration of the purified VHL recruiting HaloPROTAC **144** is the compound's  $\text{DC}_{\text{max}}$  (showing 80% knockdown of GFP). This was therefore used and then combined with increasing concentrations of the other components of the reaction to assess their effect on degradation. The HaloPROTAC was combined with either the NHS ester **175** (green), the chloroalkane acid **162** (blue), and the VHL amine **101** (red) to determine the impact of incomplete conversion (**Figure 120B**). Both the acid **162** and the ester **175** were used in this case to determine if the acid **162** was cell permeable. To mimic true incomplete conversion, both starting materials would be present alongside the HaloPROTAC **144**. As a result, the acid **162** can be dosed to the cells along with the amine **101** in increasing concentrations with final HaloPROTAC **144** (purple). The acid **162** and amine **101** would not react with one another unlike if the amine **101** and NHS ester **175** were combined, so was a suitable alternative to imitate an impure reaction mixture (**Figure 120B**). The acid **162** and amine mixture **101** (purple) also corresponds to percent conversion as calculated by molarity comparison of the “starting materials” to the “product” upon reaction component addition (if one equivalent of NHS ester **175** was used).

In this experiment, the amine **101** had little to no effect on  $\text{DC}_{\text{max}}$  of the VHL recruiting HaloPROTAC **144**. This could be a result of the possible poor cell permeability of the amine. This also could be the result of reversible binding of the amine binding to the E3 ligase, allowing the HaloPROTAC **144** to bind competitively which would lead to GFP degradation. The NHS ester **175** and the acid both have a concentration dependent effect on the GFP reduction, with increasing competition with the HaloPROTAC **144** via the covalent mechanism of HaloTag® binding (also elucidating the acid is sufficiently cell permeable). In the case of the acid **162** and amine together **101** (purple), the effect is consistent with the GFP degradation observed with the acid alone. Good GFP reduction is still observed with reaction conversion of 50% with 65% GFP degradation observed. Reaction conversion of less than 30% corresponded to poorer GFP degradation. This also explains the small difference in  $\text{DC}_{50}$  values observed in the purified versus non-purified assay (**Figure 119**) as 1.2 eq. of NHS ester **175** was used and could impede the covalent mechanism to the GFP-HaloTag®. As a result of this result, 1 equivalent of the NHS ester **175** would be desirable to ensure good HaloPROTAC concentrations in the cells without impeding the covalent attachment and will be used in the future experiments.

A)



B)

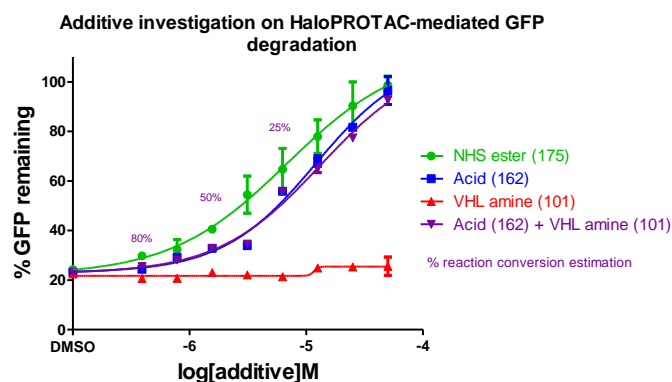


**Figure 120:** Determining the effect of varying levels of reaction components compared to the VHL recruiting HaloPROTAC **144** (A). Effect of incomplete conversion of *in-situ* HaloPROTAC **144** synthesis on GFP reduction (n=2). This was measured with the DC<sub>max</sub> of the VHL recruiting HaloPROTAC **144** of 1  $\mu$ M with increasing concentrations of NHS ester **175** (green), acid **162** (blue), VHL amine **101** (red) and acid **162** and amine **101** combined (purple) with corresponding % conversion that this would reflect (B).

In order to analyse the reaction conversion of the amine **174** to the desired HaloCompounds **176**, LCMS would be used. LCMS would be useful to determine if the target compounds had been successfully synthesised, and an estimation of reaction conversion could be attained

without the use of an internal standard. NMR techniques are not suitable for use on a large array as the reactions would be run in non-deuterated DMSO and the wells would be used directly in biological testing without purification. As a result of using reaction mixtures directly in biological assays, quantitative LCMS techniques would prove challenging, as the internal standards needed could compromise the biological readouts and therefore impair the screen. As a result, it was deemed that qualitative LCMS conversion was a suitable alternative to quantitative LCMS in this case. The bases and the NHS ester **175** are not UV active, and the DMSO peak is eluted at the solvent front and not quantified. In addition, the UV absorbance of the starting amine **174** and the product HaloCompound **176** are assumed to be comparable. As a result, the percentage area of the UV peak ratio of product to starting material will be used in the subsequent screens to determine reaction conversion. This is also a rationale for using one equivalent of the linker to the starting material, as this will streamline the percentage conversion calculation. Qualitative conversions would therefore be classed as poor (<20%), moderate (20–50%), good (50–70%) and very good (>70%) for the purpose of this screen. The good conversion category was classed with at least 50% product, as this conversion could potentially elicit a positive biological response if the compound was active, as determined in the previous experiments. In addition, due to the lack of NMR structure confirmation, HaloCompounds would be assumed as the amide for the majority of compounds. This may not always be the case, as without definite structural confirmation, the compounds synthesised could be esters (if there is an alcohol in the molecule) or an anhydride (if there is an additional acid in the molecule). As a result, the HaloCompounds arising from amine reaction would not be definitively drawn as the amide but merely referred to as a HaloCompound arising from the starting material. As the assay was phenotypic, and positive assay results would be followed up in greater detail, this was not a concern at this stage. The aim of this assay was to find HaloCompounds which could induce GFP degradation, irrespective of the compound synthesised in the well.

Testing the *in-situ* formed VHL recruiting HaloPROTAC **144** demonstrated that mixtures of compounds in this assay could give positive results without negating the biological response. This shows that the powerful technique of high-throughput chemistry could be suitable to generate many hundreds to many thousands of compounds to test in the phenotypic assay. Therefore, this could combine the well-established high-throughput fluorescence read-outs, with novel compound synthesis to find new chemical matter for protein degradation. As a result, high-throughput plate chemistry would be explored to synthesise hundreds or thousands of HaloCompounds which could then be tested in the GFP degradation assay.

### 7.3.2 Computational Chemistry Selection for the HaloTag® Degradation Screen

#### 7.3.2.1 Optimisation Set – Selecting 300 amines

The ultimate aim of the phenotypic screen would be to assess up to 100,000 HaloCompounds, similar to an HTS selection screen.<sup>229-232</sup> In order to choose suitable amines from the GSK collection to optimise and validate the assay for a large screen, computational selection methods were used. The first set of compounds would be utilised for chemistry optimisation, to validate the robustness of the reaction, and would contain up to 300 amine compounds (one 384-well microplate with a number of control wells). The second step in screen validation would be to analyse the positive hit rate from the screen, which would not be possible on a small screen of 300 compounds, as the probability of finding a hit would be too low.<sup>233</sup> Therefore, increasing the size of the screen to around 10x the chemistry optimisation set, should be sufficient to estimate a hit rate from this degradation assay. It would also be important to determine the number of false positives that arose from the assay. False positives are often problematic in phenotypic screening assays, and in this case fluorescence reduction could be a result of cytotoxicity protein synthesis inhibition, among other reasons.<sup>232,234-240</sup> In this assay, interfering compounds should theoretically be removed by screening in the GFP-HaloTag® control cell line which would highlight non-PROTAC related GFP reduction, but this would require validation on a large set of compounds to assess the counter-screen robustness. As a result, a second set, known as the validation set, would include 3000 amines from the GSK HTS screening collection to evaluate the hit rate and subsequent false positive rate. Only aliphatic amines would be utilised in the reaction screening sets, due to previous unsuccessful reactions of the NHS ester using anilines and heteroaromatic amines, which are not sufficiently nucleophilic for the reaction to efficiently take place at room temperature.<sup>241</sup> This is a caveat of using the NHS ester as the leaving group, however, reactivity in the amide coupling versus water hydrolysis is an important consideration for the amines in the GSK collection as they have been stored in hygroscopic DMSO for potentially many years.<sup>242</sup>

Including the entire GSK collection, (encompassing the HTS collection and the global chemistry synthesis collection) there are 250,000 aliphatic amine monomers from which to select the optimisation set. In order to reduce this set to 300 amines, computational methods were employed. Amines, represented by **174**, were chosen to form this diverse set and their physicochemical properties were evaluated to ensure the synthesised HaloCompounds were predicted to be cell permeable in the phenotypic assay.<sup>37,151-154</sup> As a result, a virtual compound library was created combining amines with polymethylene chloride linker **179** which was utilised to predict the final compounds' properties (**Figure 121**). The all-methylene Halo-linker was used to select the 300-amine set, as at this point, both all-methylene and PEG derived

Halo-linkers were being pursued as options (as described in **Figure 104**) for the future screening. It was later decided that the PEG derivative was more suitable due to increase solubility and will be discussed in the following section. Therefore, using the all-methylene linker, physicochemical filtering on the virtual final HaloCompound library was used as follows: clogP 4–7, cChromLogD 5–8,<sup>152</sup> promiscuity forecast index (PFI) <12,<sup>243</sup> hydrogen bond donors (hbd) <5, hydrogen bond acceptors (hba) <6, total polar surface area (tpsa) <250 were all selected to ensure cell permeability of the HaloCompounds. Aromatic rings were chosen to be included so the samples were UV active and visible by LCMS (between 1–3 rings present). The molecular weight (MW) of the HaloCompounds was selected as <750 to ensure the molecules were smaller or comparable weight with the VHL recruiting HaloPROTACs. And finally, if the small molecule compounds had measured kinetic solubility then they were selected if CLND >100  $\mu\text{M}$ . Cheminformatics was used to filter the compounds based on diversity.<sup>244,245</sup> The corresponding small molecule monomers were clustered at Tanimoto 0.6 (similarity ratio of one molecule to another) with one cluster representative selected in order to achieve diversity between the amines. Compounds which were found to be cytotoxic in GSK cell health assays were also removed. The set was then reduced further by selecting compounds which were available in DMSO stock solutions. This gave a total of 219 compounds out of 250,000 which met the desired criteria. A number of compounds were also added to the optimisation set which were not within the selection boundaries, due to containing similar substructures to literature precedented E3 ligases. As a result, 76 compounds with similar substructure similarity to VHL, cereblon, IAP and KEAP1 binders were added. After selection and addition, this gave a diverse set of 297 amines. Two positive control compounds, the VHL recruiting HaloPROTACs **11a** and **144** were also added to the set. The 297 amines selected were coined the optimisation set, or the 300-amine set.

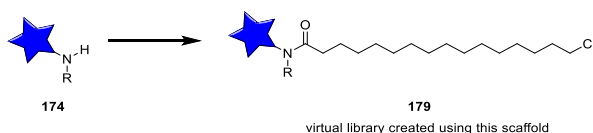


**Figure 121:** Virtual library created from the 250,000 amines at GSK and were used for various computational selection criteria to generate the chemistry optimisation set for the screen.

The selected amine's properties were analysed to ensure the set was chemically diverse. The visualisations in **Figure 122** show the ChromLogD distribution of the amine molecules in comparison with their respective molecular weights, with many molecules in the range -1.5–3 ChromLogD. As the amines contain a basic centre, which would be converted to a neutral amide after the linker addition, the compound's ChromLogD values were therefore hypothesised as acceptable to generate cellularly permeable tool HaloCompounds. The set encompasses 119 primary amines (blue), 168 secondary amines (orange), and 8 which have both a primary and secondary centre (green). The compounds which had multiple amine

centres in the same category (for example, two primary centres (3 compounds) or two secondary centres (two compounds) were not included in this visualisation/calculation for clarity but instead included in the primary or secondary categories respectively). Selected scaffolds **101**, **180–182** are shown and colour coded based on the visualisation. The set was deemed diverse with respect to the ChromLogD and molecular weight distributions and was analysed further.

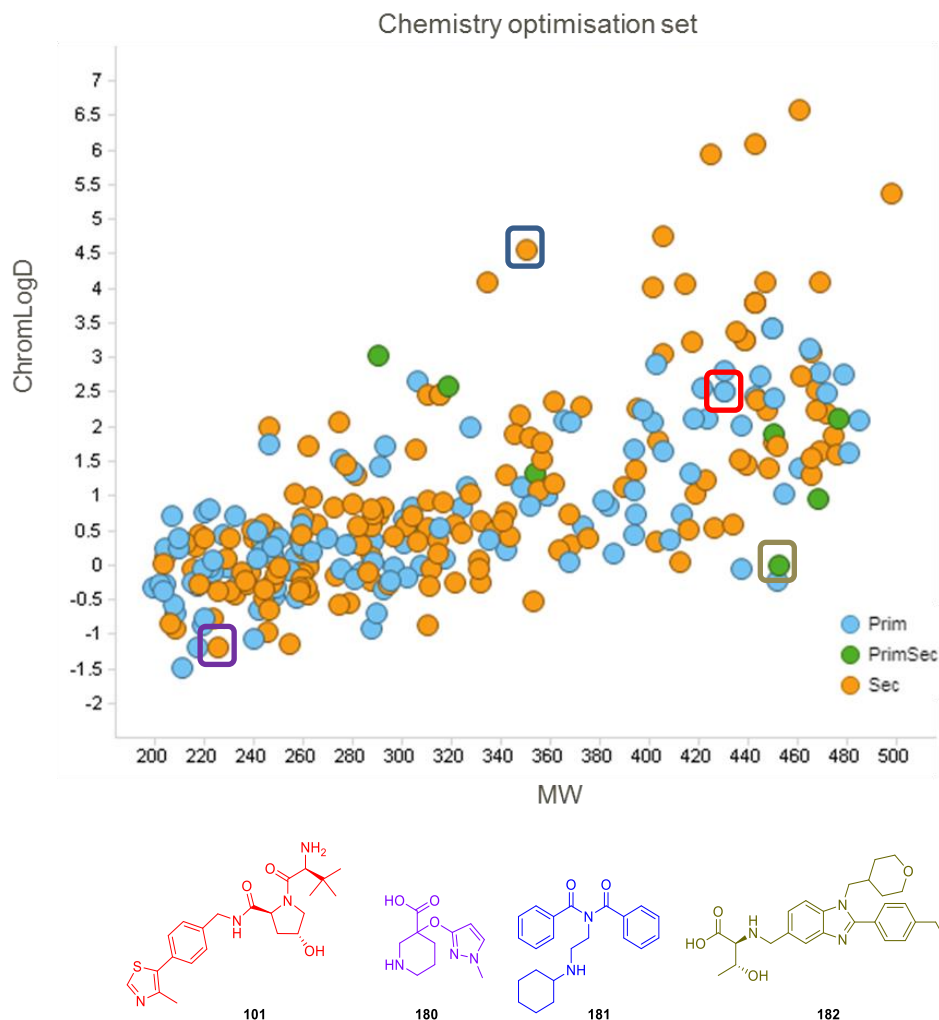


**Figure 122:** The set encompasses 119 primary amines, 168 secondary amines, and 8 which have both a primary and secondary centre. Distribution of the compounds is visualised by ChromLogD (between -2 and 7) versus MW (200–500) for the set. Compounds highlighted with colour and corresponding structure shown below.

Another measure of determining structural diversity in a compound set is by analysing the molecular shape of the compounds. This can be represented based on the lowest-energy conformations of all depicted molecules. Therefore, normalised ratios of principal moment-of-inertia (npr) descriptors were calculated and plotted on a triangular graph spanned by the three basic shape types, 'rod-like', 'disc-like' and 'spherical' (**Figure 123**).<sup>155,246-248</sup> As shown by the diagram, many of the amines selected span the rod- and disc-like states. This is a common

feature of medicinal chemistry compound sets,<sup>248</sup> and is overall representative of the amines found in the collection. Selected scaffolds **101**, **180–182** are shown and colour coded to their arrow. The set was therefore deemed well suited to explore the chemistry for the phenotypic GFP reduction screen.

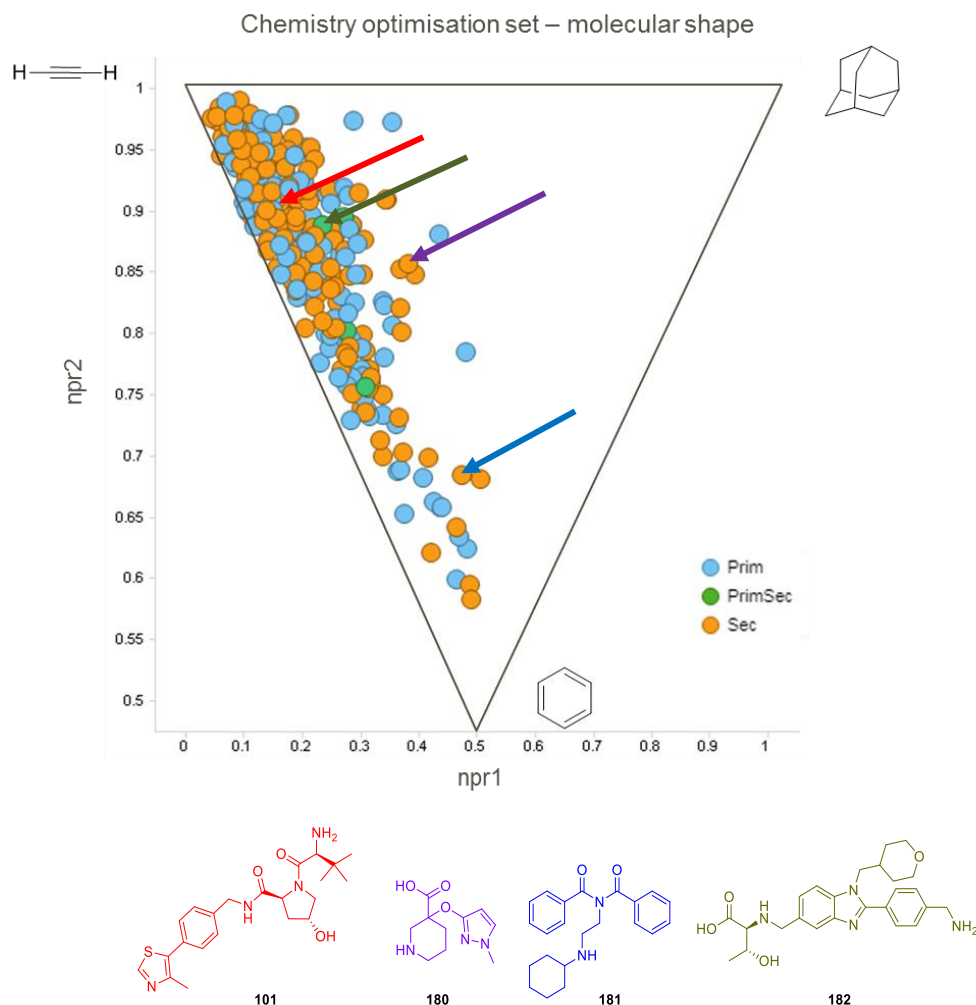


**Figure 123:** The molecular shape diversity of the optimisation set between rod, disc and sphere using moments of inertia. Compounds highlighted with colour arrow and corresponding structure shown below in analogous colour.

### 7.3.2.2 Validation Set – Selecting 3000 amines

In addition to the optimisation set, a larger set was also developed to investigate the hit rate from the phenotypic screen. The compounds were now chosen from the GSK HTS collection, which has 150,000 aliphatic amines (instead of the collective GSK collections which have 250,000 amines used previously) curated through the removal of known PAINS and other cytotoxic compounds.<sup>249</sup> This was then filtered to the desired 3000 by utilising physicochemical properties and chemical diversity. Unlike the optimisation set, a virtual library was not created,

and the amine monomers were used by first intent. This was deemed a more suitable method of filtering, as the linker was identical in each case, the amine properties would be perturbed in a constant fashion between the amines. As the physicochemical properties were measured instead of the calculated values with the previous set, this was deemed a more appropriate selection strategy. In this set, amines were filtered to contain PFI <7, hbd <4, psa <140, ChromLogD <4, MW <500, aring count 1–3 (UV activity for LCMS), and were filtered using Tanimoto 0.6 (with 1 cluster representative selected) for chemical diversity.<sup>244</sup> This gave a total of 2934 amines which were available in sufficient quantities in DMSO stock solutions. The 2934 amines selected were coined the validation set, or the 3000-amine set. The set encompasses 661 primary amines (blue), 2267 secondary amines (orange), and 6 compounds which have both two different classes of aliphatic amine centres (one primary and one secondary, green) (**Figure 124**). Those which have two primary amine centres (2 compounds) or two secondary amine centres (31 compounds) are not included in this visualisation/calculation for clarity but instead are included in the primary and secondary categories respectively. The proportion of primary to secondary amines in this selected set is reflective of the proportion of primary and secondary amines in the GSK HTS collection.

As with the previous set, the molecular diversity of the selected set can be visualised (**Figure 124**). Comparison of ChromLogD and MW shows the diversity covered by the amines selected, with more molecules now occupying the range between ChromLogD 2–5. This should ensure cellular permeability in the final HaloCompounds containing a PEG derived linker, in comparison to the lower ChromLogD values of the previous screening set, as a result of the virtual library using the lipophilic linker (**Figure 124A**). In addition, the molecular shape can be visualised as previously described (**Figure 124B**). There are now more compounds which have disc-like molecular shapes. There are also more structures closer to the sphere-like molecular shapes, indicating there are more compounds which feature more 3-dimensional shapes. There are no true “spheres” in the screening set, most likely due to the medicinal chemistry applications of the screening collection. More rod/disc features are more common as a result for the need for the protein-small molecule interactions. This set was a good reflection of the overall amines in the HTS compound collection and as a result, the validation set was therefore deemed well suited to explore the biological assay on a larger scale and to evaluate the hit rate for the phenotypic GFP degradation screen.

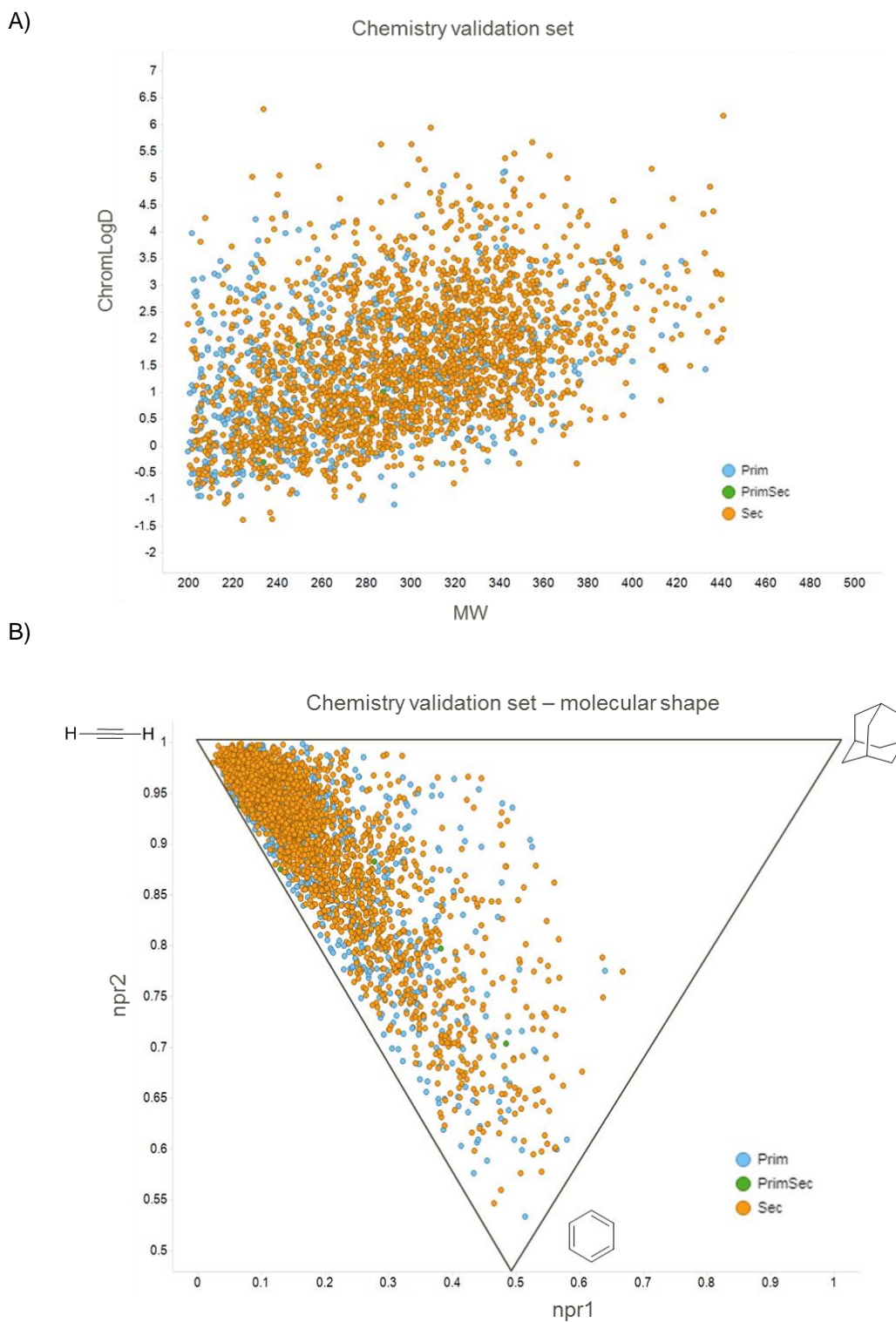


**Figure 124:** The set encompasses 661 primary amines, 2267 secondary amines, and 6 which have both a primary and secondary centre. Distribution of the compounds is visualised by ChromLogD (between -2 and 7) versus MW (200–500) for the set (A). The molecular shape diversity of the optimisation set between rod, disc and sphere using moments of inertia (B).

### 7.3.3 High-Throughput Chemistry for HaloCompound Synthesis

#### 7.3.3.1 HTE Optimisation – VHL as a Standard Amine

Plate-based high-throughput chemistry has not previously been utilised for PROTAC synthesis, therefore reaction optimisation was required. Before executing the HTE of the optimisation and validation sets, small scale high-throughput chemistry in 384-well plates required validation. As a result, the VHL recruiting HaloPROTAC **144** was used as an exemplar compound to synthesise in plate 384-well format. The chemical transformation was previously shown to be robust and reproducible in round bottom flasks and 5 mL vials. Further optimisation into small scale chemistry is required as the surface area to air ratio becomes important on nano and micromolar scales (**Figure 125**). It was envisaged that because the sterically hindered *tert*-butyl on the alpha carbon, this amine would be suitable to test the platform initially for HTE. This amine is frequently used in amide couplings in the group for PROTAC synthesis, and found relatively unreactive, therefore will be a good measure of applicability to the amines in the GSK collection for elaboration into new HaloCompounds on a small scale.

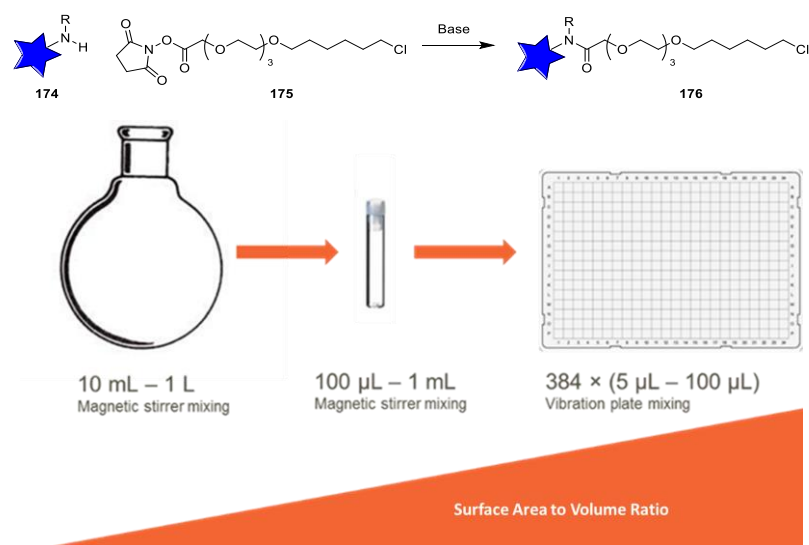
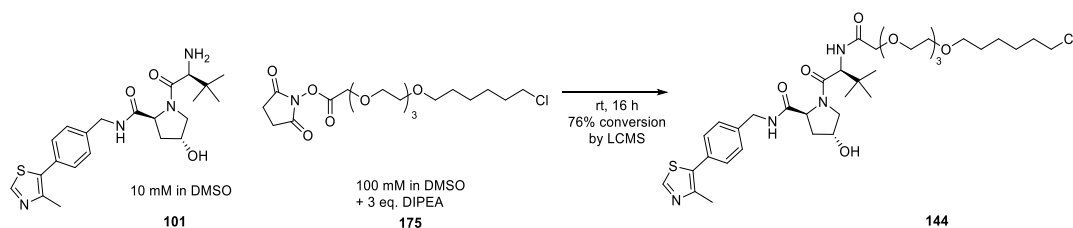


**Figure 125:** Development of HTE in microplates and the subsequent differences in mixing and surface area to volume ratio considerations which require optimisation.

HTE design and execution had to involve in a solvent which would be compatible both with the polypropylene 384-well plates and the biological assay. As the GSK compound collection is stored in 10 mM DMSO stocks frozen at -20 °C, this was envisaged as a suitable solvent to use in the reactions. Therefore, the VHL amine **101** was made up to a 10 mM DMSO stock solution to test the HaloPROTAC formation on small scale. As the reactions would be tested directly in cells, the solvent that the NHS ester **175** was dissolved in also had to be compatible

with both these systems. As a result, the NHS ester **175** was also made into a DMSO stock solution with a concentration of 100 mM. The linker was used in a concentrated stock solution in the first intent, to ensure the reaction concentration was sufficiently high for the reaction to proceed. To reduce the addition steps for the small-scale chemistry, the base was introduced to the NHS ester **175** DMSO stock solution, resulting in one simple dispense to the reaction plate containing the amine. This resulted in the VHL amine **101** in 10 mM DMSO with the addition of both the NHS ester **175** and 3 equivalents of DIPEA in 100 mM stock to give the VHL recruiting HaloPROTAC **144**. Dispensing protocols developed by Merck and Co were adopted using semi-automated electronic multichannel pipettes from a polypropylene trough.<sup>205</sup> The amine in DMSO would be added to the 384-well plate using this technique, centrifuged, and then the base and linker stock would then be added in an analogous manner, then a plate lid could be used while the reaction proceeded overnight. Traditionally, small-scale chemistry is performed in glovebox conditions, due to the increased surface to volume ratio and thus increased impact of atmospheric water and oxygen. In this case, the amines will have been stored in DMSO stock solution for multiple years, and gone through multiple freeze-thaw cycles, so the presence of water is expected. As a result, in addition to lack of glovebox availability during optimisation, these reactions needed to be robust, so were performed in a fume hood. Using this technique as an initial test in one well of the 384-well plate, the VHL recruiting HaloPROTAC **144** was synthesised in 79% conversion by LCMS. This was achieved using 10  $\mu$ L of VHL amine **101** and 1.2  $\mu$ L of the NHS ester **175** and DIPEA stock solution which equates to 1.2 equivalents of the linker and 3 equivalents of base (**Scheme 20**). The reaction was therefore deemed a success and would be attempted using the optimisation set containing 297 amines.



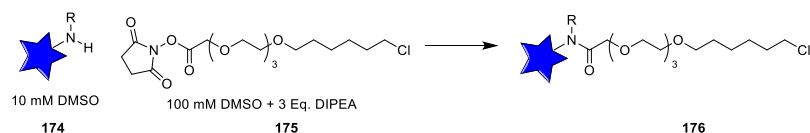
**Scheme 20:** Synthesis of VHL recruiting HaloPROTAC **144** in 384-well plate format using Thermofisher electronic multichannel pipette.

### 7.3.3.2 HaloCompound In-Situ Synthesis for the Optimisation Set

With a suitable HTE dispense technique established using VHL as an example, this was attempted using the 300-amine set selected from the GSK compound collection. Using the same conditions, the plate was loaded with the optimisation set containing the 297 unique amines in wells in a random order (0.100  $\mu$ mol, 10  $\mu$ L of 10 mM stock). Additionally, present

on the plate was a column of the *in-situ* synthesis of the VHL recruiting HaloPROTAC **144** from VHL amine **101** (containing 16 identical wells, column 18). A number of positive control compounds were also present on the plate, including 16 purified HaloPROTAC wells (column 6) as positive controls for the biological assay. The reactions were carried out by dispensing the linker and base solution from a PP trough into every well using the multichannel pipetting technique. The plates were then left to stand for 16 h, and then analysed by LCMS (**Figure 126A**). Following analysis, the reaction mixtures were categorised based on % conversion to their desired HaloCompound: poor ( $\leq 20\%$  conversion by LCMS, red), moderate (20–50% conversion, amber), good (50–70% conversion, light green) and very good ( $\geq 70\%$  conversion, dark green). As indicated by the plate map, many of the reactions were unsuccessful (96 had less than 20% conversion by LCMS) including the VHL control wells shown in column 18. Good conversion of over 50% conversion to the desired HaloCompound was observed in 156 reactions (**Figure 126B**). Example scaffolds are shown (**180–182**, **Figure 126C**), with good conversion observed with primary amine **182** and cyclic secondary amine **180**, and poor conversion observed with linear secondary compound **181**, perhaps due to steric effects (this will be discussed further in the next section). This was a disappointing result, as the reactions were less successful than anticipated for the range of compounds. Upon manual analysis, the compounds with the higher yielding conversions were more likely to be free amines not conjugated as a salt. Those compounds which were conjugated as an HCl or TFA salt, including the VHL amine **101**, had poor conversion despite a number of the amines containing a reactive primary centre expected to give good conversion. This suggested the reactions failed possibly due to insufficient base present in the reaction, despite three equivalents of DIPEA added to the NHS ester **175** stock. It was then discovered, that DIPEA and DMSO are immiscible, and therefore the reactions may not have had sufficient base in solution for the amide coupling. The DIPEA would have formed a thin layer in the trough used to hold the stock solution, and therefore was not taken up by the electronic pipette in most cases. Therefore, moving forward, a base miscible with DMSO would be used.

A)



		Amines																				
		1	2	3	4	5	6	7	8	9	10	11	12	13	14	15	16	17	18	19	20	21
A	0	74	68	93	73		86	0	81	83	90	78	55	81	13	3	83	33	90	2	67	
B	24	37	16	10	85		81	77	53	26	6	48	59	36	86	0	87	3	7	0	39	
C	91	0	18	12	84		14	91	28	48	54	84	31	79	78	40	48	3	29	52	61	
D	24	72	93	8	46		0	75	59	0	71	83	71	61	0	10	7	36	72	62	0	
E	31	16	18	13	11		87	39	67	44	94	83	86	89	10	79	28	26	0	0	78	
F	15	54	18	0	86		53	89	82	68	5	15	56	53	85	59	0	22	73	88	1	
G	100	54	0	10	3		80	66	75	0	10	60	78	78	38	83	35	6	48	70	86	
H	19	57	91	0	17		35	23	47	0	84	6	54	0	15	44	56	5	1	9	86	
I	30	47	86	20	43		42	48	72	67	79	0	87	82	21	23	0	11	49	62	2	
J	100	86	2	24	81		82	71	82	83	75	90	0	33	31	0	87	4	70	20	81	
K	31	2	54	16	58		38	83	9	72	85	86	90	0	7	44	45	3	0	40	87	
L	83	76	90	18	73		82	71	74	75	35	82	64	84	93	80	89	4	77	65		
M	65	55	36	48	6		0	81	39	78	51	78	79	28	81	0	77	13	0	16		
N	81	81	65	27	48		84	85	3	84	0	72	65	50	32	78	0	8	55	75		
O	0	82	84	89	37		2	0	1	23	5	0	85	87	81	0	3	22	8	74		
P	0	92	2	21	89		73	53	34	73	71	59	94	13	81	16	0	21	15	23		

B)

Number of reactions with >50% conversion	Number of reactions with <20% conversion	Conversion Key
156	96	

<20%
20-50%
50-70%
70-100%

C)

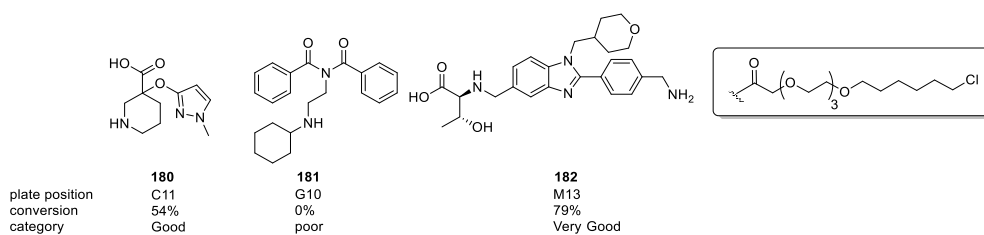
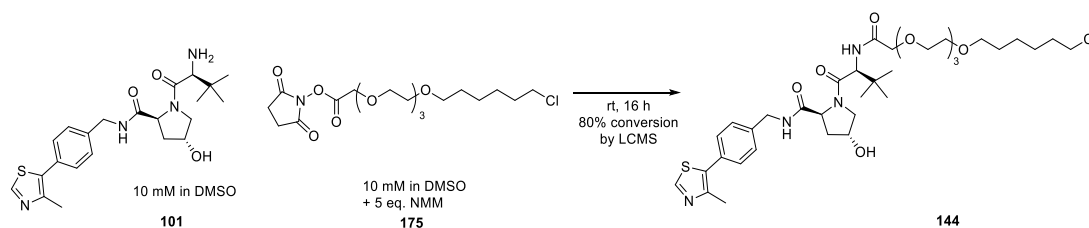


**Figure 126:** High-throughput amide coupling to generate HaloCompounds from the 300-amine set using an NHS ester and DIPEA as a base. LCMS analysis performed after overnight incubation and results depicted in colour coded key (middle). Column 18 (blue) had identical VHL amine **101** as positive control wells and cells depicted in white were either positive controls for the biological assay (column 6) or contained DMSO (column 21) (A). Overall reaction success and conversion key (B). Exemplar compounds **180–182** shown with plate position and percentage conversion and their corresponding category (C).

As a result of the failed reactions observed with the use of DIPEA, a new organic base was required. The base used in the reaction would preferably be non-UV active due to the LCMS conversion calculated by UV area, as this would streamline the analysis of LCMS data. In addition, the base had to be soluble and miscible in DMSO. Most importantly, the base had to be compatible with the biological assay, causing no GFP reduction or issues with the biological read-out. It was hypothesised that the reaction could be performed in an a DMSO mixture with the addition of aqueous buffer used in cell culture which would be inert in the biological assay. Phosphate buffer was attempted as both the co-solvent and base, but no reaction occurred. Aqueous bases may promote the hydrolysis of the NHS ester **175** instead of the intended amide coupling, so an organic base was envisaged to be more suitable. *N*-methyl morpholine (NMM) was chosen as a base for the reaction as it met all the criteria outlined. To ensure NMM had adequate solubility in DMSO the concentration of the base and NHS ester **175** stock was reduced from 100 mM to 10 mM. In addition, 5 equivalents of the base were used to guarantee sufficient base was present to allow the reaction to proceed. As an initial example, VHL derivative **101**, was used with NMM as a base in single reaction in a 384-well plate. Using the same conditions as previously described, replacing DIPEA and with NMM and using 5 equivalents, 80% conversion to the desired product was achieved (**Scheme 21**). The less concentrated solution gave satisfactory results without impeding the reaction conversion and would be used moving into the optimisation set synthesis.

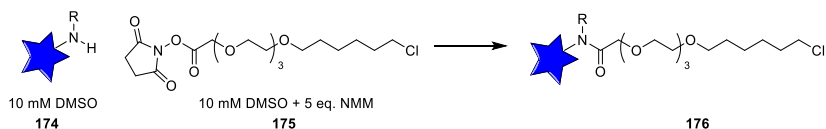


**Scheme 21:** Synthesis of VHL recruiting HaloPROTAC **144** performed in a 384-well plate using NMM as the base.

The 297 amines which were chosen for the optimisation set would subsequently be tested using the conditions established with NMM. The 297 amines were received frozen in a 384-well format with 10  $\mu$ L of 10mM DMSO solutions in a random order. In row 18, VHL amine **101** was added into every well (blue), as a positive control for the biological assay (leading to **144** synthesis *in situ*). The reactions were carried out, by dispensing the linker and base stock solution across the plate as previously described from a PP trough. This was then left to stand for 16 h and were then analysed by LCMS (**Figure 127A**). Compared to the previous example using DIPEA, the amide coupling for the HaloCompound synthesis was more successful using NMM as a base. There were 210 reactions which had more than 50% conversion, compared to 156 in the last set (**Figure 127B**). The VHL control **101** wells in column 18 previously

showed incomplete conversion with the DIPEA conditions, now showed excellent conversion with NMM. The failed reactions previously observed with 96 examples using DIPEA were reduced to 73 using NMM. Some example scaffolds are shown, with similar conversions observed with NMM in comparison to those observed when DIPEA was used (**Figure 127C**). Further analysis with respect to the rationale for the reactions' failure will be discussed below. Overall the new reaction conditions showed an improved profile, and good overall success of HaloCompound formation for the 300-amine set.

A)



		Amines																				
		1	2	3	4	5	6	7	8	9	10	11	12	13	14	15	16	17	18	19	20	21
Amines	A	43	94	81	100	100		100	92	93	94	52	86	77	89	14	3	97	85	100	86	74
	B	57	95	66	15	97		92	94	57	27	74	64	61	84	92	22	85	83	14	0	0
	C	93	13	98	19	100		22	97	30	40	64	30	82	39	75	58	93	82	96	98	38
	D	11	78	99	19	96		24	80	69	0	83	82	56	18	2	15	10	83	81	96	0
	E	21	5	20	19	88		98	82	68	31	98	98	91	98	15	97	100	81	0	6	0
	F	96	89	97	0	94		96	100	91	76	3	21	96	59	98	92	0	81	89	100	5
	G	0	84	4	67	6		99	96	84	0	10	100	95	99	97	97	100	82	96	100	96
	H	83	93	99	0	21		88	47	82	18	97	93	59	2	56	56	100	84	13	5	100
	I	82	24	100	27	61		25	56	75	74	86	0	99	91	72	100	8	87	53	91	1
	J	0	91	0	14	98		95	82	98	100	93	93	0	98	80	0	100	89	13	98	91
	K	28	68	78	14	97		32	87	4	82	99	91	100	0	3	60	92	90	0	98	100
	L	54	91	73	12	84		88	85	76	88	17	77	85	94	100	94	100	94	100	85	
	M	86	39	58	83	13		0	100	43	92	59	58	83	92	77	0	83	82	0	19	
	N	81	49	70	90	46		88	100	4	90	0	70	44	25	0	83	2	83	85	95	
	O	0	77	89	44	29		41	0	0	97	5	0	83	81	80	0	18	83	100	70	
	P	3	82	0	73	99		72	17	94	84	28	59	71	26	81	98	0	85	95	18	

B)

Number of reactions with >50% conversion	Number of reactions with <20% conversion	Conversion Key <20% 20-50% 50-70% 70-100%
210	73	

C)

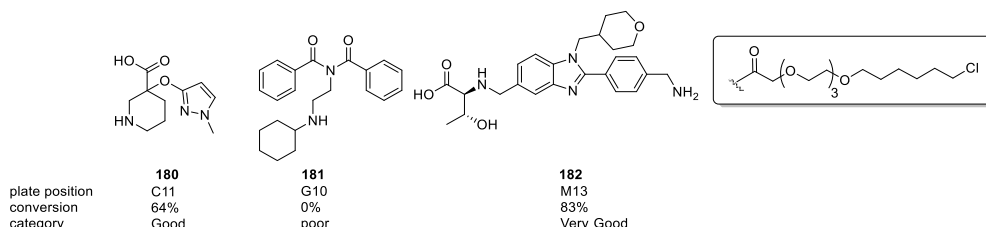


**Figure 127:** High-throughput amide coupling to generate HaloCompounds from the 300-amine set using an NHS ester and NMM as a base. LCMS analysis performed after overnight incubation and results depicted in colour coded key (middle). Column 18 (blue) had identical VHL amine **101** as positive control wells and cells depicted in white were either positive controls for the biological assay (column 6) or contained DMSO (column 21) (A). Overall reaction success and conversion key (B). Exemplar compounds **180–182** shown with plate position and percentage conversion and their corresponding category (C).

In order to ensure that the failed reactions were not a consequence of impure starting material amines, the 300 amines from the GSK collection were submitted for LCMS analysis for QC

purposes (**Figure 128**). The compounds selected have been frozen in DMSO since the initial synthesis, in some cases this may have been for multiple decades. This analysis flagged 13 compounds as very impure by LCMS (red, and amber) (<33% remaining) with 7 of those compounds giving poor results in the amide coupling (the remaining 5 gave moderate conversions). One result had moderate conversion to desired product, despite showing no starting material in this example. This could be a result of the retention time of the amine, if the compound is too polar it will elute in the solvent front and therefore would not be observed and be flagged as impure. Additionally, a poor result could be due to poor ionisation of the starting material. The analysis also showed 7 compounds as moderately pure (50–70% remaining) out of the 300. This shows that on large scale, a small number of impure starting materials should not affect the success or failure rate by a significant proportion. Of the 73 reactions which had poor conversion to the desired product, the majority contained sterically hindered secondary amines, which could explain their unreactive nature to this amide coupling, which will be discussed further. In addition, a small number of compounds which contained two amines could undergo the reaction on both centres, and this would flag as a failure (this will also be discussed further). In total, the effect of the amine starting materials which were impure represented a small proportion of the reactions and did not have a large impact on the overall success of the array. Therefore, starting material QC would not be used in a larger experiment, as it would involve significant time and costs associated with it. In addition, with 70% of the reactions producing over 50% conversion of the desired HaloCompound, this was seen as satisfactory to increase the probability of successfully finding new E3 ligases.

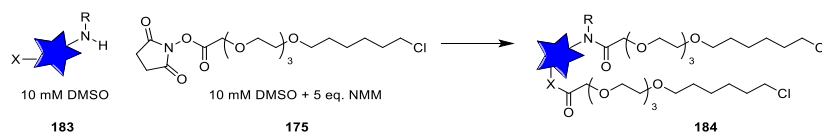
		Amines (starting material only)																				
		1	2	3	4	5	6	7	8	9	10	11	12	13	14	15	16	17	18	19	20	21
Amines (starting material only)	A	100	95	100	100	99		100	92	99	96	99	100	100	100	0	93	100	100	100	86	71
	B	84	99	100	100	97		80	99	100	100	100	100	60	77	100	100	89	100	7	100	84
	C	92	14	98	98	99		88	97	24	87	80	88	100	100	100	85	96	100	97	99	94
	D	93	93	100	89	94		77	98	100	100	86	100	100	56	93	100	97	100	100	96	94
	E	95	100	99	100	91		100	81	100	90	96	100	99	98	100	98	96	100	97	87	99
	F	100	99	100	89	100		98	99	95	86	86	15	97	100	99	86	98	100	85	100	98
	G	100	96	63	71	100		100	97	83	100	100	100	100	100	100	100	100	83	100	100	100
	H	99	95	100		30		94	99	99	99	94	97	100	98	96	94	96	100	64	84	97
	I	100	90	100	100	100		99	100	96	100	86	99	100	90	99	96	95	100	52	100	97
	J	99	92	81	93	96		100	100	98	94	100	91	85	97	81	100	100	100	88	91	89
	K	70	100	87	100	97		99	97	73	100	97	94	100		91	33	98	100	100	100	100
	L	100	100	83	86	95		90	98	91	100	100	100	82	98	100	94	100	100	86	87	
	M	95	100	100	100	99		85	92	93	90	78	100	84	96	100	98	96	100	98	17	
	N	100	100	100	93	54		89	100	86	93	84	100	78	100	97	81	95	100	96	96	
	O	100	92	90	100	5		91	97	97	98	93	7	85	93	100	100	100	100	100	83	
	P	100	91	89	100	93		82	92	93	100	0	100	70	100	89	99	100	100	94	78	

Conversion Key	
<20%	Red
20-50%	Yellow
50-70%	Light Green
70-100%	Dark Green

**Figure 128:** LCMS analysis performed on the 300-amine optimisation set starting materials as a QC measure for the reaction. Column 18 (blue) had identical VHL amine **101** as positive control wells and cells depicted in white were not populated.

In order to determine whether di-amidation was retarding the reaction conversion, the di-adducts were analysed by LCMS (**Figure 129A**). Six compounds were shown to have more than 20% conversion to the di-amide product. A further 17 compounds had detectable levels of di-adduct formation (1–20%) (**Figure 129B**). The six compounds **185–190** which had over 20% di-adduct formation are represented (**Figure 129C**). In addition to other amines which could also cause di-adduct formation, other functional groups present could also react with the NHS ester group. The other functional groups which could also undergo the reaction were highlighted in red, including additional amines, alcohols, such as phenol and hydroxyl groups. Hydroxyl groups are not predicted to undergo the amide forming reaction, due to their decreased nucleophilicity in comparison to the reactive amines, however, as <sup>1</sup>H NMR studies are not used in this reaction, they would not be discounted at this stage. Compound **187** in G11 was not envisaged to have a di-adduct formation, as only one amine is present. This compound **187** in G11 was further derivatised in other GSK projects using amide coupling without obvious issue, therefore the reason for this is unknown. One compound **190** in J7, was found to have both 95% di-adduct formation and, in the previous LCMS data, desired mono-product formation at 95% which was incorrectly identified. This illustrates a limitation of LCMS analysis, where the mono-product mass could therefore be identified as a fragment in the di-adduct product peak and subsequently misrepresented as the desired product. This, however, has only happened in one case in this example, was therefore deemed at present, not a significant issue in the screen.

A)



		Amines																				
		1	2	3	4	5	6	7	8	9	10	11	12	13	14	15	16	17	18	19	20	21
A	N.D.	N.D.	10	N.D.	N.D.			N.D.														
B	N.D.	N.D.	N.D.	N.D.	N.D.			N.D.	N.D.	N.D.	N.D.	N.D.	9	N.D.								
C	N.D.	N.D.	N.D.	N.D.	N.D.			12	N.D.													
D	N.D.	N.D.	N.D.	N.D.	N.D.			N.D.	N.D.	N.D.	N.D.	N.D.	10	N.D.								
E	N.D.	N.D.	N.D.	N.D.	N.D.			N.D.	N.D.	11	N.D.											
F	N.D.	N.D.	N.D.	N.D.	N.D.			N.D.	N.D.	N.D.	2	N.D.										
G	N.D.	N.D.	N.D.	N.D.	N.D.			N.D.	N.D.	N.D.	N.D.	55	N.D.									
H	N.D.	N.D.	N.D.	N.D.	N.D.			N.D.	4	N.D.	N.D.	N.D.	N.D.	3	N.D.	1	17	N.D.	N.D.	N.D.	N.D.	N.D.
I	7	N.D.	N.D.	N.D.	N.D.			N.D.	1	N.D.	N.D.	N.D.	N.D.	N.D.	N.D.							
J	N.D.	N.D.	N.D.	N.D.	N.D.			95	N.D.													
K	N.D.	N.D.	3	N.D.	N.D.			46	N.D.													
L	N.D.	N.D.	N.D.	N.D.	9			N.D.	3	N.D.												
M	N.D.	N.D.	N.D.	N.D.	N.D.			N.D.	N.D.	N.D.	N.D.	N.D.	N.D.	6	N.D.							
N	N.D.	N.D.	N.D.	N.D.	N.D.			N.D.	N.D.	N.D.	N.D.	24	N.D.	N.D.	N.D.	N.D.	N.D.	N.D.	90	N.D.	N.D.	N.D.
O	26	N.D.	N.D.	N.D.	N.D.			N.D.	N.D.	3	N.D.											
P	N.D.	N.D.	N.D.	N.D.	N.D.			N.D.														

B)

Number of reactions with >20% di-adduct conversion	Number of reactions with 1–20% di-adduct conversion
6	17

Conversion Key
<20%
20-50%
50-70%
70-100%

C)

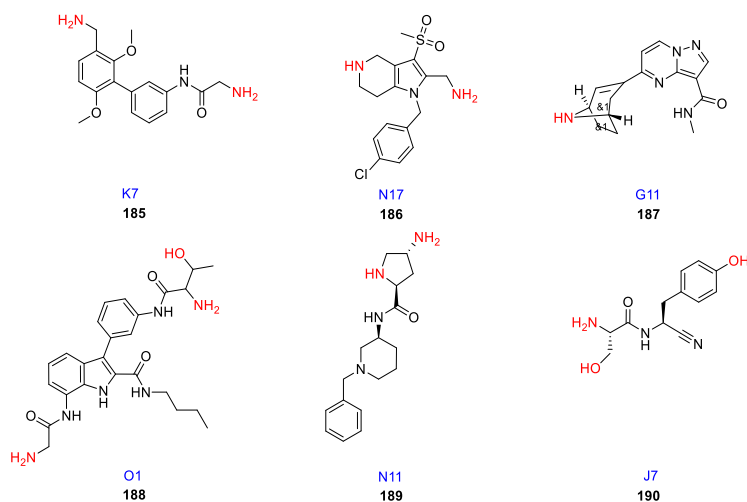


**Figure 129:** LCMS analysis performed on the 300-amine set to investigate di-addition of the linker. Column 18 (blue) had identical VHL amine **101** as positive control wells and cells depicted in white were not populated (A). Overall reaction success and conversion key (B). Analysis of the compounds which had more than 20% di-adduct formation are shown **185–190** and functional groups present in the molecules which could cause di-addition are highlighted in red and plate position (well number) is shown in blue. ND = not-detected (C).

In order to investigate the di-adduct addition further, those amines with more than one aliphatic amine were analysed. In the 300-amine set, there were a total of 13 amines which had more than one amine present, and this was a mixture of primary amines and secondary amines.

This was then correlated with their respective conversion rates to product or di-product (**Table 7**). As shown in the table, those molecules which have two amines with similar reactivity (e.g. 2 primary aliphatic amines or 2 secondary aliphatic amines) are more likely to give the di-adduct. An exception is in the case of compound in C7 where one primary centre is hindered in the alpha position and the other primary centre is non-hindered and would react preferentially with the more reactive centre. Molecules which contain both a secondary amine and a primary amine have little to no di-adduct formation, possibly due to the increased steric availability with the primary amine. Compounds which had additional alcohols and carboxylic acids were also analysed computationally, but there was no direct correlation between the presence of alcohols or acids and whether the reaction had good conversion, showing that additional amines had greater propensity to give di-adduct formation. This had already been seen as the VHL amine **101** has a secondary alcohol which has not esterified in any conditions presented thus far. Compounds with poor conversion, no di-adduct formation and no SM remaining were not well understood, so the LCMS traces were manually visualised. In cases where the di-adduct was over 1000 MW (the mass capacity for the analytical method), the  $(M+2H)/2$  ion was investigated. In some cases, this mass ion did not give a strong enough signal for the minimal mass detection and was not therefore not automatically integrated. This occurred in compound in J19 and compound in B21, where the di-adduct was present but not observed in the automatic read-out. This is a limitation of the automated analytical processing technique which produces the percent area of the product peak on the molecular weight data input. As a large number of the di-adducts in the subsequent screens would be over 1000 MW, the probability of the compounds being observed by the MS was lower. This method for di-adduct identification was therefore not a robust method for being able to determine diamidation automatically. Additionally, other limitations of the MS technique were also elucidated in the analysis of the di-adducts. In a small number of other cases, failed product/di-adduct identification could also be a result of the low UV absorbance arising from the reaction being too dilute for recognition by the automatic integration. This occurred in wells B19 and in H19 and upon manual visualisation, the peaks were significantly reduced in size, and therefore not successful in determining if the reactions had good product conversion. The two issues with the LCMS data would therefore need to be considered in the larger screen. However, as the resulting screen was phenotypic, it was envisaged that the MS read-outs had sufficient success in finding the majority of products in the previous figures. As a result, those wells which showed positive GFP reduction in the assay would be manually reviewed to ensure the activity was a result of the conversion (and then would be followed up in the GFP degradation assay with purified compounds). Additionally, due to the issues with di-adduct automated read-out, this would not be used in the further screen, and would therefore only be considered in positive hits.

**Table 7:** Analysis of the 300-amine set where 2 aliphatic amines were present in the same molecule, and comparison of percentage conversion to product versus di-adduct and the starting material purity (those highlighted in orange were identified in **Figure 129** with over 20% di-adduct formed). ND = not-detected.) SM purity reported as measured in **Figure 128**. \*denotes a manual assignment of %area- a tentative mass was found for the di-adduct, but the MS signal was too weak and was not automatically integrated. \*\*denotes a poor overall UV trace upon manual visualisation.

Well Number	Primary amine centre count	Secondary amine centre count	Total amine count	product conversion %	di-adduct conversion %	SM purity before reaction %
O1	2	0	2	0	25	100
O2	1	1	2	77	N.D.	92
C7	2	0	2	22	12	88
K7	2	0	2	32	46	99
N11	1	1	2	N.D.	24	84
H13	0	2	2	59	3	100
M13	1	1	2	83	6	84
H16	0	2	2	56	17	94
N17	1	1	2	3	90	95
B19	1	1	2	14	N.D.**	7
H19	1	1	2	13	N.D.**	64
J19	1	1	2	13	N.D. (76*)	88
B21	1	1	2	N.D.	N.D. (77*)	71

### 7.3.3.3 Computational Analysis of the Chemistry Optimisation Set

In order to understand the results of several hundred reactions performed, the amines from the optimisation set were categorised and analysed using computational methods. Amines from the GSK collection (297 total), along with the 16 VHL **101** control wells, were placed into 6 categories based on the amine's sterics to elucidate if there was correlation between steric hinderance and reaction conversion (**Figure 130**). The 6 categories include: primary non-hindered, primary hindered, secondary linear non-hindered, secondary linear hindered, secondary cyclic non-hindered and secondary cyclic hindered. Compounds were classed as hindered if they had a branched substituent in the alpha position (as shown in the figure). If there were two primary or secondary amines present, the compound was placed in the category corresponding to the least hindered substituent. There is an even number of hindered and non-hindered compounds featured in the primary category. The majority of the compounds from the secondary amine collection are cyclic and non-hindered, with 97/297 amines in this category. There are also more hindered linear secondary amines than non-hindered in the optimisation set (37 versus 19).

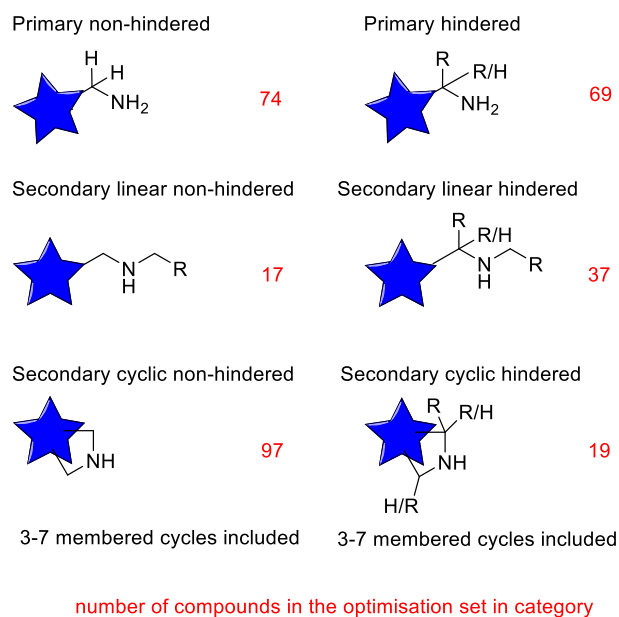
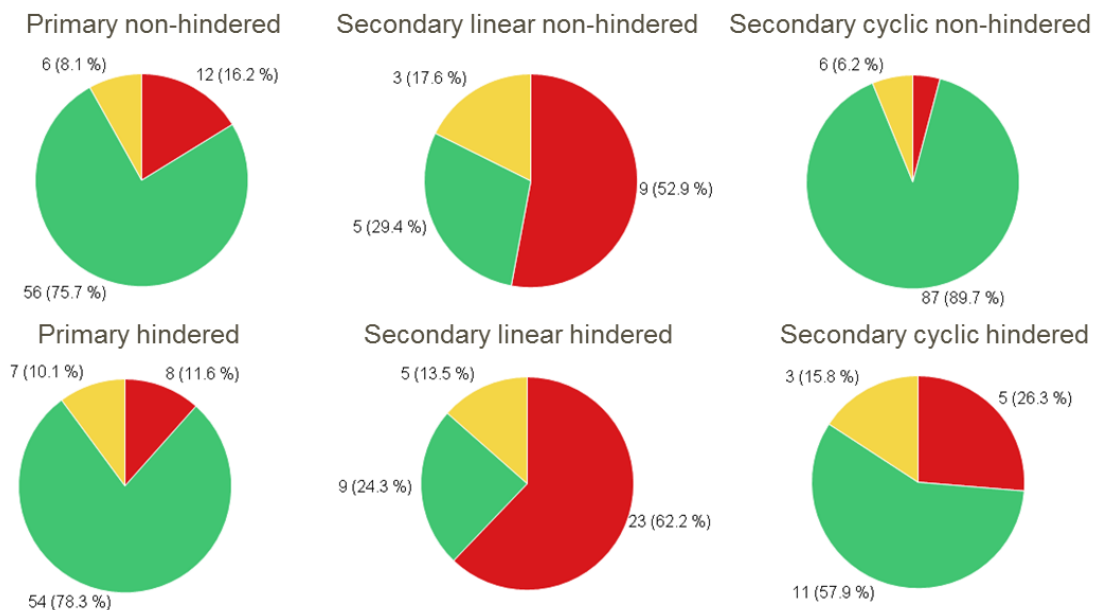


**Figure 130:** Categories used to group the amines into sets for reaction characterisation and compound numbers in each category marked in red. If there are two different amines in the same molecule, the compound is classified by its least hindered amine (8 examples).

The categories were then used to determine any correlations between the steric effects around the reactive amine and subsequent reaction conversion. As predicted, the non-hindered amines were more successful in most categories than the hindered amines (**Figure 131A**). The primary amines were the most successful, both hindered and non-hindered gave excellent responses with over 75% of the compounds resulting in good conversions to the desired HaloCompound. This result was predicted by the optimisation with the VHL amine, which is a member of the hindered primary category. The reactions of cyclic amines were more successful than the linear secondary amines. Over 57% of the sterically hindered cyclic amines were able to generate good yields with over 50% reaction conversion to the desired HaloCompound. The reactions involving secondary linear amines were more likely to have poor conversion than the other categories, both in hindered and non-hindered variations. This result could be predicted, as a result of the decreased reactivity of a sterically hindered secondary amine, more than 62% of the reactions gave less than 20% reaction conversion. However, in the secondary linear amine categories, 9 reactions (over 25%) were successful in generating good conversion of the HaloCompound. Representative compounds are also shown for each category with their reaction conversion and plate position shown (**191–196, Figure 131B**). As the subset is relatively small and may not be representative of a larger set of secondary amines, it was decided that the results of this assay would not be considered in the selection of the 3000 amines. The secondary amines contained in the 3000-amine set would therefore be utilised in the synthesis of the validation set of HaloCompounds. In addition, they

would be analysed computationally in the same manner as the optimisation set to fully understand the limitations of this HTE amide coupling.

### A) Classes of Reactions into Categories and their Respective Conversions



### B)

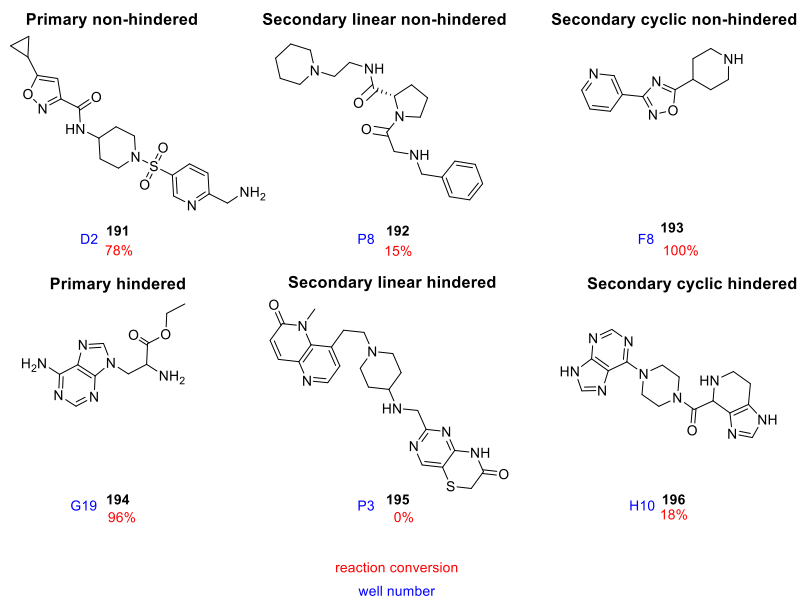
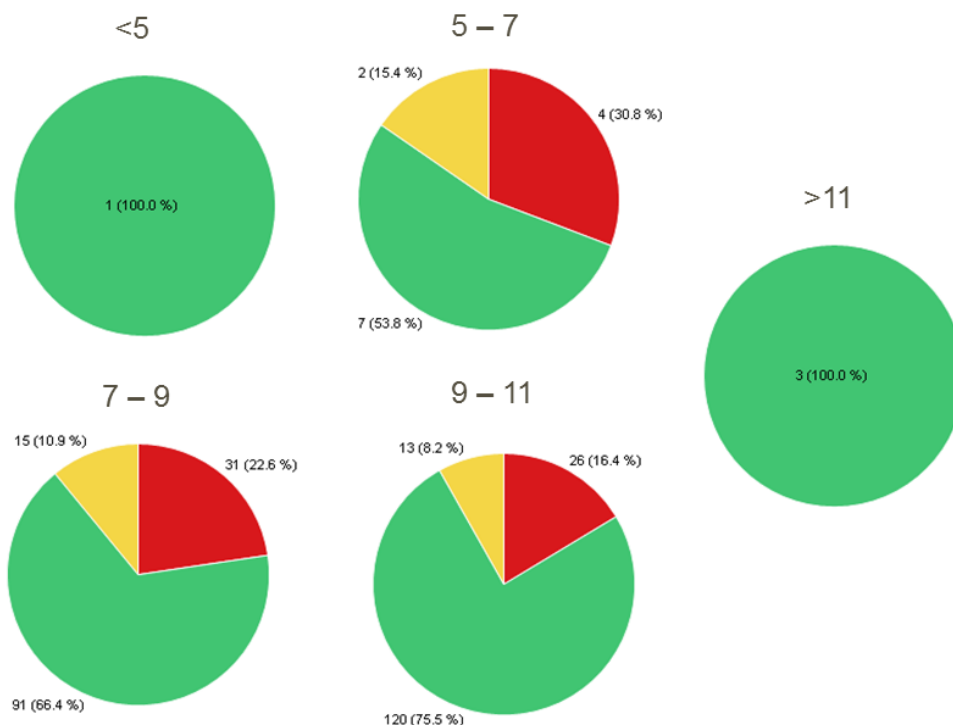


**Figure 131:** Analysis of the 300-amine optimisation set, reaction conversion over 50% good (green), between 20–50% moderate (amber) and <20% poor (red) into their respective 6 categories based on steric hinderance (A). Exemplar amines 191–196 from the class and respective conversion for each HaloCompound are shown in red, and well number is shown in blue (B).

In addition to the steric element which may influence the reactivity of the amines, the electronic effects of the amine were then considered for this small subset. In order to determine the

amine's reactivity, the  $pK_a$  values of the conjugate bases ( $pK_{aH}$ ) were calculated computationally for the most basic amine in the molecule.<sup>250</sup> Therefore, the  $pK_{aH}$  of the reactive aliphatic amine in the molecules was calculated and then compared to the reaction conversions observed in the 300-amine set (**Figure 132A**). The  $pK_{aH}$  values were categorised from less than 5 or "weakly basic" to 11 (or "highly basic") in increments of 2 logs (or a 100-fold difference). Compounds which contained the amines with higher  $pK_{aH}$  values would hypothetically be more nucleophilic and more likely to result in successful conversion to the desired HaloCompound. Exemplar amines from each of the classes and respective conversion for each HaloCompound **197–201** are also shown (**Figure 132B**). As shown in **Figure 132A**, there is not a clear correlation of  $pK_{aH}$  and reaction conversion as compounds containing very "highly basic" or "weakly basic"  $pK_{aH}$  values performed with good conversion. However, there were only 4 compounds in each of the the categories, so is not a large enough subset to be statistically significant. As there was not a significant correlation, this suggests sterics may be more likely to influence the outcome of the reaction. In order to test this hypothesis, a larger screen of compounds would be required to determine the correlation between sterics and electronics and their outcome on this reaction, and this would be carried out with the validation set (the 3000-amine set).

A) pKaH's of the 300-Amine set and Reaction Conversion



B)

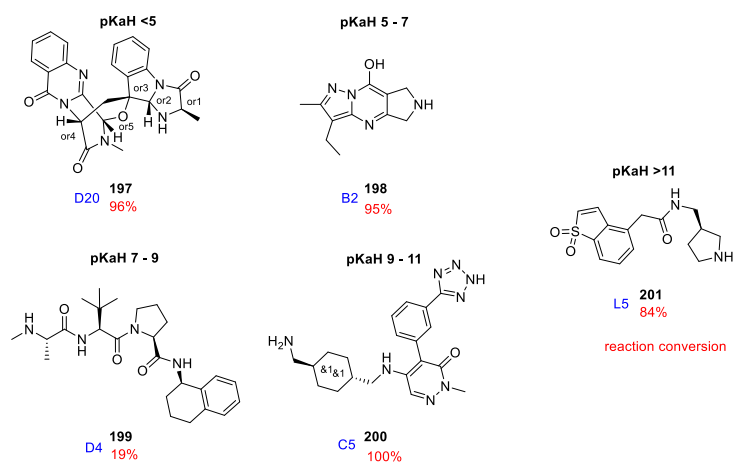


**Figure 132:** pKaH values of the 300-amine set were calculated and separate into 5 categories based on increasing pKaH values and then compared to reaction conversions observed (reaction conversion over 50% (green), between 20–50% (amber) and <20% (red)) (A). Exemplar amines **197–201** from the class and respective conversion for each HaloCompound (B).

Overall, nearly 200 HaloCompounds were synthesised in good yields using high-throughput chemistry. The compounds could therefore be tested in the GFP degradation assay, which will

be discussed in the next section. The optimisation set was analysed by both LCMS and computational techniques. Where there were two amines in a molecule, it was discovered that in most cases one amine preferentially reacted to give a monomeric HaloCompound. In a small number of cases, di-addition did occur and resulted in failed reactions to the mono-HaloCompound. The reactions which had poor conversion were further analysed to determine the reaction failure. This was hypothesised to be due to the steric bulk of the amines and was not dramatically affected by the amine's calculated pKa. As this was a relatively small test set, the validation set of 2934 amines would still be synthesised and analysed in the same manner, to determine if this was the significant driver of reaction failure. The results of the larger amine set could then be utilised to build a 100,000 amine set for further testing which would only contain amines hypothesised to be successful in this reaction.

#### **7.3.3.4 Further Chemistry Optimisation for HTE for the Validation Set**

After elucidating that the chemistry was efficient for the *in-situ* synthesis of the HaloCompounds, the next aim of the project was to synthesise thousands of compounds which could be used to assess the false positive rate for the biological assay. In a phenotypic high-throughput assay, a major source of complications is the deconvolution of hits, and the possibility of hits being false positives. Therefore, the hit rate for this assay would require investigation on a larger scale, using 3000 HaloCompounds to elucidate whether this assay would be suitable for the final HTS of 100,000 compounds. If the hit rate is too high, then the final assay would be terminated as compound follow-up would be too resource-intensive. Given the number of controls in place to reduce the false positive rate, with the mutant cell line counter screen, coupled with imaging algorithms developed in the previous chapter, it was envisaged that the screen would be suitable for a large-scale screening set, and would be evaluated with thousands of HaloPROTACs. Conversely, testing many compounds would lead to an increased probability of finding real hits for new E3 ligases for the protein degradation platform.

In order to synthesise a larger number of compounds, such as the 3000-compound validation set, introducing automation in the chemical reaction would be beneficial. A number of liquid handling robots were considered for this role. There was a requirement that the robot would need to be compact enough to be situated in a fume hood. There are many liquid handling robots that are utilised in high-throughput biology but are generally self-contained and not able to be moved into a chemistry-focused work space. Liquid handling robots that are frequently used to dispense large number of compounds include the Mosquito liquid handling robot, which has been used in a number of HTE chemistry publications which can be used in a fume hood or glovebox.<sup>204-206,217,218</sup>

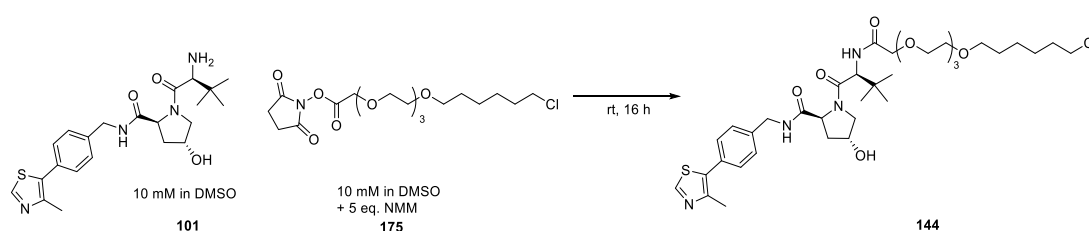
As the reaction has previously been successful in a fume hood, and due to the size of the Mosquito and lack of space in the available glovebox, the Mosquito was set up and calibrated in a fume hood and evaluated. The model of Mosquito that was employed was the LV Mosquito (low volume), where the Mosquito can dispense 1.2  $\mu\text{L}$  of solution into a 96/384/1536-well plate. The Mosquito dispenses using the 16-pipetting head into columns of the plate in positive displacement mode and it can therefore dispense into the 24 columns in a 384-well plate relatively quickly. (**Figure 133**). The Mosquito can change tips after every column dispense as programmed (the tips are stored in a reel with 36,000 tips), to ensure no cross contamination between dispenses. This was therefore envisaged as a suitable liquid handler robot to replace the semi-automated technique and would be validated in the HTE amide coupling previously described.



**Figure 133:** Mosquito Liquid handling robot, featuring a 16-pipette tip changeable head, allowing for positive displacement into entire columns of 384-well plates in one dispense with rapid tip exchange. Disposable pipette tips are held in a spool reel of 36,000 tips. Plate deck allows 5 plates (96/384/1536-wells supported) to be positioned on the robot at once. TTPLabTech®.

In order to synthesise a large number of HaloCompounds at once, it was envisaged that utilising the Mosquito could accomplish this in an extremely high-throughput manner. The Mosquito was evaluated for this HTE amide coupling by synthesising the VHL recruiting HaloPROTAC **144** *in-situ*. For the synthesis, 20  $\mu\text{L}$  total volume of reaction was previously used as this was the lowest volume that was compatible with the LCMS technique (10  $\mu\text{L}$  of the amine solution, and 10  $\mu\text{L}$  of the linker and base solution). As a result, and in addition to the Mosquito's ability to only dispense 1  $\mu\text{L}$  at a time, a repeat dispensing process was required to deliver the 10  $\mu\text{L}$  of the NHS ester **175** and NMM stock solution into the reaction plate. Therefore, this repeat dispense was achieved by dosing 10  $\times$  1  $\mu\text{L}$  from a source plate (also known as the reactant plate) onto the reaction plate. Before dosing the linker and base solution, the reaction plate was pre-dispensed with 10  $\mu\text{L}$  of 10 mM stock of VHL amine **101**

into every well, allowing for an identical 384-well plate to test the Mosquito's dispensing robustness. The total time for the Mosquito to dispense from the source plate into the reaction plate was 25 minutes per plate using the repetitive pipetting technique. In comparison, the dosing for the semi-automated electronic pipetting method was less than 5 minutes per plate. After the Mosquito dosed the linker and base solution across the plate, the plate was left to stand for 16 hours, and was then analysed by LCMS (**Figure 134**). It was previously observed that vigorously shaking the plate, compared to leaving the plate to stand, gave no additional conversion so all reaction plates were left to stand in a fume hood overnight (16 h). As the Mosquito dispensed to the columns, there was a "edge-effect" where there was incomplete reaction conversion at the edges, which was most noticeable in the latter columns (after about 20 minutes of dispensing). Conversions in the centre of the plate were as expected with >70% product observed, but for the last column the conversion was below 30% - the lowest result observed. It was hypothesised that time was the major factor in this failure, as the plates were previously complete in 5 minutes without issues. The initial hypothesis was that the NHS ester **175** could be hydrolysing during the experiment. Other NHS esters have been previously shown to be bench stable, but when **175** was stored at room temperature overnight, partial hydrolysis was observed, so was then stored in -20 °C. As a result, time dependency for dosing the reactants was further investigated.



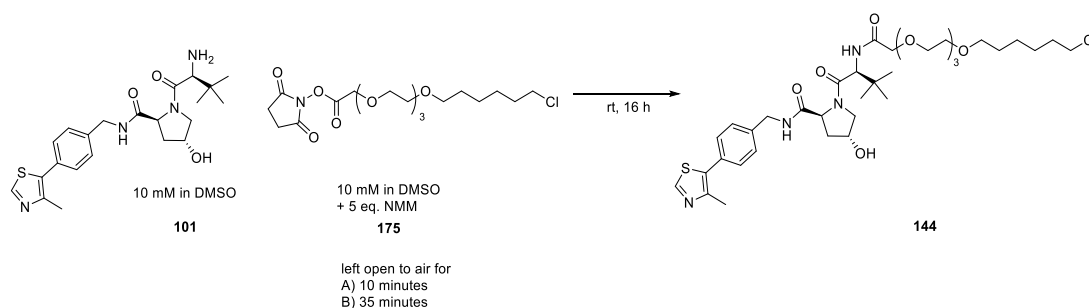
Mosquito dispense (starting from column 1)																								
	1	2	3	4	5	6	7	8	9	10	11	12	13	14	15	16	17	18	19	20	21	22	23	24
A	69	69	72	73	76	77	78	78	77	75	73	71	70	66	63	59	56	51	48	44	40	38	36	34
B	66	68	71	74	75	77	79	78	77	76	73	71	70	66	63	60	56	51	48	44	40	38	34	33
C	67	71	74	75	77	77	78	78	77	76	75	71	69	67	61	59	55	52	47	43	40	37	35	32
D	67	72	72	74	75	76	77	77	76	76	76	73	69	67	62	59	55	51	47	44	40	35	33	32
E	67	71	73	74	75	76	76	77	78	77	74	72	69	65	63	59	55	51	48	44	40	36	34	33
F	69	72	73	74	75	76	77	77	78	78	76	73	*	67	64	59	57	53	49	45	41	37	34	33
G	68	72	72	74	75	76	78	79	77	79	77	73	71	67	64	59	56	*	49	44	42	36	34	32
H	69	71	73	73	75	77	78	79	78	77	76	71	68	64	61	55	51	47	44	41	36	34	32	32
I	68	70	71	72	73	75	77	77	81	77	79	75	74	69	65	61	58	53	49	44	39	35	33	32
J	65	68	69	70	71	73	75	76	75	78	77	75	74	70	66	63	58	54	50	44	40	37	34	33
K	64	66	68	69	71	72	75	76	78	78	78	77	74	70	66	62	57	53	47	43	38	36	33	31
L	62	63	64	66	68	71	73	75	76	77	77	76	76	73	68	65	59	54	49	44	39	35	33	32
M	60	60	61	64	67	69	73	75	76	77	78	77	76	73	69	65	60	54	49	44	38	34	33	31
N	57	56	58	62	66	69	73	76	77	78	79	78	80	76	73	70	64	58	51	47	40	36	34	34
O	56	55	56	60	64	68	72	75	77	78	78	76	77	75	72	68	62	56	48	44	39	34	32	31
P	56	54	55	60	65	69	73	76	77	78	78	78	76	75	72	69	64	58	51	45	39	35	32	31

Conversion Key
80-100%
70-80%
60-70%
<60%

**Figure 134:** Formation of the VHL recruiting HaloPROTAC **144** in every well in a 384-well plate using a Mosquito liquid handling robot for dispensing the NHS ester **175** and base. The

Mosquito uses a 16-head feature, dispensing in each well in a column (A–P) at once, starting from column 1 to column 24 with a 25-minute total run time. LCMS analysis performed after overnight incubation and results depicted in colour coded key. \* denotes manual failure in dispensing VHL amine **101**, so no reaction occurred in the well.

In order to ascertain whether reactions were resulting in incomplete conversion due to the time required to dispense the linker and base stock solution, a similar experiment was conducted with the conditions previously used using the semi-automated electronic pipette. To wells containing the VHL amine **101** the linker and base stock solution was added at different time points. The linker and base stock solution were prepared and placed into a PP pipetting trough left to stand at rt for 10 minutes and was then added to the first row (A) of the reaction plate. This was then left for an additional 25 minutes in the fume hood (35-minute total), and was open to air, and then dispensed into the second row (B) (**Figure 135**). A lid was placed on the plate and it was left at room temperature for 16 hours. As suspected from the previous experiment, exposing the NHS ester **175** and base stock solution to air before dispensing had a dramatic effect on the product conversion. This ranged from around 40% conversion A) to around 10% conversion B) after leaving the stock solution for 10 and 35 minutes respectively. It was hypothesised that this may be due to the increased surface area to volume ratio of air giving rise to the potential for hydrolysis of **175**. To elucidate the issue in poor conversions, additional plates of the HaloPROTAC **144** were synthesised and <sup>1</sup>H NMR studies were subsequently carried out.

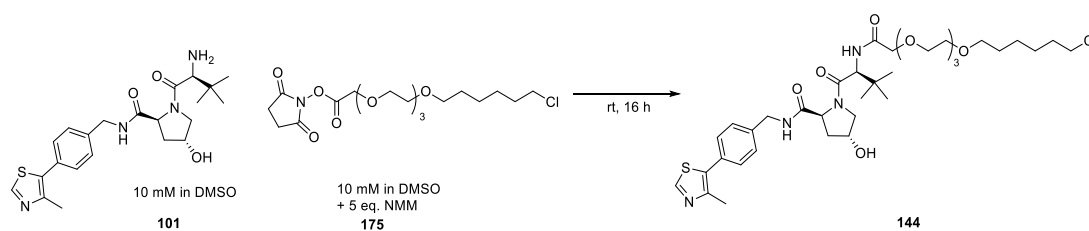


	1	2	3	4	5	6	7	8	9	10	11	12	13	14	15	16	17	18	19	20	21	22	23	24
A	47	44	42	42	43	44	45	45	45	45	44	43	39	41	41	40	40	39	40	39	38	38	40	40
B	7	7	7	8	9	10	11	11	12	13	15	15	9	9	9	9	10	11	12	13	14	15	17	17

Conversion Key
80-100%
70-80%
60-70%
<60%

**Figure 135:** Semi-automated synthesis of the VHL recruiting HaloPROTAC **144**. Time course experiment using NHS ester **175** addition onto a plate which contained identical wells featuring VHL amine **101** after ROW A) 10 minutes of NHS ester **175** stock dispensed into trough before plate addition in and after ROW B) 35 minutes. LCMS analysis performed after overnight incubation and results depicted in colour coded key.

In addition to the time course experiment, identical plates of VHL HaloPROTACs were synthesised in a fume hood using the semi-automated technique to compare the results with the Mosquito dispensing. As previously discussed, the Mosquito dispensing was 25 minutes in duration, and the semi-automated technique was less than 5 minutes for the entire plate dispense. Therefore, two identical plates of VHL HaloPROTAC **144** were synthesised in a fumehood using the traditional electronic pipetting techniques on different days to understand if the fumehood is having an impact on the reaction conversions. The air velocity at the face of the fume hood was recorded at 0.80 m/s (**Figure 136A**). This was repeated on a different occasion with the fume hood face velocity measured at 1.4 m/s which was higher than would be expected (typically velocity is between 0.40–0.60 m/s) (**Figure 136B**). Both plates carried out showed edge-effects, with incomplete conversions at the edge of the plates: with varying percentage conversions of between 50–88% depending on the location of the well on the plate. The plate prepared in the fume hood with the higher face velocity had more pronounced effects evident, with a large number of reactions having less than 60% conversion. It is not well understood why the pattern of the two plates has changed. But this was hypothesised to be due to the difference in where the plate preparation was carried out and could be a result of how the air extraction of the fume hoods operates. There are multiple factors to consider for the plate effect, but this experiment does elucidate that the fume hood technique may not be as robust as previously determined. This was not observed with the optimisation set, and the reason for this is not well understood. As a result, it was now hypothesised that the linker hydrolysis may not have been the issue for the time dependency but could have been due to evaporation of reaction components due to fume hood extraction, such as the base. This was further investigated using NMR to confirm that the fumehood was the reason for the edge effects on the identical plates.



## A) Reactions undertaken in FC with extraction measured at 0.8 m/s

	1	2	3	4	5	6	7	8	9	10	11	12	13	14	15	16	17	18	19	20	21	22	23	24
A	57	57	59	62	63	66	71	77	81	81	77	80	79	79	78	74	74	72	70	67	65	63	63	63
B	60	57	57	60	62	66	72	77	77	77	82	79	82	82	80	78	76	74	70	68	65	60	62	62
C	61	58	56	58	63	67	73	75	78	81	78	79	78	80	79	77	74	72	68	65	65	61	60	60
D	62	59	60	62	67	69	75	79	83	85	86	86	82	83	83	79	77	75	72	69	67	66	63	62
E	58	59	59	60	64	67	71	75	77	81	83	82	83	83	81	78	76	74	70	68	66	63	63	60
G	59	58	58	60	64	68	72	77	80	82	84	83	82	82	81	79	76	74	71	69	67	64	63	61
H	60	57	58	59	64	66	70	73	75	76	75	77	85	85	84	82	78	77	74	71	67	65	61	59
I	57	59	58	59	62	66	69	73	77	80	82	81	84	83	83	81	79	75	73	69	66	63	61	59
J	58	56	60	62	65	67	71	75	79	81	84	86	83	84	82	80	80	76	72	71	67	62	59	58
K	62	59	59	62	68	70	72	77	82	82	83	86	87	87	86	84	81	78	75	70	68	65	63	61
L	61	64	66	66	71	74	77	82	84	85	89	90	84	86	86	82	80	77	74	72	66	62	60	59
M	59	63	65	69	74	76	80	83	83	88	89	89	89	91	90	87	85	81	78	73	68	64	62	60
N	65	69	71	72	76	77	82	84	85	89	90	89	91	90	89	87	85	81	77	72	68	65	62	60
O	68	71	70	73	75	78	79	81	84	86	87	87	89	89	88	84	82	79	75	67	64	62	58	58
P	74	75	77	79	81	82	83	84	85	87	86	88	89	88	89	88	86	82	80	75	72	68	65	64

## B) Reactions undertaken in FC with extraction measured at 1.4 m/s

	1	2	3	4	5	6	7	8	9	10	11	12	13	14	15	16	17	18	19	20	21	22	23	24
A	54	51	49	50	48	48	49	46	50	49	49	49	50	50	53	54	57	57	58	58	57	58	57	58
B	58	52	51	52	50	49	48	47	48	49	49	48	50	52	54	57	58	59	58	59	57	57	55	55
C	56	53	53	51	49	51	50	50	50	51	50	51	51	53	54	56	59	60	61	61	59	58	59	55
D	57	55	54	51	52	52	53	51	51	54	52	54	53	56	57	59	64	62	65	64	62	59	59	57
E	57	57	58	55	54	52	52	53	53	53	54	54	56	56	58	62	61	64	65	65	63	62	60	61
F	66	64	61	59	59	57	57	58	57	58	59	58	56	58	59	61	66	67	68	68	66	65	63	64
G	63	60	57	56	57	58	57	55	54	54	55	56	61	62	64	64	69	71	70	70	69	67	66	65
H	67	64	62	61	60	59	60	59	60	60	60	62	58	59	61	64	66	69	69	68	69	66	69	67
I	67	65	64	55	62	55	56	60	60	62	61	62	65	66	68	69	73	75	76	77	75	75	75	71
J	58	59	57	57	61	64	63	65	65	67	68	68	75	77	79	82	84	85	85	83	82	80	79	79
K	62	63	63	62	63	69	71	71	71	73	74	74	73	75	77	80	82	84	86	85	84	83	81	79
L	*	67	67	67	66	67	67	68	68	69	70	73	*	76	73	79	77	79	81	86	85	83	82	79
M	61	63	59	60	65	63	63	64	65	66	67	78	71	73	79	78	80	82	87	86	85	84	80	80
N	63	60	60	61	62	62	63	64	64	64	67	67	71	71	73	76	83	85	87	83	83	81	76	74
O	62	66	65	64	65	63	62	62	64	65	66	67	71	73	74	78	83	83	84	85	84	81	81	76
P	66	65	65	64	66	66	65	60	69	70	72	72	74	72	74	81	82	87	88	88	85	84	82	79

Conversion Key
80-100%
70-80%
60-70%
<60%

**Figure 136:** Semi-automated synthesis of the VHL recruiting HaloPROTAC **144** in every well. Performed on two separate days in the same week in the same fume hood, dispensing with the plate dispensed in the FC with extraction measured at 0.8 m/s (A). The plate dispensed in the FC with extraction measured at 1.4 m/s. LCMS analysis performed after overnight incubation and results depicted in colour coded key. \* denotes dispensing error (pipette was loose and no dispense occurred and therefore no reaction took place). (B) \* denotes manual failure in dispensing VHL amine **101**, so no reaction occurred in the well.

In order to determine if the fume hood extraction of the base from the reaction was the reason for reaction failure NMR studies were carried out. Stock solutions of the NHS ester **175** and 5 eq. of NMM **202** were prepared and placed into a PP trough, mimicking the steps required to carry out the reactions previously. The solvent used was deuterated DMSO in order to analyse the stock solutions by NMR. NMR analysis was carried out at T = 0 and T = 25 minutes (**Figure 137**) after the stock solution was left to stand in the fume hood. At T = 0, surprisingly, only 3 equivalents of the base were present at the time the NMR analysis was conducted. Equivalents were determined by comparing the protons in the methylene of the linker to the

protons in the methyl group in NMM **202** (Figure 137A). At T = 25 minutes, only 1 equivalent remained in comparison to the NHS ester **175** (Figure 137B). This NMR also confirms that the NHS ester **175** appeared to be stable under the conditions required to carry out the reaction. The NHS ester methylene protons were observed at 4.60 (T = 0) and 4.56 (T = 25 minutes) and methylene protons of the acid compound **162** would be observed at 4.14 ppm, so time-dependent hydrolysis was discounted as a rationale for reaction failure. This experiment indicates the cause of the reactions failing over time, the base was evaporating under these conditions and halting the amide coupling. The VHL amine **101** was stored as a trihydrochloride salt, and without sufficient base the reaction would not proceed. NMM **202** has a boiling point of 115 °C and has a vapour pressure of 18 mmHg (20 °C).<sup>251</sup> When pipetting the linker and base solution from a trough (electronic pipetting) or a reactant plate (Mosquito dispensing) in fume hood conditions, there is a large surface area to volume ratio, which would allow the base to evaporate over time. Therefore, a more robust method of delivering the linker and base solution would be required for the 3000-amine set.

With regards to installing automation for the experiments, the time required for the Mosquito to dispense the base and NHS ester **175** stock would not be sufficient for the 3000-amine set, therefore this technique would not be utilised. Automation could be revisited with either a higher boiling point base (which would need to be screened for compatibility in the biological assay) or with NMM if the Mosquito was placed into a glovebox. It was hypothesised that the evaporation of NMM after the reaction could be advantageous prior to the subsequent biological experiments as any alternative higher boiling bases would need to be biologically evaluated before use. The 3000-amine set would therefore be synthesised using the previously established rapid pipetting technique and using increased equivalents of NMM to minimise base evaporation during reaction plate preparation.

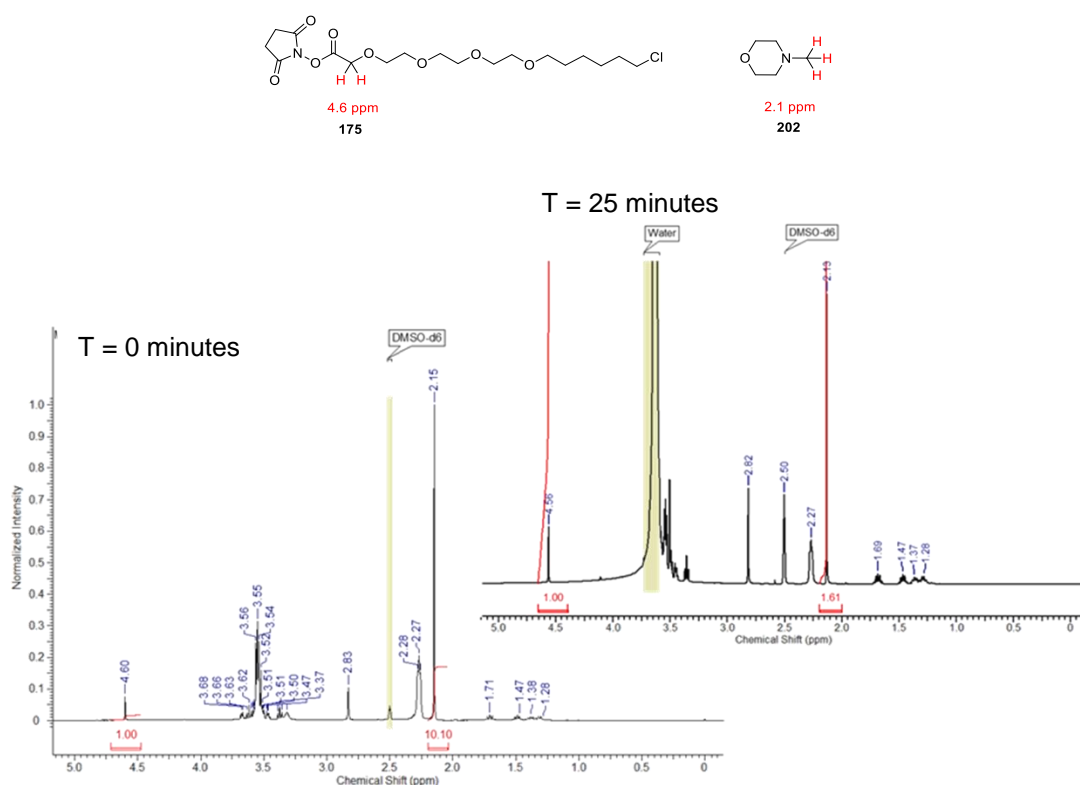
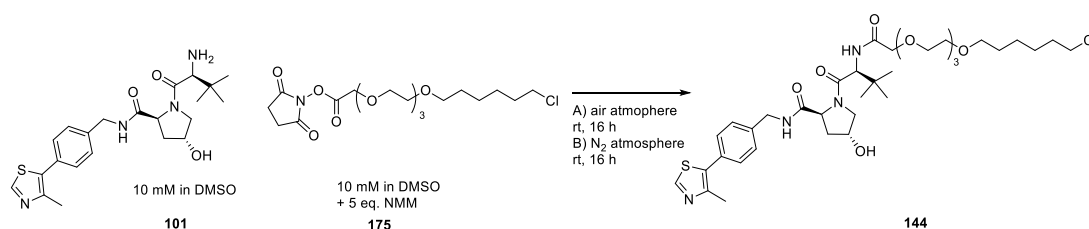


**Figure 137:** NMR study of NHS ester **175** and base **202** in DMSO-*d*<sub>6</sub> stock after dispensing into a trough then analysed by NMR at T = 0 minutes, showing approximately 3 equivalents of NMM **202** remaining (A), and T = 25 minutes of being open to the air in the fumehood, with approximately 1 equivalent of NMM remaining (B).

To synthesise the HaloCompounds from the 3000-amine set, which was contained in nine 384-well plates, a more robust dispensing method was required. As a glovebox provides a positive-pressured environment of nitrogen, this may reduce the inconsistent edge effect observed in previous experiments conducted in a fume hood. Unfortunately, the Mosquito could not be employed in an available glovebox due to the size of the machine. However, using the previous method of semi-automated electronic pipetting, the reactions could be performed in a glovebox. In order to assess the HTE amide coupling in a glovebox, two identical plates of VHL HaloPROTAC **144** were synthesised, one in a fumehood and one in a glovebox for comparison. The plate which was prepared in a fume hood is shown in **Figure 138A**, using the previously described technique with the electronic pipettes. And the other plate was also prepared in the same manner, but in a glovebox environment (**Figure 138B**). LCMS data shows a slight edge effect in the fume hood as previously seen, with one corner of the plate having moderate yields of HaloPROTAC **144** formation. This effect was less severe than previously described. This result could be due to a number of parameters, such as the equivalents of the NMM in the reaction, which has been shown to be highly dependent on the speed of pipetting, or the fumehood extraction. In contrast, the reactions in the glovebox

gave high conversion to the desired product **144**, suggesting this is a more robust method of dispensing. There were very little edge effects resulting from pipetting the linker and base solution in the glovebox. The majority of the plate had excellent conversion and good constituency was observed well to well. The small plate effect observed in one corner could be a result of reduced equivalents of base in these wells. As a result, moving forward, more equivalents of NMM would be used to mitigate this issue, for example, using 10 equivalents. This was envisaged as an alternative method to electronic pipetting in a fumehood and therefore a glovebox would be used in the larger screen.



## A) Reactions undertaken in FC

	1	2	3	4	5	6	7	8	9	10	11	12	13	14	15	16	17	18	19	20	21	22	23	24
A	88	86	87	86	87	86	86	85	84	82	81	79	75	74	71	72	68	68	67	66	64	63	63	65
B	86	83	79	81	78	83	78	81	81	77	76	70	72	71	70	69	67	66	65	64	64	62	62	62
C	87	85	83	84	83	82	81	81	79	76	76	73	74	74	73	70	70	69	68	67	66	65	65	64
D	86	84	83	83	81	82	80	79	79	78	78	77	76	76	71	73	66	70	67	67	66	64	64	67
E	88	87	86	85	84	83	**	85	82	81	82	79	80	75	75	74	72	73	71	69	69	68	68	67
F	91	84	87	87	83	84	79	79	80	80	79	76	81	81	78	73	76	75	71	72	70	70	70	70
G	87	87	88	86	85	84	85	85	84	77	78	81	80	79	77	77	75	75	75	73	73	72	71	71
H	88	87	86	86	83	84	86	85	84	84	83	77	82	81	80	82	80	79	77	78	75	75	74	75
I	88	87	88	87	86	86	86	85	86	85	84	83	84	82	84	82	82	81	80	79	77	76	75	75
J	88	86	86	85	86	86	86	86	84	83	84	84	85	83	83	84	83	81	79	79	79	77	77	77
K	88	86	86	86	83	86	85	85	86	86	86	86	83	84	85	84	84	83	82	82	81	80	79	79
L	85	84	84	83	83	83	83	83	82	82	82	82	83	83	84	83	83	83	81	82	82	81	80	81
M	87	85	85	84	83	84	83	83	83	83	83	84	85	85	86	86	86	85	84	82	81	81	81	81
N	84	84	82	82	83	83	83	83	83	83	83	83	83	84	81	84	83	84	78	79	79	82	81	81
O	85	84	84	84	84	84	84	86	85	85	87	85	85	87	87	83	87	85	87	87	86	85	85	86
P	85	80	82	81	83	84	86	85	85	86	85	82	86	88	88	84	85	89	88	88	88	88	88	87

## B) Reactions undertaken in glovebox

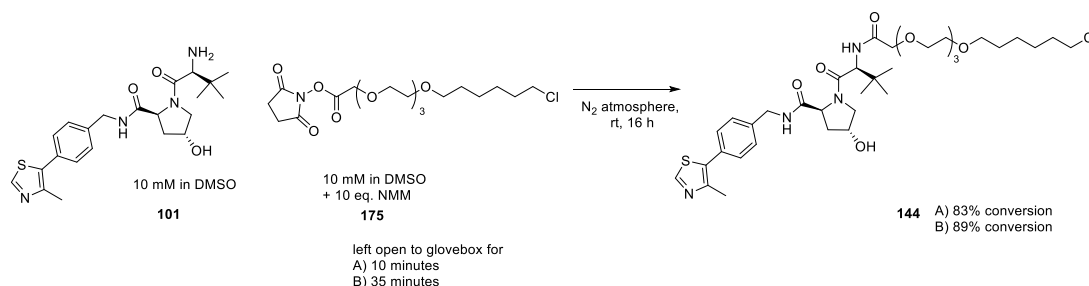
	1	2	3	4	5	6	7	8	9	10	11	12	13	14	15	16	17	18	19	20	21	22	23	24
A	88	69	73	71	72	71	72	71	71	71	74	74	78	75	73	80	80	79	80	73	78	77	73	73
B	72	73	74	77	72	76	76	76	77	79	78	79	82	82	83	79	78	79	83	79	81	82	80	77
C	77	76	79	79	80	80	80	76	81	81	83	83	84	84	85	85	85	85	85	85	83	82	81	77
D	80	81	82	82	84	82	84	82	81	83	84	84	86	84	87	86	84	86	84	85	82	81	84	78
E	82	85	86	85	86	85	86	85	81	82	83	87	87	89	88	88	87	87	89	88	87	86	85	84
F	81	83	84	81	84	84	85	86	85	84	86	86	88	89	91	90	90	91	90	91	85	88	83	82
G	82	84	85	85	87	87	87	87	80	81	88	89	88	89	87	89	87	90	89	88	88	87	87	85
H	84	85	86	85	86	85	85	86	86	87	87	87	90	90	88	89	87	88	89	86	88	84	84	85
I	85	86	86	86	82	82	87	88	88	87	89	89	87	86	92	92	87	91	91	91	87	89	88	87
J	87	84	88	87	88	86	89	88	88	88	89	84	88	90	92	92	92	92	92	91	91	90	89	88
K	86	84	86	87	88	87	88	88	87	87	89	89	89	89	92	90	92	92	89	91	89	89	89	87
L	85	86	86	87	87	87	89	89	89	89	89	90	90	91	91	92	91	92	91	89	89	89	89	87
M	86	88	88	88	85	87	88	88	87	87	89	89	87	91	91	87	91	90	85	90	89	88	86	86
N	83	86	86	87	86	87	88	88	87	87	87	87	90	90	88	90	91	91	87	90	89	88	88	85
O	84	84	85	86	87	84	85	83	86	86	87	88	90	90	90	90	90	90	89	88	87	87	85	85
P	84	87	85	85	83	86	86	86	83	83	83	86	86	86	90	85	89	89	89	88	87	86	86	83

Conversion Key
80-100%
70-80%
60-70%
<60%

**Figure 138:** Semi-automated synthesis of the VHL recruiting HaloPROTAC **144** in every well. Performed in a fumehood open to air (A) and a glovebox with a nitrogen atmosphere (B). LCMS analysis performed after overnight incubation and results depicted in colour coded key.

The time course experiment previously carried out in the fumehood was replicated in the glovebox. One row of a 384-well microplate (24 wells) of pre-dispensed VHL amine **101** was treated with the f NHS ester **175** and 10 eq of NMM from a PP dispensing trough as previously

described. After 25 minutes this was dispensed into a second row (24 wells) of pre-dispensed VHL amine **101**. This was left to stand in the glovebox for 16 h and then analysed by LCMS (A6 and B6 were chosen to represent the plate as the plate-based LCMS was unavailable) (**Scheme 22**). Both reactions gave very good conversion (over 80%) to the desired product despite the time difference in pipetting in the NHS ester **175** and base. This was considered as a suitable dispensing method to utilise in the 3000-amine synthesis as it ensured sufficient base was present for the reactions.



**Scheme 22:** Semi-automated synthesis of the VHL recruiting HaloPROTAC **144** in every well in a glovebox. Linker dispensed in A) identical row of pre-dispensed VHL amine **101** immediately after the NHS ester **175** stock was dispensed into a trough. B) 25 minutes later into another identical row of pre-dispensed VHL amine **101**. LCMS analysis performed after overnight incubation of A6 and B6 representing T = 10 minutes and T = 35 minutes after trough dispense to give conversion for (A) and (B) respectively.

### 7.3.3.5 HaloCompound In-Situ Synthesis for the Validation Set

With conditions optimised in a glovebox, ensuring the chemistry would be robust and reproducible across the plates, the HTE amide coupling could be performed on the validation set. The 3000-amine set, containing 2934 amines, were delivered in 9 plates in a random order, each with 10  $\mu$ L of the DMSO stock of the amines for the HaloCompound synthesis. The plates were also designed to contain controls for the subsequent biological assay. As a result, column 6 contained only DMSO for all plates in the validation set. Also, in each plate there were 16 replicates of the VHL amine **101** for the *in-situ* synthesis of HaloPROTAC **144** as a positive control for the biological assay (column 18). In all nine plates, this equated to 144 positive control wells, which results in 3078 amines present for the validation set including controls. The NHS ester **175** and 10 equivalents of NMM was made up to a 10 mM stock solution in DMSO. Using the glovebox conditions, the 9 plates were dispensed and left to stand for 16 h in the glovebox. The results are shown in **Figure 139** with 64% of the 3078 reactions working with over 50% conversion by LCMS (1956 reactions including the 144 positive control wells). 30% of the reactions failed with less than 20% conversion to the desired HaloCompound (936 reactions). 6% of the reactions went in moderate conversion between 20–50% (186 reactions). In the reactions which failed, around 183 of the reactions (20% of the

936 that failed) had no starting material nor product present in the LCMS trace. This could be as a result of impure starting materials, which was observed in the optimisation set or a result of insufficient UV absorbance of both the starting material and product leading to misinterpretation of the results. Due to LCMS capacity and long run time required, the starting materials from the 3000-amine set were not checked for purity by LCMS. In addition, manually visualising the LCMS traces for the 3000-amine set would require significant time, so was not carried out in this instance. Only hit compounds in the biological assay would be fully analysed by LCMS to ensure the compounds were made successfully in sufficient quantities, as this was a hit finding exercise for GFP degraders.

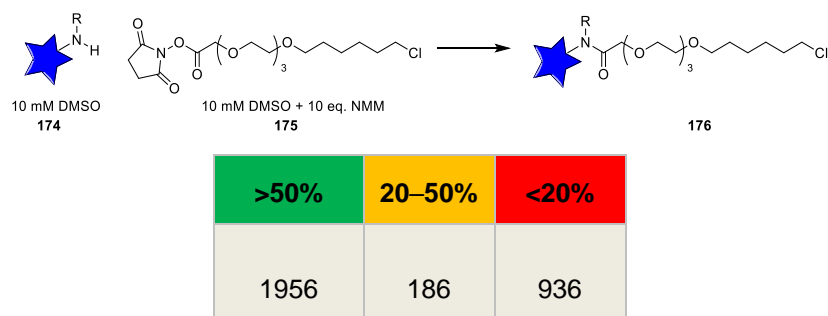
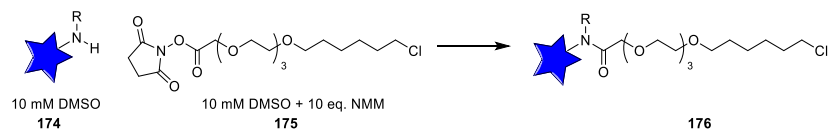


**Figure 139:** Results from synthesis of HaloCompounds from the 3000-amine set carried out in a glovebox with percentage conversion and number of wells in each category with over 50% good (green), between 20–50% moderate (amber) and <20% poor (red).

The reactions in the nine plates showed no apparent edge effects. This was confirmed with the VHL amine **101** control wells in the different plates, which had excellent conversion to the desired HaloPROTAC **144**. In **Figure 140** and **Figure 141**, there are two exemplar plates from the validation set, the best performing plate, plate 2 (**Figure 140**), and the worst performing plate, plate 4 (**Figure 141**). In plate 2, 69 of the 364 reactions had poor conversion (20%) and 275 had over 50% conversion (76%) (**Figure 140B**). In plate 4, 150 of the 368 reactions had poor conversion (41%) and 194 had over 50% conversion (53%) but in the control wells, all reactions worked well without plate effects. This result shows the poor conversion could be a result of the starting material, possibly due to poor reactivity or impure starting materials, but not the position on the plate (**Figure 141B**). The additional plates from the screen are shown in the experimental section (**Supplementary Figure 1**).

A)



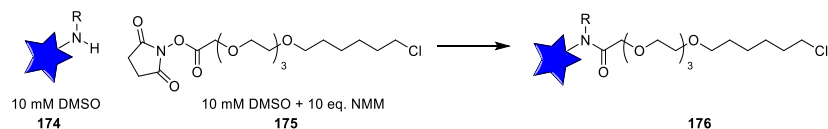
		Amines (Plate 2)																							
		1	2	3	4	5	6	7	8	9	10	11	12	13	14	15	16	17	18	19	20	21	22	23	24
Amines (Plate 2)	A	82	94	80	51	100		100	100	100	100	94	100	0	0	100	95	100	100	100		100	100	0	98
	B	0	100	93	0	84		88	100	55	88	100	40	100	100	47	100	56	100	12	0	0	100	0	0
	C	0	100	100	68	0		85	100	98	100	100	100	100	100	100	100	100	100	0	0	100	100	100	35
	D	68	100	100	95	0		25	100	100	39	0	100	48	100	0	100	87	100	100	0	100	97	100	100
	E	95	100	31	93	56		100	94	100	100	100	0	95	92	100	100	100	100	23		82	30	14	100
	F	100	100	89	100	100		100	21	100	100	0	0	0	0	100	100	100	67	100	94	36	46	54	0
	G	0	100	0	100	93		100	71	0	100	100	100	100	100	0	0	100	100	100		64	100	100	100
	H	100	89	48	100	0		100	97	100	100	0	0	0	0	0	100	100	100	100	83	100	100	0	91
	I	100	0	43	100	0		100	4	100	100	100	100	88	100	100	62	62	100	9		93	53	100	100
	J	100	37	100	100	0		100	27	100	79	0	100	100	100	98	100	89	100	0	79	14	100	63	0
	K	100	78	100	52	100		100	100	100	0	100	84	31	91	82	93	100	100	100	100	100	100	97	50
	L	100	100	100	100	100		92	0	92	0	0	100	0	97	100	100	100	100	100	0	100	100	100	100
	M	100	6	100	90	100		100	100	100	100	0	100	0	29	0	72	98	100	100	100	100	100	85	36
	N	100	0	56	100	18		100	100	100	0	0	100	68	0	100	0	100	100	88	100	0	100	100	100
	O	100	76	0	0	20		0	89	94	81	52	100	86	63	100	90	100	100	100	57	0	30	100	0
	P	93	100	100	100	6		91	87	81	100	100	100	100	100	100	100	100	100	100	90	0	100	100	56

B)

Number of reactions with >50% conversion	Number of reactions with <20% conversion	Conversion Key
275	69	
		20-50%
		50-70%
		70-100%

**Figure 140:** High-throughput amide coupling to generate HaloCompounds from the 3000-amine set using an NHS ester and NMM as a base (in a glovebox). LCMS analysis performed after overnight incubation of 9 plates and results depicted in colour coded key. Plate shown as example from the screen: LCMS data shown for the best performing plate (Plate 2, (A)). For each plate Column 18 (blue) had identical VHL amine **101** as positive control wells and cells depicted in white were not populated. Overall reaction success and conversion key (B).

A)



		Amines (Plate 4)																							
		1	2	3	4	5	6	7	8	9	10	11	12	13	14	15	16	17	18	19	20	21	22	23	24
Amines (Plate 4)	A	60	100	0	91	0		54	40	0	83	0	40	100	100	72	0	100	100	100	0	85	28	0	
	B	0	100	73	0	100		95	100	100	100	91	0	100	100	100	0	0	100	0	36	100	100	39	0
	C	0	91	15	100	100		0	36	100	0	85	0	100	0	0	0	0	100	51	0	23	87	84	0
	D	93	0	100	70	95		13	0	91	100	100	100	60	0	100	0	0	100	30	56	100	85	100	100
	E	100	0	100	0	100		46	0	100	63	100	79	0	93	0	0	11	100	0	63	100	22	60	0
	F	81	9	100	0	0		100	0	50	61	0	0	27	88	100	0	57	100	56	0	0	100	100	0
	G	52	0	100	0	100		0	100	100	10	0	0	100	100	0	15	100	100	55	100	90	100	60	0
	H	0	100	80	0	94		100	100	100	0	0	36	0	0	68	0	100	100	0	100	57	0	0	0
	I	0	100	100	100	0		100	0	0	100	0	25	100	83	100	100	66	100	100	0	89	100	0	100
	J	95	0	91	0	95		82	0	0	0	0	28	0	0	0	0	89	100	96	100	100	0	0	0
	K	0	0	100	43	100		100	4	0	0	0	0	100	0	45	100	23	100	100	100	100	100	0	96
	L	0	0	0	0	100		0	0	100	0	0	100	0	0	100	0	88	100	0	82	100	0	0	100
	M	0	53	84	0	52		100	100	0	100	0	0	100	48	100	28	100	100	100	0	84	100	0	67
	N	0	0	0	86	96		0	90	44	95	0	64	0	0	0	100	100	100	0	100	100	0	0	93
	O	0	74	0	0	90		73	85	25	100	91	12	0	100	72	0	93	100	0	0	100	100	100	0
	P	100	0	100	0	100		100	0	39	63	87	50	100	0	0	89	100	100	0	0	100	0	0	19

B)

Number of reactions with >50% conversion	Number of reactions with <20% conversion	Conversion Key <20% 20-50% 50-70% 70-100%
194	150	

**Figure 141:** High-throughput amide coupling to generate HaloCompounds from the 3000-amine set using an NHS ester and NMM as a base (in a glovebox). LCMS analysis performed after overnight incubation of 9 plates and results depicted in colour coded key. Plate shown as examples from the screen: LCMS data shown for the worst performing plate (Plate 4, (A)). For each plate Column 18 (blue) had identical VHL amine **101** as positive control wells and cells depicted in white were not populated. Overall reaction success and conversion key (B).

### 7.3.3.6 Computational Analysis of the Validation Set

In order to rationalise the outcomes of the reactions, the compounds were categorised computationally and the reaction conversions were evaluated for each category. As with the 300 amine optimisation set, the compounds were placed into one of six categories depending on the steric bulk proximal to the amine (**Figure 142**). Out of the 2934 amines, 667 contained primary centres and the rest contained secondary. If there are two amines in the same molecule, the compounds were classified by their least hindered amine (6 examples found with both a primary and secondary centre, so these are included in the primary category). There was an even split between primary hindered and non-hindered, as expected with the previous optimisation set. The majority of the amines fell into the secondary cyclic non-

hindered category with 868 out of the 2934 amines, which was reflective of the GSK compound collection as a whole. The collection comprised of many piperidine/piperazine and pyrrolidine amines which have proven useful in medicinal chemistry as solubilising groups and adding  $sp^3$  character into molecules. The second largest category was the secondary linear hindered category, with 639 amines, compared to 464 non-hindered amines. From the 3000-amine set, it will be extremely useful to understand the failed conversion of this amide coupling from this large data set. This could then feed into computational analysis for the larger phenotypic screen of 100,000 molecules. LCMS would not be possible on the entire HTS reactions but would be performed on compounds which were shown to be potential positive hits. As a result, the larger screening set would only contain amines which were hypothesised as reactive towards the HTE amide coupling to increase the probability of HaloCompounds which could find hits for E3 ligases.

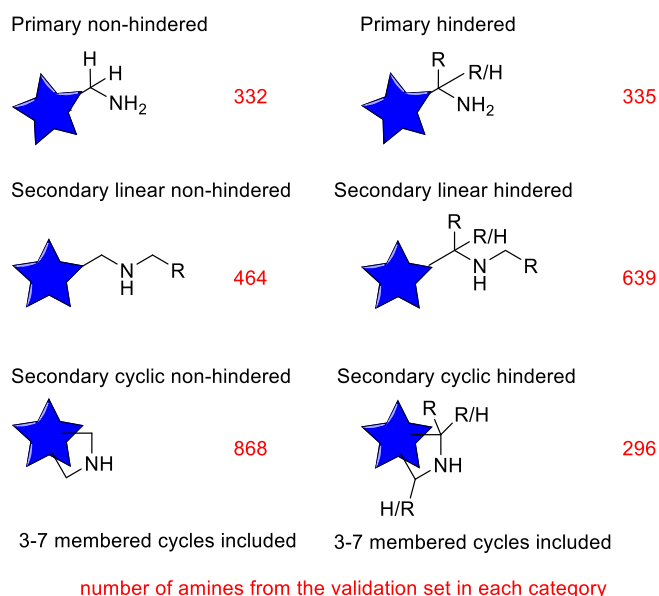
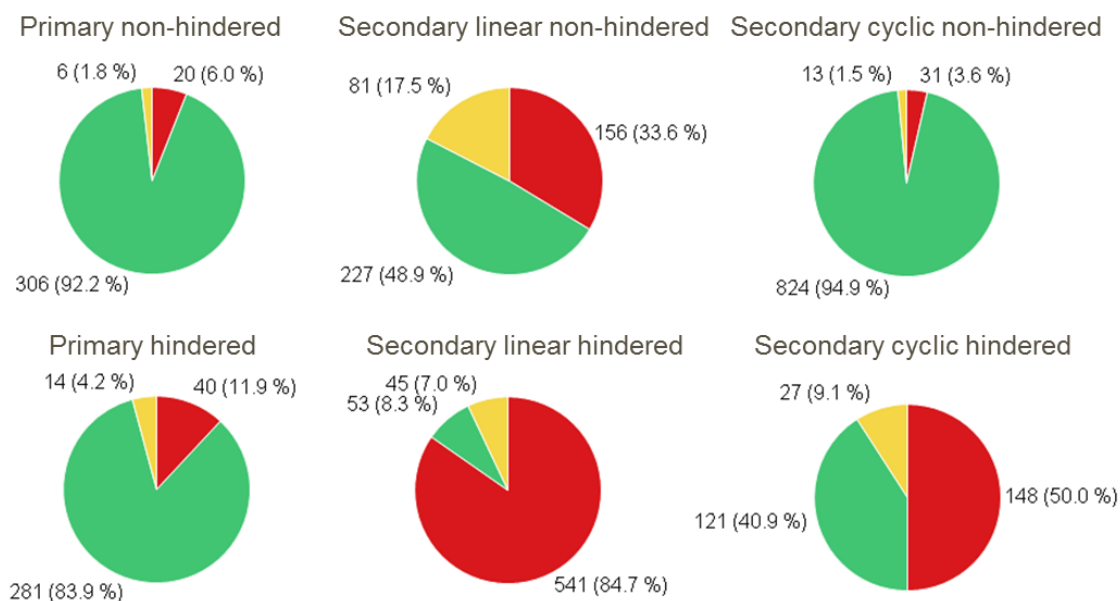


**Figure 142:** Categories of amines and number of each from the validation set and numbers featured in red. If there are two different amines in the same molecule with different categories, the compound is classified by its least hindered amine (6 examples).

The product conversions observed in the validation set were then analysed and compared to the compound's steric hindrance category (**Figure 143A**). For this set, the starting materials were not analysed by LCMS in the same manner as the optimisation set. Therefore, some reactions may have failed due to starting material impurities which has to be considered when analysing the results. The primary amines, as expected, gave good conversion regardless of steric hindrance in the alpha position, as seen in the previous set. The secondary non-hindered linear amines were successful in 49% of cases, and the hindered linear amines were only successful in 8%. This confirms that sterics are likely to play a major role in this reaction. The compounds could be too sterically encumbered to react with the NHS ester. The

secondary cyclic amines were more successful overall than secondary linear amines. The non-hindered cyclic secondary amines gave good conversion with 95% of the amines successful. The cyclic hindered secondary amines were successful in 41% of cases, with 50% having poor conversion. Example amines **203–208** from each category are shown, with respective conversions stated (**Figure 143B**). In total, 84% of the sterically hindered secondary linear amines failed, in comparison to 61% with the optimisation set. This was relatively surprising and could be a result of the small subset of the 300, giving statistically insignificant results. With these results categorised, the future screens would contain 5 categories, and remove the secondary hindered linear amines using the same conditions. In order to further improve the scope of the reaction, chemistry optimisation could be undertaken with the hindered compounds, such as by altering the activated ester, or altering temperature of the reaction.

A) Classes of Reactions into Categories and their Respective Conversions



B)

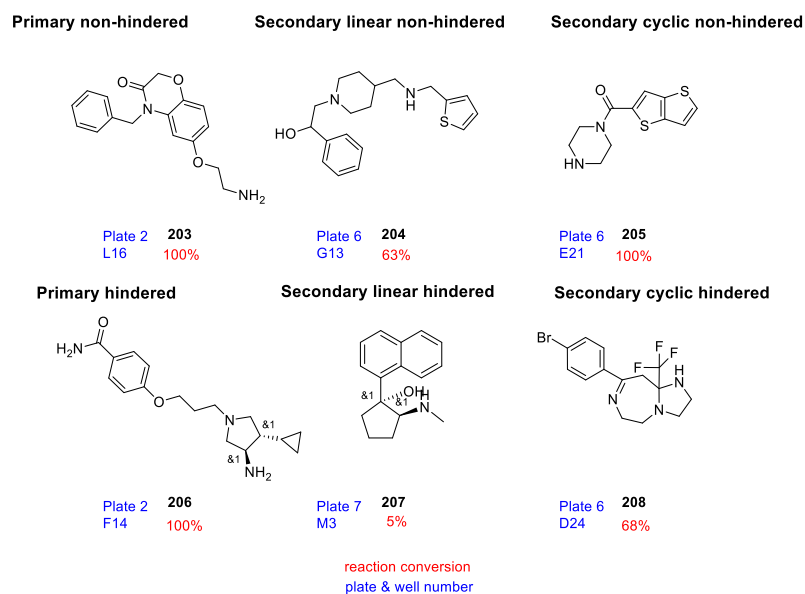
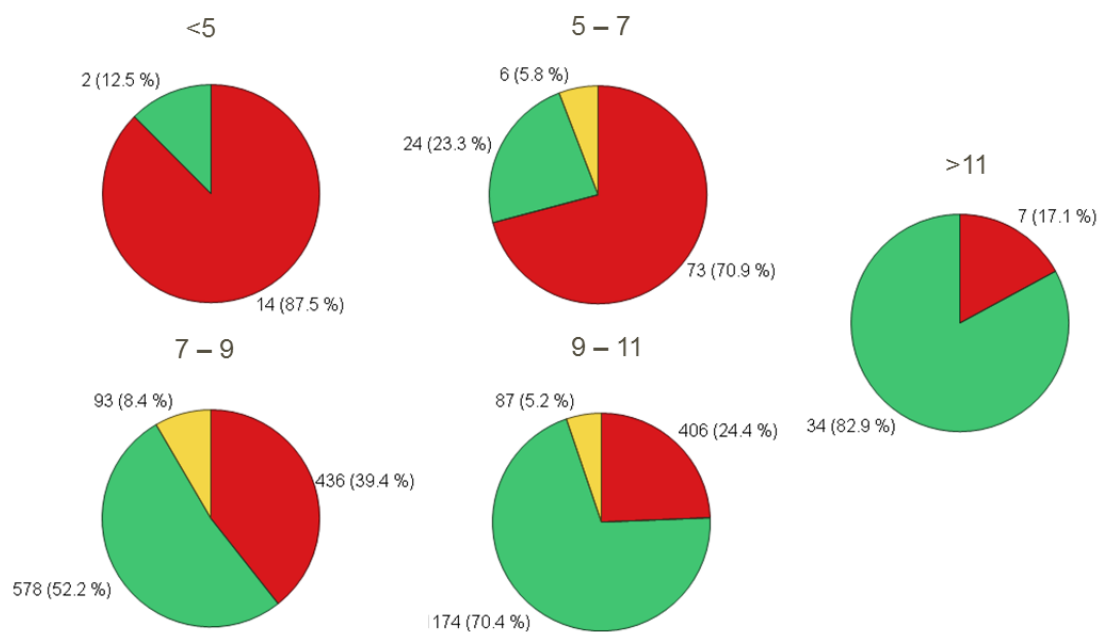


**Figure 143:** Analysis of the 3000 validation set, reaction conversion over 50% good (green), between 20–50% moderate (amber) and <20% poor (red) into their respective 6 categories based on steric hinderance. Number of reactions denoted with percentage of overall of the category in brackets (A). Exemplar amines **203–208** from the class and respective conversion for each HaloCompound (B).

In addition to the steric element which may influence the reaction, the electronics of the reactive amine were also considered. In order to determine their reactivity, the amines'  $pK_a$

values of the conjugate bases ( $pK_aH$ ) were calculated computationally<sup>250,252</sup> and then compared to the reaction conversions observed in the 3000-amine set (**Figure 144A**). The  $pK_aH$  values were classed from less than 5 or “weakly basic” to 11 (or “highly basic”) in increments of  $pK_aH = 2$  (or a 100-fold increase) in an analogous manner to the optimisation set. Example amines from each class (**204, 205, 208–210**) are shown with their respective reaction conversions (**Figure 144B**). More basic amines are expected to react with better conversion due to increased nucleophilicity. The compounds with  $pK_aH$  values less than 7 (87/119) were observed to have conversions less than 50%. This correlates well with the amines’ calculated  $pK_aH$  values. Compounds with  $pK_aH$  values of less than 5 were more likely to give poor reaction conversions. This could be a result of decreased reactivity or nucleophilicity of the amines. With a  $pK_aH$  value of between 7 and 9, there is a 50% chance the reaction would proceed with good conversion. This is hypothesised to be due to the reactivity as a result of combined electronic and steric effects. Compounds with  $pK_aH$  values over 9, were more likely to have good conversions, with 71% of the amines in this category showing over 50% conversion to the desired compound (1208/1708 reactions). Therefore, increasing the  $pK_aH$  led to increasing reactivity and better conversions overall, as expected. This information could be useful if another larger screening subset was carried out. This information, along with the steric bulk effects found on reaction conversion, could be utilised to build a reaction predictor model for future transformations using the same conditions. This would ensure the 100,000 amine screen contained compounds which were more likely to give good conversion, which could increase the probability of finding an active hit for a new E3 ligase.

## A) pKaH values of the 2934 Amines and Reaction Conversion



## B)

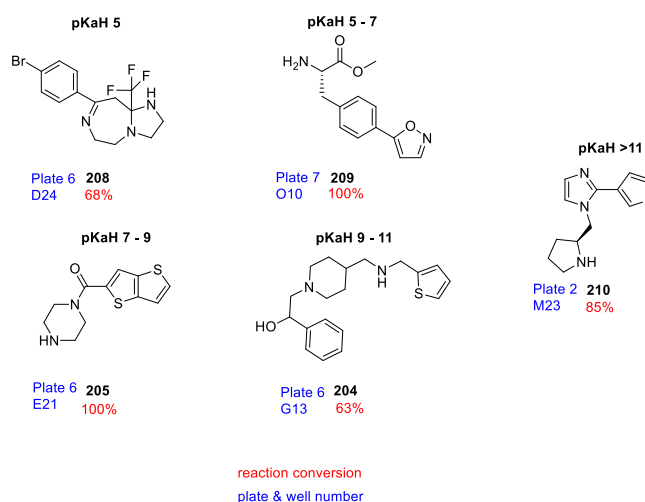


**Figure 144:** pKaH values of the 3000-amine set were calculated and separate into 5 categories based on increasing pKaH values and then compared to reaction conversions observed (reaction conversion over 50% good (green), between 20–50% moderate (amber) and <20% poor (red)) (A). Exemplar amines **204**, **205**, **208–210** from the class and respective conversion for each HaloCompound (B).

Previous analysis of the validation set does not account for molecules with multiple amine centres. In total, 39 compounds had more than one amine, and were subsequently analysed to determine if there was correlation between failure of product conversion and multiple reactive centres (**Table 8**). Overall, 30/39 reactions were found to have good conversion to

the mono-product (with 23 of the 30 having over 80% conversion to the desired HaloCompound), 3 reactions had moderate conversion and 6 had poor conversion. As previously observed, there is a small possibility (one case observed in the 300-amine set) that the mass corresponding to the desired HaloCompound could be a fragment peak in the di-adduct peak. This is a caveat of the LCMS analysis software and would have to be considered. As the phenotypic screen is not a binding assay, but looking for a pharmacological effect, mixtures of compounds should be able to induce protein degradation with one of the mixture molecules amongst the others. Therefore, after hit identification from the screening set, the compounds could be resynthesised and purified to identify the active molecule.

**Table 8:** Analysis of the reaction conversion of the compounds with 2 amines present in the same molecule with over 50% good (green), between 20–50% moderate (amber) and <20% poor (red).

>50%	20–50%	<20%
30	3	6

As a result, the high-throughput chemistry of the validation set of nearly 3000 amines was deemed successful. The analysis of the assay was able to confirm that the poorest performing amines were sterically hindered secondary amines. A number of compounds, which despite having two possibly reactive centres, were able to generate a single HaloCompound in good conversions. Overall, 1956 HaloCompounds were synthesised in good conversions, and together with the optimisation set, will allow the testing of over 2000 novel HaloCompounds in the GFP degradation assay. Utilising a high number of novel compounds, leads to an increase in the likelihood of successfully finding new E3 ligase binders for the PROTAC approach, which could be utilised in further drug discovery efforts.

### **7.3.4 Biological Evaluation of the In-Situ HaloCompounds**

#### **7.3.4.1 Biological Evaluation of the Chemistry Optimisation Set**

All of the compounds synthesised in the previous section were then tested in the GFP degradation screen. First, the optimisation set of nearly 300 HaloCompounds was tested in the two cell lines. Two test concentrations were used, with final concentrations of 1  $\mu$ M and 10  $\mu$ M each with a replicate (n=2) for the GFP-HaloTag® cells, and 10  $\mu$ M (n=1) for the GFP-HaloTag® mutant control cells. These concentrations were selected due to GFP reduction observed with the exemplar HaloPROTACs in the previous chapter showing robust degradation at these levels. It was hypothesised that 1  $\mu$ M may not be a high enough

concentration for weak binders for E3 ligases to induce GFP degradation, so 10  $\mu$ M was also used. With the higher concentration of 10  $\mu$ M, it was more likely to find compounds that induced GFP degradation via the UPS, but also that induced GFP degradation due to cytotoxicity. This was closely monitored by utilising the GFP-HaloTag® mutant cell line, which would remove compounds which induced GFP reduction non-specifically. In addition, the cell roundness algorithm would be used to detect compounds which were causing apoptosis, indicated by small round cell formation. Two different time points were also used, both 18 hours and 48 hours. As shown previously, the compounds are more likely to induce GFP degradation when incubated with the cells for longer, but this may also have unwanted cytotoxicity effects. Cellular imaging techniques can be used for both time points using the same cells, as the imaging technique is non-invasive, and the cells show no adverse effects when removed from the incubator for short periods of time. For visualisation and quantification of the GFP degraders, a Spotfire plot can be utilised, which shows one of the replicates versus the other (**Figure 145**). To simplify quantification of the results, both VHL recruiting HaloPROTACs **11a** and **144** were both included in the VHL recruiting HaloPROTACs identifiers (blue). At 1  $\mu$ M for 18 h, all control wells showed good GFP knockdown as expected with 60% knockdown, consistent with previous experiments. VHL derivative (light blue) is a structurally similar compound utilised in our laboratories.<sup>94</sup> GFP reduction was observed with the purified HaloPROTACs **144** and *in-situ* HaloPROTACs **144**, and were indistinguishable in this assay, irrespective of purification. The replicates show excellent correlation to one another showing the assay is robust on this scale. In addition to the positive control wells showing activity, the purified KEAP1 derived HaloCompound **148** (green) based on bardoxolone (the known cytotoxic compound), the IAP recruiting HaloPROTAC **145** and the DCAF HaloCompound **149** were also utilised as a positive control for the cytotoxicity read-outs. None of the 300 test HaloCompounds showed any significant decrease (>30% reduction) in GFP levels at this concentration and time point. So, the higher concentrations and longer incubation times were investigated.

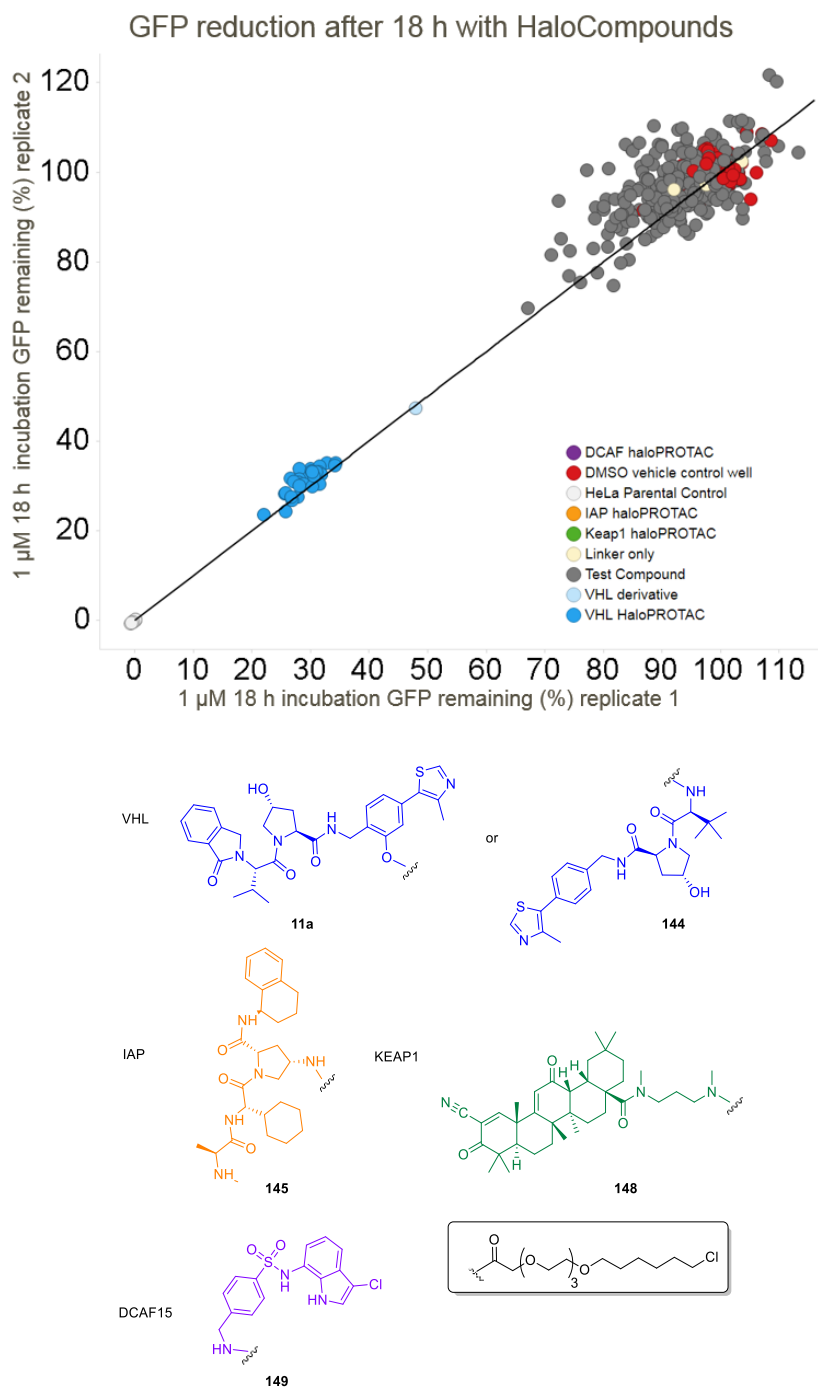
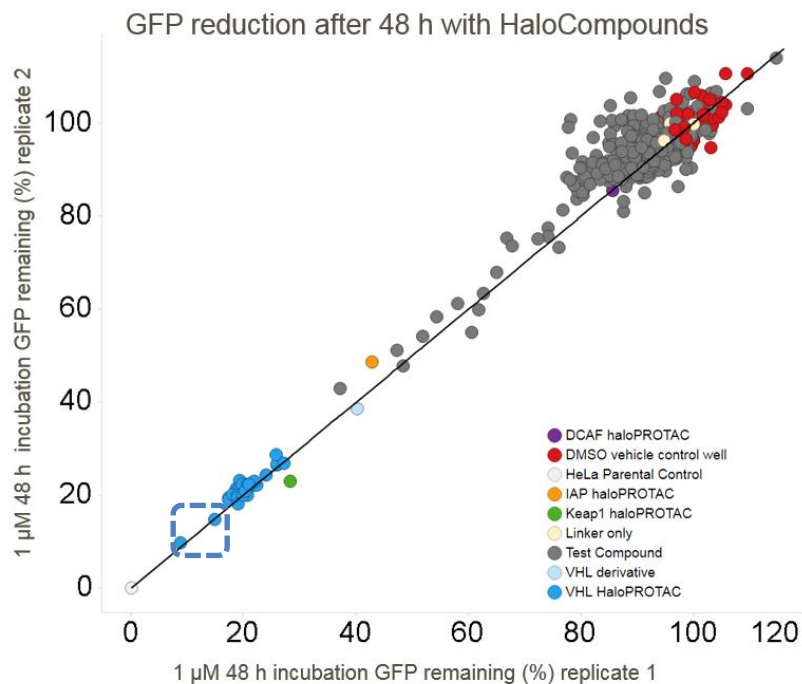


**Figure 145:** HaloCompound incubation at 1  $\mu\text{M}$  with GFP-HaloTag® cells for 18 h. GFP reduction in excel plate visualisation (top), and corresponding data converted into a Spotfire plot (bottom) showing % GFP remaining on each axis (replicate 1 versus replicate 2). Compounds shown in coloured spots in Spotfire visualisation, with corresponding structures below.

The HaloCompounds were further incubated for 48 h in order to assess if the 1  $\mu\text{M}$  test concentration would afford any hit compounds from the 300-amine set (**Figure 146A**). As expected the VHL recruiting PROTACs were more potent, affording between 70–80%

reduction in GFP levels. Differentiation between the two VHL recruiting PROTAC chemotypes is now clearer, corresponding with the activity difference observed in the previous section (**11a** circled in blue). The purified KEAP1 derived HaloCompound **148** (green) and the purified IAP recruiting HaloPROTAC **145** (orange) show GFP degradation, but this readout does not include any filtering based on cytotoxicity. In addition, 10 test HaloCompounds also showed more than 30% GFP degradation in this assay. In order to determine if the HaloCompounds were true degraders, or non-specific/cytotoxic compounds, filters were used in Spotfire (**Figure 146B**). To remove compounds that showed non-specific effects, HaloCompounds that had less than 75% GFP remaining in the GFP-HaloTag® mutant cell line were removed. In addition, compounds that caused more than 10% of the cells to become small and round (indicating apoptosis) were identified with this method and removed. As expected, the purified HaloCompounds derived from IAP **145** and KEAP1 **148** inhibitors (orange and green) were eliminated. Additionally, all but one of the 10 HaloCompounds which showed GFP reduction after 48 h with 1  $\mu$ M were also removed. One hit was therefore found at this concentration at 48 h, coined **211** (circled in red, see later). The GFP degradation screen was then repeated at higher concentrations with the 300-amine set to evaluate if any additional compounds were potential hits in this assay.

A)



B)

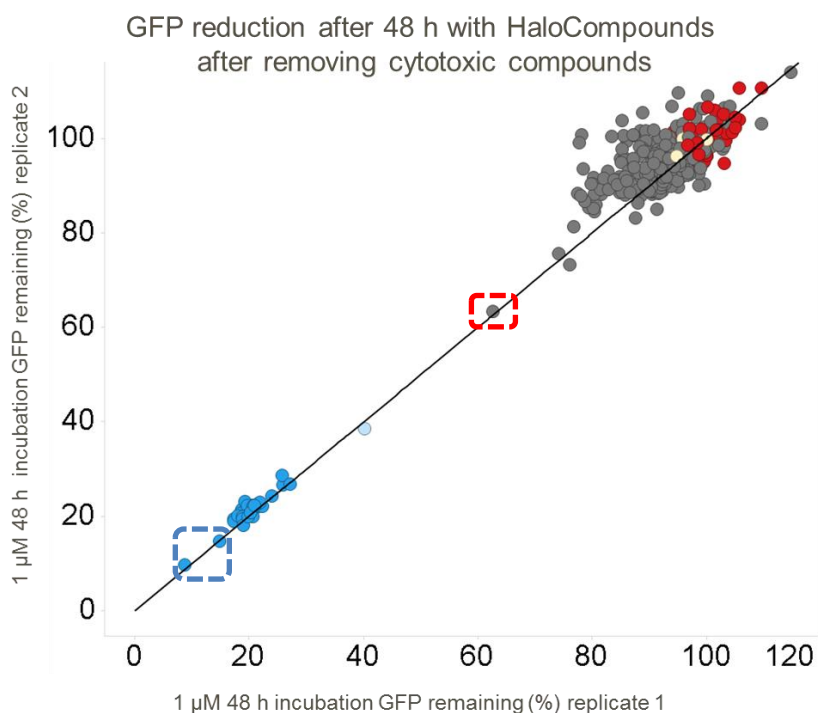
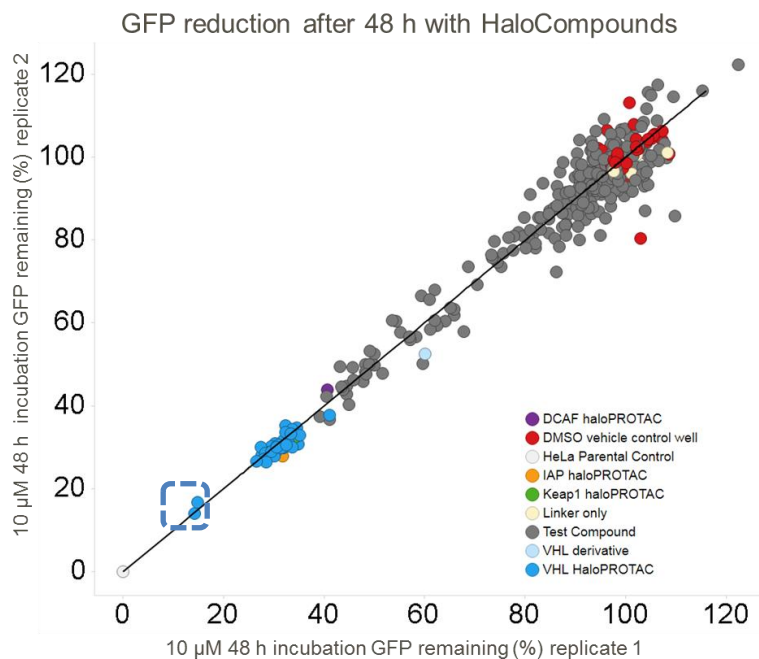


**Figure 146:** HaloCompound incubation at 1  $\mu$ M with GFP-HaloTag® cells for 48 h. GFP reduction data converted into a Spotfire plot (A) showing % GFP remaining on each axis (replicate 1 versus replicate 2). Compounds excluded which showed less than 75% GFP remaining in the GFP-HaloTag® mutant cell and more than 10% round cells forming (B). Compounds shown in coloured spots in both Spotfire visualisations. With **211** circled in red and VHL recruiting HaloPROTAC **11a** circled in blue.

The HaloCompounds were then tested at a 10  $\mu$ M concentration in the GFP degradation assay. Due to lack of degradation from the 1  $\mu$ M concentration at 18 hours, the HaloCompounds were incubated for 48 hours with the 10  $\mu$ M test concentration (**Figure 147A**). As expected, the VHL recruiting HaloPROTACs **11a** showed robust and reproducible GFP knockdown. Differentiation of the VHL recruiting HaloPROTAC **11a** and **144** were now visible with **11a** HaloPROTACs showing 10% GFP remaining and the **144** showing 30–40% GFP remaining, due to the hook effect with these compounds (see previous section, dotted line shows **11a**). Purified IAP recruiting HaloPROTAC **145** (orange), purified KEAP1 derived HaloCompound **148** (green) and purified DCAF15 derived HaloCompound **149** (purple) all show GFP degradation, which are all known to be cytotoxic at this concentration and time point. In addition, over 30 test HaloCompounds also showed GFP degradation of 30% or more. As previously discussed, filtering out the compounds based on non-specific effects can be achieved using Spotfire (**Figure 147B**). In filtering out compounds which showed less than 75% GFP present in GFP-HaloTag® mutant cell line, half of the test HaloCompounds that show activity are eliminated. In addition, removing compounds that induce more than 10% cell rounding due to apoptosis, leaves 5 HaloCompounds that can be considered as hits from this concentration and time point (n=2), one of which was also effective at the lower concentration, **211** (see next section).

A)



B)

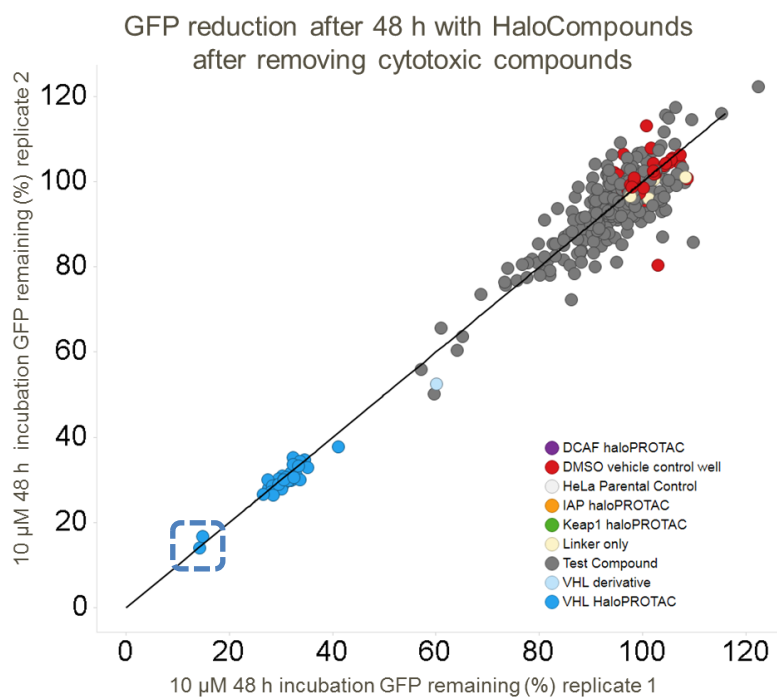
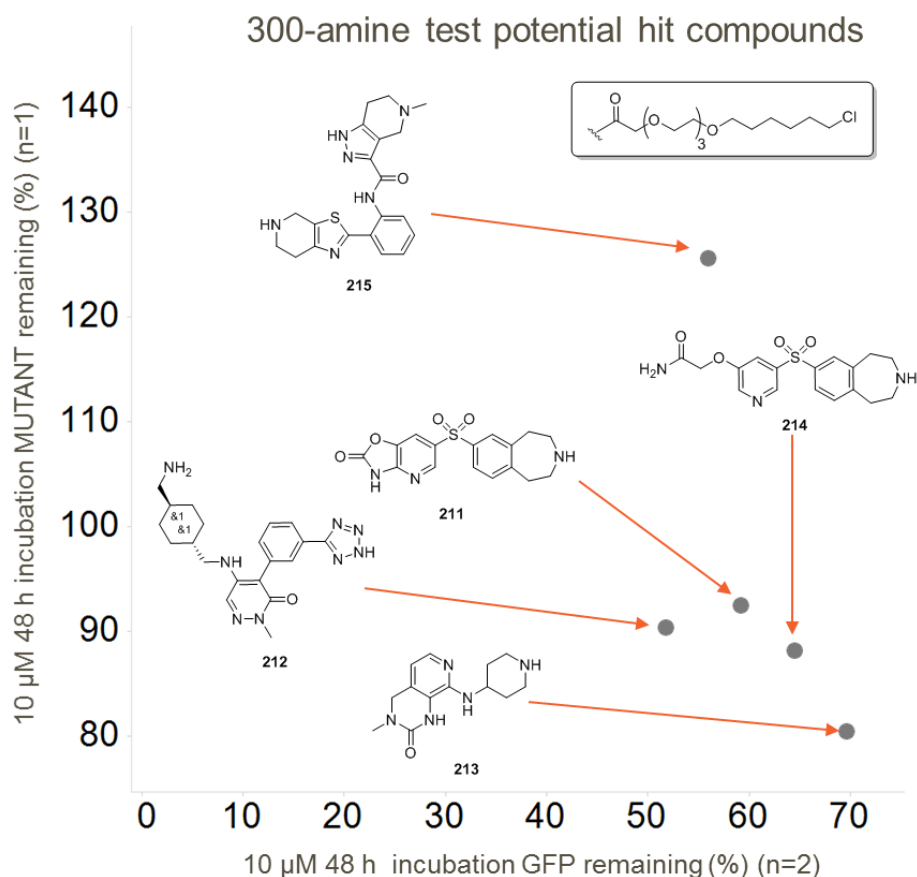


**Figure 147:** HaloCompound incubation at 10 µM with GFP-HaloTag® cells for 48 h. GFP reduction data converted into a Spotfire plot (A) showing % GFP remaining on each axis (replicate 1 versus replicate 2). Compounds excluded which showed less than 75% GFP remaining in the GFP-HaloTag® mutant cell and more than 10% round cells forming (B). Compounds shown in coloured spots in both Spotfire visualisations.

#### **7.3.4.2 Hit Evaluation from the Chemistry Optimisation Set**

The five HaloCompounds which induced more than 30% degradation in the GFP-HaloTag® cell line specifically were considered as potential hits in this assay. The compounds, which did not significantly affect the GFP-HaloTag® mutant cell line (>75% remaining) and no more than 10% cell roundness was observed, merited further study. The five compounds of the 300-amine set met the potential hit criteria and are shown in **Figure 148A**, compounds **211–215** (which is a scaled version of the previous figure containing chemical structures for **211–215**). The potential hit compounds were all from the unique amine selection from the GSK collection, and not from the compounds added which were structurally similar to known E3 ligase binders. Interestingly, two of the compounds shown have similar core structures (**211** and **214**) suggesting this pharmacophore could be potentially binding the same protein of interest, if they were real hits. Compound **213** only showed small levels of differentiation between the two cell lines (~35% reduction of GFP levels in the GFP-HaloTag® cell line, and 10–20% GFP reduction in the GFP-HaloTag® mutant control cell line), however, due to the nature of the phenotypic screen variability, they would be investigated further. If the compounds which did not show major differentiation in the two cells lines were shown to be false positives, this would elucidate the need for substantial differentiation in the future screening sets. All HaloCompounds **211–215** identified showed good conversion in the LCMS data, with more than 70% conversion for each compound **Figure 148B**.

A)



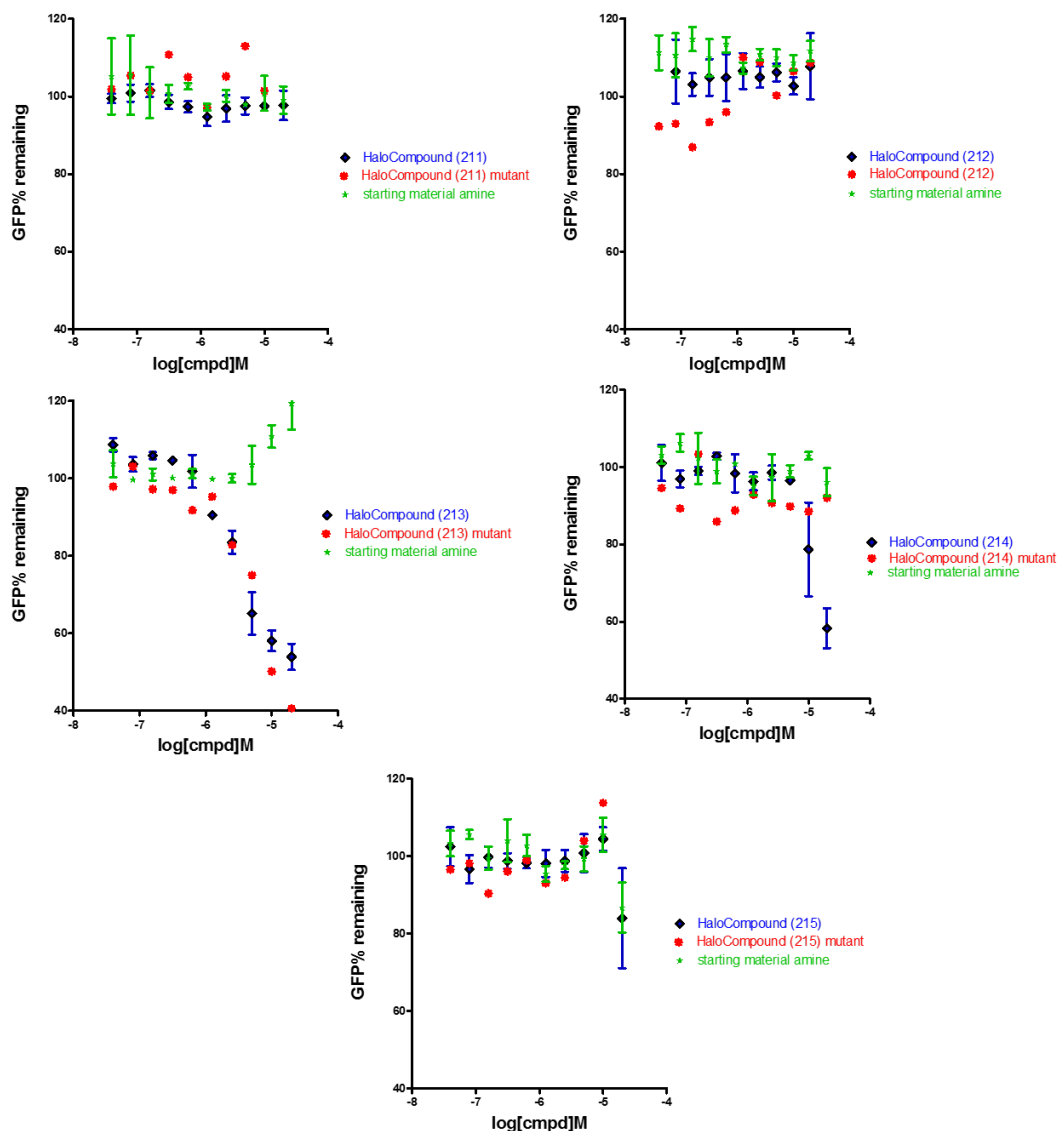
B)

Compound	% Chemical conversion experiment 1 (n=1)	Well position
211	72	P7
212	93	C1
213	70	N12
214	91	J2
215	100	C5

**Figure 148:** Analysis of GFP-HaloTag® cells and GFP-HaloTag® Mutant cells after 300-amine set 10  $\mu$ M compound treatment after 48 h (n=1 for each axis). DMSO control wells, NHS ester **175** only wells and VHL positive control HaloPROTACs **144** removed in visualisation for clarity. Compound set filtered by (<70% GFP remaining in GFP-HaloTag® cells and >75% GFP remaining in GFP-HaloTag® Mutant cells and compounds which caused more than 10% cell roundness are removed) and HaloCompounds **211–215** highlighted with structures of corresponding amine starting materials (A). Chemical conversions of the amines into the HaloCompounds by LCMS shown (B).

The HaloCompounds **211–215** were resynthesised for retesting in a concentration response in the GFP degradation assay(**Figure 149A**). All HaloCompounds were resynthesised in good conversions using the same high-throughput chemistry technique previously described. (**Figure 149B**). The reaction mixtures containing HaloCompounds **211–215** were incubated in the GFP-HaloTag® cells from the highest concentration of 20 µM using a 1 in 2 dilution series. The compounds' amine starting materials were also tested in the GFP-HaloTag® cells in order to ensure the effect was from the HaloCompound and not as a result of any residual amine in the reaction mixture. The compounds were also tested in the GFP-HaloTag® mutant cell line in concentration response. Amine starting materials derived from **213** and **215** showed no effect on GFP levels, but the HaloCompound **213** and **215** showed reduction in both the GFP-HaloTag® line and the GFP-HaloTag® mutant cell line, confirming the compound is also a false positive. The difference in effects of the amine starting materials from HaloCompounds **213** and **215** and the HaloCompounds themselves could be due to the increased cell permeability, leading to higher in-cell concentrations and subsequently the undesired cytotoxicity. As previously described, **213** was expected to be a false positive due to the small differentiation between the two cell lines. HaloCompounds **211** and **212** showed no degradation in this assay, confirming the compounds were false positives. This could be a result of well to well contamination as both compounds were situated closely to a VHL positive control well, this would have to be monitored in a bigger subset to ensure cross-contamination did not affect the outcome of GFP degradation. However as there was no LCMS analysis which showed such a contamination, this was only a hypothesis for failure. This is a disappointing result as **211** and **214** are structurally similar. HaloCompound **214** induced GFP degradation specifically, no reduction is observed in GFP-HaloTag® mutant cell line and its starting amine also showed no effect. None of the HaloCompounds **211–215** showed any cell roundness (apoptosis) at any of the concentrations. Therefore, the GFP reduction could be a result of the compounds, for example, if they were proteasome activators or protein synthesis inhibitors. The compound **214** shows 58% (n=2) reduction at 20 µM, but at 10 µM one of the experiments showed moderate knockdown of GFP of 67%, but in another there was no significant response (91% GFP remaining). This compound **214** was deemed a potential hit meriting further investigation with the purified compound. Moving forward into the larger screening set, as a result of these findings, 1) larger differentiation (>20%) between the GFP-HaloTag® and the GFP-HaloTag® control cell line would be required in order to find true degradation and 2) compounds which induce more GFP reduction than 30% would be considered as more likely to be true degraders.

A) Resynthesis and retest of the potential hits in the GFP degradation assay



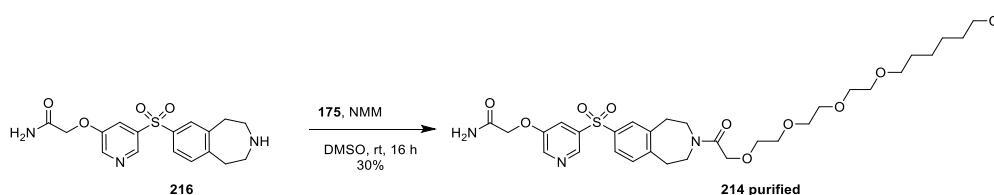
B)

Compound	% Chemical conversion in resynthesis
211	62
212	100
213	80
214	95
215	88

**Figure 149:** Retesting hit HaloCompounds 211–215 in concentration response curve in GFP-HaloTag® HeLa cells (blue), and in the GFP-HaloTag® mutant cell line (red), and testing their amine starting materials (green) (A) (n=2, technical replicates). Chemical conversions of the amines into the HaloCompounds by LCMS shown in resynthesis (B).

In order to determine if **214** was a true hit from the assay, it was resynthesised and purified and retested in the GFP degradation assay. This was achieved using the same conditions used in the 300-amine experiment but on larger scale, to afford the desired compound **214 purified** in a 30% yield (**Figure 150A**). This was retested in the two cell lines using the concentrations previously outlined, and unfortunately, there was not a significant reduction in GFP compared to the mutant cell line (**Figure 150B**). This could be due to better reproducibility in this experiment than in the previous one, where the error bars showed a significant margin of error in two experiments. The compound **214** was therefore deemed not a substantial hit from the screen and was not further investigated.

A)



B)

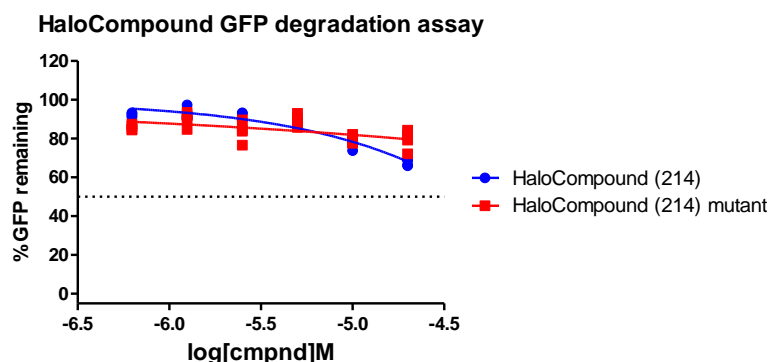


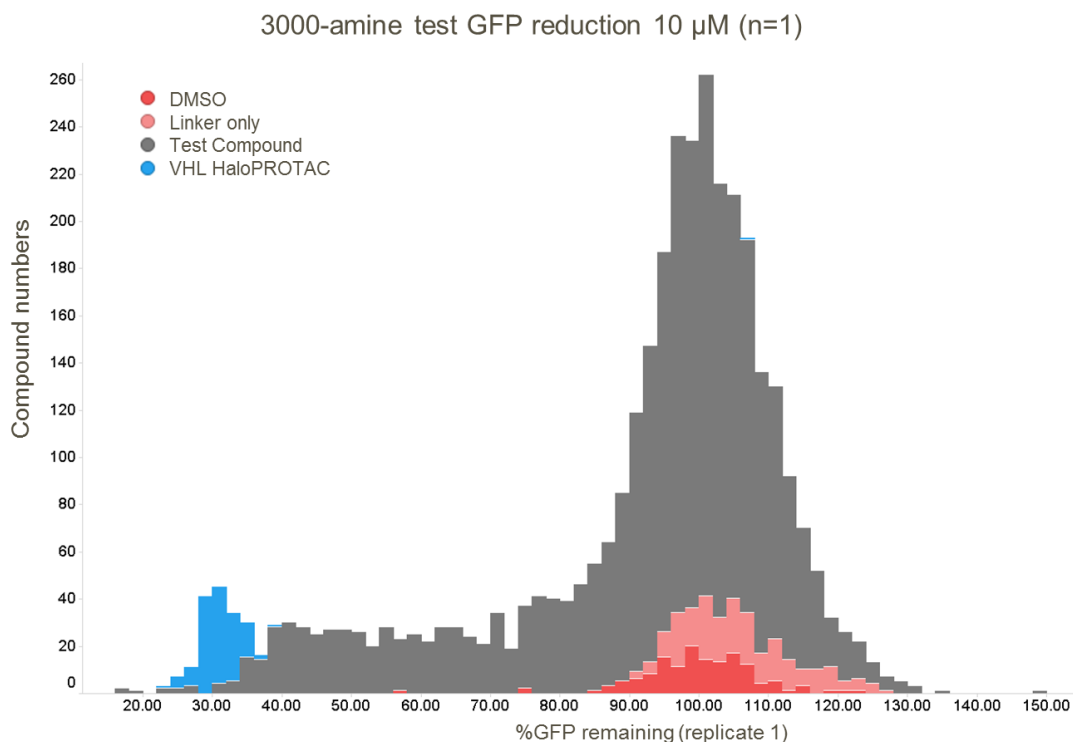
**Figure 150:** Synthesis of the hit compound **214 purified** (A), and retesting of **214 purified** in concentration response curve in GFP-HaloTag® HeLa cells (blue), and in the GFP-HaloTag® mutant cell line (red) (n=4 technical replicates) (B).

The main purpose of the 300-amine screen was to validate the high-throughput chemistry and biology required for a larger screening set. The 300-amine experiment was deemed successful and showed the potential for a powerful larger phenotypic screen. With the GFP-HaloTag® mutant cell line and the small round cell algorithm in hand, this screen was envisaged as a good method of finding specific GFP degradation. With the small number of hits from the 300-amine set showing false positive results due to contamination or non-substantial differentiation between the two cell lines, this was considered moving into a larger screening set. More careful plate handling to eliminate some false positives would therefore be employed, which consisted

of more centrifugal steps with sufficient plate cover to prevent well to well contamination during lid removal (due to biological technical inexperience). In addition, the differentiation of GFP-HaloTag® cells versus GFP-HaloTag® mutant cell line would be taken into consideration, and more than 20% difference between the two cell lines would be required. A larger screen would therefore be evaluated to determine hit rate.

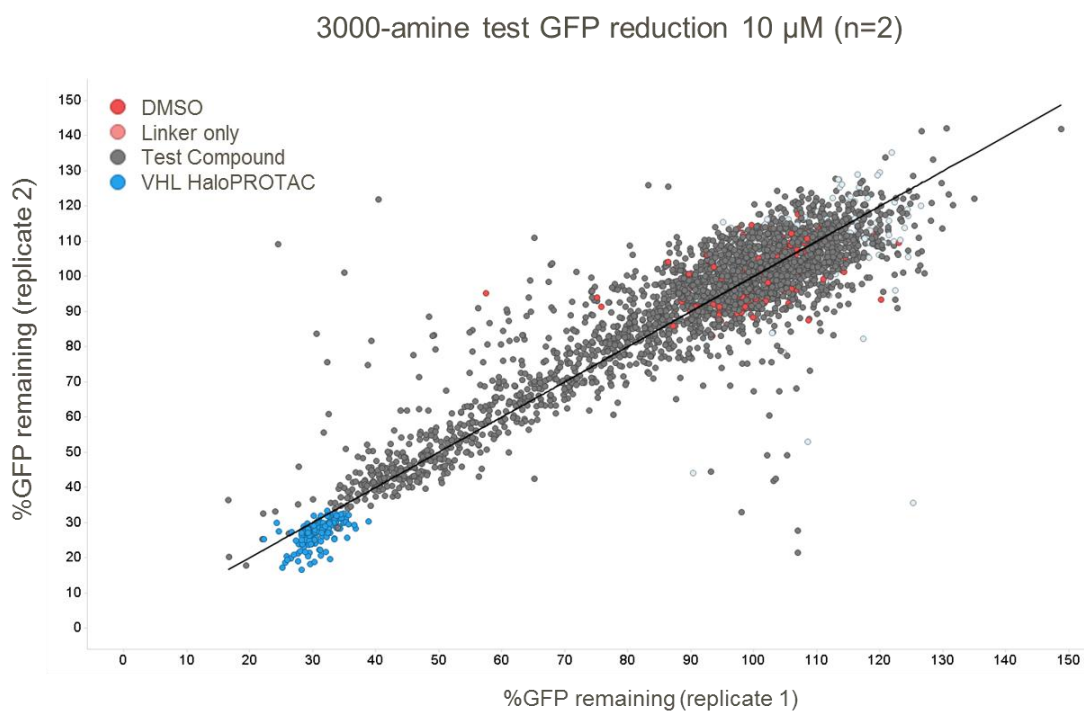
#### **7.3.4.3 Biological Evaluation of the Validation Set**

The 3000-amine set was then tested in the GFP degradation assay. As a result of the data generated for the 300-amine set, the 10 µM concentrations were chosen to evaluate the HaloCompounds each with a replicate for each of the cell lines (n=2) with an incubation time of 48 h. In replicate 1 (n=1) a histogram was used to view the distribution of the compounds and their effect on GFP levels (**Figure 151**). As predicted, the VHL recruiting HaloPROTAC **144** compounds on all 9 plates cause good degradation of GFP. DMSO control wells were used to determine the 0% effect (100% GFP remaining). As this is an in-cell phenotypic screen, with 9 plates being tested (each with DMSO and VHL recruiting HaloPROTAC **144** control wells), variability between plates was expected. As a result, within 3 standard deviations (99.7% confidence), a hit molecule would reduce GFP by a minimum of 25% compared to the average DMSO well. Over 210 test HaloCompounds out of the 3000-amine set showed significant reduction, with over 50% GFP reduction. Over 530 test HaloCompounds showed more than 25% GFP reduction. This does not include any filters to remove any non-specific reduction including cytotoxicity and this is a single test set with no replicates, so the number of hits found was expected and should be greatly reduced with the correct controls.



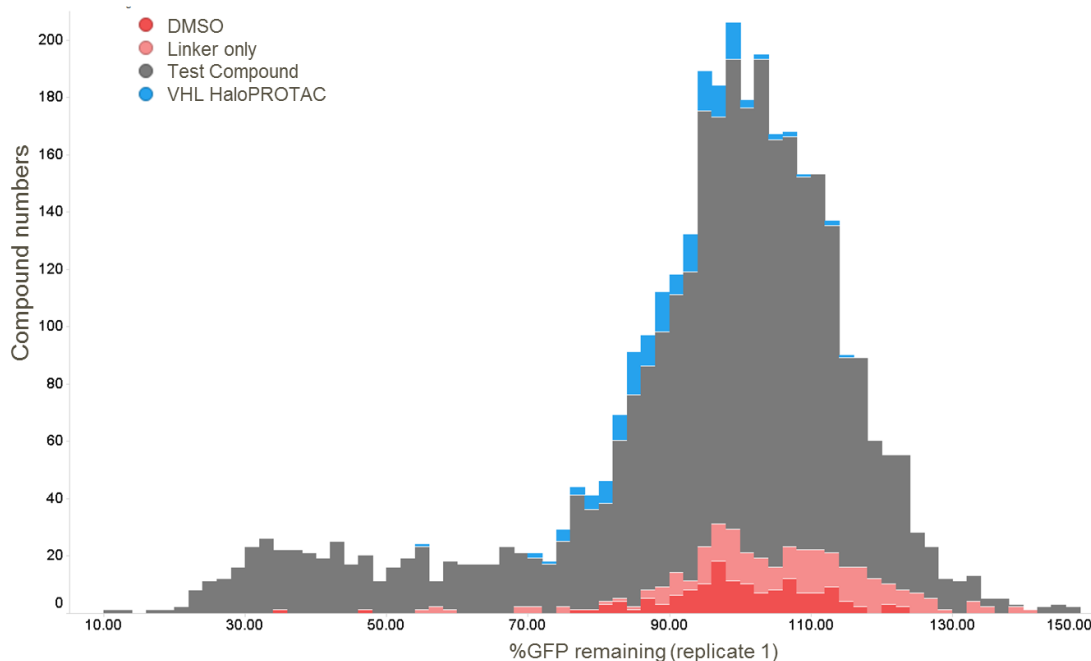
**Figure 151:** Analysis of GFP-HaloTag® cells after 3000-amine set 10  $\mu$ M compound treatment after 48 h (n=1). DMSO control wells shown in red, NHS ester **175** only wells in pale red, test HaloCompounds in grey and VHL positive control HaloPROTACs **144** in blue.

A second replicate for the 3000-amine set was carried out and compared to the replicate 1 (**Figure 152**). As expected, there was generally good agreement between the two replicates, with just under 170 HaloCompounds showing 50% GFP reduction. There were 438 test HaloCompounds which had 25% reduction in both replicates. There were a few HaloCompounds which were not replicated, this could be due to false negatives (for example, errors in compound dispense between plates which were tested) or false positives (for example, error in cell dispense leading to decreased fluorescence observed) or due to other external factors such as well contamination (by another compound in a nearby well or bacteria for example). These results still include false positives which cause compound specific cytotoxicity in the GFP-HaloTag® mutant cell line, which will be discussed.



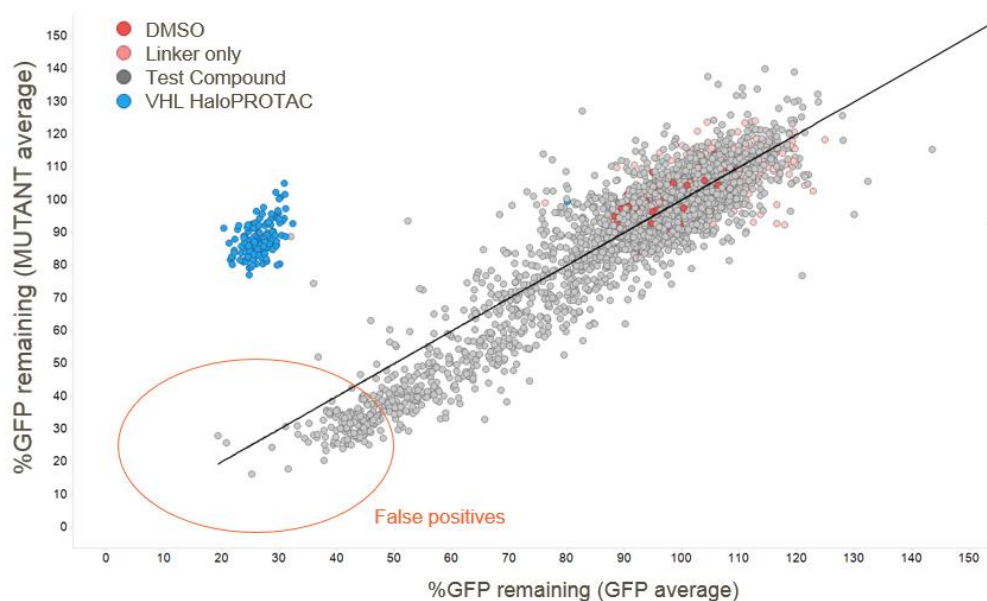
**Figure 152:** Analysis of GFP-HaloTag® cells after 3000-amine set 10  $\mu$ M compound treatment after 48 h replicate 1 versus replicate 2. DMSO control wells shown in red, NHS ester **175** only wells in pale red, test HaloCompounds in grey and VHL positive control HaloPROTACs in blue. Visualisation did not include NHS ester **175** only cells for clarity.

In addition to testing in the GFP-HaloTag® cells, the HaloCompounds were also tested in the GFP-HaloTag® mutant control cells (**Figure 153**). As the mutant cells are not as strongly fluorescing (around 5500 fluorescence counts per second versus 17000 fluorescence counts per second for the GFP line), there is more variability in this large data set than in the GFP-HaloTag® cells. For the data to be statistically significant, within 3 standard deviations (99.7% confidence), more than 36% GFP reduction in comparison to the DMSO wells had to be observed. VHL recruiting HaloPROTACs **144** did not cause significant reduction in the GFP-HaloTag® mutant cell line as expected. Over 250 HaloCompounds showed 50% GFP reduction in the GFP-HaloTag® mutant cell line, suggesting this is non-specific reduction due to cytotoxicity or inhibitors of protein synthesis. A number of these compounds were found in the GFP-HaloTag® cells and could therefore be removed as non-specific protein reduction.

3000-amine test GFP MUTANT reduction 10  $\mu$ M (n=1)

**Figure 153:** Analysis of GFP-HaloTag® Mutant cells after 3000-amine set 10  $\mu$ M compound treatment after 48 h (n=1). DMSO control wells shown in red, NHS ester **175** only wells in pale red, test HaloCompounds in grey and VHL positive control HaloPROTACs in blue. Compounds in which had >150% GFP remaining were excluded from the visualisation (7 compounds).

In comparing the GFP-HaloTag® cells and the GFP-HaloTag® mutant control cells, two replicates for each condition were carried out and the results were averaged and plotted in Spotfire (**Figure 154**). The HaloCompounds which decreased the GFP levels in the GFP-HaloTag® cells are on the “x” axis and those which decreased GFP in the GFP-HaloTag® mutant control cells are on the “y” axis. Those circled in orange show the compounds which caused GFP reduction in both cell lines, which are therefore false positives. Hit compounds would reduce the GFP specifically in the GFP-HaloTag® cells (as shown by the VHL HaloPROTACs **144**, blue) potentially through the PROTAC approach.

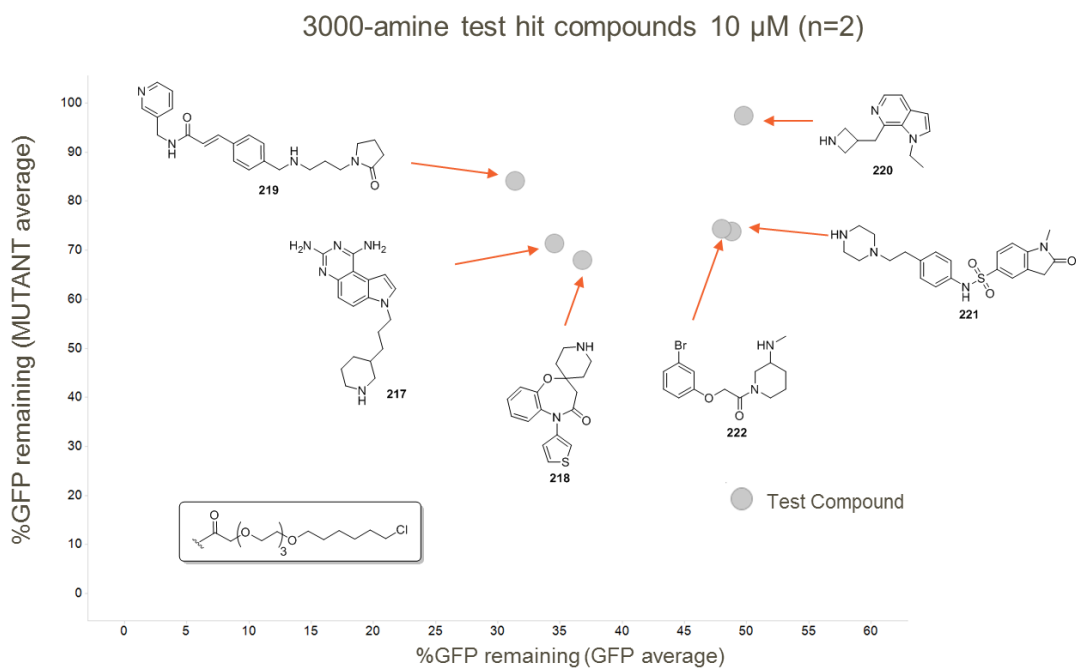
3000-amine test GFP reduction versus MUTANT 10  $\mu$ M (n=3 for both)

**Figure 154:** Analysis of GFP-HaloTag® cells and GFP-HaloTag® Mutant cells after 3000-amine set 10  $\mu$ M compound treatment after 48 h (n=2 for each axis). DMSO control wells shown in red, NHS ester **175** only wells in pale red, test HaloCompounds in grey and VHL positive control HaloPROTACs in blue. Visualisation did not include NHS ester **175** only cells for clarity. False positives circled in orange (>50% reduction in GFP-HaloTag® cells and GFP-HaloTag® Mutant Control cells).

In order to filter HaloCompounds based on the results from the two cell lines results, a number of cut-offs for active HaloCompounds were set and outlined in **Figure 155**. Compounds were removed if they did not induce significant GFP degradation (45% GFP remaining in the GFP-HaloTag® cells) and those which reduced GFP levels in the GFP-HaloTag® Mutant cells (less than 65% GFP remaining, as outlined by the variation between the plates). This was achieved using the average values (n=2) for each cell line. In addition, as a result of the 300-amine experiment, those compounds which had good differentiation between the GFP reduction in the GFP cell line and the mutant cell line control, would be deemed more likely to be a potential hit.

Shown in **Figure 155** are the six HaloCompounds **217–222** which fit the desired criteria. HaloCompound **219** shows promising results as it caused more than 70% GFP knockdown but maintained good GFP mutant control levels over 80% (n=2, average). HaloCompound **220** degraded 50% of GFP but did not affect the mutant control cell line. The resulting four HaloCompounds **217, 218, 221, 22** had moderate knockdown differentiation between the two cell lines, which were considered possible hits (at least more than 20% difference between the two cell lines as deemed by the 300-amine set) and would be further investigated due to the

small number of compounds remaining at this stage. None of the six hits **217–222** were shown to cause the cells to round up as a sign of apoptosis. The chemical conversion for the reactions are also shown in the figure, with 5 HaloCompounds having very good conversion by LCMS, compound **219** was therefore an outlier with only 42% conversion observed. As indicated by the experiments in chapter 6, despite an impure reaction mixture, the HaloCompound could induce potentially GFP reduction in lower conversions, which will be further investigated. Additionally, compound **220** was found to be next to a positive control well, which has previously been a higher indicator of a false positive which had to be further assessed. The six HaloCompounds **217–222** were therefore deemed potential hits from the GFP-HaloTag® phenotypic screen. Due to the variability observed with replicates due to the phenotypic nature of this assay, along with the chemical conversion with **219**, retesting would be required to determine if the hits were real or false positives.



Compound Number	% Conversion in initial experiment	Plate and well position
<b>217</b>	100	Plate 7, Well D9
<b>218</b>	100	Plate 5, Well O1
<b>219</b>	42	Plate 2, Well B7
<b>220</b>	100	Plate 8, Well H17
<b>221</b>	91	Plate 3, Well B11
<b>222</b>	89	Plate 8, Well F3

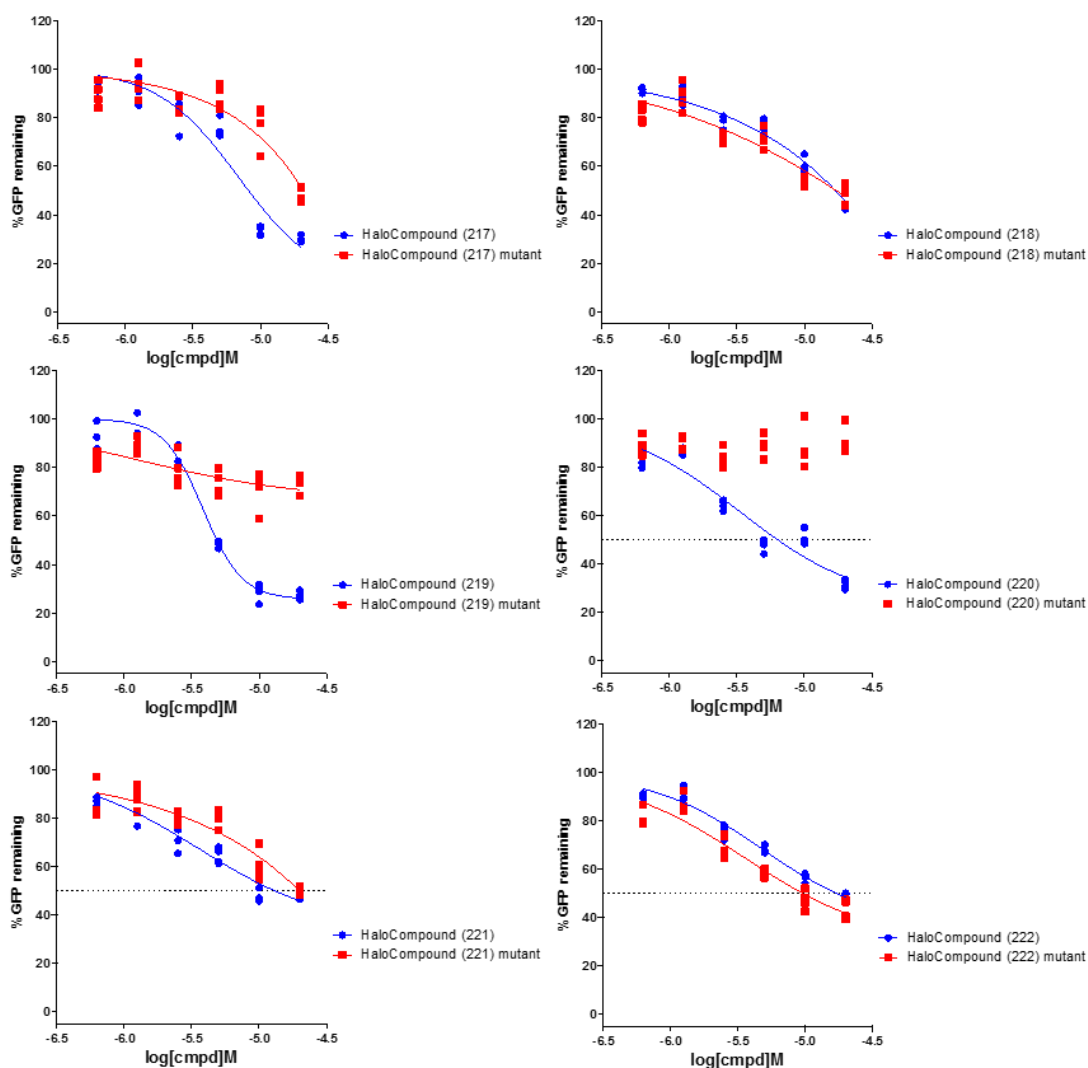
**Figure 155:** Analysis of GFP-HaloTag® cells and GFP-HaloTag® Mutant cells after 3000-amine set 10  $\mu$ M compound treatment after 48 h (n=2 for each axis). DMSO control wells, NHS ester **175** only wells and VHL positive control HaloPROTACs **144** removed in visualisation for clarity. Compound set filtered by (<50% GFP remaining in GFP-HaloTag® cells and >65% GFP remaining in GFP-HaloTag® Mutant cells) and HaloCompounds highlighted with structures of corresponding amine starting materials **217–222** (top). LCMS conversion to the potential hit HaloCompounds **217–222** and plate position is also shown (below).

#### 7.3.4.4 Hit Evaluation from the Validation Set

In order to retest the six potential hits **217–222**, they were resynthesised in an analogous manner to the previous conditions and retested in concentration response in the GFP degradation assay (**Figure 156A**). Four out of the six HaloCompounds **217**, **218**, **221**, **222** showed concentration dependent reduction in both GFP-HaloTag® cells and the GFP-HaloTag® Mutant cells, illustrating they were false positives not eliminated by the GFP-

HaloTag® Mutant cells in the first test. This was expected to be an issue in a number of examples, due to the fluorescence differences between the cell lines. In the cases of the four compounds, as the two cell lines did not have major differentiation in GFP reduction, combined with the concentration response, the compounds were therefore deemed not potential hits from the screen. Two compounds, **219** and **220** showed good GFP reduction exclusively in the GFP-HaloTag® cells, showing more confidence that they could be real hits. Despite **220** being situated next to a positive control well in the initial experiment, the resynthesis in a fresh plate and retest shows that it is a potentially real hit. This also increases the confidence in the new measures of preventing cross-contamination in the 3000-amine set. It is worth noting that the conversion to **220** was good in both reactions (initial and resynthesis), but **219** was only synthesised in a moderate yield of 34% (**Figure 156B**). As previously shown, a small concentration of the HaloCompound could induce the degradation of GFP, but in order to determine if the two HaloCompounds were real hits, they would be evaluated against their starting material amines to determine if the degradation was a result of the HaloCompound or their starting material amine.

A)



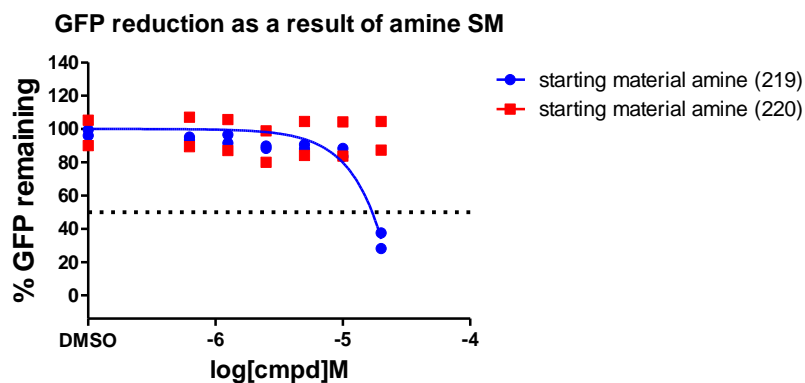
B)

Compound Number	% Conversion in resynthesis
217	98
218	98
219	34
220	95
221	83
222	59

**Figure 156:** Analysis of GFP-HaloTag® cells and GFP-HaloTag® Mutant cells after potential hit compounds **217–222** for 48 h incubation (A, n=4 technical replicates). Conversion to the potential hit HaloCompounds **217–222** is also shown for the resynthesis (B).

In order to determine that the GFP reduction of **219** and **220** were a result of the HaloCompounds and not the corresponding small molecules, the amine starting materials were also tested in the GFP-HaloTag® cells. As shown in **Figure 157A**, no significant effects are observed as a result of the amine starting material of HaloCompound **220**, leading to increased confidence in the hit HaloCompound **220**. However, **219** shows clear concentration dependent reduction in GFP with the amine alone, but this is only achieved at the top concentration of 20 µM. At high concentrations compounds are more likely to be cytotoxic. This is however a surprising result given that there was no observed toxicity in the GFP-HaloTag® Mutant cells in the previous experiment with the reaction mixture. As a result of the unexpected GFP degradation at this concentration, this was repeated at 20 µM (n=4, technical replicates) with a fresh sample of **219** starting material amine (**Figure 157B**). As indicated by the bar chart, the compound did not cause cytotoxicity in any of the 4 replicates at this concentration, with between 85% and 98% GFP remaining in this test. In the example where the GFP reduction was observed with **219**, this was discovered as a result of cross-contamination of a cytotoxic compound in an adjacent well, which can therefore be discounted. In summary, there were two compounds found out of the 3000-amine set which gave concentration dependent reduction of GFP specifically as a result of the HaloCompound.

A)



B)

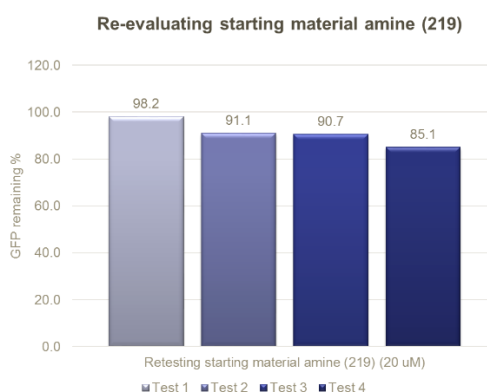


**Figure 157:** Effects of the starting material amines of the two hits **219** and **220** on GFP levels after 48 h treatment in GFP-HaloTag® cells (n=4 technical replicates) (A). Retesting the 20  $\mu$ M test concentration for compound **219** in the GFP-HaloTag® cells (n=4 technical replicates) (B).

As a result of evaluating the 3000-amine test set in the GFP degradation assay and then following up potential hits in concentration response, two HaloCompounds, **219** and **220** were found to be confident hits. The hits were shown to be active in two separate HTE syntheses, were not cytotoxic in the control cell line, and the amine starting materials did not cause GFP reduction. This increases the confidence that the two compounds could be binders for an E3 ligase or another protein involved in targeted protein degradation. The two compounds will be further evaluated in their ability to degrade GFP, and other proteins of interest, to assess their overall utility for targeted protein degradation as possible binders for E3 ligases.

## 7.4 Summary and Future Work

High-throughput chemistry was optimised and executed for the evaluation of HaloCompounds to potentially find new E3 ligases for the PROTAC approach (**Figure 158**). Computational chemistry was used in order to determine diverse test sets for the approach from the GSK and GSK HTS compound collection, and a 300-amine optimisation set (297 amines) and 3000-amine validation set (2934 amines) were found to fit criteria desirable to test. Reactions were optimised in a HTE capacity, executed for both test sets and were all evaluated by LCMS for product conversion. The 300-amine set was successfully synthesised in a fumehood. Due to issues in reproducibility in a fumehood with base evaporation, reactions were best employed in a glovebox. With HTE optimised, HaloCompounds from the 3000-amine set were successfully synthesised in good conversions, giving rise to nearly 2000 unique HaloCompounds with over 50% conversion. Compounds from both sets were evaluated in the GDP degradation assay using both the GFP-HaloTag® and GFP-HaloTag® mutant control cell lines. The 300-amine set produced a small number of hits **211–215**, which were found to be false positives. These were found to be a result of proximity to a positive control well, with possible contamination in the plate preparation stage, in addition to cytotoxic compounds which were not determined in the initial testing. In the 3000-amine set, six potential hits **217–222** were identified to induce GFP degradation more selectively, so were chosen for further experiments. Of the six potential hits, two compounds **219** and **220** were shown to degrade GFP exclusively in the GFP-HaloTag® cells, and their corresponding amines showed no effects to the GFP levels. This increases the confidence that the two compounds are showing GFP reduction as a result of the chloroalkane attachment to the HaloTag®, which could potentially recruit new E3 ligases or other proteins which cause targeted degradation of GFP.

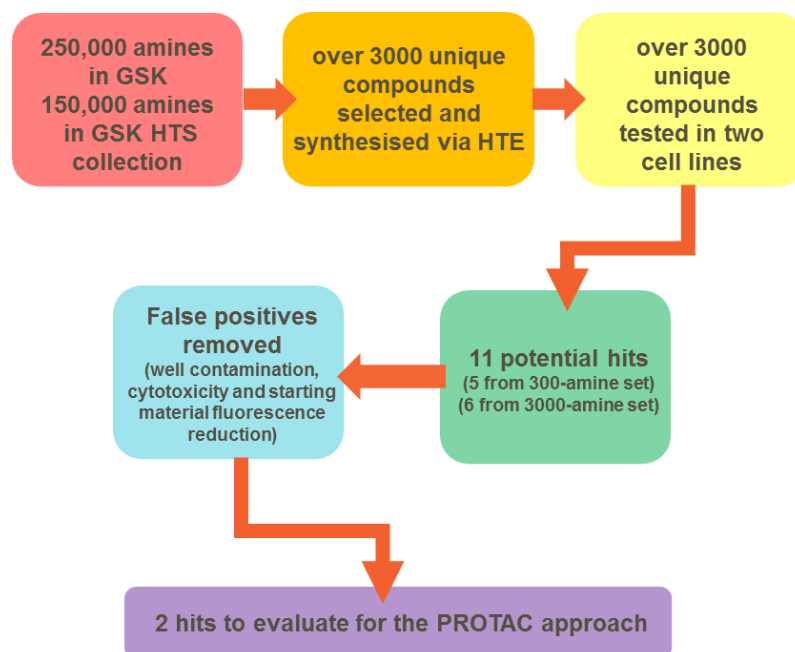
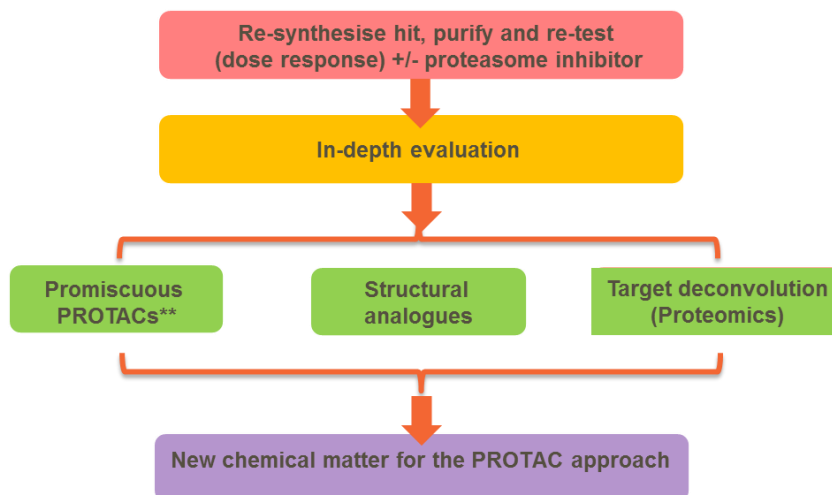


**Figure 158:** Outcome for the 300-amine and 3000-amine set starting from the compound selection through to hit identification.

In order to fully evaluate the hits from the 3000-amine set in their ability to induce protein degradation via a PROTAC approach, a potential assay cascade is described (**Figure 159A**). The compounds **219** and **220** would be resynthesised, purified and retested in the GFP degradation assay with and without the presence of a proteasome inhibitor (such as MG132) to determine if the degradation was proteasome dependent. In parallel, the amines would be evaluated in their ability to degrade other proteins of interest. To validate amines **223** and **224**, a toolbox of promiscuous POI PROTACs would be synthesised (**Figure 159B**). Using RIPK2 **75**, promiscuous kinase **76** and the JQ1 derived binder **81** this would ensure multiple proteins could be assessed with each amine. Using one exit vector (shown to be permissible from the GFP screen) and multiple linkers would increase the chance of success of creating a potent PROTAC. Linkers could include the 4-EG **112a**, 6-EG **112b** and all-methylene derived variants **113** (if required for increased permeability). To gain confidence in the hits, structural analogues could be synthesised into HaloCompounds or reversible PROTACs and tested in degradation assays. This would lead to a better understanding of the SAR of the structures with respect to their induction of protein degradation. In tandem, affinity enrichment proteomics could be utilised to determine which protein the amine is recruiting for the targeted degradation. The same linking vector for the HaloPROTAC could also be used to conjugate the amines to the bead matrix used in AEP. After compound incubation, MS experiments could then be used to identify the proteins which interact with the compound. All of these steps could lead to the elucidation of new proteins for targeted protein degradation from the two amines described.

A)



B)

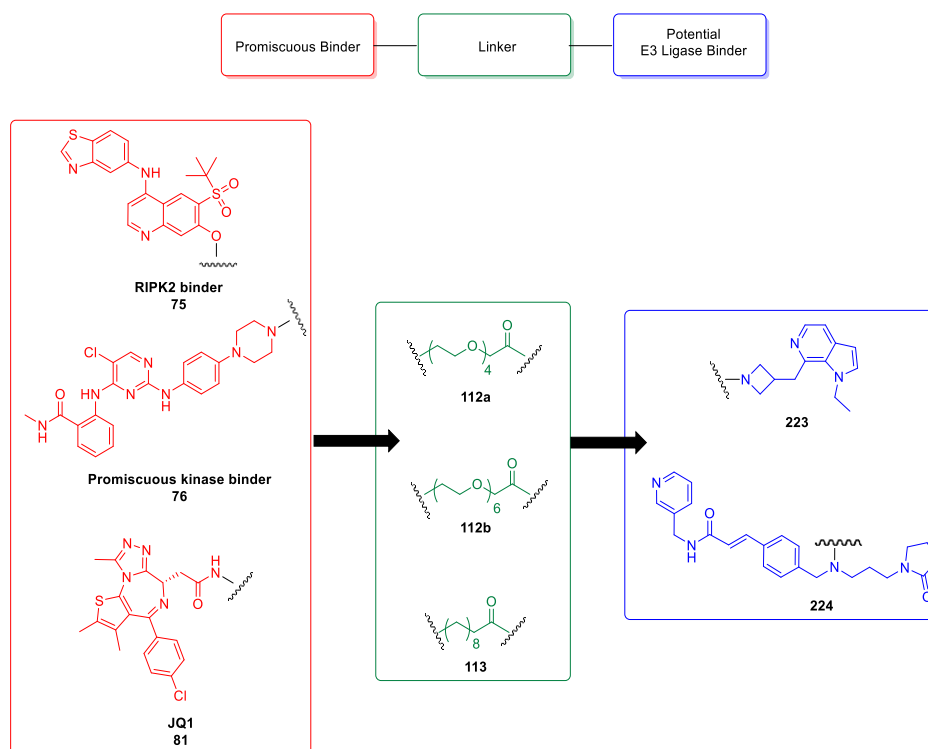


**Figure 159:** Hit triage from the phenotypic assay for the potential hit from the 3000-amine set (A). Utilising the promiscuous toolbox to evaluate the potential hit compound in PROTACs with three different linkers and protein binders (B).

Additional experiments to synthesise novel HaloCompounds derived 3000-amine set would be useful to widen the search for additional E3 ligases. The use of different linker lengths for the same 3000-amine set could increase the chances of finding an E3 ligase. Using 3–4

linkers, including different lengths and/or chemical composition, with all 2934 amines could ensure E3 ligases are less likely to be missed due to impaired ternary complex formation with the linker chosen.

The high-throughput chemistry methodology used for the approach could also be optimised in future work. In moving to a larger screen of the 100,000 amines, it would be beneficial for the chemistry to be completely automated. This would involve the optimisation of the chemical element of the screen, to employ a new base to replace NMM. The base would therefore need to be less volatile than NMM, be miscible with DMSO, and would also need to be compatible with the biological assay. Once in place, automated dispensing methods could be utilised in the larger screening set. Using the Mosquito liquid handler in a glovebox could achieve a large subset of compound testing, with multiple plates (either 384 well or 1536 well plates) being performed leading to a 100,000 HTS screen.

In addition to automation for the 100,000-amine experiment, machine learning could also be employed to determine the amine set selected. Using the information in the 3000-amine reaction conversions, cheminformatics can be used to determine which compounds failed due to structural features (e.g. sterically hindered secondary amines) and electronics (pKa) and a computational model could be built which can predict the outcome for the intended reaction. This would therefore be useful in the larger HTS screen to ensure the compounds are successfully synthesised prior to the biological experiments for finding new E3 ligases for the PROTAC approach.

This approach could also be expanded by utilising alternative chemical transformations. In this example, a high conversion amide coupling was utilised to develop this high-throughput chemical biology platform. This could be further developed by utilising plate based chemistry suitable for a number of other reactions developed, such as metal catalysed couplings and click chemistry (but would likely require compound purification prior to the phenotypic assay).<sup>204,205</sup> Using chemical matter other than aliphatic amines could expand this toolbox and open up a platform for wider utility in the search for new E3 ligases.

## 8 Conclusions

The protein degradation approach has the potential to be an extremely valuable method for therapeutic intervention in drug discovery. PROTACs have shown considerable merit as future therapeutic agents, with potent protein knockdown both *in vitro* and *in vivo* and the promises of extended duration of action, lower human doses and the ability to replicate a biological-agent effect with a small molecule. However, limited availability of chemical matter for E3 ligase recruitment may restrict the use of the PROTAC approach in future for targeting proteins not yet deemed degradable by the approach.

In the search for new chemical matter for E3 ligases several approaches have been utilised. In order to investigate E3 ligase small molecule binders which are reported in the literature, a promiscuous toolbox was envisaged and utilised for testing novel chemical matter. This involved the synthesis and systematic testing of a number of novel PROTAC molecules. The PROTACs were designed to target a range of proteins of interest, to increase the probability of achieving successful degradation as a result of E3 ligase recruitment. This approach was used for the investigation of DCAF15 as an E3 ligase but was resource intensive and ultimately resulted in no new chemical matter for the protein degradation platform. As a result, differentiated approaches to find new chemical matter for E3 ligase recruitment were assessed and executed.

This work has demonstrated the first high-throughput chemistry application to a phenotypic cellular assay. In order to assess E3 ligase recruitment in a high-throughput manner, a phenotypic screen for GFP degradation was developed and optimised. This assay was shown to be robust when recruiting validated E3 ligases for the PROTAC approach. The assay also employed a novel cell line control to distinguish between PROTAC-driven protein degradation and compound-driven cytotoxicity. With the assays in hand, an HTE method was employed through optimisation of high-throughput small scale chemistry. This method was able to deliver 100s-1000s of novel molecules which could be used directly in the phenotypic screening campaign for the search for new E3 ligase binders. Using two computationally selected chemical sets, the chemistry and biological evaluation was optimised and set up with the ultimate aim of setting up a high-throughput screening campaign of up to a hundred thousand compounds for protein degradation. During the assay optimisation, two potential hits were found to specifically reduce GFP in the GFP-HaloTag® cells, and no effects were observed in the GFP-HaloTag® mutant cell line, or by the non-conjugated small molecules. Further evaluation of the hits is ongoing to determine their utility in the PROTAC approach.

The approach could be further expanded and exploited to new areas of protein degradation, such as target identification and also beyond into other areas of chemical biology where crude

reaction mixtures can be tolerated in cells. The work carried out in this thesis shows the potential of combining high-throughput chemistry and cellular assays. It shows the ability to implement new methods of screening for novel chemical binder identification in a fast and robust manner. This screen promises to deliver a large number of novel compounds, capable of elucidating potential E3 ligase binders from the GSK collection for the protein degradation platform.

## 9 Experimental

### 9.1 General Methods

#### Nuclear Magnetic Resonance (NMR)

NMR spectra were recorded using a Bruker DPX400, DPX500, AV400 or AVIII600 (with cryoprobe). Chemical shifts ( $\delta$ ) are reported in parts per million (ppm) relative to residual solvent peaks respective to solvent used and coupling constants ( $J$ ) in Hz. The following abbreviations are used for multiplicities: s = singlet; br s = broad singlet; d = doublet; T = triplet; q = quartet; m = multiplet; dd = doublet of doublets, app = apparent. If not specifically stated, the NMR experiments were run at 30 °C. Compounds were found to be unstable to high temperature NMR so rotamers were not resolved.

#### Liquid Chromatography Mass spectrometry (LCMS)

##### LCMS Method A:

The analysis was conducted on an Acquity UPLC BEH C18 column (50 mm  $\times$  2.1 mm internal diameter 1.7  $\mu$ m packing diameter) at 40 °C.

Buffer A = 0.1% v/v solution of formic acid in water.  
Buffer B = 0.1% v/v solution of formic acid in acetonitrile.

The gradient employed was as follows:

Time (min)	Flow rate (mL/min)	% A	% B
0	1	97	3
1.5	1	5	95
1.9	1	5	95
2.0	1	97	3

The UV detection was an averaged signal from wavelength of 210 nm to 350 nm and mass spectra were recorded on a Waters ZQ mass spectrometer using alternate-scan positive and negative mode electrospray ionisation (ES +ve and ES -ve).

##### LCMS Method B:

The analysis was conducted on an XBridge C18 column (50 mm  $\times$  4.6 mm internal diameter 3.5  $\mu$ m packing diameter) at 30 °C.

The solvents employed were:

Buffer A = 10 mM ammonium bicarbonate in water adjusted to pH 10 with ammonia solution.

Buffer B = acetonitrile.

The typical gradient employed was as follows:

Time (min)	Flow Rate (mL/min)	% A	% B
0	1	97	3
0.05	1	97	3
1.50	1	5	95
1.90	1	5	95
2.00	1	97	3

The UV detection was an averaged signal from wavelength of 210 nm to 350 nm and mass spectra were recorded on a Waters ZQ mass spectrometer using alternate-scan positive and negative mode electrospray ionisation (ES +ve and ES -ve).

#### High Resolution Mass spectrometry (HRMS)

ESI (+) high resolution mass spectra were obtained on a Micromass Q-ToF 2 hybrid quadrupole time-of-flight mass spectrometer, equipped with a Z-spray interface, over a mass range of 100 – 1500 Da, with a scan time of 0.9 s and an interscan delay of 0.1 s. Reserpine was used as the external mass calibrant ( $[M+H]^+ = 609.2812$  Da). The Q-ToF 2 mass spectrometer was operated in W reflectron mode to give a resolution (FWHM) of 16000 – 20000. Ionisation was achieved with a spray voltage of 3.2 kV, a cone voltage of 50 V, with cone and desolvation gas flows of 10-20 and 600 L/h, respectively. The source block and desolvation temperatures were maintained at 120 °C and 250 °C, respectively. The elemental composition was calculated using MassLynx v4.1 for the  $[M+H]^+$  and the mass error quoted as ppm.

#### Mass Directed Auto-Preparative (MDAP)

“Mass directed automated preparative HPLC” (MDAP) was conducted on a system such as a Waters FractionLynx system comprising of a Waters 600 pump with extended pump heads, Waters 2700 autosampler, Waters 996 diode array and Gilson 202 fraction collector on an XBridge C18 column (100 mm × 30 mm i.d. 5 µm packing diameter) at ambient temperature, eluting with 10 mM ammonium bicarbonate in water adjusted to pH 10 with ammonia solution (solvent A) and acetonitrile (solvent B) using the appropriate elution gradient. The UV detection was a summed signal from wavelength of 210 nm to 350 nm. The mass spectra were recorded

on a Waters ZQ spectrometer using electrospray positive and negative mode (ES +ve and ES -ve). The software used was MassLynx 3.5 with OpenLynx and FractionLynx option or using equivalent alternative systems. Similar systems using Sunfire C18 columns and gradient of solvents such as formic acid (for) (or ammonium carbonate (HPH) or TFA (TFA)) in water (solvent A) and acetonitrile (solvent B) were also employed.

### **Infrared**

IR spectra were recorded from solid samples using a Perkin Elmer Spectrum One FTIR spectrometer fitted with a Perkin Elmer Universal ATR (attenuated total reflectance) sampling accessory. Absorption frequencies are reported in wavenumbers ( $\text{cm}^{-1}$ ).

### **Phase Separators**

'Hydrophobic frits' refer to filtration ISOLUTE® tubes sold by Biotage® (25–150 mL) containing an optimised semi-permeable frit that separates the organic phase from aqueous phase under gravity.

### **Purification by Column Chromatography**

The Flashmaster II is an automated multi-user flash chromatography system, available from Argonaut Technologies Ltd, which utilises disposable, normal phase, SPE cartridges. It provides quaternary on-line solvent mixing to enable gradient methods to be run. Samples are queued using the multi-functional open access software, which manages solvents, flow-rates, gradient profile, and collection conditions. The system is equipped with a Knauer variable wavelength UV-detector and two Gilson FC204 fraction-collectors enabling automated peak cutting, collection and tracking.

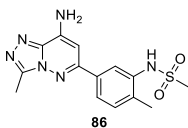
Silica chromatography techniques include either automated (Flashmaster) techniques or manual chromatography on pre-packed cartridges (SPE) or manually-packed flash columns.

## **9.2 Synthetic Procedures**

All reagents were used as purchased from commercial suppliers. Solvents were purchased from Sigma Aldrich, anhydrous, sure-seal quality, and used with no further purification. Reactions were carried out in a fumehood, under air atmosphere, unless otherwise stated.

### 9.2.1 Bromosporine-based PROTAC synthesis

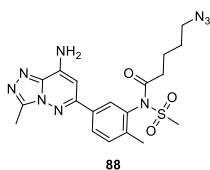
#### *N*-(5-(8-Amino-3-methyl-[1,2,4]triazolo[4,3-*b*]pyridazin-6-yl)-2-methylphenyl)methanesulfonamide, **86**.



To a stirred solution of ethyl (3-methyl-6-(4-methyl-3-(methylsulfonamido)phenyl)-[1,2,4]triazolo[4,3-*b*]pyridazin-8-yl)carbamate (bromosporine **78**) (24.0 mg, 0.0590 mmol) in MeOH (0.1 mL), toluene (0.2 mL) and NMP (0.2 mL) was added 2M NaOH aq. (59.3  $\mu$ L, 0.119 mmol). The resulting mixture was stirred at 70 °C for 4 h. The reaction mixture was concentrated under a stream of nitrogen and purified directly by reverse phase column chromatography (0–30% MeCN (0.1% NH<sub>3</sub>) in 10 mM ammonium bicarbonate) and fractions containing the pure product were concentrated under a stream of nitrogen to afford the desired product **86** (16.0 mg, 81% yield) as a white solid.

**LCMS** (Method B) (ES +ve)  $m/z$  333.1 (M + H)<sup>+</sup> Rt 0.66 min (>95% pure). **HRMS** (ES) calcd for C<sub>14</sub>H<sub>16</sub>N<sub>6</sub>O<sub>2</sub> (M + H)<sup>+</sup> 333.1134 found 333.1131. **<sup>1</sup>H NMR** (400 MHz, DMSO-*d*<sub>6</sub>)  $\delta$  = 9.24 (br. s, 1H), 7.82 (d, *J* = 2.0 Hz, 1H), 7.70 (dd, *J* = 2.0, 8.0 Hz, 1H), 7.47 (s, 2H), 7.40 (d, *J* = 8.0 Hz, 1H), 6.54 (s, 1H), 3.02 (s, 3H), 2.68 (s, 3H), 2.38 (s, 3H). **<sup>13</sup>C NMR** (101 MHz, DMSO-*d*<sub>6</sub>)  $\delta$  = 153.65, 146.72, 142.84, 139.85, 136.48, 135.48, 134.45, 131.22, 123.99, 123.96, 91.73, 39.77, 18.00, 9.55. Note that <sup>13</sup>C NMR data are reported to 2 decimal places to differentiate signals.

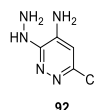
#### *N*-(5-(8-Amino-3-methyl-[1,2,4]triazolo[4,3-*b*]pyridazin-6-yl)-2-methylphenyl)-5-azido-*N*-(methylsulfonyl)pentanamide, **89**.



To a stirred solution of **86** (10.7 mg, 0.0320 mmol) in NMP (0.3 mL) was added 5-azidopentanoic acid **87** (9.22 mg, 0.0640 mmol), DIPEA (0.0170 mL, 0.0970 mmol) and HATU (12.2 mg, 0.0320 mmol). The resulting mixture was stirred at room temperature for 16 h. The crude material was purified directly by reverse phase column chromatography (10–60% MeCN (0.1% NH<sub>3</sub>) in 10 mM ammonium bicarbonate) and fractions containing the pure product were concentrated under a stream of nitrogen to afford the desired product **89** (10.0 mg, 68% yield) as a white solid.

**LCMS** (Method B) (ES +ve)  $m/z$  458.2 (M + H)<sup>+</sup> Rt 0.97 min (>95% pure). **HRMS** (ES) calcd for C<sub>19</sub>H<sub>24</sub>N<sub>9</sub>O<sub>3</sub>S (M + H)<sup>+</sup> 458.1725 found 458.1724. **<sup>1</sup>H NMR** (400 MHz, DMSO-*d*<sub>6</sub>) δ 8.00 – 7.95 (m, 2H), 7.58 (d, *J* = 8.0 Hz, 1H), 7.49 (s, 2H), 6.59 (s, 1H), 3.63 (s, 3H), 3.26 (t, *J* = 6.6 Hz, 2H), 2.70 (s, 3H), 2.35 (s, 3H), 2.29 – 1.93 (m, 2H), 1.60 – 1.40 (m, 4H). **<sup>13</sup>C NMR** (101 MHz, DMSO-*d*<sub>6</sub>) δ = 172.9, 153.0, 146.8, 142.9, 139.8, 139.7, 135.5, 135.23, 131.7, 128.6, 128.1, 92.0, 50.4, 42.3, 34.9, 27.3, 21.0, 17.8, 9.6.

**6-Chloro-3-hydrazinylpyridazin-4-amine, 92.**

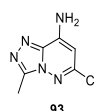


To two separate microwave vials was added 3,6-dichloropyridazin-4-amine **91** (1.50 g, 9.20 mmol) and hydrazine hydrate (9.00 mL, 183 mmol). The resulting mixtures was sealed and stirred at 120 °C for 2 h. The resulting mixture was cooled to room temperature and H<sub>2</sub>O (10 mL) was added. The solid from both mixtures was combined and filtered. The precipitate was washed with H<sub>2</sub>O (50 mL) and dried under vacuum to afford the desired product **92** (802 mg, 28%) as a brown solid.

**<sup>1</sup>H NMR** (400 MHz, DMSO-*d*<sub>6</sub>) δ = 7.29 (br. s, 1H), 6.39 (s, 1H), 6.26 (br. s, 2H), 4.26 (br. s, 2H). **<sup>13</sup>C NMR** (101 MHz, DMSO-*d*<sub>6</sub>) δ = 150.6, 146.6, 137.4, 103.8.

Consistent with literature data.<sup>253</sup>

**6-Chloro-3-methyl-[1,2,4]triazolo[4,3-*b*]pyridazin-8-amine, 93.**

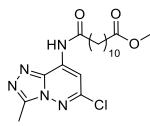


A stirred solution of 6-chloro-3-hydrazinylpyridazin-4-amine **92** (1.00 g, 3.76 mmol) in AcOH (10 mL) in a sealed microwave vial was heated to 120 °C for 5 h. The solution was cooled to room temperature and the solvent was removed *in vacuo*. The product was recrystallised with 10% EtOH in H<sub>2</sub>O to afford the desired product **93** (570 mg, 92%) as long brown needles.

**LCMS** (Method B) (ES +ve)  $m/z$  183.96 (M + H)<sup>+</sup> Rt 0.61 min (>95% pure). **HRMS** (ES) calcd for C<sub>6</sub>H<sub>7</sub>ClN<sub>5</sub> (M + H)<sup>+</sup> 184.0390 found 184.0387. **<sup>1</sup>H NMR** (400 MHz, DMSO-*d*<sub>6</sub>) δ = 7.87 (br. s, 2H), 6.12 (s, 1H), 2.59 (s, 3H). **<sup>13</sup>C NMR** (101 MHz, DMSO-*d*<sub>6</sub>) δ = 149.3, 146.7, 143.8, 139.3, 93.5, 9.4.

Consistent with literature data.<sup>253</sup>

**Methyl 12-((6-chloro-3-methyl-[1,2,4]triazolo[4,3-b]pyridazin-8-yl)amino)-12-oxododecanoate, 95.**

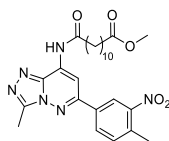


95

To a stirred solution of 6-chloro-3-methyl-[1,2,4]triazolo[4,3-b]pyridazin-8-amine **93** (450 mg, 2.45 mmol), 12-methoxy-12-oxododecanoic acid **94** (719 mg, 2.94 mmol) and DIPEA (2.14 mL, 12.3 mmol) in THF (25 mL) in a sealed microwave vial was added T3P (50% solution in EtOAc) (4.38 mL, 7.35 mmol). The resulting mixture was stirred at 85 °C for 16 h. To this mixture was added T3P (50% solution in EtOAc) (4.38 mL, 7.35 mmol) and DIPEA (2.14 mL, 12.3 mmol) and the resulting mixture was stirred at 85 °C for 7 h. The reaction mixture was diluted with CH<sub>2</sub>Cl<sub>2</sub> (100 mL) and washed with sat. Na<sub>2</sub>CO<sub>3</sub> aq. sol. (3 × 100 mL) and passed through a hydrophobic frit before concentration *in vacuo* to afford a brown solid as the crude product. The crude product was then purified by column chromatography (0–80% ethyl acetate in cyclohexane) and fractions containing the pure product were concentrated *in vacuo* to afford the desired product **95** (830 mg, 83%) as a pale yellow solid.

**LCMS** (Method B) (ES +ve) *m/z* 410.1 (M + H)<sup>+</sup> Rt 1.36 min (>95% pure). **HRMS** (ES) calcd for C<sub>19</sub>H<sub>29</sub>ClN<sub>5</sub>O<sub>3</sub> (M + H)<sup>+</sup> 410.1951 found 410.1945. **<sup>1</sup>H NMR** (400 MHz, CDCl<sub>3</sub>) δ = 9.25 (br. s, 1H), 8.08 (s, 1H), 3.69 (s, 3H), 2.78 (s, 3H), 2.56 (t, *J* = 7.3 Hz, 2H), 2.30 (t, *J* = 7.6 Hz, 2H), 1.75 (app quint, *J* = 7.5 Hz, 2H), 1.62 (app quint, *J* = 7.3 Hz, 2H), 1.41 – 1.25 (m, 12H). **<sup>13</sup>C NMR** (101 MHz, CDCl<sub>3</sub>) δ = 174.3, 173.4, 151.6, 148.2, 138.6, 133.8, 105.4, 51.4, 37.6, 34.1, 29.3, 29.3, 29.2, 29.2, 29.1, 29.1, 29.0, 24.9, 9.7.

**Methyl 12-((3-methyl-6-(4-methyl-3-nitrophenyl)-[1,2,4]triazolo[4,3-b]pyridazin-8-yl)amino)-12-oxododecanoate, 97.**



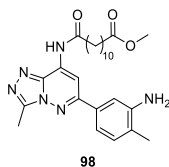
97

To a degassed and nitrogen blanketed solution of methyl 12-((6-chloro-3-methyl-[1,2,4]triazolo[4,3-b]pyridazin-8-yl)amino)-12-oxododecanoate **95** (500 mg, 1.22 mmol), sodium carbonate (1.83 mL, 3.66 mmol) and (4-methyl-3-nitrophenyl)boronic acid **96** (486 mg, 2.68 mmol) in toluene (30 mL) and EtOH (30 mL) was added Pd(dppf)Cl<sub>2</sub>.CH<sub>2</sub>Cl<sub>2</sub> adduct (498 mg, 0.610 mmol). The flask was evacuated and backfilled with nitrogen three times before heating to 90 °C for 3 h. The reaction mixture was concentrated *in vacuo*, redissolved in CH<sub>2</sub>Cl<sub>2</sub> (100 mL) and passed through a Celite® plug before concentration *in vacuo* to give the crude

product as a red gum. The crude product was purified by column chromatography (0–80% ethyl acetate in cyclohexane) and fractions containing the pure product were concentrated *in vacuo* to afford the desired product **97** (450 mg, 72%) as a yellow solid.

**LCMS** (Method B) (ES +ve)  $m/z$  511.3 (M + H)<sup>+</sup> Rt 1.46 min (>95% pure). **HRMS** (ES) calcd for C<sub>26</sub>H<sub>35</sub>N<sub>6</sub>O<sub>5</sub> (M + H)<sup>+</sup> 511.2668 found 511.2669. **<sup>1</sup>H NMR** (400 MHz, CDCl<sub>3</sub>)  $\delta$  = 9.11 (s, 1H), 8.66 (d,  $J$  = 2.0 Hz, 1H), 8.56 (s, 1H), 8.14 (dd,  $J$  = 2.0, 8.1 Hz, 1H), 7.53 (d,  $J$  = 8.1 Hz, 1H), 3.68 (s, 3H), 2.90 (s, 3H), 2.71 (s, 3H), 2.61 (t,  $J$  = 7.5 Hz, 2H), 2.32 (t,  $J$  = 7.5 Hz, 2H), 1.84 – 1.77 (m, 2H), 1.71 – 1.56 (m, 2H), 1.45 – 1.28 (m, 12H). **<sup>13</sup>C NMR** (101 MHz, CDCl<sub>3</sub>)  $\delta$  = 174.27, 173.66, 153.46, 149.84, 148.66, 138.99, 135.81, 134.39, 133.73, 133.46, 131.24, 123.39, 101.82, 51.41, 37.67, 34.09, 29.32, 29.26, 29.18, 29.10, 29.08, 24.98, 24.92, 20.32, 9.92. Note that <sup>13</sup>C NMR data are reported to 2 decimal places to differentiate signals. One signal not observed, potentially due to overlapping frequencies of methylene carbons.

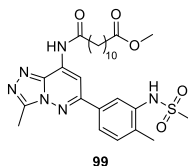
**Methyl 12-((6-(3-amino-4-methylphenyl)-3-methyl-[1,2,4]triazolo[4,3-*b*]pyridazin-8-yl)amino)-12-oxododecanoate, 98.**



To a stirred solution of methyl 12-((3-methyl-6-(4-methyl-3-nitrophenyl)-[1,2,4]triazolo[4,3-*b*]pyridazin-8-yl)amino)-12-oxododecanoate **97** (206 mg, 0.403 mmol) in EtOAc (7.8 mL) was added tin(II) chloride (306 mg, 1.61 mmol) and H<sub>2</sub>O (200  $\mu$ L). The resulting mixture was heated to 70 °C for 1.5 h. The reaction mixture was diluted with EtOAc (50 mL) and washed with sat. aq. Na<sub>2</sub>CO<sub>3</sub> solution (50 mL). The aqueous phase was back extracted with CH<sub>2</sub>Cl<sub>2</sub> (50 mL) and the combined organics were passed through a hydrophobic frit before concentrating *in vacuo* to afford the desired product methyl 12-((6-(3-amino-4-methylphenyl)-3-methyl-[1,2,4]triazolo[4,3-*b*]pyridazin-8-yl)amino)-12-oxododecanoate (190 mg, 98%) as a yellow solid.

**LCMS** (Method B) (ES +ve)  $m/z$  481.2 (M + H)<sup>+</sup> Rt 1.34 min (>95% pure). **HRMS** (ES) calcd for C<sub>26</sub>H<sub>37</sub>N<sub>6</sub>O<sub>3</sub> (M + H)<sup>+</sup> 481.2925 found 481.2927. **<sup>1</sup>H NMR** (400 MHz, CDCl<sub>3</sub>)  $\delta$  = 8.86 (s, 1H), 8.49 (s, 1H), 7.37 – 7.32 (m, 2H), 7.18 (d,  $J$  = 8.0 Hz, 1H), 3.80 (br. s, 2H), 3.67 (s, 3H), 2.86 (s, 3H), 2.59 – 2.53 (m, 2H), 2.34 – 2.28 (m, 2H), 2.25 (s, 3H), 1.82 – 1.73 (m, 2H), 1.64 – 1.62 (m, 2H), 1.45 – 1.25 (m, 12H). **<sup>13</sup>C NMR** (101 MHz, CDCl<sub>3</sub>)  $\delta$  = 174.29, 173.44, 155.96, 148.41, 145.16, 139.21, 133.85, 132.75, 131.02, 125.31, 117.72, 113.24, 102.98, 53.42, 51.41, 37.67, 34.10, 29.32, 29.27, 29.19, 29.11, 29.09, 25.02, 24.94, 17.33, 9.90. Note that <sup>13</sup>C NMR data are reported to 2 decimal places to differentiate signals.

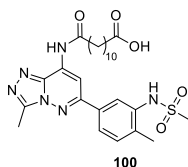
**Methyl 12-((3-methyl-6-(4-methyl-3-(methylsulfonamido)phenyl)-[1,2,4]triazolo[4,3-*b*]pyridazin-8-yl)amino)-12-oxododecanoate, 99.**



To a cooled 0 °C solution of methyl 12-((6-(3-amino-4-methylphenyl)-3-methyl-[1,2,4]triazolo[4,3-*b*]pyridazin-8-yl)amino)-12-oxododecanoate **98** (44.0 mg, 0.0920 mmol) in CH<sub>2</sub>Cl<sub>2</sub> (1.8 mL) was added pyridine (74.0 μL, 0.915 mmol) and MsCl (25.0 μL, 0.320 mmol). The reaction mixture was then stirred at this temperature for 1 h before stirring at room temperature for 16 h. The solution was diluted with CH<sub>2</sub>Cl<sub>2</sub> (25 mL), washed with H<sub>2</sub>O (25 mL), 5% aq. Copper sulfate solution (25 mL) and brine (25 mL) before passing through a hydrophobic frit. The organic phase was then concentrated *in vacuo* to afford the desired product **99** (50.0 mg, 98%) as a yellow solid.

**LCMS** (Method B) (ES +ve) *m/z* 559.2 (M + H)<sup>+</sup> Rt 1.26 min (>95% pure). **HRMS** (ES) calcd for C<sub>27</sub>H<sub>38</sub>N<sub>6</sub>O<sub>5</sub>S (M + H)<sup>+</sup> 559.2701 found 559.2703. **<sup>1</sup>H NMR** (400 MHz, CDCl<sub>3</sub>) δ = 9.71 (br. s, 1H), 8.79 – 8.67 (m, 1H), 8.14 (s, 1H), 7.75 (d, *J* = 7.9 Hz, 1H), 7.39 (d, *J* = 7.9 Hz, 1H), 7.14 – 7.08 (m, 1H), 3.66 (s, 3H), 3.11 (s, 3H), 2.90 – 2.81 (m, 3H), 2.71 – 2.65 (m, 2H), 2.46 (s, 3H), 2.32 – 2.27 (m, 2H), 1.85 – 1.76 (m, 2H), 1.65 – 1.58 (m, 2H), 1.47 – 1.40 (m, 2H), 1.38 – 1.25 (m, 10H). **<sup>13</sup>C NMR** (151 MHz, CDCl<sub>3</sub>) δ = 174.31, 174.09, 155.99, 135.74, 134.62, 134.25, 133.91, 133.33, 131.84, 127.49, 125.27, 122.62, 103.67, 51.43, 40.33, 39.42, 37.75, 34.11, 29.36, 29.33, 29.20, 29.15, 29.12, 25.09, 24.94, 18.25, 10.34. Note that <sup>13</sup>C NMR data are reported to 2 decimal places to differentiate signals.

**12-((3-Methyl-6-(4-methyl-3-(methylsulfonamido)phenyl)-[1,2,4]triazolo[4,3-*b*]pyridazin-8-yl)amino)-12-oxododecanoic acid, 100.**

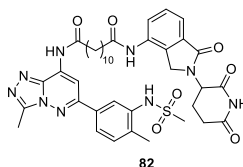


To a microwave vial was added methyl 12-((3-methyl-6-(4-methyl-3-(methylsulfonamido)phenyl)-[1,2,4]triazolo[4,3-*b*]pyridazin-8-yl)amino)-12-oxododecanoate **99** (144 mg, 0.258 mmol) in DMF (2.5 mL) and lithium chloride (54.6 mg, 1.29 mmol). The resulting mixture was sealed and heated to 150 °C for 72 h. The reaction mixture was purified directly by reverse phase chromatography (15–75% MeCN (0.1% NH<sub>3</sub>) in ammonium

bicarbonate 10 mM) and fractions containing the pure product were concentrated under a stream of nitrogen to afford the desired product **100** (33.0 mg, 24%) as an off white solid.

**LCMS** (Method B) (ES +ve)  $m/z$  545.1 (M + H)<sup>+</sup> Rt 0.78 min (>95% pure). **HRMS** (ES) calcd for C<sub>26</sub>H<sub>36</sub>N<sub>6</sub>O<sub>5</sub>S (M + H)<sup>+</sup> 557.2541 found 545.2546. **<sup>1</sup>H NMR** (600 MHz, DMSO-*d*<sub>6</sub>) δ = 11.13 (br. s, 1H), 8.46 (s, 1H), 7.89 (d, *J* = 2.0 Hz, 1H), 7.74 (dd, *J* = 2.0, 7.9 Hz, 1H), 7.46 (d, *J* = 7.9 Hz, 1H), 3.02 (s, 3H), 2.75 (s, 3H), 2.65 (t, *J* = 7.4 Hz, 2H), 2.40 (s, 3H), 2.19 – 2.15 (m, 2H), 1.65 (app quin, *J* = 7.2 Hz, 2H), 1.48 (t, *J* = 7.4 Hz, 2H), 1.37 – 1.24 (m, 12H). 2 exchangeables not observed. **<sup>13</sup>C NMR** (151 MHz, DMSO-*d*<sub>6</sub>) δ = 174.84, 174.46, 153.94, 147.43, 138.64, 136.48, 134.09, 133.50, 131.55, 124.31, 124.22, 117.98, 101.69, 40.08, 36.12, 33.71, 28.84, 28.80, 28.68, 28.67, 28.52, 24.68, 24.48, 18.08, 9.45. Note that <sup>13</sup>C NMR data are reported to 2 decimal places to differentiate signals. One signal not observed, potentially due to overlapping frequencies of methylene carbons.

**M1-(2-(2,6-Dioxopiperidin-3-yl)-1-oxoisindolin-4-yl)-M12-(3-methyl-6-(4-methyl-3-(methylsulfonamido)phenyl)-[1,2,4]triazolo[4,3-*b*]pyridazin-8-yl)dodecanediamide, **82**.**

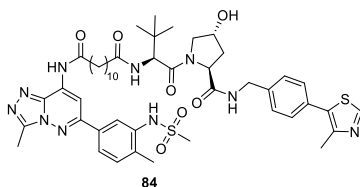


To a stirred solution of 12-((3-methyl-6-(4-methyl-3-(methylsulfonamido)phenyl)-[1,2,4]triazolo[4,3-*b*]pyridazin-8-yl)amino)-12-oxododecanoic acid **100** (14.0 mg, 0.0260 mmol) in DMF (0.6 mL) was added *N*-methylmorpholine (11.3 μL, 0.103 mmol), 3-(4-amino-1-oxoisindolin-2-yl)piperidine-2,6-dione **29** (13.3 mg, 0.0510 mmol) and HATU (19.6 mg, 0.051 mmol) sequentially. The resulting mixture was stirred at room temperature for 24 h. The reaction mixture was purified directly by reverse phase chromatography (15–55% MeCN (0.1% formic acid) in H<sub>2</sub>O (0.1% formic acid)) and fractions containing the pure product were concentrated under a stream of nitrogen to afford the desired product **82** (12.0 mg, 59%) as an off white solid.

**LCMS** (Method B) (ES +ve)  $m/z$  786.2 (M + H)<sup>+</sup> Rt 1.06 min (>95% pure). **HRMS** (ES) calcd for C<sub>39</sub>H<sub>47</sub>N<sub>9</sub>O<sub>7</sub>S (M + H)<sup>+</sup> 786.3398 found 786.3398. **<sup>1</sup>H NMR** (600 MHz, DMSO-*d*<sub>6</sub>) δ = 11.15 (br. s, 1H), 11.0 (br. s, 1H), 9.74 (s, 1H), 8.46 (s, 1H), 7.90 (d, *J* = 2.0 Hz, 1H), 7.81 (dd, *J* = 1.1, 7.4 Hz, 1H), 7.75 (dd, *J* = 2.0, 7.9 Hz, 1H), 7.51 – 7.45 (m, 3H), 5.15 (dd, *J* = 5.2, 13.3 Hz, 1H), 4.46 – 4.25 (m, 2H), 3.02 (s, 3H), 2.99 – 2.85 (m, 1H), 2.75 (s, 3H), 2.71 – 2.59 (m, 3H), 2.40 (s, 3H), 2.38 – 2.33 (m, 3H), 2.06 – 2.01 (m, 1H), 1.66 – 1.57 (m, 4H), 1.35 – 1.25 (m, 12H). one exchangeable not observed. **<sup>13</sup>C NMR** (151 MHz, DMSO-*d*<sub>6</sub>) δ = 174.82, 172.75,

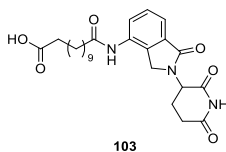
171.31, 170.98, 167.76, 153.90, 147.44, 138.63, 136.54, 136.51, 134.09, 133.76, 133.63, 133.50, 132.60, 131.57, 128.53, 125.17, 124.44, 124.32, 118.88, 101.67, 51.49, 46.43, 40.10, 36.12, 35.76, 31.16, 28.83, 28.88, 28.62, 28.53, 25.03, 24.67, 22.60, 18.05, 9.44. Note that  $^{13}\text{C}$  NMR data are reported to 2 decimal places to differentiate signals. Two signals not observed, potentially due to overlapping frequencies of methylene carbons. IR  $\nu_{\text{max}}$  (neat) 3300, 2919, 2850, 1697, 1577, 1538, 1409  $\text{cm}^{-1}$ .

***N1-((S)-1-((2S,4R)-4-Hydroxy-2-((4-(4-methylthiazol-5-yl)benzyl)carbamoyl)pyrrolidin-1-yl)-3,3-dimethyl-1-oxobutan-2-yl)-N12-(3-methyl-6-(4-methyl-3-(methylsulfonamido)phenyl)-[1,2,4]triazolo[4,3-*b*]pyridazin-8-yl)dodecanediamide, 84.***



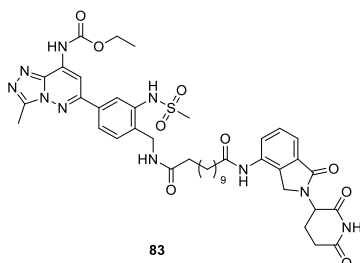
To a stirred solution of 12-((3-methyl-6-(4-methyl-3-(methylsulfonamido)phenyl)-[1,2,4]triazolo[4,3-*b*]pyridazin-8-yl)amino)-12-oxododecanoic acid **100** (14.0 mg, 0.0260 mmol) in DMF (0.9 mL) was added (2*S*,4*R*)-1-((*S*)-2-amino-3,3-dimethylbutanoyl)-4-hydroxy-*N*-(4-(4-methylthiazol-5-yl)benzyl)pyrrolidine-2-carboxamide **101** (22.1 mg, 0.0510 mmol), DIPEA (13.5  $\mu\text{L}$ , 0.0770 mmol) and HATU (10.8 mg, 0.0280 mmol) sequentially. The reaction was stirred at room temperature for 2 h. The reaction mixture was purified directly by reverse phase chromatography (15–65% MeCN (0.1%  $\text{NH}_3$ ) in ammonium bicarbonate 10 mM) and fractions containing the pure product were concentrated under a stream of nitrogen to afford the desired product **84** (12.0 mg, 49%) as an off white solid.

**LCMS** (Method B) (ES +ve)  $m/z$  957.5 ( $\text{M} + \text{H}$ ) $^+$  Rt 1.15 min (>95% pure). **HRMS** (ES) calcd for  $\text{C}_{48}\text{H}_{64}\text{N}_{10}\text{O}_7\text{S}_2$  ( $\text{M} + \text{H}$ ) $^+$  956.4401 found 957.4500.  **$^1\text{H}$  NMR** (600 MHz,  $\text{CDCl}_3$ )  $\delta$  = 9.47 (s, 1H), 8.69 (s, 1H), 8.54 (d,  $J$  = 1.9 Hz, 1H), 8.08 (m, 1H), 7.80 (dd,  $J$  = 1.9, 8.0 Hz, 1H), 7.47 – 7.33 (m, 6H), 6.29 (d,  $J$  = 8.8 Hz, 1H), 4.78 (t,  $J$  = 7.9 Hz, 1H), 4.64 – 4.54 (m, 3H), 4.43 – 4.33 (m, 1H), 4.15 (d, 11.3 Hz, 1H), 3.65 (dd,  $J$  = 3.9, 11.3 Hz, 1H), 3.10 (s, 3H), 2.86 (s, 3H), 2.65 – 2.56 (m, 3H), 2.51 (s, 3H), 2.46 (s, 3H), 2.23 – 2.15 (m, 3H), 1.85 – 1.74 (m, 2H), 1.58 – 1.55 (m, 2H), 1.42 – 1.35 (m, 2H), 1.33 – 1.22 (m, 10H), 0.96 (s, 9H). (2 exchangeables not observed).  **$^{13}\text{C}$  NMR** (151 MHz,  $\text{CDCl}_3$ )  $\delta$  = 174.02, 173.79, 172.03, 170.75, 154.96, 150.28, 148.48, 148.46, 139.17, 138.07, 135.58, 134.90, 134.44, 133.45, 131.85, 131.56, 131.00, 129.51, 128.11, 125.41, 122.93, 102.83, 70.06, 58.54, 57.51, 56.77, 43.27, 40.21, 37.57, 36.36, 35.90, 34.99, 28.89, 28.88, 28.83, 28.70, 28.62, 28.53, 26.45, 25.44, 24.97, 18.20, 16.05, 9.85. Note that  $^{13}\text{C}$  NMR data are reported to 2 decimal places to differentiate signals. IR  $\nu_{\text{max}}$  (neat) 3284, 2924, 2854, 1629, 1534, 1471, 1416  $\text{cm}^{-1}$ .

**12-((2-(2,6-Dioxopiperidin-3-yl)-1-oxoisindolin-4-yl)amino)-12-oxododecanoic acid, 103.**

To a stirred solution of 3-(4-amino-1-oxoisindolin-2-yl)piperidine-2,6-dione **29** (250 mg, 0.964 mmol) in NMP (1.1 mL) was added dodecanedioic acid **102** (666 mg, 2.89 mmol), DIPEA (674  $\mu$ L, 3.86 mmol) and HATU (1100 mg, 2.89 mmol) sequentially. The resulting mixture was stirred at room temperature for 1 h before purifying directly by reverse phase column chromatography (10–45% MeCN (0.1% formic acid) in H<sub>2</sub>O (0.1% formic acid) and fractions containing the pure product were concentrated under a stream of nitrogen. The product was then repurified via MDAP (HPH) and AcOH (50  $\mu$ L) was added to fractions containing the pure product and were concentrated under a stream of nitrogen to afford the desired product **103** (120 mg, 24%) as a white solid.

**LCMS** (Method B) (ES +ve)  $m/z$  490.2 (M + H<sub>2</sub>O + H)<sup>+</sup> Rt 0.66 min (89% pure). **HRMS** (ES) calcd for C<sub>25</sub>H<sub>33</sub>N<sub>3</sub>O<sub>6</sub> (M + H)<sup>+</sup> 490.2551 found 490.2551. **<sup>1</sup>H NMR** (400 MHz, DMSO-*d*<sub>6</sub>)  $\delta$  = 9.76 (s, 1H), 7.82 (dd,  $J$  = 1.9, 7.0 Hz, 1H), 7.56 – 7.46 (m, 2H), 5.15 (dd,  $J$  = 5.4, 13.2 Hz, 1H), 4.39 – 4.35 (m, 2H), 3.04 – 2.86 (m, 1H), 2.66 – 2.58 (m, 1H), 2.38 – 2.33 (m, 3H), 2.21 – 2.16 (m, 2H), 2.09 – 2.00 (m, 1H), 1.68 – 1.57 (m, 2H), 1.51 – 1.42 (m, 2H), 1.36 – 1.23 (m, 12H). 2 exchangeables not observed. **<sup>13</sup>C NMR** (101 MHz, DMSO-*d*<sub>6</sub>)  $\delta$  = 174.51, 172.76, 171.34, 170.98, 167.79, 133.78, 133.65, 132.62, 128.54, 125.19, 118.90, 51.52, 46.46, 35.78, 33.78, 31.17, 28.84, 28.71, 28.68, 28.63, 28.53, 25.05, 24.52, 22.62. Note that <sup>13</sup>C NMR data are reported to 2 decimal places to differentiate signals. One signal not observed, potentially due to overlapping frequencies of methylene carbons.

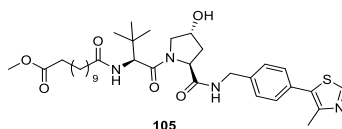
**Ethyl (6-(4-((12-((2-(2,6-dioxopiperidin-3-yl)-1-oxoisindolin-4-yl)amino)-12-oxododecanamido)methyl)-3-(methylsulfonamido)phenyl)-3-methyl-[1,2,4]triazolo[4,3-*b*]pyridazin-8-yl)carbamate, 83.**

To a stirred solution of 12-((2-(2,6-dioxopiperidin-3-yl)-1-oxoisindolin-4-yl)amino)-12-oxododecanoic acid **103** (25.0 mg, 0.0530 mmol) in NMP (0.5 mL) and to this solution was

added ethyl (6-(4-(aminomethyl)-3-(methylsulfonamido)phenyl)-3-methyl-[1,2,4]triazolo[4,3-*b*]pyridazin-8-yl)carbamate **104** (22.2 mg, 0.0530 mmol), DIPEA (27.8  $\mu$ L, 0.159 mmol) and HATU (20.2 mg, 0.0530 mmol) sequentially. The resulting mixture was stirred at room temperature for 0.5 h. The reaction mixture was purified directly by reverse phase column chromatography (20–70% MeCN (0.1% formic acid) in H<sub>2</sub>O (0.1% formic acid)) and fractions containing the pure product were concentrated under a stream of nitrogen to afford the desired product **83** (15.0 mg, 32%) as a yellow gum.

**LCMS** (Method B) (ES +ve)  $m/z$  873.4 (M + H)<sup>+</sup> Rt 0.98 min (92% pure). **HRMS** (ES) calcd for C<sub>42</sub>H<sub>52</sub>N<sub>10</sub>O<sub>9</sub>S (M + H)<sup>+</sup> 873.3718 found 873.3710. **<sup>1</sup>H NMR** (600 MHz, DMSO-*d*<sub>6</sub>)  $\delta$  = 11.05 (br. s, 1H), 9.74 (s, 1H), 8.56 – 8.50 (m, 1H), 8.28 (s, 1H), 8.11 (s, 1H), 7.95 (s, 1H), 7.81 (d,  $J$  = 7.7 Hz, 2H), 7.53 – 7.45 (m, 3H), 5.15 (dd,  $J$  = 5.1, 13.5 Hz, 2H), 4.42 – 4.25 (m, 6H), 3.07 (s, 3H), 2.97 – 2.88 (m, 1H), 2.74 (s, 3H), 2.65 – 2.59 (m, 1H), 2.39 – 2.31 (m, 3H), 2.17 (t,  $J$  = 7.4 Hz, 2H), 2.08 – 2.01 (m, 1H), 1.62 – 1.50 (m, 4H), 1.32 – 1.23 (m, 15H). One exchangeable not observed. **<sup>13</sup>C NMR** (151 MHz, DMSO-*d*<sub>6</sub>)  $\delta$  = 173.14, 172.77, 171.31, 170.99, 167.77, 153.64, 153.54, 147.41, 138.74, 136.55, 135.97, 135.01, 134.72, 133.77, 133.62, 132.60, 129.78, 128.53, 125.16, 124.21, 123.40, 118.88, 100.76, 61.68, 51.51, 46.44, 39.84, 38.65, 35.74, 35.15, 31.16, 28.87, 28.85, 28.72, 28.68, 28.62, 28.58, 25.18, 25.02, 22.61, 14.23, 9.44. Note that <sup>13</sup>C NMR data are reported to 2 decimal places to differentiate signals. **IR**  $\nu_{max}$  (neat) 3259, 2925, 2852, 1691, 1536, 1472 cm<sup>-1</sup>.

**Methyl 12-(((S)-1-((2S,4R)-4-hydroxy-2-((4-(4-methylthiazol-5-yl)benzyl)carbamoyl)pyrrolidin-1-yl)-3,3-dimethyl-1-oxobutan-2-yl)amino)-12-oxododecanoate, 105.**

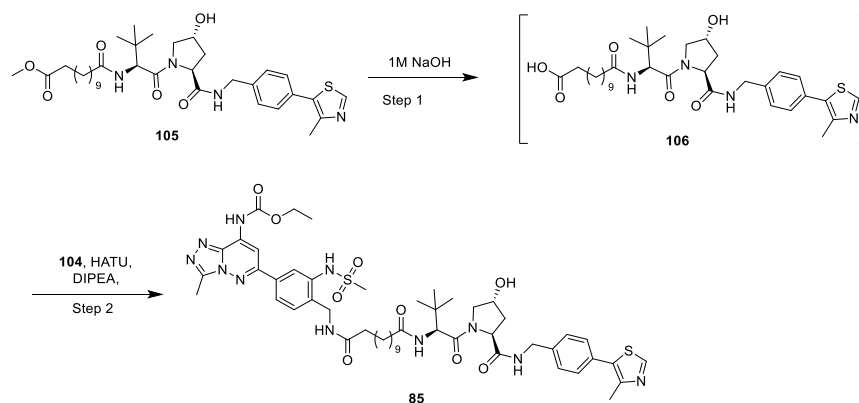


To a stirred solution of (2S,4R)-1-(((S)-2-amino-3,3-dimethylbutanoyl)-4-hydroxy-N-(4-(4-methylthiazol-5-yl)benzyl)pyrrolidine-2-carboxamide **101** (100 mg, 0.232 mmol) in NMP (1.1 mL) was added 12-methoxy-12-oxododecanoic acid **94** (56.7 mg, 0.232 mmol), DIPEA (203  $\mu$ L, 1.161 mmol) and HATU (106 mg, 0.279 mmol) sequentially. The resulting mixture was stirred at room temperature for 0.5 h before purifying directly by reverse phase column chromatography (20–75% MeCN (0.1% NH<sub>3</sub>) in 10 mM ammonium carbonate) and fractions containing the pure product were concentrated under a stream of nitrogen to afford the desired product **105** (100 mg, 66%) as a yellow gum.

**LCMS** (Method B) (ES +ve)  $m/z$  657.4 (M + H)<sup>+</sup> Rt 1.22 min (>95% pure). **HRMS** (ES) calcd for C<sub>35</sub>H<sub>52</sub>N<sub>4</sub>O<sub>6</sub>S (M + H)<sup>+</sup> 657.3686 found 657.3688. **<sup>1</sup>H NMR** (400 MHz, DMSO-*d*<sub>6</sub>)  $\delta$  = 8.99

(s, 1H), 8.57 – 8.50 (m, 1H), 7.82 – 7.80 (m, 1H), 7.46 – 7.37 (m, 4H), 5.11 (d,  $J = 3.6$  Hz, 1H), 4.55 (d,  $J = 9.4$  Hz, 1H), 4.47 – 4.34 (m, 3H), 4.26 – 4.19 (m, 1H), 3.71 – 3.62 (m, 2H), 3.58 (s, 3H), 2.45 (s, 3H), 2.37 (s, 3H), 2.15 – 2.00 (m, 2H), 1.95 – 1.88 (m, 1H), 1.56 – 1.43 (m, 4H), 1.28 – 1.20 (m, 12H), 0.97 (s, 9H).  $^{13}\text{C}$  NMR (101 MHz, DMSO- $d_6$ )  $\delta = 173.29, 172.04, 171.87, 169.67, 151.36, 147.67, 139.45, 131.11, 129.60, 128.58, 127.38, 68.81, 58.64, 56.27, 56.23, 51.08, 41.62, 37.90, 35.15, 34.83, 33.23, 28.82, 28.76, 28.65, 28.58, 28.40, 26.34, 25.37, 24.37, 15.89$ . Note that  $^{13}\text{C}$  NMR data are reported to 2 decimal places to differentiate signals. One signal not observed, potentially due to overlapping frequencies of methylene carbons.

**Ethyl (6-(4-((12-(((S)-1-((2S,4R)-4-hydroxy-2-((4-(4-methylthiazol-5-yl)benzyl)carbamoyl)pyrrolidin-1-yl)-3,3-dimethyl-1-oxobutan-2-yl)amino)-12-oxododecanamido)methyl)-3-(methylsulfonamido)phenyl)-3-methyl-[1,2,4]triazolo[4,3-*b*]pyridazin-8-yl)carbamate, 85.**



**Step 1:**

To a stirred solution of methyl 12-(((S)-1-((2S,4R)-4-hydroxy-2-((4-(4-methylthiazol-5-yl)benzyl)carbamoyl)pyrrolidin-1-yl)-3,3-dimethyl-1-oxobutan-2-yl)amino)-12-oxododecanoate **105** (40.0 mg, 0.0610 mmol) in THF (0.5 mL) was added 1M NaOH aq. (30.4  $\mu\text{L}$ , 0.0610 mmol). The resulting mixture was stirred at room temperature for 6 h. The reaction mixture was neutralised with 1M HCl aq. (30  $\mu\text{L}$ ) and concentrated under a stream of nitrogen to give **106** as a crude gum.

**LCMS** (Method B) (ES +ve)  $m/z$  643.4 ( $M + H$ ) $^+$  Rt 0.80 min (>95% pure).

**Step 2:**

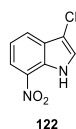
Crude product **106** was redissolved in NMP (0.5 mL) and to this solution was added ethyl (6-(4-(aminomethyl)-3-(methylsulfonamido)phenyl)-3-methyl-[1,2,4]triazolo[4,3-*b*]pyridazin-8-yl)carbamate **104** (25.5 mg, 0.0610 mmol), DIPEA (31.9  $\mu\text{L}$ , 0.183 mmol) and HATU (27.8 mg, 0.0730 mmol) sequentially. The resulting mixture was stirred at room temperature for 0.5 h.

The reaction mixture was purified directly by reverse phase column chromatography (20–70% MeCN (0.1% NH<sub>3</sub>) in 10 mM ammonium carbonate) and fractions containing the pure product were concentrated under a stream of nitrogen to afford the desired product **85** (33 mg, 52% over two steps) as a yellow gum.

**LCMS** (Method B) (ES +ve)  $m/z$  1044.5 (M + H)<sup>+</sup> Rt 1.08 min (>95% pure). **HRMS** (ES) calcd for C<sub>51</sub>H<sub>69</sub>N<sub>11</sub>O<sub>9</sub>S<sub>2</sub> (M + H)<sup>+</sup> 1044.4790 found 1044.4786. **<sup>1</sup>H NMR** (400 MHz, DMSO-*d*<sub>6</sub>)  $\delta$  = 8.97 (s, 1H), 8.56 – 8.50 (m, 2H), 8.11 (s, 1H), 7.95 (d,  $J$  = 2.0 Hz, 1H), 7.83 – 7.77 (m, 2H), 7.50 – 7.36 (m, 5H), 7.28 – 7.13 (m, 2H), 5.10 (d,  $J$  = 3.6 Hz, 1H), 4.53 (d,  $J$  = 9.4 Hz, 1H), 4.48 – 4.34 (m, 5H), 4.27 (q,  $J$  = 7.1 Hz, 2H), 4.24 – 4.21 (m, 1H), 3.69 – 3.63 (m, 2H), 3.07 (s, 3H), 2.74 (s, 3H), 2.44 (s, 3H), 2.28 – 2.11 (m, 5H), 1.95 – 1.87 (m, 1H), 1.56 – 1.40 (m, 4H), 1.30 (t,  $J$  = 7.1 Hz, 3H), 1.23 – 1.20 (m, 12H), 0.93 (s, 9H). **<sup>13</sup>C NMR** (101 MHz, DMSO-*d*<sub>6</sub>)  $\delta$  = 173.13, 172.01, 171.85, 169.65, 153.63, 153.49, 151.34, 147.65, 147.41, 139.44, 138.73, 136.62, 135.70, 135.01, 134.73, 131.09, 129.80, 129.59, 128.57, 127.37, 124.38, 123.52, 100.76, 68.80, 61.67, 58.63, 56.26, 56.22, 41.61, 39.85, 38.62, 37.89, 35.14, 34.82, 28.87, 28.69, 28.68, 28.61, 28.60, 26.32, 25.37, 25.18, 15.88, 14.24, 9.44. Note that <sup>13</sup>C NMR data are reported to 2 decimal places to differentiate signals. Two signals not observed, potentially due to overlapping frequencies of methylene carbons. **IR**  $\nu_{max}$  (neat) 3280, 2926, 2851, 1739, 1632, 1562, 1536, 1474 cm<sup>-1</sup>.

### 9.2.2 DCAF15-based PROTAC synthesis

#### 3-Chloro-7-nitro-1*H*-indole, **122**.

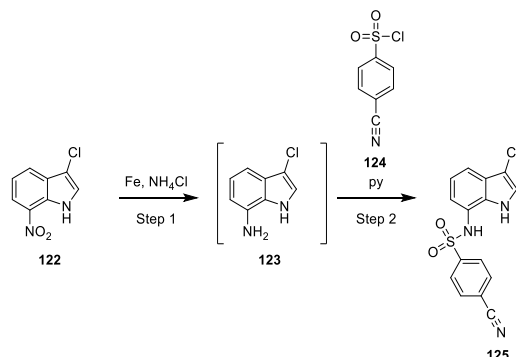


To a stirred solution of 7-nitro-1*H*-indole **121** (2.18 g, 13.4 mmol) in THF (20 mL) was added 2M HCl aq. (0.100 mL, 0.200 mmol) and NCS (2.24 g, 16.8 mmol) in one portion. The resulting mixture was stirred at room temperature for 3 h. To this mixture was added H<sub>2</sub>O (50 mL), and the resulting precipitate was filtered. The mixture was then washed with H<sub>2</sub>O (50 mL), MeOH:H<sub>2</sub>O 1:1 (50 mL) and TBME (2 × 50 mL) and then dried *in vacuo* to afford the desired product **122** (2.35 g, 89%) as a yellow solid.

**LCMS** (Method B) (ES +ve)  $m/z$  197.0 (M + H)<sup>+</sup> Rt 1.15 min (>95% pure). **<sup>1</sup>H NMR** (400 MHz, DMSO-*d*<sub>6</sub>)  $\delta$  = 12.12 (br. s, 1H), 8.21 (br. d,  $J$  = 7.8 Hz, 1H), 8.02 (br. d,  $J$  = 7.8 Hz, 1H), 7.71 (br. s, 1H), 7.49 – 7.24 (m, 1H). **<sup>13</sup>C NMR** (101 MHz, DMSO-*d*<sub>6</sub>)  $\delta$  = 132.9, 128.6, 127.1, 125.8, 125.7, 119.8, 119.6, 105.4.

Consistent with literature data.<sup>254</sup>

***N*-(3-Chloro-1*H*-indol-7-yl)-4-cyanobenzenesulfonamide, **125**.**



**Step 1:**

To a stirred solution of 3-chloro-7-nitro-1*H*-indole **122** (2.00 g, 10.2 mmol) in IPA (40 mL) and H<sub>2</sub>O (8.0 mL) was added iron powder (1.70 g, 30.5 mmol) and ammonium chloride (3.27 g, 61.0 mmol). The resulting mixture was stirred at 60 °C for 2 h. To this mixture was added activated charcoal (1.0 g) and the mixture was filtered, the precipitate was further washed with EtOAc (50 mL) before the combined filtrate was concentrated *in vacuo* to afford the reduced amine **123** as a brown gum which was used without further purification.

**LCMS** (Method B) (ES +ve) *m/z* 166.91 (M + H)<sup>+</sup> Rt 0.92 min (84% pure).

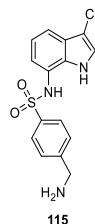
**Step 2:**

To a cooled (0 °C) solution of the **123** in THF (25 mL) was added pyridine (3.29 mL, 40.7 mmol), and 4-cyanobenzenesulfonyl chloride **124** (2.05 g, 10.17 mmol) in THF (25 mL) was added dropwise. The resulting mixture was warmed to room temperature over 16 h. The reaction mixture was concentrated *in vacuo*, redissolved in EtOAc (75 mL), washed with 5% Cu(II)SO<sub>4</sub> aq. sol. (75 mL) H<sub>2</sub>O (75 mL) and brine (75 mL) before passing through a hydrophobic frit. The organic layer was concentrated *in vacuo* to afford the desired product **125** (2.25 g, 67% over two steps) as a brown solid.

**LCMS** (Method B) (ES -ve) *m/z* 330.0 (M + H)<sup>+</sup> Rt 0.83 min (>95% pure). **<sup>1</sup>H NMR** (400 MHz, DMSO-*d*<sub>6</sub>) δ = 11.07 (br. s, 1H), 10.23 (br. s, 1H), 8.05 – 7.99 (m, 2H), 7.92 – 7.84 (m, 2H), 7.49 (d, *J* = 2.8 Hz, 1H), 7.31 (d, *J* = 7.8 Hz, 1H), 6.97 (app t, *J* = 7.8 Hz, 1H), 6.77 – 6.70 (m, 1H). **<sup>13</sup>C NMR** (101 MHz, DMSO-*d*<sub>6</sub>) δ = 143.4, 133.3, 129.7, 127.6, 126.3, 123.1, 121.1, 119.9, 117.5, 116.9, 115.4, 115.3, 103.6.

Consistent with literature data.<sup>254</sup>

**4-(Aminomethyl)-N-(3-chloro-1H-indol-7-yl)benzenesulfonamide, 115.**

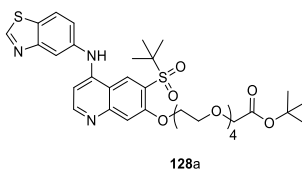


To a stirred solution of *N*-(3-chloro-1H-indol-7-yl)-4-cyanobenzenesulfonamide **125** (1.90 g, 5.73 mmol) in THF (1 mL) was added borane (1M in THF, 5.70 mL, 22.9 mmol). The resulting mixture was stirred at room temperature for 16 h. LCMS analysis of the reaction mixture indicated incomplete conversion. Therefore, additional borane (1M in THF, 5.70 mL, 22.9 mmol) was added and the resulting mixture was stirred at room temperature for a further 16 h. The reaction mixture was quenched slowly with NH<sub>4</sub>Cl sat. aq. solution (10 mL) and purified directly via SCX-2 (washed with MeOH then elution with 2M NH<sub>3</sub> in MeOH) and concentrated *in vacuo* to give the crude product as a brown oil. The crude product was further purified by reverse phase column chromatography (0–35% MeCN (0.1% NH<sub>3</sub>) in 10 mM ammonium bicarbonate) and fractions containing the pure product were concentrated *in vacuo* to afford the desired product **115** (750 mg, 39%) as a light brown solid.

**LCMS** (Method B) (ES +ve) *m/z* 335.9 (M + H)<sup>+</sup> Rt 0.77 min (>95% pure). **HRMS** (ES) calcd for C<sub>15</sub>H<sub>14</sub>ClN<sub>3</sub>O<sub>2</sub>S (M + H)<sup>+</sup> 336.0573 found 336.0568. **<sup>1</sup>H NMR** (400 MHz, DMSO-*d*<sub>6</sub>) δ = 10.94 (br. s, 1H), 7.71 (d, *J* = 8.1 Hz, 2H), 7.42 (d, *J* = 8.1 Hz, 2H), 7.36 (s, 1H), 7.05 (dd, *J* = 1.6, 7.5 Hz, 1H), 6.96 – 6.76 (m, 2H), 3.80 (s, 2H). One exchangeable not observed. **<sup>13</sup>C NMR** (101 MHz, DMSO-*d*<sub>6</sub>) δ = 145.9, 140.7, 129.7, 128.1, 127.1, 126.9, 126.1, 122.4, 120.6, 114.2, 112.1, 103.8, 44.7.

Consistent with literature data.<sup>254</sup>

***tert*-Butyl 14-((4-(benzo[*d*]thiazol-5-ylamino)-6-(*tert*-butylsulfonyl)quinolin-7-yl)oxy)-3,6,9,12-tetraoxatetradecanoate, 128a.**



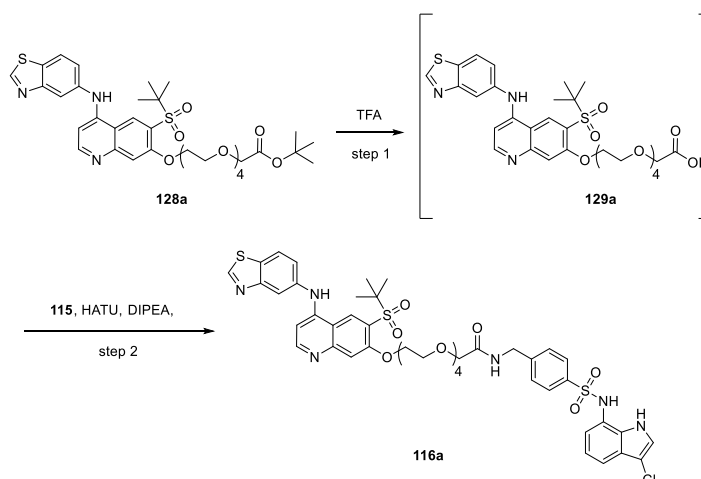
A solution of 4-(benzo[*d*]thiazol-5-ylamino)-6-(*tert*-butylsulfonyl)quinolin-7-ol **126** (120 mg, 0.290 mmol), *tert*-butyl 14-chloro-3,6,9,12-tetraoxatetradecanoate **127a** (142 mg, 0.435

mmol), sodium iodide (44.0 mg, 0.290 mmol) and DIPEA (0.15 mL, 0.871 mmol) in DMF (1.5 mL) was heated at 80 °C for 16 h. The reaction mixture was cooled to room temperature and was purified directly by reverse phase column chromatography (30–95% MeCN (0.1% NH<sub>3</sub>) in 10 mM ammonium bicarbonate) and fractions containing the pure product were concentrated under a stream of nitrogen to afford the desired product **128a** (70.0 mg, 34%) as a yellow gum.

**LCMS** (Method B) (ES +ve)  $m/z$  704.3 (M + H)<sup>+</sup> Rt 1.17 min (>95% pure). **HRMS** (ES) calcd for C<sub>34</sub>H<sub>45</sub>N<sub>3</sub>O<sub>9</sub>S<sub>2</sub> (M + H)<sup>+</sup> 704.2675 found 704.2676. **<sup>1</sup>H NMR** (400 MHz, DMSO-*d*<sub>6</sub>) δ = 9.68 (s, 1H), 9.44 (s, 1H), 8.96 (s, 1H), 8.50 (d, *J* = 5.4 Hz, 1H), 8.21 (d, *J* = 8.6 Hz, 1H), 8.04 (d, *J* = 2.1 Hz, 1H), 7.55 (dd, *J* = 2.1, 8.6 Hz, 1H), 7.48 (s, 1H), 6.90 (d, *J* = 5.4 Hz, 1H), 4.39 – 4.29 (m, 2H), 3.98 (s, 2H), 3.93 – 3.78 (m, 2H), 3.69 – 3.61 (m, 2H), 3.59 – 3.50 (m, 10H), 1.42 (s, 9H), 1.35 (s, 9H). **<sup>13</sup>C NMR** (101 MHz, DMSO-*d*<sub>6</sub>) δ = 169.27, 157.28, 156.32, 154.06, 153.97, 153.03, 149.36, 138.73, 130.66, 129.15, 123.06, 123.01, 121.64, 116.62, 113.24, 110.32, 101.26, 80.54, 69.87, 69.83, 69.81, 69.76, 69.71, 69.66, 68.53, 68.31, 68.08, 60.70, 27.71, 23.66. Note that <sup>13</sup>C NMR data are reported to 2 decimal places to differentiate signals.

Consistent with literature data.<sup>4</sup>

**14-((4-(Benzo[*d*]thiazol-5-ylamino)-6-(*tert*-butylsulfonyl)quinolin-7-yl)oxy)-*N*-(4-(*N*-(3-chloro-1*H*-indol-7-yl)sulfamoyl)benzyl)-3,6,9,12-tetraoxatetradecanamide, **116a**.**



**Step 1:**

To a vial of *tert*-butyl 14-((4-(benzo[*d*]thiazol-5-ylamino)-6-(*tert*-butylsulfonyl)quinolin-7-yl)oxy)-3,6,9,12-tetraoxatetradecanoate **128a** (70.0 mg, 0.0990 mmol) was added TFA (153 μL, 1.99 mmol). The resulting mixture was stirred at room temperature for 10 minutes before concentrating *in vacuo* and 4M HCl in dioxane (500 μL, 1.99 mmol) was added and reconcentrated to give the acid **129a** which was used directly without further purification.

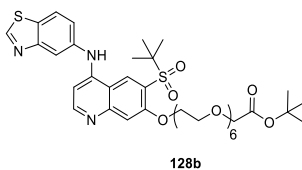
**LCMS** (Method B) (ES +ve)  $m/z$  648.2 (M + H)<sup>+</sup> Rt 0.78 min (91% pure).

Step 2:

The crude products **129a** was dissolved in DMF (0.9 mL), and was added DIPEA (87.0  $\mu$ L, 0.497 mmol), 4-(aminomethyl)-*N*-(3-chloro-1*H*-indol-7-yl)benzenesulfonamide **115** (33.0 mg, 0.0990 mmol) and HATU (38.0 mg, 0.0990 mmol) sequentially. The resulting mixture was stirred at room temperature for 1 h. The reaction mixture was purified directly by reverse phase column chromatography (20–80% MeCN (0.1% NH<sub>3</sub>) in 10 mM ammonium carbonate) and fractions containing the pure product were concentrated under a stream of nitrogen to afford the desired product **116a** (42.0 mg, 44% over two steps) as a yellow gum.

**LCMS** (Method B) (ES +ve)  $m/z$  965.2 (M + H)<sup>+</sup> Rt 1.12 min (>95% pure). **HRMS** (ES) calcd for C<sub>45</sub>H<sub>49</sub>ClN<sub>6</sub>O<sub>10</sub>S<sub>3</sub> (M + H)<sup>+</sup> 965.2439 found 965.2441. **<sup>1</sup>H NMR** (600 MHz, DMSO-*d*<sub>6</sub>)  $\delta$  = 11.02 – 10.96 (m, 1H), 9.98 (br. s, 1H), 9.68 (br. s, 1H), 9.43 (s, 1H), 8.96 (s, 1H), 8.50 (br. d,  $J$  = 5.4 Hz, 1H), 8.29 (t,  $J$  = 6.3 Hz, 1H), 8.20 (d,  $J$  = 8.6 Hz, 1H), 8.04 (br. s, 1H), 7.70 (d,  $J$  = 8.1 Hz, 2H), 7.54 (br. d,  $J$  = 8.6 Hz, 1H), 7.48 – 7.47 (m, 2H), 7.37 (d,  $J$  = 8.4 Hz, 2H), 7.22 (d,  $J$  = 8.1 Hz, 1H), 6.94 (app t,  $J$  = 7.8 Hz, 1H), 6.91 – 6.88 (m, 1H), 6.87 – 6.82 (m, 1H), 4.36 – 4.30 (m, 4H), 3.95 (s, 2H), 3.84 – 3.80 (m, 2H), 3.61 – 3.59 (m, 4H), 3.57 – 3.54 (m, 2H), 3.53 – 3.45 (m, 6H), 1.34 (s, 9H). **<sup>13</sup>C NMR** (151 MHz, DMSO-*d*<sub>6</sub>)  $\delta$  = 169.56, 157.28, 156.35, 154.08, 153.97, 153.01, 149.42, 144.75, 138.73, 137.80, 130.70, 129.17, 128.75, 127.62, 127.55, 126.83, 126.09, 123.01, 122.82, 122.17, 121.65, 119.95, 116.65, 115.27, 114.33, 113.26, 110.31, 103.61, 101.26, 70.30, 69.90, 69.84, 69.78, 69.71, 69.71, 69.49, 68.52, 68.31, 60.69, 41.20, 23.65. Note that <sup>13</sup>C NMR data are reported to 2 decimal places to differentiate signals. **IR**  $\nu_{max}$  (neat) 3338, 3074, 2888, 2799, 1656, 1611, 1572, 1525, 1444, 1356 cm<sup>-1</sup>.

**tert-Butyl 20-((4-(benzo[*d*]thiazol-5-ylamino)-6-(*tert*-butylsulfonyl)quinolin-7-yl)oxy)-3,6,9,12,15,18-hexaoxaicosanoate, 128b.**

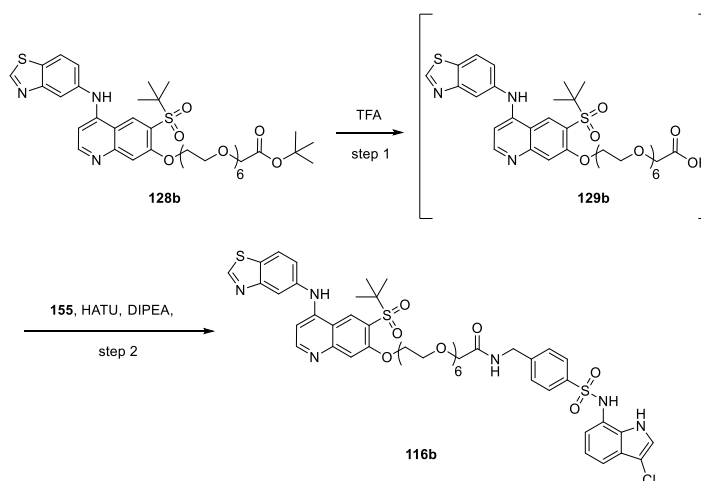


A solution of 4-(benzo[*d*]thiazol-5-ylamino)-6-(*tert*-butylsulfonyl)quinolin-7-ol **126** (120 mg, 0.290 mmol), *tert*-butyl 20-chloro-3,6,9,12,15,18-hexaoxaicosanoate **127b** (181 mg, 0.435 mmol), sodium iodide (44 mg, 0.290 mmol) and DIPEA (0.15 mL, 0.871 mmol) in DMF (1.5 mL) was heated at 80 °C for 16 h. The reaction mixture was purified directly by reverse phase column chromatography (30–85% MeCN (0.1% NH<sub>3</sub>) in 10 mM ammonium bicarbonate) and

fractions containing the pure product were concentrated *in vacuo* to afford the desired product **128b** (70.0 mg, 31%) as a yellow gum.

**LCMS** (Method B) (ES +ve)  $m/z$  792.3 (M + H)<sup>+</sup> Rt 1.16 min (>95% pure). **HRMS** (ES) calcd for C<sub>38</sub>H<sub>53</sub>N<sub>3</sub>O<sub>11</sub>S<sub>2</sub> (M + H)<sup>+</sup> 792.3200 found 792.3195. **<sup>1</sup>H NMR** (600 MHz, DMSO-*d*<sub>6</sub>) δ = 9.68 (s, 1H), 9.44 (s, 1H), 8.96 (s, 1H), 8.50 (d, *J* = 5.4 Hz, 1H), 8.21 (d, *J* = 8.6 Hz, 1H), 8.04 (d, *J* = 2.1 Hz, 1H), 7.55 (dd, *J* = 2.1, 8.6 Hz, 1H), 7.48 (s, 1H), 6.90 (d, *J* = 5.4 Hz, 1H), 4.39 – 4.28 (m, 2H), 3.98 (s, 2H), 3.90 – 3.79 (m, 2H), 3.70 – 3.61 (m, 2H), 3.59 – 3.48 (m, 18H), 1.42 (s, 9H), 1.38 – 1.31 (m, 9H). **<sup>13</sup>C NMR** (151 MHz, DMSO-*d*<sub>6</sub>) δ = 169.27, 157.28, 156.33, 154.07, 153.98, 153.03, 149.36, 138.72, 130.66, 129.15, 123.06, 123.01, 121.64, 116.62, 113.24, 110.32, 101.26, 80.54, 69.88, 69.82, 69.80, 69.77, 69.74, 69.69, 69.64, 68.53, 68.32, 68.07, 60.69, 38.34, 27.71, 23.66. Note that <sup>13</sup>C NMR data are reported to 2 decimal places to differentiate signals. Two signals not observed, potentially due to overlapping frequencies of PEG chain carbons.

**20-((4-(Benzo[*d*]thiazol-5-ylamino)-6-(*tert*-butylsulfonyl)quinolin-7-yl)oxy)-*N*-(4-(*N*-(3-chloro-1*H*-indol-7-yl)sulfamoyl)benzyl)-3,6,9,12,15,18-hexaoxaicosanamide, **116b**.**



Step 1:

To a vial of *tert*-butyl 20-((4-(benzo[*d*]thiazol-5-ylamino)-6-(*tert*-butylsulfonyl)quinolin-7-yl)oxy)-3,6,9,12,15,18-hexaoxaicosanoate **128b** (70.0 mg, 0.0880 mmol) was added TFA (153 μL, 1.99 mmol). The resulting mixture was stirred at room temperature for 10 minutes before concentrating *in vacuo* and 4M HCl in dioxane (500 μL, 1.989 mmol) was added and re-concentrated to give the acid **116b** which was used without further purification.

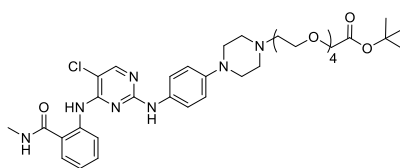
**LCMS** (Method B) (ES +ve)  $m/z$  736.2 (M + H)<sup>+</sup> Rt 0.80 min (94% pure).

## Step 2:

Crude product **116b** was dissolved in DMF (1.5 mL) and was added DIPEA (0.077 mL, 0.442 mmol), 4-(aminomethyl)-*N*-(3-chloro-1*H*-indol-7-yl)benzenesulfonamide **115** (33.0 mg, 0.0990 mmol) and HATU (38.0 mg, 0.0990 mmol) sequentially. The resulting mixture was stirred at room temperature for 1 h. The reaction mixture was purified directly by reverse phase column chromatography (20–60% MeCN (0.1% NH<sub>3</sub>) in 10 mM ammonium carbonate) and fractions containing the pure product were concentrated under a stream of nitrogen to afford the desired product **116b** (45.0 mg, 48% over two steps) as a yellow gum.

**LCMS** (Method A) (ES +ve) *m/z* 1053.3 (M + H)<sup>+</sup> Rt 0.84 min (>95% pure). **HRMS** (ES) calcd for C<sub>49</sub>H<sub>57</sub>ClN<sub>6</sub>O<sub>12</sub>S<sub>3</sub> (M + H)<sup>+</sup> 1053.2963 found 1053.2955. **<sup>1</sup>H NMR** (600 MHz, DMSO-*d*<sub>6</sub>) δ = 10.98 (br. s, 1H), 9.97 (br. s, 1H), 9.68 (s, 1H), 9.43 (s, 1H), 8.96 (s, 1H), 8.50 (br. d, *J* = 5.4 Hz, 1H), 8.28 (t, *J* = 6.3 Hz, 1H), 8.20 (d, *J* = 8.6 Hz, 1H), 8.04 (s, 1H), 7.70 (d, *J* = 8.5 Hz, 2H), 7.54 (d, *J* = 8.5 Hz, 1H), 7.49 – 7.45 (m, 2H), 7.38 – 7.35 (d, *J* = 8.0 Hz, 2H), 7.21 (d, *J* = 8.0 Hz, 1H), 6.96 – 6.87 (m, 2H), 6.84 (d, *J* = 7.7 Hz, 1H), 4.37 – 4.30 (m, 4H), 3.95 (s, 2H), 3.87 – 3.81 (m, 2H), 3.64 – 3.63 (m, 2H), 3.60 – 3.57 (m, 2H), 3.56 – 3.43 (m, 16H), 1.34 (s, 9H). **<sup>13</sup>C NMR** (151 MHz, DMSO-*d*<sub>6</sub>) δ = 169.55, 157.28, 156.33, 154.07, 153.98, 153.02, 149.38, 144.67, 138.72, 137.95, 130.67, 129.16, 128.77, 127.75, 127.53, 126.81, 126.05, 123.05, 123.01, 122.76, 121.64, 119.95, 116.64, 115.16, 114.16, 113.25, 110.33, 103.59, 101.26, 70.29, 69.86, 69.81, 69.89, 69.75, 69.72, 69.70, 69.68, 69.46, 68.52, 68.31, 60.69, 41.19, 23.66. Note that <sup>13</sup>C NMR data are reported to 2 decimal places to differentiate signals. Two signals not observed, potentially due to overlapping frequencies of PEG chain carbons. **IR** *v*<sub>max</sub> (neat) 3291, 3074, 2873, 1659, 1611, 1572, 1525, 1445, 1356 cm<sup>-1</sup>.

**tert-Butyl 14-(4-(4-((5-chloro-4-((2-(methylcarbamoyl)phenyl)amino)pyrimidin-2-yl)amino)phenyl)piperazin-1-yl)-3,6,9,12-tetraoxatetradecanoate, 131a.**



131a

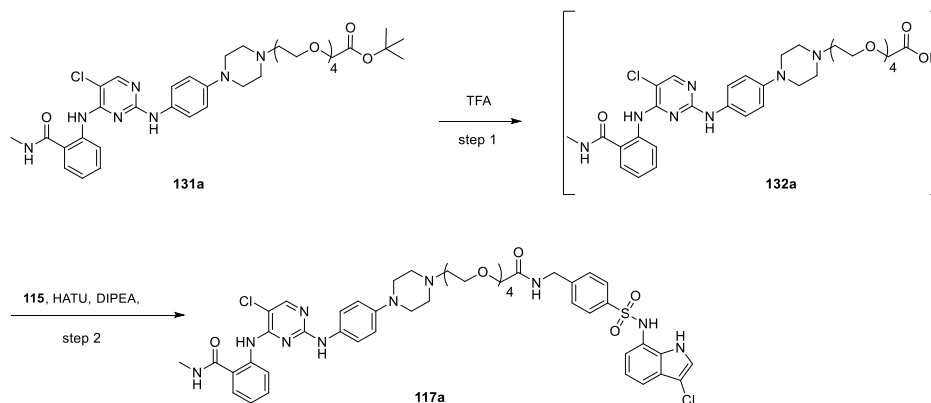
A solution of 2-((5-chloro-2-((4-(piperazin-1-yl)phenyl)amino)pyrimidin-4-yl)amino)-*N*-methylbenzamide **130** (100 mg, 0.228 mmol), *tert*-butyl 14-chloro-3,6,9,12-tetraoxatetradecanoate **127a** (90.0 mg, 0.274 mmol), sodium iodide (52.0 mg, 0.347 mmol) and DIPEA (120 μL, 0.685 mmol) in DMF (1.5 mL) was heated at 90 °C for 16 h. The reaction mixture was purified directly by reverse phase column chromatography (30–95% MeCN (0.1% NH<sub>3</sub>) in 10 mM ammonium bicarbonate)) and fractions containing the pure product were

concentrated under a stream of nitrogen to afford the desired product **131a** (110 mg, 66%) as a yellow gum.

**LCMS** (Method B) (ES +ve)  $m/z$  728.3 (M + H)<sup>+</sup> Rt 1.23 min (>95% pure). **HRMS** (ES) calcd for C<sub>36</sub>H<sub>50</sub>ClN<sub>7</sub>O<sub>7</sub> (M + H)<sup>+</sup> 727.3460 found 364.6809 which equates to ((M + 2H)/2)<sup>+</sup>. **<sup>1</sup>H NMR** (400 MHz, CDCl<sub>3</sub>)  $\delta$  = 11.07 (br. s, 1H), 8.68 – 8.63 (m, 1H), 8.11 – 7.94 (m, 1H), 7.47 (dd,  $J$  = 1.6, 7.8 Hz, 1H), 7.42 – 7.35 (m, 3H), 7.11 – 6.95 (m, 2H), 6.92 – 6.87 (m, 2H), 6.39 (br. s, 1H), 4.01 (s, 2H), 3.75 – 3.60 (m, 14H), 3.19 – 3.14 (m, 4H), 3.03 – 2.98 (m, 3H), 2.73 – 2.64 (m, 6H), 1.47 (s, 9H). **<sup>13</sup>C NMR** (101 MHz, DMSO-*d*<sub>6</sub>)  $\delta$  = 169.62, 169.59, 158.23, 155.70, 154.49, 147.59, 139.70, 131.90, 131.64, 126.62, 122.26, 122.20, 121.95, 121.37, 116.69, 106.13, 81.51, 70.69, 70.58, 70.56, 70.52, 70.37, 69.02, 68.89, 57.79, 53.60 49.75, 28.08, 26.84. Note that <sup>13</sup>C NMR data are reported to 2 decimal places to differentiate signals. One signal not observed, potentially due to overlapping frequencies of PEG chain carbons.

Consistent with literature data.<sup>80</sup>

***N*-(4-(*N*-(3-Chloro-1*H*-indol-7-yl)sulfamoyl)benzyl)-14-(4-(4-((5-chloro-4-((2-(methylcarbamoyl)phenyl)amino)pyrimidin-2-yl)amino)phenyl)piperazin-1-yl)-3,6,9,12-tetraoxatetradecanamide, 117a.**



Step 1:

To a vial of *tert*-butyl 14-(4-(4-((5-chloro-4-((2-(methylcarbamoyl)phenyl)amino)pyrimidin-2-yl)amino)phenyl)piperazin-1-yl)-3,6,9,12-tetraoxatetradecanoate **131a** (48.0 mg, 0.0660 mmol) was added TFA (500  $\mu$ L, 6.49 mmol). The resulting mixture was stirred at room temperature for 0.5 h. The reaction mixture was then concentrated under a stream of nitrogen. To this was added 4M HCl in dioxane (1.65 mL, 6.59 mmol) and this was concentrated under a stream of nitrogen to afford the crude product **132a** which was used without further purification.

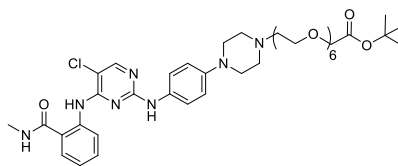
**LCMS** (Method B) (ES +ve)  $m/z$  672.3 (M + H)<sup>+</sup> Rt 0.79 min (>95% pure).

## Step 2:

The crude product **132a** was dissolved in NMP (0.5 mL) was added 4-(aminomethyl)-*N*-(3-chloro-1*H*-indol-7-yl)benzenesulfonamide **115** (18.0 mg, 0.0540 mmol), DIPEA (38.0  $\mu$ L, 0.215 mmol) and HATU (24.5 mg, 0.0640 mmol) sequentially. The resulting mixture was stirred at room temperature for 1 h. The reaction mixture was purified directly by reverse phase column chromatography (20–85% MeCN (0.1% NH<sub>3</sub>) in 10 mM ammonium carbonate) and fractions containing the pure product were concentrated under a stream of nitrogen to afford the desired product **117a** (15.0 mg, 28% over two steps) as a colourless gum.

**LCMS** (Method A) (ES +ve)  $m/z$  989.45 (M + H)<sup>+</sup> Rt 0.81 min (>95% pure). **HRMS** (ES) calcd for C<sub>47</sub>H<sub>54</sub>C<sub>12</sub>N<sub>10</sub>O<sub>8</sub>S ((M + 2H)/2)<sup>+</sup> 495.1612 found 495.1694. **<sup>1</sup>H NMR** (600 MHz, DMSO-*d*<sub>6</sub>)  $\delta$  = 11.58 (s, 1H), 10.99 (br. s, 1H), 10.06 – 9.88 (m, 1H), 9.18 (s, 1H), 8.76 (br. s, 1H), 8.75 – 8.70 (m, 1H), 8.28 (t,  $J$  = 6.2 Hz, 1H), 8.18 – 8.14 (m, 1H), 7.75 (dd,  $J$  = 1.6, 7.9 Hz, 1H), 7.71 (d,  $J$  = 8.3 Hz, 2H), 7.50 – 7.43 (m, 4H), 7.37 (d,  $J$  = 8.3 Hz, 2H), 7.22 (d,  $J$  = 7.9 Hz, 1H), 7.14 – 7.11 (m, 1H), 6.94 (app t,  $J$  = 7.9 Hz, 1H), 6.89 – 6.83 (m, 3H), 4.35 (d,  $J$  = 6.2 Hz, 2H), 3.96 (s, 2H), 3.62 – 3.58 (m, 2H), 3.58 – 3.55 (m, 2H), 3.55 – 3.43 (m, 12H), 3.10 – 3.02 (m, 4H), 2.82 (d,  $J$  = 4.5 Hz, 3H), 2.59 – 2.54 (m, 4H). **<sup>13</sup>C NMR** (151 MHz, DMSO-*d*<sub>6</sub>)  $\delta$  = 170.10, 169.41, 158.53, 155.40, 155.08, 147.09, 145.21, 139.92, 138.48, 138.43, 132.60, 131.93, 129.28, 128.38, 128.06, 127.34, 126.59, 123.30, 122.23, 121.82, 121.74, 120.97, 120.47, 116.15, 115.71, 114.74, 104.74, 104.12, 70.84, 70.43, 70.24, 70.21, 70.20, 70.12, 70.01, 68.80, 57.70, 53.64, 49.45, 41.72, 26.78. Note that <sup>13</sup>C NMR data are reported to 2 decimal places to differentiate signals. **IR**  $\nu_{max}$  (neat) 3268, 2878, 2825, 1655, 1600, 1560, 1513, 1447 cm<sup>-1</sup>.

**tert-Butyl 20-(4-(4-((5-chloro-4-((2-(methylcarbamoyl)phenyl)amino)pyrimidin-2-yl)amino)phenyl)piperazin-1-yl)-3,6,9,12,15,18-hexaoxaicosanoate, dihydrochloride, 131b.**



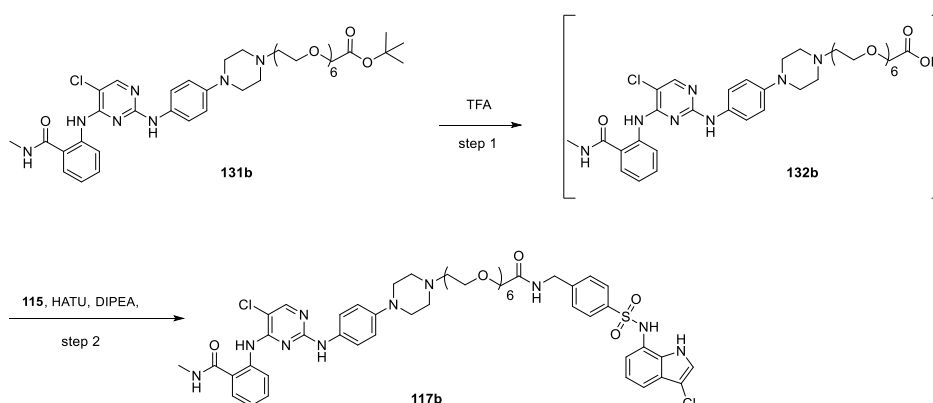
131b

To a vial of 2-((5-chloro-2-((4-(piperazin-1-yl)phenyl)amino)pyrimidin-4-yl)amino)-*N*-methylbenzamide **130** (100 mg, 0.228 mmol) in NMP (1 mL) was added DIPEA (80.0  $\mu$ L, 0.457 mmol), sodium iodide (34.0 mg, 0.228 mmol) and *tert*-butyl 20-chloro-3,6,9,12,15,18-hexaoxaicosanoate **127b** (114 mg, 0.274 mmol). The resulting mixture was stirred at 80 °C for 16 h. The reaction mixture was purified directly by reverse phase column chromatography (20–75% MeCN (0.1% NH<sub>3</sub>) in 10 mM ammonium carbonate) and fractions containing the pure

product were concentrated under a stream of nitrogen to afford the desired product **131b** (112 mg, 55%) as a colourless gum.

**LCMS** (Method B) (ES +ve)  $m/z$  816.4 (M + H)<sup>+</sup> Rt 1.20 min (>95% pure). **HRMS** (ES) calcd for C<sub>40</sub>H<sub>58</sub>ClN<sub>7</sub>O<sub>9</sub> ((M + 2H)/2)<sup>+</sup> 408.7070 found 408.7076. **<sup>1</sup>H NMR** (400 MHz, DMSO-*d*<sub>6</sub>) δ = 11.59 (s, 1H), 9.25 – 9.10 (m, 1H), 8.74 (br. s, 1H), 8.16 (s, 1H), 7.76 (br. d, *J* = 8.0 Hz, 1H), 7.60 – 7.39 (m, 4H), 7.19 – 7.09 (m, 1H), 6.95 – 6.82 (m, 2H), 3.98 (s, 2H), 3.60 – 3.51 (m, 24H), 3.11 – 3.02 (m, 4H), 2.82 (d, *J* = 4.4 Hz, 3H), 2.60 – 2.53 (m, 4H), 1.42 (s, 9H). **<sup>13</sup>C NMR** (151 MHz, DMSO-*d*<sub>6</sub>) δ = 169.26, 168.88, 158.02, 154.88, 154.54, 146.56, 139.45, 132.09, 131.40, 127.86, 121.66, 121.28, 121.22, 120.40, 115.61, 104.23, 80.53, 69.82, 69.82, 69.75, 69.76, 69.74, 69.70, 69.66, 69.65, 68.35, 68.09, 57.22, 53.15, 48.97, 27.70, 26.24. Note that <sup>13</sup>C NMR data are reported to 2 decimal places to differentiate signals. Two signals not observed, potentially due to overlapping frequencies of PEG chain carbons.

***N*-(4-(*N*-(3-Chloro-1H-indol-7-yl)sulfamoyl)benzyl)-20-(4-(4-((5-chloro-4-((2-(methylcarbamoyl)phenyl)amino)pyrimidin-2-yl)amino)phenyl)piperazin-1-yl)-3,6,9,12,15,18-hexaoxaicosanamide, 117b.**



Step 1:

To a vial of *tert*-butyl 20-(4-(4-((5-chloro-4-((2-(methylcarbamoyl)phenyl)amino)pyrimidin-2-yl)amino)phenyl)piperazin-1-yl)-3,6,9,12,15,18-hexaoxaicosanoate, dihydrochloride **131b** (44.0 mg, 0.049 mmol) was added TFA (381 μL, 4.95 mmol). The reaction mixture was concentrated under a stream of nitrogen and 4M HCl in dioxane (1.20 mL, 4.95 mmol) was added before reconcentrating to give the crude product **132b** which was used without further purification.

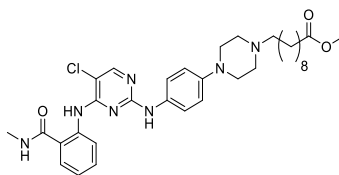
**LCMS** (Method B) (ES +ve)  $m/z$  760.3 (M + H)<sup>+</sup> Rt 0.82 min (>95% pure). **HRMS** (ES) calcd for C<sub>36</sub>H<sub>50</sub>ClN<sub>7</sub>O<sub>9</sub> ((M + 2H)/2)<sup>+</sup> 380.6773 found 380.6764.

## Step 2:

The crude products **132b** was redissolved in n NMP (0.5 mL) and was added 4-(aminomethyl)-*N*-(3-chloro-1*H*-indol-7-yl)benzenesulfonamide **115** (17.0 mg, 0.0490 mmol), DIPEA (35.0  $\mu$ L, 0.198 mmol) and HATU (23 mg, 0.0590 mmol) sequentially. The resulting mixture was stirred at room temperature for 0.5 h. The reaction mixture was purified directly by reverse phase column chromatography (20–70% MeCN (0.1% NH<sub>3</sub>) in 10 mM ammonium carbonate) and fractions containing the pure product were concentrated under a stream of nitrogen to afford the desired product **117b** (32.0 mg, 60% over two steps) as a colourless gum.

**LCMS** (Method B) (ES +ve)  $m/z$  1077.3 (M + H)<sup>+</sup> Rt 1.13 min (>95% pure). **HRMS** (ES) calcd for C<sub>51</sub>H<sub>62</sub>Cl<sub>2</sub>N<sub>10</sub>O<sub>10</sub>S ((M + 2H)/2)<sup>+</sup> 539.1952 found 539.1957. **<sup>1</sup>H NMR** (400 MHz, DMSO-*d*<sub>6</sub>)  $\delta$  = 11.59 (s, 1H), 10.98 (br. s, 1H), 10.11 – 9.83 (m, 1H), 9.18 (s, 1H), 8.87 – 8.64 (m, 2H), 8.28 (t,  $J$  = 6.2 Hz, 1H), 8.16 (s, 1H), 7.77 – 7.67 (m, 3H), 7.54 – 7.42 (m, 4H), 7.40 – 7.33 (m, 2H), 7.23 (d,  $J$  = 7.9 Hz, 1H), 7.18 – 7.07 (m, 1H), 6.99 – 6.91 (m, 1H), 6.90 – 6.83 (m, 3H), 4.35 (d,  $J$  = 6.2 Hz, 2H), 3.95 (s, 2H), 3.63 – 3.46 (m, 24H), 3.11 – 3.03 (m, 4H), 2.82 (d,  $J$  = 4.9 Hz, 3H), 2.59 – 2.56 (m, 4H). **<sup>13</sup>C NMR** (101 MHz, DMSO-*d*<sub>6</sub>)  $\delta$  = 170.09, 169.40, 158.53, 155.40, 155.09, 147.09, 145.24, 139.93, 138.54, 138.48, 132.59, 131.93, 129.28, 128.38, 128.05, 127.34, 126.59, 123.28, 122.29, 122.22, 121.82, 120.97, 120.48, 116.15, 115.72, 115.65, 104.73, 104.12, 70.83, 70.42, 70.26, 70.22, 70.16, 69.99, 68.84, 57.71, 55.36, 53.65, 49.46, 49.07, 41.72, 39.14, 26.77. Note that <sup>13</sup>C NMR data are reported to 2 decimal places to differentiate signals. Two signals not observed, potentially due to overlapping frequencies of PEG chain carbons. **IR**  $\nu_{max}$  (neat) 3275, 3116, 2899, 2836, 1649, 1599, 1558, 1513, 1447, 1412, 1091 cm<sup>-1</sup>.

**Methyl 10-(4-(4-((5-chloro-4-((2-(methylcarbamoyl)phenyl)amino)pyrimidin-2-yl)amino)phenyl)piperazin-1-yl)decanoate, 134.**

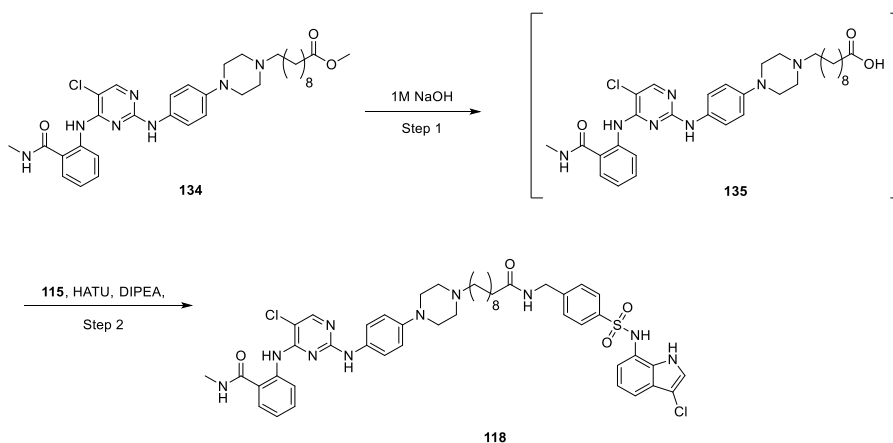


134

A solution of 2-((5-chloro-2-((4-(piperazin-1-yl)phenyl)amino)pyrimidin-4-yl)amino)-*N*-methylbenzamide **130** (155 mg, 0.354 mmol), methyl 10-bromodecanoate **133** (113 mg, 0.425 mmol), sodium iodide (52.0 mg, 0.347 mmol) and DIPEA (0.185 mL, 1.06 mmol) in DMF (1.5 mL) was heated at 70 °C for 16 h. The reaction mixture was purified directly by reverse phase column chromatography (30–95% MeCN (0.1% NH<sub>3</sub>) in 10 mM ammonium bicarbonate) and fractions containing the pure product were concentrated under a stream of nitrogen to afford the desired product **134** (137 mg, 62%) as a yellow gum.

**LCMS** (Method B) (ES +ve)  $m/z$  622.3 (M + H)<sup>+</sup> Rt 1.51 min (>95% pure). **HRMS** (ES) calcd for C<sub>33</sub>H<sub>44</sub>ClN<sub>7</sub>O<sub>3</sub> (M + H)<sup>+</sup> 622.3278 found 622.3275. **<sup>1</sup>H NMR** (400 MHz, DMSO-*d*<sub>6</sub>) δ = 11.60 (s, 1H), 9.18 (s, 1H), 8.82 – 8.69 (m, 2H), 8.16 (s, 1H), 7.75 (dd, *J* = 1.6, 7.9 Hz, 1H), 7.51 – 7.43 (m, 3H), 7.16 – 7.10 (m, 1H), 6.89 – 6.87 (m, 2H), 3.59 (s, 3H), 3.16 – 2.98 (m, 4H), 2.82 (d, *J* = 4.5 Hz, 3H), 2.49 – 2.48 (m, 2H), 2.34 – 2.26 (m, 4H), 1.58 – 1.35 (m, 4H), 1.28 – 1.24 (m, 12H). **<sup>13</sup>C NMR** (101 MHz, DMSO-*d*<sub>6</sub>) δ = 173.81, 169.40, 158.52, 155.39, 155.01, 147.11, 139.93, 132.57, 131.92, 128.37, 122.21, 121.78, 121.73, 120.94, 116.13, 104.72, 58.41, 53.34, 51.60, 49.50, 39.33, 33.76, 29.38, 29.32, 29.11, 28.92, 27.43, 26.78, 24.91. Note that <sup>13</sup>C NMR data are reported to 2 decimal places to differentiate signals.

**2-((5-Chloro-2-((4-(4-(10-((4-(*N*-(3-chloro-1*H*-indol-7-yl)sulfamoyl)benzyl)amino)-10-oxododecyl)piperazin-1-yl)phenyl)amino)pyrimidin-4-yl)amino)-*N*-methylbenzamide, 118.**



Step 1:

To a stirred solution of methyl 10-(4-(4-((5-chloro-4-((2-(methylcarbamoyl)phenyl)amino)pyrimidin-2-yl)amino)phenyl)piperazin-1-yl)decanoate **134** (55.0 mg, 0.0880 mmol) in THF (0.45 mL) was added 2M aq. NaOH (133 μL, 0.265 mmol). The resulting mixture was stirred at room temperature for 16 h. The reaction mixture was then neutralised with 2M HCl aq. (133 μL, 0.265 mmol) before concentrating under a stream of nitrogen to give the crude product **135** which was used without further purification.

**LCMS** (Method B) (ES +ve)  $m/z$  608.2 (M + H)<sup>+</sup> Rt 0.92 min (>95% pure).

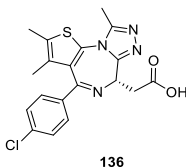
Step 2:

The crude product **135** was then dissolved in NMP (0.45 mL) and DIPEA (77.0 μL, 0.442 mmol), 4-(aminomethyl)-*N*-(3-chloro-1*H*-indol-7-yl)benzenesulfonamide **115** (33.0 mg, 0.0970 mmol) and HATU (40.0 mg, 0.106 mmol) were added sequentially. The resulting mixture was stirred at room temperature for 1 h. The reaction mixture was purified directly by reverse phase column chromatography (30–70% MeCN (0.1% NH<sub>3</sub>) in 10 mM ammonium carbonate) and

fractions containing the pure product were concentrated under a stream of nitrogen to afford the desired product **118** (21.0 mg, 26% over two steps) as a colourless gum.

**LCMS** (Method A) (ES +ve)  $m/z$  925.2 (M + H)<sup>+</sup> Rt 0.91 min (>95% pure). **HRMS** (ES) calcd for C<sub>47</sub>H<sub>54</sub>Cl<sub>2</sub>N<sub>10</sub>O<sub>4</sub>S (M + H)<sup>+</sup> 925.3506 found 925.3509. **<sup>1</sup>H NMR** (600 MHz, DMSO-*d*<sub>6</sub>)  $\delta$  = 11.59 (s, 1H), 11.00 (br. s, 1H), 10.18 – 9.71 (m, 1H), 9.18 (br. s, 1H), 8.84 – 8.66 (m, 2H), 8.31 (t,  $J$  = 6.0 Hz, 1H), 8.26 (m, 1H), 8.16 (s, 1H), 7.75 (dd,  $J$  = 1.6, 7.9 Hz, 1H), 7.70 (d,  $J$  = 8.3 Hz, 2H), 7.50 – 7.44 (m, 3H), 7.35 (d,  $J$  = 8.0 Hz, 2H), 7.23 (d,  $J$  = 7.9 Hz, 1H), 7.14 – 7.11 (m, 1H), 6.94 (app t,  $J$  = 7.9 Hz, 1H), 6.88 (d,  $J$  = 8.8 Hz, 2H), 6.83 (d,  $J$  = 7.8 Hz, 1H), 4.28 (d,  $J$  = 6.0 Hz, 2H), 3.18 – 3.04 (m, 4H), 2.82 (d,  $J$  = 4.5 Hz, 3H), 2.50 – 2.46 (m, 2H), 2.31 (t,  $J$  = 7.4 Hz, 2H), 2.13 (t,  $J$  = 7.4 Hz, 2H), 1.51 (app quint,  $J$  = 7.1 Hz, 2H), 1.47 – 1.42 (m, 2H), 1.31 – 1.21 (m, 12H). **<sup>13</sup>C NMR** (151 MHz, DMSO-*d*<sub>6</sub>)  $\delta$  = 172.28, 168.89, 158.01, 154.88, 154.57, 146.57, 145.02, 139.41, 137.91, 132.07, 131.41, 128.83, 127.86, 127.49, 126.83, 126.06, 122.77, 122.41, 121.70, 121.29, 121.22, 120.44, 119.94, 115.63, 115.24, 114.20, 104.22, 103.59, 57.88, 52.79, 48.93, 41.49, 35.23, 28.90, 28.87, 28.67, 28.59, 26.93, 26.26, 25.15. Note that <sup>13</sup>C NMR data are reported to 2 decimal places to differentiate signals. One signal not observed, potentially due to overlapping frequencies of methylene carbons. **IR**  $\nu_{max}$  (neat) 3260, 2928, 2853, 1600, 1561, 1514, 1447, 1414 cm<sup>-1</sup>.

**(S)-2-(4-(4-Chlorophenyl)-2,3,9-trimethyl-6H-thieno[3,2-*f*][1,2,4]triazolo[4,3-*a*][1,4]diazepin-6-yl)acetic acid, 81.**

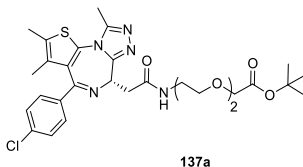


To a stirred solution of *tert*-butyl (S)-2-(4-(4-chlorophenyl)-2,3,9-trimethyl-6H-thieno[3,2-*f*][1,2,4]triazolo[4,3-*a*][1,4]diazepin-6-yl)acetate (JQ1) **14** (2.40 g, 5.25 mmol) in CH<sub>2</sub>Cl<sub>2</sub> (53 mL) was added 3M HCl in CPME (17.5 mL, 52.5 mmol). The resulting mixture was stirred at room temperature for 8 h. The reaction mixture was concentrated *in vacuo* and purified by reverse phase column chromatography (15–75% MeCN (0.1% formic acid) in H<sub>2</sub>O (0.1% formic acid) and fractions containing the pure product were concentrated under a stream of nitrogen to afford the desired product **136** (1.8 g, 85%) as a yellow solid.

**LCMS** (Method B) (ES +ve)  $m/z$  401.0 (M + H)<sup>+</sup> Rt 0.76 min (>95% pure). **HRMS** (ES) calcd for C<sub>19</sub>H<sub>17</sub>ClN<sub>4</sub>O<sub>2</sub>S (M + H)<sup>+</sup> 401.0836 found 401.0836. **<sup>1</sup>H NMR** (400 MHz, DMSO-*d*<sub>6</sub>)  $\delta$  = 7.52 – 7.43 (m, 4H), 4.50 – 4.41 (m, 1H), 3.44 – 3.41 (m, 1H), 2.61 (s, 3H), 2.42 (s, 3H), 1.64 (s, 3H). **<sup>13</sup>C NMR** (151 MHz, DMSO-*d*<sub>6</sub>)  $\delta$  = 171.9, 163.1, 154.8, 149.8, 136.6, 135.2, 132.2, 130.7, 130.1, 129.8, 129.5, 128.4, 53.6, 36.5, 14.0, 12.6, 11.2.

Consistent with literature data.<sup>255</sup>

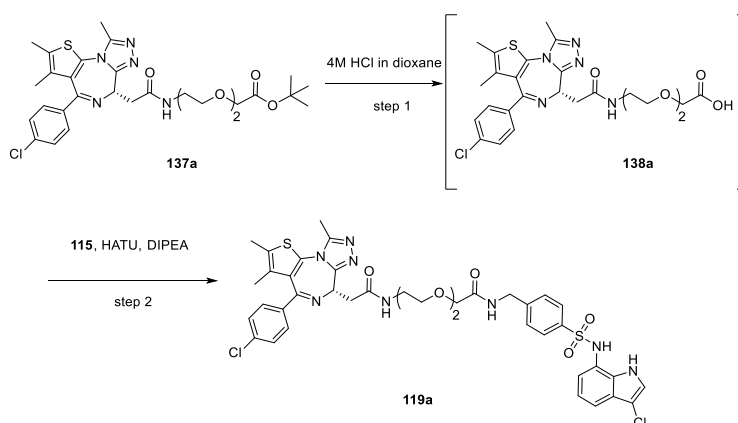
**tert-Butyl (S)-3-(2-(2-(2-(4-(4-chlorophenyl)-2,3,9-trimethyl-6H-thieno[3,2-f][1,2,4]triazolo[4,3-a][1,4]diazepin-6-yl)acetamido)ethoxy)ethoxy)propanoate, 137a.**



To a stirred solution of (S)-2-(4-(4-chlorophenyl)-2,3,9-trimethyl-6H-thieno[3,2-f][1,2,4]triazolo[4,3-a][1,4]diazepin-6-yl)acetic acid **81** (70.0 mg, 0.175 mmol) in NMP (1.8 mL) was added *tert*-butyl 3-(2-(2-aminoethoxy)ethoxy)propanoate **136a** (41.0 mg, 0.175 mmol) DIPEA (152  $\mu$ L, 0.873 mmol) and HATU (80.0 mg, 0.210 mmol) sequentially. The resulting mixture was stirred at room temperature for 1 h. The reaction mixture was purified directly by reverse phase column chromatography (30–75% MeCN (0.1% NH<sub>3</sub>) in 10 mM ammonium carbonate) and fractions containing the pure product were concentrated *in vacuo* to afford the desired product **137a** (71.0 mg, 66%) as a colourless gum.

**LCMS** (Method B) (ES +ve)  $m/z$  616.2 (M + H)<sup>+</sup> Rt 1.19 min (>95% pure). **HRMS** (ES) calcd for C<sub>30</sub>H<sub>38</sub>ClN<sub>5</sub>O<sub>5</sub>S (M + H)<sup>+</sup> 616.2360 found 616.2362. **<sup>1</sup>H NMR** (400 MHz, DMSO-*d*<sub>6</sub>)  $\delta$  = 8.28 – 8.23 (m, 1H), 7.52 – 7.47 (m, 2H), 7.46 – 7.42 (m, 2H), 4.55 – 4.48 (m, 1H), 3.64 – 3.57 (m, 2H), 3.56 – 3.50 (m, 4H), 3.49 – 3.44 (m, 2H), 3.30 – 3.18 (m, 6H), 2.60 (s, 3H), 2.43 – 2.41 (m, 3H), 1.64 (s, 3H), 1.40 (s, 9H). **<sup>13</sup>C NMR** (101 MHz, DMSO-*d*<sub>6</sub>)  $\delta$  = 170.32, 169.60, 162.92, 155.06, 149.72, 136.73, 135.17, 132.22, 130.64, 130.09, 129.77, 129.53, 128.39, 79.66, 69.56, 69.48, 69.15, 66.19, 53.81, 38.58, 37.49, 35.81, 27.71, 13.99, 12.63, 11.24. Note that <sup>13</sup>C NMR data are reported to 2 decimal places to differentiate signals.

**(S)-N-(4-(N-(3-Chloro-1H-indol-7-yl)sulfamoyl)benzyl)-3-(2-(2-(2-(4-(4-chlorophenyl)-2,3,9-trimethyl-6H-thieno[3,2-f][1,2,4]triazolo[4,3-a][1,4]diazepin-6-yl)acetamido)ethoxy)ethoxy)propanamide, 119a.**

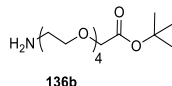
**Step 1:**

*tert*-Butyl (S)-3-(2-(2-(2-(4-(4-chlorophenyl)-2,3,9-trimethyl-6H-thieno[3,2-f][1,2,4]triazolo[4,3-a][1,4]diazepin-6-yl)acetamido)ethoxy)ethoxy)propanoate **137a** (50.0 mg, 0.0810 mmol) was dissolved in TFA (625  $\mu$ L, 8.11 mmol) and allowed to stand for 5 minutes before concentrating, to this gum was then added 4M HCl in dioxane (2.0 mL, 8.11 mmol) and this was reconcentrated to give the crude product **138a** which was used without further purification.

**Step 2:**

The crude product **138a** was dissolved in NMP (811  $\mu$ L) was added DIPEA (71.0  $\mu$ L, 0.406 mmol), 4-(aminomethyl)-*N*-(3-chloro-1*H*-indol-7-yl)benzenesulfonamide **115** (33 mg, 0.097 mmol) and HATU (46 mg, 0.122 mmol) sequentially. The resulting mixture was stirred at room temperature for 1 h. The reaction mixture was purified directly via MDAP (HPH) and fractions containing the pure product were concentrated *in vacuo* to afford the desired product **119a** (15.0 mg, 21% over two steps) as a colourless gum.

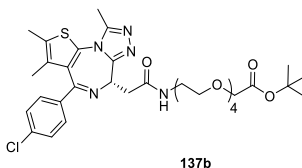
**LCMS** (Method B) (ES +ve)  $m/z$  877.1 (M + H)<sup>+</sup> Rt 1.13 min (>95% pure). **HRMS** (ES) calcd for C<sub>41</sub>H<sub>42</sub>Cl<sub>2</sub>N<sub>8</sub>O<sub>6</sub>S<sub>2</sub> (M + H)<sup>+</sup> 877.2124 found 877.2135. **<sup>1</sup>H NMR** (600 MHz, DMSO-*d*<sub>6</sub>)  $\delta$  = 11.09 – 10.95 (m, 1H), 9.97 (br. s, 1H), 8.40 (br. t,  $J$  = 5.6 Hz, 1H), 8.26 (br. t,  $J$  = 5.6 Hz, 1H), 7.69 (d,  $J$  = 8.1 Hz, 2H), 7.51 – 7.45 (m, 3H), 7.45 – 7.41 (m, 2H), 7.36 (d,  $J$  = 8.1 Hz, 2H), 7.23 (d,  $J$  = 7.7 Hz, 1H), 6.95 (app t,  $J$  = 7.7 Hz, 1H), 6.84 (d,  $J$  = 7.7 Hz, 1H), 4.52 (t,  $J$  = 7.2 Hz, 1H), 4.31 (d,  $J$  = 5.9 Hz, 2H), 3.65 (t,  $J$  = 6.2 Hz, 2H), 3.52 (s, 4H), 3.45 (t,  $J$  = 5.9 Hz, 2H), 3.31 – 3.22 (m, 4H), 2.60 (s, 3H), 2.44 – 2.37 (m, 5H), 1.62 (s, 3H). **<sup>13</sup>C NMR** (151 MHz, DMSO-*d*<sub>6</sub>)  $\delta$  = 170.38, 169.68, 162.96, 155.07, 149.74, 144.85, 137.77, 136.72, 135.17, 132.20, 130.64, 130.08, 129.78, 129.53, 128.75, 128.40, 127.44, 126.80, 126.09, 122.83, 119.97, 115.26, 114.32, 109.48, 103.62, 69.51, 69.43, 69.15, 66.76, 53.80, 41.51, 38.59, 37.48, 36.10, 13.98, 12.63, 11.24. Note that <sup>13</sup>C NMR data are reported to 2 decimal places to differentiate signals. **IR**  $\nu_{max}$  (neat) 3280, 3100, 2920, 2846, 1650, 1589, 1530, 1419, 1330, 1159 cm<sup>-1</sup>.

***tert*-Butyl 14-amino-3,6,9,12-tetraoxatetradecanoate, 136b.**

To a solution of *tert*-butyl 14-chloro-3,6,9,12-tetraoxatetradecanoate **127a** (100 mg, 0.306 mmol), and sodium iodide (55.0 mg, 0.367 mmol) in DMF (1.5 mL) was added ammonium hydroxide (35% aq., 0.306 mL, 3.06 mmol). The resulting mixture was heated at 90 °C for 16 h. The reaction mixture was cooled to room temperature and was concentrated *in vacuo*. The crude product was before purified directly via MDAP (HPH) and fractions containing the pure product were concentrated under a stream of nitrogen to afford the desired product **136b** (40.0 mg, 43%) as a colourless gum.

<sup>1</sup>H NMR (400 MHz, DMSO-*d*<sub>6</sub>) δ = 3.99 (s, 2H), 3.63 – 3.48 (m, 16H), 1.42 (s, 9H). No exchangeables observed.

Consistent with literature data.<sup>256</sup>

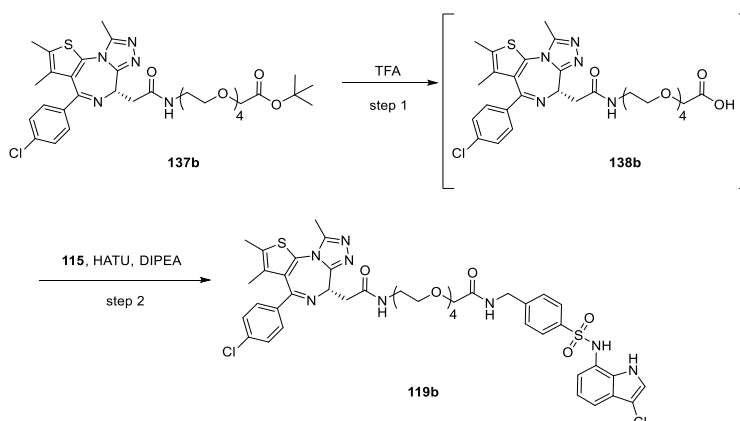
***tert*-Butyl (S)-1-(4-(4-chlorophenyl)-2,3,9-trimethyl-6*H*-thieno[3,2-*f*][1,2,4]triazolo[4,3-*a*][1,4]diazepin-6-yl)-2-oxo-6,9,12,15-tetraoxa-3-azaheptadecan-17-oate, 137b.**

To a stirred solution of (S)-2-(4-(4-chlorophenyl)-2,3,9-trimethyl-6*H*-thieno[3,2-*f*][1,2,4]triazolo[4,3-*a*][1,4]diazepin-6-yl)acetic acid **81** (39.0 mg, 0.0980 mmol) in NMP (0.5 mL) was added *tert*-butyl 14-amino-3,6,9,12-tetraoxatetradecanoate **136b** (30.0 mg, 0.0980 mmol), DIPEA (85.0 μL, 0.488 mmol) and HATU (44.0 mg, 0.117 mmol) sequentially. The resulting mixture was stirred at room temperature for 1 h. The reaction mixture was purified directly by reverse phase column chromatography (20–95% MeCN (0.1% NH<sub>3</sub>) in 10 mM ammonium carbonate) and fractions containing the pure product were concentrated under a stream of nitrogen to afford the desired product **137b** (40.0 mg, 59%) as a colourless gum.

**LCMS** (Method B) (ES +ve) *m/z* 690.4 (M + H)<sup>+</sup> Rt 1.20 min (>95% pure). **HRMS** (ES) calcd for C<sub>33</sub>H<sub>44</sub>ClN<sub>5</sub>O<sub>7</sub>S (M + H)<sup>+</sup> 690.2728 found 690.2728. <sup>1</sup>H NMR (400 MHz, DMSO-*d*<sub>6</sub>) δ = 8.25 (t, *J* = 5.6 Hz, 1H), 7.51 – 7.47 (m, 2H), 7.46 – 7.42 (m, 2H), 4.53 – 4.50 (m, 1H), 3.99 – 3.97 (m, 2H), 3.60 – 3.45 (m, 14H), 3.29 – 3.19 (m, 4H), 2.60 (s, 3H), 2.42 (s, 3H), 1.64 (s, 3H), 1.42 (s, 9H). <sup>13</sup>C NMR (101 MHz, DMSO-*d*<sub>6</sub>) δ = 170.12, 169.80, 163.44, 155.58, 150.24,

137.25, 135.68, 132.73, 131.16, 130.60, 130.29, 130.04, 128.91, 81.08, 70.33, 70.26, 70.22, 70.17, 70.09, 69.68, 68.61, 54.32, 39.12, 38.00, 28.23, 14.51, 13.15, 11.75. Note that  $^{13}\text{C}$  NMR data are reported to 2 decimal places to differentiate signals. One signal not observed, potentially due to overlapping frequencies of PEG chain carbons.

**(S)-N-(4-(N-(3-Chloro-1H-indol-7-yl)sulfamoyl)benzyl)-14-(2-(4-(4-chlorophenyl)-2,3,9-trimethyl-6H-thieno[3,2-f][1,2,4]triazolo[4,3-a][1,4]diazepin-6-yl)acetamido)-3,6,9,12-tetraoxatetradecanamide, 119b.**



#### Step 1:

To a vial of *tert*-butyl (S)-1-(4-(4-chlorophenyl)-2,3,9-trimethyl-6H-thieno[3,2-f][1,2,4]triazolo[4,3-a][1,4]diazepin-6-yl)-2-oxo-6,9,12,15-tetraoxa-3-azaheptadecan-17-oate **137b** (25.0 mg, 0.0360 mmol) was added TFA (300  $\mu\text{L}$ , 3.89 mmol). The resulting mixture was stirred at room temperature for 10 minutes before concentrating *in vacuo* and was added 4M HCl in dioxane (905  $\mu\text{L}$ , 3.62 mmol) and this was reconcentrated to afford the crude product **138b** which was used without further purification.

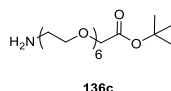
**LCMS** (Method B) (ES +ve)  $m/z$  634.1 (M + H)<sup>+</sup> Rt 0.78 min (>95% pure).

#### Step 2:

The crude product **138b** was then dissolved in NMP (0.5 mL) and DIPEA (32.0  $\mu\text{L}$ , 0.181 mmol), 4-(aminomethyl)-N-(3-chloro-1H-indol-7-yl)benzenesulfonamide **115** (12.0 mg, 0.0360 mmol) and HATU (17 mg, 0.0430 mmol) were added sequentially. The resulting mixture was stirred at room temperature for 1 h. The reaction mixture was purified directly by reverse phase column chromatography (20–80% MeCN (0.1%  $\text{NH}_3$ ) in 10 mM ammonium carbonate) and fractions containing the pure product were concentrated under a stream of nitrogen to afford the desired product **119b** (14.0 mg, 41% over two steps) as a colourless gum.

**LCMS** (Method B) (ES +ve)  $m/z$  951.2 (M + H)<sup>+</sup> Rt 1.21 min (92% pure). **HRMS** (ES) calcd for C<sub>44</sub>H<sub>49</sub>Cl<sub>2</sub>N<sub>8</sub>O<sub>8</sub>S<sub>2</sub> (M + H)<sup>+</sup> 951.2492 found 951.2490. **<sup>1</sup>H NMR** (600 MHz, DMSO-*d*<sub>6</sub>)  $\delta$  = 11.06 (br. s, 1H), 8.29 (t,  $J$  = 6.2 Hz, 1H), 8.27 – 8.23 (m, 1H), 8.18 (br. s, 1H), 7.73 – 7.68 (m, 2H), 7.64 (br. s, 1H), 7.50 – 7.45 (m, 3H), 7.44 – 7.41 (m, 2H), 7.36 (d,  $J$  = 8.4 Hz, 2H), 7.24 – 7.20 (m, 1H), 7.02 (br. s, 1H), 6.94 (app t,  $J$  = 7.7 Hz, 1H), 6.86 (app d,  $J$  = 7.0 Hz, 1H), 6.72 – 6.38 (m, 1H), 4.53 – 4.50 (m, 1H), 4.33 (d,  $J$  = 6.2 Hz, 2H), 3.95 (s, 2H), 3.66 – 3.43 (m, 16H), 2.59 (s, 3H), 2.41 (s, 3H), 1.62 (s, 3H). **<sup>13</sup>C NMR** (151 MHz, DMSO-*d*<sub>6</sub>)  $\delta$  = 170.14, 170.07, 163.45, 155.58, 150.25, 145.20, 138.43, 137.24, 135.68, 132.73, 131.15, 130.60, 130.29, 130.04, 129.21, 128.91, 128.04, 127.34, 126.58, 123.28, 122.88, 120.46, 115.63, 114.69, 104.11, 70.80, 70.42, 70.21, 70.21, 70.18, 70.06, 70.00, 69.65, 54.32, 41.71, 39.10, 38.00, 14.50, 13.14, 11.75. Note that <sup>13</sup>C NMR data are reported to 2 decimal places to differentiate signals. **IR**  $\nu_{max}$  (neat) 3248, 2931, 2883, 1652, 1589, 1530, 1487, 1419 cm<sup>-1</sup>.

**tert-Butyl 20-amino-3,6,9,12,15,18-hexaoxaicosanoate, 136c.**

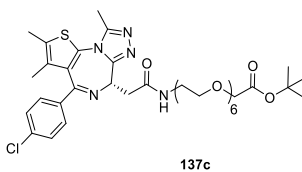


To a vial of *tert*-butyl 20-chloro-3,6,9,12,15,18-hexaoxaicosanoate **127b** (500 mg, 1.21 mmol) in NMP (1.2 mL) was added ammonium hydroxide (35% aq., 745  $\mu$ L, 12.1 mmol). The resulting mixture was stirred at 80 °C for 16 h. The reaction mixture was concentrated *in vacuo* and purified via MDAP (HPH) and fractions containing the pure product were concentrated under a stream of nitrogen to afford the desired product **136c** (120 mg, 25%) as a colourless oil.

**HRMS** (ES) calcd for C<sub>18</sub>H<sub>37</sub>NO<sub>8</sub> (M + H)<sup>+</sup> 396.2597 found 396.2593. **<sup>1</sup>H NMR** (400 MHz, DMSO-*d*<sub>6</sub>)  $\delta$  = 3.99 (s, 2H), 3.60 – 3.51 (m, 24H), 1.49 – 1.38 (m, 9H). **<sup>13</sup>C NMR** (101 MHz, DMSO-*d*<sub>6</sub>)  $\delta$  = 80.58, 69.82, 69.74, 69.70, 69.65, 69.54, 68.09, 27.72. Note that <sup>13</sup>C NMR data are reported to 2 decimal places to differentiate signals. 10 signals not observed, potentially due to overlapping frequencies of PEG chain carbons.

Consistent with literature data.<sup>257</sup>

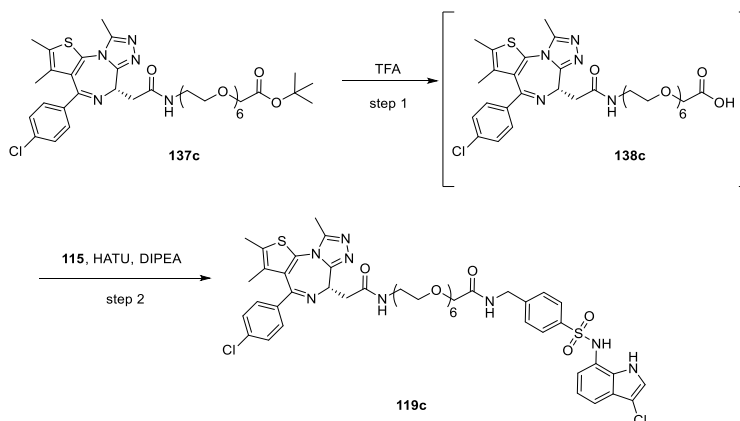
**tert-Butyl (S)-1-(4-(4-chlorophenyl)-2,3,9-trimethyl-6H-thieno[3,2-*f*][1,2,4]triazolo[4,3-*a*][1,4]diazepin-6-yl)-2-oxo-6,9,12,15,18,21-hexaoxa-3-azatricosanoate, 137c.**



To a stirred solution of methyl (S)-10-(2-(4-(4-chlorophenyl)-2,3,9-trimethyl-6H-thieno[3,2-f][1,2,4]triazolo[4,3-a][1,4]diazepin-6-yl)acetamido)decanoate **81** (30.0 mg, 0.0760 mmol) in NMP (0.5 mL) was added tert-butyl 20-amino-3,6,9,12,15,18-hexaoxaicosanoate **136c** (30.0 mg, 0.0760 mmol), DIPEA (0.040 mL, 0.228 mmol) and HATU (35.0 mg, 0.0910 mmol) sequentially. The resulting mixture was stirred at room temperature for 1 h. The reaction mixture was purified directly by reverse phase column chromatography (20–65% MeCN (0.1% NH<sub>3</sub>) in 10 mM ammonium carbonate) and fractions containing the pure product were concentrated under a stream of nitrogen to afford the desired product **137c** (50.0 mg, 85%) as a colourless gum.

**LCMS** (Method B) (ES +ve)  $m/z$  778.3 (M + H)<sup>+</sup> Rt 1.19 min (>95% pure). **HRMS** (ES) calcd for C<sub>37</sub>H<sub>52</sub>ClN<sub>5</sub>O<sub>9</sub>S (M + H)<sup>+</sup> 778.3253 found 778.3275. **<sup>1</sup>H NMR** (400 MHz, DMSO-*d*<sub>6</sub>) δ = 8.32 – 8.15 (m, 1H), 7.51 – 7.47 (m, 2H), 7.46 – 7.42 (m, 2H), 4.52 (dd, *J* = 5.9, 8.1 Hz, 1H), 3.98 (s, 2H), 3.59 – 3.51 (m, 20H), 3.47 (t, *J* = 5.9 Hz, 2H), 3.30 – 3.18 (m, 4H), 2.60 (s, 3H), 2.42 (s, 3H), 1.64 (s, 3H), 1.42 (s, 9H). **<sup>13</sup>C NMR** (101 MHz, DMSO-*d*<sub>6</sub>) δ = 169.59, 169.28, 162.92, 155.06, 149.71, 136.72, 135.15, 132.22, 130.63, 130.08, 129.77, 129.52, 128.39, 80.56, 69.81, 69.74, 69.71, 69.69, 69.64, 69.58, 69.16, 68.08, 53.80, 38.59, 37.48, 27.71, 13.99, 12.62, 11.23. Note that <sup>13</sup>C NMR data are reported to 2 decimal places to differentiate signals. Four signals not observed, potentially due to overlapping frequencies of PEG chain carbons.

**(S)-N-(4-(N-(3-chloro-1H-indol-7-yl)sulfamoyl)benzyl)-20-(2-(4-(4-chlorophenyl)-2,3,9-trimethyl-6H-thieno[3,2-f][1,2,4]triazolo[4,3-a][1,4]diazepin-6-yl)acetamido)-3,6,9,12,15,18-hexaoxaicosanamide, 119c.**



Step 1:

To a vial of *tert*-butyl (S)-1-(4-(4-chlorophenyl)-2,3,9-trimethyl-6H-thieno[3,2-f][1,2,4]triazolo[4,3-a][1,4]diazepin-6-yl)-2-oxo-6,9,12,15,18,21-hexaoxa-3-azatricosan-23-oate **137c** (50.0 mg, 0.0640 mmol) was added TFA (495 μL, 6.42 mmol). The resulting mixture was stirred at room temperature for 10 minutes before concentrating *in vacuo* and was added

4M HCl in dioxane (1.60 mL, 6.42 mmol) and this was reconcentrated to afford the crude product **138c** was used without further purification.

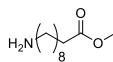
**LCMS** (Method B) (ES +ve)  $m/z$  722.2 (M + H)<sup>+</sup> Rt 0.81 min (>95% pure). **HRMS** (ES) calcd for C<sub>33</sub>H<sub>44</sub>ClN<sub>5</sub>O<sub>9</sub>S (M + H)<sup>+</sup> 722.2627 found 722.2627.

Step 2:

The crude product **138c** was then dissolved in NMP (0.5 mL), 4-(aminomethyl)-*N*-(3-chloro-1*H*-indol-7-yl)benzenesulfonamide **115** (26.0 mg, 0.0770 mmol) and DIPEA (11 μL, 0.064 mmol), and HATU (29.3 mg, 0.0770 mmol) were added sequentially. The resulting mixture was stirred at room temperature for 1 h. The reaction mixture was purified directly by reverse phase column chromatography (20–80% MeCN (0.1% NH<sub>3</sub>) in 10 mM ammonium carbonate) and fractions containing the pure product were concentrated under a stream of nitrogen to afford the desired product **119c** (28.0 mg, 42% over two steps) as a colourless gum.

**LCMS** (Method B) (ES +ve)  $m/z$  1039.2 (M + H)<sup>+</sup> Rt 1.13 min (>95% pure). **HRMS** (ES) calcd for C<sub>48</sub>H<sub>56</sub>Cl<sub>2</sub>N<sub>8</sub>O<sub>10</sub>S<sub>2</sub> (M + H)<sup>+</sup> 1039.3014 found 1039.3015. **<sup>1</sup>H NMR** (600 MHz, DMSO-*d*<sub>6</sub>) δ = 11.02 (br. s, 1H), 10.09 – 9.91 (m, 1H), 8.31 – 8.23 (m, 2H), 7.72 – 7.69 (m, 2H), 7.50 – 7.46 (m, 3H), 7.45 – 7.41 (m, 2H), 7.37 (d, *J* = 8.1 Hz, 2H), 7.23 (d, *J* = 7.9 Hz, 1H), 6.94 (app t, *J* = 7.9 Hz, 1H), 6.85 (d, *J* = 7.9 Hz, 1H), 4.52 (t, *J* = 7.0 Hz, 1H), 4.34 (d, *J* = 6.2 Hz, 2H), 3.95 (s, 2H), 3.60 – 3.43 (m, 22H), 3.32 – 3.21 (m, 4H), 2.60 (s, 3H), 2.40 (s, 3H), 1.62 (s, 3H). **<sup>13</sup>C NMR** (151 MHz, DMSO-*d*<sub>6</sub>) δ = 169.61, 169.59, 162.97, 155.06, 149.77, 144.78, 137.76, 136.70, 135.19, 132.20, 130.68, 130.10, 129.79, 129.54, 128.71, 128.40, 127.55, 126.84, 126.10, 122.83, 122.12, 119.95, 115.25, 114.36, 103.63, 70.31, 69.90, 69.75, 69.73, 69.71, 69.67, 69.69, 69.58, 69.47, 69.17, 66.32, 53.79, 41.20, 38.61, 37.47, 14.00, 12.63, 11.24. Note that <sup>13</sup>C NMR data are reported to 2 decimal places to differentiate signals. One signal not observed, potentially due to overlapping frequencies of PEG chain carbons. **IR**  $\nu_{max}$  (neat) 3269, 3074, 2920, 2878, 1651, 1589, 1530, 1419, 1089 cm<sup>-1</sup>.

**Methyl 10-aminodecanoate, 139c.**



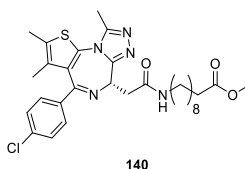
139

A solution of methyl 10-bromodecanoate **133** (315 mg, 1.19 mmol) in DMF (1.1 mL) in a microwave vial was added sodium azide (81.0 mg, 1.25 mmol) and was sealed and irradiated at 60 °C for 1 h. The reaction mixture was diluted with EtOAc (40 mL), washed with sat. aq. sodium bicarbonate (40 mL), H<sub>2</sub>O (40 mL) before passing through a hydrophobic frit and concentrating *in vacuo*. The crude mixture was dissolved in THF (1.1 mL) and were added triphenylphosphine (467 mg, 1.78 mmol) and H<sub>2</sub>O (0.1 mL). The resulting mixture was stirred

at room temperature for 16 h. TLC (50:50 EtOAc: cyclohexane) indicated consumption of SM and the mixture was then passed through an SCX-2 cartridge, washed with MeOH (3 CV) and then eluted with 2M NH<sub>3</sub> in MeOH (2 CV) and concentrated *in vacuo* to afford the desired product **139** (85.0 mg, 36%) as a colourless oil.

**<sup>1</sup>H NMR** (400 MHz, DMSO-*d*<sub>6</sub>) δ = 3.59 (s, 3H), 2.34 – 2.26 (m, 2H), 1.56 – 1.48 (m, 2H), 1.36 – 1.29 (m, 2H), 1.27 -1.25 (m, 12H). no exchangeables observed. **<sup>13</sup>C NMR** (151 MHz, DMSO-*d*<sub>6</sub>) δ = 173.50, 51.22, 41.53, 33.34, 32.96, 28.94, 28.92, 28.67, 28.49, 26.43, 24.48. Note that <sup>13</sup>C NMR data are reported to 2 decimal places to differentiate signals.

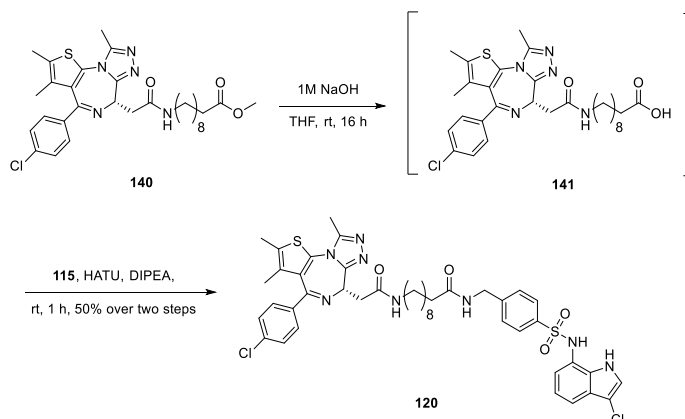
**(S)-10-(2-(4-(4-Chlorophenyl)-2,3,9-trimethyl-6H-thieno[3,2-f][1,2,4]triazolo[4,3-a][1,4]diazepin-6-yl)acetamido)decanoate, 140.**



To a stirred solution of (S)-2-(4-(4-chlorophenyl)-2,3,9-trimethyl-6H-thieno[3,2-f][1,2,4]triazolo[4,3-a][1,4]diazepin-6-yl)acetic acid **81** (50.0 mg, 0.125 mmol) in NMP (1.2 mL) was added methyl 10-aminodecanoate **139c** (25 mg, 0.125 mmol), DIPEA (109 μL, 0.624 mmol) and HATU (57.0 mg, 0.150 mmol) sequentially. The resulting mixture was stirred at room temperature for 1 h. The reaction mixture was purified directly by reverse phase column chromatography (30–75% MeCN (0.1% NH<sub>3</sub>) in 10 mM ammonium carbonate) and fractions containing the pure product were concentrated *in vacuo* to afford the desired product **140** (50.0 mg, 69%) as a colourless gum.

**LCMS** (Method B) (ES +ve) *m/z* 584.2 (M + H)<sup>+</sup> Rt 1.32 min (>95% pure). **HRMS** (ES) calcd for C<sub>30</sub>H<sub>38</sub>ClN<sub>5</sub>O<sub>3</sub>S (M + H)<sup>+</sup> 584.2462 found 584.2463. **<sup>1</sup>H NMR** (400 MHz, DMSO-*d*<sub>6</sub>) δ = 8.14 (s, 1H), 7.50 – 7.46 (m, 2H), 7.45 – 7.42 (m, 2H), 4.51 (dd, *J* = 5.9, 8.3 Hz, 1H), 3.58 (s, 3H), 3.29 – 3.03 (m, 4H), 2.60 (s, 3H), 2.42 (s, 3H), 2.28 (t, *J* = 7.6 Hz, 2H), 1.64 (s, 3H), 1.55 – 1.41 (m, 4H), 1.33 – 1.20 (m, 10H). **<sup>13</sup>C NMR** (101 MHz, DMSO-*d*<sub>6</sub>) δ = 173.26, 169.24, 162.87, 155.09, 149.71, 136.68, 135.17, 132.20, 130.66, 130.05, 129.74, 129.53, 128.37, 53.90, 51.08, 38.41, 37.65, 33.23, 29.22, 28.82, 28.71, 28.60, 28.41, 26.34, 24.37, 13.98, 12.62, 11.23. Note that <sup>13</sup>C NMR data are reported to 2 decimal places to differentiate signals.

**(S)-N-(4-(N-(3-Chloro-1H-indol-7-yl)sulfamoyl)benzyl)-10-(2-(4-(4-chlorophenyl)-2,3,9-trimethyl-6H-thieno[3,2-f][1,2,4]triazolo[4,3-a][1,4]diazepin-6-yl)acetamido)decanamide, **120**.**



**Step 1:**

To a stirred solution of methyl (S)-10-(2-(4-(4-chlorophenyl)-2,3,9-trimethyl-6H-thieno[3,2-f][1,2,4]triazolo[4,3-a][1,4]diazepin-6-yl)acetamido)decanoate **140** (45.0 mg, 0.0770 mmol) in THF (0.4 mL) was added 2M aq. NaOH (116  $\mu$ L, 0.231 mmol). The resulting mixture was stirred at room temperature for 16 h. The reaction mixture was then neutralised with 2M HCl aq. (133  $\mu$ L, 0.265 mmol) before concentrating under a stream of nitrogen to afford the crude product **141** which was used directly without further purification.

**LCMS** (Method B) (ES +ve)  $m/z$  570.1 (M + H)<sup>+</sup> Rt 0.88 min (>95% pure).

**Step 2:**

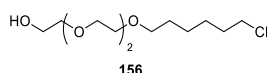
The crude product **141** was then dissolved in NMP (0.5 mL) and DIPEA (67.0  $\mu$ L, 0.385 mmol), 4-(aminomethyl)-N-(3-chloro-1H-indol-7-yl)benzenesulfonamide **115** (31 mg, 0.0920 mmol) and HATU (35.0 mg, 0.0920 mmol) were added sequentially. The resulting mixture was stirred at room temperature for 1 h. The reaction mixture was purified directly by reverse phase column chromatography (30–75% MeCN (0.1% NH<sub>3</sub>) in 10 mM ammonium carbonate) and fractions containing the pure product were concentrated under a stream of nitrogen to afford the desired product **120** (34.0 mg, 50% over two steps) as an off-white gum.

**LCMS** (Method B) (ES -ve)  $m/z$  885.1 (M – H)<sup>+</sup> Rt 1.27 min (>95% pure). **HRMS** (ES) calcd for C<sub>44</sub>H<sub>48</sub>Cl<sub>2</sub>N<sub>8</sub>O<sub>4</sub>S<sub>2</sub> (M + H)<sup>+</sup> 887.2695 found 887.2693. **<sup>1</sup>H NMR** (600 MHz, DMSO-*d*<sub>6</sub>)  $\delta$  = 10.98 (br. s, 1H), 9.92 (br. s, 1H), 8.42 – 8.26 (m, 1H), 8.14 (t,  $J$  = 5.9 Hz, 1H), 7.71 – 7.68 (m, 2H), 7.50 – 7.45 (m, 2H), 7.45 – 7.42 (m, 3H), 7.33 (d,  $J$  = 8.4 Hz, 2H), 7.18 (d,  $J$  = 7.9 Hz, 1H), 6.92 (app t,  $J$  = 7.9 Hz, 1H), 6.84 – 6.81 (m, 1H), 4.51 (dd,  $J$  = 5.9, 8.4 Hz, 1H), 4.27 (d,  $J$  = 5.9 Hz, 2H), 3.29 – 3.04 (m, 4H), 2.60 (s, 3H), 2.42 – 2.39 (m, 3H), 2.11 (t,  $J$  = 7.5 Hz, 2H), 1.63 (s, 3H), 1.53 – 1.41 (m, 4H), 1.33 – 1.16 (m, 10H). **<sup>13</sup>C NMR** (151 MHz, DMSO-*d*<sub>6</sub>)  $\delta$  =

172.24, 169.27, 162.89, 155.09, 149.71, 144.70, 138.44, 136.68, 135.18, 132.20, 130.66, 130.05, 129.75, 129.53, 128.90, 128.36, 127.42, 126.78, 125.94, 122.55, 119.97, 114.83, 113.53, 103.51, 53.91, 41.50, 39.35, 38.44, 37.66, 35.23, 29.22, 28.89, 28.75, 28.69, 28.63, 26.36, 25.15, 13.98, 12.62, 11.23. Note that  $^{13}\text{C}$  NMR data are reported to 2 decimal places to differentiate signals. IR  $\nu_{\text{max}}$  (neat) 3269, 3068, 2924, 2857, 1642, 1528, 1325, 1159  $\text{cm}^{-1}$ .

### 9.2.3 HaloPROTAC synthesis

#### 2-(2-(2-((6-Chlorohexyl)oxy)ethoxy)ethoxy)ethan-1-ol, **156**.

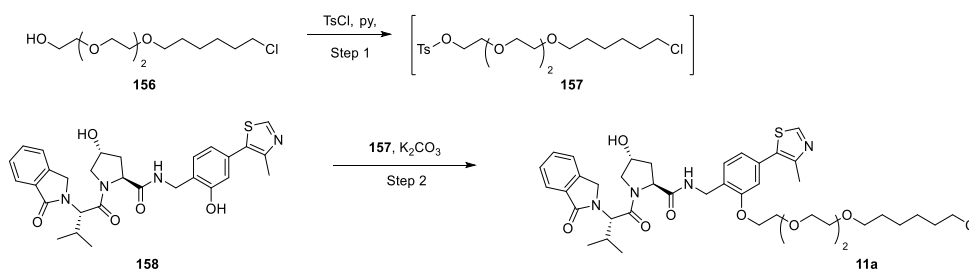


To a stirred and cooled 0 °C solution of 2,2'-(ethane-1,2-diylbis(oxy))bis(ethan-1-ol) **154** (3.66 g, 24.3 mmol) in THF (8 mL) and DMF (8 mL) was added portion wise sodium hydride (0.811 g, 20.3 mmol). After 30 minutes at this temperature 1-chloro-6-iodohexane **155** (2.00 g, 8.11 mmol) was added. The resulting mixture was warmed to room temperature over 16 h. The reaction mixture was quenched with water (10 mL) and diluted with 2M HCl aq. (10 mL). The reaction mixture was extracted with  $\text{CH}_2\text{Cl}_2$  (3  $\times$  50 mL) and the combined organics were washed with sat. aq. LiCl (100 mL) and passed through a hydrophobic frit and concentrated *in vacuo*. The reaction mixture was purified by column chromatography (0–100% cyclohexane in EtOAc) and fractions containing the pure product were concentrated *in vacuo* to afford the desired product **156** (1.50 g, 69%) as a yellow oil.

**HRMS** (ES) calcd for  $\text{C}_{12}\text{H}_{25}\text{ClO}_4$  ( $\text{M} + \text{H}$ ) $^+$  269.1520 found 269.1514.  **$^1\text{H}$  NMR** (400 MHz,  $\text{CDCl}_3$ )  $\delta$  = 3.76 – 3.58 (m, 12H), 3.54 (t,  $J$  = 6.6 Hz, 2H), 3.51 – 3.44 (m, 2H), 2.51 (br. s, 1H), 1.85 – 1.74 (m, 2H), 1.66 – 1.56 (m, 2H), 1.52 – 1.33 (m, 4H).  **$^{13}\text{C}$  NMR** (101 MHz,  $\text{CDCl}_3$ )  $\delta$  = 72.5, 71.3, 70.6, 70.6, 70.4, 70.1, 61.8, 45.0, 32.6, 29.4, 26.7, 25.4.

Consistent with literature data.<sup>63</sup>

**(2*S*,4*R*)-*N*-(2-(2-(2-(2-(6-Chlorohexyl)oxy)ethoxy)ethoxy)ethoxy)-4-(4-methylthiazol-5-yl)benzyl)-4-hydroxy-1-((*S*)-3-methyl-2-(1-oxoisindolin-2-yl)butanoyl)pyrrolidine-2-carboxamide, **11a**.**



**Step 1:**

To a stirred solution of 2-(2-(2-(2-(6-chlorohexyl)oxy)ethoxy)ethoxy)ethan-1-ol **156** (100 mg, 0.372 mmol) in THF (0.7 mL) was added pyridine (60.2  $\mu$ L, 0.744 mmol) and 4-methylbenzenesulfonyl chloride (70.9 mg, 0.372 mmol). The resulting mixture was stirred at room temperature for 16 h. The resulting mixture was diluted with CH<sub>2</sub>Cl<sub>2</sub> (50 mL) and was washed with 5% Cu(II)SO<sub>4</sub> aq. solution (2  $\times$  50 mL) and brine (50 mL). The organic layer was filtered through a hydrophobic frit and concentrated *in vacuo* to give the crude product **157** which was used without further purification.

**Step 2:**

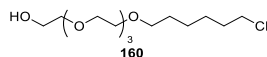
The crude product **157** was dissolved in DMF (3 mL) and was added (2*S*,4*R*)-4-hydroxy-*N*-(2-hydroxy-4-(4-methylthiazol-5-yl)benzyl)-1-((*S*)-3-methyl-2-(1-oxoisindolin-2-yl)butanoyl)pyrrolidine-2-carboxamide **158** (202 mg, 0.369 mmol) and potassium carbonate (127 mg, 0.922 mmol). The resulting mixture was stirred at 60  $^{\circ}$ C for 16 h. The reaction mixture was cooled to room temperature and purified directly via MDAP (TFA) and fractions containing the pure product were concentrated under a stream of nitrogen to afford the desired product **11a** (85 mg, 35% over two steps) as a yellow gum.

**LCMS** (Method B) (ES +ve)  $m/z$  799.2 [M + H]<sup>+</sup> Rt 1.18 min (93% pure). **HRMS** (ES) calcd for C<sub>41</sub>H<sub>55</sub>ClN<sub>4</sub>O<sub>8</sub>S (M + H)<sup>+</sup> 799.3507 found 799.3499. **<sup>1</sup>H NMR** (400 MHz, CDCl<sub>3</sub>)  $\delta$  = 8.77 (s, 1H), 7.84 – 7.75 (m, 1H), 7.58 – 7.48 (m, 1H), 7.49 – 7.41 (m, 2H), 7.37 – 7.30 (m, 2H), 6.99 (dd,  $J$  = 2.0, 7.6 Hz, 1H), 6.91 (d,  $J$  = 2.0 Hz, 1H), 4.80 – 4.73 (m, 2H), 4.63 – 4.39 (m, 6H), 4.27 – 4.15 (m, 2H), 3.98 – 3.86 (m, 2H), 3.81 – 3.56 (m, 8H), 3.55 – 3.49 (m, 3H), 3.41 (t,  $J$  = 6.6 Hz, 2H), 2.55 (s, 3H), 2.46 – 2.33 (m, 2H), 2.14 – 2.04 (m, 1H), 1.81 – 1.71 (m, 2H), 1.60 – 1.51 (m, 2H), 1.48 – 1.29 (m, 4H), 0.98 – 0.87 (m, 6H). One exchangeable not observed. **<sup>13</sup>C NMR** (101 MHz, CDCl<sub>3</sub>)  $\delta$  = 170.62, 170.09, 169.49, 156.88, 150.69, 147.89, 142.14, 132.14, 131.85, 131.75, 131.62, 129.82, 127.99, 127.13, 123.82, 122.85, 122.03, 112.73, 71.20, 70.79, 70.55, 70.54, 70.02, 69.61, 68.00, 58.69, 58.57, 56.06, 47.47, 45.01, 39.23, 36.37, 36.34, 32.52, 29.37, 28.81, 26.67, 25.38, 19.09, 15.76. Note that <sup>13</sup>C NMR data are reported

to 2 decimal places to differentiate signals. IR  $\nu_{max}$  (neat) 3328, 2941, 2862, 1667, 1643, 1469, 1446, 1408, 1124  $\text{cm}^{-1}$ .

Consistent with literature data.<sup>63</sup>

#### 18-Chloro-3,6,9,12-tetraoxaoctadecan-1-ol, **160**.

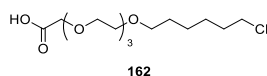


To a cooled 0 °C solution of 2,2'-((oxybis(ethane-2,1-diyl))bis(oxy))bis(ethan-1-ol) **159** (4.73 g, 24.3 mmol) in THF anhydrous (40 mL) was added portion wise sodium hydride (0.811 g, 20.3 mmol). The resulting mixture was stirred at this temperature for 0.5 h before 1-chloro-6-iodohexane **155** (2.00 g, 8.11 mmol) was added dropwise. The resulting mixture was warmed to room temperature over 16 h. The reaction was quenched with H<sub>2</sub>O (50 mL), diluted with 2M HCl aq. (50 mL) and extracted with chloroform (3 × 100 mL) and the organic layers were passed through a hydrophobic frit before concentrating *in vacuo*. The crude product was then purified via silica FCC (washed with 50:50 EtOAc in cyclohexane and eluted with 100% EtOAc) and fractions containing the pure product were concentrated *in vacuo* to afford the desired product **160** (1.00 g, 39%) as a light-yellow oil.

<sup>1</sup>H NMR (400 MHz, CDCl<sub>3</sub>)  $\delta$  = 3.74 – 3.68 (m, 2H), 3.68 – 3.55 (m, 14H), 3.52 (t,  $J$  = 6.6 Hz, 2H), 3.45 (t,  $J$  = 6.6 Hz, 2H), 2.74 (br. s, 1H), 1.84 – 1.71 (m, 2H), 1.62 – 1.53 (m, 2H), 1.50 – 1.31 (m, 4H). <sup>13</sup>C NMR (101 MHz, CDCl<sub>3</sub>)  $\delta$  = 72.47, 71.12, 70.52, 70.50, 70.26, 70.01, 61.62, 44.91, 32.46, 29.33, 26.59, 25.32. Note that <sup>13</sup>C NMR data are reported to 2 decimal places to differentiate signals.

Consistent with literature data.<sup>258</sup>

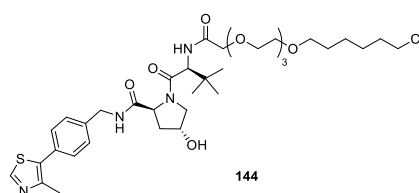
#### 18-Chloro-3,6,9,12-tetraoxaoctadecanoic acid, **162**.



To a stirred and cooled 0 °C solution of 18-chloro-3,6,9,12-tetraoxaoctadecan-1-ol **160** (1.40 g, 4.48 mmol) in acetone (10 mL) and NaHCO<sub>3</sub> (sat. aq. 12.5 mL) was added TEMPO (69.9 mg, 0.448 mmol) and potassium bromide (107 mg, 0.895 mmol). To this resulting mixture was added trichloroisocyanuric acid **161** (2.06 g, 8.95 mmol) over 15 minutes. The reaction mixture was warmed to room temperature over 16 h. The reaction mixture was then diluted with H<sub>2</sub>O (50 mL) and 2M HCl aq. (50 mL) and extracted with chloroform (3 × 100 mL) and the combined organics were concentrated *in vacuo* to give the desired product **162** (1.32 g, 90%) as a colourless oil.

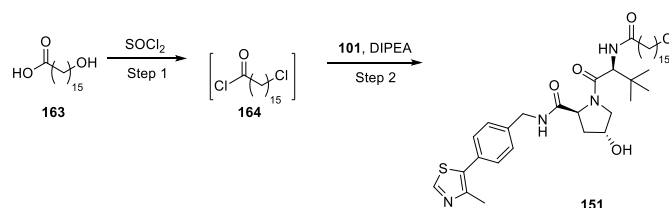
**HRMS** (ES) calcd for  $C_{14}H_{27}ClO_6$  ( $M + H$ )<sup>+</sup> 327.1574 found 327.1581. **<sup>1</sup>H NMR** (400 MHz, DMSO-*d*<sub>6</sub>)  $\delta$  = 12.46 (br. s, 1H), 4.02 (s, 2H), 3.64 – 3.46 (m, 14H), 3.38 (t,  $J$  = 6.4 Hz, 2H), 1.77 – 1.66 (m, 2H), 1.50 (app quint,  $J$  = 7.0 Hz, 2H), 1.43 – 1.27 (m, 4H). **<sup>13</sup>C NMR** (101 MHz, DMSO-*d*<sub>6</sub>)  $\delta$  = 171.54, 70.13, 69.78, 69.75, 69.70, 69.43, 67.58, 45.29, 31.97, 29.00, 26.06, 24.88. Note that <sup>13</sup>C NMR data are reported to 2 decimal places to differentiate signals. Two signals not observed, potentially due to overlapping frequencies of PEG chain carbons.

**(2*S*,4*R*)-1-((*S*)-2-(*tert*-Butyl)-21-chloro-4-oxo-6,9,12,15-tetraoxa-3-azahenicosanoyl)-4-hydroxy-*N*-(4-(4-methylthiazol-5-yl)benzyl)pyrrolidine-2-carboxamide, **144**.**



To a stirred solution of (2*S*,4*R*)-1-((*S*)-2-amino-3,3-dimethylbutanoyl)-4-hydroxy-*N*-(4-(4-methylthiazol-5-yl)benzyl)pyrrolidine-2-carboxamide **101** (39.5 mg, 0.0920 mmol) in DMF (1 mL) was added 18-chloro-3,6,9,12-tetraoxaoctadecanoic acid **162** (30.0 mg, 0.0920 mmol), DIPEA (64.1  $\mu$ L, 0.367 mmol) and HATU (34.9 mg, 0.0920 mmol) sequentially. The resulting mixture was stirred at room temperature for 1 h and purified directly via MDAP (FOR) and appropriate fractions were concentrated under a stream of nitrogen to afford the desired product **144** (12 mg, 18%) as a yellow gum.

**LCMS** (Method B) (ES +ve)  $m/z$  739.3 [ $M + H$ ]<sup>+</sup> Rt 1.15 min (>95% pure). **HRMS** (ES) calcd for  $C_{36}H_{55}ClN_4O_8S$  ( $M + H$ )<sup>+</sup> 739.3507 found 739.3502. **<sup>1</sup>H NMR** (400 MHz, DMSO-*d*<sub>6</sub>)  $\delta$  = 8.70 (br. s, 1H), 7.41 – 7.33 (m, 4H), 7.30 – 7.29 (m, 1H), 4.76 (app t,  $J$  = 8.1 Hz, 1H), 4.61 – 4.46 (m, 3H), 4.39 – 4.31 (m, 1H), 4.14 – 4.11 (m, 1H), 4.07 – 3.95 (m, 2H), 3.70 – 3.50 (m, 15H), 3.45 (t,  $J$  = 6.6 Hz, 2H), 2.64 – 2.56 (m, 1H), 2.53 (s, 3H), 2.19 – 2.09 (m, 1H), 1.85 – 1.73 (m, 2H), 1.65 – 1.55 (m, 2H), 1.51 – 1.34 (m, 4H), 0.96 (s, 9H). 2 exchangeables not observed. **<sup>13</sup>C NMR** (101 MHz, DMSO-*d*<sub>6</sub>)  $\delta$  = 171.53, 170.66, 170.58, 150.35, 148.42, 138.12, 131.63, 130.93, 129.53, 128.16, 77.20, 71.25, 71.20, 70.61, 70.59, 70.48, 70.38, 70.16, 70.07, 58.32, 57.26, 56.63, 45.01, 43.29, 35.68, 34.76, 32.54, 29.44, 26.69, 26.40, 25.41, 15.99. Note that <sup>13</sup>C NMR data are reported to 2 decimal places to differentiate signals. **IR**  $\nu_{max}$  (neat) 3312, 2931, 2865, 1633, 1524, 1435, 1105  $cm^{-1}$ .

**(2S,4R)-1-((S)-2-(16-Chlorohexadecanamido)-3,3-dimethylbutanoyl)-4-hydroxy-N-(4-(4-methylthiazol-5-yl)benzyl)pyrrolidine-2-carboxamide, 151.****Step 1:**

To a stirred solution of 16-hydroxyhexadecanoic acid **163** (300 mg, 1.10 mmol) in chloroform (2.2 mL) was added DMF (8.53  $\mu$ L, 0.110 mmol) and thionyl chloride (241  $\mu$ L, 3.30 mmol). The resulting mixture was stirred at 65 °C for 16 h. The mixture was then concentrated under a stream of nitrogen and was dried under vacuum to afford the desired product **164** (341 mg, quant.) as a colourless gum. The crude product **164** was used immediately without further purification.

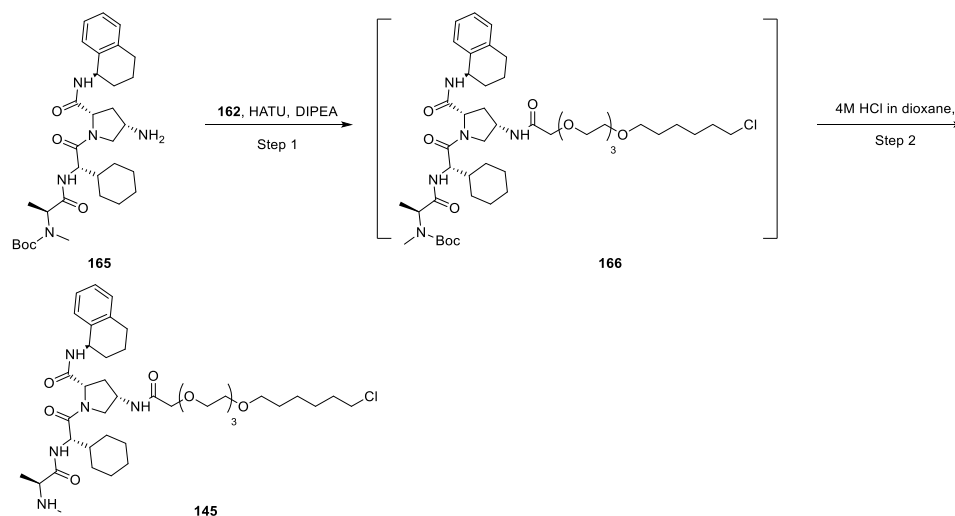
**<sup>1</sup>H NMR** (400 MHz, CDCl<sub>3</sub>)  $\delta$  = 3.55 (t,  $J$  = 6.8 Hz, 2H), 2.93 – 2.86 (m, 2H), 1.89 – 1.68 (m, 4H), 1.50 – 1.25 (m, 22H).

**Step 2:**

To a stirred solution of (2S,4R)-1-((S)-2-amino-3,3-dimethylbutanoyl)-4-hydroxy-N-(4-(4-methylthiazol-5-yl)benzyl)pyrrolidine-2-carboxamide **101** (50.0 mg, 0.116 mmol) in DMF (1 mL) was added 16-chlorohexadecanoyl chloride **164** (35.9 mg, 0.116 mmol) and DIPEA (81.0  $\mu$ L, 0.465 mmol). The resulting mixture was stirred at room temperature for 16 h. The reaction mixture was purified directly via MDAP (HPH) and fractions containing the pure product were concentrated under a stream of nitrogen to afford the desired product **151** (12.0 mg, 15% over two steps) as a yellow gum.

**LCMS** (Method B) (ES +ve)  $m/z$  703.3 (M + H)<sup>+</sup> Rt 1.59 min (>95% pure). **HRMS** (ES) calcd for C<sub>38</sub>H<sub>59</sub>ClN<sub>4</sub>O<sub>4</sub>S (M + H)<sup>+</sup> 703.4024 found 703.4025. **<sup>1</sup>H NMR** (600 MHz, CDCl<sub>3</sub>)  $\delta$  = 8.69 (s, 1H), 7.40 – 7.33 (m, 4H), 7.31 (s, 1H), 6.09 (d,  $J$  = 8.8 Hz, 1H), 4.73 (app t,  $J$  = 7.9 Hz, 1H), 4.60 – 4.49 (m, 3H), 4.36 – 4.32 (m, 1H), 4.15 – 4.10 (m, 1H), 3.60 (dd,  $J$  = 3.7, 11.4 Hz, 1H), 3.53 (t,  $J$  = 6.6 Hz, 2H), 2.60 – 2.54 (m, 1H), 2.52 (s, 3H), 2.19 (t,  $J$  = 7.5 Hz, 2H), 2.16 – 2.09 (m, 1H), 1.81 – 1.74 (m, 3H), 1.60 – 1.57 (m, 2H), 1.45 – 1.40 (m, 2H), 1.32 – 1.22 (m, 20H), 0.95 – 0.92 (m, 9H). **<sup>13</sup>C NMR** (151 MHz, CDCl<sub>3</sub>)  $\delta$  = 173.93, 172.05, 170.52, 150.29, 148.48, 138.02, 131.55, 131.02, 129.54, 128.14, 70.07, 58.37, 57.46, 56.62, 45.17, 43.29, 36.52, 35.64, 34.71, 32.65, 29.61, 29.60, 29.59, 29.57, 29.52, 28.45, 29.44, 29.27, 29.20, 28.87, 26.88, 26.40, 25.58, 16.03. **IR**  $\nu_{max}$  (neat) 3407, 3286, 2919, 2850, 1622, 1462, 1416, 1025 cm<sup>-1</sup>.

**(2S,4S)-4-(18-Chloro-3,6,9,12-tetraoxaoctadecanamido)-1-((S)-2-cyclohexyl-2-((S)-2-(methylamino)propanamido)acetyl)-N-((R)-1,2,3,4-tetrahydronaphthalen-1-yl)pyrrolidine-2-carboxamide, Hydrochloride 145.**



**Step 1:**

To a stirred solution of *tert*-butyl ((S)-1-(((S)-2-((2S,4S)-4-amino-2-(((R)-1,2,3,4-tetrahydronaphthalen-1-yl)carbamoyl)pyrrolidin-1-yl)-1-cyclohexyl-2-oxoethyl)amino)-1-oxopropan-2-yl)(methyl)carbamate **165** (268 mg, 0.459 mmol) in DMF (4.5 mL) was added DIPEA (321  $\mu$ L, 1.82 mmol), 18-chloro-3,6,9,12-tetraoxaoctadecanoic acid **162** (150 mg, 0.459 mmol) and HATU (175 mg, 0.459 mmol) sequentially. The resulting mixture was stirred at room temperature for 2 h. The reaction mixture was purified directly by MDAP (for) and fractions containing the pure product **166** were concentrated under a stream of nitrogen to give a yellow gum.

**LCMS** (Method B) (ES +ve)  $m/z$  892.4 (M + H)<sup>+</sup> Rt 1.50 min (>95% pure).

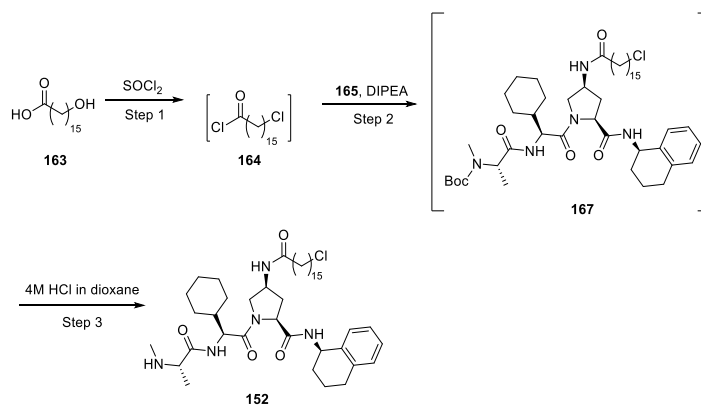
**Step 2:**

To this gum was added 4M HCl in dioxane (500  $\mu$ L) and this was allowed to stand for 4 h before concentrating *in vacuo* to afford the desired product **145** (269 mg, 71% over two steps) as a yellow gum.

**LCMS** (Method B) (ES +ve)  $m/z$  792.3 (M + H)<sup>+</sup> Rt 1.32 min (>95% pure). **HRMS** (ES) calcd for C<sub>41</sub>H<sub>66</sub>ClN<sub>5</sub>O<sub>8</sub> (M + H)<sup>+</sup> 792.4678 found 792.4673. **<sup>1</sup>H NMR** (400 MHz, CDCl<sub>3</sub>)  $\delta$  = 8.61 – 8.51 (m, 1H), 7.60 – 7.60 (m, 1H), 7.69 – 7.51 (m, 1H), 7.19 – 7.04 (m, 4H), 5.21 – 5.09 (m, 1H), 4.81 – 4.72 (m, 1H), 4.71 – 4.61 (m, 1H), 4.41 – 4.35 (m, 1H), 4.24 – 4.11 (m, 1H), 4.07 (s, 2H), 3.79 – 3.70 (m, 4H), 3.67 – 3.59 (m, 7H), 3.57 – 3.51 (m, 4H), 3.45 (t,  $J$  = 6.6 Hz, 2H), 3.09 – 3.00 (m, 1H), 2.88 – 2.70 (m, 2H), 2.54 – 2.47 (m, 1H), 2.41 – 2.35 (m, 3H), 2.27 – 2.17

(m, 1H), 2.08 – 1.98 (m, 1H), 1.90 – 1.73 (m, 5H), 1.71 – 1.34 (m, 14H), 1.31 – 1.22 (m, 3H), 1.18 – 0.84 (m, 5H). Rotamers present, therefore additional peaks observed. Unstable to high temperature NMR.  $^{13}\text{C}$  NMR (101 MHz,  $\text{CDCl}_3$ )  $\delta$  = 174.83, 174.66, 173.09, 173.04, 170.57, 170.52, 170.11, 137.16, 136.37, 136.32, 129.08, 128.29, 128.27, 127.16, 126.04, 77.31, 77.00, 76.68, 71.26, 70.68, 70.56, 70.47, 70.04, 60.20, 60.04, 60.00, 55.46, 55.43, 54.76, 54.67, 48.84, 47.69, 44.97, 40.45, 40.42, 35.26, 35.03, 32.52, 31.08, 30.01, 29.42, 29.33, 29.17, 28.48, 26.66, 25.96, 25.93, 25.80, 25.76, 25.39, 20.15, 20.11, 19.39, 19.08. Note that  $^{13}\text{C}$  NMR data are reported to 2 decimal places to differentiate signals. Rotamers present, therefore additional signals observed. Product was found to be unstable to high temperature NMR. IR  $\nu_{\text{max}}$  (neat) 3258, 2928, 2855, 1660, 1625, 1536, 1449, 1106  $\text{cm}^{-1}$ .

**(2S,4R)-4-(16-Chlorohexadecanamido)-1-((S)-2-cyclohexyl-2-((S)-2-(methylamino)propanamido)acetyl)-N-((R)-1,2,3,4-tetrahydronaphthalen-1-yl)pyrrolidine-2-carboxamide, 152.**



**Step 1:**

Synthesised previously from **163** and **164** was used immediately.

**Step 2:**

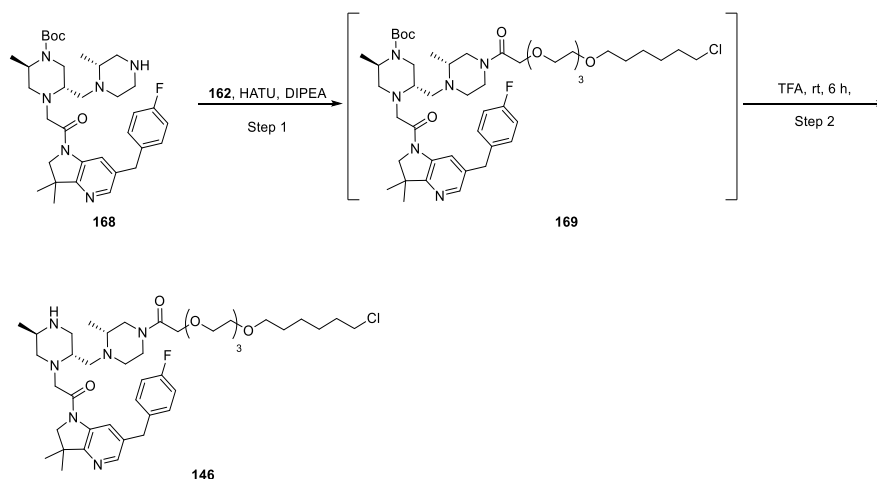
To a stirred solution to *tert*-butyl ((S)-1-(((S)-2-((2S,4R)-4-amino-2-(((R)-1,2,3,4-tetrahydronaphthalen-1-yl)carbamoyl)pyrrolidin-1-yl)-1-cyclohexyl-2-oxoethyl)amino)-1-oxopropan-2-yl)(methyl)carbamate **165** (55.0 mg, 0.0940 mmol) in DMF (0.9 mL) was added 16-chlorohexadecanoyl chloride **164** (29.1 mg, 0.0940 mmol) and DIPEA (16.5  $\mu\text{L}$ , 0.094 mmol). The resulting mixture was stirred at room temperature for 16 h.

**Step 3:**

To this mixture was added 4M HCl in dioxane (1 mL). The resulting mixture was stirred at room temperature for 2 h. The reaction mixture was concentrated *in vacuo* and purified via MDAP (HPH) and fractions containing the pure product were concentrated under a stream of nitrogen to afford the desired product **152** (14.0 mg, 20% over two steps) as a yellow gum.

**LCMS** (Method B) (ES +ve)  $m/z$  756.4 (M + H)<sup>+</sup> Rt 1.87 min (>95% pure). **HRMS** (ES) calcd for C<sub>43</sub>H<sub>70</sub>ClN<sub>5</sub>O<sub>4</sub> (M + H)<sup>+</sup> 756.5195 found 756.5190. **<sup>1</sup>H NMR** (400 MHz, CDCl<sub>3</sub>)  $\delta$  = 8.31 – 7.95 (m, 2H), 7.77 – 7.70 (m, 1H), 7.23 – 7.00 (m, 4H), 5.22 – 5.12 (m, 1H), 4.82 – 4.36 (m, 3H), 4.12 – 4.02 (m, 1H), 3.73 – 3.63 (m, 1H), 3.55 (app dt,  $J$  = 1.5, 6.8 Hz, 2H), 3.45 – 3.40 (m, 1H), 2.91 – 2.74 (m, 2H), 2.44 – 2.17 (m, 5H), 2.09 – 1.60 (m, 16H), 1.50 – 1.41 (m, 2H), 1.38 – 0.92 (m, 29H). Sample decomposed in NMR tube before carbon NMR was acquired. **IR**  $\nu_{max}$  (neat) 3267, 3062, 2922, 2852, 1650, 1627, 1449, 1536 cm<sup>-1</sup>.

**18-Chloro-1-((*R*)-4-(((2*R*,5*R*)-1-(2-(6-(4-fluorobenzyl)-3,3-dimethyl-2,3-dihydro-1H-pyrrolo[3,2-*b*]pyridin-1-yl)-2-oxoethyl)-5-methylpiperazin-2-yl)methyl)-3-methylpiperazin-1-yl)-3,6,9,12-tetraoxaocadecan-1-one, TFA salt, **146**.**



#### Step 1:

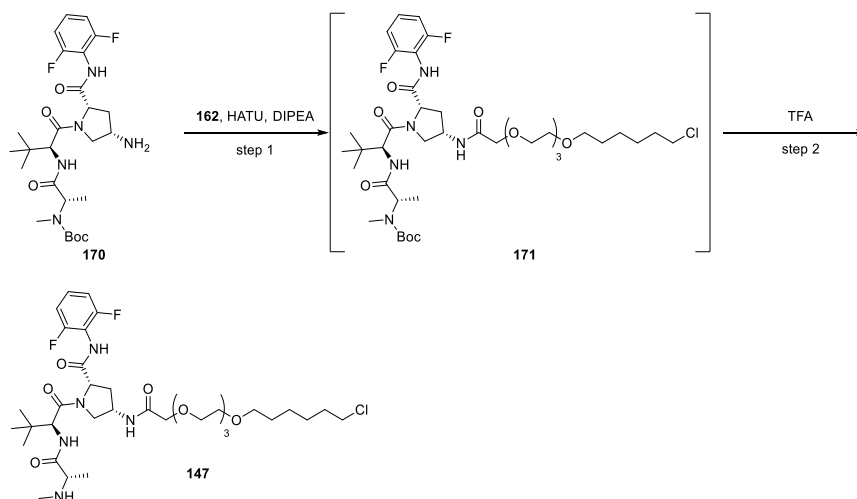
To a stirred solution of (*2R,5S*)-*tert*-butyl 4-(2-(6-(4-fluorobenzyl)-3,3-dimethyl-2,3-dihydro-1H-pyrrolo[3,2-*b*]pyridin-1-yl)-2-oxoethyl)-2-methyl-5-(((*R*)-2-methylpiperazin-1-yl)methyl)piperazine-1-carboxylate **168** (55.9 mg, 0.0920 mmol) in DMF (0.9 mL) was added 18-chloro-3,6,9,12-tetraoxaocadecanoic acid **162** (30.0 mg, 0.0920 mmol), DIPEA (64.1  $\mu$ L, 0.367 mmol) and HATU (34.9 mg, 0.0920 mmol) sequentially. The resulting mixture was stirred at room temperature for 1 h. The reaction mixture was purified directly via MDAP (HPH) to give fractions containing **169** which were carried onto the next step.

#### Step 2:

Fractions containing the pure product **169** were combined and TFA (70.7  $\mu$ L, 0.918 mmol) was added before being concentrated under a stream of nitrogen to afford the desired product **146** (12 mg, 14% over two steps) as a yellow gum.

**LCMS** (Method B) (ES +ve)  $m/z$  817.3 (M + H)<sup>+</sup> Rt 1.27 min (>95% pure). **HRMS** (ES) calcd for C<sub>43</sub>H<sub>66</sub>ClFN<sub>6</sub>O<sub>6</sub> (M + H)<sup>+</sup> 817.4794 found 817.4797. **<sup>1</sup>H NMR** (600 MHz, MeOD-*d*<sub>4</sub>)  $\delta$  = 8.24 – 8.20 (m, 1H), 8.18 (s, 1H), 7.26 – 7.22 (m, 2H), 7.06 – 6.99 (m, 2H), 4.40 – 4.27 (m, 2H), 4.08 – 3.92 (m, 7H), 3.75 – 3.34 (m, 25H), 3.21 – 2.98 (m, 4H), 2.65 – 2.52 (m, 1H), 1.78 – 1.71 (m, 2H), 1.61 – 1.51 (m, 2H), 1.47 – 1.28 (m, 16H). One exchangeable not observed. **<sup>13</sup>C NMR** (151 MHz, MeOD-*d*<sub>4</sub>)  $\delta$  = 163.21 (d,  $J_{C-F}$  = 243.3 Hz), 161.22 (q,  $J_{C-F}$  = 37.6 Hz), 159.52, 159.24, 158.96, 145.64, 138.54, 137.49 (d,  $J_{C-F}$  = 3.1 Hz), 132.06 (d,  $J_{C-F}$  = 7.7 Hz), 126.60, 117.15, 116.64 (d,  $J_{C-F}$  = 21.0 Hz), 116.35 (q,  $J_{C-F}$  = 286.4 Hz), 111.55, 72.28, 71.98, 71.66, 71.63, 71.52, 71.49, 71.28, 71.19, 61.85, 54.58, 49.72, 45.86, 42.25, 38.67, 33.89, 30.69, 27.86, 27.51, 27.47, 26.63, 17.43, 15.70. Note that <sup>13</sup>C NMR data are reported to 2 decimal places to differentiate signals. Five signals not observed, potentially due to overlapping frequencies of carbons worsened by broadening as a result of rotamers. **IR**  $\nu_{max}$  (neat) 3412, 2866, 2931, 1670, 1619, 1429, 1509, 1119 cm<sup>-1</sup>.

**(2S,4S)-4-(18-Chloro-3,6,9,12-tetraoxaoctadecanamido)-N-(2,6-difluorophenyl)-1-((S)-3,3-dimethyl-2-((S)-2 (methylamino)propanamido)butanoyl)pyrrolidine-2-carboxamide, TFA salt, 147.**



Step 1:

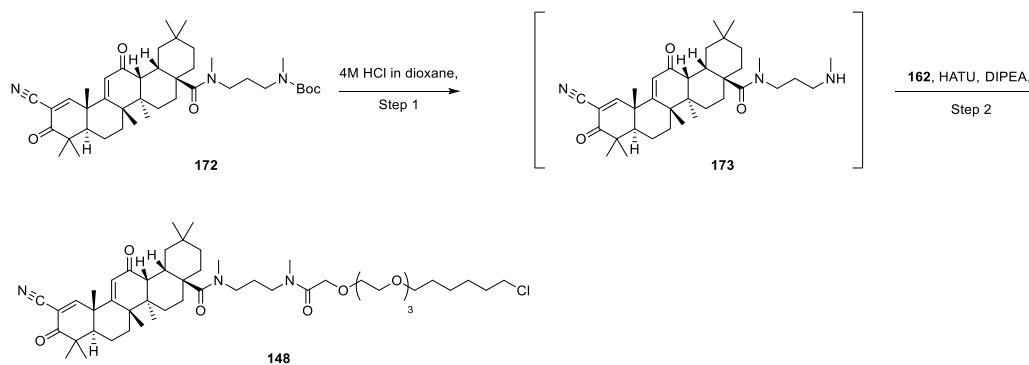
To a stirred solution of *tert*-butyl ((*S*)-1-(((*S*)-1-((2*S*,4*S*)-4-amino-2-((2,6-difluorophenyl)carbamoyl)pyrrolidin-1-yl)-3,3-dimethyl-1-oxobutan-2-yl)amino)-1-oxopropan-2-yl)(methyl)carbamate **170** (49.5 mg, 0.092 mmol) in DMF (0.9 mL) was added 18-chloro-3,6,9,12-tetraoxaoctadecanoic acid **162** (30 mg, 0.092 mmol), DIPEA (64.1  $\mu$ L, 0.367 mmol), HATU (34.9 mg, 0.092 mmol) sequentially. The resulting mixture was stirred at room temperature for 1 h. The reaction mixture was purified directly via MDAP (HPH) to give fractions containing **171** which were carried onto the next step.

Step 2:

Fractions containing the pure product **171** were combined and TFA (70.7  $\mu$ L, 0.918 mmol) was added before being concentrated under a stream of nitrogen to afford the desired product **147** (38.0 mg, 48% over two steps) as a yellow gum.

**LCMS** (Method B) (ES +ve)  $m/z$  748.3 (M + H)<sup>+</sup> Rt 1.16 min (94% pure). **HRMS** (ES) calcd for C<sub>35</sub>H<sub>56</sub>ClF<sub>2</sub>N<sub>5</sub>O<sub>8</sub> (M + H)<sup>+</sup> 748.3849 found 748.3856. **<sup>1</sup>H NMR** (600 MHz, CDCl<sub>3</sub>)  $\delta$  = 10.15 – 9.95 (m, 1H), 9.31 (br. s, 1H), 8.54 – 8.23 (m, 2H), 7.26 – 7.19 (m, 1H), 6.95 (app t,  $J$  = 8.1 Hz, 2H), 4.87 – 4.85 (m, 1H), 4.74 – 4.71 (m, 2H), 4.34 – 4.33 (m, 1H), 4.13 – 3.99 (m, 3H), 3.75 (br. d,  $J$  = 9.2 Hz, 1H), 3.66 – 3.55 (m, 12H), 3.53 (t,  $J$  = 6.8 Hz, 2H), 3.47 (t,  $J$  = 6.8 Hz, 2H), 2.66 – 2.55 (m, 4H), 2.30 – 2.21 (m, 1H), 1.80 – 1.74 (m, 2H), 1.63 – 1.56 (m, 2H), 1.49 – 1.33 (m, 7H), 0.96 (s, 9H). **<sup>13</sup>C NMR** (151 MHz, CDCl<sub>3</sub>)  $\delta$  = 171.23, 170.75, 169.31, 168.70, 160.51 (q,  $J_{C-F}$  = 38.7 Hz), 158.02 (dd,  $J_{C-F}$  = 251, 4.9 Hz), 128.17 (t,  $J_{C-F}$  = 9.4 Hz), 113.62 (t,  $J_{C-F}$  = 16.9 Hz), 115.55 (q,  $J_{C-F}$  = 289.0 Hz), 111.71 (dd,  $J_{C-F}$  = 19.6, 3.5 Hz), 71.30, 71.25, 71.23, 70.43, 70.41, 70.36, 70.14, 70.08, 70.02, 69.92, 69.86, 69.74, 69.44, 59.44, 57.84, 57.48, 57.40, 55.25, 48.67, 48.60, 45.00, 44.99, 35.94, 34.30, 33.64, 32.50, 32.44, 31.80, 29.30, 29.02, 26.65, 26.57, 26.33, 26.12, 26.00, 25.34, 25.14, 16.48. Note that <sup>13</sup>C NMR data are reported to 2 decimal places to differentiate signals. Rotamers present, therefore additional signals observed. Only clearly resolved <sup>13</sup>C-<sup>19</sup>F couplings are reported. **IR**  $\nu_{max}$  (neat) 3269, 2952, 2841, 1668, 1626, 1531, 1470, 1200, 1129 cm<sup>-1</sup>.

**18-Chloro-*N*-(3-((4a*S*,6a*R*,6b*S*,8a*R*,12a*S*,14a*R*,14b*S*)-11-cyano-*N*,2,2,6a,6b,9,9,12a-octamethyl-10,14-dioxo-1,2,3,4,4a,5,6,6a,6b,7,8,8a,9,10,12a,14,14a,14b-octadecahydropicene-4a-carboxamido)propyl)-*N*-methyl-3,6,9,12-tetraoxaoctadecanamide, **148**.**



Step 1:

*tert*-Butyl (3-((4a*S*,6a*R*,6b*S*,8a*R*,12a*S*,14a*R*,14b*S*)-11-cyano-*N*,2,2,6a,6b,9,9,12a-octamethyl-10,14-dioxo-1,2,3,4,4a,5,6,6a,6b,7,8,8a,9,10,12a,14,14a,14b-octadecahydropicene-4a-carboxamido)propyl)(methyl)carbamate **172** (62.0 mg, 0.092 mmol) was dissolved in 4M HCl in dioxane (279  $\mu$ L, 9.18 mmol) and allowed to stand for 0.5 h. The

resulting mixture was concentrated under a stream of nitrogen to give the crude product **173** which was used without further purification.

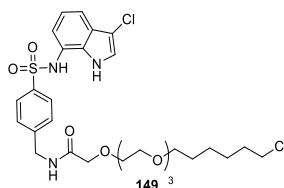
**LCMS** (Method A) (ES +ve)  $m/z$  576.3 (M + H)<sup>+</sup> Rt 0.86 min (>95% pure).

Step 2:

The crude product **173** was dissolved in DMF (1 mL) and was added DIPEA (64.1  $\mu$ L, 0.367 mmol), 18-chloro-3,6,9,12-tetraoxaoctadecanoic acid **162** (30.0 mg, 0.092 mmol) and HATU (34.9 mg, 0.092 mmol) sequentially. The resulting mixture was stirred at room temperature for 2 h. The reaction mixture was purified directly via MDAP (for) and fractions containing the pure product were concentrated under a stream of nitrogen to afford the desired product **148** (18.0 mg, 22% over two steps) as a colourless gum.

**LCMS** (Method A) (ES +ve)  $m/z$  884.4 (M + H)<sup>+</sup> Rt 1.47 min (92% pure). **HRMS** (ES) calcd for C<sub>50</sub>H<sub>78</sub>ClN<sub>3</sub>O<sub>8</sub> (M + H)<sup>+</sup> 884.5543 found 884.5549. **<sup>1</sup>H NMR** (600 MHz, CDCl<sub>3</sub>)  $\delta$  = 8.07 – 8.02 (m, 1H), 5.98 – 5.92 (m, 1H), 4.21 (s, 2H), 3.73 – 3.68 (m, 4H), 3.66 (s, 4H), 3.65 – 3.62 (m, 2H), 3.59 – 3.57 (m, 2H), 3.55 – 3.52 (m, 2H), 3.48 – 3.45 (m, 2H), 3.41 – 3.31 (m, 3H), 3.28 – 3.11 (m, 4H), 3.02 – 2.92 (m, 3H), 2.06 – 1.97 (m, 1H), 1.89 – 1.76 (m, 9H), 1.74 – 1.57 (m, 10H), 1.55 – 1.44 (m, 6H), 1.41 – 1.34 (m, 3H), 1.31 (s, 4H), 1.26 (s, 6H), 1.21 – 1.17 (m, 4H), 1.03 (d,  $J$  = 2.6 Hz, 6H), 0.94 – 0.90 (m, 3H). Rotamers present, therefore additional peaks present, unable to resolve. **<sup>13</sup>C NMR** (151 MHz, CDCl<sub>3</sub>)  $\delta$  = 199.09, 196.55, 176.02, 169.14, 165.75, 124.05, 114.51, 114.36, 71.24, 70.66, 70.63, 70.60, 70.58, 70.55, 70.42, 70.41, 70.30, 70.11, 49.67, 49.05, 47.83, 47.66, 45.83, 45.72, 45.04, 45.01, 42.50, 42.33, 36.24, 34.38, 34.33, 33.16, 32.55, 31.66, 30.45, 30.02, 29.46, 28.46, 26.95, 26.70, 26.58, 25.43, 24.53, 23.96, 21.91, 21.55, 18.26. Note that <sup>13</sup>C NMR data are reported to 2 decimal places to differentiate signals. **IR**  $\nu_{max}$  (neat) 3365, 2928, 2863, 1779, 1659, 1613, 1465, 1106 cm<sup>-1</sup>.

**18-Chloro-*N*-(4-(*N*-(3-chloro-1*H*-indol-7-yl)sulfamoyl)benzyl)-3,6,9,12-tetraoxaoctadecanamide, 149.**

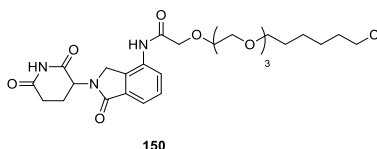


To a stirred solution of 4-(aminomethyl)-*N*-(3-chloro-1*H*-indol-7-yl)benzenesulfonamide **115** (25.7 mg, 0.0760 mmol) in DMF (0.7 mL) was added DIPEA (53.4  $\mu$ L, 0.306 mmol), 18-chloro-3,6,9,12-tetraoxaoctadecanoic acid **162** (25.0 mg, 0.0760 mmol) and HATU (29.1 mg, 0.0760 mmol). The resulting mixture was stirred at room temperature for 1 h. The reaction mixture was purified directly by MDAP (for) and fractions containing the pure product were

concentrated under a stream of nitrogen to afford the desired product **149** (19.0 mg, 39%) as a colourless gum.

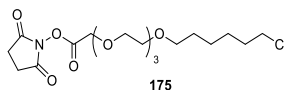
**LCMS** (Method B) (ES +ve)  $m/z$  644.1 (M + H)<sup>+</sup> Rt 1.25 min (93% pure). **HRMS** (ES) calcd for C<sub>29</sub>H<sub>39</sub>Cl<sub>2</sub>N<sub>3</sub>O<sub>7</sub>S (M + H)<sup>+</sup> 644.1964 found 644.1965 (98% pure). **<sup>1</sup>H NMR** (400 MHz, CDCl<sub>3</sub>)  $\delta$  = 9.47 (br. s, 1H), 7.77 (t,  $J$  = 5.9 Hz, 1H), 7.63 – 7.53 (m, 3H), 7.46 (app d,  $J$  = 8.3 Hz, 1H), 7.31 (d,  $J$  = 8.3 Hz, 2H), 7.17 (d,  $J$  = 2.4 Hz, 1H), 6.96 (app t,  $J$  = 7.8 Hz, 1H), 6.73 (d,  $J$  = 7.0 Hz, 1H), 4.51 (d,  $J$  = 6.4 Hz, 2H), 4.10 (s, 2H), 3.71 – 3.65 (m, 2H), 3.64 – 3.58 (m, 2H), 3.54 – 3.44 (m, 10H), 3.42 – 3.37 (m, 2H), 1.76 – 1.63 (m, 2H), 1.56 – 1.47 (m, 2H), 1.44 – 1.25 (m, 4H). **<sup>13</sup>C NMR** (101 MHz, CDCl<sub>3</sub>)  $\delta$  = 171.03, 143.96, 137.51, 130.20, 127.97, 127.42, 127.31, 121.77, 120.80, 120.44, 118.23, 116.86, 106.40, 71.31, 71.24, 71.23, 70.44, 70.25, 70.18, 70.17, 69.97, 45.00, 42.27, 32.47, 29.26, 26.62, 25.33. Note that <sup>13</sup>C NMR data are reported to 2 decimal places to differentiate signals. **IR**  $\nu_{max}$  (neat) 3238, 1931, 2863, 1644, 1527, 1442, 1410, 1330, 1159, 1091 cm<sup>-1</sup>.

**18-Chloro-N-(2-(2,6-dioxopiperidin-3-yl)-1-oxoisindolin-4-yl)-3,6,9,12-tetraoxaocetadecanamide, 150.**



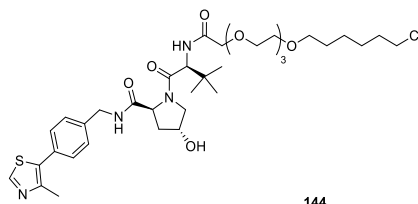
To a stirred solution of 3-(4-amino-1-oxoisindolin-2-yl)piperidine-2,6-dione **29** (127 mg, 0.490 mmol) in DMF (5 mL) was added DIPEA (342  $\mu$ L, 1.96 mmol), 18-chloro-3,6,9,12-tetraoxaocetadecanoic acid **162** (160 mg, 0.490 mmol) and HATU (186 mg, 0.490 mmol) sequentially. The resulting mixture was stirred for 6 h. The reaction mixture was purified directly by MDAP (for) and fractions containing the pure product were concentrated under a stream of nitrogen to afford the desired product **150** (100 mg, 36%) as a colourless gum.

**LCMS** (Method B) (ES +ve)  $m/z$  568.1 (M + H)<sup>+</sup> Rt 0.94 min (>95% pure). **HRMS** (ES) calcd for C<sub>27</sub>H<sub>38</sub>ClN<sub>3</sub>O<sub>8</sub> (M + H)<sup>+</sup> 568.2426 found 568.2427. **<sup>1</sup>H NMR** (400 MHz, CDCl<sub>3</sub>)  $\delta$  = 9.01 (s, 1H), 8.61 (s, 1H), 7.74 (app t,  $J$  = 7.8 Hz, 2H), 7.52 – 7.46 (m, 1H), 5.80 – 5.67 (m, 1H), 5.26 – 5.18 (m, 1H), 4.46 (s, 1H), 4.17 (d,  $J$  = 2.9 Hz, 2H), 3.82 – 3.77 (m, 2H), 3.76 – 3.72 (m, 2H), 3.71 – 3.68 (m, 2H), 3.62 – 3.59 (m, 2H), 3.54 – 3.45 (m, 6H), 3.42 – 3.37 (m, 2H), 2.93 – 2.75 (m, 2H), 2.45 – 2.31 (m, 1H), 2.24 – 2.16 (m, 1H), 1.79 – 1.70 (m, 2H), 1.59 – 1.50 (m, 2H), 1.48 – 1.27 (m, 4H). **<sup>13</sup>C NMR** (101 MHz, CDCl<sub>3</sub>)  $\delta$  = 171.37, 169.60, 168.98, 168.67, 134.57, 132.72, 131.99, 129.06, 126.33, 121.48, 71.26, 71.19, 70.58, 70.39, 70.29, 70.13, 70.03, 69.89, 51.88, 46.60, 44.99, 32.46, 31.46, 29.23, 26.59, 25.29, 23.32. Note that <sup>13</sup>C NMR data are reported to 2 decimal places to differentiate signals. **IR**  $\nu_{max}$  (neat) 3211, 3095, 2927, 2862, 1687, 1603, 1524, 1456, 1105 cm<sup>-1</sup>.

**2,5-Dioxopyrrolidin-1-yl 18-chloro-3,6,9,12-tetraoxaoctadecanoate, 175.**

To a stirred solution of 18-chloro-3,6,9,12-tetraoxaoctadecanoic acid **162** (1.40 g, 4.28 mmol) in THF (16 mL) added bis(2,5-dioxopyrrolidin-1-yl) carbonate **178** (1.65 g, 6.43 mmol) and 1-hydroxypyrrrolidine-2,5-dione **177** (493 mg, 4.28 mmol). The resulting mixture was stirred at 50 °C for 16 h. The reaction mixture was then diluted with H<sub>2</sub>O (100 mL) and extracted with CH<sub>2</sub>Cl<sub>2</sub> (3 × 100 mL) and the organic layers were passed through a hydrophobic frit and concentrated *in vacuo*. The crude product was then purified by column chromatography (50–100% EtOAc in cyclohexane) and the desired fractions were concentrated *in vacuo* to afford the desired product **175** (730 mg, 40%) as a yellow oil

**HRMS** (ES) calcd for C<sub>18</sub>H<sub>30</sub>ClNO<sub>8</sub> (M + H)<sup>+</sup> 424.1744 found 424.1741. **<sup>1</sup>H NMR** (400 MHz, CDCl<sub>3</sub>) δ = 4.53 (s, 2H), 3.82 – 3.57 (m, 12H), 3.54 (t, *J* = 6.6 Hz, 2H), 3.49 – 3.45 (m, 2H), 2.89 – 2.83 (m, 4H), 1.86 – 1.72 (m, 2H), 1.64 – 1.55 (m, 2H), 1.51 – 1.33 (m, 4H). **<sup>13</sup>C NMR** (101 MHz, CDCl<sub>3</sub>) δ = 168.66, 165.97, 71.38, 71.23, 70.68, 70.64, 70.60, 70.11, 66.55, 45.05, 32.56, 29.47, 26.70, 25.58, 25.43, 25.38. Note that <sup>13</sup>C NMR data are reported to 2 decimal places to differentiate signals.

**(2S,4R)-1-((S)-2-(tert-Butyl)-21-chloro-4-oxo-6,9,12,15-tetraoxa-3-azahenicosanoyl)-4-hydroxy-N-(4-(4-methylthiazol-5-yl)benzyl)pyrrolidine-2-carboxamide, 144.**

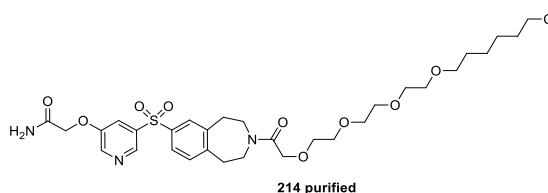
- 1) A stock solution of (2S,4R)-1-((S)-2-amino-3,3-dimethylbutanoyl)-4-hydroxy-N-(4-(4-methylthiazol-5-yl)benzyl)pyrrolidine-2-carboxamide dihydrochloride **101** (47.2 mg, 0.100 mmol) in 10 mL DMSO was prepared to give a 10 mM DMSO solution.
- 2) A stock solution of 2,5-dioxopyrrolidin-1-yl 18-chloro-3,6,9,12-tetraoxaoctadecanoate (42.4 mg, 0.100 mmol) and DIPEA (52 μL, 0.300 μmol) in DMSO (1 mL) was prepared to give a 100 mM DMSO solution.

To a small vial, (2S,4R)-1-((S)-2-amino-3,3-dimethylbutanoyl)-4-hydroxy-N-(4-(4-methylthiazol-5-yl)benzyl)pyrrolidine-2-carboxamide stock solution (100 μL, 1 μmol, 10 mM)

and 2,5-dioxopyrrolidin-1-yl 18-chloro-3,6,9,12-tetraoxaoctadecanoate and DIPEA stock solution (12  $\mu$ L, 1.2  $\mu$ mol, 100 mM) were added. The reaction was allowed to stand at rt for 16 h and used directly and featured in **Figure 119**.

**LCMS** (Method B) (ES +ve)  $m/z$  739.3 (M + H)<sup>+</sup> Rt 1.14 min (83% pure).

**2-((5-((3-(18-Chloro-3,6,9,12-tetraoxaoctadecanoyl)-2,3,4,5-tetrahydro-1H-benzo[d]azepin-7-yl)sulfonyl)pyridin-3-yl)oxy)acetamide, 214 purified.**



To a stirred solution of 2-((5-((2,3,4,5-tetrahydro-1H-benzo[d]azepin-7-yl)sulfonyl)pyridin-3-yl)oxy)acetamide **216** (14.5 mg, 0.040 mmol) in DMSO (0.5 mL) was added 2,5-dioxopyrrolidin-1-yl 18-chloro-3,6,9,12-tetraoxaoctadecanoate **175** (17.0 mg, 0.040 mmol) and NMM (22.1  $\mu$ L, 0.20 mmol). The reaction mixture was purified directly via MDAP (HPH) and appropriate fractions were concentrated under a stream of nitrogen to afford the desired product **214 purified** (8.00 mg, 30%) as a colourless gum.

**LCMS** (Method B) (ES +ve)  $m/z$  670.3 [M + H]<sup>+</sup> Rt 1.02 min (88% pure). **HRMS** (ES) calcd for C<sub>31</sub>H<sub>44</sub>ClN<sub>3</sub>O<sub>9</sub>S (M + H)<sup>+</sup> 670.2565 found 670.2555. **<sup>1</sup>H NMR** (600 MHz, DMSO-*d*<sub>6</sub>)  $\delta$  = 8.75 – 8.70 (m, 1H), 8.57 (d,  $J$  = 2.7 Hz, 1H), 7.90 – 7.78 (m, 3H), 7.69 – 7.61 (m, 1H), 7.48 – 7.40 (m, 2H), 4.69 (s, 2H), 4.20 (s, 2H), 3.61 (t,  $J$  = 6.6 Hz, 2H), 3.59 – 3.42 (m, 16H), 3.37 – 3.33 (m, 2H), 3.06 – 3.02 (m, 2H), 2.96 – 2.92 (m, 2H), 1.73 – 1.66 (m, 2H), 1.49 – 1.43 (m, 2H), 1.40 – 1.26 (m, 4H). **<sup>13</sup>C NMR** (151 MHz, DMSO-*d*<sub>6</sub>)  $\delta$  = 168.84, 167.61, 154.04, 147.66, 142.77, 140.02, 138.20, 138.12, 128.24, 128.13, 125.78, 125.63, 119.58, 70.10, 69.78, 69.74, 69.71, 69.67, 69.56, 69.41, 66.95, 46.01, 45.29, 43.48, 37.08, 36.16, 35.95, 31.96, 28.97, 26.04, 24.85.

### 9.3 High-Throughput Chemistry Experiments

#### 9.3.1 General Considerations

Reactions were carried out in a fumehood under air atmosphere unless otherwise stated. Experiments conducted in a glovebox were performed inside an Mbraun glovebox operating

with a constant N<sub>2</sub>-purge (oxygen typically <5 ppm). Reactions were completed with reaction component 1 (amine) and reaction component 2 (NHS ester and base).

All source plates were prepared by hand unless otherwise stated.

Stock solution reservoirs were purchased from Corning Costar® (polystyrene, 50 mL capacity, Cat. No. 4870). 384-well reactor plates were sourced from either Greiner Bio-One Microplates (384-well, PP, v-bottom, Cat. No. 781280) or Labcyte Echo® Qualified Microplates (384-well, PP, flat-bottom, Cat. No. P-05525). Plates were covered with a lid (without corner notch, polystyrene, Cat. No 3098).

Pipetting procedures were completed using the Thermofisher E1-ClipTip™ electronic multichannel pipette from the stock solution reservoirs (12 channels, 1 to 30 µL, Cat. No. 4671030BT) with no special modifications. Pipettes used the stepper function with one uptake and dispense per well with the standard Thermofisher ClipTip™ non-filtered 384 format pipette tips (ClipTip™ 384 30 sterile, violet, Cat. No. 94410103).

Plats were spun using a Heraeus™ Megafuge™ (8 Small Benchtop Centrifuge Series Cat. No. 75007214).

### 9.3.2 General Procedures

#### Stock solutions

Stock Solution 1 (**SS1**): **VHL amine 101**. A stock solution of (2*S*,4*R*)-1-((*S*)-2-amino-3,3-dimethylbutanoyl)-4-hydroxy-*N*-(4-(4-methylthiazol-5-yl)benzyl)pyrrolidine-2-carboxamide dihydrochloride **101** was prepared (47.2 mg, 0.100 mmol) in DMSO (10 mL) to give a 10 mM stock solution which was used immediately.

Stock Solution 2 (**SS2**): **A) NHS Ester 175 and DIPEA (3 eq)**. A stock solution of 2,5-dioxopyrrolidin-1-yl 18-chloro-3,6,9,12-tetraoxaoctadecanoate **175** (42.4 mg, 0.100 mmol) and DIPEA (52 µL, 0.300 µmol) in DMSO (1 mL) was prepared to give an overall concentration of 100 mM.

Stock Solution 3 (**SS3**): **B) NHS Ester 175 and NMM (5 eq)**. A stock solution of 2,5-dioxopyrrolidin-1-yl 18-chloro-3,6,9,12-tetraoxaoctadecanoate **175** (42.4 mg, 0.100 mmol) and *N*-methylmorpholine (54.5 µL, 0.495 µmol) in DMSO (10 mL) was prepared to give an overall concentration of 10 mM.

Stock Solution 4 (**SS4**): **C** **NHS Ester 175 and NMM (10 eq)**. A stock solution of 2,5-dioxopyrrolidin-1-yl 18-chloro-3,6,9,12-tetraoxaoctadecanoate **175** (42.4 mg, 0.100 mmol) and *N*-methylmorpholine (109  $\mu$ L, 0.991  $\mu$ mol) in DMSO (10 mL) was prepared in a glovebox under a  $N_2$  atmosphere to give a 10 mM DMSO solution and used immediately for every individual experiment.

### General Protocols

**GP1**: Plate preparation for single amine screening.

Amine stock solution was prepared according to **SS1** and dosed into a 384-well reactor plate inside a fumehood. The plate was subsequently centrifuged at 400G for 15 seconds. Subsequently, NHS ester **175** and desired base stock solutions were prepared according to **SS2–4** and dosed into the reactor plate. The reactor plate was placed into a centrifuge for 15 seconds at 400G and left to stand in the fumehood for 16 hours.

**GP2**: Plate preparation for multi-amine screening

Reactor plates were prepared by GSK compound manager as per the specification given and stored at  $-20$  °C. The plates were thawed at room temperature prior to reaction dosing. NHS ester **175** and desired base stock solutions were prepared according to **SS2–4** and dosed into the reactor plate. The reactor plate was placed into a centrifuge for 15 seconds at 400G and left to stand in the fumehood for 16 hours.

**GP3**: Plate preparation for single-amine screening in a glovebox

Amine stock solution was prepared according to **SS1** and dosed into a 384-well reactor plate inside a fumehood. The plate was subsequently centrifuged at 400G for 15 seconds and taken into a nitrogen glovebox. Within the glovebox, NHS ester **175** and desired base stock solutions were prepared according to **SS2–4** and dosed into the reactor plate. The reactor plate was then sealed and left to stand at room temperature.

**GP4**: Plate preparation for multi-amine screening in a glovebox

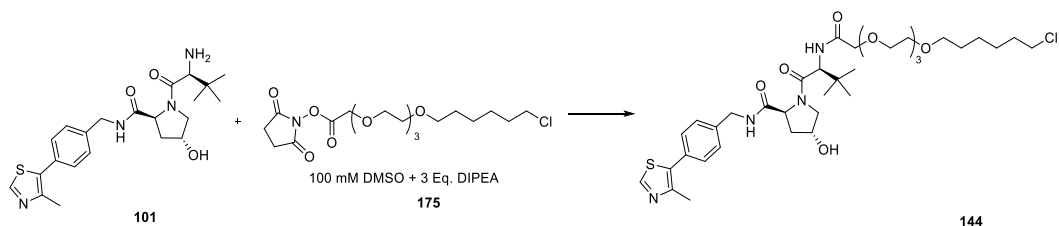
Reactor plates were prepared by GSK compound management as per the specification given and stored at  $-20$  °C. The plates were thawed at room temperature within a glovebox prior to reaction dosing. Within the glovebox, NHS ester **175** and desired base stock solutions were prepared according to **SS2–4** and dosed into the reactor plate. The reactor plate was then sealed and left to stand at room temperature.

**GP5**: Analysis protocol

Once the reaction plate had been left for the allocated time, the seal was removed. DMSO (20  $\mu$ L) was added to each well and the plate resealed using a heat sealer and PFA seal. The plate was placed directly into a sample organiser and analysed using UV/vis chromophore validated by the corresponding mass spectrometer peak. UV/vis peak integrals were used as a relative hit identification tool.

### 9.3.3 Nanoscale Synthetic Procedures

Experiments featured in **Scheme 20**, synthesis of VHL recruiting HaloPROTAC **144**.



Reactions in **Scheme 20** were performed using **GP1** with **SS1** and **SS2** modified as only one well was used. Reactions were performed in Labcyte ECHO® Microplates. After reaction time of 16 h, the plates were then diluted with DMSO (20  $\mu$ L) and analysed by LCMS.

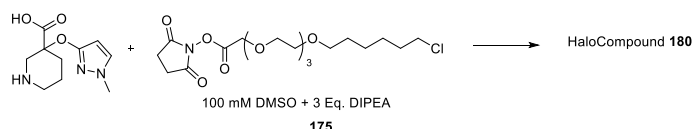
**LCMS** (Method B) (ES +ve) Product  $m/z$  739.3 (M + H)<sup>+</sup> Rt 1.15 min (76% conversion), SM  $m/z$  431.1 (M + H)<sup>+</sup> Rt 0.81 min (10% remaining).

#### Optimisation Set Synthesis - DIPEA

Reactions in **Figure 126** were performed using **GP2** with **SS2**. Reactions were performed in Labcyte ECHO® Microplates. After reaction time of 16 h, plates prepared for analysis using **GP5**.

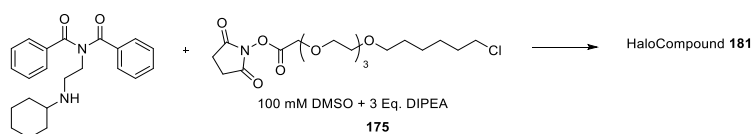
Example Analysis from **Figure 126**:

HaloCompound **180**, Well C11, derived from: 3-((1-methyl-1H-pyrazol-3-yl)oxy)piperidine-3-carboxylic acid



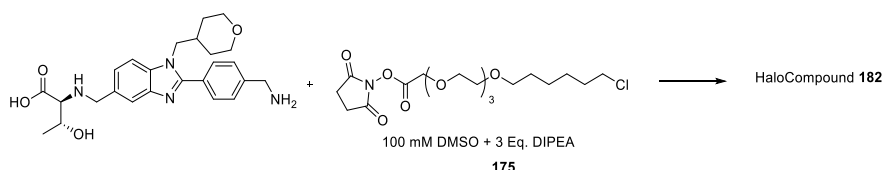
**LCMS** (Method B) (ES +ve) Product  $m/z$  534.1 (M + H)<sup>+</sup> Rt 0.84 min (54% conversion), SM not observed.

HaloCompound **181**, Well G10, derived from *N*-benzoyl-*N*-(2-(cyclohexylamino)ethyl)benzamide



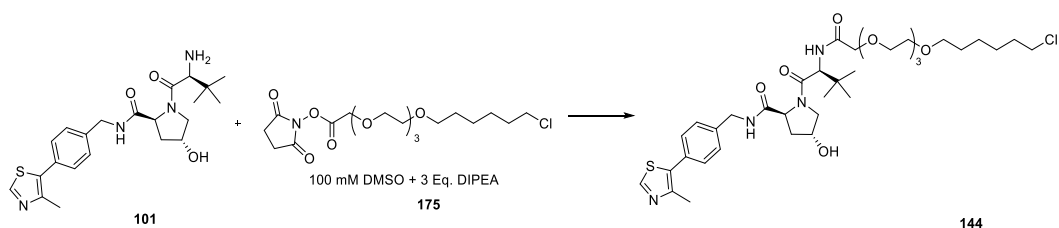
**LCMS** (Method B) (ES +ve) Product  $m/z$  659.25 (M + H)<sup>+</sup> Not found (0% conversion), SM  $m/z$  350.2 (M + H)<sup>+</sup> Rt 1.06 min (85% remaining).

HaloCompound **182**, Well M13, derived from ((2-(4-(aminomethyl)phenyl)-1-((tetrahydro-2H-pyran-4-yl)methyl)-1H-benzo[d]imidazol-5-yl)methyl)-L-threonine



**LCMS** (Method B) (ES +ve) Product  $m/z$  761.4 (M + H)<sup>+</sup> Rt 0.74 min (79% conversion), SM  $m/z$  452.2 (M + H)<sup>+</sup> Rt 0.36 min (11% remaining).

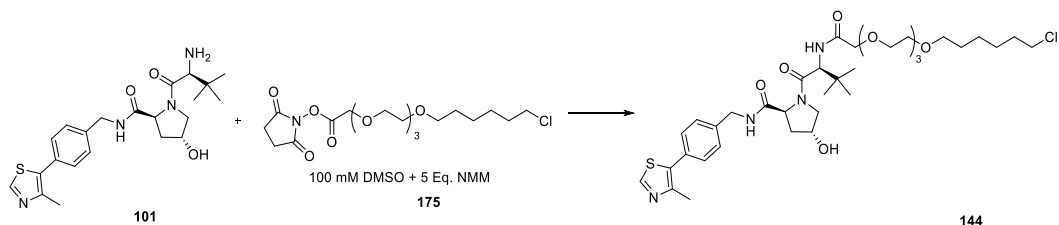
VHL HaloPROTAC **144**, Well A – P 18, derived from (2*S*,4*R*)-1-((*S*)-2-amino-3,3-dimethylbutanoyl)-4-hydroxy-*N*-(4-(4-methylthiazol-5-yl)benzyl)pyrrolidine-2-carboxamide  
**101**



Example B18 **LCMS** (Method B) (ES +ve) Product  $m/z$  739.4 (M + H)<sup>+</sup> Rt 1.06 min (3% conversion), SM  $m/z$  431.1 (M + H)<sup>+</sup> Rt 0.57 min (90% remaining).

Full LCMS analysis can be found in **Supplementary Table 1**.

Experiments featured in **Scheme 21**, synthesis of VHL recruiting HaloPROTAC **144**.



Reactions in **Scheme 21** were performed using **GP1** using **SS1** and **SS3**, modified as only one well was used. Reactions were performed in Labcyte ECHO® Microplates. After reaction time of 16 h, plates prepared for analysis using **GP5**.

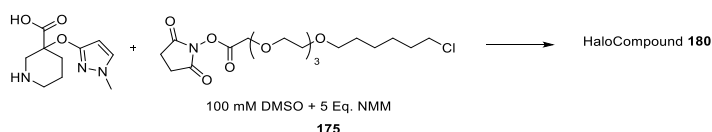
**LCMS** (Method B) (ES +ve) Product  $m/z$  739.3 (M + H)<sup>+</sup> Rt 1.14 min (80% conversion), SM  $m/z$  431.1 (M + H)<sup>+</sup> Rt 0.81 min (20% remaining).

### Optimisation Set Synthesis - NMM

Reactions in **Figure 127** were performed using **GP2** with **SS3**. Reactions were performed in Labcyte ECHO® Microplates. After reaction time of 16 h, plates prepared for analysis using **GP5**. Plates were dispensed into daughter plates by ECHO® acoustic dispensing (200 nL for 10 μM final test concentration, 20 nL for 1 μM final test concentration) and were evaluated in the biological assay (described in next section).

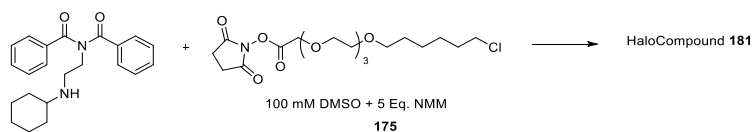
Example Analysis from **Figure 127**:

HaloCompound **180**, Well C11, derived from: 3-((1-methyl-1*H*-pyrazol-3-yl)oxy)piperidine-3-carboxylic acid



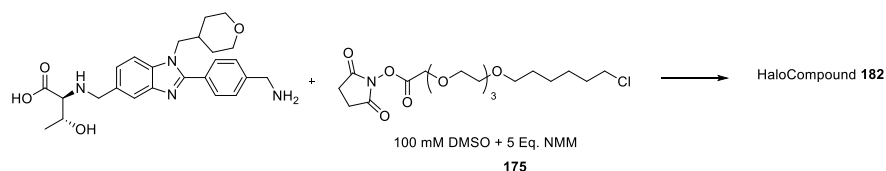
**LCMS** (Method A) (ES +ve) Product  $m/z$  534.1 (M + H)<sup>+</sup> Rt 0.84 min (64% conversion), SM not observed.

HaloCompound **181**, Well G10, derived from *N*-benzoyl-*N*-(2-(cyclohexylamino)ethyl)benzamide



**LCMS** (Method A) (ES +ve) Product  $m/z$  659.25 (M + H)<sup>+</sup> Not found (0% conversion), SM  $m/z$  350.2 (M + H)<sup>+</sup> Rt 1.06 min (100% remaining).

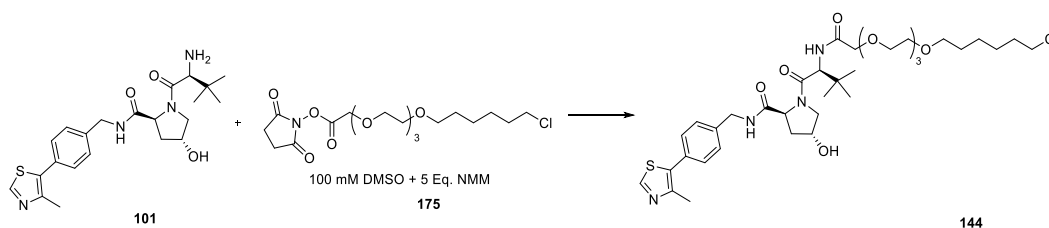
HaloCompound **182**, Well M13, derived from ((2-(4-(aminomethyl)phenyl)-1-((tetrahydro-2*H*-pyran-4-yl)methyl)-1*H*-benzo[*d*]imidazol-5-yl)methyl)-*L*-threonine



**LCMS** (Method A) (ES +ve) Product  $m/z$  761.4 (M + H)<sup>+</sup> Rt 0.74 min (83% conversion), SM not observed.

VHL HaloPROTAC **144** Well A – P 18, derived from (2*S*,4*R*)-1-((*S*)-2-amino-3,3-dimethylbutanoyl)-4-hydroxy-*N*-(4-(4-methylthiazol-5-yl)benzyl)pyrrolidine-2-carboxamide

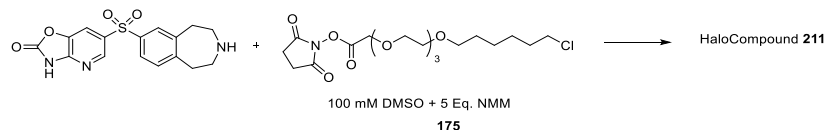
**101**



Example B18 **LCMS** (Method A) (ES +ve) Product  $m/z$  739.4 (M + H)<sup>+</sup> Rt 1.06 min (83% conversion), SM  $m/z$  431.1 (M + H)<sup>+</sup> Rt 0.57 min (17% remaining).

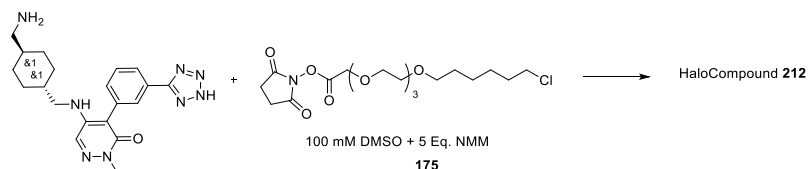
Analysis from the potential hit compounds, identified in the GFP degradation assay, are demonstrated in **Figure 148**:

HaloCompound **211**, Well P7, Derived from: 6-((2,3,4,5-tetrahydro-1*H*-benzo[*d*]azepin-7-yl)sulfonyl)oxazolo[4,5-*b*]pyridin-2(3*H*)-one



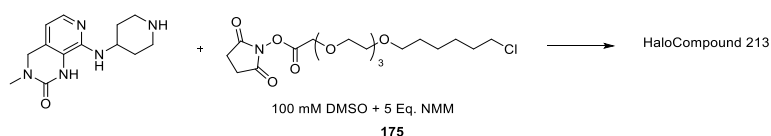
**LCMS** (Method A) (ES +ve) Product  $m/z$  652.2 (M - H)<sup>+</sup> Rt 1.02 min (72% conversion), SM  $m/z$  344.1 (M - H)<sup>+</sup> Rt 0.54 min (14% remaining). Di-adduct not observed.

HaloCompound **212**, Well C1, Derived from: rac-4-(3-(2*H*-tetrazol-5-yl)phenyl)-5-(((1*r*,4*r*)-4-(aminomethyl)cyclohexyl)methyl)amino)-2-methylpyridazin-3(2*H*)-one



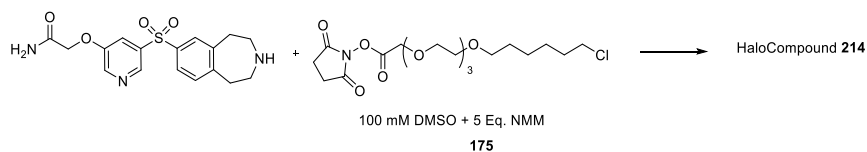
**LCMS** (Method A) (ES +ve) Product  $m/z$  703.3 (M + H)<sup>+</sup> Rt 1.01 min (93% conversion). SM and di-adduct not observed.

HaloCompound **213**, Well N12, Derived from: 3-methyl-8-(piperidin-4-ylamino)-3,4-dihydropyrido[3,4-*d*]pyrimidin-2(1*H*)-one



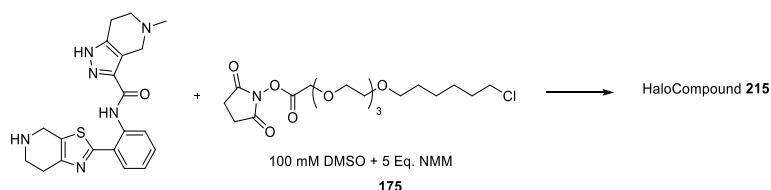
**LCMS** (Method A) (ES +ve) Product  $m/z$  570.1 (M + H)<sup>+</sup> Rt 0.73 min (70% conversion). SM and di-adduct not observed.

HaloCompound **214**, Well J2, Derived from: 2-((5-((2,3,4,5-tetrahydro-1*H*-benzo[*d*]azepin-7-yl)sulfonyl)pyridin-3-yl)oxy)acetamide



**LCMS** (Method A) (ES +ve) Product  $m/z$  670.2 (M + H)<sup>+</sup> Rt 0.95 min (91% conversion). SM  $m/z$  362.1 (M + H)<sup>+</sup> Rt 0.99 min (4% remaining). Di-adduct not observed.

HaloCompound **215**, Well C5, Derived from: 5-methyl-*N*-(2-(4,5,6,7-tetrahydrothiazolo[5,4-*c*]pyridin-2-yl)phenyl)-4,5,6,7-tetrahydro-1*H*-pyrazolo[4,3-*c*]pyridine-3-carboxamide.

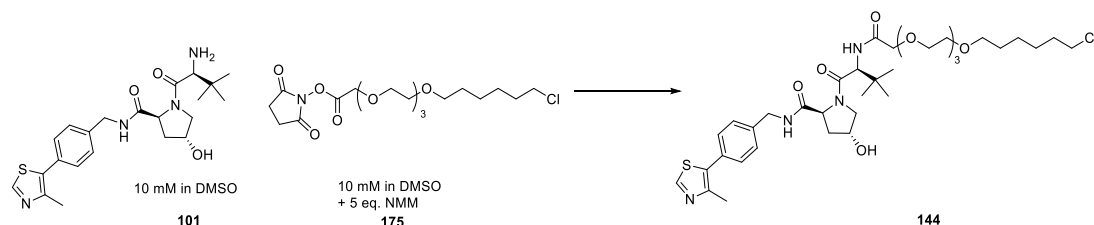


**LCMS** (Method A) (ES +ve) Product  $m/z$  703.3 (M + H)<sup>+</sup> Rt 0.87 min (100% conversion).

Full LCMS analysis can be found in **Supplementary Table 2**.

### **Further High-Throughput Chemistry Optimisation**

Experiments featured in **Figure 134**, synthesis of VHL recruiting HaloPROTAC **144** using the Mosquito liquid handling robot.



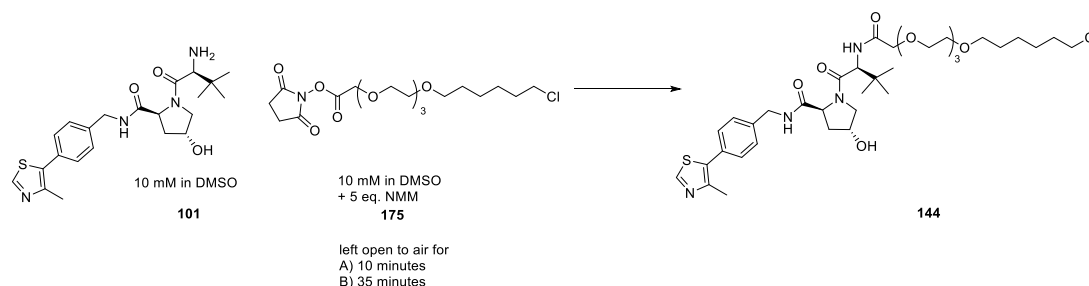
Reactions in **Figure 134** were performed using the TTP Labtech Mosquito® HTS liquid handling robot inside a fumehood.

Two 384-well source plates (Greiner Bio-One Microplates) were created containing **SS1** (every well identical 25  $\mu$ L, 10 mM) and in a separate plate **SS3** (every well identical 25  $\mu$ L, 10 mM). Dosing of **SS1** and **SS3** into their respective 384-well source plates was conducted using **GP1**. Dosing of reaction components into the 384-well reaction plate (Greiner Bio-One Microplates) was accomplished in a fumehood using the Mosquito® with no special modifications and using the TTP software in a copy function of one plate dispense from the source plate to each well of the 384 well plate of **SS1** ( $10 \times 1 \mu$ L (10 mM)) into the reaction plate.

After dosing of this component then the copy function was used in an analogous manner for **SS3** ( $10 \times 1 \mu$ L (10 mM)) into the reaction plate. Upon dosing, the 384-well plates were covered by a Corning CoStar® universal lid. The plates were centrifuged at 400G for 15 seconds. After reaction time of 16 h, plates prepared for analysis using **GP5**.

Example B18 **LCMS** (Method A) (ES +ve) Product  $m/z$  739.3 (M + H)<sup>+</sup> Rt 1.05 min (51% conversion).

Experiments featured in **Figure 135**, synthesis of VHL recruiting HaloPROTAC **144** featuring time dependence.

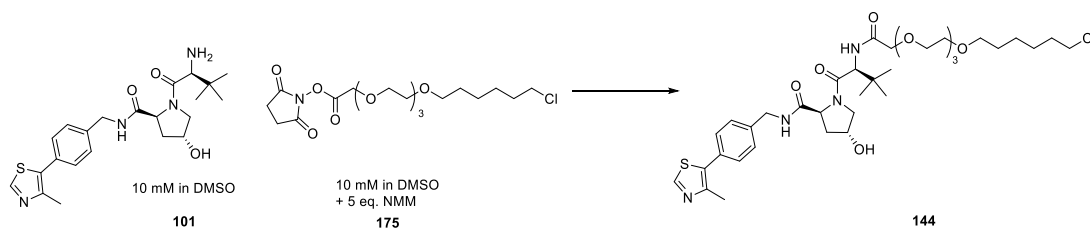


Reactions in **Figure 135** were performed using **GP1** with **SS1** and **SS3**, with modification of dispensing **SS3** from reservoirs into plates after A) T = 10 minutes and B) T = 35 minutes. Reactions were performed in Greiner Bio-One microplates. After reaction time of 16 h, plates prepared for analysis using **GP5**.

A) Example A18 **LCMS** (Method A) (ES +ve) Product  $m/z$  739.3 (M + H)<sup>+</sup> Rt 1.05 min (39% conversion).

B) Example B18 **LCMS** (Method A) (ES +ve) Product  $m/z$  739.3 (M + H)<sup>+</sup> Rt 1.05 min (11% conversion).

Experiments featured in **Figure 136**, synthesis of VHL recruiting HaloPROTAC **144**.

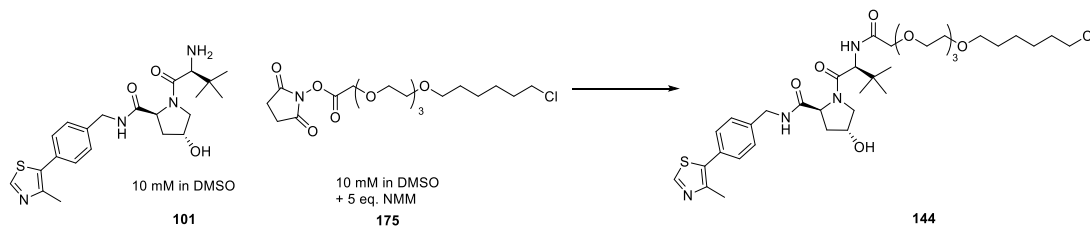


- A) Reactions in **Figure 136** were performed using **GP1** with **SS1** and **SS3**. Reactions were performed in Greiner Bio-One microplates. After reaction time of 16 h, plates prepared for analysis using **GP5**. (Fumehood velocity measured at 0.8 m/s).
- B) Reactions in **Figure 136** were performed using **GP1** with **SS1** and **SS3**. Reactions were performed in Greiner Bio-One microplates. After reaction time of 16 h, plates prepared for analysis using **GP5**. (Fumehood velocity measured at 1.4 m/s).

A) Example B18 **LCMS** (Method A) (ES +ve) Product  $m/z$  739.3 (M + H)<sup>+</sup> Rt 1.04 min (74% conversion).

B) Example B18 **LCMS** (Method A) (ES +ve) Product  $m/z$  739.3 (M + H)<sup>+</sup> Rt 1.05 min (59% conversion).

Experiments featured in **Figure 138**, synthesis of VHL recruiting HaloPROTAC **144** in a fumehood versus a glovebox.

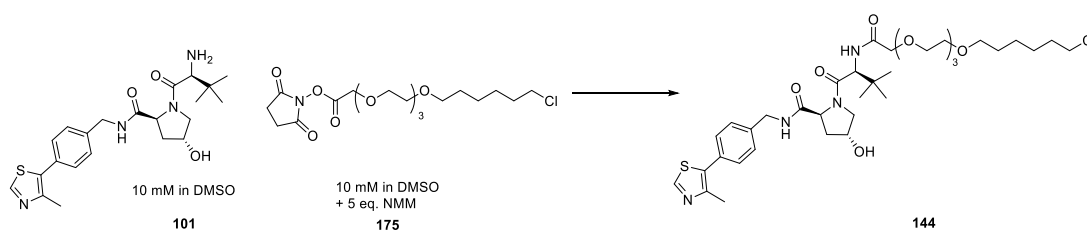


- A) Reactions in **Figure 138** were performed using **GP1** with **SS1** and **SS3** modified as no final centrifugal step and left to stand in a fumehood at rt for 16 h and not on the vibration plate. Reactions were performed in Greiner Bio-One microplates. After reaction time of 16 h, plates prepared for analysis using **GP5**.
- B) Reactions in **Figure 138** were performed using **GP3** with **SS1** and **SS3**. Reactions were performed in Greiner Bio-One microplates. After reaction time of 16 h, plates prepared for analysis using **GP5**.

A) Example B18 **LCMS** (Method A) (ES +ve) Product  $m/z$  739.3 (M + H)<sup>+</sup> Rt 1.06 min (66% conversion).

B) Example B18 **LCMS** (Method A) (ES +ve) Product  $m/z$  739.3 (M + H)<sup>+</sup> Rt 1.06 min (79% conversion).

Experiments featured in **Scheme 22**, synthesis of VHL recruiting HaloPROTAC **144** in a glovebox with time dependence.



Reactions in **Scheme 22** were performed using **GP3** with **SS1** and **SS3** with modification of dispensing **SS3** from reservoirs into plates after A) T = 10 minutes and B) T = 35 minutes. Reactions were performed in Greiner Bio-One microplates. After reaction time of 16 h, plates prepared for analysis using **GP5**.

A) Example A6 **LCMS** (Method B) (ES +ve) Product  $m/z$  739.3 (M + H)<sup>+</sup> Rt 1.14 min (83% conversion), SM  $m/z$  431.1 (M + H)<sup>+</sup> Rt 0.79 min (12% remaining).

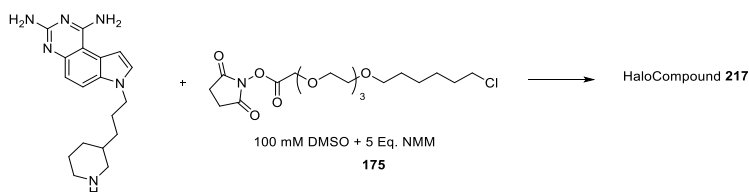
B) Example B6 **LCMS** (Method B) (ES +ve) Product  $m/z$  739.3 (M + H)<sup>+</sup> Rt 1.14 min (89% conversion), SM  $m/z$  431.1 (M + H)<sup>+</sup> Rt 0.79 min (9% remaining).

### Validation Set Synthesis

Reactions in **Figure 139** were performed using **GP4** with **SS4**. Reactions were performed in Labcyte ECHO® Microplates. After reaction time of 16 h, plates were then diluted to final concentration of 2.5 mM with DMSO (20  $\mu$ L in every well) using a Matrix WellMate™ microplate dispenser (all plates were placed in a stacker unit feeding into the dispenser). The plate resealed using a heat sealer and PFA seal and were then analysed by LCMS. Plates were dispensed into daughter plates by ECHO® acoustic dispensing (200 nL for 10  $\mu$ M final test concentration, 20 nL for 1  $\mu$ M final test concentration) and were evaluated in the biological assay (described in next section).

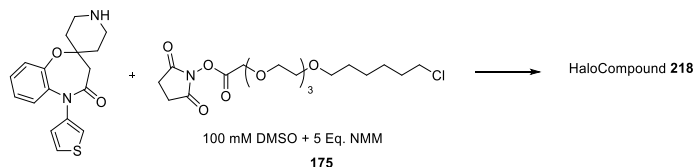
Analysis from the potential hit compounds, identified in the GFP degradation assay, are demonstrated in **Figure 155**:

HaloCompound **217**, Plate 3, well D9, derived from 7-(3-(piperidin-3-yl)propyl)-7H-pyrrolo[3,2-f]quinazoline-1,3-diamine



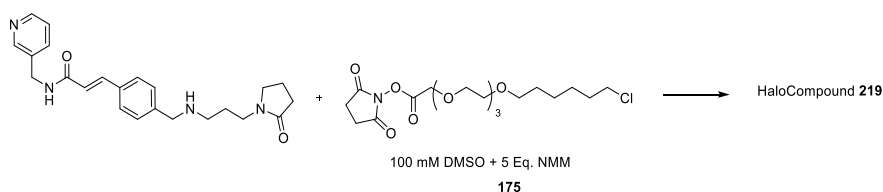
**LCMS** (Method B) (ES +ve) Product  $m/z$  633.4 (M + H)<sup>+</sup> Rt 0.85 min (100% conversion). SM not observed.

HaloCompound **218**, Plate 5, well O1, derived from 5-(thiophen-3-yl)-3*H*-spiro[benzo[*b*][1,4]oxazepine-2,4'-piperidin]-4(5*H*)-one



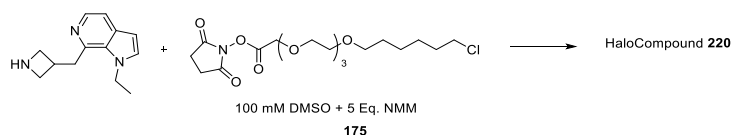
**LCMS** (Method B) (ES +ve) Product  $m/z$  623.3 (M + H)<sup>+</sup> Rt 1.18min (100% conversion). SM not observed.

HaloCompound **219**, Plate 6, well B7, derived from (*E*)-3-(4-(((3-(2-oxopyrrolidin-1-yl)propyl)amino)methyl)phenyl)-*N*-(pyridin-3-ylmethyl)acrylamide



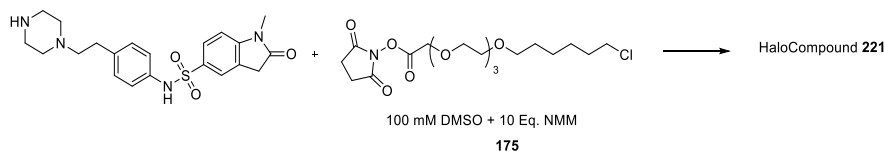
**LCMS** (Method B) (ES +ve) Product  $m/z$  700.3 (M + H)<sup>+</sup> Rt 0.78 min (42% conversion).

HaloCompound **220**, Plate 2, well H17, derived from 7-(azetidin-3-ylmethyl)-1-ethyl-1*H*-pyrrolo[2,3-*c*]pyridine



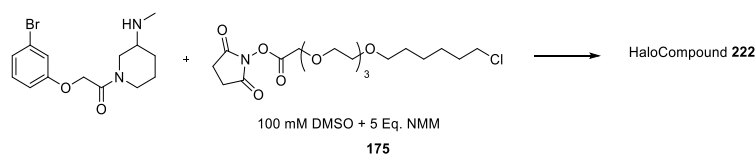
**LCMS** (Method B) (ES +ve) Product  $m/z$  524.3 (M + H)<sup>+</sup> Rt 0.80 min (100% conversion).

HaloCompound **221**, Plate 4, well B11, 1-methyl-2-oxo-*N*-(4-(2-(piperazin-1-yl)ethyl)phenyl)indoline-5-sulfonamide



**LCMS** (Method B) (ES +ve) Product  $m/z$  723.3 (M + H)<sup>+</sup> Rt 0.81 min (91% conversion). SM and di-adduct not observed.

HaloCompound **222**, Plate 2, well F3, derived from 2-(3-bromophenoxy)-1-(3-(methylamino)piperidin-1-yl)ethan-1-one



**LCMS** (Method B) (ES +ve) Product  $m/z$  635.2 (M + H)<sup>+</sup> Rt 1.17 min (89% conversion), SM  $m/z$  327.1 (M + H)<sup>+</sup> Rt 0.61 min (11% remaining).

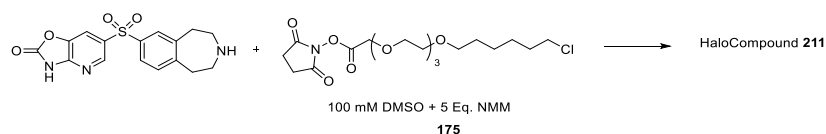
Full LCMS analysis can be found in **Supplementary Tables 4–12**.

### Hit Resynthesis from the Optimisation set

Reactions in **Figure 149** were performed using **GP2** with **SS3**. Reactions were performed in Labcyte ECHO® Microplates. After reaction time of 16 h, plates prepared for analysis using **GP5**.

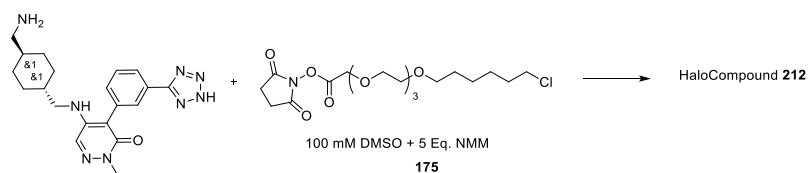
Analysis from **Figure 149**:

HaloCompound **211** resynthesis, Derived from: 6-((2,3,4,5-tetrahydro-1H-benzo[d]azepin-7-yl)sulfonyl)oxazolo[4,5-b]pyridin-2(3H)-one



**LCMS** (Method B) (ES +ve) Product  $m/z$  652.2 (M - H)<sup>+</sup> Rt 0.86 min (62% conversion), SM  $m/z$  344.1 (M - H)<sup>+</sup> Rt 0.54 min (22% remaining). Di-adduct not observed.

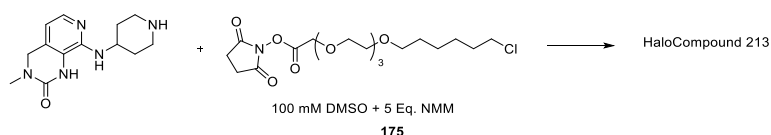
HaloCompound **212** resynthesis, Derived from: rac-4-(3-(2H-tetrazol-5-yl)phenyl)-5-((((1*r*,4*r*)-4-(aminomethyl)cyclohexyl)methyl)amino)-2-methylpyridazin-3(2H)-one



**LCMS** (Method B) (ES +ve) Product  $m/z$  703.3 (M + H)<sup>+</sup> Rt 0.87 min (>95% conversion). SM and di-adduct not observed.

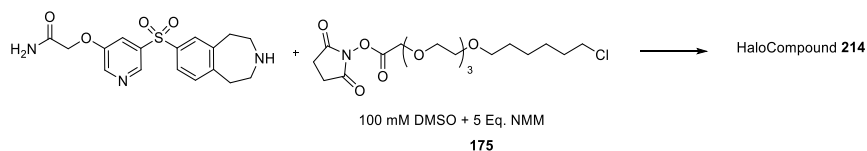
HaloCompound **213** resynthesis, Derived from: 3-methyl-8-(piperidin-4-ylamino)-3,4-dihydropyrido[3,4-d]pyrimidin-2(1H)-one

Confidential – Do Not Copy



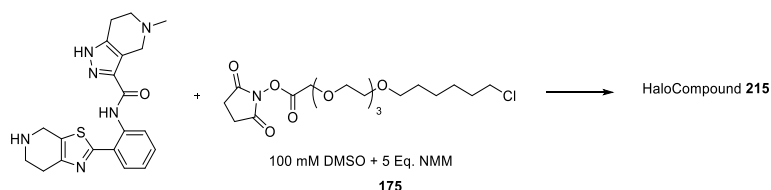
**LCMS** (Method B) (ES +ve) Product  $m/z$  570.1 (M + H)<sup>+</sup> Rt 1.01 min (80% conversion). SM and di-adduct not observed.

HaloCompound **214** resynthesis, Derived from: 2-((5-((2,3,4,5-tetrahydro-1*H*-benzo[*d*]azepin-7-yl)sulfonyl)pyridin-3-yl)oxy)acetamide



**LCMS** (Method B) (ES +ve) Product  $m/z$  670.2 (M + H)<sup>+</sup> Rt 1.03 min (>95% conversion). SM and di-adduct not observed.

HaloCompound **215** resynthesis, Derived from: 5-methyl-*N*-(2-(4,5,6,7-tetrahydrothiazolo[5,4-*c*]pyridin-2-yl)phenyl)-4,5,6,7-tetrahydro-1*H*-pyrazolo[4,3-*c*]pyridine-3-carboxamide.



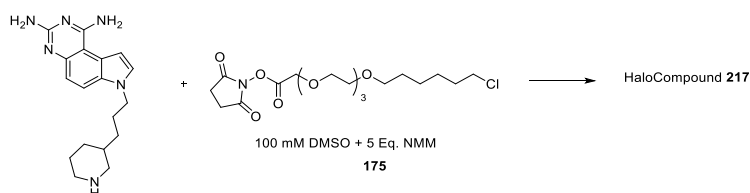
**LCMS** (Method B) (ES +ve) Product  $m/z$  703.3 (M + H)<sup>+</sup> Rt 1.27 min (88% conversion), SM  $m/z$  395.1 (M + H)<sup>+</sup> Rt 0.96 min (6% remaining), Di-adduct  $m/z$  507.2 ((M + 2H)/2)<sup>+</sup> Rt 1.58 min (4% remaining).

### Hit resynthesis from the Validation Set

Reactions in **Figure 156** were performed using **GP2** and **SS4**. Reactions were performed in Labcyte ECHO® Microplates. After reaction time of 16 h, plates prepared for analysis using **GP5**. Plates were dispensed into daughter plates and were evaluated in the biological assay (described in next section).

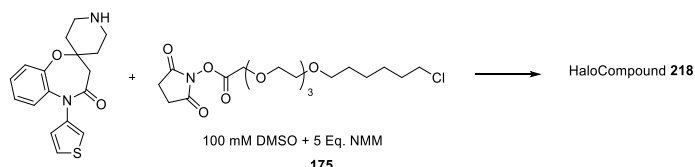
Analysis from **Figure 156**:

HaloCompound **217** resynthesis, derived from 7-(3-(piperidin-3-yl)propyl)-7*H*-pyrrolo[3,2-*f*]quinazoline-1,3-diamine



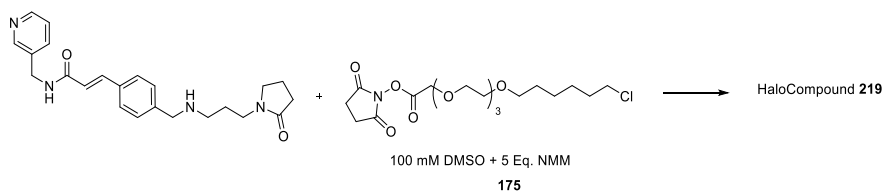
**LCMS** (Method B) (ES +ve) Product  $m/z$  633.2 (M + H)<sup>+</sup> Rt 1.08 min (98% conversion).

HaloCompound **218** resynthesis, derived from 5-(thiophen-3-yl)-3*H*-spiro[benzo[*b*][1,4]oxazepine-2,4'-piperidin]-4(5*H*)-one



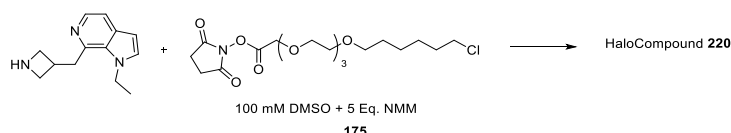
**LCMS** (Method B) (ES +ve) Product  $m/z$  623.2 (M + H)<sup>+</sup> Rt 1.27 min (98% conversion).

HaloCompound **219** resynthesis, derived from (*E*)-3-(4-(((3-(2-oxopyrrolidin-1-yl)propyl)amino)methyl)phenyl)-*N*-(pyridin-3-ylmethyl)acrylamide



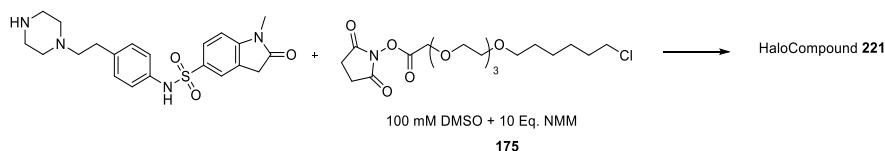
**LCMS** (Method B) (ES +ve) Product  $m/z$  701.3 (M + H)<sup>+</sup> Rt 1.01 min (34% conversion), SM  $m/z$  393.1 (M + H)<sup>+</sup> Rt 0.70 min (47% remaining).

HaloCompound **220** resynthesis, derived from 7-(azetidin-3-ylmethyl)-1-ethyl-1*H*-pyrrolo[2,3-*c*]pyridine



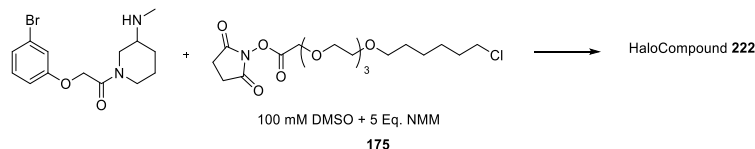
**LCMS** (Method B) (ES +ve) Product  $m/z$  524.2 (M + H)<sup>+</sup> Rt 1.11 min (100% conversion).

HaloCompound **221** resynthesis, 1-methyl-2-oxo-*N*-(4-(2-(piperazin-1-yl)ethyl)phenyl)indoline-5-sulfonamide



LCMS (Method B) (ES +ve) Product  $m/z$  723.3 (M + H)<sup>+</sup> Rt 1.06 min (83% conversion), SM and di-adduct not observed.

HaloCompound **222** resynthesis, derived from 2-(3-bromophenoxy)-1-(3-(methylamino)piperidin-1-yl)ethan-1-one



LCMS (Method B) (ES +ve) Product  $m/z$  636.0 (M + H)<sup>+</sup> Rt 1.25 min (59% pure), SM  $m/z$  328.0 (M + H)<sup>+</sup> Rt 0.90 min (39% remaining).

All other examples of HaloCompounds synthesised can be found in the **Supplementary Tables**.

#### 9.4 Supplementary Figures

**Supplementary Figure 1:** LCMS conversion to desired product of the nine reaction 384-well plates containing 2934 unique amines (known as the 3000-amine set). White wells denote where DMSO was used and no reaction occurring (column 6 in every plate and partial wells in other plates) and blue wells containing the positive control **SS1** “VHL amine **101**”.

Analysis shown with % conversion in conversion key: dark green more than 70%, light green 50–70%, amber 20–50% and red less than 20%.

Total number of wells containing good conversion versus poor conversion for each plate shown in table below plate map.

		Amines (Plate 1)																								
		1	2	3	4	5	6	7	8	9	10	11	12	13	14	15	16	17	18	19	20	21	22	23	24	
Amines (Plate 1)	A	0	100	100	25	100		100	100	0	100	0	0	0	100	100	100	95	94	0	89	97	100	100	0	
	B	27	58	100	100	100		26	100	7	100	0	0	96	100	100	1	90	97	64	0	0	100	0	0	
	C	84	5	33	23	5		0	100	93	100	100	100	0	16	56	29	83	97	100	80	0	52	100	100	
	D	0	100	100	0	0		44	93	0	100	96	94	96	100	68	0	100	85	0	0	0	63	100	100	
	E	0	95	100	0	18		97	0	100	100	19	51	100	77	0	6	0	93	0	100	91	89	100	0	
	F	0	100	100	34	0		0	88	0	100	0	47	100	100	0	74	62	96	76	0	100	0	100	0	
	G	0	100	0	100	0		100	100	53	0	100	100	100	76	100	100	98	96	100	0	96	45	0	100	
	H	24	37	0	0	0		0	0	0	9	0	0	0	0	97	0	0	100	95	0	81	100	100	92	100
	I	100	93	0	100	0		17	0	94	0	0	100	0	100	0	60	83	26	93	85	95	0	100	100	16
	J	0	0	100	0	0		0	100	0	100	54	100	0	91	72	0	95	95	0	100	0	43	100	0	0
	K	0	100	100	100	0		0	0	0	12	100	76	0	0	13	100	100	95	55	100	27	100	0	67	0
	L	100	100	100	92	17		0	0	0	0	92	0	100	0	12	39	0	97	100	54	70	100	0	77	0
	M	100	100	81	92	0		56	100	100	0	0	100	77	100	42	0	100	95	0	100	100	0	100	100	0
	N	100	100	0	100	100		59	0	0	100	54	100	0	100	100	83	100	95	100	0	90	100	77	0	0
	O	0	100	83	100	100		100	13	0	38	0	100	100	11	42	100	0	96	94	0	0	100	59	0	0
	P	85	100	0	100	0		100	100	0	100	100	94	100	18	100	52	100	96	90	95	0	100	100	100	0

Number of reactions with >50% conversion	Number of reactions with <20% conversion
216	133

Conversion Key
<20%
20-50%
50-70%
70-100%

		Amines (Plate 2)																							
		1	2	3	4	5	6	7	8	9	10	11	12	13	14	15	16	17	18	19	20	21	22	23	24
Amines (Plate 2)	A	82	94	80	51	100		100	100	100	100	94	100	0	0	100	95	100	100	100		100	100	0	98
	B	0	100	93	0	84		88	100	55	88	100	40	100	100	47	100	56	100	12	0	0	100	0	0
	C	0	100	100	68	0		85	100	98	100	100	100	100	100	100	100	100	100	100	0	100	100	100	35
	D	68	100	100	95	0		25	100	100	39	0	100	48	100	0	100	87	100	100	0	100	97	100	100
	E	95	100	31	93	56		100	94	100	100	100	0	95	92	100	100	100	100	23		82	30	14	100
	F	100	100	89	100	100		100	21	100	100	0	0	0	0	100	100	100	67	100	94	36	46	54	0
	G	0	100	0	100	93		100	71	0	100	100	100	100	100	0	0	100	100	100		64	100	100	100
	H	100	89	48	100	0		100	97	100	100	0	0	0	0	0	100	100	100	100	83	100	100	0	91
	I	100	0	43	100	0		100	4	100	100	100	100	88	100	100	62	62	100	9		93	53	100	100
	J	100	37	100	100	0		100	27	100	79	0	100	100	100	98	100	89	100	0	79	14	100	63	0
	K	100	78	100	52	100		100	100	100	0	100	84	31	91	82	93	100	100	100	100	100	100	97	50
	L	100	100	100	100	100		92	0	92	0	0	100	0	97	100	100	100	100	100	0	100	100	100	100
	M	100	6	100	90	100		100	100	100	100	0	100	0	29	0	72	98	100	100	100	100	100	85	36
	N	100	0	56	100	18		100	100	100	0	0	100	68	0	100	0	100	100	88	100	0	100	100	100
	O	100	76	0	0	20		0	89	94	81	52	100	86	63	100	90	100	100	100	57	0	30	100	0
	P	93	100	100	100	6		91	87	81	100	100	100	100	100	100	100	100	100	100	90	0	100	100	56

Number of reactions with >50% conversion	Number of reactions with <20% conversion
275	69

Conversion Key
<20%
20-50%
50-70%
70-100%

		Amines (Plate 3)																							
		1	2	3	4	5	6	7	8	9	10	11	12	13	14	15	16	17	18	19	20	21	22	23	24
Amines (Plate 3)	A	100	90	0	100	86		100	46	68	100	100	100	0	90	100	100	96	100	86	0	100	100	100	70
	B	87	6	0	100	37		84	100	100	0	100	100	8	15	57	85	84	100	81	0	0	38	0	0
	C	84	100	91	100	100		0	100	0	14	88	100	100	0	100	2	0	100	0	100	20	0	86	100
	D	100	0	0	76	100		100	71	100	0	0	97	0	100	100	100	0	100	18	0	100	100	100	58
	E	100	100	0	100	8		52	98	100	100	100	100	100	82	84	100	100	100	100	100	88	34	0	100
	F	100	100	100	100	89		81	48	100	100	91	100	0	100	0	0	0	100	100	100	100	80	0	0
	G	0	0	84	0	100		100	82	76	100	100	100	100	33	0	0	100	100	0	39	0	37	96	100
	H	0	100	100	78	58		100	100	0	40	25	100	0	97	60	68	9	100	0	0	100	100	34	
	I	0	100	100	27	100		0	0	100	100	78	45	100	100	100	85	0	100	52	92	0	82	100	
	J	89	0	0	100	0		0	100	44	100	100	93	0	100	92	100	100	100	0	0	93	55	83	
	K	0	0	0	17	77		100	100	60	100	0	100	89	100	0	44	7	100	0	69	36	100	100	
	L	11	100	100	76	100		100	0	32	100	0	100	0	0	79	100	50	100	0	14	0	100	0	
	M	0	100	100	0	0		100	100	100	100	47	100	100	13	28	100	100	28	0	100	100	0		
	N	100	100	100	100	0		95	30	80	100	70	46	0	31	100	100	48	100	46	0	19	100	0	
	O	0	47	100	82	0		100	100	0	100	15	100	100	0	100	100	0	100	94	100	96	95	100	
	P	0	100	0	0	87		0	12	52	100	85	26	0	0	100	100	0	100	100	100	100	37	0	

Number of reactions with >50% conversion	Number of reactions with <20% conversion
224	106

Conversion Key
<20%
20-50%
50-70%
70-100%

		Amines (Plate 4)																							
		1	2	3	4	5	6	7	8	9	10	11	12	13	14	15	16	17	18	19	20	21	22	23	24
Amines (Plate 4)	A	60	100	0	91	0		54	40	0	83	0	40	100	100	72	0	100	100	100	100	0	85	28	0
	B	0	100	73	0	100		95	100	100	100	91	0	100	100	100	0	0	100	0	36	100	100	39	0
	C	0	91	15	100	100		0	36	100	0	85	0	100	0	0	0	0	100	51	0	23	87	84	0
	D	93	0	100	70	95		13	0	91	100	100	100	60	0	100	0	0	100	30	56	100	85	100	100
	E	100	0	100	0	100		46	0	100	63	100	79	0	93	0	0	11	100	0	63	100	22	60	0
	F	81	9	100	0	0		100	0	50	61	0	0	27	88	100	0	57	100	56	0	0	100	100	0
	G	52	0	100	0	100		0	100	100	10	0	0	100	100	0	15	100	100	55	100	90	100	60	0
	H	0	100	80	0	94		100	100	100	0	0	36	0	0	68	0	100	100	0	100	57	0	0	0
	I	0	100	100	100	0		100	0	0	100	0	25	100	83	100	100	66	100	100	0	89	100	0	100
	J	95	0	91	0	95		82	0	0	0	0	28	0	0	0	0	89	100	96	100	100	0	0	0
	K	0	0	100	43	100		100	4	0	0	0	0	0	100	0	45	100	23	100	100	100	100	0	96
	L	0	0	0	0	100		0	0	100	0	0	100	0	0	100	0	88	100	0	82	100	0	0	100
	M	0	53	84	0	52		100	100	0	100	0	0	100	48	100	28	100	100	100	0	84	100	0	67
	N	0	0	0	86	96		0	90	44	95	0	64	0	0	0	100	100	100	0	100	100	0	0	93
	O	0	74	0	0	90		73	85	25	100	91	12	0	100	72	0	93	100	0	0	100	100	100	0
	P	100	0	100	0	100		100	0	39	63	87	50	100	0	0	89	100	100	0	0	100	0	0	19

Number of reactions with >50% conversion	Number of reactions with <20% conversion
194	150

Conversion Key
<20%
20-50%
50-70%
70-100%

		Amines (Plate 5)																								
		1	2	3	4	5	6	7	8	9	10	11	12	13	14	15	16	17	18	19	20	21	22	23	24	
Amines (Plate 5)	A	100	100	0	100	100		100	0	0	0	92	16	100	100	100		11	100	100	100	100	100	0	93	
	B	100	100	0	45	100		100	0	0	0	100	100	100	100	7	40	60	100	100	58	100	0	0	21	
	C	0	100	8	0	0		0	100	97	0	100	100	86	0	100		0	100	0	100	61	0	96	0	
	D	0	84	100	89	100		0	100	0	100	60	100	0	0	0	25	100	100	70	0	36	30	100	0	
	E	100	91	100	0	79		100	90	92	96	92	97	100	100	95		100	100	97	100	0	0	100	100	
	F	37	0	21	100	100		100	100	5	0	100	100	0	100	96	100	0	100	100	0	6	100	100	0	
	G	100	100	0	41	100		100	100	100	100	100	54	100	100	100		0	100	0	0	100	0	100	0	
	H	92	85	46	100	0		0	100	0	100	100	13	100	0	97	100	100	100	100	100	100	100	100	100	
	I	100	91	39	100	100		100	0	100	100	25	54	100	100	100		100	100	0	0	0	0	100	0	
	J	32	100	0	29	100		0	100	0	6	0	0	100	0	100	0	0	100	100	100	100	0	100	9	
	K	100	100	0	100	100		83	0	0	78	100	34	100	100	0		100	100	0	53	100	100	0	0	
	L	0	100	100	0	0		100	100	82	100	100	0	0	0	51	100	100	100	46	100	85	100	8	0	
	M	73	42	8	100	0		0	86	0	100	100	100	0	100	34	100	100	100	100	100	98	100	0	0	
	N	0	50	0	100	17		100	100	30	100	0	97	0	0	0	93	100	100	0	0	100	100	100	100	
	O	100	0	100	0	0		0	0	100	0	100	0	0	0	71	100	100	84	71	85	83	100	44	100	97
	P	100	100	100	94	100		100	100	100	88	100	0	100	0	40	100	0	100	0	0	100	13	0	0	

Number of reactions with >50% conversion	Number of reactions with <20% conversion
220	120

Conversion Key
<20%
20-50%
50-70%
70-100%

		Amines (Plate 6)																							
		1	2	3	4	5	6	7	8	9	10	11	12	13	14	15	16	17	18	19	20	21	22	23	24
Amines (Plate 6)	A	81	100	100	89	100		100	66	71	100	27	100	0	23	89	0	0	100	100	100	100	100	0	0
	B	0	9	100	33	0		100	0	100	0	0	0	100	100	100	0	78	100	0	0	0	100	0	100
	C	0	0	100	0	58		57	100	61	100	100	100	100	100	100	96	100	100	100	100	0	100	0	82
	D	92	0	100	100	93		62	100	100	100	100	0	100	100	100	90	100	100	7	100	0	0	68	
	E	100	100	0	60	100		100	100	100	91	100	66	100	100	0	70	100	100	100	30	100	100	97	100
	F	58	100	0	37	100		96	100	100	100	100	0	71	100	100	100	67	100	100	100	100	100	83	
	G	0	20	65	100	100		100	0	100	90	0	0	63	0	100	0	0	100	0	0	100	100	100	100
	H	100	100	0	100	0		81	100	73	72	100	0	65	88	100	0	70	100	100	100	60	73	100	100
	I	50	98	86	86	32		100	81	0	100	0	100	0	0	82	53	0	100	100	94	100	0	0	100
	J	48	69	34	56	100		0	0	87	100	98	100	0	0	100	96	100	100	0	100	100	91	100	100
	K	47	0	0	100	65		10	100	100	0	0	77	54	100	94	100	100	100	66	100	0	100	100	0
	L	0	87	100	46	0		100	100	0	0	0	68	100	0	93	100	100	100	100	100	71	90	100	0
	M	91	0	100	0	100		59	100	0	100	100	100	0	100	100	100	100	95	97	65	90	71	8	
	N	0	0	100	66	100		100	66	100	53	28	96	0	100	0	100	100	100	100	46	0	62	19	100
	O	87	100	100	100	63		100	22	100	58	100	100	99	68	0	100	95	100	100	100	100	86	0	100
	P	100	54	0	0	100		100	30	0	21	95	96	100	78	0	100	44	100	100	70	0	100	100	100

Number of reactions with >50% conversion	Number of reactions with <20% conversion
263	88

Conversion Key
<20%
20-50%
50-70%
70-100%

		Amines (Plate 7)																							
		1	2	3	4	5	6	7	8	9	10	11	12	13	14	15	16	17	18	19	20	21	22	23	24
Amines (Plate 7)	A	0	100	81	0	100		91	100	100	0	100	0	0	100	100	100	85	100	95	100	49	100	100	90
	B	34	97	7	0	64		100	100	100	96	100	97	100	96	35	100	94	100	100	0	100	100	55	0
	C	94	90	100	0	0		0	9	0	100	100	100	0	100	0	100	75	100	100	100	19	100	100	0
	D	0	100	100	15	100		100	100	87	100	100	87	100	100	100	55	100	100	100	78	100	0	96	
	E	66	100	0	0	0		66	100	22	0	100	0	0	79	0	88	0	100	0	81	0	0	72	
	F	88	0	100	0	100		61	0	25	72	100	41	100	100	100	13	90	100	0	0	100	100	100	
	G	100	100	100	81	72		0	100	89	97	100	100	0	100	100	0	100	100	0	100	93	100	100	
	H	0	0	100	59	100		0	100	89	73	15	0	94	54	100	93	100	100	100	18	63	31	0	
	I	86	100	100	54	82		0	100	87	0	45	100	100	100	0	91	100	100	0	100	100	100	100	
	J	47	100	100	100	0		0	15	81	0	54	100	95	89	0	100	100	100	100	64	100	100	93	
	K	100	100	100	100	15		0	36	95	100	100	100	100	100	0	44	100	100	100	94	100	53	100	
	L	100	100	100	94	0		100	100	0	100	100	0	100	97	100	0	91	100	0	100	12	0	0	
	M	100	100	5	84	93		100	96	92	100	82	0	100	45	100	100	0	100	100	57	83	100	0	
	N	20	0	100	0	37		100	91	84	100	53	100	74	100	100	0	0	100	0	100	40	100	100	
	O	100	0	100	100	100		100	100	100	100	100	100	0	0	100	52	100	100	0	100	100	0	95	
	P	100	9	59	12	100		100	100	100	100	100	100	100	100	93	52	100	100	94	100	100	100	100	

Number of reactions with >50% conversion	Number of reactions with <20% conversion
194	150

Conversion Key
<20%
20-50%
50-70%
70-100%

		Amines (Plate 8)																							
		1	2	3	4	5	6	7	8	9	10	11	12	13	14	15	16	17	18	19	20	21	22	23	24
Amines (Plate 8)	A	100	0	59	0	100		100	60	0	100	0	85	0	91	100	0	0	100	100	0	0	7	100	94
	B	100	100	95	100	31		42	53	100	0	11	48	100	100	97	0	0	100	30	100	100	100	69	0
	C	0	0	0	27	0		64	100	0	0	100	100	0	100	54	96	0	100	28	30	0	11	0	21
	D	20	100	100	0	92		38	0	0	0	0	0	100	0	100	91	100	100	0	100	88	100	47	87
	E	89	57	100	0	94		0	100	0	78	0	100	100	0	100	12	100	100	100	100	100	100	43	100
	F	84	100	100	100	100		44	12	0	23	68	25	87	100	94	25	100	100	100	10	0	100	100	0
	G	0	0	0	100	0		0	0	0	0	0	78	73	100	0	53	100	100	9	100	15	41	33	100
	H	78	0	81	100	6		100	0	100	0	0	0	100	100	100	0	0	100	100	96	97	100	100	0
	I	100	66	96	100	100		0	100	74	86	96	100	100	0	100	100	0	100	0	100	100	100	0	0
	J	11	86	100	100	100		100	0	100	99	100	0	95	70	91	100	100	100	100	100	100	97	100	52
	K	0	0	97	69	100		48	100	0	100	100	100	95	99	0	8	54	100	100	100	0	0	95	0
	L	18	100	37	100	62		100	10	53	100	0	89	0	32	0	100	100	100	7	100	0	100	0	100
	M	0	100	0	92	100		41	100	100	100	100	13	0	7	100	95	0	100	100	100	0	100	100	0
	N	0	100	0	100	100		0	0	100	35	34	100	0	100	100	93	100	100	62	100	0	0	0	100
	O	100	0	0	0	100		100	100	0	36	98	0	0	54	0	100	64	100	100	100	0	98	100	0
	P	79	0	0	100	0		90	100	0	70	0	61	27	100	100	0	0	100	100	100	60	0	100	0

Number of reactions with >50% conversion	Number of reactions with <20% conversion
247	125

Conversion Key
<20%
20-50%
50-70%
70-100%

		Amines (Plate 9)											
		1	2	3	4	5	6	7	8	9	10	11	12
Amines (Plate 9)	A	100	0	48	100	0		0	40	0	69	96	96
	B	22	96	0	0	0		0	100	0	100	0	97
	C	100	100	100	75	83		27	0	5	100	94	100
	D	100	18	0	0	0		100	100	90	0	83	100
	E	57	100	100	96	79		9	88	100	0	0	100
	F	0	23	100	30	100		5	84	0	0	75	100
	G	47	80	100	100	100		100	100	97	100	100	100
	H	100	4	100	0	100		100	29	83	100	88	98
	I	58	84	100	100	0		100	100	14	0		97
	J	0	19	0	100	31		0	100	0	100		100
	K	0	0	0	95	0		15	0	0	0		97
	L	35	100	100	5	43		100	80	100	100		97
	M	0	30	0	100	100		100	0	0	82		97
	N	0	100	0	100	100		0	0	51	100		97
	O	100	0	26	0	0		0	96	96	91		95
	P	0	0	0	0	0		0	39	0	88		89

Number of reactions with >50% conversion	Number of reactions with <20% conversion
92	62

Conversion Key
<20%
20-50%
50-70%
70-100%

## 9.5 Biological Experiments

### 9.5.1 Cell culture

Cell line	Media
THP-1	RPMI
HeLa GFP-HaloTag®	DMEM
A549	DMEM
K562	RPMI

All cells were cultured and supplemented by 2 mM Glutamax, 10% heat inactivated foetal bovine serum, 100 units/mL penicillin and 100 µg/mL streptomycin. They were grown at 37 °C with 5% CO<sub>2</sub>. All cell culture reagents were purchased from Thermofisher. Cells were passaged every 3-4 days, typically used 1:20 split ratio.

### 9.5.2 Compound preparation

All compounds were suspended in 100% dimethyl sulfoxide (DMSO, Sigma-Aldrich), aliquoted and stored at -20°C as 10 mM stock solutions. 3-fold or half log unit increment dilution series

in 100% DMSO in a polypropylene 96 well plate (1000× final concentration) were carried out. A 1 in 100 aqueous dilution from this in Fluorobrite DMEM basal medium without serum (ThermoFisher) gave an aqueous daughter plate (10× final concentration, 1% DMSO). 5 µL of the aqueous daughter plate was placed into the assay plate. Alternatively, compounds were obtained pre-dispensed in 100% DMSO in the assay plate dispensed by ECHO acoustic dispense (e.g. 200 nL per well for 10 µM test concentration, 20 nL per well for 1 µM test concentration, 100% DMSO).

The human biological samples were sourced ethically, and their research use was in accord with the terms of the informed consents under an IRB/EC approved protocol.

### **9.5.3 Cell lysis**

Cells were incubated with PROTACs at indicated time and concentrations. After incubation, cells were resuspended and collected in 15 mL falcon tubes. Wells were then washed once with PBS and washout added. Cells were centrifuged using a Heraeus™ Megafuge™ (400g for 5 min). Supernatants were discarded, and cell pellets were resuspended in 1 mL of PBS and transferred to Eppendorf. Cells were centrifuged once more (400g for 5 min), PBS was aspirated, and the cell pellets were resuspended in 50 µL of RIPA buffer (ThermoScientific) containing protease inhibitors (Roche) and 1% Triton-X 100. Cell lysates were incubated at 0 °C for 45 min and vortexed vigorously every 10 min. After centrifugation (16000g for 15 min) at 4 °C, supernatants were transferred and stored at -80°C until analysis.

### **9.5.4 Protein Concentration Measurement**

Total protein concentrations were assessed using the Pierce BCA Protein Assay Kit (ThermoScientific) following the manufacturer's instructions. Samples were diluted 1:10 and pipetted in triplicate. The absorbance was measured at 562 nm on a plate reader (Molecular Devices, SPECTRA max Plus, Biomax) using SoftMax Pro 5.2 software.

Standard curve and linear regression was determined by GraphPad software 5.04. A linear regression line has an equation of the form  $Y = a + bX$ , where  $X$  is the explanatory variable and  $Y$  is the dependent variable. The slope of the line is  $b$ , and  $a$  is the intercept (the value of  $y$  when  $x = 0$ ). Interpolated values ( $X$ ) were multiplied with dilution factor 10 and the volume for 60 µg total protein calculated accordingly with the formula:  $60 / (\frac{x}{1000}) = \text{vol } (\mu\text{L})$ .

### **9.5.5 PAGE Electrophoresis**

30 µg of total protein were loaded onto the gels. 4 × Western LDS sample buffer (Invitrogen), 10 × reducing agent (Invitrogen) and sterile water was added into the protein sample mixture. Samples were then boiled for 10 min at 75 °C and cooled down by centrifugation (15,000g) at 4 °C. Samples were loaded on 4–12% NuPAGE Bis-Tris Mini Gels, 1 mm thick, 12 wells (Invitrogen) and run in MES SDS Running Buffer (Invitrogen) for 1 hour and 30 min at 150 V. The molecular marker used was SeeBlue Plus2 Pre-Stained Protein Standard (Invitrogen). Samples were run in duplicate on two separate gels, the first one to be probed with BRD4 antibody, the second to be probed with tubulin antibody.

### **9.5.6 Western Blotting Experiments**

Gels were then placed onto iBlot2 PVDF mini stacks (Life Technologies). The iBlot2 Electrophoretic Transfer Cell (Life Technologies) for wet transfer was used to transfer proteins. Odyssey PVDF Membrane (Li-COR; P/N 926-31092) was cut to a size of 9 cm × 7 cm and placed in a tray containing transfer buffer for 20 min. To start a stack, one provided thick blotting paper pre-soaked in transfer buffer was placed on the fiber pad on the transparent side of the cassette and rolled to remove bubbles. The membrane was added next and rolled. The gel was then placed on the membrane and rolled to remove air bubbles. The second blotting paper was added on top of the stack and rolled. The second fiber pad was placed on top of the sandwich. The cassette was locked, and the transfer was started. Wet transfer run at 15 V for 12 minutes.

Membranes were blocked in Odyssey Blocking Buffer (PBS) (Li-Cor) for 1 hour at room temperature. Membranes were then incubated overnight at 4°C with the following primary antibody diluted in Odyssey Blocking Buffer + 0.1% Tween (Sigma). membranes were washed four times for 10 min in PBS containing 0.1% Tween-20 and incubated for 1 hour with the following secondary antibodies (diluted 1:5000 in Odyssey Blocking Buffer + 0.1% Tween).

### **9.5.7 Western Blot Quantification**

The intensity of the infrared signal obtained with the different antibodies was quantified using Odyssey Image Analyzer software (LI-COR Biosciences). The bands of interest were selected, and the values calculated were exported to an Excel file.

### **9.5.8 GFP Degradation Assay**

Tryple express (ThermoFisher) was used to harvest the GFP and GFP mutant cells. HeLa cells were thawed prior to harvest, all cell types were centrifugated using a Heraeus™ Megafuge™ (400g for 5 min) and the mother liquid was disposed, and the cell pellet was re-suspended in assay medium at a concentration of 20,000 cells per 45 µL of media (or 20,000 cells per 50 µL of media if using low volume 100% DMSO aliquot alternative by ECHO dispense) for all cell types.

Cells were added to the test plate in buffer solution either by electronic pipetting (ThermoScientific) or using a Multidrop™ Combi Reagent Dispenser (ThermoScientific). 45 µL of GFP cells suspended in media (20,000 cells per well) were added to the assay plate containing the 5 µL of aqueous dilution of compound and DMSO vehicle wells, 0% effect wells (i.e. 0.1% final DMSO). This is repeated for GFP mutant in an analogous plate. (Note: 50 µL (20,000 cells per well) was used if the low volume DMSO aliquot was used.) 45 µL of HeLa parental cells were added to an assay plate which was absent of test compounds and were used to determine the background fluorescence for both end-point reading and cellular imaging and as 100% effect wells. Assay plates were then centrifuged using a Heraeus™ Megafuge™ at 200 g for 5 seconds. The plates were incubated at 37 °C with 5% CO<sub>2</sub> for the required time e.g. 24 or 48 hours. Plates were then visualised by GFP fluorescence endpoint on PHERAstar reader and/or cellular imaging on Incell 6000 GE Healthcare.

### **9.5.9 Fluorescence measurements in 384 well assay plates**

GFP fluorescence was measured directly in live cells in assay plates using both a PHERAstar microplate reader (BMG lab technologies) and an Incell 6000 imager (GE Healthcare).

PHERAstar reader settings: Bottom optic; matrix scan mode 2x2 with scan width at 2mm; excitation filter 485 nm, emission 520 nm; gain 500; focal height 3.9mm.

Incell 6000 imager: A single non-confocal image was taken per well using a 20x primary objective with a GFP/FITC filter set. Exposure time was 0.5 sec. The raw image value was reduced in file size by setting the binning parameter in the Incell reader software to 2x2. Images were analysed using the Columbus image analysis software package (Perkin Elmer). Areas of the image containing individual cells were identified using the standard algorithm in the Columbus software, and the average pixel fluorescence intensity in the cells exported. For an indication of cytotoxicity, parameters corresponding to cell area and “roundness” were also taken. For quantification of compound effects, units from both reader types were converted to

a percentage of DMSO vehicle treated control wells after subtraction of blank well values corresponding to HeLa parental cells expressing no GFP.

## 10 References

- (1) Ma, H.; Deacon, S.; Horiuchi, K. *Expert Opin. Drug Discov.* **2008**, *3*, 607.
- (2) Law, R. P.; Atkinson, S. J.; Bamborough, P.; Chung, C.-w.; Demont, E. H.; Gordon, L. J.; Lindon, M.; Prinjha, R. K.; Watson, A. J. B.; Hirst, D. J. *J. Med. Chem.* **2018**, *61*, 4317.
- (3) Nachbur, U.; Stafford, C. A.; Bankovacki, A.; Zhan, Y.; Lindqvist, L. M.; Fiil, B. K.; Khakham, Y.; Ko, H. J.; Sandow, J. J.; Falk, H.; Holien, J. K.; Chau, D.; Hildebrand, J.; Vince, J. E.; Sharp, P. P.; Webb, A. I.; Jackman, K. A.; Muhlen, S.; Kennedy, C. L.; Lowes, K. N.; Murphy, J. M.; Gyrd-Hansen, M.; Parker, M. W.; Hartland, E. L.; Lew, A. M.; Huang, D. C.; Lessene, G.; Silke, J. *Nat Commun* **2015**, *6*, 6442.
- (4) Bondeson, D. P.; Mares, A.; Smith, I. E.; Ko, E.; Campos, S.; Miah, A. H.; Mulholland, K. E.; Routly, N.; Buckley, D. L.; Gustafson, J. L.; Zinn, N.; Grandi, P.; Shimamura, S.; Bergamini, G.; Faeth-Savitski, M.; Bantscheff, M.; Cox, C.; Gordon, D. A.; Willard, R. R.; Flanagan, J. J.; Casillas, L. N.; Votta, B. J.; den Besten, W.; Famm, K.; Kruidenier, L.; Carter, P. S.; Harling, J. D.; Churcher, I.; Crews, C. M. *Nat. Chem. Biol.* **2015**, *11*, 611.
- (5) Tinworth, C. P.; Lithgow, H.; Dittus, L.; Bassi, Z. I.; Hughes, S. E.; Muelbaier, M.; Dai, H.; Smith, I. E. D.; Kerr, W. J.; Burley, G. A.; Bantscheff, M.; Harling, J. D. *ACS Chem. Bio.* **2019**, *14*, 342.
- (6) Hill, A. P.; Young, R. J. *Drug Discov. Today* **2010**, *15*, 648.
- (7) Chen, D.; Dou, Q. P. *Curr. Protein. Pept. Sci.* **2010**, *11*, 459.
- (8) Wilkinson, K. D. *Proc. Natl. Acad. Sci. USA.* **2005**, *102*, 15280.
- (9) Ciechanover, A. *Nat. Rev. Mol. Cell. Biol.* **2005**, *6*, 79.
- (10) Voges, D.; Zwickl, P.; Baumeister, W. *Annu. Rev. Biochem.* **1999**, *68*, 1015.
- (11) Lecker, S. H.; Goldberg, A. L.; Mitch, W. E. *J. Am. Soc. Nephrol.* **2006**, *17*, 1807.
- (12) Swatek, K. N.; Komander, D. *Cell. Res.* **2016**, *26*, 399.
- (13) Buckley, D. L.; Crews, C. M. *Angew. Chem. Int. Edit.* **2014**, *53*, 2312.
- (14) Crews, C. M. *Chem. Biol.* **2010**, *17*, 551.
- (15) Pickart, C. M.; Eddins, M. J. *BBA-Mol. Cell. Res.* **2004**, *1695*, 55.
- (16) Hershko, A. *Angew. Chem. Int. Ed.* **2005**, *44*, 5932.
- (17) Cohen, P.; Tcherpakov, M. *Cell.* **2010**, *143*, 686.
- (18) Ardley, H. C.; Robinson, P. A. *Essays. Biochem.* **2005**, *41*, 15.
- (19) Berndsen, C. E.; Wolberger, C. *Nat. Struct. Mol. Biol.* **2014**, *21*, 301.
- (20) Naujokat, C.; Hoffmann, S. *Lab. Invest.* **2002**, *82*, 965.
- (21) Martejn, J. A.; Jansen, J. H.; van der Reijden, B. A. *Leukemia.* **2006**, *20*, 1511.
- (22) Baumeister, W.; Cejka, Z.; Kania, M.; Seemüller, E. *J. Biol. Chem.* **1997**, *378*, 121.
- (23) Adjei, A. A. *J. Clin. Oncol.* **2006**, *24*, 4054.
- (24) Kristensen, A. R.; Gsponer, J.; Foster, L. J. *Mol. Syst. Biol.* **2013**, *9*.
- (25) Resnier, P.; Montier, T.; Mathieu, V.; Benoit, J.-P.; Passirani, C. *Biomaterials.* **2013**, *34*, 6429.
- (26) Xue, H. Y.; Liu, S.; Wong, H. L. *Nanomedicine.* **2014**, *9*, 295.
- (27) Wang, J.; Lu, Z.; Wientjes, M. G.; Au, J. L. S. *AAPS. J.* **2010**, *12*, 492.
- (28) Sander, J. D.; Joung, J. K. *Nat. Biotech.* **2014**, *32*, 347.
- (29) Ishino, Y.; Krupovic, M.; Forterre, P. *J. Bacteriol.* **2018**, *200*.
- (30) Cox, D. B. T.; Platt, R. J.; Zhang, F. *Nat. Med.* **2015**, *21*, 121.
- (31) Sakamoto, K. M.; Kim, K. B.; Kumagai, A.; Mercurio, F.; Crews, C. M.; Deshaies, R. J. *Proc. Natl. Acad. Sci. USA.* **2001**, *98*, 8554.
- (32) Tinworth, C. P., Lithgow, H., Churcher, I. *Med. Chem. Comm.* **2016**, *7*, 2206.

- (33) Rodriguez-Gonzalez, A.; Cyrus, K.; Salcius, M.; Kim, K.; Crews, C. M.; Deshaies, R. J.; Sakamoto, K. M. *Oncogene*. **2008**, *27*, 7201.
- (34) Sakamoto, K. M. *Methods Enzymol.* **2005**, *399*, 833.
- (35) Deshaies, R. J. *Nat. Chem. Biol.* **2015**, *11*, 634.
- (36) Churcher, I. J. *Med. Chem.* **2018**, *61*, 444.
- (37) Doak, Bradley C.; Over, B.; Giordanetto, F.; Kihlberg, J. *Chem. Biol.* **2014**, *21*, 1115.
- (38) Pajouhesh, H.; Lenz, G. R. *NeuroRx*. **2005**, *2*, 541.
- (39) Hopkins, A. L.; Groom, C. R. *Nat. Rev. Drug. Discov.* **2002**, *1*, 727.
- (40) Toure, M.; Crews, C. M. *Angew. Chem. Int. Ed.* **2016**, In Press.
- (41) Sakamoto, K. M.; Kim, K. B.; Verma, R.; Ransick, A.; Stein, B.; Crews, C. M.; Deshaies, R. J. *Mol. Cell. Proteomics.* **2003**, *2*, 1350.
- (42) Schneekloth, J. S.; Fonseca, F. N.; Koldobskiy, M.; Mandal, A.; Deshaies, R.; Sakamoto, K.; Crews, C. M. *J. Am. Chem. Soc.* **2004**, *126*, 3748.
- (43) Schneekloth, J. S.; Crews, C. M. *Chem. Bio. Chem.* **2005**, *6*, 40.
- (44) Schneekloth, A. R.; Pucheault, M.; Tae, H. S.; Crews, C. M. *Bioorg. Med. Chem. Lett.* **2008**, *18*, 5904.
- (45) Buckley, D. L.; Gustafson, J. L.; Van Molle, I.; Roth, A. G.; Tae, H. S.; Gareiss, P. C.; Jorgensen, W. L.; Ciulli, A.; Crews, C. M. *Angew. Chem. Int. Ed.* **2012**, *51*, 11463.
- (46) Jang, E. R.; Lee, W.; Kim, K. B. *Curr. Protoc. Chem. Biol.* **2010**, *2*, 71.
- (47) Lu, M.; Liu, T.; Jiao, Q.; Ji, J.; Tao, M.; Liu, Y.; You, Q.; Jiang, Z. *Eur. J. Med. Chem.* **2018**, *146*, 251.
- (48) Toto, R. D. *J. Am. Soc. Nephrol.* **2018**, *29*, 360.
- (49) Hisamichi, M.; Kamijo-Ikemori, A.; Sugaya, T.; Hoshino, S.; Kimura, K.; Shibagaki, Y. *Hypertens. Res.* **2018**, *41*, 8.
- (50) Wang, X. Y.; Zhang, X. H.; Peng, L.; Liu, Z.; Yang, Y. X.; He, Z. X.; Dang, H. W.; Zhou, S. F. *Am. J. Transl. Res.* **2017**, *9*, 4652.
- (51) Wang, Y. Y.; Yang, Y. X.; Zhao, R.; Pan, S. T.; Zhe, H.; He, Z. X.; Duan, W.; Zhang, X.; Yang, T.; Qiu, J. X.; Zhou, S. F. *Drug. Des. Devel. Ther.* **2015**, *9*, 993.
- (52) Abed, D. A.; Goldstein, M.; Albanyan, H.; Jin, H.; Hu, L. *Acta. Pharm. Sin. B.* **2015**, *5*, 285.
- (53) Cleasby, A.; Yon, J.; Day, P. J.; Richardson, C.; Tickle, I. J.; Williams, P. A.; Callahan, J. F.; Carr, R.; Concha, N.; Kerns, J. K.; Qi, H.; Sweitzer, T.; Ward, P.; Davies, T. G. *PLoS One.* **2014**, *9*, e98896.
- (54) Zhang, D. D. *Antioxid. Redox. Signal.* **2013**, *19*, 517.
- (55) Ward, G. A.; Lewis, E. J.; Ahn, J. S.; Johnson, C. N.; Lyons, J. F.; Martins, V.; Munck, J. M.; Rich, S. J.; Smyth, T.; Thompson, N. T.; Williams, P. A.; Wilsher, N. E.; Wallis, N. G.; Chessari, G. *Mol. Cancer. Ther.* **2018**, *17*, 1381.
- (56) Zhuang, C.; Wu, Z.; Xing, C.; Miao, Z. *Med. Chem. Comm.* **2017**, *8*, 286.
- (57) Jiang, Z.-Y.; Xu, L.-L.; Lu, M.-C.; Pan, Y.; Huang, H.-Z.; Zhang, X.-J.; Sun, H.-P.; You, Q.-D. *J. Comput. Aided. Mol. Des.* **2014**, *28*, 1233.
- (58) Hon, W. C.; Wilson, M. I.; Harlos, K.; Claridge, T. D. W.; Schofield, C. J.; Pugh, C. W.; Maxwell, P. H.; Ratcliffe, P. J.; Stuart, D. I.; Jones, E. Y. *Nature.* **2002**, *417*, 975.
- (59) Buckley, D. L.; Van Molle, I.; Gareiss, P. C.; Tae, H. S.; Michel, J.; Noblin, D. J.; Jorgensen, W. L.; Ciulli, A.; Crews, C. M. *J. Am. Chem. Soc.* **2012**, *134*, 4465.
- (60) Galdeano, C.; Gadd, M. S.; Soares, P.; Scaffidi, S.; Van Molle, I.; Birced, I.; Hewitt, S.; Dias, D. M.; Ciulli, A. *J. Med. Chem.* **2014**, *57*, 8657.
- (61) Crews, C. M.; Buckley, D.; Ciulli, A.; Jorgensen, W.; Gareiss, P. C.; Van Molle, I.; Gustafson, J.; Tae, H. S.; Michel, J.; Hoyer, D. W. *WO 2013106643 A2.* **2013**.
- (62) Raina, K.; Crews, C. M. *J. Biol. Chem.* **2010**, *285*, 11057.

- (63) Buckley, D. L.; Raina, K.; Darricarrere, N.; Hines, J.; Gustafson, J. L.; Smith, I. E.; Miah, A. H.; Harling, J. D.; Crews, C. M. *ACS. Chem. Biol.* **2015**, *10*, 1831.
- (64) Nichols, P. L.; Eatherton, A. J.; Bamborough, P.; Jandu, K. S.; Philps, O. J.; Andreotti, D. *WO 2011/038872 A1*. **2011**.
- (65) Zengerle, M.; Chan, K. H.; Ciulli, A. *ACS. Chem. Biol.* **2015**, *10*, 1770.
- (66) Wurz, R. P.; Dellamaggiore, K.; Dou, H.; Javier, N.; Lo, M. C.; McCarter, J. D.; Mohl, D.; Sastri, C.; Lipford, J. R.; Cee, V. J. *J. Med. Chem.* **2018**, *61*, 453.
- (67) Raina, K.; Lu, J.; Qian, Y.; Altieri, M.; Gordon, D.; Rossi, A. M.; Wang, J.; Chen, X.; Dong, H.; Siu, K.; Winkler, J. D.; Crew, A. P.; Crews, C. M.; Coleman, K. G. *Proc. Natl. Acad. Sci. USA*. **2016**, *113*, 7124.
- (68) Chan, K. H.; Zengerle, M.; Testa, A.; Ciulli, A. *J. Med. Chem.* **2018**, *61*, 504.
- (69) Gadd, M. S.; Testa, A.; Lucas, X.; Chan, K. H.; Chen, W.; Lamont, D. J.; Zengerle, M.; Ciulli, A. *Nat Chem Biol* **2017**, *13*, 514.
- (70) Gechijian, L. N.; Buckley, D. L.; Lawlor, M. A.; Reyes, J. M.; Paulk, J.; Ott, C. J.; Winter, G. E.; Erb, M. A.; Scott, T. G.; Xu, M.; Seo, H. S.; Dhe-Paganon, S.; Kwiatkowski, N. P.; Perry, J. A.; Qi, J.; Gray, N. S.; Bradner, J. E. *Nat. Chem. Biol.* **2018**, *14*, 405.
- (71) Gadd, M. S.; Testa, A.; Lucas, X.; Chan, K. H.; Chen, W.; Lamont, D. J.; Zengerle, M.; Ciulli, A. *Nat. Chem. Biol.* **2017**, *13*, 514.
- (72) Palmer, W. S.; Poncet-Montange, G.; Liu, G.; Petrocchi, A.; Reyna, N.; Subramanian, G.; Theroff, J.; Yau, A.; Kost-Alimova, M.; Bardenhagen, J. P.; Leo, E.; Shepard, H. E.; Tieu, T. N.; Shi, X.; Zhan, Y.; Zhao, S.; Barton, M. C.; Draetta, G.; Toniatti, C.; Jones, P.; Geck Do, M.; Andersen, J. N. *J. Med. Chem.* **2016**, *59*, 1440.
- (73) Lai, A. C.; Toure, M.; Hellerschmied, D.; Salami, J.; Jaime-Figueroa, S.; Ko, E.; Hines, J.; Crews, C. M. *Angew. Chem. Int. Ed.* **2015**.
- (74) Burslem, G. M.; Smith, B. E.; Lai, A. C.; Jaime-Figueroa, S.; McQuaid, D. C.; Bondeson, D. P.; Toure, M.; Dong, H.; Qian, Y.; Wang, J.; Crew, A. P.; Hines, J.; Crews, C. M. *Cell. Chem. Biol.* **2018**, *25*, 67.
- (75) Bondeson, D. P.; Smith, B. E.; Burslem, G. M.; Buhimschi, A. D.; Hines, J.; Jaime-Figueroa, S.; Wang, J.; Hamman, B. D.; Ishchenko, A.; Crews, C. M. *Cell. Chem. Biol.* **2018**, *25*, 78.
- (76) Kataoka, Y.; Mukohara, T.; Tomioka, H.; Funakoshi, Y.; Kiyota, N.; Fujiwara, Y.; Yashiro, M.; Hirakawa, K.; Hirai, M.; Minami, H. *Invest. New. Drugs.* **2012**, *30*, 1352.
- (77) Seiwert, T.; Sarantopoulos, J.; Kallender, H.; McCallum, S.; Keer, H. N.; Blumenschein, G., Jr. *Invest. New. Drugs.* **2013**, *31*, 417.
- (78) Chen, G. Z.; Dai, W. S.; Zhu, H. C.; Song, H. M.; Yang, X.; Wang, Y. D.; Min, H.; Lu, Q.; Liu, S.; Sun, X. C.; Zeng, X. N. *J. Cancer.* **2017**, *8*, 983.
- (79) Kogata, Y.; Tanaka, T.; Ono, Y. J.; Hayashi, M.; Terai, Y.; Ohmichi, M. *Oncotarget.* **2018**, *9*, 22769.
- (80) Tinworth, C. P. *Thesis.* **2016**.
- (81) Zhang, L.; Holmes, I. P.; Hochgrafe, F.; Walker, S. R.; Ali, N. A.; Humphrey, E. S.; Wu, J.; de Silva, M.; Kersten, W. J.; Connor, T.; Falk, H.; Allan, L.; Street, I. P.; Bentley, J. D.; Pilling, P. A.; Monahan, B. J.; Peat, T. S.; Daly, R. J. *J. Proteome. Res.* **2013**, *12*, 3104.
- (82) Salami, J.; Alabi, S.; Willard, R. R.; Vitale, N. J.; Wang, J.; Dong, H.; Jin, M.; McDonnell, D. P.; Crew, A. P.; Neklesa, T. K.; Crews, C. M. *Commun. Biol.* **2018**, *1*, 100.
- (83) Ito, T.; Ando, H.; Suzuki, T.; Ogura, T.; Hotta, K.; Imamura, Y.; Yamaguchi, Y.; Handa, H. *Science.* **2010**, *327*, 1345.
- (84) Zhu, Y. X.; Kortuem, K. M.; Stewart, A. K. *Leuk. Lymphoma.* **2013**, *54*, 683.
- (85) Che, Y.; Gilbert, A. M.; Shanmugasundaram, V.; Noe, M. C. *Bioorg. Med. Chem. Lett.* **2018**, *28*, 2585.
- (86) Krönke, J.; Hurst, S. N.; Ebert, B. L. *Oncoimmunology.* **2014**, *3*, e941742.

- (87) Anderson, K. C.; Prince, H. M. *Semin. Hematology*. **2005**, *42*, Supplement 4, S1.
- (88) Lu, J.; Qian, Y.; Altieri, M.; Dong, H.; Wang, J.; Raina, K.; Hines, J.; Winkler, J. D.; Crew, A. P.; Coleman, K.; Crews, C. M. *Chem. Biol.* **2015**, *22*, 755.
- (89) Winter, G. E.; Buckley, D. L.; Paulk, J.; Roberts, J. M.; Souza, A.; Dhe-Paganon, S.; Bradner, J. E. *Science*. **2015**, *348*, 1376.
- (90) Nowak, R. P.; DeAngelo, S. L.; Buckley, D.; He, Z.; Donovan, K. A.; An, J.; Safaei, N.; Jedrychowski, M. P.; Ponthier, C. M.; Ishoey, M.; Zhang, T.; Mancias, J. D.; Gray, N. S.; Bradner, J. E.; Fischer, E. S. *Nat. Chem. Biol.* **2018**, *14*, 706.
- (91) Qin, C.; Hu, Y.; Zhou, B.; Fernandez-Salas, E.; Yang, C. Y.; Liu, L.; McEachern, D.; Przybranowski, S.; Wang, M.; Stuckey, J.; Meagher, J.; Bai, L.; Chen, Z.; Lin, M.; Yang, J.; Ziazadeh, D. N.; Xu, F.; Hu, J.; Xiang, W.; Huang, L.; Li, S.; Wen, B.; Sun, D.; Wang, S. *J. Med. Chem.* **2018**, *61*, 6685.
- (92) Bassi, Z. I.; Fillmore, M. C.; Miah, A. H.; Chapman, T. D.; Maller, C.; Roberts, E. J.; Davis, L. C.; Lewis, D. E.; Galwey, N. W.; Waddington, K. E.; Parravicini, V.; Macmillan-Jones, A. L.; Gongora, C.; Humphreys, P. G.; Churcher, I.; Prinjha, R. K.; Tough, D. F. *ACS. Chem. Biol.* **2018**, *13*, 2862.
- (93) Remillard, D.; Buckley, D. L.; Paulk, J.; Brien, G. L.; Sonnett, M.; Seo, H. S.; Dastjerdi, S.; Wühr, M.; Dhe-Paganon, S.; Armstrong, S. A.; Bradner, J. E. *Angew. Chem. Int. Ed. Engl.* **2017**, *56*, 5738.
- (94) Smith, I. E. M., A.; Mares, A.; Harling, J.; Churcher, I. *Unpublished Results*. **2016**.
- (95) Huang, H. T.; Dobrovolsky, D.; Paulk, J.; Yang, G.; Weisberg, E. L.; Doctor, Z. M.; Buckley, D. L.; Cho, J. H.; Ko, E.; Jang, J.; Shi, K.; Choi, H. G.; Griffin, J. D.; Li, Y.; Treon, S. P.; Fischer, E. S.; Bradner, J. E.; Tan, L.; Gray, N. S. *Cell. Chem. Biol.* **2018**, *25*, 88.
- (96) Sun, Y.; Zhao, X.; Ding, N.; Gao, H.; Wu, Y.; Yang, Y.; Zhao, M.; Hwang, J.; Song, Y.; Liu, W.; Rao, Y. *Cell. Res.* **2018**, *28*, 779.
- (97) Zorba, A.; Nguyen, C.; Xu, Y.; Starr, J.; Borzilleri, K.; Smith, J.; Zhu, H.; Farley, K. A.; Ding, W.; Schiemer, J.; Feng, X.; Chang, J. S.; Uccello, D. P.; Young, J. A.; Garcia-Irrizary, C. N.; Czabaniuk, L.; Schuff, B.; Oliver, R.; Montgomery, J.; Hayward, M. M.; Coe, J.; Chen, J.; Niosi, M.; Luthra, S.; Shah, J. C.; El-Kattan, A.; Qiu, X.; West, G. M.; Noe, M. C.; Shanmugasundaram, V.; Gilbert, A. M.; Brown, M. F.; Calabrese, M. F. *Proc. Natl. Acad. Sci. USA*. **2018**, *115*, E7285.
- (98) Buhimschi, A. D.; Armstrong, H. A.; Toure, M.; Jaime-Figueroa, S.; Chen, T. L.; Lehman, A. M.; Woyach, J. A.; Johnson, A. J.; Byrd, J. C.; Crews, C. M. *Biochem. J.* **2018**, *57*, 3564.
- (99) Raghu, N. S.; Reddy, Y. R.; Naresh, V.; Suryanarayana Rao, V.; Ravindranath, L. K. *J. Liq. Chromatogr. R. T.* **2010**, *33*, 654.
- (100) Reist, M.; Carrupt, P.-A.; Francotte, E.; Testa, B. *Chem. Res. Toxicol.* **1998**, *11*, 1521.
- (101) Hoffmann, M.; Kasserra, C.; Reyes, J.; Schafer, P.; Kosek, J.; Capone, L.; Parton, A.; Kim-Kang, H.; Surapaneni, S.; Kumar, G. *Cancer. Chemother. Pharmacol.* **2013**, *71*, 489.
- (102) Jacques, V.; Czarnik, A. W.; Judge, T. M.; Van der Ploeg, L. H. T.; DeWitt, S. H. *Proc. Natl. Acad. Sci. USA*. **2015**, *112*, E1471.
- (103) Erin, R. L.; Nicola, F. S.; Michael, C. C.; Charity, D. S.; William, D. F. *Curr. Drug. Metab.* **2006**, *7*, 677.
- (104) Fischer, E. S.; Bohm, K.; Lydeard, J. R.; Yang, H.; Stadler, M. B.; Cavadini, S.; Nagel, J.; Serluca, F.; Acker, V.; Lingaraju, G. M.; Tichkule, R. B.; Schebesta, M.; Forrester, W. C.; Schirle, M.; Hassiepen, U.; Ottl, J.; Hild, M.; Beckwith, R. E.; Harper, J. W.; Jenkins, J. L.; Thoma, N. H. *Nature*. **2014**, *512*, 49.

- (105) Tisato, V.; Voltan, R.; Gonelli, A.; Secchiero, P.; Zauli, G. *J. Hematol. Oncol.* **2017**, *10*, 133.
- (106) Neochoritis, C.; Estrada-Ortiz, N.; Khoury, K.; Dömling, A. *Annu. Rep. Med. Chem.* **2014**, *49*, 167.
- (107) Marhefka, C. A.; Gao, W.; Chung, K.; Kim, J.; He, Y.; Yin, D.; Bohl, C.; Dalton, J. T.; Miller, D. D. *J. Med. Chem.* **2004**, *47*, 993.
- (108) Hines, J.; Lartigue, S.; Dong, H.; Qian, Y.; Crews, C. M. *Cancer. Res.* **2018**.
- (109) Wang, P.; Zhou, J. *Curr. Top. Med. Chem.* **2018**.
- (110) Fulda, S. *Semin. Cell. Dev. Biol.* **2015**, *39*, 132.
- (111) Fulda, S. *Clin. Cancer Res.* **2015**, *21*, 5030.
- (112) Bai, L.; Smith, D. C.; Wang, S. *Pharmacol. Ther.* **2014**, *144*, 82.
- (113) Silke, J.; Meier, P. *Cold Spring Harb. Perspect. Biol.* **2013**, *5*.
- (114) Dueber, E. C.; Schoeffler, A. J.; Lingel, A.; Elliott, J. M.; Fedorova, A. V.; Giannetti, A. M.; Zobel, K.; Maurer, B.; Varfolomeev, E.; Wu, P.; Wallweber, H. J. A.; Hymowitz, S. G.; Deshayes, K.; Vucic, D.; Fairbrother, W. J. *Science.* **2011**, *334*, 376.
- (115) Itoh, Y.; Ishikawa, M.; Kitaguchi, R.; Sato, S.; Naito, M.; Hashimoto, Y. *Bioorg. Med. Chem.* **2011**, *19*, 3229.
- (116) Sekine, K.; Takubo, K.; Kikuchi, R.; Nishimoto, M.; Kitagawa, M.; Abe, F.; Nishikawa, K.; Tsuruo, T.; Naito, M. *J. Biol. Chem.* **2008**, *283*, 8961.
- (117) Sato, S.; Tetsuhashi, M.; Sekine, K.; Miyachi, H.; Naito, M.; Hashimoto, Y.; Aoyama, H. *Bioorg. Med. Chem.* **2008**, *16*, 4685.
- (118) Okuhira, K.; Shoda, T.; Omura, R.; Ohoka, N.; Hattori, T.; Shibata, N.; Demizu, Y.; Sugihara, R.; Ichino, A.; Kawahara, H.; Itoh, Y.; Ishikawa, M.; Hashimoto, Y.; Kurihara, M.; Itoh, S.; Saito, H.; Naito, M. *Mol. Pharmacol.* **2017**, *91*, 159.
- (119) Tomoshige, S.; Hashimoto, Y.; Ishikawa, M. *Bioorg. Med. Chem.* **2016**, *24*, 3144.
- (120) Shibata, N.; Nagai, K.; Morita, Y.; Ujikawa, O.; Ohoka, N.; Hattori, T.; Koyama, R.; Sano, O.; Imaeda, Y.; Nara, H.; Cho, N.; Naito, M. *J. Med. Chem.* **2018**, *61*, 543.
- (121) Ohoka, N.; Ujikawa, O.; Shimokawa, K.; Sameshima, T.; Shibata, N.; Hattori, T.; Nara, H.; Cho, N.; Naito, M. *Chem. Pharm. Bull. (Tokyo)* **2018**.
- (122) Ohoka, N.; Okuhira, K.; Ito, M.; Nagai, K.; Shibata, N.; Hattori, T.; Ujikawa, O.; Shimokawa, K.; Sano, O.; Koyama, R.; Fujita, H.; Teratani, M.; Matsumoto, H.; Imaeda, Y.; Nara, H.; Cho, N.; Naito, M. *J. Biol. Chem.* **2017**, *292*, 4556.
- (123) Shibata, N.; Miyamoto, N.; Nagai, K.; Shimokawa, K.; Sameshima, T.; Ohoka, N.; Hattori, T.; Imaeda, Y.; Nara, H.; Cho, N.; Naito, M. *Cancer. Sci.* **2017**, *108*, 1657.
- (124) Ohoka, N.; Morita, Y.; Nagai, K.; Shimokawa, K.; Ujikawa, O.; Fujimori, I.; Ito, M.; Hayase, Y.; Okuhira, K.; Shibata, N.; Hattori, T.; Sameshima, T.; Sano, O.; Koyama, R.; Imaeda, Y.; Nara, H.; Cho, N.; Naito, M. *J. Biol. Chem.* **2018**, *293*, 6776.
- (125) Kim, K. S.; Zhang, L.; Williams, D.; Perez, H. L.; Stang, E.; Borzilleri, R. M.; Posy, S.; Lei, M.; Chaudhry, C.; Emanuel, S.; Talbott, R. *Bioorg. Med. Chem. Lett.* **2014**, *24*, 5022.
- (126) Bantscheff, M.; Eberhard, D.; Abraham, Y.; Bastuck, S.; Boesche, M.; Hobson, S.; Mathieson, T.; Perrin, J.; Raida, M.; Rau, C.; Reader, V.; Sweetman, G.; Bauer, A.; Bouwmeester, T.; Hopf, C.; Kruse, U.; Neubauer, G.; Ramsden, N.; Rick, J.; Kuster, B.; Drewes, G. *Nat. Biotechnol.* **2007**, *25*, 1035.
- (127) Bantscheff, M.; Hopf, C.; Savitski, M. M.; Dittmann, A.; Grandi, P.; Michon, A. M.; Schlegl, J.; Abraham, Y.; Becher, I.; Bergamini, G.; Boesche, M.; Dellling, M.; Dumpelfeld, B.; Eberhard, D.; Huthmacher, C.; Mathieson, T.; PoECKel, D.; Reader, V.; Strunk, K.; Sweetman, G.; Kruse, U.; Neubauer, G.; Ramsden, N. G.; Drewes, G. *Nat. Biotechnol.* **2011**, *29*, 255.
- (128) Kester, R. F.; Donnell, A. F.; Lou, Y.; Remiszewski, S. W.; Lombardo, L. J.; Chen, S.; Le, N. T.; Lo, J.; Moliterni, J. A.; Han, X.; Hogg, J. H.; Liang, W.; Michoud, C.;

- Rupert, K. C.; Mischke, S.; Le, K.; Weisel, M.; Janson, C. A.; Lukacs, C. M.; Fretland, A. J.; Hong, K.; Polonskaia, A.; Gao, L.; Li, S.; Solis, D. S.; Aguilar, D.; Tardell, C.; Dvorozniak, M.; Tannu, S.; Lee, E. C.; Schutt, A. D.; Goggin, B. *J. Med. Chem.* **2013**, *56*, 7788.
- (129) Liu, Y.; Huang, X.; He, X.; Zhou, Y.; Jiang, X.; Chen-Kiang, S.; Jaffrey, S. R.; Xu, G. *FASEB J.* **2015**, *29*, 4829.
- (130) Chamberlain, P. P.; Lopez-Girona, A.; Miller, K.; Carmel, G.; Pagarigan, B.; Chie-Leon, B.; Rychak, E.; Corral, L. G.; Ren, Y. J.; Wang, M.; Riley, M.; Delker, S. L.; Ito, T.; Ando, H.; Mori, T.; Hirano, Y.; Handa, H.; Hakoshima, T.; Daniel, T. O.; Cathers, B. E. *Nat. Struct. Mol. Biol.* **2014**, *21*, 803.
- (131) Semeraro, M.; Galluzzi, L. *Oncoimmunology.* **2014**, *3*, e28386.
- (132) Lopez-Girona, A.; Mendy, D.; Ito, T.; Miller, K.; Gandhi, A. K.; Kang, J.; Karasawa, S.; Carmel, G.; Jackson, P.; Abbasian, M.; Mahmoudi, A.; Cathers, B.; Rychak, E.; Gaidarova, S.; Chen, R.; Schafer, P. H.; Handa, H.; Daniel, T. O.; Evans, J. F.; Chopra, R. *Leukemia.* **2012**, *26*, 2326.
- (133) Chang, X. B.; Stewart, A. K. *Int. J. Biochem. Mol. Biol.* **2011**, *2*, 287.
- (134) Zhu, Y. X.; Braggio, E.; Shi, C. X.; Bruins, L. A.; Schmidt, J. E.; Van Wier, S.; Chang, X. B.; Bjorklund, C. C.; Fonseca, R.; Bergsagel, P. L.; Orłowski, R. Z.; Stewart, A. K. *Blood.* **2011**, *118*, 4771.
- (135) Han, T.; Goralski, M.; Gaskill, N.; Capota, E.; Kim, J.; Ting, T. C.; Xie, Y.; Williams, N. S.; Nijhawan, D. *Science.* **2017**, 356.
- (136) Uehara, T.; Minoshima, Y.; Sagane, K.; Sugi, N. H.; Mitsuhashi, K. O.; Yamamoto, N.; Kamiyama, H.; Takahashi, K.; Kotake, Y.; Uesugi, M.; Yokoi, A.; Inoue, A.; Yoshida, T.; Mabuchi, M.; Tanaka, A.; Owa, T. *Nat. Chem. Biol.* **2017**, *13*, 675.
- (137) Assi, R.; Kantarjian, H. M.; Kadia, T. M.; Pemmaraju, N.; Jabbour, E.; Jain, N.; Daver, N.; Estrov, Z.; Uehara, T.; Owa, T.; Cortes, J. E.; Borthakur, G. *Cancer.* **2018**, *124*, 2758.
- (138) Yuan, L.; Han, J.; Meng, Q.; Xi, Q.; Zhuang, Q.; Jiang, Y.; Han, Y.; Zhang, B.; Fang, J.; Wu, G. *Oncol Rep* **2015**, *33*, 2261.
- (139) Belyanskaya, S. L.; Ding, Y.; Callahan, J. F.; Lazaar, A. L.; Israel, D. I. *Chem. Bio. Chem.* **2017**, *18*, 837.
- (140) Kollmann, C. S.; Bai, X.; Tsai, C. H.; Yang, H.; Lind, K. E.; Skinner, S. R.; Zhu, Z.; Israel, D. I.; Cuzzo, J. W.; Morgan, B. A.; Yuki, K.; Xie, C.; Springer, T. A.; Shimaoka, M.; Evindar, G. *Bioorg. Med. Chem.* **2014**, *22*, 2353.
- (141) Encinas, L.; O'Keefe, H.; Neu, M.; Remuinan, M. J.; Patel, A. M.; Guardia, A.; Davie, C. P.; Perez-Macias, N.; Yang, H.; Convery, M. A.; Messer, J. A.; Perez-Herran, E.; Centrella, P. A.; Alvarez-Gomez, D.; Clark, M. A.; Huss, S.; O'Donovan, G. K.; Ortega-Muro, F.; McDowell, W.; Castaneda, P.; Arico-Muendel, C. C.; Pajk, S.; Rullas, J.; Angulo-Barturen, I.; Alvarez-Ruiz, E.; Mendoza-Losana, A.; Ballell Pages, L.; Castro-Pichel, J.; Evindar, G. *J. Med. Chem.* **2014**, *57*, 1276.
- (142) Bostrom, J.; Brown, D. G.; Young, R. J.; Keseru, G. M. *Nat. Rev. Drug. Discov.* **2018**, *17*, 709.
- (143) Kang, C. H.; Lee, D. H.; Lee, C. O.; Du Ha, J.; Park, C. H.; Hwang, J. Y. *Biochem. Biophys. Res. Commun.* **2018**, *505*, 542.
- (144) Brand, M.; Measures, A. R.; Wilson, B. G.; Cortopassi, W. A.; Alexander, R.; Hoss, M.; Hewings, D. S.; Rooney, T. P.; Paton, R. S.; Conway, S. J. *ACS. Chem. Biol.* **2015**, *10*, 22.
- (145) Pan, H.; Lu, P.; Shen, Y.; Wang, Y.; Jiang, Z.; Yang, X.; Zhong, Y.; Yang, H.; Khan, I. U.; Zhou, M.; Li, B.; Zhang, Z.; Xu, J.; Lu, H.; Zhu, H. *Oncotarget.* **2017**, *8*, 94104.
- (146) Picaud, S.; Leonards, K.; Lambert, J. P.; Dovey, O.; Wells, C.; Fedorov, O.; Monteiro, O.; Fujisawa, T.; Wang, C. Y.; Lingard, H.; Tallant, C.; Nikbin, N.; Guetzoyan, L.;

- Ingham, R.; Ley, S. V.; Brennan, P.; Muller, S.; Samsonova, A.; Gingras, A. C.; Schwaller, J.; Vassiliou, G.; Knapp, S.; Filippakopoulos, P. *Sci. Adv.* **2016**, *2*, e1600760.
- (147) Bantscheff, M.; Muelbaier, M.; Zinn, N. *Unpublished Results* **2017**.
- (148) Bondeson, D. P.; Smith, B. E.; Burslem, G. M.; Buhimschi, A. D.; Hines, J.; Jaime-Figueroa, S.; Wang, J.; Hamman, B. D.; Ishchenko, A.; Crews, C. M. *Cell. Chem. Biol.* **2018**, *25*, 78.
- (149) Thompson, A.; Schafer, J.; Kuhn, K.; Kienle, S.; Schwarz, J.; Schmidt, G.; Neumann, T.; Johnstone, R.; Mohammed, A. K.; Hamon, C. *Anal. Chem.* **2003**, *75*, 1895.
- (150) Dayon, L.; Hainard, A.; Licker, V.; Turck, N.; Kuhn, K.; Hochstrasser, D. F.; Burkhard, P. R.; Sanchez, J. C. *Anal. Chem.* **2008**, *80*, 2921.
- (151) DeGoey, D. A.; Chen, H. J.; Cox, P. B.; Wendt, M. D. *J. Med. Chem.* **2018**, *61*, 2636.
- (152) Bergstrom, C. A. S.; Porter, C. J. H. *Adv Drug Deliv Rev* **2016**, *101*, 1.
- (153) Matsson, P.; Doak, B. C.; Over, B.; Kihlberg, J. *Adv. Drug. Deliv. Rev.* **2016**, *101*, 42.
- (154) Yang, N. J.; Hinner, M. J. *Methods Mol. Biol.* **2015**, *1266*, 29.
- (155) Molecular Operating Environment (MOE) 2019.
- (156) Belkina, A. C.; Nikolajczyk, B. S.; Denis, G. V. *J. Immunol.* **2013**, *190*, 3670.
- (157) Nguyen, T. H.; Maltby, S.; Eyers, F.; Foster, P. S.; Yang, M. *PLoS One.* **2016**, *11*, e0163392.
- (158) Ghosh, R.; Gilda, J. E.; Gomes, A. V. *Expert. Rev. Proteomics.* **2014**, *11*, 549.
- (159) Wang, L.; Wu, X.; Wang, R.; Yang, C.; Li, Z.; Wang, C.; Zhang, F.; Yang, P. *Biol. Res.* **2017**, *50*, 19.
- (160) Sedgmen, B. J.; Papalia, L.; Wang, L.; Dyson, A. R.; McCallum, H. A.; Simson, C. M.; Pearse, M. J.; Maraskovsky, E.; Hung, D.; Eomois, P. P.; Hartel, G.; Barnden, M. J.; Rockman, S. P. *Clin. Dev. Immunol.* **2013**, *2013*, 186420.
- (161) Savitski, M. M.; Zinn, N.; Faelth-Savitski, M.; Poeckel, D.; Gade, S.; Becher, I.; Muelbaier, M.; Wagner, A. J.; Strohmer, K.; Werner, T.; Melchert, S.; Petretich, M.; Rutkowska, A.; Vappiani, J.; Franken, H.; Steidel, M.; Sweetman, G. M.; Gilan, O.; Lam, E. Y. N.; Dawson, M. A.; Prinjha, R. K.; Grandi, P.; Bergamini, G.; Bantscheff, M. *Cell.* **2018**, *173*, 260.
- (162) Zinn, N.; Hopf, C.; Drewes, G.; Bantscheff, M. *Methods.* **2012**, *57*, 430.
- (163) Heap, R. E.; Gant, M. S.; Lamoliatte, F.; Peltier, J.; Trost, M. *Biochem. Soc. Trans.* **2017**, *45*, 1137.
- (164) Iconomou, M.; Saunders, D. N. *Biochem. J.* **2016**, *473*, 4083.
- (165) Deshaies, R. J.; Joazeiro, C. A. *Annu. Rev. Biochem.* **2009**, *78*, 399.
- (166) Sun, B.; Fiskus, W.; Qian, Y.; Rajapakshe, K.; Raina, K.; Coleman, K. G.; Crew, A. P.; Shen, A.; Saenz, D. T.; Mill, C. P.; Nowak, A. J.; Jain, N.; Zhang, L.; Wang, M.; Khoury, J. D.; Coarfa, C.; Crews, C. M.; Bhalla, K. N. *Leukemia* **2018**, *32*, 343.
- (167) Zhang, X.; Lee, H. C.; Shirazi, F.; Baladandayuthapani, V.; Lin, H.; Kuitse, I.; Wang, H.; Jones, R. J.; Berkova, Z.; Singh, R. K.; Lu, J.; Qian, Y.; Raina, K.; Coleman, K. G.; Crews, C. M.; Li, B.; Wang, H.; Hailemichael, Y.; Thomas, S. K.; Wang, Z.; Davis, R. E.; Orlowski, R. Z. *Leukemia.* **2018**, *32*, 2224.
- (168) Zhang, X.; Lee, H. C.; Shirazi, F.; Baladandayuthapani, V.; Lin, H.; Kuitse, I.; Wang, H.; Jones, R. J.; Berkova, Z.; Singh, R. K.; Lu, J.; Qian, Y.; Raina, K.; Coleman, K. G.; Crews, C. M.; Li, B.; Wang, H.; Hailemichael, Y.; Thomas, S. K.; Wang, Z.; Davis, R. E.; Orlowski, R. Z. *Leukemia* **2018**, *32*, 2224.
- (169) Lebraud, H.; Wright, D. J.; Johnson, C. N.; Heightman, T. D. *ACS. Cent. Sci.* **2016**, *2*, 927.
- (170) DeMars, K. M.; Yang, C.; Castro-Rivera, C. I.; Candelario-Jalil, E. *Biochem. Biophys. Res. Commun.* **2018**, *497*, 410.

- (171) Farkas, L.; Stoelcker, B.; Jentsch, N.; Heitzer, S.; Pfeifer, M.; Schulz, C. *Scand. J. Immunol.* **2008**, *68*, 315.
- (172) Jeong, Y. J.; Kang, M. J.; Lee, S. J.; Kim, C. H.; Kim, J. C.; Kim, T. H.; Kim, D. J.; Kim, D.; Nunez, G.; Park, J. H. *Immunology.* **2014**, *143*, 269.
- (173) Yang, Y.; Yin, C.; Pandey, A.; Abbott, D.; Sasseti, C.; Kelliher, M. A. *J. Biol. Chem.* **2007**, *282*, 36223.
- (174) Pan, Q.; Mathison, J.; Fearn, C.; Kravchenko, V. V.; Da Silva Correia, J.; Hoffman, H. M.; Kobayashi, K. S.; Bertin, J.; Grant, E. P.; Coyle, A. J.; Sutterwala, F. S.; Ogura, Y.; Flavell, R. A.; Ulevitch, R. J. *J. Leukoc. Biol.* **2007**, *82*, 177.
- (175) Windheim, M.; Lang, C.; Pegg, M.; Plater, L. A.; Cohen, P. *Biochem. J.* **2007**, *404*, 179.
- (176) Stoddart, L. A.; Kilpatrick, L. E.; Hill, S. J. *Trends. Pharmacol. Sci.* **2018**, *39*, 136.
- (177) Machleidt, T.; Woodroffe, C. C.; Schwinn, M. K.; Mendez, J.; Robers, M. B.; Zimmerman, K.; Otto, P.; Daniels, D. L.; Kirkland, T. A.; Wood, K. V. *ACS. Chem. Biol.* **2015**, *10*, 1797.
- (178) Riching, K. M.; Mahan, S.; Corona, C. R.; McDougall, M.; Vasta, J. D.; Robers, M. B.; Urh, M.; Daniels, D. L. *ACS. Chem. Biol.* **2018**, *13*, 2758.
- (179) Benink, H. A.; Urh, M. *Methods. Mol. Biol.* **2015**, *1266*, 119.
- (180) Urh, M.; Rosenberg, M. *Curr. Chem. Genomics.* **2012**, *6*, 72.
- (181) Cong, M. *Curr. Chem. Genomics.* **2012**, *6*, 6.
- (182) Neklesa, T. K.; Tae, H. S.; Schneekloth, A. R.; Stulberg, M. J.; Corson, T. W.; Sundberg, T. B.; Raina, K.; Holley, S. A.; Crews, C. M. *Nat. Chem. Biol.* **2011**, *7*, 538.
- (183) Taniguchi, Y.; Kawakami, M. *Langmuir.* **2010**, *26*, 10433.
- (184) Los, G. V.; Wood, K. *Methods. Mol. Biol.* **2007**, *356*, 195.
- (185) Lang, C.; Schulze, J.; Mendel, R. R.; Hansch, R. *J. Exp. Bot.* **2006**, *57*, 2985.
- (186) Chessari, G.; Buck, I. M.; Day, J. E.; Day, P. J.; Iqbal, A.; Johnson, C. N.; Lewis, E. J.; Martins, V.; Miller, D.; Reader, M.; Rees, D. C.; Rich, S. J.; Tamanini, E.; Vitorino, M.; Ward, G. A.; Williams, P. A.; Williams, G.; Wilsher, N. E.; Woolford, A. J. *J. Med. Chem.* **2015**, *58*, 6574.
- (187) Perez, H. L.; Chaudhry, C.; Emanuel, S. L.; Fanslau, C.; Fargnoli, J.; Gan, J.; Kim, K. S.; Lei, M.; Naglich, J. G.; Traeger, S. C.; Vuppugalla, R.; Wei, D. D.; Vite, G. D.; Talbott, R. L.; Borzilleri, R. M. *J. Med. Chem.* **2015**, *58*, 1556.
- (188) Zhang, Y.; Seigal, B. A.; Terrett, N. K.; Talbott, R. L.; Fargnoli, J.; Naglich, J. G.; Chaudhry, C.; Posy, S. L.; Vuppugalla, R.; Cornelius, G.; Lei, M.; Wang, C.; Zhang, Y.; Schmidt, R. J.; Wei, D. D.; Miller, M. M.; Allen, M. P.; Li, L.; Carter, P. H.; Vite, G. D.; Borzilleri, R. M. *ACS. Med. Chem. Lett.* **2015**, *6*, 770.
- (189) Chaguturu, R. *Comb. Chem. High Throughput Screen.* **2013**, *16*, 1.
- (190) Kennedy, J. P.; Williams, L.; Bridges, T. M.; Daniels, R. N.; Weaver, D.; Lindsley, C. W. *J. Comb. Chem.* **2008**, *10*, 345.
- (191) Fonseca, M. H.; List, B. *Curr. Opin. Chem. Biol.* **2004**, *8*, 319.
- (192) Seneci, P.; Miertus, S. *Mol. Divers.* **2000**, *5*, 75.
- (193) Burgess, K.; Lim, D.; Mousa, S. A. *J. Med. Chem.* **1996**, *39*, 4520.
- (194) Molander, G. A.; Wisniewski, S. R. *J. Am. Chem. Soc.* **2012**, *134*, 16856.
- (195) Molander, G. A.; Trice, S. L.; Dreher, S. D. *J. Am. Chem. Soc.* **2010**, *132*, 17701.
- (196) Vara, B. A.; Li, X.; Berritt, S.; Walters, C. R.; Petersson, E. J.; Molander, G. A. *Chem. Sci.* **2018**, *9*, 336.
- (197) Tschäen, B. A.; Schmink, J. R.; Molander, G. A. *Org. Lett.* **2013**, *15*, 500.
- (198) Molander, G. A.; Wisniewski, S. R.; Hosseini-Sarvari, M. *Adv. Synth. Catal.* **2013**, *355*, 3037.

- (199) Molander, G. A.; Cavalcanti, L. N.; Garcia-Garcia, C. *J. Org. Chem.* **2013**, 78, 6427.
- (200) McGrew, G. I.; Stanciu, C.; Zhang, J.; Carroll, P. J.; Dreher, S. D.; Walsh, P. *J. Angew. Chem. Int. Ed. Engl.* **2012**, 51, 11510.
- (201) McNally, A.; Prier, C. K.; MacMillan, D. W. *Science.* **2011**, 334, 1114.
- (202) Jaman, Z.; Mufti, A.; Sah, S.; Avramova, L.; Thompson, D. H. *Chemistry* **2018**, 24, 9546.
- (203) Ganesan, L.; Shieh, P.; Bertozzi, C. R.; Levental, I. *Sci. Rep.* **2017**, 7, 41147.
- (204) Krska, S. W.; DiRocco, D. A.; Dreher, S. D.; Shevlin, M. *Acc. Chem. Res.* **2017**, 50, 2976.
- (205) Shevlin, M. *ACS. Med. Chem. Lett.* **2017**, 8, 601.
- (206) Cernak, T.; Gesmundo, N. J.; Dykstra, K.; Yu, Y.; Wu, Z.; Shi, Z. C.; Vachal, P.; Sperbeck, D.; He, S.; Murphy, B. A.; Sonatore, L.; Williams, S.; Madeira, M.; Verras, A.; Reiter, M.; Lee, C. H.; Cuff, J.; Sherer, E. C.; Kuethe, J.; Goble, S.; Perrotto, N.; Pinto, S.; Shen, D. M.; Nargund, R.; Balkovec, J.; DeVita, R. J.; Dreher, S. D. *J. Med. Chem.* **2017**, 60, 3594.
- (207) Shevlin, M.; Friedfeld, M. R.; Sheng, H.; Pierson, N. A.; Hoyt, J. M.; Campeau, L. C.; Chirik, P. J. *J. Am. Chem. Soc.* **2016**, 138, 3562.
- (208) Montgomery, J. *Science.* **2011**, 333, 1387.
- (209) Caschera, F.; Gazzola, G.; Bedau, M. A.; Bosch Moreno, C.; Buchanan, A.; Cawse, J.; Packard, N.; Hanczyc, M. M. *PLoS One.* **2010**, 5, e8546.
- (210) Srinivasan, R.; Tan, L. P.; Wu, H.; Yang, P. Y.; Kalesh, K. A.; Yao, S. Q. *Org. Biomol. Chem.* **2009**, 7, 1821.
- (211) Yang, X.; Parker, D.; Whitehead, L.; Ryder, N. S.; Weidmann, B.; Stabile-Harris, M.; Kizer, D.; McKinnon, M.; Smellie, A.; Powers, D. *Comb. Chem. High Throughput Screen.* **2006**, 9, 123.
- (212) DiRocco, D. A.; Dykstra, K.; Krska, S.; Vachal, P.; Conway, D. V.; Tudge, M. *Angew. Chem. Int. Ed. Engl.* **2014**, 53, 4802.
- (213) Kramer, R.; Cohen, D. *Nat. Rev. Drug. Discov.* **2004**, 3, 965.
- (214) Cernak, T.; Dykstra, K. D.; Tyagarajan, S.; Vachal, P.; Krska, S. W. *Chem. Soc. Rev.* **2017**, 46, 1760.
- (215) Kutchukian, P. S.; Dropinski, J. F.; Dykstra, K. D.; Li, B.; DiRocco, D. A.; Streckfuss, E. C.; Campeau, L. C.; Cernak, T.; Vachal, P.; Davies, I. W.; Krska, S. W.; Dreher, S. D. *Chem. Sci.* **2016**, 7, 2604.
- (216) Buitrago Santanilla, A.; Regalado, E. L.; Pereira, T.; Shevlin, M.; Bateman, K.; Campeau, L. C.; Schneeweis, J.; Berritt, S.; Shi, Z. C.; Nantermet, P.; Liu, Y.; Helmy, R.; Welch, C. J.; Vachal, P.; Davies, I. W.; Cernak, T.; Dreher, S. D. *Science.* **2015**, 347, 49.
- (217) Lin, S.; Dikler, S.; Blincoe, W. D.; Ferguson, R. D.; Sheridan, R. P.; Peng, Z.; Conway, D. V.; Zawatzky, K.; Wang, H.; Cernak, T.; Davies, I. W.; DiRocco, D. A.; Sheng, H.; Welch, C. J.; Dreher, S. D. *Science.* **2018**, 361.
- (218) Gesmundo, N. J.; Sauvagnat, B.; Curran, P. J.; Richards, M. P.; Andrews, C. L.; Dandliker, P. J.; Cernak, T. *Nature.* **2018**, 557, 228.
- (219) Cabrera-Pardo, J. R.; Chai, D. I.; Liu, S.; Mrksich, M.; Kozmin, S. A. *Nat. Chem.* **2013**, 5, 423.
- (220) Haslam, C.; Hellicar, J.; Dunn, A.; Fuetterer, A.; Hardy, N.; Marshall, P.; Paape, R.; Pemberton, M.; Resemannand, A.; Leveridge, M. *J. Biomol. Screen.* **2016**, 21, 176.
- (221) Hughes, I.; Hunter, D. *Curr. Opin. Chem. Biol.* **2001**, 5, 243.
- (222) Ripka, W. C.; Barker, G.; Krakover, J. *Drug. Discov. Today.* **2001**, 6, 471.
- (223) Peng, S. X.; Henson, C.; Strojnowski, M. J.; Golebiowski, A.; Klopfenstein, S. R. *Anal. Chem.* **2000**, 72, 261.
- (224) Kelley, B. D.; Switzer, M.; Bastek, P.; Kramarczyk, J. F.; Molnar, K.; Yu, T.; Coffman, J. *Biotechnol. Bioeng.* **2008**, 100, 950.

- (225) Yan, B.; Collins, N.; Wheatley, J.; Irving, M.; Leopold, K.; Chan, C.; Shornikov, A.; Fang, L.; Lee, A.; Stock, M.; Zhao, J. *J. Comb. Chem.* **2004**, *6*, 255.
- (226) Irving, M.; Krueger, C. A.; Wade, J. V.; Hodges, J. C.; Leopold, K.; Collins, N.; Chan, C.; Shaqair, S.; Shornikov, A.; Yan, B. *J. Comb. Chem.* **2004**, *6*, 478.
- (227) Dittus, L.; Werner, T.; Muelbaier, M.; Bantscheff, M. *ACS. Chem. Biol.* **2017**, *12*, 2515.
- (228) Werner, T.; Becher, I.; Sweetman, G.; Doce, C.; Savitski, M. M.; Bantscheff, M. *Anal. Chem.* **2012**, *84*, 7188.
- (229) Wagner, B. K.; Schreiber, S. L. *Cell. Chem. Biol.* **2016**, *23*, 3.
- (230) Mullard, A. *Nat. Rev. Drug. Discov.* **2015**, *14*, 807.
- (231) Reisen, F.; Sauty de Chalon, A.; Pfeifer, M.; Zhang, X.; Gabriel, D.; Selzer, P. *Assay. Drug. Dev. Technol.* **2015**, *13*, 415.
- (232) Etzion, Y.; Muslin, A. J. *Trends. Cardiovasc. Med.* **2009**, *19*, 207.
- (233) Lowe, D. *Med. Chem. Comm.* **2018**, *9*, 1397.
- (234) An, W. F.; Tolliday, N. *Mol. Biotechnol.* **2010**, *45*, 180.
- (235) An, W. F.; Tolliday, N. J. *Methods. Mol. Biol.* **2009**, 486, 1.
- (236) Dikici, E.; Deo, S. K.; Daunert, S. *Anal. Bioanal. Chem.* **2008**, 390, 2073.
- (237) Maddox, C. B.; Rasmussen, L.; White, E. L. *JALA Charlottesv. Va.* **2008**, *13*, 168.
- (238) Kolossov, E.; Lemon, A. *Eur. J. Med. Chem.* **2006**, *41*, 166.
- (239) Brandish, P. E.; Chiu, C. S.; Schneeweis, J.; Brandon, N. J.; Leech, C. L.; Kornienko, O.; Scolnick, E. M.; Strulovici, B.; Zheng, W. *J. Biomol. Screen.* **2006**, *11*, 481.
- (240) Lembo, D.; Donalisio, M.; De Andrea, M.; Cornaglia, M.; Scutera, S.; Musso, T.; Landolfo, S. *FASEB. J.* **2006**, *20*, 148.
- (241) Boss, C.; Hazemann, J.; Kimmerlin, T.; von Korff, M.; Luthi, U.; Peter, O.; Sander, T.; Siegrist, R. *Chimia (Aarau).* **2017**, *71*, 667.
- (242) Cline, G. W.; Hanna, S. B. *J. Am. Chem. Soc.* **1987**, *109*, 3087.
- (243) Leeson, P. D.; Young, R. J. *ACS. Med. Chem. Lett.* **2015**, *6*, 722.
- (244) Bajusz, D.; Racz, A.; Heberger, K. *J. Cheminform.* **2015**, *7*, 20.
- (245) Zhang, B.; Vogt, M.; Maggiora, G. M.; Bajorath, J. *J. Comput. Aided. Mol. Des.* **2015**, *29*, 595.
- (246) Akella, L. B.; DeCaprio, D. *Curr. Opin. Chem. Biol.* **2010**, *14*, 325.
- (247) Aldeghi, M.; Malhotra, S.; Selwood, D. L.; Chan, A. W. *Chem. Biol. Drug. Des.* **2014**, *83*, 450.
- (248) Carles, F.; Bourg, S.; Meyer, C.; Bonnet, P. *Molecules.* **2018**, *23*.
- (249) Chakravorty, S. J.; Chan, J.; Greenwood, M. N.; Popa-Burke, I.; Remlinger, K. S.; Pickett, S. D.; Green, D. V. S.; Fillmore, M. C.; Dean, T. W.; Luengo, J. I.; Macarron, R. *SLAS Discov.* **2018**, *23*, 532.
- (250) Csizmadia, J. S. a. F. *ACS. Spring. Meeting.* **2007**, *Presentation*.
- (251) Aldrich, S.  
<https://www.sigmaaldrich.com/catalog/product/aldrich/407704?lang=en&region=GB> **2019**,  
 Accessed February
- (252) Dixon, S. L.; Jurs, P. C. *J. Comput. Chem.* **1993**, *14*, 1460.
- (253) Suh, J. L.; Watts, B.; Stuckey, J. I.; Norris-Drouin, J. L.; Cholensky, S. H.; Dickson, B. M.; An, Y.; Mathea, S.; Salah, E.; Knapp, S.; Khan, A.; Adams, A. T.; Strahl, B. D.; Sagum, C. A.; Bedford, M. T.; James, L. I.; Kireev, D. B.; Frye, S. V. *Biochemistry.* **2018**, *57*, 2140.
- (254) Owa, T.; Yoshino, H.; Okauchi, T.; Yoshimatsu, K.; Ozawa, Y.; Sugi, N. H.; Nagasu, T.; Koyanagi, N.; Kitoh, K. *J. Med. Chem.* **1999**, *42*, 3789.
- (255) Fidanze, S. D.; Liu, D.; Mantel, R. A.; Hasvold, L. A.; Pratt, J. K.; Sheppard, G. S.; Wang, L.; Holms, J. H.; Dai, Y.; Aguirre, A.; Bogdan, A.; Dietrich, J. D.; Marjanovic, J.; Park, C. H.; Hutchins, C. W.; Lin, X.; Bui, M. H.; Huang, X.; Wilcox, D.; Li, L.; Wang, R.;

Kovar, P.; Magoc, T. J.; Rajaraman, G.; Albert, D. H.; Shen, Y.; Kati, W. M.; McDaniel, K. F. *Bioorg. Med. Chem. Lett.* **2018**, *28*, 1804.

(256) Yue, X., Feng, Y., Yu, B. *J. Fluorine Chem.* **2013**, *152*, 173.

(257) Dif, A.; Boulmedais, F.; Pinot, M.; Roullier, V.; Baudy-Floc'h, M.; Coquelle, F. M.; Clarke, S.; Neveu, P.; Vignaux, F.; Le Borgne, R.; Dahan, M.; Gueroui, Z.; Marchi-artzner, V. *J. Am. Chem. Soc.* **2009**, *131*, 14738.

(258) Aonbangkhen, C.; Zhang, H.; Wu, D. Z.; Lampson, M. A.; Chenoweth, D. M. *J. Am. Chem. Soc.* **2018**, *140*, 11926.

## 11. Supplementary information

**Supplementary Table 1:** LCMS data from **Figure 160**. Column 6 featured a control well, and column 18 featured positive control VHL amine **101**. Performed using standard conditions as outlined in General Methods, using LCMS method (A).

Well Number	SM Mass	Rt	% Area	Product Mass	Rt	% Area
DIPEA-A1	417.31	ND	0	726.37	ND	0
DIPEA-B1	430.2	0.57	71.88	739.36	1.06	24.45
DIPEA-C1	394.22	0.49	3.12	703.27	1	91.08
DIPEA-D1	424.23	0.66	72.01	733.33	1.15	23.6
DIPEA-E1	414.21	0.6	61.53	723.3	1.11	31.42
DIPEA-F1	444.22	0.59	84.59	753.4	1.11	15.41
DIPEA-G1	738.34	1.06	100	739.36	1.06	100
DIPEA-H1	554.26	0.44	74.68	863.4	0.67	19.1
DIPEA-I1	460.21	0.53	51.94	769.4	1	29.92
DIPEA-J1	798.34	1.12	100	799.41	1.12	100
DIPEA-K1	415.07	ND	0	724.65	0.96	31.03
DIPEA-L1	262.18	ND	0	571.16	0.67	83.31
DIPEA-M1	262.14	0.55	25.57	571.11	1.14	65.44
DIPEA-N1	204.1	0.35	2.7	513.03	0.82	80.84
DIPEA-O1	480.25	1.23	73.56	789.37	ND	0
DIPEA-P1	356.18	0.5	54.15	665.2	ND	0
DIPEA-A2	383.17	0.43	10.49	692.2	0.85	73.85
DIPEA-B2	218.12	0.39	55.9	527.05	0.9	37.39
DIPEA-C2	438.25	0.82	16.92	747.37	ND	0
DIPEA-D2	405.15	0.61	24.28	714.28	1.09	71.9
DIPEA-E2	337.17	0.36	57.95	646.18	0.86	16.35
DIPEA-F2	330.06	0.48	39.41	639.59	0.96	54.44
DIPEA-G2	434.1	0.99	3.6	744.12	1.19	53.89
DIPEA-H2	212.11	0.37	34.48	521.06	0.93	56.57
DIPEA-I2	446.13	0.75	31.54	755.39	1.25	47.39
DIPEA-J2	361.11	0.98	3.12	670.22	0.94	85.65
DIPEA-K2	277.1	0.35	94.05	586.15	0.77	2.29
DIPEA-L2	307.1	0.4	18.33	616.16	0.92	76.18
DIPEA-M2	295.15	0.44	19.65	604.13	0.91	55.22
DIPEA-N2	421.21	ND	0	730.3	1.08	81.1
DIPEA-O2	468.27	0.58	2.92	777.39	0.82	81.82
DIPEA-P2	240.07	ND	0	549.08	0.74	92.39
DIPEA-A3	223.14	0.6	1.83	532.08	0.81	68.27
DIPEA-B3	239.11	0.54	19.98	548.15	0.84	16.4
DIPEA-C3	289.17	0.36	80.79	598.14	0.86	17.93
DIPEA-D3	220.04	ND	0	529.06	1.07	93.08
DIPEA-E3	324.03	0.39	74	633.23	0.82	18.1

Confidential – Do Not Copy

DIPEA-F3	416.19	0.48	80.61	725.35	0.93	18.38
DIPEA-G3	438.25	0.83	59.64	747.37	ND	0
DIPEA-H3	451.25	ND	0	760.36	0.99	90.58
DIPEA-I3	245.15	ND	0	554.12	1.01	86.1
DIPEA-J3	263.11	0.42	71.52	572.07	1.01	1.55
DIPEA-K3	311.19	0.66	54.44	620.18	0.66	54.44
DIPEA-L3	209.04	0.41	3.3	518.43	1.01	89.78
DIPEA-M3	354.14	0.47	33.25	663.16	0.96	35.8
DIPEA-N3	225.12	0.95	64.59	534.04	0.95	64.59
DIPEA-O3	471.13	0.41	1.56	780.4	0.79	84.22
DIPEA-P3	465.19	0.35	76.35	774.38	0.74	2
DIPEA-A4	206.12	ND	0	515.05	0.72	93
DIPEA-B4	468.31	0.75	80.94	777.44	1.26	10.27
DIPEA-C4	442.29	0.72	82.94	751.4	1.23	11.63
DIPEA-D4	442.29	0.71	74.03	751.4	1.22	8.26
DIPEA-E4	442.29	0.7	81.6	751.4	1.21	12.7
DIPEA-F4	292.07	ND	0	601.53	ND	0
DIPEA-G4	269.15	0.39	61.09	578.14	0.95	10.4
DIPEA-H4	235.08	ND	0	544.11	ND	0
DIPEA-I4	259.22	0.36	47.96	568.21	0.87	20
DIPEA-J4	460.13	0.78	64.11	769.37	1.32	23.83
DIPEA-K4	288.18	0.38	49.28	597.18	0.87	16.33
DIPEA-L4	442.14	0.77	66.23	751.4	1.32	18.27
DIPEA-M4	237.07	0.35	32.33	546.07	0.88	47.56
DIPEA-N4	417.14	0.5	65.52	726.17	0.97	27.45
DIPEA-O4	258.15	ND	0	567.12	0.79	88.93
DIPEA-P4	290.21	0.43	67.56	599.2	0.96	20.78
DIPEA-A5	287.14	0.53	19.31	596.12	1.03	73.05
DIPEA-B5	249.15	0.74	3.92	558.11	0.98	85.23
DIPEA-C5	394.16	0.45	3.71	703.3	0.86	84.47
DIPEA-D5	223.13	0.42	45.35	532.07	1.03	46.09
DIPEA-E5	373.12	0.39	80.48	682.22	0.85	10.74
DIPEA-F5	375.14	ND	0	684.24	0.73	85.96
DIPEA-G5	368.16	ND	0	677.2	0.64	2.96
DIPEA-H5	242.08	ND	0	551.09	0.86	17.05
DIPEA-I5	260.15	0.45	15.42	569.13	0.99	42.85
DIPEA-J5	363.22	ND	0	672.25	0.9	81.25
DIPEA-K5	381.17	0.49	34.57	690.28	0.99	57.56
DIPEA-L5	306.1	0.41	9.34	615.19	0.93	72.99
DIPEA-M5	433.26	0.42	43.45	742.34	0.74	5.67
DIPEA-N5	327.09	0.61	2.22	636.07	1.13	48.37
DIPEA-O5	405.24	0.69	26.87	714.3	1.09	37.2
DIPEA-P5	302.1	0.37	2.6	611.15	0.93	89.15

Confidential – Do Not Copy

DIPEA-A6	Control	Control	Control	Control	Control	Control
DIPEA-B6	Control	Control	Control	Control	Control	Control
DIPEA-C6	Control	Control	Control	Control	Control	Control
DIPEA-D6	Control	Control	Control	Control	Control	Control
DIPEA-E6	Control	Control	Control	Control	Control	Control
DIPEA-F6	Control	Control	Control	Control	Control	Control
DIPEA-G6	Control	Control	Control	Control	Control	Control
DIPEA-H6	Control	Control	Control	Control	Control	Control
DIPEA-I6	Control	Control	Control	Control	Control	Control
DIPEA-J6	Control	Control	Control	Control	Control	Control
DIPEA-K6	Control	Control	Control	Control	Control	Control
DIPEA-L6	Control	Control	Control	Control	Control	Control
DIPEA-M6	Control	Control	Control	Control	Control	Control
DIPEA-N6	Control	Control	Control	Control	Control	Control
DIPEA-O6	Control	Control	Control	Control	Control	Control
DIPEA-P6	Control	Control	Control	Control	Control	Control
DIPEA-A7	247.17	0.72	86.02	556.14	0.72	86.02
DIPEA-B7	426.15	0.49	3.87	735.29	0.98	81.25
DIPEA-C7	396.19	0.43	23.9	705.72	0.86	14.07
DIPEA-D7	475.23	0.4	79.22	784.34	ND	0
DIPEA-E7	244.13	ND	0	553.09	0.75	87.47
DIPEA-F7	340.16	0.54	40.24	649.24	1.08	53.33
DIPEA-G7	280.15	0.4	4.34	589.12	0.73	79.93
DIPEA-H7	263.09	0.39	56.6	572.05	0.94	34.84
DIPEA-I7	305.15	0.48	44.81	614.15	1.04	42.29
DIPEA-J7	249.11	ND	0	558.07	0.91	82.36
DIPEA-K7	315.16	0.99	1.8	624.17	0.79	37.92
DIPEA-L7	247.1	ND	0	556.05	0.94	81.87
DIPEA-M7	246.17	0.48	79.48	555.15	ND	0
DIPEA-N7	209.04	ND	0	518.43	1.05	83.94
DIPEA-O7	430.2	0.57	91.31	739.36	1.06	1.81
DIPEA-P7	345.08	0.47	7.64	654.17	1.01	72.94
DIPEA-A8	326.19	0.65	4.79	635.2	ND	0
DIPEA-B8	365.14	0.58	17.12	674.24	1.1	76.52
DIPEA-C8	464.28	ND	0	773.41	1.19	90.99
DIPEA-D8	257.1	0.54	15.15	566.52	0.95	75.32
DIPEA-E8	478.29	0.81	13.86	787.44	1.22	39.2
DIPEA-F8	230.12	0.69	4.61	539.07	0.99	89.04
DIPEA-G8	232.12	0.51	25.33	541.08	1.12	66.34
DIPEA-H8	240.09	0.36	64.76	549.12	0.89	22.75
DIPEA-I8	468.31	ND	0	777.45	1.26	47.85
DIPEA-J8	272.16	0.4	14.69	581.15	0.92	70.84
DIPEA-K8	275.13	0.66	12.1	584.11	1.07	83.11

Confidential – Do Not Copy

DIPEA-L8	321.09	0.36	15.2	630.16	0.89	71.42
DIPEA-M8	405.24	ND	0	714.32	1.27	81.34
DIPEA-N8	300.16	0.45	4.08	609.16	1.03	85.4
DIPEA-O8	465.2	0.39	97.66	774.31	ND	0
DIPEA-P8	372.25	0.37	25.24	681.3	0.85	53.48
DIPEA-A9	246.12	ND	0	555.07	0.79	81.02
DIPEA-B9	250.18	ND	0	559.14	0.7	53.02
DIPEA-C9	323.06	0.6	6.62	632.6	0.94	27.76
DIPEA-D9	244.13	0.37	7.12	553.09	0.71	58.57
DIPEA-E9	385.23	1.05	3.17	694.28	0.71	66.53
DIPEA-F9	230.12	ND	0	539.07	0.91	81.74
DIPEA-G9	454.22	0.69	6.46	763.32	0.97	75.21
DIPEA-H9	262.15	0.47	46.79	571.11	1.09	47.14
DIPEA-I9	316.15	0.4	11.64	625.16	0.88	72.27
DIPEA-J9	243.14	0.5	3.02	552.11	1.07	82.46
DIPEA-K9	219.1	0.5	68.46	528.04	0.88	9.42
DIPEA-L9	401.21	0.61	1.01	710.26	1.08	74.28
DIPEA-M9	450.19	0.47	1.84	759.35	0.79	38.92
DIPEA-N9	274.17	0.57	86.99	583.16	1.22	2.96
DIPEA-O9	467.26	0.55	96.41	776.38	1	1.05
DIPEA-P9	241.1	0.35	59.41	550.06	0.85	34.09
DIPEA-A10	245.12	0.41	1.57	554.08	1	82.78
DIPEA-B10	222.11	0.5	21.2	531.04	1.1	25.6
DIPEA-C10	437.21	0.58	37.28	746.3	1.03	48.49
DIPEA-D10	465.23	0.51	96.33	774.34	ND	0
DIPEA-E10	300.11	0.51	42.75	609.17	1.09	44.09
DIPEA-F10	273.16	ND	0	582.13	0.78	67.74
DIPEA-G10	350.2	1.06	84.81	659.25	ND	0
DIPEA-H10	353.17	0.35	84.79	662.18	ND	0
DIPEA-I10	243.11	0.52	16.74	552.06	0.84	66.76
DIPEA-J10	358.24	ND	0	667.28	0.74	83.45
DIPEA-K10	227.05	0.7	2.66	536.45	0.89	72.12
DIPEA-L10	300.16	0.45	11.49	609.16	0.96	74.98
DIPEA-M10	296.15	ND	0	605.12	0.89	77.91
DIPEA-N10	254.13	0.44	8.48	563.08	0.96	83.62
DIPEA-O10	287.15	0.37	65.06	596.12	0.87	23.47
DIPEA-P10	211.08	ND	0	520.01	0.78	72.73
DIPEA-A11	358.24	0.43	2.22	667.28	0.75	89.65
DIPEA-B11	229.11	0.36	93.05	538.04	0.84	5.59
DIPEA-C11	225.11	ND	0	534.05	0.84	54.14
DIPEA-D11	216.09	0.42	14.84	525.04	1.04	70.84
DIPEA-E11	281.13	0.75	1.69	590.12	1.09	93.52
DIPEA-F11	393.22	ND	0	702.29	1.06	4.5

Confidential – Do Not Copy

DIPEA-G11	283.14	ND	0	592.13	0.94	9.96
DIPEA-H11	484.19	ND	0	793.32	0.99	84
DIPEA-I11	451.19	0.53	4.24	760.29	0.98	78.85
DIPEA-J11	223.14	0.42	7.94	532.08	0.8	74.58
DIPEA-K11	203.11	ND	0	512.04	0.96	84.71
DIPEA-L11	296.26	0.52	14.85	605.25	0.67	34.87
DIPEA-M11	447.12	0.58	2.33	756.74	1	51.27
DIPEA-N11	302.21	ND	0	611.21	ND	0
DIPEA-O11	412.21	0.45	84.37	721.28	0.89	4.91
DIPEA-P11	471.36	0.61	28.72	780.47	0.93	71.28
DIPEA-A12	199.07	0.36	1.79	508.07	0.97	77.83
DIPEA-B12	402.26	0.56	32.47	711.33	1.08	48.14
DIPEA-C12	288.18	ND	0	597.18	1.06	84.12
DIPEA-D12	222.1	ND	0	531.03	0.83	83.11
DIPEA-E12	202.12	ND	0	511.05	0.75	83.15
DIPEA-F12	232.13	ND	0	541.08	0.9	15.48
DIPEA-G12	442.33	ND	0	751.44	0.9	60.13
DIPEA-H12	342.17	0.35	91.31	651.19	0.78	6.14
DIPEA-I12	334.17	0.66	98.79	643.22	ND	0
DIPEA-J12	449.24	ND	0	758.36	1.2	90.37
DIPEA-K12	244.13	0.37	2.39	553.09	0.94	85.89
DIPEA-L12	449.24	0.96	2.26	758.36	1.19	82.07
DIPEA-M12	280.15	0.68	9.97	589.12	0.96	77.91
DIPEA-N12	261.16	ND	0	570.12	0.72	72.46
DIPEA-O12	423.23	0.99	5.79	732.32	ND	0
DIPEA-P12	262.14	0.37	23.91	571.11	0.78	59.03
DIPEA-A13	256.11	0.43	36.64	565.53	1	55.46
DIPEA-B13	310.14	ND	0	619.15	0.85	58.92
DIPEA-C13	284.14	0.35	63.86	593.13	0.8	30.76
DIPEA-D13	306.19	0.66	7.39	615.2	1.21	71.35
DIPEA-E13	238.14	0.61	1.1	547.09	0.83	86.24
DIPEA-F13	259.13	0.37	39.49	568.11	0.94	55.64
DIPEA-G13	204.08	0.35	4.67	512.98	0.94	78.3
DIPEA-H13	247.13	0.38	3.39	556.09	0.76	53.99
DIPEA-I13	422.21	0.67	5.44	731.28	0.92	86.7
DIPEA-J13	401.27	0.81	71.15	710.34	ND	0
DIPEA-K13	447.24	ND	0	756.33	1.1	90.16
DIPEA-L13	203.11	0.39	30.76	512.04	0.96	64.46
DIPEA-M13	452.24	0.36	11.88	761.35	0.74	78.89
DIPEA-N13	361.08	0.52	15.82	670.13	1.1	64.7
DIPEA-O13	247.17	0.55	6.11	556.14	0.99	85.19
DIPEA-P13	233.12	0.52	1.08	542.07	0.95	93.51
DIPEA-A14	215.12	ND	0	524.05	0.78	81.46

Confidential – Do Not Copy

DIPEA-B14	468.13	0.46	46.77	777.77	0.95	36.09
DIPEA-C14	280.14	ND	0	589.12	1.09	79.34
DIPEA-D14	287.16	0.44	60.66	596.16	0.44	60.66
DIPEA-E14	274.14	ND	0	583.12	0.85	89.13
DIPEA-F14	287.11	0.45	12.06	596.14	0.88	53.35
DIPEA-G14	301.15	0.52	13.96	610.15	1.12	77.93
DIPEA-H14	254.13	0.36	92.13	563.08	ND	0
DIPEA-I14	215.07	0.58	9.19	524.07	0.98	81.8
DIPEA-J14	259.14	0.42	61.28	568.11	0.98	33.46
DIPEA-K14	236.13	0.61	9.85	545.07	ND	0
DIPEA-L14	403.21	0.96	0.87	712.27	1	84.48
DIPEA-M14	246.15	0.37	67.48	555.11	0.92	28.04
DIPEA-N14	207.14	ND	0	516.08	0.7	49.77
DIPEA-O14	260.16	0.83	2.95	569.14	1.03	86.91
DIPEA-P14	367.17	0.35	20.65	676.27	0.75	12.7
DIPEA-A15	368.1	0.9	11.07	677.27	1.08	12.96
DIPEA-B15	208.1	0.61	0.99	517.02	0.8	85.6
DIPEA-C15	356.22	0.8	9.64	665.26	0.76	77.63
DIPEA-D15	258.14	0.43	79.78	567.12	ND	0
DIPEA-E15	331.23	0.75	10.26	640.25	0.75	10.26
DIPEA-F15	287.17	1.14	5.05	596.17	1.22	85.41
DIPEA-G15	393.23	0.35	57.59	702.28	0.7	38.31
DIPEA-H15	327.06	0.36	77.27	636.58	0.77	14.7
DIPEA-I15	310.17	0.36	57.58	619.15	0.7	21.35
DIPEA-J15	282.15	0.4	47.05	591.15	0.92	31.32
DIPEA-K15	395.13	0.59	73.58	704.25	1.06	6.7
DIPEA-L15	260.14	ND	0	569.09	0.73	93.44
DIPEA-M15	245.13	ND	0	554.07	0.82	80.67
DIPEA-N15	330.15	0.59	3.14	639.16	0.88	31.56
DIPEA-O15	217.1	0.35	5.71	526.03	0.88	81.49
DIPEA-P15	288.17	0.57	2.43	597.15	0.91	80.66
DIPEA-A16	402.18	0.46	75.48	711.24	0.81	2.68
DIPEA-B16	335.2	ND	0	644.21	ND	0
DIPEA-C16	294.17	0.7	5.16	603.15	0.72	39.58
DIPEA-D16	278.14	0.38	76.13	587.11	0.91	9.88
DIPEA-E16	317.14	0.45	15.17	626.14	0.93	78.67
DIPEA-F16	304.19	0.49	21.9	613.19	0.94	58.57
DIPEA-G16	331.18	0.61	83.31	640.18	0.61	83.31
DIPEA-H16	367.19	0.43	37.27	676.24	0.79	44.37
DIPEA-I16	342.16	0.49	70.78	651.17	1	22.67
DIPEA-J16	291.14	0.7	96.41	600.12	ND	0
DIPEA-K16	311.09	1.18	30.63	620.16	0.94	44.36
DIPEA-L16	280.1	0.9	79.66	589.15	0.9	79.66

Confidential – Do Not Copy

DIPEA-M16	218.11	0.53	90.59	527.06	ND	0
DIPEA-N16	275.16	0.37	8.03	584.15	0.89	78.35
DIPEA-O16	314.19	0.37	34.81	623.18	ND	0
DIPEA-P16	277.18	0.48	80.38	586.15	0.88	15.97
DIPEA-A17	219.11	0.38	4.43	528.05	0.8	82.64
DIPEA-B17	437.17	0.82	1.09	746.26	0.94	87.09
DIPEA-C17	265.09	0.41	39.39	574.13	0.99	48.45
DIPEA-D17	467.12	0.63	77.63	776.27	1.12	7.19
DIPEA-E17	217.12	0.4	68.29	526.07	0.96	28.41
DIPEA-F17	347.2	0.48	70.34	656.23	ND	0
DIPEA-G17	436.22	0.58	59.39	745.31	1.03	34.75
DIPEA-H17	204.13	0.48	32.6	513.07	1.03	55.69
DIPEA-I17	497.12	0.59	94.14	806.4	ND	0
DIPEA-J17	439.23	ND	0	748.31	0.92	87.18
DIPEA-K17	246.14	0.57	51	555.11	1.22	45.32
DIPEA-L17	283.1	0.84	1.56	592.15	1	89.24
DIPEA-M17	407.2	ND	0	716.74	0.85	77.35
DIPEA-N17	353.1	0.84	8.46	662.67	ND	0
DIPEA-O17	355.19	0.4	93.63	664.22	0.88	2.81
DIPEA-P17	315.19	0.47	75.88	624.21	ND	0
DIPEA-A18	430.2	0.57	57.6	739.36	1.06	32.97
DIPEA-B18	430.2	0.57	89.94	739.36	1.06	2.9
DIPEA-C18	430.2	0.57	89.91	739.36	1.06	3.1
DIPEA-D18	430.2	0.57	55.11	739.36	1.06	36.48
DIPEA-E18	430.2	0.57	66.82	739.36	1.06	25.92
DIPEA-F18	430.2	0.57	71.63	739.36	1.06	21.69
DIPEA-G18	430.2	0.57	87.01	739.36	1.06	6.13
DIPEA-H18	430.2	0.57	88.63	739.36	1.06	4.52
DIPEA-I18	430.2	0.57	84.28	739.36	1.06	11.19
DIPEA-J18	430.2	0.57	87.1	739.36	1.06	4.22
DIPEA-K18	430.2	0.57	88.27	739.36	1.06	3.25
DIPEA-L18	430.2	0.57	86.08	739.36	1.06	4.2
DIPEA-M18	430.2	0.57	78.58	739.36	1.06	12.78
DIPEA-N18	430.2	0.57	85.57	739.36	1.06	8.01
DIPEA-O18	430.2	0.57	70.34	739.36	1.06	22.23
DIPEA-P18	430.2	0.57	70.04	739.36	1.06	21.29
DIPEA-A19	430.29	ND	0	739.4	1.19	90.32
DIPEA-B19	290.24	0.46	80.18	599.24	0.93	6.8
DIPEA-C19	288.16	0.42	60.63	597.15	0.9	29.43
DIPEA-D19	208.11	0.61	1.72	517.02	0.75	71.63
DIPEA-E19	292.1	0.41	98.8	601.16	ND	0
DIPEA-F19	461.24	0.99	2.57	770.37	1.11	72.88
DIPEA-G19	250.12	0.35	41.24	559.06	0.82	48.21

Confidential – Do Not Copy

DIPEA-H19	318.27	0.59	8.51	627.3	1	1.02
DIPEA-I19	393.15	0.48	6.76	702.26	0.74	49.07
DIPEA-J19	450.24	0.5	1.24	759.34	0.84	70.08
DIPEA-K19	304.16	0.35	92.11	613.15	ND	0
DIPEA-L19	348.23	0.93	77.03	657.26	0.93	77.03
DIPEA-M19	351.18	0.41	86.84	660.19	ND	0
DIPEA-N19	356.16	0.53	27.43	665.15	1.03	55.21
DIPEA-O19	220.17	0.36	90.32	529.11	0.89	7.83
DIPEA-P19	259.14	0.45	75.06	568.11	1.01	14.81
DIPEA-A20	418.26	0.36	4.41	727.34	0.79	2.38
DIPEA-B20	315.19	0.47	88.87	624.21	ND	0
DIPEA-C20	299.16	0.42	39.61	608.17	0.94	52.44
DIPEA-D20	248.13	0.38	24.22	557.07	0.88	62
DIPEA-E20	314.17	0.46	82.19	623.17	ND	0
DIPEA-F20	321.13	ND	0	630.2	1.03	88.14
DIPEA-G20	287.15	0.4	70.35	596.12	0.4	70.35
DIPEA-H20	412.04	0.55	82.13	722.03	0.97	9.05
DIPEA-I20	207.11	0.37	18.34	516.04	0.97	61.56
DIPEA-J20	220.11	0.31	76.35	529.02	0.78	20.16
DIPEA-K20	229.13	0.36	48.55	538.09	0.79	39.76
DIPEA-L20	310.14	0.61	18.56	619.15	1.16	64.81
DIPEA-M20	241.1	ND	0	550.04	1.04	16.22
DIPEA-N20	257.08	0.38	13.16	566.11	0.94	75.29
DIPEA-O20	293.15	0.5	21.16	602.14	1.08	73.68
DIPEA-P20	342.14	0.49	0.9	651.22	1.04	22.76
DIPEA-A21	351.14	0.7	17.71	660.22	0.9	67.17
DIPEA-B21	476.25	ND	0	785.38	0.86	38.53
DIPEA-C21	389.23	0.6	1.82	698.28	1.12	61.2
DIPEA-D21	443.16	0.8	94.64	752.26	ND	0
DIPEA-E21	474.19	0.61	3.85	783.28	1.05	78.25
DIPEA-F21	256.13	0.4	90.16	565.09	0.83	1.38
DIPEA-G21	286.18	ND	0	595.18	0.71	85.92
DIPEA-H21	450.26	ND	0	759.39	1.15	86.2
DIPEA-I21	258.14	0.36	90.12	567.12	0.84	1.67
DIPEA-J21	343.12	ND	0	652.19	1.1	80.5
DIPEA-K21	310.1	ND	0	619.17	1	87.29

**Supplementary Table 2:** LCMS data from **Figure 126**. Column 6 featured a control well, and column 18 featured positive control VHL amine **101**. Performed using standard conditions as outlined in General Methods, using LCMS method (A). To determine di-adduct formation, input mass was (M + H) if the compounds mass was <1000 Da, and if over 1000, then (M + 2H)/2 was used to search for the compound.

Well Number	SM Mass	Rt	% Area	Product Mass	Rt	% Area	Di-adduct mass	Rt	% Area
NMM-A1	417.31	N.D.	0	725.45	0.67	43.03	516.5	N.D.	0
NMM-B1	430.2	0.58	6.47	738.34	1.07	57.19	523	N.D.	0
NMM-C1	394.22	N.D.	0	702.36	1.01	93.12	505	N.D.	0
NMM-D1	424.23	0.67	76.79	732.37	1.16	10.88	520	N.D.	0
NMM-E1	414.21	0.61	62.75	722.34	1.12	21.4	515	N.D.	0
NMM-F1	444.22	0.61	4.45	752.36	1.12	95.55	530	N.D.	0
NMM-G1	738.34	1.07	100	523	N.D.	0	677	N.D.	0
NMM-H1	554.26	0.45	11.16	862.4	0.68	82.89	585	N.D.	0
NMM-I1	460.21	0.54	2.56	768.35	1.01	81.55	538	1.28	7.03
NMM-J1	798.34	1.13	98.7	553	N.D.	0	707	N.D.	0
NMM-K1	415.07	N.D.	0	723.21	0.96	28.03	515.5	N.D.	0
NMM-L1	262.18	N.D.	0	570.32	0.68	53.56	878.46	N.D.	0
NMM-M1	262.14	N.D.	0	570.28	1.15	85.96	878.42	N.D.	0
NMM-N1	204.1	N.D.	0	512.24	0.83	80.75	820.38	N.D.	0
NMM-O1	480.25	N.D.	0	788.39	N.D.	0	548	0.83	25.54
NMM-P1	356.18	0.51	36.56	664.32	0.96	2.74	972.45	N.D.	0
NMM-A2	383.17	N.D.	0	691.31	0.85	93.68	999.45	N.D.	0
NMM-B2	218.12	N.D.	0	526.26	0.9	94.72	834.39	N.D.	0
NMM-C2	438.25	0.87	29.32	746.39	1.08	12.7	527	N.D.	0
NMM-D2	405.15	1.01	4.64	713.29	1.1	78.49	510.5	N.D.	0
NMM-E2	337.17	0.45	13.11	645.31	0.87	5.01	953.45	N.D.	0
NMM-F2	330.06	0.86	4.25	638.19	0.97	89.35	946.33	N.D.	0
NMM-G2	434.1	N.D.	0	742.24	1.2	84.11	507.5	N.D.	0
NMM-H2	212.11	N.D.	0	520.25	0.94	92.62	828.38	N.D.	0
NMM-I2	446.13	0.75	58	754.27	1.26	23.85	531	N.D.	0
NMM-J2	361.11	0.99	3.64	669.25	0.95	91.25	977.39	N.D.	0
NMM-K2	277.1	0.4	4.04	585.24	0.78	68.25	877.38	N.D.	0
NMM-L2	307.1	N.D.	0	615.24	0.93	91.02	923.38	N.D.	0
NMM-M2	295.15	N.D.	0	603.29	0.92	38.79	911.43	N.D.	0
NMM-N2	421.21	N.D.	0	729.35	1.08	48.87	518.5	N.D.	0
NMM-O2	468.27	N.D.	0	776.41	0.83	77.09	542	N.D.	0
NMM-P2	240.07	0.51	4.7	548.21	0.75	81.59	856.35	N.D.	0
NMM-A3	223.14	N.D.	0	531.28	0.82	81.15	839.42	1.16	10.28
NMM-B3	239.11	0.78	1.82	547.25	0.85	65.74	855.39	N.D.	0
NMM-C3	289.17	N.D.	0	597.3	0.87	98.21	905.44	N.D.	0

Confidential – Do Not Copy

NMM-D3	220.04	N.D.	0	528.18	1.08	98.83	836.32	N.D.	0
NMM-E3	324.03	0.4	77.73	632.17	0.83	20	940.31	N.D.	0
NMM-F3	416.19	0.49	1.51	724.33	0.94	96.93	516	N.D.	0
NMM-G3	438.25	0.84	54.32	746.39	1.05	3.97	527	N.D.	0
NMM-H3	451.25	N.D.	0	759.39	1	98.98	533.5	N.D.	0
NMM-I3	245.15	N.D.	0	553.29	1.02	100	861.43	N.D.	0
NMM-J3	263.11	0.43	64.94	571.25	N.D.	0	879.39	N.D.	0
NMM-K3	311.19	0.86	5.31	619.32	0.73	78.09	927.46	1.02	3.47
NMM-L3	209.04	N.D.	0	517.17	1.02	72.75	825.31	N.D.	0
NMM-M3	354.14	N.D.	0	662.28	0.97	58.35	970.42	N.D.	0
NMM-N3	225.12	N.D.	0	533.26	0.96	70.37	841.4	N.D.	0
NMM-O3	471.13	0.42	1.39	779.27	0.8	88.78	543.5	N.D.	0
NMM-P3	465.19	0.36	73.41	773.33	N.D.	0	540.5	N.D.	0
NMM-A4	206.12	N.D.	0	514.26	0.73	100	822.39	N.D.	0
NMM-B4	468.31	0.76	51.65	776.45	1.27	15.21	542	N.D.	0
NMM-C4	442.29	0.73	80.8	750.43	1.24	19.2	529	N.D.	0
NMM-D4	442.29	0.71	68.97	750.43	1.23	18.98	529	N.D.	0
NMM-E4	442.29	0.71	80.69	750.43	1.22	19.31	529	N.D.	0
NMM-F4	292.07	N.D.	0	600.21	N.D.	0	908.35	N.D.	0
NMM-G4	269.15	0.4	1.93	577.29	0.96	66.61	885.43	N.D.	0
NMM-H4	235.08	0.94	87.09	543.22	N.D.	0	851.36	N.D.	0
NMM-I4	259.22	N.D.	0	567.36	0.88	27.43	875.5	N.D.	0
NMM-J4	460.13	0.79	71.25	768.27	1.33	13.71	538	N.D.	0
NMM-K4	288.18	0.38	22.76	596.32	0.88	13.76	904.46	N.D.	0
NMM-L4	442.14	0.78	69.45	750.28	1.33	12.2	529	N.D.	0
NMM-M4	237.07	0.48	3.07	545.21	0.89	83.12	837.35	N.D.	0
NMM-N4	417.14	0.89	3.4	725.28	0.98	90.29	516.5	N.D.	0
NMM-O4	258.15	N.D.	0	566.29	0.8	44.41	874.43	N.D.	0
NMM-P4	290.21	0.44	5.51	598.35	0.97	72.98	906.49	N.D.	0
NMM-A5	287.14	N.D.	0	595.28	1.04	100	903.42	N.D.	0
NMM-B5	249.15	N.D.	0	557.29	0.99	97.47	865.43	N.D.	0
NMM-C5	394.16	N.D.	0	702.3	0.87	100	505	N.D.	0
NMM-D5	223.13	N.D.	0	531.27	1.04	95.7	839.41	N.D.	0
NMM-E5	373.12	N.D.	0	681.26	0.86	88.33	989.4	N.D.	0
NMM-F5	375.14	N.D.	0	683.28	0.74	94.35	991.41	N.D.	0
NMM-G5	368.16	0.64	6.02	676.3	0.64	6.02	984.44	N.D.	0
NMM-H5	242.08	N.D.	0	550.22	0.87	20.58	858.36	N.D.	0
NMM-I5	260.15	N.D.	0	568.29	1	60.71	876.43	N.D.	0
NMM-J5	363.22	N.D.	0	671.35	0.91	97.99	979.49	N.D.	0
NMM-K5	381.17	N.D.	0	689.31	1	97.18	997.45	N.D.	0
NMM-L5	306.1	N.D.	0	614.24	0.94	84.32	922.38	0.84	9.47
NMM-M5	433.26	0.43	41.34	741.4	0.75	12.65	524.5	N.D.	0
NMM-N5	327.09	0.89	1.49	635.23	1.14	45.93	943.37	N.D.	0

Confidential – Do Not Copy

NMM-O5	405.24	0.69	13.86	713.38	1.1	29.44	510.5	N.D.	0
NMM-P5	302.1	N.D.	0	610.24	0.94	98.53	918.38	N.D.	0
NMM-A6	No Target	N.D.	0	308.14	N.D.	0	616.28	N.D.	0
NMM-B6	No Target	N.D.	0	308.14	N.D.	0	616.28	N.D.	0
NMM-C6	No Target	N.D.	0	308.14	N.D.	0	616.28	N.D.	0
NMM-D6	No Target	N.D.	0	308.14	N.D.	0	616.28	N.D.	0
NMM-E6	No Target	N.D.	0	308.14	N.D.	0	616.28	N.D.	0
NMM-F6	No Target	N.D.	0	308.14	N.D.	0	616.28	N.D.	0
NMM-G6	No Target	N.D.	0	308.14	N.D.	0	616.28	N.D.	0
NMM-H6	No Target	N.D.	0	308.14	N.D.	0	616.28	N.D.	0
NMM-I6	No Target	N.D.	0	308.14	N.D.	0	616.28	N.D.	0
NMM-J6	No Target	N.D.	0	308.14	N.D.	0	616.28	N.D.	0
NMM-K6	No Target	N.D.	0	308.14	N.D.	0	616.28	N.D.	0
NMM-L6	No Target	N.D.	0	308.14	N.D.	0	616.28	N.D.	0
NMM-M6	No Target	N.D.	0	308.14	N.D.	0	616.28	N.D.	0
NMM-N6	No Target	N.D.	0	308.14	N.D.	0	616.28	N.D.	0
NMM-O6	No Target	N.D.	0	308.14	N.D.	0	616.28	N.D.	0
NMM-P6	No Target	N.D.	0	308.14	N.D.	0	616.28	N.D.	0
NMM-A7	247.17	N.D.	0	555.31	0.73	100	863.45	N.D.	0
NMM-B7	426.15	0.5	2.62	734.29	0.99	92.05	521	N.D.	0
NMM-C7	396.19	0.38	0.58	704.33	0.81	21.68	506	1.27	11.81
NMM-D7	475.23	0.43	25.56	783.37	0.75	24.31	545.5	N.D.	0
NMM-E7	244.13	N.D.	0	552.27	0.76	98.38	860.41	N.D.	0
NMM-F7	340.16	0.55	3.52	648.3	1.09	96.48	956.43	N.D.	0
NMM-G7	280.15	N.D.	0	588.29	0.74	98.93	896.43	N.D.	0
NMM-H7	263.09	N.D.	0	571.23	0.95	87.96	879.37	N.D.	0
NMM-I7	305.15	0.49	60.63	613.29	1.05	24.82	921.43	N.D.	0
NMM-J7	249.11	N.D.	0	557.25	0.92	95.06	865.39	0.92	95.06
NMM-K7	315.16	0.4	10.9	623.3	0.8	32.16	931.44	1.24	45.69
NMM-L7	247.1	N.D.	0	555.23	0.95	88	863.37	N.D.	0
NMM-M7	246.17	0.49	92.1	554.31	N.D.	0	862.45	N.D.	0
NMM-N7	209.04	N.D.	0	517.17	1.06	88.14	825.31	N.D.	0
NMM-O7	430.2	0.57	51.09	738.34	1.07	41	523	N.D.	0
NMM-P7	345.08	0.48	13.98	653.22	1.02	72.44	961.36	N.D.	0
NMM-A8	326.19	0.66	4.05	634.32	0.75	91.91	942.46	N.D.	0
NMM-B8	365.14	1.11	94.17	673.28	1.11	94.17	981.42	N.D.	0
NMM-C8	464.28	N.D.	0	772.42	1.2	96.91	540	N.D.	0
NMM-D8	257.1	N.D.	0	565.24	0.96	80.34	873.38	N.D.	0
NMM-E8	478.29	N.D.	0	786.43	1.23	82.22	547	N.D.	0
NMM-F8	230.12	N.D.	0	538.26	1	100	846.39	N.D.	0
NMM-G8	232.12	N.D.	0	540.26	1.13	95.96	848.4	N.D.	0

Confidential – Do Not Copy

NMM-H8	240.09	0.36	45.45	548.23	0.89	46.55	856.37	1.24	3.81
NMM-I8	468.31	N.D.	0	776.45	1.27	55.52	542	N.D.	0
NMM-J8	272.16	0.41	17.04	580.3	0.94	81.95	888.44	N.D.	0
NMM-K8	275.13	0.67	12.62	583.27	1.08	87.38	891.41	N.D.	0
NMM-L8	321.09	0.36	10.66	629.23	0.89	85.07	937.37	1.2	3.28
NMM-M8	405.24	N.D.	0	713.38	1.28	100	510.5	N.D.	0
NMM-N8	300.16	N.D.	0	608.3	1.04	100	916.44	N.D.	0
NMM-O8	465.2	0.4	100	773.34	N.D.	0	540.5	N.D.	0
NMM-P8	372.25	0.4	80.53	680.39	0.86	17.02	988.53	N.D.	0
NMM-A9	246.12	N.D.	0	554.26	0.8	93.33	862.4	N.D.	0
NMM-B9	250.18	N.D.	0	558.32	0.71	57.36	866.46	N.D.	0
NMM-C9	323.06	0.6	7.12	631.2	0.95	29.76	939.34	N.D.	0
NMM-D9	244.13	0.65	1.46	552.27	0.72	68.75	860.41	N.D.	0
NMM-E9	385.23	N.D.	0	693.37	0.72	67.54	500.5	0.92	10.69
NMM-F9	230.12	N.D.	0	538.26	0.92	90.86	846.39	N.D.	0
NMM-G9	454.22	0.69	5.71	762.36	0.98	84.15	535	N.D.	0
NMM-H9	262.15	0.47	17.98	570.29	1.1	82.02	878.43	N.D.	0
NMM-I9	316.15	0.41	14.88	624.29	0.89	75.23	932.43	N.D.	0
NMM-J9	243.14	N.D.	0	551.28	1.08	98.21	859.42	N.D.	0
NMM-K9	219.1	0.5	75.99	527.24	0.89	3.58	835.38	N.D.	0
NMM-L9	401.21	N.D.	0	709.35	1.09	76.38	508.5	N.D.	0
NMM-M9	450.19	0.94	4.57	758.33	0.8	42.78	533	N.D.	0
NMM-N9	274.17	0.58	86.06	582.31	1.23	3.62	890.45	N.D.	0
NMM-O9	467.26	0.56	93.75	775.4	N.D.	0	541.5	0.7	2.88
NMM-P9	241.1	N.D.	0	549.24	0.86	93.64	857.37	N.D.	0
NMM-A10	245.12	0.41	0.95	553.26	1	94.47	861.39	N.D.	0
NMM-B10	222.11	0.51	23.85	530.25	1.11	27.13	838.39	N.D.	0
NMM-C10	437.21	0.59	20.9	745.35	1.04	40.19	526.5	N.D.	0
NMM-D10	465.23	0.52	96.05	773.37	N.D.	0	540.5	N.D.	0
NMM-E10	300.11	0.52	53.74	608.25	1.1	30.58	916.39	N.D.	0
NMM-F10	273.16	N.D.	0	581.3	0.79	76.09	889.44	1.23	1.69
NMM-G10	350.2	1.07	100	658.34	N.D.	0	966.48	N.D.	0
NMM-H10	353.17	0.35	62.28	661.31	0.67	17.59	969.45	N.D.	0
NMM-I10	243.11	0.53	16.7	551.25	0.85	74.43	859.39	N.D.	0
NMM-J10	358.24	N.D.	0	666.38	0.75	100	974.52	N.D.	0
NMM-K10	227.05	0.66	3.96	535.19	0.9	82.14	843.32	N.D.	0
NMM-L10	300.16	0.46	10.65	608.3	0.97	88.11	916.44	N.D.	0
NMM-M10	296.15	N.D.	0	604.29	0.9	92.07	912.43	N.D.	0
NMM-N10	254.13	N.D.	0	562.27	0.97	90.32	870.4	N.D.	0
NMM-O10	287.15	N.D.	0	595.29	0.88	96.9	903.43	N.D.	0
NMM-P10	211.08	N.D.	0	519.22	0.79	84.01	869.37	N.D.	0
NMM-A11	358.24	N.D.	0	666.38	0.84	51.63	974.52	N.D.	0
NMM-B11	229.11	0.35	15.07	537.25	0.84	74.23	845.39	N.D.	0

Confidential – Do Not Copy

NMM-C11	225.11	N.D.	0	533.25	0.85	63.95	841.39	N.D.	0
NMM-D11	216.09	0.52	1.64	524.23	1.05	83.2	832.37	N.D.	0
NMM-E11	281.13	N.D.	0	589.27	1.1	97.81	897.41	N.D.	0
NMM-F11	393.22	N.D.	0	701.36	1.06	2.7	504.5	N.D.	0
NMM-G11	283.14	N.D.	0	591.28	0.95	10.28	899.42	0.72	54.55
NMM-H11	484.19	N.D.	0	792.33	1	97.13	550	N.D.	0
NMM-I11	451.19	N.D.	0	759.32	0.98	85.99	533.5	N.D.	0
NMM-J11	223.14	0.76	1.8	531.28	0.81	92.86	839.42	N.D.	0
NMM-K11	203.11	N.D.	0	511.24	0.97	98.51	819.38	N.D.	0
NMM-L11	296.26	N.D.	0	604.4	0.69	16.54	912.54	N.D.	0
NMM-M11	447.12	1.01	58.91	755.26	1.01	58.91	531.5	N.D.	0
NMM-N11	302.21	0.69	5.54	610.35	N.D.	0	918.49	1.01	24.14
NMM-O11	412.21	0.46	88.34	720.35	0.87	5.43	514	N.D.	0
NMM-P11	471.36	N.D.	0	779.5	0.93	28.26	543.5	N.D.	0
NMM-A12	199.07	N.D.	0	507.21	0.98	86.29	829.35	N.D.	0
NMM-B12	402.26	N.D.	0	710.4	1.09	64.35	509	0.98	8.59
NMM-C12	288.18	0.85	14.74	596.32	1.07	30.29	904.46	N.D.	0
NMM-D12	222.1	N.D.	0	530.24	0.84	82.28	838.38	1.17	10.27
NMM-E12	202.12	N.D.	0	510.26	0.75	98.43	818.4	N.D.	0
NMM-F12	232.13	N.D.	0	540.27	0.9	20.87	848.41	N.D.	0
NMM-G12	442.33	N.D.	0	750.47	0.91	100	529	N.D.	0
NMM-H12	342.17	N.D.	0	650.31	0.78	92.65	958.45	N.D.	0
NMM-I12	334.17	0.67	98.56	642.31	N.D.	0	950.45	N.D.	0
NMM-J12	449.24	N.D.	0	757.38	1.2	93.04	532.5	N.D.	0
NMM-K12	244.13	N.D.	0	552.27	0.95	91.38	860.41	N.D.	0
NMM-L12	449.24	N.D.	0	757.38	1.2	76.97	532.5	N.D.	0
NMM-M12	280.15	1.02	1.68	588.29	0.97	57.92	896.43	N.D.	0
NMM-N12	261.16	N.D.	0	569.3	0.73	70.34	877.44	N.D.	0
NMM-O12	423.23	0.97	4.43	731.37	N.D.	0	519.5	N.D.	0
NMM-P12	262.14	0.36	33.31	570.28	0.78	59.04	878.42	N.D.	0
NMM-A13	256.11	0.44	11.63	564.25	1.01	76.73	872.39	N.D.	0
NMM-B13	310.14	N.D.	0	618.28	0.86	61.19	926.42	N.D.	0
NMM-C13	284.14	N.D.	0	592.28	0.8	81.97	900.42	N.D.	0
NMM-D13	306.19	0.86	5.69	614.33	1.22	56.37	922.47	N.D.	0
NMM-E13	238.14	N.D.	0	546.28	0.84	91.16	854.42	N.D.	0
NMM-F13	259.13	0.38	1.65	567.27	0.95	96.49	875.41	N.D.	0
NMM-G13	204.08	0.5	4.09	512.22	0.94	94.95	820.35	N.D.	0
NMM-H13	247.13	0.71	3.76	555.27	0.77	59.24	863.41	1.21	3.44
NMM-I13	422.21	N.D.	0	730.35	0.92	98.86	519	N.D.	0
NMM-J13	401.27	0.82	90.38	709.41	N.D.	0	508.5	N.D.	0
NMM-K13	447.24	N.D.	0	755.38	1.11	100	531.5	N.D.	0
NMM-L13	203.11	N.D.	0	511.24	0.97	85.01	819.38	N.D.	0
NMM-M13	452.24	N.D.	0	760.38	0.75	83.32	534	0.97	5.85

Confidential – Do Not Copy

NMM-N13	361.08	0.53	14.35	669.22	1.11	43.62	977.36	N.D.	0
NMM-O13	247.17	0.51	5.32	555.31	1	82.78	863.45	N.D.	0
NMM-P13	233.12	0.53	1.65	541.26	0.96	70.97	849.39	N.D.	0
NMM-A14	215.12	N.D.	0	523.26	0.78	88.79	831.4	N.D.	0
NMM-B14	468.13	0.47	10.59	776.27	0.96	83.66	542	N.D.	0
NMM-C14	280.14	1.01	6.27	588.28	1.1	38.66	896.42	N.D.	0
NMM-D14	287.16	0.45	45.5	595.3	1.01	17.98	903.44	N.D.	0
NMM-E14	274.14	N.D.	0	582.28	0.86	97.76	890.42	N.D.	0
NMM-F14	287.11	0.46	13.65	595.24	0.89	59.06	903.38	N.D.	0
NMM-G14	301.15	N.D.	0	609.29	1.13	98.5	917.43	N.D.	0
NMM-H14	254.13	0.36	97.75	562.27	0.89	2.25	870.4	N.D.	0
NMM-I14	215.07	N.D.	0	523.21	0.99	91.4	831.35	N.D.	0
NMM-J14	259.14	N.D.	0	567.28	0.99	98.42	875.42	N.D.	0
NMM-K14	236.13	N.D.	0	544.27	N.D.	0	852.41	N.D.	0
NMM-L14	403.21	N.D.	0	711.35	1.01	94.03	509.5	N.D.	0
NMM-M14	246.15	1.04	1.58	554.29	0.92	92.27	862.43	N.D.	0
NMM-N14	207.14	N.D.	0	515.28	0.71	24.74	823.42	N.D.	0
NMM-O14	260.16	0.45	2.68	568.3	1.04	80.66	876.44	N.D.	0
NMM-P14	367.17	0.75	25.51	675.31	0.75	25.51	983.45	N.D.	0
NMM-A15	368.1	0.91	13.93	676.24	1.08	13.97	984.38	N.D.	0
NMM-B15	208.1	0.69	1.29	516.24	0.81	91.73	824.37	N.D.	0
NMM-C15	356.22	N.D.	0	664.36	0.77	74.57	972.5	N.D.	0
NMM-D15	258.14	0.43	79.46	566.28	0.97	1.71	874.41	N.D.	0
NMM-E15	331.23	0.76	14.87	639.37	0.76	14.87	947.5	N.D.	0
NMM-F15	287.17	N.D.	0	595.31	1.23	98.38	903.45	N.D.	0
NMM-G15	393.23	N.D.	0	701.37	0.71	96.68	504.5	N.D.	0
NMM-H15	327.06	0.36	24.31	635.19	0.78	56.13	943.33	1.1	1.2
NMM-I15	310.17	0.35	23.45	618.3	0.75	71.75	926.44	1.08	0.95
NMM-J15	282.15	0.89	3.31	590.29	0.93	79.9	898.43	N.D.	0
NMM-K15	395.13	0.6	83.72	703.27	1.07	2.56	505.5	N.D.	0
NMM-L15	260.14	N.D.	0	568.28	0.73	100	876.42	N.D.	0
NMM-M15	245.13	N.D.	0	553.27	0.82	77.19	861.41	N.D.	0
NMM-N15	330.15	0.89	35.65	638.28	N.D.	0	946.42	N.D.	0
NMM-O15	217.1	N.D.	0	525.24	0.89	80.36	833.37	N.D.	0
NMM-P15	288.17	0.58	1.48	596.31	0.92	80.5	904.45	N.D.	0
NMM-A16	402.18	0.47	78.54	710.32	0.81	2.98	509	N.D.	0
NMM-B16	335.2	N.D.	0	643.33	0.72	22.41	951.47	N.D.	0
NMM-C16	294.17	N.D.	0	602.31	0.72	58.1	910.45	N.D.	0
NMM-D16	278.14	0.39	64.11	586.28	0.92	15.08	894.42	N.D.	0
NMM-E16	317.14	N.D.	0	625.28	0.94	96.62	933.42	N.D.	0
NMM-F16	304.19	N.D.	0	612.33	0.95	91.86	920.47	N.D.	0
NMM-G16	331.18	0.62	96.67	639.31	0.62	96.67	947.45	N.D.	0
NMM-H16	367.19	0.44	17.47	675.33	0.8	55.71	983.47	1.22	16.83

Confidential – Do Not Copy

NMM-I16	342.16	N.D.	0	650.3	1.01	100	958.44	N.D.	0
NMM-J16	291.14	0.71	100	599.28	N.D.	0	907.42	N.D.	0
NMM-K16	311.09	1.19	36.1	619.23	0.95	59.51	927.37	N.D.	0
NMM-L16	280.1	N.D.	0	588.24	0.91	94.23	896.38	N.D.	0
NMM-M16	218.11	0.54	84.01	526.24	N.D.	0	834.38	N.D.	0
NMM-N16	275.16	N.D.	0	583.3	0.9	83.21	891.44	N.D.	0
NMM-O16	314.19	0.48	17.1	622.32	N.D.	0	930.46	N.D.	0
NMM-P16	277.18	N.D.	0	585.32	0.89	98.47	893.46	N.D.	0
NMM-A17	219.11	0.5	1.05	527.25	0.81	97.39	835.39	N.D.	0
NMM-B17	437.17	N.D.	0	745.31	0.95	84.52	526.5	N.D.	0
NMM-C17	265.09	0.42	1.41	573.23	1	92.84	881.37	N.D.	0
NMM-D17	467.12	0.64	76.97	775.26	1.13	10.04	541.5	N.D.	0
NMM-E17	217.12	N.D.	0	525.26	0.97	100	833.4	N.D.	0
NMM-F17	347.2	0.49	71.53	655.34	N.D.	0	963.48	N.D.	0
NMM-G17	436.22	N.D.	0	744.36	1.04	100	526	N.D.	0
NMM-H17	204.13	N.D.	0	512.27	1.04	100	820.4	N.D.	0
NMM-I17	497.12	0.6	84.51	805.26	1.09	7.86	556.5	N.D.	0
NMM-J17	439.23	N.D.	0	747.37	0.93	100	527.5	N.D.	0
NMM-K17	246.14	0.58	6.58	554.28	1.23	91.67	862.41	N.D.	0
NMM-L17	283.1	N.D.	0	591.24	1.01	100	899.38	N.D.	0
NMM-M17	407.2	N.D.	0	715.34	0.86	82.55	511.5	N.D.	0
NMM-N17	353.1	N.D.	0	661.24	0.86	2.46	969.37	1.31	90.27
NMM-O17	355.19	0.41	79.65	663.33	0.89	18.31	971.47	N.D.	0
NMM-P17	315.19	0.48	84.46	623.33	N.D.	0	931.47	N.D.	0
NMM-A18	430.56	0.58	14.52	738.34	1.07	85.48	523	N.D.	0
NMM-B18	430.56	0.58	17.04	738.34	1.07	82.96	523	N.D.	0
NMM-C18	430.56	0.58	18.4	738.34	1.07	81.6	523	N.D.	0
NMM-D18	430.56	0.58	16.96	738.34	1.07	83.04	523	N.D.	0
NMM-E18	430.56	0.58	19.07	738.34	1.07	80.93	523	N.D.	0
NMM-F18	430.56	0.58	19.02	738.34	1.07	80.98	523	N.D.	0
NMM-G18	430.56	0.58	17.58	738.34	1.07	82.42	523	N.D.	0
NMM-H18	430.56	0.58	13.76	738.34	1.07	84.29	523	N.D.	0
NMM-I18	430.56	0.58	10.97	738.34	1.07	86.78	523	N.D.	0
NMM-J18	430.56	0.58	10.66	738.34	1.07	89.34	523	N.D.	0
NMM-K18	430.56	0.58	10.38	738.34	1.07	89.62	523	N.D.	0
NMM-L18	430.56	0.58	6.48	738.34	1.07	93.52	523	N.D.	0
NMM-M18	430.56	0.58	17.66	738.34	1.07	82.34	523	N.D.	0
NMM-N18	430.56	0.58	17.25	738.34	1.07	82.75	523	N.D.	0
NMM-O18	430.56	0.58	17.13	738.34	1.07	82.87	523	N.D.	0
NMM-P18	430.56	0.58	14.9	738.34	1.07	85.1	523	N.D.	0
NMM-A19	430.6	N.D.	0	738.43	1.2	100	523	N.D.	0
NMM-B19	290.24	0.47	74.03	598.37	1	14	906.51	N.D.	0
NMM-C19	288.16	N.D.	0	596.3	0.91	96.1	904.44	N.D.	0

Confidential – Do Not Copy

NMM-D19	208.11	N.D.	0	516.25	0.76	81.12	824.39	N.D.	0
NMM-E19	292.1	0.42	100	600.24	N.D.	0	908.38	N.D.	0
NMM-F19	461.24	N.D.	0	769.38	1.12	89.11	538.5	N.D.	0
NMM-G19	250.12	N.D.	0	558.26	0.83	96.37	866.4	N.D.	0
NMM-H19	318.27	N.D.	0	626.41	1	12.7	934.55	N.D.	0
NMM-I19	393.15	0.45	24.28	701.29	0.75	53.32	504.5	N.D.	0
NMM-J19	450.24	0.96	2.41	758.38	0.85	12.72	533	N.D.	0
NMM-K19	304.16	0.35	98.12	612.3	N.D.	0	920.44	N.D.	0
NMM-L19	348.23	0.94	100	656.37	0.94	100	964.51	N.D.	0
NMM-M19	351.18	0.42	100	659.31	N.D.	0	967.45	N.D.	0
NMM-N19	356.16	0.54	7.17	664.3	1.04	85.46	972.44	N.D.	0
NMM-O19	220.17	N.D.	0	528.31	0.9	100	836.45	N.D.	0
NMM-P19	259.14	N.D.	0	567.28	1.02	94.72	875.42	N.D.	0
NMM-A20	418.26	0.39	1.76	726.4	0.78	85.65	517	N.D.	0
NMM-B20	315.19	0.48	53.44	623.33	N.D.	0	931.47	N.D.	0
NMM-C20	299.16	0.57	1.19	607.3	0.95	97.75	915.44	N.D.	0
NMM-D20	248.13	N.D.	0	556.27	0.89	96	864.41	N.D.	0
NMM-E20	314.17	0.47	68.31	622.31	0.96	6.1	930.45	N.D.	0
NMM-F20	321.13	N.D.	0	629.27	1.04	100	937.4	N.D.	0
NMM-G20	287.15	N.D.	0	595.29	0.94	100	903.43	N.D.	0
NMM-H20	412.04	0.56	85.18	720.18	0.98	5.32	514	N.D.	0
NMM-I20	207.11	N.D.	0	515.25	0.98	90.88	823.39	N.D.	0
NMM-J20	220.11	N.D.	0	528.25	0.79	98	836.39	N.D.	0
NMM-K20	229.13	0.41	1.69	537.27	0.8	98.31	845.41	N.D.	0
NMM-L20	310.14	0.63	2.35	618.28	1.18	85.47	926.42	N.D.	0
NMM-M20	241.1	0.62	19.19	549.24	1.05	18.77	857.37	N.D.	0
NMM-N20	257.08	N.D.	0	565.22	0.95	95.36	873.36	N.D.	0
NMM-O20	293.15	N.D.	0	601.29	1.09	70.25	909.43	N.D.	0
NMM-P20	342.14	N.D.	0	650.28	1.05	17.92	958.41	N.D.	0
NMM-A21	351.14	0.91	73.84	659.28	0.91	73.84	967.41	N.D.	0
NMM-B21	476.25	N.D.	0	784.39	N.D.	0	546	N.D.	0
NMM-C21	389.23	N.D.	0	697.37	1.13	38.4	502.5	N.D.	0
NMM-D21	443.16	0.81	95.95	751.3	N.D.	0	529.5	N.D.	0
NMM-E21	474.19	N.D.	0	782.33	N.D.	0	545	N.D.	0
NMM-F21	256.13	0.4	93.61	564.27	0.84	4.83	872.41	N.D.	0
NMM-G21	286.18	0.64	1.16	594.32	0.72	95.65	902.46	N.D.	0
NMM-H21	450.26	N.D.	0	758.4	1.16	100	533	N.D.	0
NMM-I21	258.14	0.36	93.56	566.28	0.86	1.34	874.41	N.D.	0
NMM-J21	343.12	N.D.	0	651.26	1.11	91.3	959.39	N.D.	0
NMM-K21	310.1	N.D.	0	618.24	1.01	100	926.38	N.D.	0

**Supplementary Table 3:** LCMS data from **Figure 127**. Starting material only. Column 6 and 18 featured a control well. Performed using standard conditions as outlined in General Methods, using LCMS method (A).

Well Number	Mass	Rt	% Area
NMM-SM-A1	418.31	0.17	100
NMM-SM-A2	384.17	0.37	95
NMM-SM-A3	224.14	0.15	100
NMM-SM-A4	207.12	0.15	100
NMM-SM-A5	288.14	0.48	99
NMM-SM-A6	control	control	control
NMM-SM-A7	248.17	0.14	100
NMM-SM-A8	327.19	0.26	92
NMM-SM-A9	247.12	0.28	99
NMM-SM-A10	246.12	0.35	96
NMM-SM-A11	359.24	0.27	99
NMM-SM-A12	200.07	0.26	100
NMM-SM-A13	257.11	0.38	100
NMM-SM-A14	216.12	0.15	100
NMM-SM-A15	ND	ND	0
NMM-SM-A16	403.18	0.42	93
NMM-SM-A17	220.11	0.19	100
NMM-SM-A18	control	control	control
NMM-SM-A19	431.29	0.7	100
NMM-SM-A20	419.26	0.29	86
NMM-SM-A21	352.14	0.45	71
NMM-SM-B1	431.2	0.53	84
NMM-SM-B2	219.12	0.32	99
NMM-SM-B3	240.11	0.25	100
NMM-SM-B4	469.31	0.72	100
NMM-SM-B5	250.15	0.36	97
NMM-SM-B6	control	control	control
NMM-SM-B7	427.15	0.45	80
NMM-SM-B8	366.14	0.53	99
NMM-SM-B9	251.18	0.2	100
NMM-SM-B10	223.11	0.4	100
NMM-SM-B11	230.11	0.27	100
NMM-SM-B12	403.26	0.52	100
NMM-SM-B13	311.14	0.31	60
NMM-SM-B14	469.13	0.41	77
NMM-SM-B15	209.1	0.13	100
NMM-SM-B16	336.2	0.15	100
NMM-SM-B17	438.17	0.47	89
NMM-SM-B18	control	control	control

<b>NMM-SM-B19</b>	291.24	0.42	7
<b>NMM-SM-B20</b>	316.19	0.43	100
<b>NMM-SM-B21</b>	477.25	0.48	84
<b>NMM-SM-C1</b>	395.22	0.45	92
<b>NMM-SM-C2</b>	439.25	0.79	14
<b>NMM-SM-C3</b>	290.17	0.29	98
<b>NMM-SM-C4</b>	443.29	0.68	98
<b>NMM-SM-C5</b>	395.16	0.4	99
<b>NMM-SM-C6</b>	control	control	control
<b>NMM-SM-C7</b>	397.19	0.38	88
<b>NMM-SM-C8</b>	465.28	0.7	97
<b>NMM-SM-C9</b>	324.06	0.37	24
<b>NMM-SM-C10</b>	438.21	0.54	87
<b>NMM-SM-C11</b>	226.11	0.22	80
<b>NMM-SM-C12</b>	289.18	0.48	88
<b>NMM-SM-C13</b>	285.14	0.27	100
<b>NMM-SM-C14</b>	281.14	0.46	100
<b>NMM-SM-C15</b>	357.22	0.23	100
<b>NMM-SM-C16</b>	295.17	0.14	85
<b>NMM-SM-C17</b>	266.09	0.36	96
<b>NMM-SM-C18</b>	control	control	control
<b>NMM-SM-C19</b>	289.16	0.37	97
<b>NMM-SM-C20</b>	300.16	0.37	99
<b>NMM-SM-C21</b>	390.23	0.58	94
<b>NMM-SM-D1</b>	425.23	0.62	93
<b>NMM-SM-D2</b>	406.15	0.56	93
<b>NMM-SM-D3</b>	221.04	0.39	100
<b>NMM-SM-D4</b>	443.29	0.67	89
<b>NMM-SM-D5</b>	224.13	0.36	94
<b>NMM-SM-D6</b>	control	control	control
<b>NMM-SM-D7</b>	476.23	0.36	77
<b>NMM-SM-D8</b>	258.1	0.3	98
<b>NMM-SM-D9</b>	245.13	0.19	100
<b>NMM-SM-D10</b>	466.23	0.47	100
<b>NMM-SM-D11</b>	217.09	0.36	86
<b>NMM-SM-D12</b>	223.1	0.14	100
<b>NMM-SM-D13</b>	307.19	0.62	100
<b>NMM-SM-D14</b>	288.16	0.39	56
<b>NMM-SM-D15</b>	259.14	0.37	93
<b>NMM-SM-D16</b>	279.14	0.32	100
<b>NMM-SM-D17</b>	468.12	0.59	97
<b>NMM-SM-D18</b>	control	control	control
<b>NMM-SM-D19</b>	209.11	0.14	100

<b>NMM-SM-D20</b>	249.13	0.32	96
<b>NMM-SM-D21</b>	444.16	0.77	94
<b>NMM-SM-E1</b>	415.21	0.56	95
<b>NMM-SM-E2</b>	338.18	0.28	100
<b>NMM-SM-E3</b>	325.03	0.32	99
<b>NMM-SM-E4</b>	443.29	0.67	100
<b>NMM-SM-E5</b>	374.12	0.34	91
<b>NMM-SM-E6</b>	control	control	control
<b>NMM-SM-E7</b>	245.13	0.14	100
<b>NMM-SM-E8</b>	479.29	0.74	81
<b>NMM-SM-E9</b>	386.23	0.29	100
<b>NMM-SM-E10</b>	301.11	0.46	90
<b>NMM-SM-E11</b>	282.13	0.5	96
<b>NMM-SM-E12</b>	203.12	0.13	100
<b>NMM-SM-E13</b>	239.14	0.27	99
<b>NMM-SM-E14</b>	275.14	0.28	98
<b>NMM-SM-E15</b>	332.23	0.28	100
<b>NMM-SM-E16</b>	318.14	0.4	98
<b>NMM-SM-E17</b>	218.12	0.34	96
<b>NMM-SM-E18</b>	control	control	control
<b>NMM-SM-E19</b>	293.1	0.36	97
<b>NMM-SM-E20</b>	315.17	0.42	87
<b>NMM-SM-E21</b>	475.19	0.57	99
<b>NMM-SM-F1</b>	445.22	0.55	100
<b>NMM-SM-F2</b>	331.06	0.43	99
<b>NMM-SM-F3</b>	417.19	0.44	100
<b>NMM-SM-F4</b>	ND	ND	0
<b>NMM-SM-F5</b>	376.14	0.25	100
<b>NMM-SM-F6</b>	ND	0.86	100
<b>NMM-SM-F7</b>	341.16	0.49	98
<b>NMM-SM-F8</b>	231.12	0.31	99
<b>NMM-SM-F9</b>	231.12	0.29	95
<b>NMM-SM-F10</b>	274.16	0.28	86
<b>NMM-SM-F11</b>	ND	ND	0
<b>NMM-SM-F12</b>	233.13	0.26	15
<b>NMM-SM-F13</b>	260.13	0.31	97
<b>NMM-SM-F14</b>	288.11	0.2	100
<b>NMM-SM-F15</b>	288.17	0.54	99
<b>NMM-SM-F16</b>	305.19	0.45	86
<b>NMM-SM-F17</b>	348.2	0.44	98
<b>NMM-SM-F18</b>	control	control	control
<b>NMM-SM-F19</b>	462.24	0.62	85
<b>NMM-SM-F20</b>	322.13	0.42	100

<b>NMM-SM-F21</b>	257.13	0.34	98
<b>NMM-SM-G1</b>	739.34	1.03	100
<b>NMM-SM-G2</b>	435.1	0.63	96
<b>NMM-SM-G3</b>	439.25	0.8	63
<b>NMM-SM-G4</b>	270.15	0.33	71
<b>NMM-SM-G5</b>	369.16	0.15	100
<b>NMM-SM-G6</b>	control	control	control
<b>NMM-SM-G7</b>	281.15	0.15	100
<b>NMM-SM-G8</b>	233.12	0.47	97
<b>NMM-SM-G9</b>	455.22	0.49	83
<b>NMM-SM-G10</b>	351.2	0.7	100
<b>NMM-SM-G11</b>	284.14	0.29	100
<b>NMM-SM-G12</b>	443.33	0.47	100
<b>NMM-SM-G13</b>	205.08	0.24	100
<b>NMM-SM-G14</b>	302.15	0.47	100
<b>NMM-SM-G15</b>	394.23	0.14	100
<b>NMM-SM-G16</b>	332.18	0.13	100
<b>NMM-SM-G17</b>	437.22	0.53	100
<b>NMM-SM-G18</b>	control	control	control
<b>NMM-SM-G19</b>	251.12	0.19	100
<b>NMM-SM-G20</b>	288.15	0.35	100
<b>NMM-SM-G21</b>	287.18	0.13	100
<b>NMM-SM-H1</b>	555.26	0.4	99
<b>NMM-SM-H2</b>	213.11	0.29	95
<b>NMM-SM-H3</b>	452.25	0.51	100
<b>NMM-SM-H4</b>	236.08	0.29	0
<b>NMM-SM-H5</b>	243.08	0.27	30
<b>NMM-SM-H6</b>	control	control	control
<b>NMM-SM-H7</b>	264.09	0.34	94
<b>NMM-SM-H8</b>	241.09	0.28	99
<b>NMM-SM-H9</b>	263.15	0.41	99
<b>NMM-SM-H10</b>	354.17	0.27	99
<b>NMM-SM-H11</b>	485.19	0.56	94
<b>NMM-SM-H12</b>	343.17	0.29	97
<b>NMM-SM-H13</b>	248.13	0.28	100
<b>NMM-SM-H14</b>	255.13	0.28	98
<b>NMM-SM-H15</b>	328.06	0.28	96
<b>NMM-SM-H16</b>	368.19	0.38	94
<b>NMM-SM-H17</b>	205.13	0.43	96
<b>NMM-SM-H18</b>	control	control	control
<b>NMM-SM-H19</b>	319.27	0.56	64
<b>NMM-SM-H20</b>	413.04	0.51	84
<b>NMM-SM-H21</b>	451.26	0.66	97

<b>NMM-SM-I1</b>	461.21	0.49	100
<b>NMM-SM-I2</b>	447.13	0.71	90
<b>NMM-SM-I3</b>	246.15	0.4	100
<b>NMM-SM-I4</b>	260.22	0.3	100
<b>NMM-SM-I5</b>	261.15	0.39	100
<b>NMM-SM-I6</b>	control	control	control
<b>NMM-SM-I7</b>	306.15	0.43	99
<b>NMM-SM-I8</b>	469.31	0.69	100
<b>NMM-SM-I9</b>	317.15	0.35	96
<b>NMM-SM-I10</b>	244.11	0.28	100
<b>NMM-SM-I11</b>	452.19	0.49	86
<b>NMM-SM-I12</b>	335.17	0.63	99
<b>NMM-SM-I13</b>	423.21	0.44	100
<b>NMM-SM-I14</b>	216.07	0.27	90
<b>NMM-SM-I15</b>	311.17	0.28	99
<b>NMM-SM-I16</b>	343.16	0.45	96
<b>NMM-SM-I17</b>	498.12	0.55	95
<b>NMM-SM-I18</b>	control	control	control
<b>NMM-SM-I19</b>	394.15	0.33	52
<b>NMM-SM-I20</b>	208.11	0.29	100
<b>NMM-SM-I21</b>	259.14	0.28	97
<b>NMM-SM-J1</b>	799.34	1.09	99
<b>NMM-SM-J2</b>	362.11	0.38	92
<b>NMM-SM-J3</b>	264.11	0.36	81
<b>NMM-SM-J4</b>	461.13	0.74	93
<b>NMM-SM-J5</b>	364.22	0.4	96
<b>NMM-SM-J6</b>	control	control	control
<b>NMM-SM-J7</b>	250.11	0.3	100
<b>NMM-SM-J8</b>	273.16	0.35	100
<b>NMM-SM-J9</b>	244.14	0.45	98
<b>NMM-SM-J10</b>	359.24	0.27	94
<b>NMM-SM-J11</b>	224.14	0.22	100
<b>NMM-SM-J12</b>	450.24	0.71	91
<b>NMM-SM-J13</b>	402.27	0.78	85
<b>NMM-SM-J14</b>	260.14	0.37	97
<b>NMM-SM-J15</b>	283.15	0.34	81
<b>NMM-SM-J16</b>	292.14	0.67	100
<b>NMM-SM-J17</b>	440.23	0.39	100
<b>NMM-SM-J18</b>	control	control	control
<b>NMM-SM-J19</b>	451.24	0.45	88
<b>NMM-SM-J20</b>	221.11	0.17	91
<b>NMM-SM-J21</b>	344.12	0.49	89
<b>NMM-SM-K1</b>	416.07	0.4	70

<b>NMM-SM-K2</b>	278.1	0.23	100
<b>NMM-SM-K3</b>	312.19	0.17	87
<b>NMM-SM-K4</b>	289.18	0.31	100
<b>NMM-SM-K5</b>	382.17	0.44	97
<b>NMM-SM-K6</b>	control	control	control
<b>NMM-SM-K7</b>	316.16	0.35	99
<b>NMM-SM-K8</b>	276.13	0.46	97
<b>NMM-SM-K9</b>	220.1	0.27	73
<b>NMM-SM-K10</b>	228.05	0.23	100
<b>NMM-SM-K11</b>	204.11	0.28	97
<b>NMM-SM-K12</b>	245.13	0.3	94
<b>NMM-SM-K13</b>	448.24	0.59	100
<b>NMM-SM-K14</b>	ND	ND	0
<b>NMM-SM-K15</b>	396.13	0.55	91
<b>NMM-SM-K16</b>	312.09	0.33	33
<b>NMM-SM-K17</b>	247.14	0.52	98
<b>NMM-SM-K18</b>	control	control	control
<b>NMM-SM-K19</b>	305.16	0.2	100
<b>NMM-SM-K20</b>	230.13	0.27	100
<b>NMM-SM-K21</b>	311.1	0.39	100
<b>NMM-SM-L1</b>	263.18	0.14	100
<b>NMM-SM-L2</b>	308.1	0.34	100
<b>NMM-SM-L3</b>	210.04	0.34	83
<b>NMM-SM-L4</b>	443.14	0.73	86
<b>NMM-SM-L5</b>	307.1	0.35	95
<b>NMM-SM-L6</b>	control	control	control
<b>NMM-SM-L7</b>	248.1	0.32	90
<b>NMM-SM-L8</b>	322.09	0.29	98
<b>NMM-SM-L9</b>	402.21	0.56	91
<b>NMM-SM-L10</b>	301.16	0.4	100
<b>NMM-SM-L11</b>	297.26	0.23	100
<b>NMM-SM-L12</b>	450.24	0.7	100
<b>NMM-SM-L13</b>	204.11	0.32	82
<b>NMM-SM-L14</b>	404.21	0.48	98
<b>NMM-SM-L15</b>	261.14	0.15	100
<b>NMM-SM-L16</b>	281.1	0.34	94
<b>NMM-SM-L17</b>	284.1	0.34	100
<b>NMM-SM-L18</b>	control	control	control
<b>NMM-SM-L19</b>	349.23	0.56	86
<b>NMM-SM-L20</b>	311.14	0.57	87
<b>NMM-SM-M1</b>	263.14	0.5	95
<b>NMM-SM-M2</b>	296.15	0.39	100
<b>NMM-SM-M3</b>	355.14	0.43	100

<b>NMM-SM-M4</b>	238.07	0.24	100
<b>NMM-SM-M5</b>	434.26	0.37	99
<b>NMM-SM-M6</b>	control	control	control
<b>NMM-SM-M7</b>	247.17	0.43	85
<b>NMM-SM-M8</b>	406.24	0.78	92
<b>NMM-SM-M9</b>	451.19	0.4	93
<b>NMM-SM-M10</b>	297.15	0.32	90
<b>NMM-SM-M11</b>	448.12	0.51	78
<b>NMM-SM-M12</b>	281.15	0.34	100
<b>NMM-SM-M13</b>	453.24	0.28	84
<b>NMM-SM-M14</b>	247.15	0.31	96
<b>NMM-SM-M15</b>	246.13	0.15	100
<b>NMM-SM-M16</b>	219.11	0.49	98
<b>NMM-SM-M17</b>	408.2	0.38	96
<b>NMM-SM-M18</b>	control	control	control
<b>NMM-SM-M19</b>	352.18	0.36	98
<b>NMM-SM-M20</b>	242.1	0.39	17
<b>NMM-SM-N1</b>	205.1	0.14	100
<b>NMM-SM-N2</b>	422.21	0.58	100
<b>NMM-SM-N3</b>	226.12	0.24	100
<b>NMM-SM-N4</b>	418.14	0.46	93
<b>NMM-SM-N5</b>	328.09	0.53	54
<b>NMM-SM-N6</b>	control	control	control
<b>NMM-SM-N7</b>	210.04	0.4	89
<b>NMM-SM-N8</b>	301.16	0.4	100
<b>NMM-SM-N9</b>	275.17	0.53	86
<b>NMM-SM-N10</b>	255.13	0.38	93
<b>NMM-SM-N11</b>	303.21	0.13	84
<b>NMM-SM-N12</b>	262.16	0.25	100
<b>NMM-SM-N13</b>	362.08	0.46	78
<b>NMM-SM-N14</b>	208.14	0.12	100
<b>NMM-SM-N15</b>	332.15	0.4	97
<b>NMM-SM-N16</b>	276.16	0.29	81
<b>NMM-SM-N17</b>	354.1	0.3	95
<b>NMM-SM-N18</b>	control	control	control
<b>NMM-SM-N19</b>	357.16	0.48	96
<b>NMM-SM-N20</b>	258.08	0.32	96
<b>NMM-SM-O1</b>	481.25	0.45	100
<b>NMM-SM-O2</b>	469.27	0.42	92
<b>NMM-SM-O3</b>	472.13	0.37	90
<b>NMM-SM-O4</b>	259.15	0.15	100
<b>NMM-SM-O5</b>	406.24	0.49	5
<b>NMM-SM-O6</b>	control	control	control

NMM-SM-O7	431.2	0.53	91
NMM-SM-O8	466.2	0.35	97
NMM-SM-O9	468.26	0.51	97
NMM-SM-O10	288.15	0.3	98
NMM-SM-O11	413.21	0.41	93
NMM-SM-O12	424.23	0.55	7
NMM-SM-O13	248.17	0.42	85
NMM-SM-O14	261.16	0.44	93
NMM-SM-O15	218.1	0.2	100
NMM-SM-O16	315.19	0.23	100
NMM-SM-O17	356.19	0.34	100
NMM-SM-O18	control	control	control
NMM-SM-O19	221.17	0.27	100
NMM-SM-O20	294.15	0.45	83
NMM-SM-P1	357.18	0.41	100
NMM-SM-P2	241.07	0.19	91
NMM-SM-P3	466.19	0.28	89
NMM-SM-P4	291.21	0.39	100
NMM-SM-P5	303.1	0.29	93
NMM-SM-P6	control	control	control
NMM-SM-P7	346.08	0.42	82
NMM-SM-P8	373.25	0.31	92
NMM-SM-P9	242.1	0.27	93
NMM-SM-P10	212.08	0.22	100
NMM-SM-P11	ND	ND	0
NMM-SM-P12	263.14	0.3	100
NMM-SM-P13	234.12	0.33	70
NMM-SM-P14	368.17	0.25	100
NMM-SM-P15	289.17	0.35	89
NMM-SM-P16	278.18	0.44	99
NMM-SM-P17	316.19	0.43	100
NMM-SM-P18	control	control	control
NMM-SM-P19	260.14	0.4	94
NMM-SM-P20	343.14	0.44	78

**Supplementary Table 4: Plate 1:** LCMS data from Chapter 7.3.3.5, HaloCompound *In-Situ* Synthesis for the Validation Set. Column 6 featured a control well, and column 18 featured positive control VHL amine **101**. Performed using standard conditions as outlined in General Methods, using LCMS method (A).

Well Number	SM mass	Rt	% Area	Product Mass	Rt	% Area
VALIDATION-P1-A1	255.15	0.36	100	563.29	ND	0
VALIDATION-P1-A2	252.16	ND	0	560.30	0.91	100

Confidential – Do Not Copy

VALIDATION-P1-A3	219.13	ND	0	527.27	1.21	100
VALIDATION-P1-A4	376.15	0.51	71	684.28	1.10	25
VALIDATION-P1-A5	369.17	ND	0	677.31	1.02	100
VALIDATION-P1-A7	221.15	ND	0	529.29	0.95	100
VALIDATION-P1-A8	367.27	ND	0	675.41	0.87	100
VALIDATION-P1-A9	347.18	0.57	100	655.32	ND	0
VALIDATION-P1-A10	241.13	ND	0	549.27	0.87	100
VALIDATION-P1-A11	324.20	0.65	100	632.34	ND	0
VALIDATION-P1-A12	340.19	0.57	100	648.33	ND	0
VALIDATION-P1-A13	345.04	0.63	100	653.18	ND	0
VALIDATION-P1-A14	247.14	ND	0	555.28	0.80	100
VALIDATION-P1-A15	262.99	ND	0	571.13	0.90	100
VALIDATION-P1-A16	403.10	ND	0	711.24	1.31	100
VALIDATION-P1-A17	355.21	ND	0	663.35	0.71	95
VALIDATION-P1-A18	430.00	0.58	6	738.00	1.06	94
VALIDATION-P1-A19	409.18	0.71	100	717.32	ND	0
VALIDATION-P1-A20	227.09	0.57	11	535.23	1.17	89
VALIDATION-P1-A21	258.15	ND	0	566.29	0.72	97
VALIDATION-P1-A22	266.08	ND	0	574.22	0.96	100
VALIDATION-P1-A23	327.17	ND	0	635.31	1.11	100
VALIDATION-P1-A24	295.19	0.57	100	603.33	ND	0
VALIDATION-P1-B1	313.06	0.76	73	621.20	1.36	27
VALIDATION-P1-B2	341.22	0.39	37	649.36	0.81	58
VALIDATION-P1-B3	318.22	0.54	100	626.36	0.54	100
VALIDATION-P1-B4	316.06	ND	0	624.20	1.17	100
VALIDATION-P1-B5	377.22	ND	0	685.36	0.79	100
VALIDATION-P1-B7	346.19	0.38	74	654.33	0.86	26
VALIDATION-P1-B8	243.15	0.77	100	551.29	0.77	100
VALIDATION-P1-B9	270.15	0.56	93	578.29	1.13	7
VALIDATION-P1-B10	290.12	ND	0	598.26	1.17	100
VALIDATION-P1-B11	318.22	0.56	70	626.36	ND	0
VALIDATION-P1-B12	347.18	0.52	89	655.32	ND	0
VALIDATION-P1-B13	397.04	ND	0	705.18	1.24	96
VALIDATION-P1-B14	289.18	ND	0	597.32	0.91	100
VALIDATION-P1-B15	362.12	0.97	100	670.26	0.97	100
VALIDATION-P1-B16	380.22	0.41	99	688.36	0.84	1
VALIDATION-P1-B17	219.10	ND	0	527.24	0.89	90
VALIDATION-P1-B18	430.00	0.58	3	738.00	1.06	97
VALIDATION-P1-B19	239.16	0.44	36	547.30	0.88	64
VALIDATION-P1-B20	304.19	ND	0	612.33	ND	0

Confidential – Do Not Copy

VALIDATION-P1-B21	291.17	0.53	100	599.31	ND	0
VALIDATION-P1-B22	291.14	ND	0	599.28	1.20	100
VALIDATION-P1-B23	383.25	ND	0	691.39	ND	0
VALIDATION-P1-B24	282.14	0.52	100	590.28	ND	0
VALIDATION-P1-C1	282.10	ND	0	590.24	1.08	84
VALIDATION-P1-C2	335.07	1.21	5	643.21	1.21	5
VALIDATION-P1-C3	293.17	0.38	67	601.31	0.88	33
VALIDATION-P1-C4	256.13	0.51	77	564.27	0.93	23
VALIDATION-P1-C5	307.14	0.58	95	615.27	0.94	5
VALIDATION-P1-C7	369.24	ND	0	677.38	ND	0
VALIDATION-P1-C8	308.07	0.80	100	616.20	0.80	100
VALIDATION-P1-C9	354.19	0.69	7	662.33	1.13	93
VALIDATION-P1-C10	211.04	ND	0	519.18	1.09	100
VALIDATION-P1-C11	244.03	1.07	100	552.16	1.07	100
VALIDATION-P1-C12	276.20	ND	0	584.33	0.73	100
VALIDATION-P1-C13	354.21	0.55	91	662.34	ND	0
VALIDATION-P1-C14	301.14	0.52	84	609.28	1.10	16
VALIDATION-P1-C15	235.16	0.66	44	543.30	1.23	56
VALIDATION-P1-C16	253.12	0.54	38	561.26	0.85	29
VALIDATION-P1-C17	305.17	ND	0	613.31	0.74	83
VALIDATION-P1-C18	430.00	0.58	3	738.00	1.06	97
VALIDATION-P1-C19	249.00	ND	0	557.14	1.02	100
VALIDATION-P1-C20	318.21	ND	0	626.34	0.70	80
VALIDATION-P1-C21	330.15	0.63	100	638.29	ND	0
VALIDATION-P1-C22	326.15	0.86	52	634.29	0.86	52
VALIDATION-P1-C23	317.02	ND	0	625.16	1.13	100
VALIDATION-P1-C24	240.09	ND	0	548.23	0.94	100
VALIDATION-P1-D1	249.18	0.47	100	557.32	ND	0
VALIDATION-P1-D2	243.15	0.80	100	551.29	0.80	100
VALIDATION-P1-D3	250.17	ND	0	558.31	1.28	100
VALIDATION-P1-D4	316.19	0.56	100	624.33	ND	0
VALIDATION-P1-D5	367.23	0.38	100	675.37	ND	0
VALIDATION-P1-D7	351.17	0.36	56	659.31	0.84	44
VALIDATION-P1-D8	364.20	0.92	93	672.34	0.92	93
VALIDATION-P1-D9	298.18	0.65	100	606.32	ND	0
VALIDATION-P1-D10	363.18	0.92	100	671.31	0.92	100
VALIDATION-P1-D11	316.20	ND	0	624.34	0.94	96
VALIDATION-P1-D12	284.15	0.94	4	592.29	0.60	94
VALIDATION-P1-D13	228.14	0.32	4	536.28	0.93	96
VALIDATION-P1-D14	290.04	ND	0	598.18	1.07	100

Confidential – Do Not Copy

VALIDATION-P1-D15	254.13	1.06	68	562.27	1.06	68
VALIDATION-P1-D16	380.23	0.49	100	688.37	ND	0
VALIDATION-P1-D17	312.16	ND	0	620.30	1.11	100
VALIDATION-P1-D18	430.00	0.58	15	738.00	1.06	85
VALIDATION-P1-D19	313.15	0.45	100	621.28	ND	0
VALIDATION-P1-D20	326.16	0.72	100	634.30	ND	0
VALIDATION-P1-D21	311.17	0.37	100	619.31	ND	0
VALIDATION-P1-D22	412.10	0.65	29	720.24	1.14	63
VALIDATION-P1-D23	263.20	0.62	100	571.34	0.62	100
VALIDATION-P1-D24	212.08	ND	0	520.22	0.75	100
VALIDATION-P1-E1	333.21	0.61	100	641.34	ND	0
VALIDATION-P1-E2	230.13	0.41	5	538.27	1.00	95
VALIDATION-P1-E3	320.04	ND	0	628.18	1.11	100
VALIDATION-P1-E4	308.09	0.56	100	616.23	ND	0
VALIDATION-P1-E5	307.18	0.56	82	615.32	1.16	18
VALIDATION-P1-E7	368.20	0.83	3	676.34	0.92	97
VALIDATION-P1-E8	332.21	0.58	100	640.35	ND	0
VALIDATION-P1-E9	344.12	1.15	100	652.26	1.15	100
VALIDATION-P1-E10	248.16	ND	0	556.30	0.89	100
VALIDATION-P1-E11	343.18	0.44	81	651.32	0.95	19
VALIDATION-P1-E12	390.29	0.65	49	698.43	1.00	51
VALIDATION-P1-E13	372.25	ND	0	680.39	0.81	100
VALIDATION-P1-E14	256.17	0.42	23	564.31	1.03	77
VALIDATION-P1-E15	263.19	0.53	100	571.33	ND	0
VALIDATION-P1-E16	345.15	0.69	71	653.29	1.23	6
VALIDATION-P1-E17	229.11	0.37	100	537.25	ND	0
VALIDATION-P1-E18	430.00	0.58	7	738.00	1.06	93
VALIDATION-P1-E19	334.24	0.65	100	642.38	ND	0
VALIDATION-P1-E20	268.13	ND	0	576.27	1.03	100
VALIDATION-P1-E21	264.21	0.37	9	572.35	0.85	91
VALIDATION-P1-E22	367.20	1.08	11	675.34	1.01	89
VALIDATION-P1-E23	265.19	ND	0	573.33	0.71	100
VALIDATION-P1-E24	277.18	0.33	100	585.32	ND	0
VALIDATION-P1-F1	323.10	0.54	95	631.24	ND	0
VALIDATION-P1-F2	269.15	ND	0	577.29	1.26	100
VALIDATION-P1-F3	269.12	ND	0	577.26	1.13	100
VALIDATION-P1-F4	286.18	0.62	66	594.32	1.15	34
VALIDATION-P1-F5	317.22	0.49	100	625.36	ND	0
VALIDATION-P1-F7	369.26	0.41	96	677.40	ND	0
VALIDATION-P1-F8	347.17	0.48	12	655.31	1.03	88

Confidential – Do Not Copy

VALIDATION-P1-F9	352.08	0.60	100	660.22	ND	0
VALIDATION-P1-F10	360.20	ND	0	668.33	1.03	100
VALIDATION-P1-F11	297.19	ND	0	605.33	ND	0
VALIDATION-P1-F12	328.11	0.43	53	636.25	0.79	47
VALIDATION-P1-F13	251.13	ND	0	559.27	1.25	100
VALIDATION-P1-F14	325.17	ND	0	633.31	1.23	100
VALIDATION-P1-F15	381.11	0.71	100	689.24	ND	0
VALIDATION-P1-F16	395.28	0.37	21	703.42	0.81	74
VALIDATION-P1-F17	319.14	ND	0	627.27	1.10	62
VALIDATION-P1-F18	430.00	0.58	4	738.00	1.06	96
VALIDATION-P1-F19	295.14	ND	0	603.28	0.69	76
VALIDATION-P1-F20	369.22	0.42	100	677.36	ND	0
VALIDATION-P1-F21	340.19	ND	0	648.33	1.21	100
VALIDATION-P1-F22	217.16	ND	0	525.30	ND	0
VALIDATION-P1-F23	265.19	ND	0	573.33	0.72	100
VALIDATION-P1-F24	258.13	0.52	100	566.27	ND	0
VALIDATION-P1-G1	331.27	ND	0	639.41	ND	0
VALIDATION-P1-G2	393.14	ND	0	701.28	1.17	100
VALIDATION-P1-G3	241.11	0.54	100	549.25	ND	0
VALIDATION-P1-G4	300.20	ND	0	608.33	0.77	100
VALIDATION-P1-G5	303.24	ND	0	611.38	ND	0
VALIDATION-P1-G7	302.17	ND	0	610.31	1.07	100
VALIDATION-P1-G8	287.16	ND	0	595.30	1.03	100
VALIDATION-P1-G9	292.19	0.81	53	600.33	0.81	53
VALIDATION-P1-G10	319.17	0.46	100	627.31	ND	0
VALIDATION-P1-G11	284.13	ND	0	592.27	0.95	100
VALIDATION-P1-G12	295.15	ND	0	603.29	0.92	100
VALIDATION-P1-G13	265.14	ND	0	573.28	0.94	100
VALIDATION-P1-G14	357.12	0.40	24	665.26	0.98	76
VALIDATION-P1-G15	246.15	ND	0	554.29	0.74	100
VALIDATION-P1-G16	370.12	ND	0	678.26	1.02	100
VALIDATION-P1-G17	340.18	ND	0	648.32	0.69	98
VALIDATION-P1-G18	430.00	0.58	4	738.00	1.06	96
VALIDATION-P1-G19	268.10	ND	0	576.24	0.76	100
VALIDATION-P1-G20	354.16	0.63	100	662.30	ND	0
VALIDATION-P1-G21	357.16	0.82	4	665.30	0.86	96
VALIDATION-P1-G22	247.18	0.29	22	555.32	0.82	45
VALIDATION-P1-G23	258.07	ND	0	566.21	ND	0
VALIDATION-P1-G24	321.11	ND	0	629.25	1.11	100
VALIDATION-P1-H1	262.17	0.62	42	570.31	1.17	24

Confidential – Do Not Copy

VALIDATION-P1-H2	357.20	0.37	63	665.34	0.86	37
VALIDATION-P1-H3	340.03	0.67	100	648.17	ND	0
VALIDATION-P1-H4	315.17	0.45	100	623.31	ND	0
VALIDATION-P1-H5	237.18	0.42	100	545.32	ND	0
VALIDATION-P1-H7	351.16	1.16	100	659.29	ND	0
VALIDATION-P1-H8	252.18	0.53	100	560.32	ND	0
VALIDATION-P1-H9	247.18	0.48	100	555.32	ND	0
VALIDATION-P1-H10	319.20	0.48	87	627.34	1.13	9
VALIDATION-P1-H11	208.12	0.35	100	516.26	ND	0
VALIDATION-P1-H12	311.17	ND	0	619.31	ND	0
VALIDATION-P1-H13	346.04	0.58	100	654.17	ND	0
VALIDATION-P1-H14	354.19	0.42	3	662.33	1.12	97
VALIDATION-P1-H15	312.15	0.31	100	620.29	ND	0
VALIDATION-P1-H16	223.16	0.48	100	531.30	ND	0
VALIDATION-P1-H17	233.10	ND	0	541.24	0.88	100
VALIDATION-P1-H18	430.00	0.58	5	738.00	1.06	95
VALIDATION-P1-H19	323.23	0.39	100	631.37	ND	0
VALIDATION-P1-H20	278.13	0.42	19	586.27	0.95	81
VALIDATION-P1-H21	213.06	ND	0	521.19	1.08	100
VALIDATION-P1-H22	226.11	ND	0	534.25	1.27	100
VALIDATION-P1-H23	310.18	0.44	3	618.32	0.97	92
VALIDATION-P1-H24	235.08	ND	0	543.22	1.10	100
VALIDATION-P1-I1	247.13	ND	0	555.27	1.05	100
VALIDATION-P1-I2	396.06	0.67	4	704.20	0.98	93
VALIDATION-P1-I3	339.06	0.48	100	647.20	ND	0
VALIDATION-P1-I4	218.12	ND	0	526.26	0.75	100
VALIDATION-P1-I5	333.17	0.63	100	641.31	ND	0
VALIDATION-P1-I7	328.18	0.63	84	636.32	0.92	17
VALIDATION-P1-I8	279.18	0.51	100	587.32	ND	0
VALIDATION-P1-I9	250.10	0.82	6	558.24	1.18	94
VALIDATION-P1-I10	356.07	0.51	100	664.21	ND	0
VALIDATION-P1-I11	240.06	0.28	100	548.20	ND	0
VALIDATION-P1-I12	320.13	ND	0	628.27	1.23	100
VALIDATION-P1-I13	284.19	0.62	100	592.33	ND	0
VALIDATION-P1-I14	268.17	ND	0	576.31	1.21	100
VALIDATION-P1-I15	203.12	0.32	41	511.26	0.92	60
VALIDATION-P1-I16	302.16	ND	0	610.30	1.25	83
VALIDATION-P1-I17	307.11	0.67	74	615.25	1.22	26
VALIDATION-P1-I18	430.00	0.58	7	738.00	1.06	93
VALIDATION-P1-I19	213.08	0.47	15	521.22	1.10	85

Confidential – Do Not Copy

VALIDATION-P1-I20	243.14	0.49	5	551.28	1.03	95
VALIDATION-P1-I21	278.20	0.48	100	586.34	ND	0
VALIDATION-P1-I22	239.14	ND	0	547.28	0.78	100
VALIDATION-P1-I23	312.16	ND	0	620.30	1.02	100
VALIDATION-P1-I24	303.18	0.61	84	611.32	1.20	16
VALIDATION-P1-J1	342.21	0.62	100	650.34	ND	0
VALIDATION-P1-J2	290.17	0.44	100	598.31	ND	0
VALIDATION-P1-J3	251.16	ND	0	559.30	1.02	100
VALIDATION-P1-J4	320.18	0.34	100	628.32	ND	0
VALIDATION-P1-J5	298.17	0.62	100	606.31	ND	0
VALIDATION-P1-J7	340.19	ND	0	648.33	ND	0
VALIDATION-P1-J8	248.13	ND	0	556.27	0.75	100
VALIDATION-P1-J9	293.08	0.60	100	601.21	ND	0
VALIDATION-P1-J10	276.06	ND	0	584.20	1.08	100
VALIDATION-P1-J11	267.17	1.08	54	575.31	1.08	54
VALIDATION-P1-J12	222.10	1.00	100	530.24	1.00	100
VALIDATION-P1-J13	282.15	0.37	100	590.29	ND	0
VALIDATION-P1-J14	340.17	1.03	91	648.31	1.03	91
VALIDATION-P1-J15	318.19	0.46	13	626.33	0.89	72
VALIDATION-P1-J16	209.05	ND	0	517.19	ND	0
VALIDATION-P1-J17	216.10	0.37	5	524.24	1.01	95
VALIDATION-P1-J18	430.00	0.58	5	738.00	1.07	95
VALIDATION-P1-J19	217.09	ND	0	525.23	ND	0
VALIDATION-P1-J20	245.12	ND	0	553.26	1.01	100
VALIDATION-P1-J21	259.16	0.49	100	567.30	ND	0
VALIDATION-P1-J22	287.16	ND	0	595.30	1.13	43
VALIDATION-P1-J23	305.07	ND	0	613.21	1.19	100
VALIDATION-P1-J24	211.07	ND	0	519.21	ND	0
VALIDATION-P1-K1	326.06	0.49	100	634.20	ND	0
VALIDATION-P1-K2	239.13	ND	0	547.27	0.84	100
VALIDATION-P1-K3	302.09	ND	0	610.23	1.12	100
VALIDATION-P1-K4	231.14	ND	0	539.28	0.77	100
VALIDATION-P1-K5	297.20	0.44	100	605.33	ND	0
VALIDATION-P1-K7	375.21	0.33	42	683.35	ND	0
VALIDATION-P1-K8	352.19	0.33	100	660.33	ND	0
VALIDATION-P1-K9	297.04	ND	0	605.18	ND	0
VALIDATION-P1-K10	330.25	0.31	88	638.39	0.68	12
VALIDATION-P1-K11	357.21	ND	0	665.34	1.08	100
VALIDATION-P1-K12	345.22	0.75	76	653.36	0.75	76
VALIDATION-P1-K13	219.11	0.36	100	527.25	ND	0

Confidential – Do Not Copy

VALIDATION-P1-K14	270.11	0.55	100	578.25	ND	0
VALIDATION-P1-K15	234.15	0.47	87	542.29	1.12	13
VALIDATION-P1-K16	333.10	ND	0	641.24	1.12	100
VALIDATION-P1-K17	301.13	ND	0	609.27	0.83	100
VALIDATION-P1-K18	430.00	0.58	5	738.00	1.06	95
VALIDATION-P1-K19	305.17	0.37	39	613.31	0.81	55
VALIDATION-P1-K20	271.18	0.95	100	579.32	0.95	100
VALIDATION-P1-K21	344.13	0.49	73	652.27	0.97	27
VALIDATION-P1-K22	322.07	ND	0	630.21	1.11	100
VALIDATION-P1-K23	311.16	0.71	100	619.29	ND	0
VALIDATION-P1-K24	344.25	1.30	67	652.39	1.30	67
VALIDATION-P1-L1	348.17	0.85	100	656.31	0.85	100
VALIDATION-P1-L2	233.15	ND	0	541.29	0.92	100
VALIDATION-P1-L3	235.13	ND	0	543.27	0.73	100
VALIDATION-P1-L4	267.14	0.40	8	575.28	0.98	92
VALIDATION-P1-L5	353.22	0.36	78	661.36	0.79	17
VALIDATION-P1-L7	275.11	0.54	100	583.25	ND	0
VALIDATION-P1-L8	259.13	0.55	100	567.27	ND	0
VALIDATION-P1-L9	303.17	ND	0	611.31	ND	0
VALIDATION-P1-L10	209.15	0.32	42	517.29	ND	0
VALIDATION-P1-L11	361.01	0.68	8	669.15	1.23	92
VALIDATION-P1-L12	361.20	0.31	87	669.34	ND	0
VALIDATION-P1-L13	338.17	ND	0	646.31	1.17	100
VALIDATION-P1-L14	281.13	0.50	100	589.27	ND	0
VALIDATION-P1-L15	269.03	0.60	88	577.17	1.24	12
VALIDATION-P1-L16	440.27	0.61	61	748.41	0.93	39
VALIDATION-P1-L17	374.18	0.55	100	682.32	ND	0
VALIDATION-P1-L18	430.00	0.58	3	738.00	1.06	97
VALIDATION-P1-L19	213.08	ND	0	521.22	1.02	100
VALIDATION-P1-L20	290.12	0.53	40	598.26	1.04	54
VALIDATION-P1-L21	285.06	0.65	30	593.20	1.26	70
VALIDATION-P1-L22	211.07	ND	0	519.21	1.04	100
VALIDATION-P1-L23	300.23	0.60	100	608.37	ND	0
VALIDATION-P1-L24	350.13	0.40	6	658.27	0.85	77
VALIDATION-P1-M1	320.22	ND	0	628.36	1.13	100
VALIDATION-P1-M2	354.21	ND	0	662.34	0.80	100
VALIDATION-P1-M3	396.16	0.38	6	704.30	0.80	81
VALIDATION-P1-M4	334.15	1.13	92	642.29	1.13	92
VALIDATION-P1-M5	217.10	0.43	100	525.24	ND	0
VALIDATION-P1-M7	264.15	0.87	22	572.29	0.91	56

Confidential – Do Not Copy

VALIDATION-P1-M8	202.06	ND	0	510.20	0.97	100
VALIDATION-P1-M9	363.17	0.83	100	671.31	0.83	100
VALIDATION-P1-M10	264.14	0.53	100	572.28	ND	0
VALIDATION-P1-M11	316.93	0.95	100	625.07	ND	0
VALIDATION-P1-M12	366.17	ND	0	674.31	1.06	100
VALIDATION-P1-M13	384.03	0.68	23	692.16	1.25	77
VALIDATION-P1-M14	299.21	ND	0	607.35	0.82	100
VALIDATION-P1-M15	305.12	0.73	58	613.26	1.31	42
VALIDATION-P1-M16	316.23	0.68	100	624.37	ND	0
VALIDATION-P1-M17	231.14	ND	0	539.28	0.76	100
VALIDATION-P1-M18	430.00	0.58	5	738.00	1.06	95
VALIDATION-P1-M19	200.06	0.31	100	508.20	ND	0
VALIDATION-P1-M20	393.23	ND	0	701.37	1.38	100
VALIDATION-P1-M21	350.13	ND	0	658.27	1.04	100
VALIDATION-P1-M22	331.19	0.32	53	639.33	ND	0
VALIDATION-P1-M23	205.13	ND	0	513.27	0.76	100
VALIDATION-P1-M24	293.07	ND	0	601.21	1.16	100
VALIDATION-P1-N1	330.15	0.88	100	638.29	0.88	100
VALIDATION-P1-N2	273.16	ND	0	581.30	0.79	100
VALIDATION-P1-N3	262.09	0.48	100	570.23	ND	0
VALIDATION-P1-N4	265.14	ND	0	573.28	0.64	100
VALIDATION-P1-N5	329.14	ND	0	637.28	1.03	100
VALIDATION-P1-N7	303.16	0.79	41	611.30	0.97	59
VALIDATION-P1-N8	280.16	ND	0	588.30	ND	0
VALIDATION-P1-N9	330.12	0.46	97	638.25	ND	0
VALIDATION-P1-N10	268.09	ND	0	576.23	1.07	100
VALIDATION-P1-N11	311.19	0.95	54	619.32	0.95	54
VALIDATION-P1-N12	364.20	ND	0	672.34	0.76	100
VALIDATION-P1-N13	330.14	0.57	100	638.28	ND	0
VALIDATION-P1-N14	261.10	0.95	100	569.24	0.95	100
VALIDATION-P1-N15	303.15	0.80	100	611.29	0.80	100
VALIDATION-P1-N16	331.19	0.89	83	639.33	0.89	83
VALIDATION-P1-N17	342.22	ND	0	650.36	0.74	100
VALIDATION-P1-N18	430.00	0.58	5	738.00	1.06	95
VALIDATION-P1-N19	288.17	ND	0	596.31	0.91	100
VALIDATION-P1-N20	322.09	0.47	90	630.23	ND	0
VALIDATION-P1-N21	316.19	ND	0	624.33	0.96	90
VALIDATION-P1-N22	329.21	0.78	100	637.35	0.78	100
VALIDATION-P1-N23	332.13	0.47	23	640.27	0.87	77
VALIDATION-P1-N24	271.13	0.48	100	579.27	ND	0

Confidential – Do Not Copy

VALIDATION-P1-O1	343.20	0.57	100	651.34	ND	0
VALIDATION-P1-O2	219.11	ND	0	527.25	0.86	100
VALIDATION-P1-O3	289.14	0.55	6	597.28	1.09	83
VALIDATION-P1-O4	253.11	ND	0	561.25	1.14	100
VALIDATION-P1-O5	334.19	ND	0	642.33	0.84	100
VALIDATION-P1-O7	218.02	ND	0	526.16	0.95	100
VALIDATION-P1-O8	318.14	0.58	68	626.28	1.12	13
VALIDATION-P1-O9	414.18	0.59	100	722.32	ND	0
VALIDATION-P1-O10	267.12	0.49	62	575.26	1.02	38
VALIDATION-P1-O11	275.16	0.46	100	583.30	ND	0
VALIDATION-P1-O12	246.08	ND	0	554.22	1.22	100
VALIDATION-P1-O13	344.13	1.06	100	652.27	1.06	100
VALIDATION-P1-O14	253.15	0.48	5	561.29	0.90	11
VALIDATION-P1-O15	223.12	0.46	58	531.26	1.08	42
VALIDATION-P1-O16	253.14	ND	0	561.28	0.76	100
VALIDATION-P1-O17	338.16	0.72	100	646.30	ND	0
VALIDATION-P1-O18	430.00	0.58	4	738.00	1.06	96
VALIDATION-P1-O19	272.16	ND	0	580.30	0.76	94
VALIDATION-P1-O20	376.05	0.60	100	684.18	ND	0
VALIDATION-P1-O21	302.17	ND	0	610.31	ND	0
VALIDATION-P1-O22	267.14	ND	0	575.28	0.85	100
VALIDATION-P1-O23	302.17	ND	0	610.31	0.77	59
VALIDATION-P1-O24	282.15	0.47	100	590.29	ND	0
VALIDATION-P1-P1	283.13	0.58	15	591.27	1.12	85
VALIDATION-P1-P2	311.20	0.70	100	619.34	0.70	100
VALIDATION-P1-P3	273.98	0.63	100	582.12	ND	0
VALIDATION-P1-P4	330.15	ND	0	638.29	0.81	100
VALIDATION-P1-P5	310.10	0.51	100	618.24	ND	0
VALIDATION-P1-P7	229.12	ND	0	537.26	1.06	100
VALIDATION-P1-P8	265.19	0.72	100	573.33	0.72	100
VALIDATION-P1-P9	273.15	0.44	68	581.29	ND	0
VALIDATION-P1-P10	235.16	ND	0	543.30	1.17	100
VALIDATION-P1-P11	325.18	ND	0	633.32	1.15	100
VALIDATION-P1-P12	384.15	ND	0	692.29	1.13	94
VALIDATION-P1-P13	261.16	ND	0	569.30	0.72	100
VALIDATION-P1-P14	246.06	0.53	82	554.20	1.07	18
VALIDATION-P1-P15	287.06	ND	0	595.20	1.06	100
VALIDATION-P1-P16	263.01	0.59	48	571.15	1.25	52
VALIDATION-P1-P17	216.07	ND	0	524.21	0.86	100
VALIDATION-P1-P18	430.00	0.58	4	738.00	1.06	96

VALIDATION-P1-P19	311.16	0.80	90	619.30	0.80	90
VALIDATION-P1-P20	350.20	1.12	95	658.34	1.12	95
VALIDATION-P1-P21	309.19	0.39	100	617.32	ND	0
VALIDATION-P1-P22	251.07	ND	0	559.21	0.95	100
VALIDATION-P1-P23	261.10	ND	0	569.24	1.09	100
VALIDATION-P1-P24	395.20	ND	0	703.34	0.81	100

**Supplementary Table 5: Plate 2:** LCMS data from Chapter 7.3.3.5, HaloCompound *In-Situ* Synthesis for the Validation Set. Column 6 featured a control well, and column 18 featured positive control VHL amine **101**. Performed using standard conditions as outlined in General Methods, using LCMS method (A). Shown in **Figure 140**.

Well Number	SM mass	Rt	% Area	Product Mass	Rt	% Area
VALIDATION-P2-A1	329.16	0.55	18	637.3	1.16	82
VALIDATION-P2-A2	263.11	ND	0	571.3	1.13	94
VALIDATION-P2-A3	233.14	0.57	20	541.3	1.23	80
VALIDATION-P2-A4	307.11	0.39	49	615.3	0.88	51
VALIDATION-P2-A5	250.11	ND	0	558.3	1.13	100
VALIDATION-P2-A7	203.14	ND	0	511.3	1.15	100
VALIDATION-P2-A8	297.17	ND	0	605.3	1.30	100
VALIDATION-P2-A9	222.10	ND	0	530.2	1.07	100
VALIDATION-P2-A10	320.13	ND	0	628.3	1.26	100
VALIDATION-P2-A11	225.01	0.48	6	533.2	1.22	94
VALIDATION-P2-A12	233.12	ND	0	541.3	0.98	100
VALIDATION-P2-A13	272.11	0.51	100	580.3	ND	0
VALIDATION-P2-A14	251.16	ND	0	559.3	ND	0
VALIDATION-P2-A15	257.14	ND	0	565.3	1.29	100
VALIDATION-P2-A16	262.15	0.46	5	570.3	1.01	95
VALIDATION-P2-A17	255.13	ND	0	563.3	1.26	100
VALIDATION-P2-A18	430.00	ND	0	738.0	1.06	100
VALIDATION-P2-A19	227.13	ND	0	535.3	1.12	100
VALIDATION-P2-A21	231.11	ND	0	539.2	1.28	100
VALIDATION-P2-A22	205.09	1.00	100	513.2	1.00	100
VALIDATION-P2-A23	319.21	ND	0	627.3	ND	0
VALIDATION-P2-A24	221.09	ND	0	529.2	1.29	98
VALIDATION-P2-B1	296.05	ND	0	604.2	ND	0
VALIDATION-P2-B2	227.14	ND	0	535.3	1.03	100
VALIDATION-P2-B3	339.19	0.72	7	647.3	1.25	93
VALIDATION-P2-B4	320.05	ND	0	628.2	ND	0
VALIDATION-P2-B5	304.19	ND	0	612.3	0.85	84

Confidential – Do Not Copy

VALIDATION-P2-B7	360.14	0.79	12	668.3	1.13	88
VALIDATION-P2-B8	417.11	ND	0	725.2	0.95	100
VALIDATION-P2-B9	299.20	0.30	45	607.3	0.89	55
VALIDATION-P2-B10	300.20	ND	0	608.3	0.80	88
VALIDATION-P2-B11	217.16	ND	0	525.3	0.80	100
VALIDATION-P2-B12	254.12	0.36	60	562.3	0.87	40
VALIDATION-P2-B13	337.20	ND	0	645.3	0.82	100
VALIDATION-P2-B14	292.18	ND	0	600.3	1.10	100
VALIDATION-P2-B15	231.16	0.50	53	539.3	0.90	47
VALIDATION-P2-B16	268.16	ND	0	576.3	1.09	100
VALIDATION-P2-B17	342.09	0.51	44	650.2	0.94	56
VALIDATION-P2-B18	430.00	ND	0	738.0	1.06	100
VALIDATION-P2-B19	232.13	0.53	88	540.3	1.14	12
VALIDATION-P2-B20	286.12	0.67	100	594.3	ND	0
VALIDATION-P2-B21	342.15	0.64	100	650.3	ND	0
VALIDATION-P2-B22	234.17	ND	0	542.3	1.12	100
VALIDATION-P2-B23	305.21	0.54	100	613.4	ND	0
VALIDATION-P2-B24	333.19	0.37	100	641.3	ND	0
VALIDATION-P2-C1	234.18	ND	0	542.3	ND	0
VALIDATION-P2-C2	211.04	ND	0	519.2	0.96	100
VALIDATION-P2-C3	214.13	ND	0	522.3	0.85	100
VALIDATION-P2-C4	271.16	0.65	32	579.3	1.22	68
VALIDATION-P2-C5	219.09	ND	0	527.2	ND	0
VALIDATION-P2-C7	236.12	1.01	16	544.3	0.95	85
VALIDATION-P2-C8	257.10	ND	0	565.2	1.12	100
VALIDATION-P2-C9	373.18	ND	0	681.3	0.83	98
VALIDATION-P2-C10	217.16	ND	0	525.3	0.75	100
VALIDATION-P2-C11	316.15	ND	0	624.3	1.23	100
VALIDATION-P2-C12	346.13	0.95	100	654.3	0.95	100
VALIDATION-P2-C13	286.13	ND	0	594.3	1.13	100
VALIDATION-P2-C14	206.11	ND	0	514.2	1.10	100
VALIDATION-P2-C15	252.13	ND	0	560.3	0.87	100
VALIDATION-P2-C16	272.13	ND	0	580.3	1.17	100
VALIDATION-P2-C17	280.16	0.88	100	588.3	0.88	100
VALIDATION-P2-C18	430.00	ND	0	738.0	1.06	100
VALIDATION-P2-C19	209.10	ND	0	517.2	1.03	100
VALIDATION-P2-C20	264.16	ND	0	572.3	ND	0
VALIDATION-P2-C21	220.17	ND	0	528.3	0.81	100
VALIDATION-P2-C22	290.15	ND	0	598.3	1.15	100
VALIDATION-P2-C23	295.07	ND	0	603.2	1.20	100

Confidential – Do Not Copy

VALIDATION-P2-C24	341.10	0.83	65	649.2	1.46	35
VALIDATION-P2-D1	312.14	0.65	32	620.3	1.20	68
VALIDATION-P2-D2	206.12	ND	0	514.3	1.28	100
VALIDATION-P2-D3	202.11	ND	0	510.3	1.16	100
VALIDATION-P2-D4	311.16	1.17	95	619.3	1.17	95
VALIDATION-P2-D5	270.17	ND	0	578.3	ND	0
VALIDATION-P2-D7	280.07	0.58	59	588.2	1.21	25
VALIDATION-P2-D8	337.16	ND	0	645.3	1.19	100
VALIDATION-P2-D9	340.08	ND	0	648.2	1.20	100
VALIDATION-P2-D10	250.17	0.30	61	558.3	0.86	39
VALIDATION-P2-D11	203.13	0.36	100	511.3	ND	0
VALIDATION-P2-D12	273.16	ND	0	581.3	0.84	100
VALIDATION-P2-D13	337.18	0.56	52	645.3	0.89	48
VALIDATION-P2-D14	324.15	ND	0	632.3	1.04	100
VALIDATION-P2-D15	314.04	0.51	100	641.2	ND	0
VALIDATION-P2-D16	209.14	ND	0	517.3	1.12	100
VALIDATION-P2-D17	227.14	ND	0	535.3	1.25	87
VALIDATION-P2-D18	430.00	ND	0	738.0	1.06	100
VALIDATION-P2-D19	223.17	0.81	100	531.3	0.81	100
VALIDATION-P2-D20	284.10	0.34	100	592.2	ND	0
VALIDATION-P2-D21	220.95	ND	0	529.1	1.11	100
VALIDATION-P2-D22	318.11	ND	0	626.3	1.22	97
VALIDATION-P2-D23	326.21	0.89	100	634.4	0.89	100
VALIDATION-P2-D24	314.12	ND	0	622.3	0.93	100
VALIDATION-P2-E1	302.07	ND	0	610.2	1.27	95
VALIDATION-P2-E2	207.10	0.83	100	515.2	0.83	100
VALIDATION-P2-E3	295.20	ND	0	603.3	0.83	31
VALIDATION-P2-E4	296.13	ND	0	604.3	1.01	93
VALIDATION-P2-E5	337.22	0.55	16	645.4	0.98	56
VALIDATION-P2-E7	255.10	ND	0	563.2	1.25	100
VALIDATION-P2-E8	292.11	ND	0	600.3	1.25	94
VALIDATION-P2-E9	208.07	ND	0	516.2	1.11	100
VALIDATION-P2-E10	209.16	ND	0	517.3	0.78	100
VALIDATION-P2-E11	201.13	ND	0	509.3	1.14	100
VALIDATION-P2-E12	271.17	0.34	100	579.3	ND	0
VALIDATION-P2-E13	304.15	ND	0	612.3	0.93	95
VALIDATION-P2-E14	233.15	0.85	8	541.3	0.75	92
VALIDATION-P2-E15	204.02	ND	0	512.2	1.26	100
VALIDATION-P2-E16	237.11	ND	0	545.3	1.17	100
VALIDATION-P2-E17	211.05	ND	0	519.2	1.09	100

Confidential – Do Not Copy

VALIDATION-P2-E18	430.00	ND	0	738.0	1.06	100
VALIDATION-P2-E19	294.15	ND	0	602.3	0.92	23
VALIDATION-P2-E21	292.16	0.72	82	600.3	0.72	82
VALIDATION-P2-E22	202.15	0.58	50	510.3	1.28	30
VALIDATION-P2-E23	314.19	0.43	86	622.3	0.87	14
VALIDATION-P2-E24	216.96	ND	0	525.1	1.21	100
VALIDATION-P2-F1	218.11	ND	0	526.2	1.22	100
VALIDATION-P2-F2	296.95	ND	0	605.1	1.20	100
VALIDATION-P2-F3	326.06	0.61	11	634.2	1.17	89
VALIDATION-P2-F4	330.04	1.17	100	657.2	1.17	100
VALIDATION-P2-F5	225.15	ND	0	533.3	1.29	100
VALIDATION-P2-F7	262.14	0.83	100	570.3	0.83	100
VALIDATION-P2-F8	301.22	0.31	79	609.4	0.82	21
VALIDATION-P2-F9	294.11	ND	0	602.3	1.18	100
VALIDATION-P2-F10	280.13	ND	0	588.3	1.24	100
VALIDATION-P2-F11	347.18	0.35	100	655.3	ND	0
VALIDATION-P2-F12	285.18	0.52	100	593.3	ND	0
VALIDATION-P2-F13	288.18	0.54	87	596.3	ND	0
VALIDATION-P2-F14	303.19	ND	0	611.3	0.80	100
VALIDATION-P2-F15	306.04	ND	0	614.2	1.19	100
VALIDATION-P2-F16	272.08	ND	0	580.2	1.18	100
VALIDATION-P2-F17	319.19	0.33	33	627.3	0.83	67
VALIDATION-P2-F18	430.00	ND	0	738.0	1.07	100
VALIDATION-P2-F19	287.21	ND	0	595.4	0.75	94
VALIDATION-P2-F20	269.10	0.40	64	577.2	0.73	36
VALIDATION-P2-F21	325.12	0.41	54	633.3	0.91	46
VALIDATION-P2-F22	310.15	1.19	54	618.3	1.19	54
VALIDATION-P2-F23	330.19	0.40	4	638.3	ND	0
VALIDATION-P2-F24	227.14	ND	0	535.3	0.84	100
VALIDATION-P2-G1	249.13	0.55	100	557.3	ND	0
VALIDATION-P2-G2	227.09	ND	0	535.2	1.07	100
VALIDATION-P2-G3	257.14	ND	0	565.3	ND	0
VALIDATION-P2-G4	273.13	ND	0	581.3	1.17	100
VALIDATION-P2-G5	231.12	0.54	2	539.3	0.87	93
VALIDATION-P2-G7	229.05	ND	0	537.2	1.07	100
VALIDATION-P2-G8	259.17	0.60	13	567.3	1.20	71
VALIDATION-P2-G9	254.07	0.61	100	562.2	ND	0
VALIDATION-P2-G10	239.13	ND	0	547.3	1.20	100
VALIDATION-P2-G11	292.16	ND	0	600.3	1.15	100
VALIDATION-P2-G12	226.09	ND	0	534.2	0.99	100

Confidential – Do Not Copy

VALIDATION-P2-G13	201.13	ND	0	509.3	0.81	100
VALIDATION-P2-G14	257.15	ND	0	565.3	1.08	100
VALIDATION-P2-G15	223.17	ND	0	531.3	ND	0
VALIDATION-P2-G16	338.14	0.63	95	646.3	ND	0
VALIDATION-P2-G17	293.21	ND	0	601.4	0.82	100
VALIDATION-P2-G18	430.00	ND	0	738.0	1.06	100
VALIDATION-P2-G19	302.12	ND	0	610.3	0.90	100
VALIDATION-P2-G21	285.18	0.47	23	593.3	0.91	64
VALIDATION-P2-G22	268.16	0.89	100	576.3	0.89	100
VALIDATION-P2-G23	277.09	ND	0	585.2	1.22	100
VALIDATION-P2-G24	276.18	ND	0	584.3	1.32	100
VALIDATION-P2-H1	286.18	ND	0	594.3	0.72	100
VALIDATION-P2-H2	432.18	ND	0	740.3	1.29	89
VALIDATION-P2-H3	270.18	0.38	37	578.3	0.87	48
VALIDATION-P2-H4	349.19	0.90	100	657.3	0.90	100
VALIDATION-P2-H5	303.23	0.43	55	611.4	ND	0
VALIDATION-P2-H7	281.15	ND	0	589.3	1.07	100
VALIDATION-P2-H8	284.12	0.80	3	592.3	1.03	97
VALIDATION-P2-H9	316.16	ND	0	624.3	0.92	100
VALIDATION-P2-H10	246.09	ND	0	554.2	1.04	100
VALIDATION-P2-H11	344.03	ND	0	652.2	ND	0
VALIDATION-P2-H12	209.12	ND	0	517.3	ND	0
VALIDATION-P2-H13	264.16	0.53	100	572.3	ND	0
VALIDATION-P2-H14	203.13	0.41	100	511.3	ND	0
VALIDATION-P2-H15	315.08	0.65	100	623.2	ND	0
VALIDATION-P2-H16	278.20	ND	0	586.3	0.88	100
VALIDATION-P2-H17	215.14	ND	0	523.3	0.80	100
VALIDATION-P2-H18	430.00	ND	0	738.0	1.06	100
VALIDATION-P2-H19	346.20	1.00	100	654.3	1.00	100
VALIDATION-P2-H20	231.10	0.40	17	539.2	1.01	83
VALIDATION-P2-H21	235.13	ND	0	543.3	1.01	100
VALIDATION-P2-H22	202.11	ND	0	510.3	1.14	100
VALIDATION-P2-H23	288.05	0.61	100	596.2	ND	0
VALIDATION-P2-H24	235.11	ND	0	543.3	1.02	91
VALIDATION-P2-I1	261.08	ND	0	569.2	1.09	100
VALIDATION-P2-I2	316.23	0.51	73	624.4	ND	0
VALIDATION-P2-I3	352.22	0.64	57	660.4	1.23	43
VALIDATION-P2-I4	218.18	ND	0	526.3	0.88	100
VALIDATION-P2-I5	325.08	0.56	100	633.2	ND	0
VALIDATION-P2-I7	228.03	ND	0	536.2	1.13	100

Confidential – Do Not Copy

VALIDATION-P2-I8	337.18	0.67	88	645.3	0.57	4
VALIDATION-P2-I9	208.10	ND	0	516.2	1.08	100
VALIDATION-P2-I10	237.11	ND	0	545.3	1.17	100
VALIDATION-P2-I11	246.11	ND	0	554.3	1.17	100
VALIDATION-P2-I12	231.10	ND	0	539.2	1.01	100
VALIDATION-P2-I13	252.11	0.45	10	560.3	1.01	88
VALIDATION-P2-I14	213.12	ND	0	521.3	1.30	100
VALIDATION-P2-I15	214.12	ND	0	522.3	1.01	100
VALIDATION-P2-I16	233.10	0.52	22	541.2	0.86	62
VALIDATION-P2-I17	243.11	1.39	10	551.2	1.32	62
VALIDATION-P2-I18	430.00	ND	0	738.0	1.06	100
VALIDATION-P2-I19	232.16	ND	0	540.3	0.76	9
VALIDATION-P2-I21	316.14	0.67	7	624.3	1.19	93
VALIDATION-P2-I22	342.14	0.68	47	650.3	1.23	53
VALIDATION-P2-I23	267.10	ND	0	575.2	1.01	100
VALIDATION-P2-I24	313.18	ND	0	621.3	0.85	100
VALIDATION-P2-J1	221.12	ND	0	529.3	0.83	100
VALIDATION-P2-J2	228.14	0.74	37	536.3	0.74	37
VALIDATION-P2-J3	264.10	ND	0	572.2	1.14	100
VALIDATION-P2-J4	296.13	ND	0	604.3	1.28	100
VALIDATION-P2-J5	247.16	0.61	100	555.3	ND	0
VALIDATION-P2-J7	329.14	ND	0	637.3	1.00	100
VALIDATION-P2-J8	202.11	0.72	51	510.3	1.16	27
VALIDATION-P2-J9	320.05	ND	0	628.2	1.18	100
VALIDATION-P2-J10	273.15	ND	0	581.3	1.03	79
VALIDATION-P2-J11	289.22	0.49	100	597.4	ND	0
VALIDATION-P2-J12	365.21	ND	0	673.4	0.84	100
VALIDATION-P2-J13	263.20	ND	0	571.3	0.81	100
VALIDATION-P2-J14	205.11	ND	0	513.3	1.13	100
VALIDATION-P2-J15	229.15	1.18	2	537.3	1.30	98
VALIDATION-P2-J16	419.00	ND	0	727.1	1.40	100
VALIDATION-P2-J17	315.19	0.90	89	623.3	0.90	89
VALIDATION-P2-J18	430.00	ND	0	738.0	1.06	100
VALIDATION-P2-J19	238.17	ND	0	546.3	ND	0
VALIDATION-P2-J20	275.14	ND	0	583.3	0.82	79
VALIDATION-P2-J21	346.18	0.37	84	654.3	0.86	14
VALIDATION-P2-J22	340.08	ND	0	648.2	1.25	100
VALIDATION-P2-J23	356.21	0.45	37	664.4	0.95	63
VALIDATION-P2-J24	262.20	ND	0	570.3	ND	0
VALIDATION-P2-K1	302.17	ND	0	610.3	0.90	100

Confidential – Do Not Copy

VALIDATION-P2-K2	340.17	ND	0	648.3	1.15	78
VALIDATION-P2-K3	254.14	ND	0	562.3	0.86	100
VALIDATION-P2-K4	330.17	0.96	52	638.3	0.96	52
VALIDATION-P2-K5	244.12	ND	0	552.3	0.94	100
VALIDATION-P2-K7	214.11	ND	0	522.3	0.88	100
VALIDATION-P2-K8	266.14	ND	0	574.3	1.09	100
VALIDATION-P2-K9	233.10	ND	0	541.2	1.18	100
VALIDATION-P2-K10	328.16	0.73	100	636.3	ND	0
VALIDATION-P2-K11	244.02	ND	0	552.2	1.15	100
VALIDATION-P2-K12	218.11	0.52	16	526.2	1.15	84
VALIDATION-P2-K13	245.06	0.63	69	553.2	1.31	31
VALIDATION-P2-K14	236.20	0.75	9	544.3	0.64	91
VALIDATION-P2-K15	228.13	ND	0	536.3	0.88	82
VALIDATION-P2-K16	256.13	0.65	3	564.3	1.20	93
VALIDATION-P2-K17	206.14	ND	0	514.3	0.83	100
VALIDATION-P2-K18	430.00	ND	0	738.0	1.06	100
VALIDATION-P2-K19	319.07	ND	0	627.2	0.87	100
VALIDATION-P2-K20	365.11	ND	0	673.3	1.25	100
VALIDATION-P2-K21	245.13	ND	0	553.3	1.11	100
VALIDATION-P2-K22	219.12	ND	0	527.3	1.17	100
VALIDATION-P2-K23	262.13	0.39	3	570.3	0.77	97
VALIDATION-P2-K24	321.01	0.73	50	629.2	1.37	50
VALIDATION-P2-L1	230.18	ND	0	538.3	1.31	100
VALIDATION-P2-L2	415.11	ND	0	723.3	1.35	100
VALIDATION-P2-L3	205.10	ND	0	513.2	1.11	100
VALIDATION-P2-L4	285.14	ND	0	593.3	1.26	100
VALIDATION-P2-L5	206.14	0.83	100	514.3	0.83	100
VALIDATION-P2-L7	234.17	0.41	8	542.3	0.99	92
VALIDATION-P2-L8	260.00	0.44	100	568.1	ND	0
VALIDATION-P2-L9	257.11	ND	0	565.2	1.12	92
VALIDATION-P2-L10	252.13	0.50	100	560.3	ND	0
VALIDATION-P2-L11	348.12	ND	0	656.3	ND	0
VALIDATION-P2-L12	251.15	ND	0	559.3	1.22	100
VALIDATION-P2-L13	252.18	ND	0	560.3	ND	0
VALIDATION-P2-L14	205.12	0.80	97	513.3	0.80	97
VALIDATION-P2-L15	242.15	ND	0	550.3	0.97	100
VALIDATION-P2-L16	298.13	ND	0	606.3	1.17	100
VALIDATION-P2-L17	242.11	ND	0	550.3	1.06	100
VALIDATION-P2-L18	430.00	ND	0	738.0	1.06	100
VALIDATION-P2-L19	212.13	ND	0	520.3	0.96	100

Confidential – Do Not Copy

VALIDATION-P2-L20	289.14	0.48	100	597.3	ND	0
VALIDATION-P2-L21	233.13	ND	0	541.3	1.11	100
VALIDATION-P2-L22	307.15	ND	0	615.3	1.17	100
VALIDATION-P2-L23	342.21	ND	0	650.3	0.82	100
VALIDATION-P2-L24	254.15	ND	0	562.3	0.67	100
VALIDATION-P2-M1	276.18	ND	0	584.3	1.16	100
VALIDATION-P2-M2	311.20	0.39	91	619.3	0.56	6
VALIDATION-P2-M3	213.13	ND	0	521.3	0.83	100
VALIDATION-P2-M4	279.07	0.87	10	587.2	1.11	90
VALIDATION-P2-M5	219.13	ND	0	527.3	1.15	100
VALIDATION-P2-M7	274.11	ND	0	582.3	1.14	100
VALIDATION-P2-M8	236.19	ND	0	544.3	0.89	100
VALIDATION-P2-M9	338.21	ND	0	646.4	1.29	100
VALIDATION-P2-M10	311.13	1.15	100	619.3	1.15	100
VALIDATION-P2-M11	209.14	0.55	100	517.3	ND	0
VALIDATION-P2-M12	229.07	ND	0	537.2	1.45	100
VALIDATION-P2-M13	281.14	0.60	100	589.3	ND	0
VALIDATION-P2-M14	263.12	0.48	71	571.3	1.09	29
VALIDATION-P2-M15	200.08	ND	0	508.2	ND	0
VALIDATION-P2-M16	292.10	0.89	72	600.2	0.89	72
VALIDATION-P2-M17	270.02	ND	0	578.2	0.98	98
VALIDATION-P2-M18	430.00	ND	0	738.0	1.06	100
VALIDATION-P2-M19	334.14	ND	0	642.3	0.88	100
VALIDATION-P2-M20	238.13	ND	0	546.3	0.80	100
VALIDATION-P2-M21	234.15	ND	0	542.3	0.99	100
VALIDATION-P2-M22	205.16	ND	0	513.3	0.78	100
VALIDATION-P2-M23	233.10	ND	0	541.2	0.80	85
VALIDATION-P2-M24	305.11	0.58	64	613.3	1.19	36
VALIDATION-P2-N1	226.09	ND	0	534.2	1.26	100
VALIDATION-P2-N2	267.18	0.42	100	575.3	ND	0
VALIDATION-P2-N3	248.10	0.53	44	556.2	1.22	56
VALIDATION-P2-N4	325.15	0.87	100	633.3	0.87	100
VALIDATION-P2-N5	274.20	ND	0	582.3	0.86	18
VALIDATION-P2-N7	270.14	ND	0	578.3	1.19	100
VALIDATION-P2-N8	314.24	ND	0	622.4	0.85	100
VALIDATION-P2-N9	276.11	ND	0	584.3	1.12	100
VALIDATION-P2-N10	277.22	ND	0	585.4	ND	0
VALIDATION-P2-N11	361.24	0.40	100	669.4	ND	0
VALIDATION-P2-N12	230.10	ND	0	538.2	1.30	100
VALIDATION-P2-N13	200.98	0.72	19	509.1	1.03	68

Confidential – Do Not Copy

VALIDATION-P2-N14	278.25	ND	0	586.4	ND	0
VALIDATION-P2-N15	316.15	ND	0	624.3	0.81	100
VALIDATION-P2-N16	340.23	ND	0	648.4	ND	0
VALIDATION-P2-N17	303.08	ND	0	611.2	1.24	100
VALIDATION-P2-N18	430.00	ND	0	738.0	1.06	100
VALIDATION-P2-N19	257.12	ND	0	565.3	1.34	88
VALIDATION-P2-N20	213.13	ND	0	521.3	0.78	100
VALIDATION-P2-N21	309.19	0.55	100	617.3	ND	0
VALIDATION-P2-N22	315.14	ND	0	623.3	1.17	100
VALIDATION-P2-N23	274.20	ND	0	582.3	0.98	100
VALIDATION-P2-N24	219.16	ND	0	527.3	1.20	100
VALIDATION-P2-O1	264.10	ND	0	572.2	1.13	100
VALIDATION-P2-O2	251.13	ND	0	559.3	1.22	76
VALIDATION-P2-O3	244.16	0.55	100	552.3	ND	0
VALIDATION-P2-O4	348.12	0.56	100	656.3	ND	0
VALIDATION-P2-O5	324.18	0.61	80	632.3	1.21	20
VALIDATION-P2-O7	299.01	0.59	87	607.2	ND	0
VALIDATION-P2-O8	260.10	0.77	6	568.2	1.15	89
VALIDATION-P2-O9	214.11	ND	0	522.3	0.94	94
VALIDATION-P2-O10	254.16	ND	0	562.3	1.17	81
VALIDATION-P2-O11	316.22	ND	0	624.4	1.22	52
VALIDATION-P2-O12	279.16	0.89	100	587.3	0.89	100
VALIDATION-P2-O13	278.17	ND	0	586.3	0.74	86
VALIDATION-P2-O14	320.16	0.51	15	628.3	0.92	63
VALIDATION-P2-O15	234.08	ND	0	542.2	0.92	100
VALIDATION-P2-O16	324.13	ND	0	632.3	1.13	90
VALIDATION-P2-O17	227.13	ND	0	535.3	1.33	100
VALIDATION-P2-O18	430.00	ND	0	738.0	1.06	100
VALIDATION-P2-O19	205.16	ND	0	513.3	0.92	100
VALIDATION-P2-O20	258.14	0.46	43	566.3	1.08	57
VALIDATION-P2-O21	280.20	ND	0	588.3	ND	0
VALIDATION-P2-O22	273.20	0.45	70	581.3	1.01	30
VALIDATION-P2-O23	287.14	ND	0	595.3	1.09	100
VALIDATION-P2-O24	330.09	ND	0	638.2	ND	0
VALIDATION-P2-P1	279.04	1.25	93	587.2	1.25	93
VALIDATION-P2-P2	252.10	ND	0	560.2	1.12	100
VALIDATION-P2-P3	238.11	ND	0	546.3	1.02	100
VALIDATION-P2-P4	271.14	ND	0	579.3	1.21	100
VALIDATION-P2-P5	238.13	0.55	94	546.3	1.28	6
VALIDATION-P2-P7	424.20	ND	0	732.3	0.94	91

VALIDATION-P2-P8	233.15	ND	0	541.3	0.83	87
VALIDATION-P2-P9	325.16	0.57	19	633.3	1.09	81
VALIDATION-P2-P10	314.16	ND	0	622.3	1.23	100
VALIDATION-P2-P11	301.12	ND	0	609.3	1.17	100
VALIDATION-P2-P12	205.16	ND	0	513.3	0.85	100
VALIDATION-P2-P13	231.14	ND	0	539.3	1.09	100
VALIDATION-P2-P14	351.19	1.16	100	659.3	1.16	100
VALIDATION-P2-P15	227.03	ND	0	535.2	1.35	100
VALIDATION-P2-P16	306.05	ND	0	614.2	1.09	100
VALIDATION-P2-P17	229.16	ND	0	537.3	0.84	100
VALIDATION-P2-P18	430.00	ND	0	738.0	1.06	100
VALIDATION-P2-P19	222.08	0.91	4	530.2	1.04	90
VALIDATION-P2-P20	228.16	0.61	100	536.3	ND	0
VALIDATION-P2-P21	241.13	ND	0	549.3	1.03	100
VALIDATION-P2-P22	275.05	ND	0	583.2	1.14	100
VALIDATION-P2-P23	356.26	0.43	44	664.4	0.91	56
VALIDATION-P2-P24	239.13	ND	0	547.3	0.87	100

**Supplementary Table 6: Plate 3:** LCMS data from Chapter 7.3.3.5, HaloCompound *In-Situ* Synthesis for the Validation Set. Column 6 featured a control well, and column 18 featured positive control VHL amine **101**. Performed using standard conditions as outlined in General Methods, using LCMS method (A).

Well Number	SM mass	Rt	% Area	Product Mass	Rt	% Area
VALIDATION-P3-A1	293.21	ND	0	601.35	1.02	100
VALIDATION-P3-A2	300.15	0.60	10	608.29	1.10	90
VALIDATION-P3-A3	338.17	0.47	100	646.31	ND	0
VALIDATION-P3-A4	357.24	ND	0	665.38	0.84	100
VALIDATION-P3-A5	282.18	ND	0	590.32	0.94	86
VALIDATION-P3-A7	206.15	ND	0	514.29	1.10	100
VALIDATION-P3-A8	275.10	0.63	54	583.23	1.18	46
VALIDATION-P3-A9	309.16	0.38	68	617.30	0.38	68
VALIDATION-P3-A10	288.08	ND	0	596.22	1.13	100
VALIDATION-P3-A11	202.12	ND	0	510.26	1.05	100
VALIDATION-P3-A12	272.13	ND	0	580.27	1.04	100
VALIDATION-P3-A13	209.11	ND	0	517.24	ND	0
VALIDATION-P3-A14	325.14	ND	0	633.28	1.07	90
VALIDATION-P3-A15	345.15	1.06	100	653.29	1.06	100
VALIDATION-P3-A16	225.15	ND	0	533.29	0.82	100
VALIDATION-P3-A17	329.12	0.90	4	637.26	1.02	96
VALIDATION-P3-A18	430.00	ND	0	738.00	1.06	100

Confidential – Do Not Copy

VALIDATION-P3-A19	370.20	0.72	8	678.34	0.99	86
VALIDATION-P3-A20	306.21	0.37	96	614.34	ND	0
VALIDATION-P3-A21	235.12	ND	0	543.26	1.03	100
VALIDATION-P3-A22	240.16	ND	0	548.30	1.01	100
VALIDATION-P3-A23	336.15	ND	0	644.29	1.03	100
VALIDATION-P3-A24	362.18	0.62	30	670.31	1.17	70
VALIDATION-P3-B1	208.13	0.88	13	516.27	0.83	87
VALIDATION-P3-B2	371.23	0.31	91	679.37	0.78	6
VALIDATION-P3-B3	257.15	0.42	100	565.29	ND	0
VALIDATION-P3-B4	359.23	0.71	100	667.37	0.71	100
VALIDATION-P3-B5	219.14	0.29	61	527.28	0.84	37
VALIDATION-P3-B7	350.23	ND	0	658.37	0.76	84
VALIDATION-P3-B8	208.13	ND	0	516.27	0.75	100
VALIDATION-P3-B9	297.20	0.89	100	605.33	0.89	100
VALIDATION-P3-B10	234.15	0.46	100	542.29	ND	0
VALIDATION-P3-B11	277.19	ND	0	585.33	0.76	100
VALIDATION-P3-B12	316.15	ND	0	624.29	1.19	100
VALIDATION-P3-B13	354.11	0.60	92	662.25	0.94	8
VALIDATION-P3-B14	332.18	0.58	81	640.32	1.07	15
VALIDATION-P3-B15	324.16	0.68	43	632.30	1.19	57
VALIDATION-P3-B16	385.21	0.33	15	693.35	0.79	85
VALIDATION-P3-B17	330.10	0.94	84	638.24	0.94	84
VALIDATION-P3-B18	430.00	ND	0	738.00	1.06	100
VALIDATION-P3-B19	299.17	0.44	19	607.31	0.92	81
VALIDATION-P3-B20	269.12	0.34	100	577.26	ND	0
VALIDATION-P3-B21	343.14	0.49	70	651.28	ND	0
VALIDATION-P3-B22	327.16	0.43	62	635.30	1.00	38
VALIDATION-P3-B23	288.11	0.83	64	596.25	ND	0
VALIDATION-P3-B24	353.22	0.52	100	661.36	ND	0
VALIDATION-P3-C1	257.16	ND	0	565.30	0.80	84
VALIDATION-P3-C2	249.15	ND	0	557.29	0.97	100
VALIDATION-P3-C3	338.19	0.48	7	646.32	0.90	91
VALIDATION-P3-C4	315.14	ND	0	623.28	0.99	100
VALIDATION-P3-C5	296.15	ND	0	604.29	0.96	100
VALIDATION-P3-C7	272.07	0.65	100	580.21	ND	0
VALIDATION-P3-C8	251.13	ND	0	559.27	1.06	100
VALIDATION-P3-C9	206.15	0.38	100	514.29	ND	0
VALIDATION-P3-C10	356.21	0.53	86	664.35	0.91	14
VALIDATION-P3-C11	327.17	0.78	88	635.31	0.78	88
VALIDATION-P3-C12	269.16	ND	0	577.30	0.89	100

Confidential – Do Not Copy

VALIDATION-P3-C13	229.11	ND	0	537.25	0.98	100
VALIDATION-P3-C14	237.08	0.38	100	545.22	ND	0
VALIDATION-P3-C15	254.17	0.74	100	562.31	0.74	100
VALIDATION-P3-C16	414.17	0.69	98	722.31	1.22	2
VALIDATION-P3-C17	273.10	0.41	100	581.24	ND	0
VALIDATION-P3-C18	430.00	ND	0	738.00	1.06	100
VALIDATION-P3-C19	337.12	0.63	100	645.26	ND	0
VALIDATION-P3-C20	259.04	ND	0	567.18	1.23	100
VALIDATION-P3-C21	312.15	ND	0	620.29	0.95	20
VALIDATION-P3-C22	316.14	0.53	100	624.28	ND	0
VALIDATION-P3-C23	281.12	0.83	14	589.26	0.92	86
VALIDATION-P3-C24	343.25	ND	0	651.39	0.60	100
VALIDATION-P3-D1	244.13	ND	0	552.27	1.02	100
VALIDATION-P3-D2	342.21	0.34	96	650.34	ND	0
VALIDATION-P3-D3	265.12	0.31	100	573.26	ND	0
VALIDATION-P3-D4	437.15	0.82	13	745.29	0.99	76
VALIDATION-P3-D5	283.03	ND	0	591.17	1.10	100
VALIDATION-P3-D7	230.12	ND	0	538.26	1.06	100
VALIDATION-P3-D8	413.30	0.63	18	721.44	0.92	71
VALIDATION-P3-D9	324.21	0.85	100	632.35	0.85	100
VALIDATION-P3-D10	292.23	ND	0	600.37	ND	0
VALIDATION-P3-D11	221.15	0.41	100	529.29	ND	0
VALIDATION-P3-D12	275.11	0.57	3	583.25	0.87	97
VALIDATION-P3-D13	320.18	0.60	100	628.32	ND	0
VALIDATION-P3-D14	333.10	ND	0	641.24	1.19	100
VALIDATION-P3-D15	330.17	ND	0	638.31	1.08	100
VALIDATION-P3-D16	299.17	1.02	100	607.31	1.02	100
VALIDATION-P3-D17	248.15	0.38	100	556.29	ND	0
VALIDATION-P3-D18	430.00	ND	0	738.00	1.06	100
VALIDATION-P3-D19	316.17	0.49	82	624.31	1.00	18
VALIDATION-P3-D20	313.23	0.55	100	621.37	ND	0
VALIDATION-P3-D21	259.04	ND	0	567.18	1.04	100
VALIDATION-P3-D22	288.99	ND	0	597.13	0.99	100
VALIDATION-P3-D23	275.15	ND	0	583.29	1.07	100
VALIDATION-P3-D24	314.10	0.64	42	622.24	1.14	58
VALIDATION-P3-E1	203.12	ND	0	511.26	0.72	100
VALIDATION-P3-E2	223.13	ND	0	531.27	0.91	100
VALIDATION-P3-E3	307.23	0.56	100	615.37	ND	0
VALIDATION-P3-E4	357.22	ND	0	665.36	0.84	100
VALIDATION-P3-E5	338.18	0.54	92	646.32	0.92	8

Confidential – Do Not Copy

VALIDATION-P3-E7	301.15	0.61	48	609.29	1.12	52
VALIDATION-P3-E8	275.15	0.37	2	583.29	0.81	98
VALIDATION-P3-E9	258.15	ND	0	566.29	1.08	100
VALIDATION-P3-E10	338.21	ND	0	646.35	1.07	100
VALIDATION-P3-E11	371.20	ND	0	679.34	1.20	100
VALIDATION-P3-E12	216.10	ND	0	524.24	0.84	100
VALIDATION-P3-E13	276.08	ND	0	584.22	1.07	100
VALIDATION-P3-E14	296.13	ND	0	604.27	1.03	82
VALIDATION-P3-E15	290.09	ND	0	598.23	1.09	84
VALIDATION-P3-E16	286.18	ND	0	594.32	0.80	100
VALIDATION-P3-E17	250.11	ND	0	558.25	0.89	100
VALIDATION-P3-E18	430.00	ND	0	738.00	1.06	100
VALIDATION-P3-E19	228.09	ND	0	536.23	1.07	100
VALIDATION-P3-E20	249.15	ND	0	557.29	0.80	100
VALIDATION-P3-E21	356.04	ND	0	664.18	1.11	88
VALIDATION-P3-E22	290.21	0.42	66	598.35	0.99	34
VALIDATION-P3-E23	288.20	0.30	100	596.33	ND	0
VALIDATION-P3-E24	363.26	0.63	100	671.40	0.63	100
VALIDATION-P3-F1	282.12	ND	0	590.26	0.99	100
VALIDATION-P3-F2	238.18	ND	0	546.32	0.75	100
VALIDATION-P3-F3	344.18	1.08	100	652.32	1.08	100
VALIDATION-P3-F4	270.14	1.12	100	578.28	1.12	100
VALIDATION-P3-F5	341.22	0.35	11	649.36	0.82	89
VALIDATION-P3-F7	306.12	ND	0	614.25	1.02	81
VALIDATION-P3-F8	296.15	ND	0	604.29	1.08	48
VALIDATION-P3-F9	337.11	ND	0	645.25	1.03	100
VALIDATION-P3-F10	363.17	ND	0	671.31	0.77	100
VALIDATION-P3-F11	262.12	0.57	9	570.26	1.04	91
VALIDATION-P3-F12	286.18	ND	0	594.32	0.81	100
VALIDATION-P3-F13	321.22	0.47	100	629.36	ND	0
VALIDATION-P3-F14	328.14	1.02	100	636.28	1.02	100
VALIDATION-P3-F15	296.15	0.55	100	604.29	ND	0
VALIDATION-P3-F16	285.15	0.34	100	593.29	ND	0
VALIDATION-P3-F17	333.21	0.43	100	641.34	ND	0
VALIDATION-P3-F18	430.00	ND	0	738.00	1.06	100
VALIDATION-P3-F19	298.14	ND	0	606.27	1.17	100
VALIDATION-P3-F20	280.19	ND	0	588.33	0.69	100
VALIDATION-P3-F21	223.06	ND	0	531.20	1.13	100
VALIDATION-P3-F22	224.13	0.35	14	532.27	0.93	80
VALIDATION-P3-F23	350.21	0.61	87	658.35	ND	0

Confidential – Do Not Copy

VALIDATION-P3-F24	274.18	ND	0	582.32	ND	0
VALIDATION-P3-G1	317.13	0.58	52	625.27	ND	0
VALIDATION-P3-G2	250.14	ND	0	558.28	ND	0
VALIDATION-P3-G3	319.12	0.60	16	627.26	1.17	84
VALIDATION-P3-G4	241.09	0.40	100	549.23	ND	0
VALIDATION-P3-G5	289.14	ND	0	597.28	0.77	100
VALIDATION-P3-G7	250.13	ND	0	558.27	1.03	100
VALIDATION-P3-G8	266.14	0.59	7	574.28	1.12	82
VALIDATION-P3-G9	298.18	1.00	76	606.32	1.00	76
VALIDATION-P3-G10	289.18	ND	0	597.32	1.06	100
VALIDATION-P3-G11	345.19	ND	0	653.32	1.12	100
VALIDATION-P3-G12	204.10	ND	0	512.24	0.84	100
VALIDATION-P3-G13	361.18	ND	0	669.32	1.08	100
VALIDATION-P3-G14	299.14	0.47	23	607.28	0.87	33
VALIDATION-P3-G15	293.12	0.43	100	601.26	ND	0
VALIDATION-P3-G16	254.17	ND	0	562.31	ND	0
VALIDATION-P3-G17	332.27	0.74	100	640.41	0.74	100
VALIDATION-P3-G18	430.00	ND	0	738.00	1.06	100
VALIDATION-P3-G19	348.10	ND	0	656.24	ND	0
VALIDATION-P3-G20	305.08	0.71	61	613.22	1.27	39
VALIDATION-P3-G21	370.18	0.59	100	678.32	ND	0
VALIDATION-P3-G22	278.17	0.42	37	586.31	1.06	37
VALIDATION-P3-G23	273.16	ND	0	581.30	0.83	96
VALIDATION-P3-G24	317.17	ND	0	625.30	1.00	100
VALIDATION-P3-H1	313.18	0.64	100	621.32	ND	0
VALIDATION-P3-H2	227.11	ND	0	535.25	0.76	100
VALIDATION-P3-H3	324.17	ND	0	632.31	0.69	100
VALIDATION-P3-H4	245.15	ND	0	553.29	0.79	78
VALIDATION-P3-H5	421.27	ND	0	729.41	0.97	58
VALIDATION-P3-H7	333.14	ND	0	641.27	1.18	100
VALIDATION-P3-H8	205.10	1.02	100	513.24	1.02	100
VALIDATION-P3-H9	266.17	0.42	100	574.31	ND	0
VALIDATION-P3-H10	257.16	0.48	47	565.30	1.09	40
VALIDATION-P3-H11	243.13	0.39	75	551.27	0.87	25
VALIDATION-P3-H12	225.09	ND	0	533.23	0.93	100
VALIDATION-P3-H13	277.18	ND	0	585.32	ND	0
VALIDATION-P3-H14	251.11	0.40	3	559.25	0.94	97
VALIDATION-P3-H15	216.06	ND	0	524.20	0.91	60
VALIDATION-P3-H16	300.18	0.80	25	608.32	0.86	68
VALIDATION-P3-H17	344.14	0.55	81	652.28	1.06	9

Confidential – Do Not Copy

VALIDATION-P3-H18	430.00	ND	0	738.00	1.06	100
VALIDATION-P3-H19	236.16	0.39	100	544.30	ND	0
VALIDATION-P3-H20	355.11	0.58	100	663.25	ND	0
VALIDATION-P3-H21	264.20	ND	0	572.33	0.85	100
VALIDATION-P3-H22	208.05	1.13	100	516.19	1.13	100
VALIDATION-P3-H23	348.14	0.51	50	656.28	1.01	34
VALIDATION-P3-I1	323.15	0.58	76	631.29	ND	0
VALIDATION-P3-I2	224.14	ND	0	532.28	0.68	100
VALIDATION-P3-I3	209.16	ND	0	517.30	1.12	100
VALIDATION-P3-I4	225.09	0.47	73	533.23	1.10	27
VALIDATION-P3-I5	375.14	ND	0	683.28	1.03	100
VALIDATION-P3-I7	264.10	0.41	100	572.24	ND	0
VALIDATION-P3-I8	246.15	ND	0	554.29	ND	0
VALIDATION-P3-I9	278.21	ND	0	586.35	0.82	100
VALIDATION-P3-I10	329.21	0.78	100	637.35	0.78	100
VALIDATION-P3-I11	223.08	0.40	22	531.22	1.01	78
VALIDATION-P3-I12	245.13	0.34	9	553.27	0.81	45
VALIDATION-P3-I13	295.17	ND	0	603.31	1.03	100
VALIDATION-P3-I14	250.17	ND	0	558.31	0.81	100
VALIDATION-P3-I15	259.18	ND	0	567.32	0.81	100
VALIDATION-P3-I16	285.20	ND	0	593.33	1.09	85
VALIDATION-P3-I17	251.06	0.48	81	559.20	ND	0
VALIDATION-P3-I18	430.00	ND	0	738.00	1.06	100
VALIDATION-P3-I19	332.14	ND	0	640.28	0.90	52
VALIDATION-P3-I20	271.13	ND	0	579.27	1.16	92
VALIDATION-P3-I21	288.10	0.56	100	596.24	ND	0
VALIDATION-P3-I22	248.16	1.13	8	556.30	0.96	82
VALIDATION-P3-I23	241.12	ND	0	549.26	0.77	100
VALIDATION-P3-J1	359.18	0.58	11	667.32	0.95	89
VALIDATION-P3-J2	321.15	0.60	94	629.29	ND	0
VALIDATION-P3-J3	303.16	0.58	100	611.30	ND	0
VALIDATION-P3-J4	286.09	ND	0	594.23	0.99	100
VALIDATION-P3-J5	242.99	ND	0	551.13	ND	0
VALIDATION-P3-J7	282.21	ND	0	590.34	ND	0
VALIDATION-P3-J8	294.14	ND	0	602.28	1.03	100
VALIDATION-P3-J9	342.21	0.57	56	650.34	1.08	44
VALIDATION-P3-J10	228.14	0.79	100	536.28	0.79	100
VALIDATION-P3-J11	342.12	ND	0	650.25	1.16	100
VALIDATION-P3-J12	339.21	ND	0	647.34	0.95	93
VALIDATION-P3-J13	363.14	0.64	100	671.28	ND	0

Confidential – Do Not Copy

VALIDATION-P3-J14	265.17	ND	0	573.31	1.22	100
VALIDATION-P3-J15	325.17	0.84	92	633.30	0.84	92
VALIDATION-P3-J16	254.11	ND	0	562.25	1.08	100
VALIDATION-P3-J17	356.18	ND	0	664.32	0.87	100
VALIDATION-P3-J18	430.00	ND	0	738.00	1.06	100
VALIDATION-P3-J19	319.20	0.68	73	627.34	ND	0
VALIDATION-P3-J20	287.21	0.43	100	595.35	ND	0
VALIDATION-P3-J21	366.12	0.43	7	674.26	1.25	93
VALIDATION-P3-J22	245.12	0.36	45	553.26	0.93	55
VALIDATION-P3-J23	262.14	0.36	17	570.28	0.88	83
VALIDATION-P3-K1	314.21	0.55	100	622.35	ND	0
VALIDATION-P3-K2	254.11	0.48	100	562.25	ND	0
VALIDATION-P3-K3	332.21	ND	0	640.35	ND	0
VALIDATION-P3-K4	320.18	0.66	84	628.32	1.18	17
VALIDATION-P3-K5	278.17	0.48	10	586.31	0.86	77
VALIDATION-P3-K7	222.15	ND	0	530.29	0.91	100
VALIDATION-P3-K8	302.20	ND	0	610.34	1.13	100
VALIDATION-P3-K9	246.16	0.72	40	554.30	0.88	60
VALIDATION-P3-K10	270.18	ND	0	578.32	0.82	100
VALIDATION-P3-K11	340.18	ND	0	648.32	ND	0
VALIDATION-P3-K12	355.20	0.64	100	663.34	0.64	100
VALIDATION-P3-K13	264.20	0.31	11	572.33	0.78	89
VALIDATION-P3-K14	311.05	1.19	100	619.18	1.19	100
VALIDATION-P3-K15	290.19	0.39	100	598.32	ND	0
VALIDATION-P3-K16	327.23	0.64	44	635.37	0.64	44
VALIDATION-P3-K17	262.13	0.47	93	570.27	1.05	7
VALIDATION-P3-K18	430.00	ND	0	738.00	1.06	100
VALIDATION-P3-K19	354.17	0.53	100	662.31	ND	0
VALIDATION-P3-K20	219.01	ND	0	527.15	1.12	69
VALIDATION-P3-K21	240.14	0.43	64	548.28	1.05	36
VALIDATION-P3-K22	265.18	0.61	100	573.32	0.61	100
VALIDATION-P3-K23	233.13	ND	0	541.27	0.80	100
VALIDATION-P3-L1	221.08	0.36	89	529.22	1.13	11
VALIDATION-P3-L2	274.18	ND	0	582.32	1.12	100
VALIDATION-P3-L3	351.19	ND	0	659.33	0.99	100
VALIDATION-P3-L4	287.16	0.48	24	595.30	1.03	76
VALIDATION-P3-L5	325.11	ND	0	633.25	1.14	100
VALIDATION-P3-L7	297.16	ND	0	605.30	0.93	100
VALIDATION-P3-L8	302.16	0.56	100	610.30	ND	0
VALIDATION-P3-L9	326.13	0.51	68	634.27	1.11	32

Confidential – Do Not Copy

VALIDATION-P3-L10	271.18	ND	0	579.32	1.08	100
VALIDATION-P3-L11	370.24	0.32	100	678.38	ND	0
VALIDATION-P3-L12	379.19	ND	0	687.33	1.05	100
VALIDATION-P3-L13	333.22	0.61	100	641.36	ND	0
VALIDATION-P3-L14	265.19	0.32	98	573.33	ND	0
VALIDATION-P3-L15	289.18	0.70	21	597.32	0.72	79
VALIDATION-P3-L16	357.25	ND	0	665.39	0.89	100
VALIDATION-P3-L17	259.16	0.63	50	567.30	1.25	50
VALIDATION-P3-L18	430.00	ND	0	738.00	1.06	100
VALIDATION-P3-L19	293.13	0.63	100	601.27	ND	0
VALIDATION-P3-L20	324.05	0.64	78	632.19	1.23	14
VALIDATION-P3-L21	297.18	0.68	100	605.32	ND	0
VALIDATION-P3-L22	273.13	ND	0	581.27	1.27	100
VALIDATION-P3-L23	388.19	ND	0	696.33	ND	0
VALIDATION-P3-M1	345.09	0.53	100	653.23	ND	0
VALIDATION-P3-M2	277.19	ND	0	585.33	0.82	100
VALIDATION-P3-M3	337.19	ND	0	645.33	1.10	100
VALIDATION-P3-M4	355.20	0.66	100	663.34	ND	0
VALIDATION-P3-M5	224.17	0.38	94	532.31	ND	0
VALIDATION-P3-M7	276.16	0.76	100	584.30	0.76	100
VALIDATION-P3-M8	326.09	ND	0	634.23	1.23	100
VALIDATION-P3-M9	303.23	ND	0	611.37	0.83	100
VALIDATION-P3-M10	261.09	ND	0	569.23	0.97	100
VALIDATION-P3-M11	315.22	ND	0	623.36	0.74	100
VALIDATION-P3-M12	239.08	0.42	53	547.22	1.08	47
VALIDATION-P3-M13	323.17	ND	0	631.31	0.76	100
VALIDATION-P3-M14	224.16	ND	0	532.30	1.02	100
VALIDATION-P3-M15	313.19	0.40	74	621.33	0.85	13
VALIDATION-P3-M16	263.08	0.54	72	571.22	1.18	28
VALIDATION-P3-M17	313.18	ND	0	621.32	1.24	100
VALIDATION-P3-M18	430.00	ND	0	738.00	1.06	100
VALIDATION-P3-M19	294.17	0.66	72	602.31	1.15	28
VALIDATION-P3-M20	338.17	0.55	100	646.31	ND	0
VALIDATION-P3-M21	278.13	ND	0	586.27	1.02	100
VALIDATION-P3-M22	231.07	ND	0	539.21	0.98	100
VALIDATION-P3-M23	359.18	0.53	100	667.32	ND	0
VALIDATION-P3-N1	204.11	ND	0	512.25	0.81	100
VALIDATION-P3-N2	203.11	ND	0	511.24	1.13	100
VALIDATION-P3-N3	320.22	ND	0	628.36	1.02	100
VALIDATION-P3-N4	235.13	ND	0	543.27	1.02	100

Confidential – Do Not Copy

VALIDATION-P3-N5	225.16	ND	0	533.30	ND	0
VALIDATION-P3-N7	283.14	0.66	5	591.27	1.25	95
VALIDATION-P3-N8	323.17	0.63	70	631.31	1.16	30
VALIDATION-P3-N9	370.24	ND	0	678.38	0.87	80
VALIDATION-P3-N10	352.11	ND	0	660.25	0.93	100
VALIDATION-P3-N11	222.08	1.05	70	530.22	1.05	70
VALIDATION-P3-N12	305.13	0.64	54	613.27	1.24	46
VALIDATION-P3-N13	319.15	0.57	100	627.29	ND	0
VALIDATION-P3-N14	348.25	0.66	69	656.39	1.16	31
VALIDATION-P3-N15	261.15	ND	0	569.29	0.77	100
VALIDATION-P3-N16	297.18	ND	0	605.32	1.21	100
VALIDATION-P3-N17	252.11	0.35	52	560.25	0.99	48
VALIDATION-P3-N18	430.00	ND	0	738.00	1.06	100
VALIDATION-P3-N19	238.13	0.57	54	546.27	1.15	46
VALIDATION-P3-N20	324.21	0.53	100	632.35	ND	0
VALIDATION-P3-N21	349.22	0.38	51	657.36	0.87	19
VALIDATION-P3-N22	385.20	ND	0	693.34	1.07	100
VALIDATION-P3-N23	320.10	0.52	100	628.24	ND	0
VALIDATION-P3-O1	283.18	0.61	100	591.32	ND	0
VALIDATION-P3-O2	300.15	0.32	53	608.29	0.83	47
VALIDATION-P3-O3	341.16	ND	0	649.30	1.29	100
VALIDATION-P3-O4	330.21	0.71	82	638.34	0.71	82
VALIDATION-P3-O5	208.12	ND	0	516.26	ND	0
VALIDATION-P3-O7	276.20	ND	0	584.33	1.25	100
VALIDATION-P3-O8	355.19	ND	0	663.33	0.84	100
VALIDATION-P3-O9	351.20	0.44	100	659.34	ND	0
VALIDATION-P3-O10	354.13	ND	0	662.27	1.13	100
VALIDATION-P3-O11	379.10	0.55	78	687.24	0.93	15
VALIDATION-P3-O12	231.07	ND	0	539.21	0.93	100
VALIDATION-P3-O13	295.17	ND	0	603.31	0.83	100
VALIDATION-P3-O14	272.17	ND	0	580.31	ND	0
VALIDATION-P3-O15	295.11	ND	0	603.25	1.12	100
VALIDATION-P3-O16	243.15	ND	0	551.29	1.24	100
VALIDATION-P3-O17	294.14	0.64	100	602.28	ND	0
VALIDATION-P3-O18	430.00	ND	0	738.00	1.06	100
VALIDATION-P3-O19	273.10	ND	0	581.24	1.23	94
VALIDATION-P3-O20	294.21	ND	0	602.34	1.02	100
VALIDATION-P3-O21	256.13	ND	0	564.27	0.95	96
VALIDATION-P3-O22	232.14	0.76	95	540.28	0.76	95
VALIDATION-P3-O23	278.16	ND	0	586.30	0.86	100

VALIDATION-P3-P1	264.14	0.43	48	572.28	ND	0
VALIDATION-P3-P2	347.22	0.88	100	655.36	0.88	100
VALIDATION-P3-P3	326.17	0.57	100	634.31	ND	0
VALIDATION-P3-P4	295.15	0.63	100	603.29	ND	0
VALIDATION-P3-P5	319.16	ND	0	627.30	0.94	87
VALIDATION-P3-P7	290.15	0.55	38	598.29	ND	0
VALIDATION-P3-P8	325.19	0.49	78	633.33	0.83	12
VALIDATION-P3-P9	366.01	ND	0	674.15	1.34	52
VALIDATION-P3-P10	257.11	ND	0	565.25	1.15	100
VALIDATION-P3-P11	209.15	0.31	15	517.29	0.86	85
VALIDATION-P3-P12	340.24	0.70	68	648.38	1.19	26
VALIDATION-P3-P13	293.13	0.47	92	601.27	ND	0
VALIDATION-P3-P14	375.15	0.58	100	683.29	ND	0
VALIDATION-P3-P15	288.18	ND	0	596.32	1.19	100
VALIDATION-P3-P16	297.20	ND	0	605.33	0.79	100
VALIDATION-P3-P17	283.18	ND	0	591.32	ND	0
VALIDATION-P3-P18	430.00	ND	0	738.00	1.06	100
VALIDATION-P3-P19	221.12	ND	0	529.26	0.91	100
VALIDATION-P3-P20	262.07	ND	0	570.21	1.21	100
VALIDATION-P3-P21	235.08	ND	0	543.22	1.05	100
VALIDATION-P3-P22	368.22	0.37	63	676.36	0.77	37
VALIDATION-P3-P23	281.16	0.37	58	589.30	ND	0

**Supplementary Table 7: Plate 4:** LCMS data from Chapter 7.3.3.5, HaloCompound *In-Situ* Synthesis for the Validation Set. Column 6 featured a control well, and column 18 featured positive control VHL amine **101**. Performed using standard conditions as outlined in General Methods, using LCMS method (A). Shown in **Figure 141**.

Well Number	SM mass	Rt	% Area	Product Mass	Rt	% Area
VALIDATION-P4-A1	299.21	0.65	40	607.35	1.22	60
VALIDATION-P4-A2	332.18	ND	0	640.32	0.83	100
VALIDATION-P4-A3	221.15	0.39	100	529.29	ND	0
VALIDATION-P4-A4	320.13	ND	0	628.27	1.01	91
VALIDATION-P4-A5	281.22	ND	0	589.36	ND	0
VALIDATION-P4-A7	345.20	0.90	54	653.34	0.90	54
VALIDATION-P4-A8	244.13	ND	0	552.27	1.03	40
VALIDATION-P4-A9	323.21	ND	0	631.35	ND	0
VALIDATION-P4-A10	304.17	0.55	17	612.31	1.01	83
VALIDATION-P4-A11	222.15	0.29	100	530.29	ND	0
VALIDATION-P4-A12	320.15	0.56	60	628.29	0.91	40
VALIDATION-P4-A13	329.15	ND	0	637.29	0.93	100

Confidential – Do Not Copy

VALIDATION-P4-A14	303.12	ND	0	611.26	0.96	100
VALIDATION-P4-A15	289.14	0.61	28	597.28	1.21	72
VALIDATION-P4-A16	285.18	0.32	83	593.32	ND	0
VALIDATION-P4-A17	314.21	0.65	100	622.35	0.65	100
VALIDATION-P4-A18	430.00	ND	0	738.00	1.06	100
VALIDATION-P4-A19	352.14	ND	0	660.28	1.22	100
VALIDATION-P4-A20	388.14	ND	0	696.28	1.11	100
VALIDATION-P4-A21	309.14	0.64	100	617.28	ND	0
VALIDATION-P4-A22	335.05	0.72	15	643.19	1.26	85
VALIDATION-P4-A23	305.20	0.58	72	613.34	1.21	28
VALIDATION-P4-A24	283.05	0.43	100	591.19	ND	0
VALIDATION-P4-B1	297.09	0.42	88	605.23	ND	0
VALIDATION-P4-B2	285.14	ND	0	593.28	1.17	100
VALIDATION-P4-B3	236.13	ND	0	544.27	0.75	73
VALIDATION-P4-B4	230.12	0.41	100	538.26	ND	0
VALIDATION-P4-B5	235.13	0.78	100	543.27	0.78	100
VALIDATION-P4-B7	317.08	0.61	5	625.22	1.17	95
VALIDATION-P4-B8	358.18	ND	0	666.32	1.12	100
VALIDATION-P4-B9	310.14	ND	0	618.28	1.15	100
VALIDATION-P4-B10	298.15	ND	0	606.29	0.69	100
VALIDATION-P4-B11	414.17	ND	0	722.31	0.81	91
VALIDATION-P4-B12	314.21	0.28	88	622.35	ND	0
VALIDATION-P4-B13	293.16	ND	0	601.30	0.79	100
VALIDATION-P4-B14	303.11	ND	0	611.25	1.20	100
VALIDATION-P4-B15	263.16	ND	0	571.30	0.75	100
VALIDATION-P4-B16	322.10	0.57	100	630.24	ND	0
VALIDATION-P4-B17	295.11	0.34	100	603.25	ND	0
VALIDATION-P4-B18	430.00	ND	0	738.00	1.06	100
VALIDATION-P4-B19	269.17	ND	0	577.30	ND	0
VALIDATION-P4-B20	319.14	0.55	64	627.27	1.15	36
VALIDATION-P4-B21	241.11	ND	0	549.25	1.10	100
VALIDATION-P4-B22	244.13	ND	0	552.27	0.99	100
VALIDATION-P4-B23	295.08	0.55	61	603.22	1.17	39
VALIDATION-P4-B24	280.19	ND	0	588.33	ND	0
VALIDATION-P4-C1	314.12	0.47	100	622.26	ND	0
VALIDATION-P4-C2	317.15	ND	0	625.29	1.01	91
VALIDATION-P4-C3	364.05	0.39	85	672.19	0.85	15
VALIDATION-P4-C4	289.15	ND	0	597.29	0.80	100
VALIDATION-P4-C5	376.12	ND	0	684.26	0.89	100
VALIDATION-P4-C7	331.19	0.56	94	639.33	ND	0

Confidential – Do Not Copy

VALIDATION-P4-C8	279.19	0.31	64	587.33	0.83	36
VALIDATION-P4-C9	425.19	ND	0	733.33	0.90	100
VALIDATION-P4-C10	340.08	0.53	100	648.22	ND	0
VALIDATION-P4-C11	246.14	0.43	4	554.28	1.02	85
VALIDATION-P4-C12	321.18	0.34	94	629.32	ND	0
VALIDATION-P4-C13	273.15	ND	0	581.29	0.96	100
VALIDATION-P4-C14	263.12	0.46	100	571.26	ND	0
VALIDATION-P4-C15	358.22	0.40	100	666.36	ND	0
VALIDATION-P4-C16	342.18	0.77	100	650.31	ND	0
VALIDATION-P4-C17	338.17	ND	0	646.31	ND	0
VALIDATION-P4-C18	430.00	ND	0	738.00	1.06	100
VALIDATION-P4-C19	282.14	0.55	49	590.28	1.11	51
VALIDATION-P4-C20	294.19	0.51	100	602.32	ND	0
VALIDATION-P4-C21	354.23	0.82	77	662.37	1.32	23
VALIDATION-P4-C22	291.12	ND	0	599.25	1.04	87
VALIDATION-P4-C23	338.14	ND	0	646.28	0.83	84
VALIDATION-P4-C24	331.13	0.67	100	639.27	ND	0
VALIDATION-P4-D1	292.15	ND	0	600.29	0.91	93
VALIDATION-P4-D2	315.21	0.38	55	623.34	ND	0
VALIDATION-P4-D3	320.11	ND	0	628.24	1.00	100
VALIDATION-P4-D4	210.10	0.44	30	518.24	1.07	70
VALIDATION-P4-D5	305.22	ND	0	613.36	0.79	95
VALIDATION-P4-D7	273.17	0.59	74	581.31	0.95	13
VALIDATION-P4-D8	367.16	ND	0	675.30	ND	0
VALIDATION-P4-D9	324.20	0.60	9	632.33	1.09	91
VALIDATION-P4-D10	326.15	ND	0	634.29	1.15	100
VALIDATION-P4-D11	250.18	ND	0	558.32	0.77	100
VALIDATION-P4-D12	244.13	ND	0	552.27	1.13	100
VALIDATION-P4-D13	269.02	ND	0	577.16	1.03	60
VALIDATION-P4-D14	338.09	0.54	87	646.23	ND	0
VALIDATION-P4-D15	341.13	ND	0	649.27	0.92	100
VALIDATION-P4-D16	254.13	0.49	100	562.27	ND	0
VALIDATION-P4-D17	350.03	0.72	100	658.16	ND	0
VALIDATION-P4-D18	430.00	ND	0	738.00	1.06	100
VALIDATION-P4-D19	251.12	0.50	70	559.25	1.13	30
VALIDATION-P4-D20	257.14	0.64	44	565.28	1.24	56
VALIDATION-P4-D21	203.12	ND	0	511.26	0.98	100
VALIDATION-P4-D22	417.16	ND	0	725.30	1.24	85
VALIDATION-P4-D23	271.14	ND	0	579.28	0.88	100
VALIDATION-P4-D24	232.17	ND	0	540.31	0.76	100

Confidential – Do Not Copy

VALIDATION-P4-E1	328.23	0.65	100	636.37	0.65	100
VALIDATION-P4-E2	330.08	0.60	100	638.22	ND	0
VALIDATION-P4-E3	390.18	ND	0	698.32	0.86	100
VALIDATION-P4-E4	299.20	0.60	100	607.34	ND	0
VALIDATION-P4-E5	258.08	ND	0	566.22	1.10	100
VALIDATION-P4-E7	323.19	0.79	39	631.33	1.31	46
VALIDATION-P4-E8	315.17	0.45	100	623.31	ND	0
VALIDATION-P4-E9	404.17	ND	0	712.31	1.26	100
VALIDATION-P4-E10	293.09	0.60	37	601.23	1.20	63
VALIDATION-P4-E11	281.12	ND	0	589.26	0.89	100
VALIDATION-P4-E12	389.19	ND	0	697.33	1.22	79
VALIDATION-P4-E13	332.23	0.45	100	640.37	ND	0
VALIDATION-P4-E14	302.17	ND	0	610.31	0.81	93
VALIDATION-P4-E15	340.15	0.62	89	648.28	ND	0
VALIDATION-P4-E16	316.22	0.61	100	624.35	ND	0
VALIDATION-P4-E17	346.18	0.58	13	654.32	1.06	11
VALIDATION-P4-E18	430.00	ND	0	738.00	1.06	100
VALIDATION-P4-E19	279.15	0.45	100	587.29	ND	0
VALIDATION-P4-E20	246.11	0.51	37	554.25	1.13	63
VALIDATION-P4-E21	296.16	ND	0	604.29	1.03	100
VALIDATION-P4-E22	356.22	0.45	78	664.36	0.92	22
VALIDATION-P4-E23	332.16	ND	0	640.29	1.18	60
VALIDATION-P4-E24	250.18	ND	0	558.32	ND	0
VALIDATION-P4-F1	325.14	0.54	14	633.28	0.92	81
VALIDATION-P4-F2	248.10	0.45	91	556.24	0.88	9
VALIDATION-P4-F3	302.12	ND	0	610.26	1.09	100
VALIDATION-P4-F4	338.17	0.63	100	646.31	ND	0
VALIDATION-P4-F5	349.08	0.67	100	657.22	ND	0
VALIDATION-P4-F7	333.25	0.76	100	641.39	0.76	100
VALIDATION-P4-F8	388.16	0.70	87	696.29	ND	0
VALIDATION-P4-F9	351.13	0.49	48	659.27	0.97	50
VALIDATION-P4-F10	378.02	0.56	39	686.16	1.12	61
VALIDATION-P4-F11	247.12	ND	0	555.26	ND	0
VALIDATION-P4-F12	288.15	0.64	89	596.29	ND	0
VALIDATION-P4-F13	299.15	0.63	65	607.29	1.23	27
VALIDATION-P4-F14	340.16	0.63	12	648.30	1.16	88
VALIDATION-P4-F15	290.17	ND	0	598.31	0.87	100
VALIDATION-P4-F16	341.17	0.51	100	649.31	ND	0
VALIDATION-P4-F17	314.21	0.51	43	622.35	1.03	57
VALIDATION-P4-F18	430.00	ND	0	738.00	1.06	100

Confidential – Do Not Copy

VALIDATION-P4-F19	262.06	0.55	44	570.20	0.94	56
VALIDATION-P4-F20	296.16	0.60	100	604.29	ND	0
VALIDATION-P4-F21	296.16	0.54	100	604.29	ND	0
VALIDATION-P4-F22	283.03	ND	0	591.17	0.97	100
VALIDATION-P4-F23	292.16	ND	0	600.30	0.94	100
VALIDATION-P4-F24	340.12	0.42	90	648.26	ND	0
VALIDATION-P4-G1	224.06	ND	0	532.20	0.93	52
VALIDATION-P4-G2	381.21	0.72	89	689.34	ND	0
VALIDATION-P4-G3	289.18	ND	0	597.32	0.88	100
VALIDATION-P4-G4	274.22	ND	0	582.35	ND	0
VALIDATION-P4-G5	378.02	ND	0	686.16	1.14	100
VALIDATION-P4-G7	281.19	0.57	100	589.32	ND	0
VALIDATION-P4-G8	327.21	0.85	100	635.34	0.85	100
VALIDATION-P4-G9	335.20	ND	0	643.34	0.78	100
VALIDATION-P4-G10	314.21	0.32	55	622.35	0.82	10
VALIDATION-P4-G11	288.16	ND	0	596.30	ND	0
VALIDATION-P4-G12	354.16	0.51	69	662.30	ND	0
VALIDATION-P4-G13	306.09	ND	0	614.23	0.99	100
VALIDATION-P4-G14	318.15	ND	0	626.29	1.08	100
VALIDATION-P4-G15	348.12	0.83	100	656.26	ND	0
VALIDATION-P4-G16	290.16	0.40	20	598.30	0.85	15
VALIDATION-P4-G17	368.22	ND	0	676.36	1.09	100
VALIDATION-P4-G18	430.00	ND	0	738.00	1.06	100
VALIDATION-P4-G19	251.11	0.43	34	559.25	0.99	55
VALIDATION-P4-G20	318.19	ND	0	626.33	1.23	100
VALIDATION-P4-G21	302.15	0.55	10	610.29	1.08	90
VALIDATION-P4-G22	319.14	ND	0	627.28	1.04	100
VALIDATION-P4-G23	304.17	0.32	40	612.31	0.83	60
VALIDATION-P4-G24	210.14	0.32	87	518.28	ND	0
VALIDATION-P4-H1	326.14	0.54	100	634.28	ND	0
VALIDATION-P4-H2	260.14	ND	0	568.28	0.94	100
VALIDATION-P4-H3	322.15	0.43	20	630.29	0.93	80
VALIDATION-P4-H4	290.12	0.60	95	598.26	ND	0
VALIDATION-P4-H5	266.15	0.77	94	574.29	0.77	94
VALIDATION-P4-H7	285.16	ND	0	593.30	0.74	100
VALIDATION-P4-H8	230.12	ND	0	538.26	1.01	100
VALIDATION-P4-H9	265.22	ND	0	573.35	1.19	100
VALIDATION-P4-H10	336.07	0.59	100	644.21	ND	0
VALIDATION-P4-H11	238.13	0.35	89	546.26	ND	0
VALIDATION-P4-H12	344.22	0.35	52	652.36	0.79	36

Confidential – Do Not Copy

VALIDATION-P4-H13	347.17	0.56	100	655.31	ND	0
VALIDATION-P4-H14	330.16	0.63	100	638.30	ND	0
VALIDATION-P4-H15	236.13	0.44	32	544.27	0.88	68
VALIDATION-P4-H16	338.17	0.59	100	646.31	ND	0
VALIDATION-P4-H17	320.19	ND	0	628.33	1.06	100
VALIDATION-P4-H18	430.00	ND	0	738.00	1.06	100
VALIDATION-P4-H19	352.09	0.63	100	660.22	ND	0
VALIDATION-P4-H20	331.14	ND	0	639.27	1.11	100
VALIDATION-P4-H21	412.05	0.68	40	720.19	1.20	57
VALIDATION-P4-H22	302.20	0.60	100	610.34	ND	0
VALIDATION-P4-H23	265.22	ND	0	573.35	ND	0
VALIDATION-P4-H24	331.14	0.56	100	639.28	ND	0
VALIDATION-P4-I1	292.03	ND	0	600.17	ND	0
VALIDATION-P4-I2	322.15	ND	0	630.29	0.97	100
VALIDATION-P4-I3	364.18	ND	0	672.32	1.11	100
VALIDATION-P4-I4	210.11	ND	0	518.25	0.84	100
VALIDATION-P4-I5	314.16	0.52	100	622.29	ND	0
VALIDATION-P4-I7	273.12	ND	0	581.26	0.91	100
VALIDATION-P4-I8	324.02	0.60	87	632.16	ND	0
VALIDATION-P4-I9	306.11	0.48	100	614.25	ND	0
VALIDATION-P4-I10	303.17	ND	0	611.31	0.92	100
VALIDATION-P4-I11	306.19	0.50	100	614.33	ND	0
VALIDATION-P4-I12	309.15	0.29	75	617.29	0.81	25
VALIDATION-P4-I13	300.09	ND	0	608.23	0.98	100
VALIDATION-P4-I14	249.05	0.76	11	557.18	1.16	83
VALIDATION-P4-I15	313.18	ND	0	621.32	0.93	100
VALIDATION-P4-I16	336.15	ND	0	644.29	1.07	100
VALIDATION-P4-I17	261.15	1.28	34	569.29	0.99	66
VALIDATION-P4-I18	430.00	ND	0	738.00	1.06	100
VALIDATION-P4-I19	304.11	ND	0	612.25	1.12	100
VALIDATION-P4-I20	251.15	0.39	100	559.29	ND	0
VALIDATION-P4-I21	301.11	0.38	11	609.25	0.93	89
VALIDATION-P4-I22	241.09	ND	0	549.23	1.01	100
VALIDATION-P4-I23	276.16	0.57	100	584.30	ND	0
VALIDATION-P4-I24	237.18	ND	0	545.32	0.86	100
VALIDATION-P4-J1	330.13	ND	0	638.27	0.97	95
VALIDATION-P4-J2	300.09	0.36	100	608.23	ND	0
VALIDATION-P4-J3	388.09	ND	0	696.22	1.36	91
VALIDATION-P4-J4	323.16	0.47	100	631.29	ND	0
VALIDATION-P4-J5	244.14	ND	0	552.28	0.74	95

Confidential – Do Not Copy

VALIDATION-P4-J7	331.15	0.56	18	639.29	1.06	82
VALIDATION-P4-J8	324.20	0.68	95	632.33	ND	0
VALIDATION-P4-J9	266.18	0.57	61	574.32	ND	0
VALIDATION-P4-J10	316.24	0.36	100	624.38	ND	0
VALIDATION-P4-J11	263.16	0.50	100	571.30	ND	0
VALIDATION-P4-J12	337.18	0.57	72	645.32	1.10	28
VALIDATION-P4-J13	370.17	ND	0	678.31	ND	0
VALIDATION-P4-J14	288.16	0.48	100	596.30	ND	0
VALIDATION-P4-J15	301.16	0.54	100	609.30	ND	0
VALIDATION-P4-J16	327.21	0.45	100	635.34	ND	0
VALIDATION-P4-J17	334.14	0.57	11	642.28	0.90	89
VALIDATION-P4-J18	430.00	ND	0	738.00	1.06	100
VALIDATION-P4-J19	359.17	ND	0	667.31	0.82	96
VALIDATION-P4-J20	353.12	ND	0	661.26	1.02	100
VALIDATION-P4-J21	311.19	ND	0	619.32	0.81	100
VALIDATION-P4-J22	288.21	0.46	55	596.35	ND	0
VALIDATION-P4-J23	288.20	0.58	100	596.33	ND	0
VALIDATION-P4-J24	313.18	0.56	47	621.32	ND	0
VALIDATION-P4-K1	369.96	ND	0	690.09	ND	0
VALIDATION-P4-K2	292.12	0.44	100	600.26	ND	0
VALIDATION-P4-K3	305.17	ND	0	613.31	0.96	100
VALIDATION-P4-K4	320.16	0.78	57	628.29	1.36	43
VALIDATION-P4-K5	278.12	ND	0	586.26	1.22	100
VALIDATION-P4-K7	263.16	ND	0	571.30	0.82	100
VALIDATION-P4-K8	391.21	0.60	96	699.35	0.91	4
VALIDATION-P4-K9	354.12	0.44	100	662.25	ND	0
VALIDATION-P4-K10	208.16	0.30	100	516.30	ND	0
VALIDATION-P4-K11	344.22	ND	0	652.36	ND	0
VALIDATION-P4-K12	354.19	0.61	100	662.33	ND	0
VALIDATION-P4-K13	208.13	ND	0	516.27	1.00	100
VALIDATION-P4-K14	269.16	0.61	100	577.30	ND	0
VALIDATION-P4-K15	277.17	0.56	51	585.31	1.14	45
VALIDATION-P4-K16	289.18	ND	0	597.32	1.15	100
VALIDATION-P4-K17	305.15	0.46	77	613.29	0.88	23
VALIDATION-P4-K18	430.00	ND	0	738.00	1.06	100
VALIDATION-P4-K19	270.16	ND	0	578.30	0.83	100
VALIDATION-P4-K20	251.17	ND	0	559.31	0.79	100
VALIDATION-P4-K21	387.22	ND	0	695.35	1.04	100
VALIDATION-P4-K22	361.15	ND	0	669.28	0.99	100
VALIDATION-P4-K23	297.18	0.55	100	605.32	ND	0

Confidential – Do Not Copy

VALIDATION-P4-K24	277.18	ND	0	585.32	0.81	96
VALIDATION-P4-L1	292.14	0.58	74	600.27	ND	0
VALIDATION-P4-L2	312.21	0.30	100	620.35	ND	0
VALIDATION-P4-L3	217.11	ND	0	525.25	ND	0
VALIDATION-P4-L4	322.19	0.42	100	630.33	ND	0
VALIDATION-P4-L5	234.14	ND	0	542.28	0.80	100
VALIDATION-P4-L7	243.11	0.46	100	551.25	ND	0
VALIDATION-P4-L8	256.12	0.41	100	564.26	ND	0
VALIDATION-P4-L9	263.11	ND	0	571.25	1.18	100
VALIDATION-P4-L10	287.16	0.50	94	595.30	ND	0
VALIDATION-P4-L11	289.18	0.62	100	597.32	ND	0
VALIDATION-P4-L12	260.11	ND	0	568.25	1.07	100
VALIDATION-P4-L13	235.12	0.43	100	543.26	ND	0
VALIDATION-P4-L14	276.22	ND	0	584.36	ND	0
VALIDATION-P4-L15	304.19	ND	0	612.33	0.75	100
VALIDATION-P4-L16	282.18	0.54	100	590.32	ND	0
VALIDATION-P4-L17	336.20	0.42	12	644.33	0.82	88
VALIDATION-P4-L18	430.00	ND	0	738.00	1.06	100
VALIDATION-P4-L19	310.20	0.59	100	618.34	ND	0
VALIDATION-P4-L20	411.11	ND	0	719.25	1.17	82
VALIDATION-P4-L21	283.17	ND	0	591.31	1.23	100
VALIDATION-P4-L22	392.18	0.71	100	700.32	ND	0
VALIDATION-P4-L23	317.09	0.60	100	625.22	ND	0
VALIDATION-P4-L24	320.21	ND	0	628.35	0.75	100
VALIDATION-P4-M1	318.24	0.54	100	626.38	ND	0
VALIDATION-P4-M2	334.23	0.73	47	642.36	1.23	53
VALIDATION-P4-M3	346.13	ND	0	654.27	1.01	84
VALIDATION-P4-M4	292.18	0.45	100	600.32	ND	0
VALIDATION-P4-M5	348.16	0.60	48	656.30	1.13	52
VALIDATION-P4-M7	292.19	ND	0	600.33	0.87	100
VALIDATION-P4-M8	251.07	ND	0	559.21	0.96	100
VALIDATION-P4-M9	345.17	0.35	100	653.31	ND	0
VALIDATION-P4-M10	371.17	ND	0	679.31	1.08	100
VALIDATION-P4-M11	342.17	0.56	54	650.31	ND	0
VALIDATION-P4-M12	290.14	0.49	100	598.28	ND	0
VALIDATION-P4-M13	318.00	ND	0	626.14	1.08	100
VALIDATION-P4-M14	302.17	0.50	6	610.31	1.03	48
VALIDATION-P4-M15	282.11	ND	0	590.25	1.14	100
VALIDATION-P4-M16	256.13	0.42	63	564.27	1.02	28
VALIDATION-P4-M17	325.15	ND	0	633.28	0.95	100

Confidential – Do Not Copy

VALIDATION-P4-M18	430.00	ND	0	738.00	1.06	100
VALIDATION-P4-M19	248.20	ND	0	556.34	1.21	100
VALIDATION-P4-M20	315.16	0.45	100	623.29	ND	0
VALIDATION-P4-M21	344.18	0.41	16	652.32	0.82	84
VALIDATION-P4-M22	340.08	ND	0	648.22	1.24	100
VALIDATION-P4-M23	323.11	0.56	100	631.25	ND	0
VALIDATION-P4-M24	315.19	ND	0	623.33	1.03	67
VALIDATION-P4-N1	436.05	ND	0	744.18	ND	0
VALIDATION-P4-N2	310.17	0.50	100	618.31	ND	0
VALIDATION-P4-N3	264.20	ND	0	572.33	ND	0
VALIDATION-P4-N4	412.26	ND	0	720.40	0.76	86
VALIDATION-P4-N5	308.17	0.74	96	616.31	0.74	96
VALIDATION-P4-N7	323.20	0.44	100	631.33	ND	0
VALIDATION-P4-N8	331.15	0.53	10	639.29	1.09	90
VALIDATION-P4-N9	369.19	0.62	44	677.32	1.05	44
VALIDATION-P4-N10	343.21	ND	0	651.35	0.75	95
VALIDATION-P4-N11	320.16	0.53	100	628.29	ND	0
VALIDATION-P4-N12	323.19	0.65	36	631.33	0.99	64
VALIDATION-P4-N13	292.23	ND	0	600.37	ND	0
VALIDATION-P4-N14	327.14	0.44	100	635.28	ND	0
VALIDATION-P4-N15	329.15	0.47	100	637.29	ND	0
VALIDATION-P4-N16	304.19	ND	0	612.33	0.97	100
VALIDATION-P4-N17	238.11	ND	0	546.25	1.12	100
VALIDATION-P4-N18	430.00	ND	0	738.00	1.06	100
VALIDATION-P4-N19	310.23	0.33	100	618.36	ND	0
VALIDATION-P4-N20	233.11	ND	0	541.24	1.00	100
VALIDATION-P4-N21	221.07	ND	0	529.21	0.88	100
VALIDATION-P4-N22	363.23	0.68	100	671.37	ND	0
VALIDATION-P4-N23	322.13	0.53	76	630.27	ND	0
VALIDATION-P4-N24	391.10	ND	0	699.24	1.10	93
VALIDATION-P4-O1	284.16	0.45	100	592.30	ND	0
VALIDATION-P4-O2	320.16	0.82	26	628.29	1.41	74
VALIDATION-P4-O3	291.14	0.55	100	599.28	ND	0
VALIDATION-P4-O4	349.18	0.59	100	657.32	ND	0
VALIDATION-P4-O5	358.24	ND	0	666.38	0.88	90
VALIDATION-P4-O7	279.14	0.50	27	587.28	1.09	73
VALIDATION-P4-O8	333.25	0.81	85	641.39	0.81	85
VALIDATION-P4-O9	336.16	0.51	75	644.30	1.00	25
VALIDATION-P4-O10	315.16	ND	0	623.30	1.36	100
VALIDATION-P4-O11	344.95	ND	0	653.09	1.21	91

VALIDATION-P4-O12	329.10	0.47	54	637.24	0.89	12
VALIDATION-P4-O13	290.11	ND	0	598.25	ND	0
VALIDATION-P4-O14	270.15	1.03	100	578.29	1.03	100
VALIDATION-P4-O15	435.22	0.70	28	743.35	0.94	72
VALIDATION-P4-O16	356.21	0.67	100	664.35	ND	0
VALIDATION-P4-O17	308.12	ND	0	616.26	1.19	93
VALIDATION-P4-O18	430.00	ND	0	738.00	1.06	100
VALIDATION-P4-O19	331.15	0.51	100	639.29	ND	0
VALIDATION-P4-O20	233.11	0.66	100	541.24	ND	0
VALIDATION-P4-O21	333.24	ND	0	641.38	0.65	100
VALIDATION-P4-O22	286.14	ND	0	594.28	1.16	100
VALIDATION-P4-O23	277.12	ND	0	585.26	1.04	100
VALIDATION-P4-O24	338.10	0.38	100	646.24	ND	0
VALIDATION-P4-P1	237.12	ND	0	545.26	0.96	100
VALIDATION-P4-P2	236.15	0.47	51	544.29	ND	0
VALIDATION-P4-P3	295.13	ND	0	603.27	1.18	100
VALIDATION-P4-P4	340.98	1.03	100	649.12	ND	0
VALIDATION-P4-P5	393.07	ND	0	701.21	1.13	100
VALIDATION-P4-P7	231.11	ND	0	539.25	0.81	100
VALIDATION-P4-P8	325.18	0.46	100	633.32	ND	0
VALIDATION-P4-P9	318.09	0.53	54	626.23	1.07	39
VALIDATION-P4-P10	439.27	0.33	37	747.41	0.69	63
VALIDATION-P4-P11	434.20	ND	0	742.34	1.28	87
VALIDATION-P4-P12	274.14	0.52	50	582.28	1.05	50
VALIDATION-P4-P13	247.09	ND	0	555.23	0.83	100
VALIDATION-P4-P14	331.06	0.56	100	639.20	ND	0
VALIDATION-P4-P15	376.21	0.41	100	684.35	ND	0
VALIDATION-P4-P16	221.06	0.34	11	529.20	0.96	89
VALIDATION-P4-P17	317.14	ND	0	625.28	1.01	100
VALIDATION-P4-P18	430.00	ND	0	738.00	1.06	100
VALIDATION-P4-P19	288.20	0.56	100	596.33	ND	0
VALIDATION-P4-P20	265.14	0.60	100	573.28	ND	0
VALIDATION-P4-P21	212.10	ND	0	520.23	0.78	100
VALIDATION-P4-P22	418.09	0.73	100	726.23	ND	0
VALIDATION-P4-P23	356.26	0.34	100	664.40	ND	0
VALIDATION-P4-P24	268.12	1.02	23	576.26	1.11	19

**Supplementary Table 8: Plate 5:** LCMS data from Chapter 7.3.3.5, HaloCompound *In-Situ* Synthesis for the Validation Set. Column 6 featured a control well, and column 18 featured

positive control VHL amine **101**. Performed using standard conditions as outlined in General Methods, using LCMS method (A).

Well Number	SM mass	Rt	% Area	Product Mass	Rt	% Area
VALIDATION-P5-A1	260.07	ND	0	568.21	1.06	100
VALIDATION-P5-A2	243.15	ND	0	551.29	0.85	100
VALIDATION-P5-A3	366.01	0.54	100	674.15	ND	0
VALIDATION-P5-A4	252.16	ND	0	560.30	0.78	100
VALIDATION-P5-A5	243.15	ND	0	551.29	0.80	100
VALIDATION-P5-A7	280.12	ND	0	588.26	1.11	100
VALIDATION-P5-A8	290.21	ND	0	598.35	ND	0
VALIDATION-P5-A9	308.19	ND	0	616.33	ND	0
VALIDATION-P5-A10	274.18	0.60	100	582.32	ND	0
VALIDATION-P5-A11	356.18	ND	0	664.32	1.03	92
VALIDATION-P5-A12	353.17	0.65	84	661.31	1.18	16
VALIDATION-P5-A13	396.23	ND	0	704.37	0.84	100
VALIDATION-P5-A14	295.14	ND	0	603.27	1.16	100
VALIDATION-P5-A15	257.15	ND	0	565.29	1.01	100
VALIDATION-P5-A17	218.12	0.33	89	526.26	0.91	11
VALIDATION-P5-A18	430.00	ND	0	738.00	1.06	100
VALIDATION-P5-A19	282.08	ND	0	590.21	1.15	100
VALIDATION-P5-A20	364.13	ND	0	672.27	1.22	100
VALIDATION-P5-A21	261.09	ND	0	569.23	0.99	100
VALIDATION-P5-A22	329.11	ND	0	637.25	1.11	100
VALIDATION-P5-A23	284.10	0.51	15	592.24	ND	0
VALIDATION-P5-A24	319.16	ND	0	627.30	0.77	93
VALIDATION-P5-B1	247.14	ND	0	555.28	0.75	100
VALIDATION-P5-B2	317.21	ND	0	625.35	0.79	100
VALIDATION-P5-B3	272.12	0.61	70	580.26	ND	0
VALIDATION-P5-B4	312.20	ND	0	620.33	1.08	45
VALIDATION-P5-B5	234.15	ND	0	542.29	0.99	100
VALIDATION-P5-B7	357.15	ND	0	665.29	1.15	100
VALIDATION-P5-B8	318.16	0.37	100	626.29	ND	0
VALIDATION-P5-B9	306.15	0.54	100	614.29	ND	0
VALIDATION-P5-B10	274.17	0.50	100	582.31	ND	0
VALIDATION-P5-B11	237.07	ND	0	545.21	1.18	100
VALIDATION-P5-B12	289.14	ND	0	597.28	0.95	100
VALIDATION-P5-B13	286.11	ND	0	594.25	0.94	100
VALIDATION-P5-B14	357.21	0.60	89	665.34	1.08	7
VALIDATION-P5-B15	300.21	0.60	60	608.35	1.25	40
VALIDATION-P5-B16	209.15	0.64	40	517.29	0.74	60

Confidential – Do Not Copy

VALIDATION-P5-B17	350.18	ND	0	658.32	1.09	100
VALIDATION-P5-B18	430.00	ND	0	738.00	1.06	100
VALIDATION-P5-B19	313.18	0.50	38	621.32	1.03	58
VALIDATION-P5-B20	319.12	ND	0	627.26	1.13	100
VALIDATION-P5-B21	323.13	0.57	100	631.27	ND	0
VALIDATION-P5-B22	226.13	ND	0	534.26	ND	0
VALIDATION-P5-B23	265.18	ND	0	573.32	ND	0
VALIDATION-P5-B24	325.09	0.53	79	633.23	1.12	21
VALIDATION-P5-C1	294.17	0.56	100	602.31	ND	0
VALIDATION-P5-C2	232.11	ND	0	540.25	0.96	100
VALIDATION-P5-C3	297.16	0.58	89	605.30	1.11	8
VALIDATION-P5-C4	338.17	0.61	63	646.31	ND	0
VALIDATION-P5-C5	343.24	0.40	100	651.38	ND	0
VALIDATION-P5-C7	325.18	0.44	100	633.32	ND	0
VALIDATION-P5-C8	348.14	ND	0	656.28	0.96	100
VALIDATION-P5-C9	258.15	ND	0	566.29	0.77	97
VALIDATION-P5-C10	297.14	0.63	100	605.28	ND	0
VALIDATION-P5-C11	308.12	ND	0	616.26	0.98	100
VALIDATION-P5-C12	375.18	ND	0	683.32	0.77	100
VALIDATION-P5-C13	283.13	0.54	4	591.27	1.05	86
VALIDATION-P5-C14	254.03	0.45	100	562.17	ND	0
VALIDATION-P5-C15	221.15	ND	0	529.29	1.03	100
VALIDATION-P5-C17	327.17	0.29	100	635.31	ND	0
VALIDATION-P5-C18	430.00	ND	0	738.00	1.06	100
VALIDATION-P5-C19	269.16	ND	0	577.30	ND	0
VALIDATION-P5-C20	275.14	ND	0	583.28	0.73	100
VALIDATION-P5-C21	317.10	0.44	39	625.24	1.11	61
VALIDATION-P5-C22	295.08	0.62	89	603.22	ND	0
VALIDATION-P5-C23	302.21	ND	0	610.35	0.75	96
VALIDATION-P5-C24	330.05	0.76	100	638.19	ND	0
VALIDATION-P5-D1	332.07	0.64	100	640.21	ND	0
VALIDATION-P5-D2	251.14	ND	0	559.28	0.74	84
VALIDATION-P5-D3	321.16	ND	0	629.30	1.10	100
VALIDATION-P5-D4	313.19	0.52	11	621.33	1.05	89
VALIDATION-P5-D5	298.18	ND	0	606.32	0.82	100
VALIDATION-P5-D7	260.15	ND	0	568.29	ND	0
VALIDATION-P5-D8	299.15	ND	0	607.29	0.85	100
VALIDATION-P5-D9	309.16	0.60	93	617.30	ND	0
VALIDATION-P5-D10	285.15	ND	0	593.29	0.75	100
VALIDATION-P5-D11	239.15	0.40	23	547.29	0.84	60

Confidential – Do Not Copy

VALIDATION-P5-D12	304.15	ND	0	612.29	0.98	100
VALIDATION-P5-D13	306.09	0.60	100	614.23	ND	0
VALIDATION-P5-D14	263.16	ND	0	571.30	ND	0
VALIDATION-P5-D15	293.19	0.47	100	601.32	ND	0
VALIDATION-P5-D16	279.12	0.50	75	587.25	1.14	25
VALIDATION-P5-D17	205.09	ND	0	513.22	0.96	100
VALIDATION-P5-D18	430.00	ND	0	738.00	1.06	100
VALIDATION-P5-D19	324.20	ND	0	632.33	0.81	70
VALIDATION-P5-D20	265.09	0.42	100	573.23	ND	0
VALIDATION-P5-D21	312.20	ND	0	620.34	0.73	36
VALIDATION-P5-D22	303.10	0.70	70	611.24	1.26	30
VALIDATION-P5-D23	387.21	ND	0	695.35	0.89	100
VALIDATION-P5-D24	272.11	ND	0	580.25	ND	0
VALIDATION-P5-E1	291.17	ND	0	599.31	0.92	100
VALIDATION-P5-E2	282.17	ND	0	590.31	0.93	91
VALIDATION-P5-E3	275.16	ND	0	583.30	0.75	100
VALIDATION-P5-E4	265.17	ND	0	573.31	ND	0
VALIDATION-P5-E5	346.20	ND	0	654.34	0.82	79
VALIDATION-P5-E7	315.08	ND	0	623.22	1.28	100
VALIDATION-P5-E8	331.18	ND	0	639.32	1.15	90
VALIDATION-P5-E9	295.17	ND	0	603.31	0.78	92
VALIDATION-P5-E10	359.18	0.57	4	667.32	0.95	96
VALIDATION-P5-E11	340.19	ND	0	648.33	0.65	92
VALIDATION-P5-E12	240.14	ND	0	548.28	1.00	97
VALIDATION-P5-E13	304.22	ND	0	612.35	0.84	100
VALIDATION-P5-E14	364.18	ND	0	672.32	1.22	100
VALIDATION-P5-E15	309.11	ND	0	617.25	1.03	95
VALIDATION-P5-E17	244.10	ND	0	552.24	0.96	100
VALIDATION-P5-E18	430.00	ND	0	738.00	1.07	100
VALIDATION-P5-E19	284.16	ND	0	592.30	1.10	97
VALIDATION-P5-E20	305.22	ND	0	613.36	0.87	100
VALIDATION-P5-E21	291.09	0.37	91	599.23	ND	0
VALIDATION-P5-E22	309.13	0.49	100	617.27	ND	0
VALIDATION-P5-E23	300.14	ND	0	608.28	0.76	100
VALIDATION-P5-E24	238.14	ND	0	546.28	0.89	100
VALIDATION-P5-F1	332.12	0.51	17	640.26	0.95	37
VALIDATION-P5-F2	263.09	0.52	100	571.23	ND	0
VALIDATION-P5-F3	307.15	0.47	60	615.29	1.06	21
VALIDATION-P5-F4	262.17	ND	0	570.31	1.19	100
VALIDATION-P5-F5	293.15	ND	0	601.29	1.13	100

Confidential – Do Not Copy

VALIDATION-P5-F7	343.20	ND	0	651.34	0.73	100
VALIDATION-P5-F8	203.05	ND	0	511.19	0.96	100
VALIDATION-P5-F9	308.11	0.50	88	616.25	1.09	5
VALIDATION-P5-F10	303.16	0.48	100	611.30	ND	0
VALIDATION-P5-F11	378.05	ND	0	686.19	1.20	100
VALIDATION-P5-F12	330.17	ND	0	638.31	1.03	100
VALIDATION-P5-F13	345.17	0.35	100	653.31	ND	0
VALIDATION-P5-F14	257.05	ND	0	565.18	1.11	100
VALIDATION-P5-F15	326.16	0.91	4	634.30	1.08	96
VALIDATION-P5-F16	328.19	ND	0	636.33	0.80	100
VALIDATION-P5-F17	233.14	0.56	100	541.28	ND	0
VALIDATION-P5-F18	430.00	ND	0	738.00	1.06	100
VALIDATION-P5-F19	289.18	ND	0	597.32	0.86	100
VALIDATION-P5-F20	342.22	0.42	100	650.36	ND	0
VALIDATION-P5-F21	353.16	0.66	94	661.30	0.96	6
VALIDATION-P5-F22	252.10	ND	0	560.24	1.05	100
VALIDATION-P5-F23	255.08	ND	0	563.22	1.00	100
VALIDATION-P5-F24	256.17	0.53	100	564.31	ND	0
VALIDATION-P5-G1	210.14	ND	0	518.28	0.95	100
VALIDATION-P5-G2	282.14	ND	0	590.28	0.84	100
VALIDATION-P5-G3	299.21	0.34	90	607.35	ND	0
VALIDATION-P5-G4	326.17	0.52	59	634.31	1.12	41
VALIDATION-P5-G5	325.18	0.86	100	633.32	0.86	100
VALIDATION-P5-G7	243.14	ND	0	551.28	1.05	100
VALIDATION-P5-G8	324.08	ND	0	632.21	1.23	100
VALIDATION-P5-G9	337.20	ND	0	645.34	0.73	100
VALIDATION-P5-G10	234.15	ND	0	542.29	0.91	100
VALIDATION-P5-G11	222.15	ND	0	530.29	0.80	100
VALIDATION-P5-G12	349.19	0.39	46	657.33	0.82	54
VALIDATION-P5-G13	341.18	ND	0	649.32	1.29	100
VALIDATION-P5-G14	374.03	ND	0	682.17	1.14	100
VALIDATION-P5-G15	308.08	ND	0	616.22	1.19	100
VALIDATION-P5-G17	291.16	0.52	100	599.30	ND	0
VALIDATION-P5-G18	430.00	ND	0	738.00	1.06	100
VALIDATION-P5-G19	353.20	0.71	92	661.34	ND	0
VALIDATION-P5-G20	216.14	0.29	100	524.28	ND	0
VALIDATION-P5-G21	346.25	0.73	100	654.39	0.73	100
VALIDATION-P5-G22	330.16	0.46	100	638.30	ND	0
VALIDATION-P5-G23	313.04	ND	0	621.18	0.94	100
VALIDATION-P5-G24	294.21	ND	0	602.34	ND	0

Confidential – Do Not Copy

VALIDATION-P5-H1	348.16	0.48	8	656.30	0.90	92
VALIDATION-P5-H2	233.12	ND	0	541.26	1.34	85
VALIDATION-P5-H3	325.08	0.52	54	633.22	1.10	46
VALIDATION-P5-H4	296.12	ND	0	604.26	1.04	100
VALIDATION-P5-H5	349.14	0.91	100	657.28	ND	0
VALIDATION-P5-H7	334.24	0.33	100	642.38	ND	0
VALIDATION-P5-H8	223.13	ND	0	531.27	1.15	100
VALIDATION-P5-H9	308.23	0.45	100	616.37	ND	0
VALIDATION-P5-H10	260.13	ND	0	568.27	0.88	100
VALIDATION-P5-H11	221.08	ND	0	529.22	1.03	100
VALIDATION-P5-H12	284.17	0.53	87	592.31	0.86	13
VALIDATION-P5-H13	377.07	ND	0	685.21	1.19	100
VALIDATION-P5-H14	330.17	0.50	100	638.31	ND	0
VALIDATION-P5-H15	300.17	ND	0	608.31	0.72	97
VALIDATION-P5-H16	327.21	ND	0	635.34	0.61	100
VALIDATION-P5-H17	375.03	ND	0	683.16	1.03	100
VALIDATION-P5-H18	430.00	ND	0	738.00	1.06	100
VALIDATION-P5-H19	237.14	ND	0	545.28	1.23	100
VALIDATION-P5-H20	319.20	ND	0	627.34	0.71	100
VALIDATION-P5-H21	327.21	ND	0	635.34	1.03	100
VALIDATION-P5-H22	335.16	ND	0	643.30	0.88	100
VALIDATION-P5-H23	271.14	ND	0	579.28	0.99	100
VALIDATION-P5-H24	320.22	ND	0	628.36	0.81	100
VALIDATION-P5-I1	288.14	ND	0	596.28	1.13	100
VALIDATION-P5-I2	350.12	ND	0	658.26	1.10	91
VALIDATION-P5-I3	296.15	0.30	61	604.29	0.81	39
VALIDATION-P5-I4	235.17	ND	0	543.31	0.85	100
VALIDATION-P5-I5	319.15	ND	0	627.29	0.95	100
VALIDATION-P5-I7	350.18	ND	0	658.32	0.94	100
VALIDATION-P5-I8	297.12	0.46	76	605.26	ND	0
VALIDATION-P5-I9	211.07	ND	0	519.21	1.05	100
VALIDATION-P5-I10	323.13	ND	0	631.27	1.02	100
VALIDATION-P5-I11	308.17	0.53	75	616.31	0.90	25
VALIDATION-P5-I12	398.23	ND	0	706.37	0.95	54
VALIDATION-P5-I13	288.17	ND	0	596.31	0.71	100
VALIDATION-P5-I14	261.08	ND	0	569.22	1.00	100
VALIDATION-P5-I15	274.22	ND	0	582.35	0.77	100
VALIDATION-P5-I17	309.14	ND	0	617.28	1.04	100
VALIDATION-P5-I18	430.00	ND	0	738.00	1.06	100
VALIDATION-P5-I19	261.09	0.45	100	569.23	ND	0

Confidential – Do Not Copy

VALIDATION-P5-I20	347.18	0.51	100	655.32	ND	0
VALIDATION-P5-I21	300.16	0.57	100	608.30	ND	0
VALIDATION-P5-I22	230.15	0.46	100	538.29	ND	0
VALIDATION-P5-I23	274.09	ND	0	582.23	1.06	100
VALIDATION-P5-I24	344.19	0.65	100	652.33	ND	0
VALIDATION-P5-J1	275.07	0.47	68	583.21	0.89	32
VALIDATION-P5-J2	294.12	ND	0	602.25	0.85	100
VALIDATION-P5-J3	332.22	ND	0	640.36	ND	0
VALIDATION-P5-J4	272.12	0.56	71	580.26	1.13	29
VALIDATION-P5-J5	331.27	ND	0	639.41	0.96	100
VALIDATION-P5-J7	335.11	0.69	100	643.25	ND	0
VALIDATION-P5-J8	386.21	ND	0	694.35	1.15	100
VALIDATION-P5-J9	288.20	0.48	100	596.33	ND	0
VALIDATION-P5-J10	330.14	0.59	94	638.28	1.17	6
VALIDATION-P5-J11	303.15	0.41	94	611.29	ND	0
VALIDATION-P5-J12	242.16	ND	0	550.30	ND	0
VALIDATION-P5-J13	253.14	ND	0	561.28	0.87	100
VALIDATION-P5-J14	300.20	0.48	100	608.33	ND	0
VALIDATION-P5-J15	276.04	ND	0	584.18	1.10	100
VALIDATION-P5-J16	286.17	0.53	100	594.31	ND	0
VALIDATION-P5-J17	317.19	0.56	85	625.33	ND	0
VALIDATION-P5-J18	430.00	ND	0	738.00	1.06	100
VALIDATION-P5-J19	239.13	ND	0	547.27	0.93	100
VALIDATION-P5-J20	349.18	ND	0	657.32	1.02	100
VALIDATION-P5-J21	236.16	ND	0	544.30	0.95	100
VALIDATION-P5-J22	225.18	ND	0	533.32	ND	0
VALIDATION-P5-J23	214.12	ND	0	522.26	0.95	100
VALIDATION-P5-J24	331.18	0.65	84	639.32	0.98	9
VALIDATION-P5-K1	320.12	ND	0	628.26	1.08	100
VALIDATION-P5-K2	210.15	ND	0	518.29	0.82	100
VALIDATION-P5-K3	350.18	0.54	100	658.32	ND	0
VALIDATION-P5-K4	233.15	ND	0	541.29	0.77	100
VALIDATION-P5-K5	373.18	ND	0	681.32	0.87	100
VALIDATION-P5-K7	339.24	ND	0	647.38	0.69	83
VALIDATION-P5-K8	354.21	0.57	92	662.34	ND	0
VALIDATION-P5-K9	344.22	ND	0	652.36	ND	0
VALIDATION-P5-K10	350.18	0.87	78	658.32	0.87	78
VALIDATION-P5-K11	315.22	ND	0	623.36	0.83	100
VALIDATION-P5-K12	337.15	0.48	66	645.28	1.10	34
VALIDATION-P5-K13	281.12	ND	0	589.26	0.76	100

Confidential – Do Not Copy

VALIDATION-P5-K14	422.23	ND	0	730.37	1.20	100
VALIDATION-P5-K15	304.22	0.68	100	612.35	ND	0
VALIDATION-P5-K17	307.17	ND	0	615.31	0.93	100
VALIDATION-P5-K18	430.00	ND	0	738.00	1.06	100
VALIDATION-P5-K19	305.15	0.38	100	613.29	ND	0
VALIDATION-P5-K20	306.19	0.50	27	614.33	0.89	53
VALIDATION-P5-K21	317.22	ND	0	625.36	0.62	100
VALIDATION-P5-K22	289.09	ND	0	597.23	1.04	100
VALIDATION-P5-K23	311.17	0.53	100	619.31	ND	0
VALIDATION-P5-K24	233.03	ND	0	541.17	ND	0
VALIDATION-P5-L1	264.16	ND	0	572.30	ND	0
VALIDATION-P5-L2	354.12	ND	0	662.26	1.06	100
VALIDATION-P5-L3	320.22	ND	0	628.36	1.04	100
VALIDATION-P5-L4	343.16	0.47	100	651.30	ND	0
VALIDATION-P5-L5	249.16	0.56	100	557.30	ND	0
VALIDATION-P5-L7	270.10	ND	0	578.24	1.10	100
VALIDATION-P5-L8	346.24	ND	0	654.38	1.19	100
VALIDATION-P5-L9	330.12	ND	0	638.25	1.17	82
VALIDATION-P5-L10	220.08	ND	0	528.22	0.97	100
VALIDATION-P5-L11	235.13	ND	0	543.27	0.90	100
VALIDATION-P5-L12	283.18	0.57	100	591.32	ND	0
VALIDATION-P5-L13	327.15	0.65	100	635.29	ND	0
VALIDATION-P5-L14	278.22	ND	0	586.36	ND	0
VALIDATION-P5-L15	273.07	ND	0	581.21	1.09	51
VALIDATION-P5-L16	231.15	ND	0	539.29	0.63	100
VALIDATION-P5-L17	241.09	ND	0	549.23	1.13	100
VALIDATION-P5-L18	430.00	ND	0	738.00	1.06	100
VALIDATION-P5-L19	296.06	0.60	54	604.20	1.14	46
VALIDATION-P5-L20	351.19	ND	0	659.33	1.01	100
VALIDATION-P5-L21	267.05	ND	0	575.19	1.25	85
VALIDATION-P5-L22	339.24	ND	0	647.38	0.84	100
VALIDATION-P5-L23	344.17	0.47	82	652.31	0.89	8
VALIDATION-P5-L24	231.10	ND	0	539.24	ND	0
VALIDATION-P5-M1	231.10	0.31	27	539.24	0.94	73
VALIDATION-P5-M2	346.15	0.56	58	654.29	1.08	42
VALIDATION-P5-M3	306.19	0.30	92	614.33	0.84	8
VALIDATION-P5-M4	264.20	ND	0	572.33	1.08	100
VALIDATION-P5-M5	300.15	0.48	100	608.29	ND	0
VALIDATION-P5-M7	344.21	0.59	93	652.35	ND	0
VALIDATION-P5-M8	221.12	ND	0	529.26	0.95	86

Confidential – Do Not Copy

VALIDATION-P5-M9	369.22	ND	0	677.36	ND	0
VALIDATION-P5-M10	321.22	ND	0	629.36	1.06	100
VALIDATION-P5-M11	252.16	ND	0	560.30	0.73	100
VALIDATION-P5-M12	268.17	ND	0	576.31	0.83	100
VALIDATION-P5-M13	305.05	0.61	100	613.19	ND	0
VALIDATION-P5-M14	247.08	ND	0	555.22	0.79	100
VALIDATION-P5-M15	334.16	0.38	66	642.30	0.85	34
VALIDATION-P5-M17	278.11	ND	0	586.25	1.20	100
VALIDATION-P5-M18	430.00	ND	0	738.00	1.06	100
VALIDATION-P5-M19	275.16	ND	0	583.30	0.90	100
VALIDATION-P5-M20	305.07	ND	0	613.21	1.09	100
VALIDATION-P5-M21	236.16	ND	0	544.30	0.90	100
VALIDATION-P5-M22	311.17	ND	0	619.31	0.78	98
VALIDATION-P5-M23	236.08	ND	0	544.22	0.76	100
VALIDATION-P5-M24	356.16	0.69	100	664.29	ND	0
VALIDATION-P5-N1	262.18	ND	0	570.32	ND	0
VALIDATION-P5-N2	261.18	0.40	100	569.32	ND	0
VALIDATION-P5-N3	310.13	ND	0	618.27	1.18	50
VALIDATION-P5-N4	368.23	ND	0	676.37	ND	0
VALIDATION-P5-N5	277.18	ND	0	585.32	0.83	100
VALIDATION-P5-N7	286.18	0.55	83	594.32	0.89	17
VALIDATION-P5-N8	315.14	ND	0	623.28	1.19	100
VALIDATION-P5-N9	246.16	ND	0	554.30	0.90	100
VALIDATION-P5-N10	294.02	ND	0	602.16	1.25	30
VALIDATION-P5-N11	374.03	ND	0	682.17	1.07	100
VALIDATION-P5-N12	275.08	ND	0	583.22	ND	0
VALIDATION-P5-N13	315.21	ND	0	623.34	0.83	97
VALIDATION-P5-N14	303.16	0.52	100	611.30	ND	0
VALIDATION-P5-N15	300.16	0.36	64	608.30	ND	0
VALIDATION-P5-N16	311.19	0.47	100	619.32	ND	0
VALIDATION-P5-N17	249.18	ND	0	557.32	0.76	93
VALIDATION-P5-N18	430.00	ND	0	738.00	1.06	100
VALIDATION-P5-N19	227.08	ND	0	535.22	0.89	100
VALIDATION-P5-N20	368.23	0.42	100	676.37	ND	0
VALIDATION-P5-N21	276.16	0.51	100	584.30	ND	0
VALIDATION-P5-N22	206.12	ND	0	514.26	0.94	100
VALIDATION-P5-N23	354.22	ND	0	662.36	0.77	100
VALIDATION-P5-N24	321.17	ND	0	629.31	0.71	100
VALIDATION-P5-O1	323.20	ND	0	631.34	0.83	100
VALIDATION-P5-O2	233.13	ND	0	541.27	0.76	100

Confidential – Do Not Copy

VALIDATION-P5-O3	332.21	0.55	100	640.35	ND	0
VALIDATION-P5-O4	320.13	ND	0	628.27	0.92	100
VALIDATION-P5-O5	265.19	0.35	100	573.33	ND	0
VALIDATION-P5-O7	249.11	1.19	42	557.25	ND	0
VALIDATION-P5-O8	245.05	0.38	100	553.19	ND	0
VALIDATION-P5-O9	291.17	0.64	100	599.31	ND	0
VALIDATION-P5-O10	325.23	ND	0	633.37	1.04	100
VALIDATION-P5-O11	246.10	0.61	100	554.24	ND	0
VALIDATION-P5-O12	220.17	ND	0	528.31	0.73	100
VALIDATION-P5-O13	264.14	0.55	100	572.28	ND	0
VALIDATION-P5-O14	326.17	0.44	100	634.31	ND	0
VALIDATION-P5-O15	297.15	ND	0	605.29	0.89	71
VALIDATION-P5-O17	266.16	ND	0	574.30	1.13	100
VALIDATION-P5-O18	430.00	ND	0	738.00	1.06	100
VALIDATION-P5-O19	278.09	ND	0	586.23	1.19	84
VALIDATION-P5-O20	210.15	ND	0	518.29	0.97	71
VALIDATION-P5-O21	268.12	ND	0	576.26	1.10	85
VALIDATION-P5-O22	368.18	ND	0	676.32	0.98	83
VALIDATION-P5-O23	262.13	ND	0	570.27	1.02	100
VALIDATION-P5-O24	362.26	0.66	56	670.40	0.98	44
VALIDATION-P5-P1	287.13	ND	0	595.27	0.78	100
VALIDATION-P5-P2	224.15	ND	0	532.29	0.98	97
VALIDATION-P5-P3	343.17	ND	0	651.31	1.14	100
VALIDATION-P5-P4	222.15	ND	0	530.29	0.72	100
VALIDATION-P5-P5	251.16	ND	0	559.30	1.12	100
VALIDATION-P5-P7	296.17	ND	0	604.31	0.78	94
VALIDATION-P5-P8	316.13	ND	0	624.26	0.82	100
VALIDATION-P5-P9	239.12	ND	0	547.25	1.09	100
VALIDATION-P5-P10	341.21	ND	0	649.35	0.92	100
VALIDATION-P5-P11	212.07	ND	0	520.21	0.93	100
VALIDATION-P5-P12	349.15	0.57	12	657.28	1.08	88
VALIDATION-P5-P13	276.17	ND	0	584.31	0.83	100
VALIDATION-P5-P14	249.17	0.63	100	557.31	ND	0
VALIDATION-P5-P15	316.12	ND	0	624.26	1.19	100
VALIDATION-P5-P16	245.16	0.34	100	553.30	ND	0
VALIDATION-P5-P17	349.13	0.56	60	657.27	1.13	40
VALIDATION-P5-P18	430.00	ND	0	738.00	1.06	100
VALIDATION-P5-P19	314.17	0.64	100	622.31	ND	0
VALIDATION-P5-P20	274.15	ND	0	582.29	0.75	100
VALIDATION-P5-P21	303.21	0.30	100	611.34	ND	0

VALIDATION-P5-P22	337.03	0.60	100	645.17	ND	0
VALIDATION-P5-P23	276.15	ND	0	584.29	1.04	100
VALIDATION-P5-P24	285.18	0.57	87	593.32	1.08	13

**Supplementary Table 9: Plate 6:** LCMS data from Chapter 7.3.3.5, HaloCompound *In-Situ* Synthesis for the Validation Set. Column 6 featured a control well, and column 18 featured positive control VHL amine **101**. Performed using standard conditions as outlined in General Methods, using LCMS method (A).

Well Number	SM mass	Rt	% Area	Product Mass	Rt	% Area
VALIDATION-P6-A1	223.10	ND	0	531.24	1.26	81
VALIDATION-P6-A2	228.13	ND	0	536.27	1.17	100
VALIDATION-P6-A3	399.26	ND	0	707.40	0.63	100
VALIDATION-P6-A4	301.19	ND	0	609.33	0.84	89
VALIDATION-P6-A5	203.11	ND	0	511.24	1.22	100
VALIDATION-P6-A7	386.20	ND	0	694.33	1.19	100
VALIDATION-P6-A8	207.07	0.43	34	515.21	1.20	66
VALIDATION-P6-A9	308.12	0.33	29	616.26	0.74	71
VALIDATION-P6-A10	201.01	ND	0	509.15	1.26	100
VALIDATION-P6-A11	272.20	0.30	66	580.34	0.84	27
VALIDATION-P6-A12	235.09	ND	0	543.23	0.88	100
VALIDATION-P6-A13	253.15	0.60	100	561.29	ND	0
VALIDATION-P6-A14	225.12	0.74	33	533.26	1.29	23
VALIDATION-P6-A15	244.16	ND	0	552.30	1.18	89
VALIDATION-P6-A16	329.14	0.65	100	637.28	ND	0
VALIDATION-P6-A17	245.19	0.64	100	553.33	ND	0
VALIDATION-P6-A18	430.00	ND	0	738.00	1.06	100
VALIDATION-P6-A19	289.18	ND	0	597.32	0.87	100
VALIDATION-P6-A20	373.08	ND	0	681.22	1.22	100
VALIDATION-P6-A21	285.01	ND	0	593.15	1.26	100
VALIDATION-P6-A22	233.18	ND	0	541.32	1.47	100
VALIDATION-P6-A23	276.03	0.43	100	584.17	ND	0
VALIDATION-P6-A24	325.19	ND	0	633.33	ND	0
VALIDATION-P6-B1	320.12	0.63	50	628.26	ND	0
VALIDATION-P6-B2	317.21	0.28	91	625.35	0.79	9
VALIDATION-P6-B3	274.13	ND	0	582.27	1.03	100
VALIDATION-P6-B4	360.16	0.73	67	668.30	1.25	33
VALIDATION-P6-B5	302.24	0.64	100	610.37	ND	0
VALIDATION-P6-B7	264.09	ND	0	572.23	1.22	100
VALIDATION-P6-B8	314.20	0.36	90	622.34	ND	0

Confidential – Do Not Copy

VALIDATION-P6-B9	221.07	ND	0	529.21	1.15	100
VALIDATION-P6-B10	356.20	0.52	100	664.34	ND	0
VALIDATION-P6-B11	222.08	ND	0	530.22	ND	0
VALIDATION-P6-B12	214.99	ND	0	523.13	ND	0
VALIDATION-P6-B13	284.15	ND	0	592.29	0.97	100
VALIDATION-P6-B14	223.15	ND	0	531.29	1.01	100
VALIDATION-P6-B15	231.06	ND	0	539.20	0.78	100
VALIDATION-P6-B16	308.20	0.60	100	616.34	ND	0
VALIDATION-P6-B17	263.15	0.60	22	571.29	1.20	78
VALIDATION-P6-B18	430.00	ND	0	738.00	1.06	100
VALIDATION-P6-B19	239.11	ND	0	547.25	ND	0
VALIDATION-P6-B20	250.17	0.54	100	558.31	ND	0
VALIDATION-P6-B21	283.16	0.63	100	591.30	ND	0
VALIDATION-P6-B22	316.25	ND	0	624.39	0.95	100
VALIDATION-P6-B23	298.15	0.57	100	606.29	ND	0
VALIDATION-P6-B24	269.04	ND	0	577.18	1.21	100
VALIDATION-P6-C1	329.21	0.45	100	637.35	ND	0
VALIDATION-P6-C2	257.04	0.51	100	565.18	ND	0
VALIDATION-P6-C3	212.07	ND	0	520.21	1.03	100
VALIDATION-P6-C4	271.16	ND	0	579.30	ND	0
VALIDATION-P6-C5	255.14	ND	0	563.28	0.94	58
VALIDATION-P6-C7	219.09	0.52	43	527.23	1.13	57
VALIDATION-P6-C8	239.03	ND	0	547.17	1.30	100
VALIDATION-P6-C9	303.10	ND	0	611.24	1.16	61
VALIDATION-P6-C10	218.14	ND	0	526.28	1.01	100
VALIDATION-P6-C11	242.12	ND	0	550.26	0.96	100
VALIDATION-P6-C12	244.04	ND	0	552.18	1.08	100
VALIDATION-P6-C13	320.18	ND	0	628.32	0.99	100
VALIDATION-P6-C14	353.19	ND	0	661.32	1.08	100
VALIDATION-P6-C15	353.25	ND	0	661.39	0.90	100
VALIDATION-P6-C16	300.18	ND	0	608.32	0.87	96
VALIDATION-P6-C17	243.09	ND	0	551.23	1.15	100
VALIDATION-P6-C18	430.00	ND	0	738.00	1.06	100
VALIDATION-P6-C19	221.11	ND	0	529.24	1.18	100
VALIDATION-P6-C20	306.16	0.86	100	614.30	0.86	100
VALIDATION-P6-C21	233.10	ND	0	541.24	ND	0
VALIDATION-P6-C22	239.11	ND	0	547.25	1.21	100
VALIDATION-P6-C23	254.12	0.49	100	562.26	ND	0
VALIDATION-P6-C24	219.12	0.46	18	527.26	0.96	82
VALIDATION-P6-D1	371.22	0.86	92	679.36	0.86	92

Confidential – Do Not Copy

VALIDATION-P6-D2	316.26	ND	0	624.40	ND	0
VALIDATION-P6-D3	314.16	ND	0	622.30	0.89	100
VALIDATION-P6-D4	285.18	ND	0	593.32	1.23	100
VALIDATION-P6-D5	319.12	ND	0	627.26	0.95	93
VALIDATION-P6-D7	247.12	0.56	38	555.26	1.17	62
VALIDATION-P6-D8	298.11	ND	0	606.25	1.31	100
VALIDATION-P6-D9	325.22	0.83	100	633.35	0.83	100
VALIDATION-P6-D10	334.23	ND	0	642.36	0.86	100
VALIDATION-P6-D11	207.08	ND	0	515.22	0.88	100
VALIDATION-P6-D12	267.17	0.37	100	575.31	ND	0
VALIDATION-P6-D13	358.16	ND	0	666.30	0.97	100
VALIDATION-P6-D14	241.08	ND	0	549.22	1.03	100
VALIDATION-P6-D15	249.09	ND	0	557.23	1.14	100
VALIDATION-P6-D16	304.12	ND	0	612.26	1.18	100
VALIDATION-P6-D17	290.18	ND	0	598.32	0.88	90
VALIDATION-P6-D18	430.00	ND	0	738.00	1.06	100
VALIDATION-P6-D19	280.16	ND	0	588.30	1.14	100
VALIDATION-P6-D20	275.13	0.70	87	583.27	1.02	7
VALIDATION-P6-D21	207.09	ND	0	515.23	1.07	100
VALIDATION-P6-D22	230.97	ND	0	539.11	ND	0
VALIDATION-P6-D23	237.15	0.32	93	545.29	ND	0
VALIDATION-P6-D24	361.04	ND	0	669.18	0.96	68
VALIDATION-P6-E1	302.16	ND	0	610.30	1.29	100
VALIDATION-P6-E2	289.22	ND	0	597.35	1.18	100
VALIDATION-P6-E3	321.26	0.34	100	629.40	ND	0
VALIDATION-P6-E4	247.17	0.53	40	555.31	1.06	60
VALIDATION-P6-E5	239.10	ND	0	547.24	1.18	100
VALIDATION-P6-E7	212.15	ND	0	520.29	0.77	100
VALIDATION-P6-E8	245.05	ND	0	553.19	1.07	100
VALIDATION-P6-E9	204.13	ND	0	512.27	1.09	100
VALIDATION-P6-E10	325.22	0.42	9	633.35	0.90	91
VALIDATION-P6-E11	205.11	ND	0	513.25	1.16	100
VALIDATION-P6-E12	340.22	0.71	23	648.35	1.27	66
VALIDATION-P6-E13	200.10	ND	0	508.23	0.98	100
VALIDATION-P6-E14	231.10	ND	0	539.24	1.19	100
VALIDATION-P6-E15	274.06	0.54	44	582.20	ND	0
VALIDATION-P6-E16	233.14	ND	0	541.28	1.26	70
VALIDATION-P6-E17	207.13	ND	0	515.27	1.22	100
VALIDATION-P6-E18	430.00	ND	0	738.00	1.06	100
VALIDATION-P6-E19	208.12	ND	0	516.26	0.99	100

Confidential – Do Not Copy

VALIDATION-P6-E20	326.16	0.85	70	634.30	1.41	30
VALIDATION-P6-E21	252.04	ND	0	560.18	1.08	100
VALIDATION-P6-E22	212.08	ND	0	520.22	1.06	100
VALIDATION-P6-E23	313.10	ND	0	621.24	1.15	97
VALIDATION-P6-E24	344.16	ND	0	652.29	1.28	100
VALIDATION-P6-F1	324.18	0.86	58	632.32	0.86	58
VALIDATION-P6-F2	228.13	ND	0	536.27	1.18	100
VALIDATION-P6-F3	278.16	ND	0	586.30	ND	0
VALIDATION-P6-F4	229.16	0.35	63	537.30	0.89	37
VALIDATION-P6-F5	248.20	0.63	100	556.34	0.63	100
VALIDATION-P6-F7	219.13	ND	0	527.27	1.15	96
VALIDATION-P6-F8	237.13	ND	0	545.27	0.99	100
VALIDATION-P6-F9	283.16	ND	0	591.30	1.37	100
VALIDATION-P6-F10	242.15	ND	0	550.29	0.68	100
VALIDATION-P6-F11	260.15	ND	0	568.29	1.28	100
VALIDATION-P6-F12	281.13	0.56	100	589.27	ND	0
VALIDATION-P6-F13	241.10	0.30	29	549.24	0.92	71
VALIDATION-P6-F14	287.20	ND	0	595.34	1.08	100
VALIDATION-P6-F15	201.13	ND	0	509.27	0.84	100
VALIDATION-P6-F16	250.14	ND	0	558.28	0.88	100
VALIDATION-P6-F17	201.13	ND	0	509.27	0.88	67
VALIDATION-P6-F18	430.00	ND	0	738.00	1.06	100
VALIDATION-P6-F19	306.17	ND	0	614.31	1.33	100
VALIDATION-P6-F20	215.14	ND	0	523.28	0.87	100
VALIDATION-P6-F21	215.14	ND	0	523.28	1.16	100
VALIDATION-P6-F22	218.09	ND	0	526.23	1.19	100
VALIDATION-P6-F23	301.22	ND	0	609.35	1.14	100
VALIDATION-P6-F24	288.11	0.64	17	596.25	1.28	83
VALIDATION-P6-G1	335.20	0.41	100	643.34	ND	0
VALIDATION-P6-G2	270.18	0.59	80	578.32	1.25	20
VALIDATION-P6-G3	278.16	ND	0	586.30	1.13	65
VALIDATION-P6-G4	215.11	ND	0	523.24	1.01	100
VALIDATION-P6-G5	339.19	ND	0	647.33	1.05	100
VALIDATION-P6-G7	228.13	ND	0	536.27	1.09	100
VALIDATION-P6-G8	215.11	0.46	100	523.25	ND	0
VALIDATION-P6-G9	217.13	ND	0	525.27	0.89	100
VALIDATION-P6-G10	260.15	0.53	10	568.29	1.11	90
VALIDATION-P6-G11	285.18	0.53	86	593.32	ND	0
VALIDATION-P6-G12	237.12	ND	0	545.26	ND	0
VALIDATION-P6-G13	330.18	0.37	37	638.32	0.91	63

Confidential – Do Not Copy

VALIDATION-P6-G14	269.09	0.62	100	577.23	ND	0
VALIDATION-P6-G15	395.26	ND	0	703.40	0.91	100
VALIDATION-P6-G16	303.23	0.56	97	611.37	ND	0
VALIDATION-P6-G17	275.20	ND	0	583.34	ND	0
VALIDATION-P6-G18	430.00	ND	0	738.00	1.06	100
VALIDATION-P6-G19	243.11	0.75	24	551.25	ND	0
VALIDATION-P6-G20	217.15	ND	0	525.29	ND	0
VALIDATION-P6-G21	300.15	ND	0	608.29	1.18	100
VALIDATION-P6-G22	214.07	ND	0	522.21	1.18	100
VALIDATION-P6-G23	245.13	ND	0	553.27	0.97	100
VALIDATION-P6-G24	287.16	ND	0	595.30	0.89	100
VALIDATION-P6-H1	219.09	ND	0	527.23	1.13	100
VALIDATION-P6-H2	284.19	ND	0	592.33	1.00	100
VALIDATION-P6-H3	342.22	ND	0	650.36	ND	0
VALIDATION-P6-H4	293.12	ND	0	601.26	1.06	100
VALIDATION-P6-H5	353.21	ND	0	661.35	ND	0
VALIDATION-P6-H7	296.20	ND	0	604.34	0.65	81
VALIDATION-P6-H8	255.14	ND	0	563.28	1.05	100
VALIDATION-P6-H9	235.12	ND	0	543.26	1.24	73
VALIDATION-P6-H10	348.19	0.90	11	656.33	1.00	72
VALIDATION-P6-H11	215.14	ND	0	523.28	0.87	100
VALIDATION-P6-H12	284.15	0.56	100	592.29	ND	0
VALIDATION-P6-H13	307.17	0.62	35	615.31	1.17	65
VALIDATION-P6-H14	317.21	ND	0	625.35	0.88	88
VALIDATION-P6-H15	342.06	ND	0	650.19	1.25	100
VALIDATION-P6-H16	335.10	1.04	100	643.24	ND	0
VALIDATION-P6-H17	312.23	0.35	30	620.37	0.74	70
VALIDATION-P6-H18	430.00	ND	0	738.00	1.06	100
VALIDATION-P6-H19	275.07	ND	0	583.21	1.09	100
VALIDATION-P6-H20	245.10	ND	0	553.24	1.15	100
VALIDATION-P6-H21	349.22	ND	0	657.35	1.02	60
VALIDATION-P6-H22	269.04	ND	0	577.18	1.24	73
VALIDATION-P6-H23	244.16	ND	0	552.30	1.06	100
VALIDATION-P6-H24	220.12	ND	0	528.26	1.06	100
VALIDATION-P6-I1	430.00	ND	0	738.14	0.99	50
VALIDATION-P6-I2	228.13	ND	0	536.27	1.18	98
VALIDATION-P6-I3	369.22	ND	0	677.36	0.82	86
VALIDATION-P6-I4	334.10	ND	0	642.24	1.11	86
VALIDATION-P6-I5	246.12	0.53	21	554.26	0.92	32
VALIDATION-P6-I7	262.17	ND	0	570.31	1.16	100

Confidential – Do Not Copy

VALIDATION-P6-I8	211.10	0.59	19	519.24	1.30	81
VALIDATION-P6-I9	274.20	0.38	52	582.34	ND	0
VALIDATION-P6-I10	238.11	ND	0	546.25	1.13	100
VALIDATION-P6-I11	271.13	0.69	100	579.27	ND	0
VALIDATION-P6-I12	279.18	ND	0	587.32	1.26	100
VALIDATION-P6-I13	257.19	0.39	100	565.33	ND	0
VALIDATION-P6-I14	321.19	0.67	100	629.33	ND	0
VALIDATION-P6-I15	199.09	ND	0	507.23	0.77	82
VALIDATION-P6-I16	286.07	ND	0	594.21	0.95	53
VALIDATION-P6-I17	267.18	ND	0	575.32	ND	0
VALIDATION-P6-I18	430.00	ND	0	738.00	1.06	100
VALIDATION-P6-I19	283.17	ND	0	591.31	0.83	100
VALIDATION-P6-I20	350.17	ND	0	658.31	1.02	94
VALIDATION-P6-I21	243.09	ND	0	551.23	1.14	100
VALIDATION-P6-I22	273.22	ND	0	581.36	ND	0
VALIDATION-P6-I23	299.05	0.64	100	607.19	ND	0
VALIDATION-P6-I24	302.11	ND	0	610.25	1.15	100
VALIDATION-P6-J1	231.14	ND	0	539.28	0.87	48
VALIDATION-P6-J2	289.19	0.49	31	597.33	1.00	69
VALIDATION-P6-J3	299.21	0.34	63	607.35	0.79	34
VALIDATION-P6-J4	276.22	0.60	44	584.36	1.21	56
VALIDATION-P6-J5	311.15	ND	0	619.29	1.14	100
VALIDATION-P6-J7	318.23	0.43	100	626.37	ND	0
VALIDATION-P6-J8	318.10	0.98	100	626.24	ND	0
VALIDATION-P6-J9	221.11	ND	0	529.24	1.14	87
VALIDATION-P6-J10	268.12	ND	0	576.26	1.16	100
VALIDATION-P6-J11	344.22	ND	0	652.36	0.77	98
VALIDATION-P6-J12	222.17	ND	0	530.31	0.98	100
VALIDATION-P6-J13	324.15	0.54	100	632.29	ND	0
VALIDATION-P6-J14	361.24	ND	0	669.38	ND	0
VALIDATION-P6-J15	297.12	1.01	100	605.26	1.01	100
VALIDATION-P6-J16	346.16	0.88	96	654.30	0.88	96
VALIDATION-P6-J17	240.13	ND	0	548.27	0.99	100
VALIDATION-P6-J18	430.00	ND	0	738.00	1.06	100
VALIDATION-P6-J19	245.19	ND	0	553.33	ND	0
VALIDATION-P6-J20	292.18	ND	0	600.32	1.16	100
VALIDATION-P6-J21	218.06	ND	0	526.20	1.20	100
VALIDATION-P6-J22	299.16	ND	0	607.30	1.25	91
VALIDATION-P6-J23	222.10	ND	0	530.24	1.01	100
VALIDATION-P6-J24	297.18	ND	0	605.32	1.33	100

Confidential – Do Not Copy

VALIDATION-P6-K1	285.07	0.66	53	593.21	0.97	47
VALIDATION-P6-K2	303.22	0.77	100	611.36	ND	0
VALIDATION-P6-K3	327.15	0.60	100	635.29	ND	0
VALIDATION-P6-K4	204.10	ND	0	512.24	0.70	100
VALIDATION-P6-K5	283.18	0.47	28	591.32	1.07	65
VALIDATION-P6-K7	203.11	0.41	79	511.24	0.95	10
VALIDATION-P6-K8	287.24	ND	0	595.38	0.93	100
VALIDATION-P6-K9	296.05	ND	0	604.19	1.15	100
VALIDATION-P6-K10	320.19	0.34	100	628.33	ND	0
VALIDATION-P6-K11	207.14	ND	0	515.28	ND	0
VALIDATION-P6-K12	229.12	ND	0	537.26	1.01	77
VALIDATION-P6-K13	214.11	ND	0	522.25	0.82	54
VALIDATION-P6-K14	272.15	ND	0	580.29	1.16	100
VALIDATION-P6-K15	218.09	ND	0	526.23	1.25	94
VALIDATION-P6-K16	278.14	ND	0	586.28	1.17	100
VALIDATION-P6-K17	229.08	ND	0	537.22	1.23	100
VALIDATION-P6-K18	430.00	ND	0	738.00	1.06	100
VALIDATION-P6-K19	392.12	ND	0	700.26	0.98	66
VALIDATION-P6-K20	221.14	ND	0	529.28	1.30	100
VALIDATION-P6-K21	329.28	ND	0	637.42	ND	0
VALIDATION-P6-K22	252.14	ND	0	560.28	0.99	100
VALIDATION-P6-K23	275.10	ND	0	583.24	1.19	100
VALIDATION-P6-K24	315.19	0.52	100	623.33	ND	0
VALIDATION-P6-L1	304.18	0.34	100	612.32	ND	0
VALIDATION-P6-L2	374.19	ND	0	682.33	0.89	87
VALIDATION-P6-L3	291.23	ND	0	599.37	1.25	100
VALIDATION-P6-L4	285.18	0.61	54	593.32	0.98	46
VALIDATION-P6-L5	231.09	0.64	100	539.23	ND	0
VALIDATION-P6-L7	326.09	ND	0	634.22	1.22	100
VALIDATION-P6-L8	241.16	ND	0	549.30	0.79	100
VALIDATION-P6-L9	233.14	0.51	100	541.28	ND	0
VALIDATION-P6-L10	322.17	0.32	100	630.31	ND	0
VALIDATION-P6-L11	221.14	ND	0	529.28	ND	0
VALIDATION-P6-L12	215.11	ND	0	523.24	0.79	68
VALIDATION-P6-L13	247.13	ND	0	555.27	0.80	100
VALIDATION-P6-L14	284.15	0.50	100	592.29	ND	0
VALIDATION-P6-L15	203.08	ND	0	511.22	1.29	93
VALIDATION-P6-L16	221.15	ND	0	529.29	1.09	100
VALIDATION-P6-L17	229.07	1.30	100	537.21	1.30	100
VALIDATION-P6-L18	430.00	ND	0	738.00	1.06	100

Confidential – Do Not Copy

VALIDATION-P6-L19	273.18	ND	0	581.32	1.01	100
VALIDATION-P6-L20	383.24	ND	0	691.38	0.90	100
VALIDATION-P6-L21	294.10	0.66	24	602.24	0.96	71
VALIDATION-P6-L22	262.11	ND	0	570.25	1.11	90
VALIDATION-P6-L23	289.16	ND	0	597.30	0.96	100
VALIDATION-P6-L24	276.22	0.38	100	584.36	ND	0
VALIDATION-P6-M1	258.14	0.52	9	566.28	1.12	91
VALIDATION-P6-M2	258.14	0.63	100	566.28	ND	0
VALIDATION-P6-M3	209.11	ND	0	517.24	1.00	100
VALIDATION-P6-M4	308.19	0.37	100	616.33	ND	0
VALIDATION-P6-M5	244.16	ND	0	552.30	1.06	100
VALIDATION-P6-M7	342.17	0.73	41	650.31	1.26	59
VALIDATION-P6-M8	296.19	ND	0	604.33	0.95	100
VALIDATION-P6-M9	227.13	0.56	100	535.27	ND	0
VALIDATION-P6-M10	232.08	ND	0	540.22	1.08	100
VALIDATION-P6-M11	279.17	ND	0	587.31	1.19	100
VALIDATION-P6-M12	267.16	ND	0	575.30	1.35	100
VALIDATION-P6-M13	326.15	0.87	100	634.28	0.87	100
VALIDATION-P6-M14	318.28	0.46	100	626.42	ND	0
VALIDATION-P6-M15	313.18	ND	0	621.32	0.82	100
VALIDATION-P6-M16	236.10	ND	0	544.24	1.03	100
VALIDATION-P6-M17	302.14	ND	0	610.28	0.97	100
VALIDATION-P6-M18	430.00	ND	0	738.00	1.06	100
VALIDATION-P6-M19	235.17	ND	0	543.31	1.05	95
VALIDATION-P6-M20	242.14	ND	0	550.28	0.90	97
VALIDATION-P6-M21	368.25	ND	0	676.39	0.94	65
VALIDATION-P6-M22	314.06	0.60	10	622.20	1.21	90
VALIDATION-P6-M23	255.03	0.63	29	563.16	1.33	71
VALIDATION-P6-M24	204.13	0.48	87	512.27	1.15	8
VALIDATION-P6-N1	216.16	0.41	100	524.30	ND	0
VALIDATION-P6-N2	261.18	0.34	100	569.32	ND	0
VALIDATION-P6-N3	299.15	ND	0	607.29	1.18	100
VALIDATION-P6-N4	344.19	0.43	34	652.33	0.95	66
VALIDATION-P6-N5	316.09	ND	0	624.22	1.13	100
VALIDATION-P6-N7	227.13	ND	0	535.27	1.21	100
VALIDATION-P6-N8	273.09	0.45	34	581.23	1.01	66
VALIDATION-P6-N9	239.11	ND	0	547.24	1.11	100
VALIDATION-P6-N10	288.08	ND	0	596.22	0.93	53
VALIDATION-P6-N11	269.19	ND	0	577.33	0.83	28
VALIDATION-P6-N12	288.08	ND	0	596.22	1.00	96

Confidential – Do Not Copy

VALIDATION-P6-N13	294.04	0.66	89	602.18	ND	0
VALIDATION-P6-N14	284.15	ND	0	592.29	1.10	100
VALIDATION-P6-N15	205.07	ND	0	513.21	ND	0
VALIDATION-P6-N16	273.10	ND	0	581.24	1.10	100
VALIDATION-P6-N17	286.20	ND	0	594.34	0.83	100
VALIDATION-P6-N18	430.00	ND	0	738.00	1.06	100
VALIDATION-P6-N19	332.15	ND	0	640.29	0.88	100
VALIDATION-P6-N20	333.29	0.40	54	641.43	0.74	46
VALIDATION-P6-N21	303.23	0.34	100	611.37	ND	0
VALIDATION-P6-N22	245.12	ND	0	553.26	1.17	62
VALIDATION-P6-N23	221.10	0.50	81	529.24	1.16	19
VALIDATION-P6-N24	211.12	ND	0	519.26	1.23	100
VALIDATION-P6-O1	329.25	ND	0	637.39	0.97	87
VALIDATION-P6-O2	216.13	ND	0	524.27	1.18	100
VALIDATION-P6-O3	274.13	ND	0	582.26	0.80	100
VALIDATION-P6-O4	207.14	ND	0	515.28	0.86	100
VALIDATION-P6-O5	220.10	0.53	37	528.24	1.17	63
VALIDATION-P6-O7	342.27	ND	0	650.41	0.93	100
VALIDATION-P6-O8	319.12	0.63	78	627.26	1.21	22
VALIDATION-P6-O9	265.02	ND	0	573.16	1.18	100
VALIDATION-P6-O10	201.13	0.48	42	509.27	0.83	58
VALIDATION-P6-O11	234.14	ND	0	542.28	1.20	100
VALIDATION-P6-O12	393.25	ND	0	701.39	0.64	100
VALIDATION-P6-O13	291.04	ND	0	599.18	0.82	99
VALIDATION-P6-O14	290.20	0.68	32	598.34	1.22	68
VALIDATION-P6-O15	355.26	0.49	100	663.40	ND	0
VALIDATION-P6-O16	261.15	ND	0	569.29	1.04	100
VALIDATION-P6-O17	338.12	ND	0	646.26	1.23	95
VALIDATION-P6-O18	430.00	ND	0	738.00	1.06	100
VALIDATION-P6-O19	239.14	ND	0	547.28	0.83	100
VALIDATION-P6-O20	243.15	ND	0	551.29	0.77	100
VALIDATION-P6-O21	247.17	ND	0	555.31	1.14	100
VALIDATION-P6-O22	266.14	ND	0	574.28	1.08	86
VALIDATION-P6-O23	304.10	0.66	100	612.24	ND	0
VALIDATION-P6-O24	222.10	ND	0	530.24	1.11	100
VALIDATION-P6-P1	257.07	ND	0	565.21	1.13	100
VALIDATION-P6-P2	224.07	0.33	46	532.21	0.88	54
VALIDATION-P6-P3	241.11	0.48	100	549.25	ND	0
VALIDATION-P6-P4	298.22	0.34	100	606.35	ND	0
VALIDATION-P6-P5	321.20	0.81	100	629.33	0.81	100

VALIDATION-P6-P7	311.18	ND	0	619.32	1.22	100
VALIDATION-P6-P8	406.09	0.76	65	714.23	1.29	30
VALIDATION-P6-P9	208.14	ND	0	516.28	ND	0
VALIDATION-P6-P10	345.24	0.49	79	653.38	0.91	21
VALIDATION-P6-P11	240.14	ND	0	548.28	0.82	95
VALIDATION-P6-P12	235.11	ND	0	543.25	0.86	96
VALIDATION-P6-P13	211.12	ND	0	519.26	1.10	100
VALIDATION-P6-P14	255.13	0.77	18	563.27	1.18	78
VALIDATION-P6-P15	354.24	0.45	92	662.38	ND	0
VALIDATION-P6-P16	203.11	ND	0	511.24	1.12	100
VALIDATION-P6-P17	309.18	0.65	56	617.32	1.23	44
VALIDATION-P6-P18	430.00	ND	0	738.00	1.06	100
VALIDATION-P6-P19	226.05	ND	0	534.19	1.15	100
VALIDATION-P6-P20	299.20	0.60	30	607.34	1.18	70
VALIDATION-P6-P21	308.19	ND	0	616.33	ND	0
VALIDATION-P6-P22	221.07	ND	0	529.21	0.89	100
VALIDATION-P6-P23	205.15	ND	0	513.29	1.08	100
VALIDATION-P6-P24	236.10	ND	0	544.24	1.12	100

**Supplementary Table 10: Plate 7:** LCMS data from Chapter 7.3.3.5, HaloCompound *In-Situ* Synthesis for the Validation Set. Column 6 featured a control well, and column 18 featured positive control VHL amine **101**. Performed using standard conditions as outlined in General Methods, using LCMS method (A).

Well Number	SM mass	Rt	% Area	Product Mass	Rt	% Area
VALIDATION-P7-A1	315.19	ND	0	623.33	ND	0
VALIDATION-P7-A2	262.17	ND	0	570.31	1.13	100
VALIDATION-P7-A3	205.09	0.99	81	513.22	0.99	81
VALIDATION-P7-A4	330.19	0.58	100	638.33	ND	0
VALIDATION-P7-A5	268.17	0.74	100	576.31	0.74	100
VALIDATION-P7-A7	302.14	1.12	9	610.28	1.16	91
VALIDATION-P7-A8	260.17	0.71	100	568.31	0.71	100
VALIDATION-P7-A9	277.20	ND	0	585.34	1.28	100
VALIDATION-P7-A10	306.11	0.66	94	614.25	ND	0
VALIDATION-P7-A11	260.00	ND	0	568.14	1.15	100
VALIDATION-P7-A12	320.18	0.68	100	628.32	ND	0
VALIDATION-P7-A13	321.01	0.69	65	641.15	ND	0
VALIDATION-P7-A14	264.14	ND	0	572.28	0.76	100
VALIDATION-P7-A15	322.07	ND	0	630.21	1.16	100
VALIDATION-P7-A16	222.18	ND	0	530.32	0.76	100
VALIDATION-P7-A17	389.12	0.80	15	697.26	1.27	85

Confidential – Do Not Copy

VALIDATION-P7-A18	430.00	ND	0	738.00	1.06	100
VALIDATION-P7-A19	275.13	0.77	5	583.27	1.13	95
VALIDATION-P7-A20	309.16	1.23	100	617.30	1.23	100
VALIDATION-P7-A21	355.21	0.57	51	663.34	0.92	49
VALIDATION-P7-A22	272.16	ND	0	580.30	0.81	100
VALIDATION-P7-A23	260.16	ND	0	568.30	0.94	100
VALIDATION-P7-A24	301.22	ND	0	609.35	1.32	90
VALIDATION-P7-B1	255.17	ND	0	563.31	0.75	34
VALIDATION-P7-B2	353.14	0.77	3	661.27	1.25	97
VALIDATION-P7-B3	292.18	0.73	93	600.32	1.39	7
VALIDATION-P7-B4	233.18	0.62	100	541.32	ND	0
VALIDATION-P7-B5	304.20	0.60	36	612.33	1.17	64
VALIDATION-P7-B7	262.17	ND	0	570.31	1.11	100
VALIDATION-P7-B8	247.18	ND	0	555.32	0.86	100
VALIDATION-P7-B9	250.15	ND	0	558.29	0.92	100
VALIDATION-P7-B10	278.15	0.34	3	586.29	0.84	96
VALIDATION-P7-B11	202.96	ND	0	511.10	1.08	100
VALIDATION-P7-B12	228.14	0.98	97	536.28	0.98	97
VALIDATION-P7-B13	254.14	ND	0	562.28	1.08	100
VALIDATION-P7-B14	302.16	ND	0	610.30	0.82	96
VALIDATION-P7-B15	303.18	0.40	63	611.32	0.92	35
VALIDATION-P7-B16	259.18	ND	0	567.32	1.15	100
VALIDATION-P7-B17	201.12	ND	0	509.25	1.15	94
VALIDATION-P7-B18	430.00	ND	0	738.00	1.06	100
VALIDATION-P7-B19	270.17	ND	0	578.31	0.90	100
VALIDATION-P7-B20	267.14	0.82	100	575.28	ND	0
VALIDATION-P7-B21	290.12	ND	0	598.26	0.79	100
VALIDATION-P7-B22	201.01	ND	0	509.15	1.29	100
VALIDATION-P7-B23	332.16	0.64	45	640.29	1.22	55
VALIDATION-P7-B24	327.16	0.43	98	635.30	ND	0
VALIDATION-P7-C1	217.12	0.76	6	525.26	0.81	94
VALIDATION-P7-C2	210.12	0.92	6	518.25	0.95	90
VALIDATION-P7-C3	215.07	ND	0	523.21	0.73	100
VALIDATION-P7-C4	340.19	0.41	100	648.33	ND	0
VALIDATION-P7-C5	294.18	0.69	100	602.32	ND	0
VALIDATION-P7-C7	240.14	0.62	100	548.28	ND	0
VALIDATION-P7-C8	439.28	0.47	80	747.42	0.75	9
VALIDATION-P7-C9	275.18	0.66	100	583.32	ND	0
VALIDATION-P7-C10	262.13	ND	0	570.27	1.00	100
VALIDATION-P7-C11	349.22	0.86	100	657.36	0.86	100

Confidential – Do Not Copy

VALIDATION-P7-C12	250.09	ND	0	558.23	1.14	100
VALIDATION-P7-C13	294.06	0.65	91	602.20	ND	0
VALIDATION-P7-C14	273.18	ND	0	581.32	1.03	100
VALIDATION-P7-C15	217.16	ND	0	525.30	ND	0
VALIDATION-P7-C16	328.17	ND	0	636.31	1.10	100
VALIDATION-P7-C17	301.17	0.60	25	609.31	1.16	75
VALIDATION-P7-C18	430.00	ND	0	738.00	1.06	100
VALIDATION-P7-C19	280.17	ND	0	588.31	0.76	100
VALIDATION-P7-C20	221.14	ND	0	529.28	1.15	100
VALIDATION-P7-C21	316.14	0.51	72	624.28	1.11	19
VALIDATION-P7-C22	353.25	ND	0	661.39	0.87	100
VALIDATION-P7-C23	328.18	ND	0	636.32	1.34	100
VALIDATION-P7-C24	337.18	0.53	100	645.32	ND	0
VALIDATION-P7-D1	298.19	ND	0	606.32	ND	0
VALIDATION-P7-D2	396.25	ND	0	704.39	0.83	100
VALIDATION-P7-D3	281.15	ND	0	589.29	1.32	100
VALIDATION-P7-D4	206.14	0.42	66	514.28	0.78	15
VALIDATION-P7-D5	266.09	ND	0	574.23	1.08	100
VALIDATION-P7-D7	274.20	ND	0	582.34	1.30	100
VALIDATION-P7-D8	344.09	0.88	100	652.23	0.88	100
VALIDATION-P7-D9	269.05	ND	0	577.19	0.92	87
VALIDATION-P7-D10	226.15	ND	0	534.29	0.86	100
VALIDATION-P7-D11	255.10	ND	0	563.24	0.91	100
VALIDATION-P7-D12	300.16	0.44	13	608.30	0.83	87
VALIDATION-P7-D13	330.24	0.89	100	638.38	0.89	100
VALIDATION-P7-D14	249.18	ND	0	557.32	0.81	100
VALIDATION-P7-D15	327.09	0.92	100	635.23	0.92	100
VALIDATION-P7-D16	253.15	0.69	45	561.29	1.27	55
VALIDATION-P7-D17	302.15	ND	0	610.29	0.99	100
VALIDATION-P7-D18	430.00	ND	0	738.00	1.06	100
VALIDATION-P7-D19	298.17	ND	0	606.31	0.96	100
VALIDATION-P7-D20	266.12	ND	0	574.26	0.95	78
VALIDATION-P7-D21	241.10	ND	0	549.24	0.93	100
VALIDATION-P7-D22	285.07	0.74	100	593.21	ND	0
VALIDATION-P7-D23	336.14	ND	0	644.27	0.82	96
VALIDATION-P7-E1	334.14	0.61	34	642.28	0.98	66
VALIDATION-P7-E2	314.16	ND	0	622.30	1.32	100
VALIDATION-P7-E3	251.14	0.41	100	559.28	ND	0
VALIDATION-P7-E4	312.13	0.58	100	620.27	ND	0
VALIDATION-P7-E5	246.18	0.94	100	554.32	ND	0

Confidential – Do Not Copy

VALIDATION-P7-E7	292.10	0.79	66	600.24	0.79	66
VALIDATION-P7-E8	346.12	ND	0	654.26	1.29	100
VALIDATION-P7-E9	289.20	0.50	78	597.33	1.04	22
VALIDATION-P7-E10	255.10	0.58	100	563.24	ND	0
VALIDATION-P7-E11	286.14	ND	0	594.28	1.01	100
VALIDATION-P7-E12	249.10	0.60	100	557.24	ND	0
VALIDATION-P7-E13	257.15	ND	0	565.29	ND	0
VALIDATION-P7-E14	266.14	0.50	15	574.28	1.09	79
VALIDATION-P7-E15	312.23	0.37	100	620.37	ND	0
VALIDATION-P7-E16	257.08	ND	0	565.22	1.26	88
VALIDATION-P7-E17	199.99	0.72	100	508.13	ND	0
VALIDATION-P7-E18	430.00	ND	0	738.00	1.06	100
VALIDATION-P7-E19	219.17	ND	0	527.31	ND	0
VALIDATION-P7-E20	213.13	0.49	19	521.27	1.09	81
VALIDATION-P7-E21	206.14	0.43	100	514.28	ND	0
VALIDATION-P7-E22	286.15	0.56	100	594.29	ND	0
VALIDATION-P7-E23	288.23	ND	0	596.37	0.64	72
VALIDATION-P7-F1	203.11	0.99	88	511.24	0.99	88
VALIDATION-P7-F2	268.04	0.94	100	576.18	ND	0
VALIDATION-P7-F3	260.11	ND	0	568.25	1.06	100
VALIDATION-P7-F4	330.16	0.92	100	638.29	ND	0
VALIDATION-P7-F5	266.16	ND	0	574.30	1.09	100
VALIDATION-P7-F7	328.23	0.39	20	636.37	0.72	61
VALIDATION-P7-F8	229.09	0.47	94	537.22	ND	0
VALIDATION-P7-F9	274.17	0.66	60	582.31	1.27	25
VALIDATION-P7-F10	293.17	0.34	28	601.31	0.86	72
VALIDATION-P7-F11	253.04	ND	0	561.18	1.01	100
VALIDATION-P7-F12	219.14	0.75	59	527.28	1.21	41
VALIDATION-P7-F13	202.97	ND	0	511.11	1.20	100
VALIDATION-P7-F14	282.18	ND	0	590.32	0.85	100
VALIDATION-P7-F15	212.98	ND	0	521.12	1.17	100
VALIDATION-P7-F16	330.04	0.38	87	638.18	0.93	13
VALIDATION-P7-F17	233.10	0.63	90	541.24	0.63	90
VALIDATION-P7-F18	430.00	ND	0	738.00	1.06	100
VALIDATION-P7-F19	303.16	0.59	87	611.30	ND	0
VALIDATION-P7-F20	207.03	ND	0	515.17	ND	0
VALIDATION-P7-F21	236.15	ND	0	544.29	1.19	100
VALIDATION-P7-F22	205.15	ND	0	513.29	1.32	100
VALIDATION-P7-F23	316.24	ND	0	624.38	0.88	100
VALIDATION-P7-G1	204.13	ND	0	512.27	1.17	100

Confidential – Do Not Copy

VALIDATION-P7-G2	205.07	ND	0	513.21	1.09	100
VALIDATION-P7-G3	204.16	ND	0	512.30	0.83	100
VALIDATION-P7-G4	423.27	0.40	19	731.41	0.71	81
VALIDATION-P7-G5	320.25	0.48	28	628.39	0.96	72
VALIDATION-P7-G7	285.13	0.60	100	593.27	ND	0
VALIDATION-P7-G8	268.13	ND	0	576.27	0.95	100
VALIDATION-P7-G9	286.14	ND	0	594.28	0.74	89
VALIDATION-P7-G10	227.14	ND	0	535.28	0.82	97
VALIDATION-P7-G11	250.15	ND	0	558.29	1.24	100
VALIDATION-P7-G12	297.10	ND	0	605.24	0.83	100
VALIDATION-P7-G13	290.15	0.48	83	598.28	ND	0
VALIDATION-P7-G14	343.20	ND	0	651.34	0.67	100
VALIDATION-P7-G15	340.24	0.66	100	648.38	0.66	100
VALIDATION-P7-G16	203.13	0.44	100	511.27	ND	0
VALIDATION-P7-G17	280.19	ND	0	588.33	0.79	100
VALIDATION-P7-G18	430.00	ND	0	738.00	1.06	100
VALIDATION-P7-G19	348.24	0.59	100	656.38	ND	0
VALIDATION-P7-G20	237.05	ND	0	545.19	1.17	100
VALIDATION-P7-G21	220.11	0.41	7	528.25	0.80	93
VALIDATION-P7-G22	315.13	ND	0	623.27	0.97	100
VALIDATION-P7-G23	211.14	ND	0	519.28	1.38	100
VALIDATION-P7-H1	225.09	0.49	100	533.23	ND	0
VALIDATION-P7-H2	201.06	ND	0	509.20	ND	0
VALIDATION-P7-H3	342.24	ND	0	650.38	0.85	100
VALIDATION-P7-H4	230.15	ND	0	538.29	0.85	59
VALIDATION-P7-H5	223.06	ND	0	531.20	1.12	100
VALIDATION-P7-H7	320.19	0.63	100	628.33	ND	0
VALIDATION-P7-H8	232.16	ND	0	540.30	0.99	100
VALIDATION-P7-H9	242.01	0.43	11	550.14	1.08	89
VALIDATION-P7-H10	207.14	0.39	5	515.28	0.79	73
VALIDATION-P7-H11	302.17	0.57	85	610.31	0.92	15
VALIDATION-P7-H12	399.22	0.69	100	707.35	ND	0
VALIDATION-P7-H13	328.02	1.35	6	636.16	1.22	94
VALIDATION-P7-H14	202.11	0.47	46	510.25	1.00	54
VALIDATION-P7-H15	243.14	ND	0	551.28	1.13	100
VALIDATION-P7-H16	223.15	0.48	7	531.29	0.86	93
VALIDATION-P7-H17	244.12	ND	0	552.26	1.22	100
VALIDATION-P7-H18	430.00	ND	0	738.00	1.06	100
VALIDATION-P7-H19	349.17	ND	0	657.31	1.04	100
VALIDATION-P7-H20	337.03	0.64	82	645.17	1.24	18

Confidential – Do Not Copy

VALIDATION-P7-H21	317.16	0.53	21	625.30	0.93	63
VALIDATION-P7-H22	330.18	0.77	44	638.32	1.35	31
VALIDATION-P7-H23	254.18	ND	0	562.32	ND	0
VALIDATION-P7-I1	241.06	ND	0	549.20	1.22	86
VALIDATION-P7-I2	237.10	ND	0	545.24	1.04	100
VALIDATION-P7-I3	275.20	0.79	100	583.34	0.79	100
VALIDATION-P7-I4	327.24	0.91	54	635.38	0.91	54
VALIDATION-P7-I5	312.08	0.59	18	620.22	1.01	82
VALIDATION-P7-I7	271.12	0.47	100	579.26	ND	0
VALIDATION-P7-I8	270.14	ND	0	578.28	0.87	100
VALIDATION-P7-I9	303.16	ND	0	611.30	1.02	87
VALIDATION-P7-I10	205.15	0.49	100	513.29	ND	0
VALIDATION-P7-I11	261.13	0.63	55	569.27	0.93	45
VALIDATION-P7-I12	209.12	ND	0	517.26	1.19	100
VALIDATION-P7-I13	280.16	ND	0	588.30	1.11	100
VALIDATION-P7-I14	216.14	ND	0	524.28	0.73	100
VALIDATION-P7-I15	275.10	0.55	100	583.24	ND	0
VALIDATION-P7-I16	235.20	ND	0	543.34	0.95	91
VALIDATION-P7-I17	215.07	ND	0	523.21	1.24	100
VALIDATION-P7-I18	430.00	ND	0	738.00	1.06	100
VALIDATION-P7-I19	267.16	0.70	100	575.30	ND	0
VALIDATION-P7-I20	244.17	ND	0	552.31	1.05	100
VALIDATION-P7-I21	287.13	ND	0	595.27	0.82	100
VALIDATION-P7-I22	222.15	ND	0	530.29	0.71	100
VALIDATION-P7-I23	358.12	ND	0	666.26	0.97	100
VALIDATION-P7-J1	323.03	0.54	53	631.17	1.13	47
VALIDATION-P7-J2	280.10	ND	0	588.24	1.15	100
VALIDATION-P7-J3	238.13	ND	0	546.27	1.14	100
VALIDATION-P7-J4	330.23	ND	0	638.37	1.16	100
VALIDATION-P7-J5	227.10	0.38	100	535.24	ND	0
VALIDATION-P7-J7	274.22	0.50	100	582.35	ND	0
VALIDATION-P7-J8	345.19	0.46	85	653.33	0.95	15
VALIDATION-P7-J9	206.09	1.27	11	514.23	1.18	81
VALIDATION-P7-J10	276.16	0.50	100	584.30	ND	0
VALIDATION-P7-J11	232.13	0.83	54	540.27	0.83	54
VALIDATION-P7-J12	324.99	ND	0	633.13	1.15	100
VALIDATION-P7-J13	239.06	1.32	5	547.20	1.18	95
VALIDATION-P7-J14	205.07	0.32	6	513.21	0.87	89
VALIDATION-P7-J15	280.12	0.64	100	588.26	ND	0
VALIDATION-P7-J16	315.19	ND	0	623.33	0.99	100

Confidential – Do Not Copy

VALIDATION-P7-J17	249.10	ND	0	557.24	1.16	100
VALIDATION-P7-J18	430.00	ND	0	738.00	1.06	100
VALIDATION-P7-J19	291.21	0.77	100	599.34	0.77	100
VALIDATION-P7-J20	264.14	ND	0	572.28	0.90	64
VALIDATION-P7-J21	205.01	ND	0	513.15	1.23	100
VALIDATION-P7-J22	303.11	ND	0	611.25	1.22	100
VALIDATION-P7-J23	244.17	0.39	7	552.31	0.84	93
VALIDATION-P7-K1	359.17	ND	0	667.31	0.95	100
VALIDATION-P7-K2	227.08	ND	0	535.22	1.08	100
VALIDATION-P7-K3	269.16	ND	0	577.30	0.89	100
VALIDATION-P7-K4	301.14	ND	0	609.28	1.09	100
VALIDATION-P7-K5	258.12	0.46	85	566.26	1.08	15
VALIDATION-P7-K7	262.17	0.49	100	570.31	ND	0
VALIDATION-P7-K8	264.10	0.65	64	572.24	1.22	36
VALIDATION-P7-K9	321.16	0.60	5	629.30	0.94	95
VALIDATION-P7-K10	219.10	ND	0	527.24	1.05	100
VALIDATION-P7-K11	236.11	ND	0	544.25	1.00	100
VALIDATION-P7-K12	328.11	0.86	100	636.25	0.86	100
VALIDATION-P7-K13	316.10	ND	0	624.24	1.05	100
VALIDATION-P7-K14	240.03	ND	0	548.17	1.26	100
VALIDATION-P7-K15	298.22	ND	0	606.35	ND	0
VALIDATION-P7-K16	248.05	ND	0	556.19	0.93	44
VALIDATION-P7-K17	254.15	ND	0	562.29	0.69	100
VALIDATION-P7-K18	430.00	ND	0	738.00	1.06	100
VALIDATION-P7-K19	265.17	ND	0	573.31	1.34	100
VALIDATION-P7-K20	317.13	ND	0	625.27	1.15	94
VALIDATION-P7-K21	315.14	ND	0	623.28	0.91	100
VALIDATION-P7-K22	202.15	0.39	47	510.29	0.96	53
VALIDATION-P7-K23	216.06	ND	0	524.20	1.01	100
VALIDATION-P7-L1	250.22	ND	0	558.35	0.74	100
VALIDATION-P7-L2	230.10	ND	0	538.24	1.17	100
VALIDATION-P7-L3	231.09	ND	0	539.23	1.13	100
VALIDATION-P7-L4	262.18	0.87	6	570.32	0.84	94
VALIDATION-P7-L5	327.16	ND	0	635.29	ND	0
VALIDATION-P7-L7	224.13	ND	0	532.27	0.72	100
VALIDATION-P7-L8	247.17	ND	0	555.31	0.76	100
VALIDATION-P7-L9	275.19	0.74	100	583.33	ND	0
VALIDATION-P7-L10	231.10	ND	0	539.24	0.93	100
VALIDATION-P7-L11	231.17	ND	0	539.31	0.89	100
VALIDATION-P7-L12	312.26	ND	0	620.40	ND	0

Confidential – Do Not Copy

VALIDATION-P7-L13	333.13	ND	0	641.27	1.10	100
VALIDATION-P7-L14	205.10	ND	0	513.24	1.14	97
VALIDATION-P7-L15	358.20	ND	0	666.34	1.01	100
VALIDATION-P7-L16	306.10	0.54	100	614.24	ND	0
VALIDATION-P7-L17	232.02	0.56	9	540.16	1.25	91
VALIDATION-P7-L18	430.00	ND	0	738.00	1.06	100
VALIDATION-P7-L19	276.22	ND	0	584.36	ND	0
VALIDATION-P7-L20	299.21	ND	0	607.35	0.84	100
VALIDATION-P7-L21	230.15	0.81	12	538.29	0.81	12
VALIDATION-P7-L22	328.21	ND	0	636.35	ND	0
VALIDATION-P7-L23	322.13	ND	0	630.27	ND	0
VALIDATION-P7-M1	342.16	ND	0	650.29	1.31	100
VALIDATION-P7-M2	309.18	ND	0	617.32	1.15	100
VALIDATION-P7-M3	241.15	0.48	95	549.29	1.15	5
VALIDATION-P7-M4	213.13	ND	0	521.27	0.99	84
VALIDATION-P7-M5	355.24	0.45	7	663.38	0.88	93
VALIDATION-P7-M7	381.16	ND	0	689.30	0.95	100
VALIDATION-P7-M8	263.09	ND	0	571.23	1.23	96
VALIDATION-P7-M9	272.13	ND	0	580.27	1.33	92
VALIDATION-P7-M10	200.06	ND	0	508.20	1.00	100
VALIDATION-P7-M11	260.06	0.67	9	568.20	1.28	82
VALIDATION-P7-M12	336.18	0.61	100	644.32	ND	0
VALIDATION-P7-M13	242.14	ND	0	550.28	1.19	100
VALIDATION-P7-M14	295.03	0.56	42	603.17	1.15	45
VALIDATION-P7-M15	329.11	ND	0	637.25	0.86	100
VALIDATION-P7-M16	291.14	ND	0	599.28	1.21	100
VALIDATION-P7-M17	211.16	0.49	100	519.30	ND	0
VALIDATION-P7-M18	430.00	ND	0	738.00	1.06	100
VALIDATION-P7-M19	327.17	ND	0	635.31	0.80	100
VALIDATION-P7-M20	344.20	1.03	57	652.34	1.03	57
VALIDATION-P7-M21	226.11	ND	0	534.25	1.08	83
VALIDATION-P7-M22	325.14	0.88	100	633.27	0.88	100
VALIDATION-P7-M23	234.21	ND	0	542.35	ND	0
VALIDATION-P7-N1	306.12	0.52	80	614.26	1.11	20
VALIDATION-P7-N2	284.20	0.47	88	592.34	ND	0
VALIDATION-P7-N3	355.17	ND	0	663.31	0.89	100
VALIDATION-P7-N4	265.16	0.42	100	573.30	ND	0
VALIDATION-P7-N5	324.20	0.57	61	632.33	0.97	37
VALIDATION-P7-N7	205.03	ND	0	513.17	1.23	100
VALIDATION-P7-N8	231.02	ND	0	539.16	1.14	91

Confidential – Do Not Copy

VALIDATION-P7-N9	285.03	ND	0	593.17	1.18	84
VALIDATION-P7-N10	284.15	ND	0	592.29	1.21	100
VALIDATION-P7-N11	324.15	ND	0	632.29	1.21	53
VALIDATION-P7-N12	258.10	ND	0	566.24	1.01	100
VALIDATION-P7-N13	257.15	0.29	21	565.29	0.80	74
VALIDATION-P7-N14	230.15	ND	0	538.29	0.79	100
VALIDATION-P7-N15	264.17	0.76	100	572.31	0.76	100
VALIDATION-P7-N16	379.24	0.43	100	687.38	ND	0
VALIDATION-P7-N17	242.15	ND	0	550.29	ND	0
VALIDATION-P7-N18	430.00	ND	0	738.00	1.06	100
VALIDATION-P7-N19	266.18	0.41	100	574.32	ND	0
VALIDATION-P7-N20	326.16	ND	0	634.30	0.93	100
VALIDATION-P7-N21	305.21	0.62	46	613.35	1.17	40
VALIDATION-P7-N22	258.17	ND	0	566.31	1.25	100
VALIDATION-P7-N23	274.18	ND	0	582.32	0.73	100
VALIDATION-P7-O1	314.11	ND	0	622.25	1.18	100
VALIDATION-P7-O2	355.19	ND	0	663.33	ND	0
VALIDATION-P7-O3	294.08	ND	0	602.22	1.07	100
VALIDATION-P7-O4	302.21	ND	0	610.35	1.07	100
VALIDATION-P7-O5	331.20	ND	0	639.34	0.85	100
VALIDATION-P7-O7	260.19	ND	0	568.33	0.85	100
VALIDATION-P7-O8	231.17	0.79	100	539.31	0.79	100
VALIDATION-P7-O9	276.20	ND	0	584.33	0.92	100
VALIDATION-P7-O10	246.10	ND	0	554.24	1.13	100
VALIDATION-P7-O11	279.08	1.00	100	587.22	1.00	100
VALIDATION-P7-O12	246.14	ND	0	554.28	1.12	100
VALIDATION-P7-O13	320.11	0.49	100	628.25	ND	0
VALIDATION-P7-O14	265.09	0.43	100	573.23	ND	0
VALIDATION-P7-O15	265.14	ND	0	573.28	1.23	100
VALIDATION-P7-O16	289.07	ND	0	597.21	1.17	52
VALIDATION-P7-O17	271.12	ND	0	579.26	0.98	100
VALIDATION-P7-O18	430.00	ND	0	738.00	1.06	100
VALIDATION-P7-O19	248.19	ND	0	556.33	ND	0
VALIDATION-P7-O20	287.11	ND	0	595.25	1.32	100
VALIDATION-P7-O21	243.15	0.78	100	551.29	0.78	100
VALIDATION-P7-O22	331.17	0.38	100	639.31	ND	0
VALIDATION-P7-O23	299.15	ND	0	607.29	0.92	95
VALIDATION-P7-P1	226.15	ND	0	534.29	0.88	100
VALIDATION-P7-P2	330.19	0.37	91	638.33	0.91	9
VALIDATION-P7-P3	330.04	0.60	41	638.18	1.15	59

VALIDATION-P7-P4	268.16	0.72	84	576.30	1.27	12
VALIDATION-P7-P5	207.17	0.79	100	515.31	0.79	100
VALIDATION-P7-P7	219.10	ND	0	527.24	1.00	100
VALIDATION-P7-P8	239.15	ND	0	547.29	1.17	100
VALIDATION-P7-P9	368.26	ND	0	676.40	0.66	100
VALIDATION-P7-P10	300.03	ND	0	608.16	1.50	100
VALIDATION-P7-P11	228.14	ND	0	536.28	1.09	100
VALIDATION-P7-P12	301.19	0.83	100	609.33	0.83	100
VALIDATION-P7-P13	280.16	ND	0	588.30	0.76	100
VALIDATION-P7-P14	290.16	ND	0	598.30	0.81	100
VALIDATION-P7-P15	341.25	0.87	93	649.39	0.87	93
VALIDATION-P7-P16	310.07	1.16	52	618.21	1.16	52
VALIDATION-P7-P17	216.99	ND	0	525.13	1.24	100
VALIDATION-P7-P18	430.00	ND	0	738.00	1.06	100
VALIDATION-P7-P19	281.07	1.00	6	589.21	1.13	94
VALIDATION-P7-P20	222.10	1.00	100	530.24	1.00	100
VALIDATION-P7-P21	291.19	ND	0	599.33	0.84	100
VALIDATION-P7-P22	272.19	ND	0	580.33	0.87	100
VALIDATION-P7-P23	199.11	ND	0	507.25	0.81	100

**Supplementary Table 11: Plate 8:** LCMS data from Chapter 7.3.3.5, HaloCompound *In-Situ* Synthesis for the Validation Set. Column 6 featured a control well, and column 18 featured positive control VHL amine **101**. Performed using standard conditions as outlined in General Methods, using LCMS method (A).

Well Number	SM mass	Rt	% Area	Product Mass	Rt	% Area
VALIDATION-P8-A1	255.14	ND	0	563.28	1.24	100
VALIDATION-P8-A2	322.10	0.49	100	630.24	ND	0
VALIDATION-P8-A3	333.16	0.55	35	641.30	0.93	59
VALIDATION-P8-A4	330.28	0.29	60	638.42	ND	0
VALIDATION-P8-A5	327.21	ND	0	635.34	0.81	100
VALIDATION-P8-A7	370.19	ND	0	678.33	0.86	100
VALIDATION-P8-A8	232.12	0.47	40	540.26	1.10	60
VALIDATION-P8-A9	282.18	0.63	100	590.32	ND	0
VALIDATION-P8-A10	361.25	ND	0	669.39	0.72	100
VALIDATION-P8-A11	269.14	0.58	100	577.28	ND	0
VALIDATION-P8-A12	435.12	ND	0	743.26	1.22	85
VALIDATION-P8-A13	313.13	0.46	91	621.27	ND	0
VALIDATION-P8-A14	259.13	ND	0	567.27	1.03	91
VALIDATION-P8-A15	364.03	ND	0	672.16	1.20	100
VALIDATION-P8-A16	376.12	0.72	95	684.26	ND	0

Confidential – Do Not Copy

VALIDATION-P8-A17	337.15	0.45	100	645.28	ND	0
VALIDATION-P8-A18	430.00	ND	0	738.00	1.06	100
VALIDATION-P8-A19	363.23	ND	0	671.37	0.90	100
VALIDATION-P8-A20	340.13	0.52	100	648.27	ND	0
VALIDATION-P8-A21	370.20	0.59	100	678.34	ND	0
VALIDATION-P8-A22	287.19	0.72	90	595.33	1.32	7
VALIDATION-P8-A23	217.13	ND	0	525.27	0.90	100
VALIDATION-P8-A24	326.07	0.62	6	634.21	1.13	94
VALIDATION-P8-B1	321.16	ND	0	629.30	0.87	100
VALIDATION-P8-B2	318.17	0.69	100	626.31	0.69	100
VALIDATION-P8-B3	218.15	0.33	5	526.29	0.75	95
VALIDATION-P8-B4	306.10	ND	0	614.24	1.11	100
VALIDATION-P8-B5	306.09	0.63	69	614.23	1.16	31
VALIDATION-P8-B7	392.22	0.78	42	700.36	0.78	42
VALIDATION-P8-B8	345.21	0.89	53	653.34	0.89	53
VALIDATION-P8-B9	282.15	ND	0	590.29	1.08	100
VALIDATION-P8-B10	377.16	0.67	71	685.30	ND	0
VALIDATION-P8-B11	284.17	0.60	89	592.31	0.94	11
VALIDATION-P8-B12	263.17	0.88	13	571.31	1.17	48
VALIDATION-P8-B13	303.16	ND	0	611.30	0.84	100
VALIDATION-P8-B14	269.16	ND	0	577.30	0.79	100
VALIDATION-P8-B15	381.01	0.59	3	689.15	1.16	97
VALIDATION-P8-B16	254.16	0.45	100	562.30	ND	0
VALIDATION-P8-B17	313.13	0.47	100	621.27	ND	0
VALIDATION-P8-B18	430.00	ND	0	738.00	1.06	100
VALIDATION-P8-B19	412.30	0.31	38	720.43	0.64	30
VALIDATION-P8-B20	300.17	ND	0	608.31	0.90	100
VALIDATION-P8-B21	268.12	1.02	100	576.26	1.02	100
VALIDATION-P8-B22	247.08	ND	0	555.22	1.08	100
VALIDATION-P8-B23	293.17	0.37	31	601.31	0.89	69
VALIDATION-P8-B24	290.13	0.56	100	598.27	ND	0
VALIDATION-P8-C1	311.16	ND	0	619.30	ND	0
VALIDATION-P8-C2	380.19	0.61	100	688.33	ND	0
VALIDATION-P8-C3	266.20	0.32	100	574.34	ND	0
VALIDATION-P8-C4	431.27	0.93	73	739.41	1.47	27
VALIDATION-P8-C5	331.20	0.47	100	639.34	ND	0
VALIDATION-P8-C7	253.12	0.49	36	561.26	1.02	64
VALIDATION-P8-C8	259.13	ND	0	567.27	1.05	100
VALIDATION-P8-C9	340.23	0.34	95	648.37	ND	0
VALIDATION-P8-C10	317.05	0.60	100	625.19	ND	0

Confidential – Do Not Copy

VALIDATION-P8-C11	211.13	ND	0	519.27	1.04	100
VALIDATION-P8-C12	285.16	ND	0	593.30	0.74	100
VALIDATION-P8-C13	369.11	0.59	100	677.25	ND	0
VALIDATION-P8-C14	251.16	ND	0	559.30	1.07	100
VALIDATION-P8-C15	328.18	0.58	31	636.32	1.11	54
VALIDATION-P8-C16	344.14	ND	0	652.28	1.16	96
VALIDATION-P8-C17	323.14	0.64	75	631.28	ND	0
VALIDATION-P8-C18	430.00	ND	0	738.00	1.06	100
VALIDATION-P8-C19	351.16	0.51	72	659.30	0.91	28
VALIDATION-P8-C20	231.11	0.81	30	539.25	0.81	30
VALIDATION-P8-C21	236.10	0.38	100	544.24	ND	0
VALIDATION-P8-C22	263.09	0.33	84	571.23	0.89	11
VALIDATION-P8-C23	255.09	0.42	100	563.23	ND	0
VALIDATION-P8-C24	291.13	0.42	79	599.27	0.99	21
VALIDATION-P8-D1	337.14	0.48	80	645.28	0.97	20
VALIDATION-P8-D2	278.19	ND	0	586.32	0.70	100
VALIDATION-P8-D3	341.19	ND	0	649.32	1.11	100
VALIDATION-P8-D4	319.23	ND	0	627.37	ND	0
VALIDATION-P8-D5	304.11	1.24	3	612.25	1.06	92
VALIDATION-P8-D7	231.09	0.47	62	539.23	1.13	38
VALIDATION-P8-D8	323.19	0.62	100	631.33	ND	0
VALIDATION-P8-D9	339.19	0.41	95	647.33	ND	0
VALIDATION-P8-D10	375.18	0.71	100	683.32	ND	0
VALIDATION-P8-D11	345.19	0.37	77	653.32	ND	0
VALIDATION-P8-D12	323.22	0.56	100	631.36	ND	0
VALIDATION-P8-D13	304.14	ND	0	612.27	1.15	100
VALIDATION-P8-D14	324.20	0.67	90	632.34	ND	0
VALIDATION-P8-D15	346.26	ND	0	654.40	1.31	100
VALIDATION-P8-D16	338.12	0.58	9	646.26	1.11	91
VALIDATION-P8-D17	288.14	ND	0	596.28	0.77	100
VALIDATION-P8-D18	430.00	ND	0	738.00	1.06	100
VALIDATION-P8-D19	311.16	0.60	50	619.29	ND	0
VALIDATION-P8-D20	288.16	ND	0	596.30	0.96	100
VALIDATION-P8-D21	264.16	0.40	6	572.30	0.99	88
VALIDATION-P8-D22	267.21	ND	0	575.34	0.81	100
VALIDATION-P8-D23	298.15	0.36	53	606.29	0.83	47
VALIDATION-P8-D24	297.15	0.54	13	605.29	1.16	87
VALIDATION-P8-E1	310.17	0.76	11	618.31	1.26	89
VALIDATION-P8-E2	305.12	0.53	43	613.26	1.12	57
VALIDATION-P8-E3	297.12	ND	0	605.26	1.13	100

Confidential – Do Not Copy

VALIDATION-P8-E4	269.14	0.47	100	577.28	ND	0
VALIDATION-P8-E5	277.12	0.76	6	585.26	1.28	94
VALIDATION-P8-E7	380.19	0.50	100	688.33	ND	0
VALIDATION-P8-E8	344.18	1.21	100	652.32	1.21	100
VALIDATION-P8-E9	295.13	0.59	100	603.27	ND	0
VALIDATION-P8-E10	250.14	0.60	8	558.28	1.03	78
VALIDATION-P8-E11	300.15	0.59	100	608.29	ND	0
VALIDATION-P8-E12	257.15	ND	0	565.29	0.79	100
VALIDATION-P8-E13	280.19	0.89	100	588.33	0.89	100
VALIDATION-P8-E14	319.14	0.65	100	627.27	ND	0
VALIDATION-P8-E15	325.07	ND	0	633.20	1.05	100
VALIDATION-P8-E16	291.16	0.43	79	599.30	0.81	12
VALIDATION-P8-E17	302.11	ND	0	610.25	1.23	100
VALIDATION-P8-E18	430.00	ND	0	738.00	1.06	100
VALIDATION-P8-E19	324.20	ND	0	632.33	1.29	100
VALIDATION-P8-E20	224.13	ND	0	532.27	1.03	100
VALIDATION-P8-E21	234.14	ND	0	542.28	1.04	100
VALIDATION-P8-E22	326.14	0.87	100	634.27	0.87	100
VALIDATION-P8-E23	311.14	0.60	57	619.28	1.14	43
VALIDATION-P8-E24	219.14	ND	0	527.28	0.93	100
VALIDATION-P8-F1	222.15	ND	0	530.29	0.96	84
VALIDATION-P8-F2	273.13	ND	0	581.27	1.01	100
VALIDATION-P8-F3	414.11	ND	0	722.25	1.30	100
VALIDATION-P8-F4	311.17	0.76	100	619.31	0.76	100
VALIDATION-P8-F5	266.11	ND	0	574.25	0.98	100
VALIDATION-P8-F7	242.15	0.47	56	550.29	1.03	44
VALIDATION-P8-F8	361.19	0.51	88	669.33	1.02	12
VALIDATION-P8-F9	275.11	0.53	100	583.25	ND	0
VALIDATION-P8-F10	305.11	0.57	63	613.25	1.13	23
VALIDATION-P8-F11	280.19	0.39	32	588.33	0.94	68
VALIDATION-P8-F12	339.21	0.46	47	647.34	0.97	25
VALIDATION-P8-F13	318.15	1.09	87	626.29	1.09	87
VALIDATION-P8-F14	408.20	ND	0	716.34	0.99	100
VALIDATION-P8-F15	260.13	0.45	6	568.27	1.00	94
VALIDATION-P8-F16	272.13	0.43	75	580.27	0.92	25
VALIDATION-P8-F17	307.13	ND	0	615.27	1.35	100
VALIDATION-P8-F18	430.00	ND	0	738.00	1.06	100
VALIDATION-P8-F19	325.19	ND	0	633.33	0.83	100
VALIDATION-P8-F20	295.16	0.66	90	603.30	1.23	10
VALIDATION-P8-F21	314.09	0.49	100	622.23	ND	0

Confidential – Do Not Copy

VALIDATION-P8-F22	251.13	ND	0	559.27	1.06	100
VALIDATION-P8-F23	312.15	ND	0	620.29	1.14	100
VALIDATION-P8-F24	337.22	0.33	100	645.35	ND	0
VALIDATION-P8-G1	285.15	0.66	100	593.29	ND	0
VALIDATION-P8-G2	274.14	0.46	89	582.28	ND	0
VALIDATION-P8-G3	390.11	ND	0	698.25	ND	0
VALIDATION-P8-G4	352.20	ND	0	660.34	0.75	100
VALIDATION-P8-G5	365.12	0.47	100	673.26	ND	0
VALIDATION-P8-G7	277.22	0.54	100	585.35	ND	0
VALIDATION-P8-G8	240.13	0.44	100	548.27	ND	0
VALIDATION-P8-G9	253.14	0.36	100	561.28	ND	0
VALIDATION-P8-G10	220.12	0.32	100	528.26	ND	0
VALIDATION-P8-G11	284.13	0.36	100	592.27	ND	0
VALIDATION-P8-G12	325.20	0.39	12	633.34	0.81	78
VALIDATION-P8-G13	255.14	0.53	15	563.28	1.18	73
VALIDATION-P8-G14	321.07	ND	0	629.21	1.21	100
VALIDATION-P8-G15	225.10	ND	0	533.24	ND	0
VALIDATION-P8-G16	247.17	ND	0	555.31	1.12	53
VALIDATION-P8-G17	241.09	ND	0	549.23	0.75	100
VALIDATION-P8-G18	430.00	ND	0	738.00	1.06	100
VALIDATION-P8-G19	332.09	0.74	91	640.23	1.23	9
VALIDATION-P8-G20	241.13	ND	0	549.27	0.85	100
VALIDATION-P8-G21	337.13	0.41	85	645.27	0.84	15
VALIDATION-P8-G22	241.13	0.37	51	549.27	0.99	41
VALIDATION-P8-G23	336.16	0.55	67	644.30	1.12	33
VALIDATION-P8-G24	220.08	ND	0	528.22	0.99	100
VALIDATION-P8-H1	271.17	1.13	78	579.31	1.13	78
VALIDATION-P8-H2	323.11	0.66	93	631.25	ND	0
VALIDATION-P8-H3	266.11	ND	0	574.25	1.10	81
VALIDATION-P8-H4	225.09	ND	0	533.23	0.92	100
VALIDATION-P8-H5	399.22	0.58	91	707.35	0.90	6
VALIDATION-P8-H7	269.16	ND	0	577.30	1.05	100
VALIDATION-P8-H8	322.17	0.36	100	630.31	ND	0
VALIDATION-P8-H9	378.10	ND	0	686.24	1.15	100
VALIDATION-P8-H10	298.15	0.44	100	606.29	ND	0
VALIDATION-P8-H11	300.20	ND	0	608.33	ND	0
VALIDATION-P8-H12	343.19	0.61	100	651.33	ND	0
VALIDATION-P8-H13	344.17	1.11	100	652.31	1.11	100
VALIDATION-P8-H14	352.23	ND	0	660.37	0.86	100
VALIDATION-P8-H15	225.15	ND	0	533.29	1.14	100

Confidential – Do Not Copy

VALIDATION-P8-H16	290.08	ND	0	598.22	ND	0
VALIDATION-P8-H17	254.11	0.36	100	562.25	ND	0
VALIDATION-P8-H18	430.00	ND	0	738.00	1.06	100
VALIDATION-P8-H19	290.20	ND	0	598.34	0.78	100
VALIDATION-P8-H20	229.12	ND	0	537.26	1.18	96
VALIDATION-P8-H21	391.13	ND	0	699.27	1.01	97
VALIDATION-P8-H22	287.17	ND	0	595.31	0.82	100
VALIDATION-P8-H23	378.21	ND	0	686.35	0.84	100
VALIDATION-P8-H24	335.17	0.52	80	643.31	ND	0
VALIDATION-P8-I1	357.03	ND	0	665.17	1.25	100
VALIDATION-P8-I2	233.12	ND	0	541.26	1.11	66
VALIDATION-P8-I3	383.13	ND	0	691.27	1.21	96
VALIDATION-P8-I4	273.11	ND	0	581.25	0.98	100
VALIDATION-P8-I5	341.20	ND	0	649.34	0.93	100
VALIDATION-P8-I7	289.18	0.41	100	597.32	ND	0
VALIDATION-P8-I8	302.15	ND	0	610.29	0.80	100
VALIDATION-P8-I9	306.19	0.37	27	614.33	0.81	74
VALIDATION-P8-I10	289.09	0.46	14	597.23	1.07	86
VALIDATION-P8-I11	288.21	0.32	4	596.35	0.62	96
VALIDATION-P8-I12	288.16	0.43	100	596.30	0.43	100
VALIDATION-P8-I13	307.20	0.74	100	615.34	0.74	100
VALIDATION-P8-I14	288.10	0.47	100	596.24	ND	0
VALIDATION-P8-I15	207.13	ND	0	515.27	1.11	100
VALIDATION-P8-I16	235.16	ND	0	543.30	1.18	100
VALIDATION-P8-I17	265.11	0.74	100	573.25	ND	0
VALIDATION-P8-I18	430.00	ND	0	738.00	1.06	100
VALIDATION-P8-I19	382.24	ND	0	690.38	ND	0
VALIDATION-P8-I20	261.18	ND	0	569.32	0.75	100
VALIDATION-P8-I21	249.14	ND	0	557.28	1.09	100
VALIDATION-P8-I22	211.11	ND	0	519.25	0.87	100
VALIDATION-P8-I23	355.09	0.61	100	663.23	ND	0
VALIDATION-P8-I24	317.12	0.58	100	625.26	ND	0
VALIDATION-P8-J1	339.14	0.49	81	647.27	0.83	11
VALIDATION-P8-J2	342.21	0.83	86	650.34	0.83	86
VALIDATION-P8-J3	230.13	ND	0	538.27	0.82	100
VALIDATION-P8-J4	262.18	0.87	100	570.32	0.87	100
VALIDATION-P8-J5	235.13	ND	0	543.27	1.06	100
VALIDATION-P8-J7	303.19	ND	0	611.33	0.94	100
VALIDATION-P8-J8	331.13	0.44	100	639.27	ND	0
VALIDATION-P8-J9	276.20	ND	0	584.33	0.72	100

Confidential – Do Not Copy

VALIDATION-P8-J10	232.14	0.39	1	540.28	0.79	99
VALIDATION-P8-J11	332.12	ND	0	640.26	1.12	100
VALIDATION-P8-J12	358.14	0.63	100	666.27	ND	0
VALIDATION-P8-J13	314.15	ND	0	622.29	1.02	95
VALIDATION-P8-J14	354.18	0.42	26	662.32	0.81	70
VALIDATION-P8-J15	343.15	ND	0	651.29	1.11	91
VALIDATION-P8-J16	328.03	ND	0	636.16	1.18	100
VALIDATION-P8-J17	362.21	ND	0	670.35	0.85	100
VALIDATION-P8-J18	430.00	ND	0	738.00	1.06	100
VALIDATION-P8-J19	380.12	ND	0	688.26	1.13	100
VALIDATION-P8-J20	342.11	ND	0	650.25	1.23	100
VALIDATION-P8-J21	305.12	ND	0	613.26	1.14	100
VALIDATION-P8-J22	286.14	ND	0	594.28	0.85	97
VALIDATION-P8-J23	302.09	ND	0	610.22	1.16	100
VALIDATION-P8-J24	294.13	ND	0	602.27	0.88	52
VALIDATION-P8-K1	262.12	0.62	94	570.26	ND	0
VALIDATION-P8-K2	362.22	0.51	100	670.36	ND	0
VALIDATION-P8-K3	260.15	0.63	3	568.29	0.99	97
VALIDATION-P8-K4	268.17	0.33	31	576.31	0.84	69
VALIDATION-P8-K5	332.21	ND	0	640.35	1.14	100
VALIDATION-P8-K7	279.16	0.46	52	587.30	1.00	48
VALIDATION-P8-K8	223.11	ND	0	531.25	0.77	100
VALIDATION-P8-K9	295.14	0.47	100	603.28	ND	0
VALIDATION-P8-K10	204.10	ND	0	512.24	0.85	100
VALIDATION-P8-K11	301.20	ND	0	609.34	0.78	100
VALIDATION-P8-K12	233.15	ND	0	541.29	0.75	100
VALIDATION-P8-K13	341.15	ND	0	649.29	1.08	95
VALIDATION-P8-K14	357.09	1.04	99	665.23	1.04	99
VALIDATION-P8-K15	345.15	0.45	100	653.29	ND	0
VALIDATION-P8-K16	368.15	0.73	92	676.29	1.01	8
VALIDATION-P8-K17	346.27	0.83	46	654.41	1.47	54
VALIDATION-P8-K18	430.00	ND	0	738.00	1.06	100
VALIDATION-P8-K19	361.24	ND	0	669.38	1.05	100
VALIDATION-P8-K20	315.22	ND	0	623.36	0.77	100
VALIDATION-P8-K21	346.22	0.74	100	654.36	ND	0
VALIDATION-P8-K22	318.24	ND	0	626.38	ND	0
VALIDATION-P8-K23	232.14	ND	0	540.28	0.92	95
VALIDATION-P8-K24	248.15	ND	0	556.29	ND	0
VALIDATION-P8-L1	292.11	0.47	82	600.24	1.03	18
VALIDATION-P8-L2	317.17	ND	0	625.31	1.13	100

Confidential – Do Not Copy

VALIDATION-P8-L3	304.15	0.46	52	612.29	0.95	37
VALIDATION-P8-L4	358.15	ND	0	666.29	1.04	100
VALIDATION-P8-L5	429.22	0.63	38	737.36	0.94	62
VALIDATION-P8-L7	275.13	ND	0	583.27	0.97	100
VALIDATION-P8-L8	340.15	0.41	71	648.29	0.83	10
VALIDATION-P8-L9	318.14	0.58	31	626.28	1.13	53
VALIDATION-P8-L10	304.19	ND	0	612.33	1.02	100
VALIDATION-P8-L11	320.17	0.39	95	628.31	ND	0
VALIDATION-P8-L12	326.12	ND	0	634.26	0.76	89
VALIDATION-P8-L13	380.23	0.70	92	688.37	ND	0
VALIDATION-P8-L14	308.12	0.59	68	616.26	1.19	32
VALIDATION-P8-L15	268.09	0.51	89	576.23	ND	0
VALIDATION-P8-L16	312.16	ND	0	620.30	0.92	100
VALIDATION-P8-L17	288.17	ND	0	596.31	0.81	100
VALIDATION-P8-L18	430.00	ND	0	738.00	1.06	100
VALIDATION-P8-L19	395.11	0.58	93	703.25	0.92	7
VALIDATION-P8-L20	352.13	ND	0	660.26	1.23	100
VALIDATION-P8-L21	313.19	0.31	100	621.33	ND	0
VALIDATION-P8-L22	334.14	ND	0	642.28	0.97	100
VALIDATION-P8-L23	294.21	0.46	100	602.34	ND	0
VALIDATION-P8-L24	407.16	ND	0	715.30	0.99	100
VALIDATION-P8-M1	354.21	0.73	100	662.34	ND	0
VALIDATION-P8-M2	238.05	ND	0	546.19	1.12	100
VALIDATION-P8-M3	342.16	0.67	100	650.30	ND	0
VALIDATION-P8-M4	317.17	ND	0	625.31	0.90	92
VALIDATION-P8-M5	401.16	ND	0	709.30	1.22	100
VALIDATION-P8-M7	323.09	0.54	59	631.23	0.88	41
VALIDATION-P8-M8	288.20	ND	0	596.33	1.02	100
VALIDATION-P8-M9	210.15	ND	0	518.29	0.70	100
VALIDATION-P8-M10	314.17	ND	0	622.31	1.24	100
VALIDATION-P8-M11	332.03	ND	0	640.17	1.13	100
VALIDATION-P8-M12	417.22	0.39	87	725.36	0.81	13
VALIDATION-P8-M13	237.15	0.34	100	545.29	ND	0
VALIDATION-P8-M14	399.22	0.51	93	707.35	0.83	7
VALIDATION-P8-M15	319.15	ND	0	627.29	1.01	100
VALIDATION-P8-M16	346.18	0.42	5	654.32	0.87	95
VALIDATION-P8-M17	293.12	0.64	100	601.26	ND	0
VALIDATION-P8-M18	430.00	ND	0	738.00	1.06	100
VALIDATION-P8-M19	222.10	ND	0	530.24	0.99	100
VALIDATION-P8-M20	263.14	ND	0	571.28	1.02	100

Confidential – Do Not Copy

VALIDATION-P8-M21	384.25	0.51	100	692.39	ND	0
VALIDATION-P8-M22	277.18	ND	0	585.32	0.71	100
VALIDATION-P8-M23	334.12	ND	0	642.25	1.22	100
VALIDATION-P8-M24	223.16	ND	0	531.30	ND	0
VALIDATION-P8-N1	288.10	ND	0	596.24	ND	0
VALIDATION-P8-N2	297.15	ND	0	605.29	1.10	100
VALIDATION-P8-N3	261.15	ND	0	569.29	ND	0
VALIDATION-P8-N4	260.13	0.89	100	568.27	0.89	100
VALIDATION-P8-N5	271.14	0.67	100	579.28	0.67	100
VALIDATION-P8-N7	316.14	0.35	14	624.27	ND	0
VALIDATION-P8-N8	347.23	ND	0	655.37	ND	0
VALIDATION-P8-N9	423.03	ND	0	731.16	1.12	100
VALIDATION-P8-N10	286.15	0.45	65	594.29	0.95	35
VALIDATION-P8-N11	362.14	0.69	52	670.28	1.24	34
VALIDATION-P8-N12	390.21	ND	0	698.34	0.83	100
VALIDATION-P8-N13	372.10	0.61	100	680.24	ND	0
VALIDATION-P8-N14	234.14	ND	0	542.28	0.76	100
VALIDATION-P8-N15	246.13	ND	0	554.27	1.02	100
VALIDATION-P8-N16	343.00	ND	0	651.14	1.19	93
VALIDATION-P8-N17	287.13	ND	0	595.27	1.14	100
VALIDATION-P8-N18	430.00	ND	0	738.00	1.06	100
VALIDATION-P8-N19	336.18	ND	0	644.32	1.01	62
VALIDATION-P8-N20	362.12	ND	0	670.26	1.15	100
VALIDATION-P8-N21	266.21	ND	0	574.35	ND	0
VALIDATION-P8-N22	347.17	ND	0	655.31	ND	0
VALIDATION-P8-N23	345.12	0.62	100	653.26	ND	0
VALIDATION-P8-N24	217.13	ND	0	525.27	0.74	100
VALIDATION-P8-O1	287.14	0.58	100	595.28	0.58	100
VALIDATION-P8-O2	371.27	0.48	87	679.41	ND	0
VALIDATION-P8-O3	350.15	0.59	94	658.29	ND	0
VALIDATION-P8-O4	344.13	0.43	100	652.27	ND	0
VALIDATION-P8-O5	266.21	ND	0	574.35	0.68	100
VALIDATION-P8-O7	334.14	ND	0	642.27	1.11	100
VALIDATION-P8-O8	308.22	0.66	100	616.36	0.66	100
VALIDATION-P8-O9	314.21	ND	0	622.35	ND	0
VALIDATION-P8-O10	316.10	0.62	64	624.24	1.22	36
VALIDATION-P8-O11	291.17	0.35	2	599.31	0.81	98
VALIDATION-P8-O12	392.18	0.47	100	700.32	ND	0
VALIDATION-P8-O13	227.10	0.43	100	535.24	ND	0
VALIDATION-P8-O14	275.05	0.60	46	583.19	1.24	54

VALIDATION-P8-O15	346.11	0.64	100	654.25	ND	0
VALIDATION-P8-O16	234.18	ND	0	542.32	0.82	100
VALIDATION-P8-O17	257.12	0.57	36	565.26	0.94	64
VALIDATION-P8-O18	430.00	ND	0	738.00	1.06	100
VALIDATION-P8-O19	283.02	ND	0	591.16	1.11	100
VALIDATION-P8-O20	363.11	ND	0	671.24	1.12	100
VALIDATION-P8-O21	299.06	ND	0	607.20	ND	0
VALIDATION-P8-O22	267.14	0.98	98	575.28	0.98	98
VALIDATION-P8-O23	295.08	ND	0	603.22	1.14	100
VALIDATION-P8-O24	315.17	0.42	100	623.31	ND	0
VALIDATION-P8-P1	292.10	0.47	21	600.24	1.07	79
VALIDATION-P8-P2	329.21	ND	0	637.35	ND	0
VALIDATION-P8-P3	333.12	0.61	100	641.26	ND	0
VALIDATION-P8-P4	316.22	ND	0	624.35	1.13	100
VALIDATION-P8-P5	316.10	0.53	100	624.24	ND	0
VALIDATION-P8-P7	330.21	0.54	10	638.34	1.08	90
VALIDATION-P8-P8	333.13	ND	0	641.27	1.13	100
VALIDATION-P8-P9	421.25	0.53	93	729.39	ND	0
VALIDATION-P8-P10	395.08	0.80	30	703.22	1.32	70
VALIDATION-P8-P11	275.13	0.42	100	583.27	ND	0
VALIDATION-P8-P12	232.17	ND	0	540.31	1.01	61
VALIDATION-P8-P13	386.27	0.45	71	694.41	0.75	27
VALIDATION-P8-P14	328.19	0.74	100	636.33	0.74	100
VALIDATION-P8-P15	236.12	ND	0	544.26	0.96	100
VALIDATION-P8-P16	386.07	0.69	100	694.21	ND	0
VALIDATION-P8-P17	327.09	0.81	100	635.23	ND	0
VALIDATION-P8-P18	430.00	ND	0	738.00	1.06	100
VALIDATION-P8-P19	280.23	ND	0	588.37	1.09	100
VALIDATION-P8-P20	235.17	ND	0	543.31	0.62	100
VALIDATION-P8-P21	267.15	0.78	60	575.29	0.78	60
VALIDATION-P8-P22	302.21	0.49	100	610.35	ND	0
VALIDATION-P8-P23	270.15	ND	0	578.29	1.20	100
VALIDATION-P8-P24	260.13	0.43	89	568.27	ND	0

**Supplementary Table 12: Plate 9:** LCMS data from Chapter 7.3.3.5, HaloCompound *In-Situ* Synthesis for the Validation Set. Column 6 featured a control well, and column 18 featured positive control VHL amine **101**. Performed using standard conditions as outlined in General Methods, using LCMS method (A).

Well Number	SM mass	Rt	% Area	Product Mass	Rt	% Area
VALIDATION-P9-A1	265.15	0.83	100	573.29	0.83	100

Confidential – Do Not Copy

VALIDATION-P9-A2	407.05	0.74	81	715.19	ND	0
VALIDATION-P9-A3	329.16	0.44	42	637.30	0.88	48
VALIDATION-P9-A4	263.14	ND	0	571.28	0.91	100
VALIDATION-P9-A5	331.18	0.34	100	639.32	ND	0
VALIDATION-P9-A7	408.26	0.47	67	716.40	ND	0
VALIDATION-P9-A8	288.16	ND	0	596.30	1.20	40
VALIDATION-P9-A9	297.14	0.47	100	605.28	ND	0
VALIDATION-P9-A10	328.15	1.09	69	636.29	1.09	69
VALIDATION-P9-A11	437.21	0.72	4	745.35	1.18	96
VALIDATION-P9-A18	430.00	0.58	4	738.00	1.06	96
VALIDATION-P9-B1	391.19	0.77	78	699.33	1.33	22
VALIDATION-P9-B2	228.14	0.75	96	536.28	0.75	96
VALIDATION-P9-B3	239.13	0.44	100	547.27	ND	0
VALIDATION-P9-B4	319.12	0.44	100	627.26	ND	0
VALIDATION-P9-B5	310.18	0.41	100	618.32	ND	0
VALIDATION-P9-B7	304.14	0.36	91	612.27	ND	0
VALIDATION-P9-B8	335.16	ND	0	643.30	1.23	100
VALIDATION-P9-B9	303.16	ND	0	611.29	ND	0
VALIDATION-P9-B10	228.14	ND	0	536.28	0.98	100
VALIDATION-P9-B11	373.14	0.64	100	681.28	ND	0
VALIDATION-P9-B18	430.00	0.58	3	738.00	1.06	97
VALIDATION-P9-C1	248.07	ND	0	556.21	1.04	100
VALIDATION-P9-C2	326.22	ND	0	634.36	0.81	100
VALIDATION-P9-C3	331.14	ND	0	639.27	1.35	100
VALIDATION-P9-C4	349.16	0.42	25	657.30	0.93	75
VALIDATION-P9-C5	205.11	0.41	17	513.25	1.02	83
VALIDATION-P9-C7	305.20	0.67	73	613.34	1.27	27
VALIDATION-P9-C8	281.16	0.39	80	589.30	ND	0
VALIDATION-P9-C9	333.11	0.61	95	641.25	1.21	5
VALIDATION-P9-C10	280.19	ND	0	588.33	0.91	100
VALIDATION-P9-C11	328.08	0.93	94	636.22	0.93	94
VALIDATION-P9-C18	430.00	ND	0	738.00	1.06	100
VALIDATION-P9-D1	340.19	ND	0	648.33	0.78	100
VALIDATION-P9-D2	327.15	0.59	82	635.29	1.14	18
VALIDATION-P9-D3	299.17	0.44	100	607.31	ND	0
VALIDATION-P9-D4	291.11	0.61	100	599.25	ND	0
VALIDATION-P9-D5	340.19	0.39	89	648.33	ND	0
VALIDATION-P9-D7	280.16	1.03	100	588.30	1.03	100
VALIDATION-P9-D8	274.15	ND	0	582.29	1.01	100
VALIDATION-P9-D9	355.14	ND	0	663.27	1.16	90

Confidential – Do Not Copy

VALIDATION-P9-D10	263.20	ND	0	571.34	ND	0
VALIDATION-P9-D11	327.19	0.35	17	635.33	0.78	83
VALIDATION-P9-D18	430.00	ND	0	738.00	1.06	100
VALIDATION-P9-E1	231.11	0.33	43	539.25	0.95	57
VALIDATION-P9-E2	300.09	ND	0	608.23	1.07	100
VALIDATION-P9-E3	298.12	ND	0	606.25	1.32	100
VALIDATION-P9-E4	255.14	ND	0	563.28	0.88	96
VALIDATION-P9-E5	344.06	0.53	21	652.20	1.08	79
VALIDATION-P9-E7	287.10	0.58	91	595.24	1.18	9
VALIDATION-P9-E8	329.19	ND	0	637.32	1.17	88
VALIDATION-P9-E9	385.16	1.15	100	693.30	1.15	100
VALIDATION-P9-E10	318.10	0.60	100	626.24	ND	0
VALIDATION-P9-E11	345.15	0.55	75	653.29	ND	0
VALIDATION-P9-E18	430.00	ND	0	738.00	1.06	100
VALIDATION-P9-F1	384.14	0.56	83	692.27	ND	0
VALIDATION-P9-F2	270.10	0.44	77	578.24	1.11	23
VALIDATION-P9-F3	244.13	ND	0	552.27	0.69	100
VALIDATION-P9-F4	273.11	0.53	64	581.25	1.18	30
VALIDATION-P9-F5	390.22	ND	0	698.36	0.88	100
VALIDATION-P9-F7	318.21	0.47	84	626.34	0.86	5
VALIDATION-P9-F8	313.19	ND	0	621.33	0.83	84
VALIDATION-P9-F9	314.06	0.52	100	622.20	ND	0
VALIDATION-P9-F10	265.18	0.37	100	573.32	ND	0
VALIDATION-P9-F11	316.14	0.86	75	624.27	0.86	75
VALIDATION-P9-F18	430.00	ND	0	738.00	1.06	100
VALIDATION-P9-G1	254.11	0.35	53	562.25	1.05	47
VALIDATION-P9-G2	297.16	0.29	20	605.30	0.75	80
VALIDATION-P9-G3	325.20	ND	0	633.34	1.08	100
VALIDATION-P9-G4	277.18	0.79	100	585.32	0.79	100
VALIDATION-P9-G5	311.17	0.77	100	619.31	0.77	100
VALIDATION-P9-G7	276.12	ND	0	584.26	0.95	100
VALIDATION-P9-G8	349.10	1.31	100	657.24	1.31	100
VALIDATION-P9-G9	319.16	0.89	3	627.30	1.12	97
VALIDATION-P9-G10	374.17	ND	0	682.31	1.30	100
VALIDATION-P9-G11	299.03	ND	0	607.17	0.93	100
VALIDATION-P9-G18	430.00	ND	0	738.00	1.06	100
VALIDATION-P9-H1	246.05	ND	0	554.19	1.13	100
VALIDATION-P9-H2	307.09	0.51	85	615.23	1.12	4
VALIDATION-P9-H3	251.16	ND	0	559.30	0.98	100
VALIDATION-P9-H4	440.19	0.91	100	748.33	ND	0

Confidential – Do Not Copy

VALIDATION-P9-H5	357.15	ND	0	665.29	0.91	100
VALIDATION-P9-H7	237.15	ND	0	545.29	0.99	100
VALIDATION-P9-H8	365.21	0.68	63	673.35	1.25	29
VALIDATION-P9-H9	374.23	ND	0	682.37	0.79	83
VALIDATION-P9-H10	202.12	ND	0	510.26	0.74	100
VALIDATION-P9-H11	433.17	ND	0	741.31	1.04	88
VALIDATION-P9-H18	430.00	0.58	2	738.00	1.06	98
VALIDATION-P9-I1	339.19	ND	0	647.33	1.15	58
VALIDATION-P9-I2	249.16	0.34	16	557.30	0.94	84
VALIDATION-P9-I3	207.14	0.91	100	515.28	0.91	100
VALIDATION-P9-I4	240.10	ND	0	548.24	0.93	100
VALIDATION-P9-I5	314.17	0.57	100	622.31	ND	0
VALIDATION-P9-I7	277.19	ND	0	585.33	0.80	100
VALIDATION-P9-I8	324.14	ND	0	632.28	0.94	100
VALIDATION-P9-I9	329.23	0.61	41	637.37	0.65	14
VALIDATION-P9-I10	324.13	0.52	100	632.27	ND	0
VALIDATION-P9-I18	430.00	0.58	3	738.00	1.06	97
VALIDATION-P9-J1	317.04	0.52	100	625.18	ND	0
VALIDATION-P9-J2	308.16	0.35	81	616.30	0.85	19
VALIDATION-P9-J3	287.07	0.57	100	595.21	ND	0
VALIDATION-P9-J4	336.17	0.63	100	644.31	0.63	100
VALIDATION-P9-J5	269.08	0.44	69	577.22	1.13	31
VALIDATION-P9-J7	328.19	0.43	100	636.33	ND	0
VALIDATION-P9-J8	315.16	ND	0	623.30	1.18	100
VALIDATION-P9-J9	344.17	0.95	100	652.31	ND	0
VALIDATION-P9-J10	349.06	ND	0	657.19	1.09	100
VALIDATION-P9-J18	430.00	ND	0	738.00	1.06	100
VALIDATION-P9-K1	292.11	0.43	100	600.25	ND	0
VALIDATION-P9-K2	357.24	0.49	100	665.38	ND	0
VALIDATION-P9-K3	317.04	0.54	100	625.18	ND	0
VALIDATION-P9-K4	288.16	ND	0	596.30	0.99	95
VALIDATION-P9-K5	276.18	0.58	73	584.32	ND	0
VALIDATION-P9-K7	391.26	0.56	77	699.40	1.04	15
VALIDATION-P9-K8	326.21	ND	0	634.35	ND	0
VALIDATION-P9-K9	336.15	0.54	63	644.29	ND	0
VALIDATION-P9-K10	234.17	ND	0	542.31	ND	0
VALIDATION-P9-K18	430.00	0.58	3	738.00	1.06	97
VALIDATION-P9-L1	288.16	0.40	65	596.30	0.93	35
VALIDATION-P9-L2	246.16	ND	0	554.30	0.70	100
VALIDATION-P9-L3	265.13	ND	0	573.27	1.06	100

Confidential – Do Not Copy

VALIDATION-P9-L4	382.21	0.43	95	690.34	0.94	5
VALIDATION-P9-L5	300.15	0.63	52	608.29	1.14	43
VALIDATION-P9-L7	215.11	ND	0	523.24	0.99	100
VALIDATION-P9-L8	390.23	0.81	11	698.37	1.40	80
VALIDATION-P9-L9	337.11	ND	0	645.25	0.85	100
VALIDATION-P9-L10	351.11	ND	0	659.25	1.42	100
VALIDATION-P9-L18	430.00	0.58	3	738.00	1.06	97
VALIDATION-P9-M1	337.98	0.44	100	646.11	ND	0
VALIDATION-P9-M2	306.01	0.45	70	614.15	1.01	30
VALIDATION-P9-M3	312.12	0.50	81	620.26	ND	0
VALIDATION-P9-M4	395.24	0.57	100	689.37	0.57	100
VALIDATION-P9-M5	309.14	0.50	100	617.28	0.50	100
VALIDATION-P9-M7	271.10	ND	0	579.24	1.08	100
VALIDATION-P9-M8	281.14	0.62	100	589.28	ND	0
VALIDATION-P9-M9	263.07	0.43	100	571.21	ND	0
VALIDATION-P9-M10	439.22	0.73	9	747.36	1.26	82
VALIDATION-P9-M18	430.00	0.58	3	738.00	1.06	97
VALIDATION-P9-N1	237.14	0.44	100	545.28	ND	0
VALIDATION-P9-N2	360.24	0.62	100	668.38	0.62	100
VALIDATION-P9-N3	328.08	0.58	87	636.22	ND	0
VALIDATION-P9-N4	314.21	ND	0	622.35	1.16	100
VALIDATION-P9-N5	337.19	ND	0	645.33	1.12	100
VALIDATION-P9-N7	260.13	0.34	91	568.27	ND	0
VALIDATION-P9-N8	269.13	ND	0	577.27	ND	0
VALIDATION-P9-N9	387.19	0.52	48	695.33	0.82	51
VALIDATION-P9-N10	208.17	0.87	100	516.31	0.87	100
VALIDATION-P9-N18	430.00	0.58	3	738.00	1.06	97
VALIDATION-P9-O1	302.16	ND	0	610.30	1.07	100
VALIDATION-P9-O2	290.12	0.35	100	598.26	ND	0
VALIDATION-P9-O3	317.17	0.54	69	625.31	1.14	26
VALIDATION-P9-O4	256.16	ND	0	564.30	ND	0
VALIDATION-P9-O5	318.11	0.53	100	626.25	ND	0
VALIDATION-P9-O7	310.14	0.55	100	618.27	ND	0
VALIDATION-P9-O8	327.14	0.90	3	635.28	1.01	96
VALIDATION-P9-O9	235.09	0.48	4	543.23	1.16	96
VALIDATION-P9-O10	229.13	0.51	4	537.27	1.09	91
VALIDATION-P9-O18	430.00	0.58	5	738.00	1.06	95
VALIDATION-P9-P1	338.04	0.71	100	646.17	ND	0
VALIDATION-P9-P2	252.13	0.36	100	560.27	ND	0
VALIDATION-P9-P3	341.22	0.28	100	649.36	ND	0

Confidential – Do Not Copy

VALIDATION-P9-P4	340.01	0.65	100	648.15	ND	0
VALIDATION-P9-P5	244.13	0.45	59	566.27	ND	0
VALIDATION-P9-P7	300.15	0.55	100	608.29	ND	0
VALIDATION-P9-P8	303.19	0.62	61	611.33	1.12	39
VALIDATION-P9-P9	297.18	0.30	100	605.32	ND	0
VALIDATION-P9-P10	302.16	0.36	12	610.30	0.81	88
VALIDATION-P9-P18	430.00	1.06	89	738.00	1.06	89